Metabolic and transcriptomic response to hyperosmotic stimulus reveals strategies for optimization of antibody producing Chinese hamster ovary cells

Von der Fakultät Energie-, Verfahrens- und Biotechnik

der Universität Stuttgart zur Erlangung der Würde eines Doktors

der Naturwissenschaften (Dr. rer. nat.) genehmigte Abhandlung

Vorgelegt von

Jennifer Isabelle Pfizenmaier-Wu

geb. Pfizenmaier

aus Ludwigsburg

Hauptberichter: Prof. Dr.-Ing. Ralf Takors

Mitberichter: Prof. Dr. Monilola Olayioye

Tag der mündlichen Prüfung: 18. April 2017

Institut für Bioverfahrenstechnik

Universität Stuttgart

2017

MEINER FAMILIE

Danksagung

Table of Contents

Declaration of Academic Honesty

I hereby assure that I performed this work independently and without further help or other materials than stated.

Munich, May 2017
Jennifer Isabelle Pfizenmaier-Wu

Parts of this thesis have already been published.

Pfizenmaier, J., J.-C. Matuszczyk & R. Takors (2015). Changes in Intracellular ATP-content of CHO Cells as Response to Hyperosmolality. **Biotechnol. Prog. 31**(5):1212-1216

Pfizenmaier, J., L. Junghans, A. Teleki & R. Takors (2016). Hyperosmotic Stimulus Study Discloses Benefits in ATP Supply and Reveals miRNA/mRNA Targets to Improve Recombinant Protein Production of CHO Cells. **Biotechnol. J. 11**:1037-1047

Nomenclature

Γ	Number of counts of a gene
λ	Wavelength [nm]
ξ	Osmolality [mOsmol kg^{-1}]
π	Osmotic pressure [Pa]
ϕ_c	Cell diameter [µm]
$\phi_{impeller}$	Diameter of impeller [mm]
Ψ	Fluorescence intensity
ω	Osmotic coefficient
µ	Specific growth rate [d^{-1}]
%	Percent (per hundred)
ADP	Adenosine diphosphate
AEC	Adenylate energy charge
AMP	Adenosine monophosphate
Asn	Asparagine
ATCC	American type culture collection
ATP	Adenosine triphosphate
BSA	Bovine serum albumin
BCV	Biological coefficient of variation
c	Concentration of a compound
CDK	Cyclin dependent kinase
CDK1A	Cyclin dependent kinase inhibitor protein 1A
C. elegans	*Caenorhabditis elegans*
cgr-miR	*Cricetulus griseus* microRNA
CHO	Chinese hamster ovary
cis-aco	*cis*-aconitate
CO_2	Carbon dioxide
CoA	Coenzyme A

const.	Constant
CPM	Counts per million
cyt	Cytosolic
d	Day
DEG	Significantly differentially expressed gene
DHFR	Dihydrofolate reductase
DMSO	Dimethyl sulfoxide
DNA	Deoxyribonucleic acid
DO	Dissolved oxygen [%]
E. coli	*Escherichia coli*
EDTA	Ethylenediaminetetraacetic acid
ELISA	Enzyme linked immunosorbent assay
Eq.	Equation
ER	Endoplasmic reticulum
F6P	Fructose-6-phosphate
$F_{aeration}$	Aeration rate of bioreactor [sL h^{-1}]
FAD/FADH$_2$	Oxidized/reduced state of flavin adenine dinucleotide
FC	Fold-change in gene expression
FDR	False Discovery Rate
Fig.	Figure
FL-2,-3	Fluorescence channel-2, -3 (575 nm, 620 nm)
FS	Forward scatter
g	Gravitational acceleration
g	Gram
G418	Geneticin
G6P	Glucose-6-phosphate
GC-MS	Gas chromatography-mass spectrometry
GFP	Green fluorescent protein
Glc	Glucose
GlcNAc	N-acetylglucosamine
Gln	Glutamine
Glu	Glutamate
GOI	Gene of interest
h	Hour

HCl	Hydrochloric acid
HILIC-ESI-MS/MS	Hydrophilic interaction liquid chromatography-electrospray ionization-tandem mass spectrometry
HPLC	High performance liquid chromatography
hsa-miR	*Homo sapiens* microRNA
HSP	Heat shock protein
IDMS	Isotope dilution mass spectrometry
IgG1	Immunoglobulin G1
IL-8	Interleukin-8
IMM	Inner mitochondrial membrane
iso	Isotype control
KOH	Potassium hydroxide
Lac	Lactate
lin	Linear
log	Logarithmic
log2(FC)	Logarithm to the base 2 of the fold-change in gene expression
m	Mass of a compound [g]
M	Molarity [mol L^{-1}]
mAb	Monoclonal antibody
Man	Mannose
min	Minute
miR	microRNA
mit	Mitochondrial compartment
mmu-miR	*Mus musculus* microRNA
MRM	Multiple reaction monitoring
mRNA	Messenger RNA
MSX	Methionine sulphoximine
MTX	Methotrexate
N	Agitation Speed [rpm]
n	Molar amount of a compound [mol]
N_2	Nitrogen
N_{cells}	Number of cells
NaCl	Sodium chloride
Na_2CO_3	Sodium carbonate

NAD^+/NADH	Oxidized/reduced state of nicotinamide adenine dinucleotide
$NaHCO_3$	Sodium hydrogen carbonate
NaOH	Sodium hydroxide
NGS	Next generation sequencing
NH_4^+	Ammonium
nt	Nucleotides
O_2	Oxygen
OMM	Outer mitochondrial membrane
P	P-value
p	Pressure [mbar]
PBS	Phosphate buffered saline
pCO_2	Dissolved carbon dioxide level [bar]
PE	Phycoerythrin
pH	Negative logarithm to the base 10 of the proton concentration
PTM	Post translational modification
q	Specific metabolic formation rate
QbD	Quality by design
qRT-PCR	Quantitative real time polymerase chain reaction
R	Ideal gas constant
RISC	RNA-induced silencing complex
RNA	Ribonucleic acid
rpm	Rounds per minute
RVI	Regulatory volume increase
S. cerevisiae	*Saccharomyces cerevisiae*
SS	Sidewards scatter
STR	Stirred tank bioreactor
T	Temperature [℃]
Tab.	Table
TIM	Translocase of the inner mitochondrial membrane
TOM	Translocase of the outer mitochondrial membrane
TBS	Tris buffered saline
U	Voltage [V]
UQ	ubiquinone
UQH_2	ubiquinol

V	volume [L]
VCD	Viable cell density
VCD_{max}	Maximal viable cell density
V_R	Working volume of bioreactor cultivation [L]
vs.	Versus
(v/v)	Proportion of volume to volume
(w/v)	Proportion of weight to volume
x_{O_2}	Oxygen in inlet air [%]
$X_{O/C}$	Ratio of oxygen and carbon in a metabolite
$Y_{Lac/Glc}$	Molar yield in lactate per consumed mol of glucose [$mol_{Lac}\ mol_{Glc}^{-1}$]
$Y_{NH_4^+/Gln}$	Molar yield in ammonium per consumed mol of glutamine [$mol_{NH_4^+}\ mol_{Gln}^{-1}$]

List of Figures

List of Tables

Abstract

Cellular stress conditions, e. g. hyperosmolality or hypothermia, may occur in micro-environments of non-ideally mixed large scale bioreactors (1,000 - 20,000 L) during biopharmaceutical manufacturing. Although cell growth is inhibited by stress conditions, it has been shown that specific product formation rates (q_P) of Chinese hamster ovary (CHO) producer cell lines enhanced upon cellular stress.

This thesis deciphers the reasons behind the aforementioned phenomenon based on a hyperosmotically stressed antibody producing CHO DP-12 cell line and utilizes the gained knowledge in order to identify potential cell line engineering strategies to further improve cellular performance. Characterization of the phenotype of the CHO DP-12 cell line upon osmotic upshift (+ 100/ + 150 mOsmol kg^{-1}) exhibited well-known effects like reduced cell growth due to cell cycle arrest, increased cell specific consumption of the substrate glucose or formation of the by-product lactate as well as enhanced q_P. Considering the energy demand of recombinant protein production, this thesis particularly focused on intracellular adenine nucleotide pools and ATP formation rates (q_{ATP}) as a measure of cellular energetic capacity. Thereby, it was shown that hyperosmotically stressed CHO DP-12 cells do not exhibit reduced mitochondrial activity, disproving a previous hypothesis that was made on basis of significantly decreased antibody-mediated mitochondrial fluorescence intensities. Noteworthy, 20 - 39% increased q_{ATP} at 390 mOsmol kg^{-1} or 140 - 176% enhanced q_{ATP} at 430 mOsmol kg^{-1} and significantly elevated intracellular ATP pools mirrored improved ATP supply upon hyperosmotic stimulus whereby adenylate energy charges and ADP/ATP ratios were not affected at all. This picture was refined by a compartment specific metabolomics approach showing that both cytosolic and mitochondrial ATP pools increased in response to osmotic upshift.

Next generation sequencing for analysis of mRNA and miRNA expression dynamics linked hyperosmolality mediated G1-arrest and enhanced q_P to the immediate and long term upregulation of the gene encoding cyclin dependent kinase inhibitor protein 1A (*CDK1A*). The significantly upregulated miRNAs miR-132, miR-194 and miR-215 may play decisive roles in the aforementioned context as overexpression of these miRNAs correlated with increased *CDK1A* expression in independent cancer studies. With respect to the results of a previous independent CHO study, the hyperosmotically induced upregulation of miR-183 seemed as well to contribute to cell cycle arrest and enhanced q_P.

Concluding, improved ATP supply in combination with a presumably decreased energy demand of arrested CHO cells was anticipated to result in increased q_P. Accordingly, enhancement of ATP supply was the central focus for the identification of potential cell line engineering targets to improve productivity of CHO cells. Strikingly, several genes encoding glycosylated proteins with strictly tissue related function exhibited significantly elevated expression levels upon hyperosmotic stimulus. Therefore, deletion of genes with presumably dispensable function in suspension cultures may contribute to an improvement of q_P of CHO producer cell lines by enhanced ATP supply. Furthermore, miR-132, miR-183, miR-194 and miR-215 are hypothesized to be suitable targets to increase q_P by stable overexpression as these miRNAs were associated with CDK1A-dependent or independent cell cycle arrest. Thereby miR-183 may be the most promising target due to the fact that a q_P enhancing function has already been described for a transient expression of human miR-183 in an antibody producing CHO cell line.

Zusammenfassung

Stressbedingungen, wie beispielsweise Hyperosmolalität oder Hypothermie, können im Rahmen der Herstellung von Biopharmazeutika in Mikroumgebungen nicht-ideal durchmischter, großvolumiger Bioreaktoren (1.000 - 20.000 L) auftreten. Obwohl das Zellwachstum durch diese Stressbedingungen inhibiert wird, zeigten aus den Ovarien des chinesischen Hamsters stammende Produktionszelllinien (CHO-Zellen) infolge des zellulären Stresses verbesserte spezifische Produktbildungsraten (q_P).

In dieser Arbeit werden die Ursachen für das zuvor beschriebene Phänomen auf Basis einer hyperosmotisch gestressten Antikörper produzierenden CHO DP-12 Zelllinie aufgeklärt. Die gewonnenen Erkenntnisse werden außerdem zur Identifizierung potentieller Strategien für die Zelllinienentwicklung herangezogen, um Möglichkeiten für eine weitere Steigerung der zellulären Leistungsfähigkeit aufzuzeigen. Die phänotypische Charakterisierung der Zelllinie CHO DP-12 zeigte bei Erhöhung der Osmolalität ($+100/+150$ mOsmol kg^{-1}) bereits bekannte Effekte, wie verringertes Zellwachstum aufgrund von Zellzyklusarrest, erhöhter zellspezifischer Verbrauch des Substrats Glucose und erhöhte Bildung des Nebenprodukts Laktat, sowie eine verbesserte q_P. In Anbetracht des Energiebedarfs der Produktion rekombinanter Proteine, lag das Augenmerk dieser Arbeit insbesondere auf den intrazellulären Gehalten an Adenin-Nukleotiden, sowie auf den ATP-Bildungsraten (q_{ATP}) als Maß für das energetische Leistungsvermögen der Zellen. Dadurch wurde gezeigt, dass hyperosmotisch gestresste CHO DP-12 Zellen keine verringerte mitochondriale Aktivtät aufweisen, womit eine auf einer verringerten Antikörper-vermittelten mitochondrialen Fluoreszenzintensität basierende vorangegangene Hypothese widerlegt wurde. Erstaunlicherweise, spiegelten 20 - 39% erhöhte q_{ATP} bei 390 mOsmol kg^{-1} beziehungsweise 140 - 176% verstärkte q_{ATP} bei 430 mOsmol kg^{-1} und signifikant erhöhte intrazelluläre

ATP-Gehalte eine verbesserte ATP-Bereitstellung infolge des hyperosmolalen Stimulus wider, wobei Energieladung und ADP/ATP Verhältnisse unverändert blieben. Anhand eines kompartimentspezifischen Metabolomik-Ansatzes wurde dieses Bild näher charakterisiert, wobei gezeigt wurde, dass sich sowohl die cytosolischen als auch die mitochondrialen ATP-Gehalte im Zuge des hyperosmotischen Stimulus erhöhten.

Die mittels einer Sequenzierungstechnologie der nächsten Generation analysierten mRNA und miRNA Expressionsdynamiken verknüpften den durch Hyperosmolalität induzierten G1-Arrest und die gesteigerte q_P mit der unmittelbaren und langfristigen Hochregulierung des Gens *CDK1A*, welches einen Inhibitor Cyclin-abhängiger Kinasen codiert. Die signifikant hochregulierten miRNAs miR-132, miR-194 und miR-215 könnten eine entscheidende Rolle im zuvor erwähnten Kontext spielen, da diese miRNAs in unabhängigen Krebsstudien mit einer erhöhten *CDK1A*-Expression korrelierten. Unter Berücksichtigung der Ergebnisse eines vorangegangenen, unabhängigen CHO-Forschungsprojekts, schien die hyperosmotisch induzierte Hochregulation der miR-183 ebenfalls zum Zellzyklusarrest und der Erhöhung der q_P beizutragen.

Abschließend wurde angenommen, dass die verstärkte ATP-Bereitstellung in Kombination mit einem wahrscheinlich verminderten Energiebedarf arretierter CHO-Zellen zu den erhöhten q_P führte. Dementsprechend lag der zentrale Fokus für die Identifizierung potentieller Ansatzpunkte für die Zelllinienentwicklung auf einer Verstärkung der ATP-Bereitstellung, um dadurch die Produktivität von CHO-Zellen zu vebessern. Auffälligerweise, führte der hyperosmotische Stimulus zu einer signifikant erhöhten Expression von Genen, welche glycosylierte Proteine mit grundsätzlich gewebespezifischer Funktion codieren. Daher könnte die Deletion von Genen mit vermutlich überflüssiger Funktion in Suspensionskulturen zu einer verstärkten Bereitstellung von ATP beitragen und somit die q_P erhöhen. Des Weiteren könntenen miR-132, miR-183, miR-194 und miR-215 geeignete Ansatzpunkte für eine Erhöhung der q_P durch stabile Überexpression sein, da diese miRNAs mit einem CDK1A-abhängigen oder -unabhängigen Zellzyklusarrest assoziiert wurden. Dabei wird angenommen, dass miR-183 die vielversprechendste miRNA ist, da in einer unabhängigen Studie bereits gezeigt wurde, dass eine transiente Expression der humanen miR-183 in einer Antikörper produzierenden CHO-Zelllinie zu einer Erhöhung der q_P führte.

1 Introduction

The biotechnological production of therapeutic proteins for the treatment of diseases, e. g. cancer or autoimmune diseases, is a steadily increasing market. From \$94 billion in 2007, the global annual sales increased 7 - 12% per year and reached \$140 billion in 2013 (Walsh, 2010a, 2014). Thereof $\sim 50\%$ were commonly apportioned on the United States (US) biotech market (Aggarwal, 2014; Walsh, 2014). Biopharmaceutical products encompass the categories monoclonal antibodies (mAbs), hormones, fusion proteins, cytokines, therapeutic enzymes, blood factors, recombinant vaccines and anti-coagulants in the order of declining US market volume (Aggarwal, 2014). These biopharmaceuticals are produced by mammalian, microbial and insect cell lines. *Escherichia coli* (*E. coli*) is the predominant microbial expression system which was used for the production of three (Lantus, Neulasta and Lucen-tis) of the 10 top-selling biopharmaceutical products in 2013 (Tab. 1.1). Besides *E. coli*, biopharmaceu-ticals are mainly produced by mammalian cell cultures ($\sim 70\%$). This percentage is steadily increas-ing as more and more products require complex post-translational modifications (e. g. glycosylation) which are insufficient in prokaryotic microorganisms like *E. coli* (Walsh, 2014). Cells from human em-bryo kidney (HEK293), murine myeloma (NS0, SP2/0), baby hamster kidney (BHK) and from Chinese hamster ovary (CHO) are typical mammalian host cell lines (Jayapal et al., 2007). Seven of the 10 top-selling biopharmaceutical products in 2013 were produced by mammalian cells, predominantly CHO cell lines (6 of 7).

Research activities continually focus on the enhancement of cellular productivity. Since the ap-proval of the first product expressed by a CHO cell line (tissue plasminogen activator, 1987, Genentech) specific product formation rates (q_P) improved from less than 10 pg cell^{-1} d^{-1} to ~ 40 - 100 pg cell^{-1} d^{-1} (Seth et al., 2006; Tabuchi and Sugiyama, 2013; Wurm, 2004). In addition, product titers increased

by more than 100-fold (c_P, > 5 g L^{-1}) (Schaub et al., 2012; Wurm, 2004). Enhancements in q_P and c_P were achieved by e. g. process optimization, cell line engineering and by improved cultivation media and feeding supplements (Jayapal et al., 2007; Schaub et al., 2012; Seth et al., 2006; Tabuchi and Sugiyama, 2013; Wurm, 2004).

TABLE 1.1: The 10 top-selling biopharmaceutical products in 2013. With changes to Walsh (2014). TNF = tumor necrosis factor, VEGF = vascular endothelial growth factor.

ranking	product	Sales [$ billions][a]	Year first approved	company
1	Humira (adalimumab; anti-TNF)	11.00	2002	AbbVie & Eisai
2	Enbrel (etanercept; anti-TNF)	8.76	1998	Amgen, Pfizer, Takeda Pharmaceuticals
3	Remicade (infliximab; anti-TNF)	8.37	1998	J&J, Merck & Mitsubishi, Tanabe Pharma
4	Lantus (insulin glargine)	7.95	2000	Sanofi
5	Rituxan/MabThera (rituximab; antiCD20)	7.91	1997	Biogen-IDEC, Roche
6	Avastin (bevacizumab; anti-VEGF)	6.97	2004	Roche/Genentech
7	Herceptin (anti-HER2)	6.91	1998	Roche/Genentech
8	Neulasta (pegfilgrastim)	4.39	2002	Amgen
9	Lucentis (ranibizumab; anti-VEGF)	4.27	2006	Roche/Genentech, Novartis
10	Epogen/Procrit/Eprex/ESPO (epoetin alfa)	3.35	1989	Amgen, J&J, KHK

[a] Financial data from LaMerie Business Intelligence. J&J, Johnson & Johnson

However, optimization strategies intensified culture conditions, thus facilitating the occurrence of cellular stress. Strikingly, stress conditions, e. g. low culture temperature or hyperosmolality, were

shown to enhance q_P (Fox et al., 2004; Furukawa and Ohsuye, 1998; Han et al., 2009; Kaufmann et al., 1999; Lee et al., 2003a; Ryu et al., 2000; Shen et al., 2010). Deciphering the fundamentals of the q_P enhancing effect of hyperosmotic culture conditions is expected to reveal potential strategies for a further improvement of cellular performance. As a consequence this research project focuses on the effects of hyperosmotic culture conditions on energetic capacity and transcriptomic response of an antibody producing CHO cell line to elucidate the underlying reason for the q_P and to identify suitable cell line engineering strategies.

2 Theoretical Background

2.1 Chinese Hamster Ovary Cells

The predominantly used mammalian host cell lines for heterologous protein expression in the biotech industry are CHO cells. These cells date back to the year 1957 when Puck et al. isolated cells from different organs (kidney, lung, ovary and spleen) of *Cricetulus griseus* (Chinese hamster) and cultivated them *in vitro*. Surprisingly, the cellular morphology and growth rate of CHO cells were not affected by a long-term *in vitro* cultivation of $\sim$ 10 months (Puck et al., 1958). For about two decades CHO cells were mainly used to investigate the cell cycle and the effects of mutagenesis on cellular functions and structure, until in the 1980s Urlaub et al. generated two dihydrofolate reductase (DHFR) lacking cell lines (CHO DXB11, CHO DG44) which later became the main parental hosts of today's industrial production cell lines (Urlaub and Chasin, 1980; Urlaub et al., 1983, 1986). CHO DXB11 and CHO DG44 were generated by mutagenesis of CHO K1 and CHO pro-3 which had both been isolated by Puck et al. in 1957. While both *DHFR* loci were deleted in CHO DG44, CHO DXB11 cells still possess one inactive *DHFR* locus (Urlaub and Chasin, 1980; Urlaub et al., 1983, 1986; Wurm and Hacker, 2011). DHFR catalyzes the reduction of folate to dihydrofolate and finally to tetrahydrofolate which is an important carbon-carrier. As a cofactor tetrahydrofolate provides one-carbon-groups, e. g. methyl, methylene or formyl groups, for the synthesis of amino acids, purines or pyrimidines (e. g. hypoxanthine, thymidine) (Berg et al., 2003; Hamlin and Ma, 1990).

The DHFR deficiency of CHO DXB11 and CHO DG44 established the basis for a widely applied selection system (2.5) for the isolation of strains with high expression of recombinant protein.

2.2 Cell Cycle and Genome

Mammalian cell cycle is a defined and highly regulated chronology of cellular processes that finally result in the division of one cell into two identical daughter cells (Fig 2.1). In cell culture, this process of multiplying by cell division is commonly defined as cell growth and is the basis of biotechnological production.

Cell Cycle

Cell cycle is divided into four phases - gap phase 1 (G1), DNA-synthesis (S), gap phase 2 (G2) and mitosis (M) (Fig. 2.1-A). Extracellular mitogenic stimuli (e. g. growth factors) are required for the induction of the highly regulated process of cell cycle (Fig. 2.1). At the beginning of each cycle, cells enter G1-phase and prepare for the subsequent DNA replication in S-phase until they finally reach a checkpoint ("restriction point") that decides on commitment of further cell cycle progression or entering of cells into a quiescent/arrested state (G0/G1) (Bertoli et al., 2013; Malumbres and Barbacid, 2005; Poon, 2016; Zetterberg et al., 1995). As part of positive and negative feedback loops, complexes of cyclin and cyclin-dependent kinases (cyclin D/CDK 4/6, cyclin E/CDK 2, cyclin A/CDK 2) inactivate transcription factors or associated inhibitors (pRb) and corepressors (p107, p130) by phosphorylation, thereby enabling transcription of S-phase specific genes and passage of the "restriction point" (Bertoli et al., 2013; Malumbres and Barbacid, 2005; Poon, 2016). Thereafter, cells are committed for cell cycle progression and continue with semi-conservative replication of chromosomal DNA (Alexandrow and Hamlin, 2004; Dimitrova et al., 1999; Masai et al., 2010; Poon, 2016).

The further progression in cell cycle after DNA replication is dependent on a second checkpoint at the end of G2-phase. Cyclin B/CDK 1 is a major complex of the G2-M regulatory system whereby its phosphorylated, inactive form mediates cell cycle arrest in G2-phase (Malumbres and Barbacid, 2005; Poon, 2016; Stark and Taylor, 2006). G2-M transition is therefore based on the functional interaction of G2 checkpoint kinases and phosphatases with CDK 1 (Malumbres and Barbacid, 2005; Poon, 2016; Stark and Taylor, 2006). Furthermore, CDK 1 in turn is capable of regulating the activity of its activators

or repressors via a feedback loop (Ma and Poon, 2011; Poon, 2016; Stark and Taylor, 2006).

The final M-phase is characterized by the equal separation of chromosomes and other cellular components to two daughter cells. This involves the mitotic processes spindle assembly, nuclear envelope breakdown and chromosome movement which are regulated by a variety of kinases (Ma and Poon, 2011; Nigg, 2001; Poon, 2016).
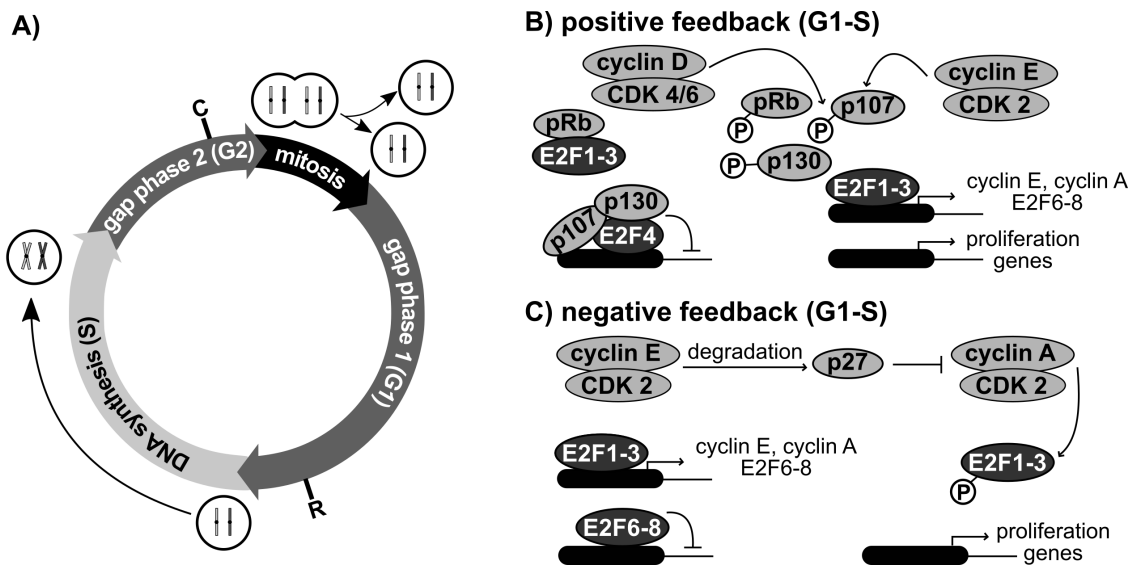
FIGURE 2.1: Cell cycle phases (A) and positive (B) and negative feedback loop (C) during G1-S transition. A) An exemplary cell with two chromosomes enters a new round of cell cycle. In gap phase 1 (G1) the cell prepares for the subsequent DNA replication and either passes the "restriction point" (R) or enters an arrested or quiescent state (G0). Further cell cycle progression leads to DNA replication and a second gap phase (G2). Another checkpoint (C) in G2-phase regulates whether the cell enters mitosis or arrests in G2-phase. Mitosis is characterized by equal distribution of cellular components to two daughter cells. **B-C)** pRb inhibits the transcription factors E2F1-3 while p107 and p130 are corepressors of E2F4. pRb, p107 and p130 are inactivated by phosphorylation which is mediated by cyclin/cyclin-dependent kinase (CDK) complexes. Cyclin D/CDK 4/6 is specific for G1-phase while cyclin E/CDK 2 and cyclin A/CDK 2 are related to S-phase. Passing of the "restriction point" is regulated by positive and negative feedback loops. Cyclin D/CDK 4/6 inactivates pRb, p107 and p130 and enables transcription of S-phase specific genes. Cyclin E/CDK 2 itself stimulates transcription by phosphorylating pRb, p107 and p130 (positive feedback). This complex further targets p27 for degradation and thereby the inactivation of E2F1-3 by cyclin A/CDK 2 is enhanced. This leads to a decreased transcription of cyclin E/A and the transcription factors E2F6-8 (negative feedback). (Poon, 2016). B) and C) with modifications to Bertoli et al. (2013).

DNA Damage Checkpoints

DNA damage is a commonly occurring cellular effect upon exposure of cells to stress conditions, e. g. hyperosmolality and radiation (Bertoli et al., 2013; Burg et al., 2007; Han et al., 2010; Leung and Sharp, 2010; Sieck et al., 2013). Specific DNA damage checkpoints in G1- and G2-phase of cell cycle can induce cell cycle arrest in order to provide time for DNA repair mechanisms. DNA damage activates the protein kinases ataxia telangiectasia mutated (ATM) and ataxia telangiectasia and Rad3 related (ATR) which activate the subsequent checkpoint kinases 1 and 2 (CHK1/2) (Bertoli et al., 2013; Ma and Poon, 2011; Poon, 2016). CHK1/2 induce transcriptional activity of tumor suppressor protein 53 (p53) by hampering the binding to its regulator MDM2, thus inducing either cell cycle arrest or p53-mediated apoptosis (Poon, 2016). p53 is a transcriptional activator of the CDK-inhibitor CDK1A/p21 which induces G1-arrest by inhibiting cyclin A/E/CDK 2 and cyclin D/CDK 4 (Fig. 2.1B/C) (He et al., 2005; Poon, 2016).

Genome

Cell cycle includes the replication of the cellular genome in S-phase. In general the Chinese hamster genome is characterized by a small but highly variable chromosome set of 2n = 19 - 23 chromosomes (Cao et al., 2012; Derouazi et al., 2006; Puck et al., 1958; Worton et al., 1977). Derouazi et al. (2006) analyzed the karyotype of 16 recombinant CHO DG44 cell lines thereby showing that more than half of the cell lines contained chromosomal aberrations, e. g. rearrangements, aneuploidy or deletions. Nevertheless, the comparison of chromosomal sequences of the primary Chinese hamster cells CHO K1 and CHO DG44 by Cao et al. (2012) revealed the conservation of eight of 20 chromosomes.

Although the preparation of CHO expressed sequencing tag (EST) libraries (Kantardjieff et al., 2009; Wlaschin et al., 2005), CHO-specific gene sequences (Birzele et al., 2010) and CHO cDNA microarrays (Nissom et al., 2006; Schaub et al., 2010) had been described in literature, almost no CHO sequence information was publicly available until Xu et al. (2011) published a draft genomic sequence comprising 24,383 predicted genes for the cell line CHO K1. In general, a variety of next generation sequencing (NGS) and Sanger-based sequencing studies for Chinese hamster, CHO K1, CHO DXB11

and CHO DG44 cell lines predicted gene/transcript numbers between $\sim$ 24,000 and $\sim$ 29,000 (Becker et al., 2011; Kantardjieff et al., 2009; Le et al., 2015; Lewis et al., 2013; Rupp et al., 2014; Xu et al., 2011). While in the past, gene annotation was commonly performed by mapping CHO sequencing data to reference genomes of *Homo sapiens*, *Mus musculus* and *Rattus norvegicus* (Hammond et al., 2011; Kantardjieff et al., 2009; Wlaschin and Hu, 2006; Wlaschin et al., 2005; Xu et al., 2011), this approach was rejected by the public availability of Chinese hamster genomes (Hammond et al., 2012; Le et al., 2015; Lewis et al., 2013; Rupp et al., 2014). Besides the protein encoding segments, the CHO genome contains small non-coding microRNAs (miRNAs) which are involved in messenger RNA (mRNA) degradation and silencing of mRNA translation (2.7). Based on NGS of small cDNA libraries from different CHO cell lines, Hackl et al. (2011) identified 387 and Johnson et al. (2011) 350 mature miRNAs. For 319 of these previously determined mature miRNAs distinct genomic loci were identified by mapping miRNA sequences to CHO reference genomes (Hackl et al., 2012). Recently, Diendorfer et al. (2015) identified another 71 novel CHO miRNAs by NGS of cDNA libraries from parental and recombinant CHO K1 and CHO DXB11 cell lines. Nevertheless, the public miRNA database "miRBase" (release 21) (Kozomara and Griffiths-Jones, 2011) currently contains 307 mature and 200 precursor miRNAs of Chinese hamster.

2.3 Mitochondria

Mammalian cells are eukaryotic organisms which are characterized by a complex subcellular compartmentalization (Fig. 2.2). Several distinct cell organelles, e. g. nucleus, endoplasmic reticulum (ER) and mitochondria, provide appropriate conditions for various cellular processes.

The metabolic pathways tricarboxylic acid (TCA) cycle, electron transport chain, oxidative phosphorylation (2.4) and β-oxidation of fatty acids are located in the mitochondrial compartment and provide precursor metabolites and energy for anabolic processes. The latter therefore gives rise to the fact that mitochondria are commonly defined as cellular "powerhouses". Furthermore, these cell

organelles play a central role in amino acid metabolism, ion homeostasis and programmed cell death. (Friedman and Nunnari, 2014; Hock and Kralli, 2009; Scheffler, 2001; Shi, 2001)
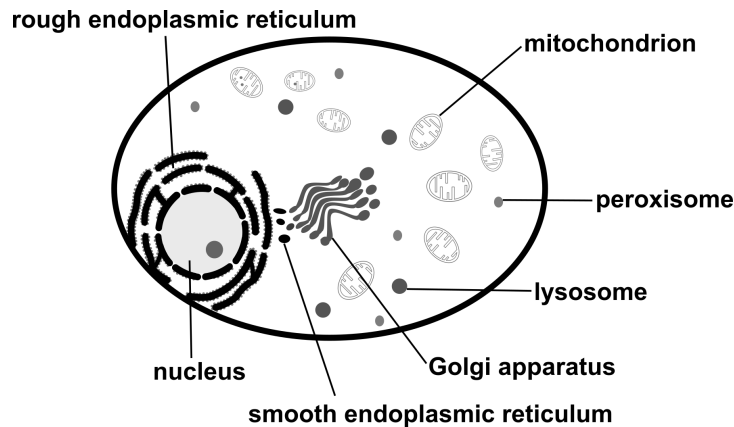
FIGURE 2.2: Schematic drawing of mammalian cell. The nucleus, host of genetic information, is the cell organelle where DNA replication and transcription of DNA occur. A small genome is as well found in mitochondria where important metabolic pathways, e.g. TCA cycle, oxidative phosphorylation and β-oxidation, take place. A variety of acid hydrolases enables the degradation of all kinds of macromolecules in the cell's lysosomes. The degradation of hydrogen peroxide and β-oxidation of fatty acids occurs in the peroxisomes. The rough endoplasmic reticulum (studded with ribosomes) represents the site for protein synthesis, processing and translocation, while the smooth endoplasmic reticulum is often involved in assembly of vesicles for transport to the Golgi apparatus. Glycosyltransferases, kinases and proteases modify proteins or lipids on their way through the Golgi apparatus until they are finally delivered to their cellular destinations. With modification to Pfizenmaier and Takors (2016).

According to the endosymbiotic theory, mitochondria originate from the uptake of an α-proteobacterium by a proto-eukaryotic cell (Pernas and Scorrano, 2016; Scheffler, 2001). This theory was supported by the discovery of mitochondrial DNA by Nass and Nass (1963). However, the 16,284 bp circular mitochondrial genome of CHO cells was shown to encode only 13 of the $\sim$ 1,100 to 1,500 mitochondrial proteins as well as two ribosomal RNAs (rRNA) and 22 transfer RNAs (tRNA) (Hock and Kralli, 2009; Partridge et al., 2007; Wenz et al., 2015).

Apart from 13 proteins of the electron transport chain, e. g. cytochrome c oxidase and ATP synthase, the majority of mitochondrial proteins is nuclear encoded and synthesized in the form of preproteins in the cytosol. These mitochondrial precursor proteins contain either N-terminal prepep-

tides or internal targeting sequences which direct them to their predestined mitochondrial location. (Endo and Kohda, 2002; Neupert and Herrmann, 2007; Wenz et al., 2015)

Mitochondrial Transport - Nuclear Encoded Proteins, Metabolites and Ions

The mitochondrial morphology is characterized by an extensively folded and protein-rich inner mitochondrial membrane (IMM) surrounded by a smooth outer mitochondrial membrane (OMM) (Bauer et al., 2015; Passarella et al., 2003; Pernas and Scorrano, 2016; Scheffler, 2001). The characteristic invaginations of the IMM are commonly defined as cristae and extend into the IMM enclosed space which is defined as mitochondrial matrix (Cogliati et al., 2013; Passarella et al., 2003; Pernas and Scorrano, 2016; Scheffler, 2001). Concluding, mitochondrial proteins can be located in the OMM, in the IMM, in the matrix or in the intermembrane space (IMS) which forms between IMM and OMM.

The precursors of nuclear encoded proteins of the mitochondrial matrix, e. g. enzymes of the TCA cycle, possess N-terminal targeting sequences of about 10 - 80 amino acids which are capable to form amphipathic α-helices. These targeting sequences are commonly cleaved from the preproteins by the mitochondrial processing peptidase upon entry into the mitochondrial matrix. In contrast to the preproteins of the mitochondrial matrix, nuclear encoded proteins of the OMM, IMM or the intermembrane space usually contain internal targeting sequences which are individually specific for their final mitochondrial location, e. g. precursors of the OMM proteins TOM5 and BCL-2 possess positive charges at the N-terminus and signal-anchor domains with moderate hydrophobicity. Furthermore, heat shock proteins (e. g. HSP70, HSP90) associate with the cytosolic precursor proteins and keep them in an unfolded import-capable state. (Bauer et al., 2015; Endo and Kohda, 2002; Hartl et al., 1989; Neupert and Herrmann, 2007; Wenz et al., 2015)

The transport of nuclear encoded mitochondrial preproteins from the cytosol to their final location is mediated by several translocases. The translocase of the outer mitochondrial membrane (TOM) complex represents the entry gate for almost all nuclear encoded mitochondrial proteins (Ahting et al., 1999; Neupert and Herrmann, 2007; Pfanner et al., 1998; Schmitt et al., 2005; Wenz et al.,

2015; Yano et al., 2000). Components of the OMM, e. g. β-barrel proteins/porins, enter the IMS via the TOM complex and are then transferred to the topogenesis of mitochondrial outer membrane β-barrel proteins (TOB) complex, also named sorting and assembly machinery (SAM) complex, which mediates folding of the OMM proteins as well as their integration into the OMM. (Neupert and Herrmann, 2007; Wenz et al., 2015; Wiedemann et al., 2003). The transport of IMM proteins is either mediated by the TOM and the TIM22 complex (e. g. carrier proteins) or by the TOM and the TIM23 complex (e. g. proteins with only one transmembrane span) whereby small TIM proteins in the IMS assist in protein transport from the TOM to the TIM22 complex (Moro et al., 1999; Neupert and Herrmann, 2007; Sirrenberg et al., 1996; Wenz et al., 2015). The protein transport from the IMS into the mitochondrial matrix is an energy-consuming process and is also dependent on the mitochondrial membrane potential (2.4) (Bauer et al., 1996; Moro et al., 1999; Neupert and Herrmann, 2007; Wenz et al., 2015).

Porins in the OMM and carriers in the IMM enable the exchange of metabolites and ions between the cytosol and the mitochondrial matrix which is of utmost importance for the cellular metabolism (2.4). While the OMM is permeable for molecules with low molecular weight (< 5 kDa), the IMM functions as a selective permeability barrier, thus requiring a variety of different carriers for metabolite and ion exchange (LaNoue and Schoolwerth, 1979; Mannella, 1992; Mitchell, 1966; Passarella et al., 2003). Exemplary mitochondrial transporters are pyruvate carriers (MPC1/MPC2) transporting the product of the Embden-Meyerhof-Parnas pathway of glycolysis from the cytosol into the mitochondrial matrix (Fig. 2.3) (Bricker et al., 2012) or the ATP/ADP carrier which exchanges mitochondrial ATP with cytosolic ADP (Klingenberg and Rottenberg, 1977; Passarella et al., 2003).

Mitochondrial Dynamics

The mitochondrial compartment is a dynamic network which continuously changes its shape by fusion and fission thereby forming a continuous reticulum or discrete isolated cell organelles (Campello and Scorrano, 2010; Hoitzing et al., 2015; Pernas and Scorrano, 2016; Scheffler, 2001). Morphological changes and the cytosolic localization are characteristic for the cellular needs. For ex-

ample, mitochondria accumulate at locations where high amounts of ATP are required and cristae folds proliferate in order to increase the surface area for oxidative phosphorylation (Campello and Scorrano, 2010; Cogliati et al., 2013; Pernas and Scorrano, 2016). Furthermore, mitochondria may form hyperfused networks to regulate calcium signaling or fragment and release cytochrome c as response to apoptotic stimuli (Mitra et al., 2009; Pernas and Scorrano, 2016). Investigations on mitochondrial mass and number are highly related to morphological changes and were studied likewise on basis of electron microscopy and fluorescent labeling of mitochondria in combination with laser-scanning confocal microscopy (Dewey and Fuhr, 1976; Lee et al., 2007, 2002b; McClatchey et al., 2015; Mitra et al., 2009; Ross and Mel, 1972; Santel and Fuller, 2001).

Mitochondrial Pathway of Apoptosis

The programmed cell death, named apoptosis, is characterized by cell shrinkage, chromatin condensation, nuclear DNA fragmentation, blebbing of cytoplasmic membrane, cell fragmentation (apoptotic bodies) and phagocytosis of apoptotic bodies by adjacent cells (Fulda and Debatin, 2006; Shi, 2001). Induction of the apoptotic pathway is either mediated by death receptors of the tumor necrosis factor (TNF) receptor superfamily , e. g. TNF-related apoptosis-inducing ligand (TRAIL) or CD95, (extrinsic pathway) or by mitochondria (intrinsic pathway) (Fulda and Debatin, 2006; Shi, 2001).

BCL-2 family members play an important role in controlling mitochondria-mediated apoptosis as this group includes interacting proteins of pro- (e. g. BAX, BAK, BID) or anti-apoptotic function (e. g. BCL-2, BCL-XL) (Bhola and Letai, 2016; Gross et al., 1999). While anti-apoptotic members of the BCL-2 family are commonly located in the membrane of cell organelles, e. g. mitochondria, ER and nucleus, pro-apoptotic members are usually found in the cytosol or attached to cell organelles via BCL-2 unless apoptotic stimuli are absent (Gross et al., 1999; Wolter et al., 1997). However, upon induction of apoptosis by e. g. DNA damage (2.2), lack in growth factors or starvation, BAX and BAK were shown to be activated by BID and BIM resulting in the formation of multimeric pores in the OMM (Bhola and Letai, 2016; Kuwana et al., 2002; Shi, 2001). Bellot et al. (2007) and Renault et al. (2012)

elucidated that TOM22 is required as receptor for BAX in order to be integrated in the OMM. OMM permeabilization by BAX and BAK causes release of the apoptogenic IMS proteins cytochrome c, apoptosis induction factor (AIF), endonuclease G and second mitochondrial apoptotic factor (SMAC) (Bhola and Letai, 2016; Fulda and Debatin, 2006; Gross et al., 1999; Kuwana et al., 2002; Shi, 2001).

Apoptosis is mediated by an intracellular proteolytic cascade, named caspase cascade which is activated by the release of apoptogenic IMS proteins. Upon entry into the cytosol, cytochrome c binds to the C-terminal region of the apoptotic protease activating factor 1 (APAF1), thus facilitating dATP/ ATP-association and the formation of a sevenfold symmetric, wheel-like complex called apoptosome (Acehan et al., 2002; Saelens et al., 2004; Srinivasula et al., 1998; Zou et al., 1999). Central N-terminal caspase-recruitment domains (CARDs) enable binding and activation of procaspase-9 which then in turn activates effector caspase-3 and -7, thus inducing the characteristic effects of apoptosis by cleavage of specific cellular substrates (Lavrik et al., 2005; Saelens et al., 2004; Srinivasula et al., 1998). The caspase cascade can also be activated by SMAC-mediated inhibition of the inhibitor of apoptosis protein (IAP) which normally inhibits caspase-3 as well as caspase-9-mediated activation of effector caspases (Du et al., 2000; Shi, 2001).

In addition to the caspase-dependent apoptotic pathway, nuclear DNA damage can be induced by the IMS proteins AIF and endonuclease G via a caspase-independent process (Candé et al., 2004; Saelens et al., 2004).

2.4 Metabolism

CHO cells grow aerobically on the common main substrates glucose and glutamine which are fueled into Emden-Meyerhof-Parnas pathway of glycolysis and tricarboxylic acid cycle (TCA), respectively (Fig. 2.3). In conjunction with further catabolic pathways, e. g. pentose-phosphate pathway, anaplerotic pathways, oxidative phosphorylation and β-oxidation, glycolysis and TCA provide 12 precursor metabolites: glucose-6-phosphate, fructose-6-phosphate, glyceraldehyde-3-phosphate,

3-phosphoglycerate, phosphoenolpyruvate, pyruvate, ribose-5-phosphate, erythrose-4-phosphate, acetyl-CoA, α-ketoglutarate, succinyl-CoA and oxaloacetate. Precursor metabolites serve as substrates for biosynthesis of e. g. nucleotides and amino acids which are essential building blocks for the synthesis of macromolecules (e. g. proteins, DNA, RNA). (Nielsen and Jewett, 2008; Seth et al., 2006)

Central Carbon Metabolism

Glucose uptake is based on facilitated diffusion via glucose transporter 1 (GLUT1) which is also known as solute carrier family 2 member 1 (SLC2A1) (Baldwin, 1993; Mulukutla et al., 2010). Cellular uptake of glutamine is mediated by two types of transporters: alanine serine cysteine transporter (ASCT, *SLC1* gene family) and sodium-coupled neutral amino acid transporter (SNAT, *SLC38* gene family) (Shotwell et al., 1981; Zander et al., 2015). SNAT2 is a symporter and transports glutamine together with one sodium ion (Na$^+$) whereas ASCT1 and 2 are amino acid antiporters. Glutamine and Na$^+$ are imported in exchange for a cytosolic amino acid (Shotwell et al., 1981; Zander et al., 2015). In mitochondria, glutamine is deamidated by glutaminase to form glutamate which in turn is converted to α-ketoglutarate by either oxidative deamination (glutamate dehydrogenase) or transamination with oxaloacetate (glutamic-oxaloacetic transaminase) (Lane and Fan, 2015). α-ketoglutarate is fueled into TCA cycle and converted to malate. Oxidative decarboxylation of malate to form pyruvate might occur in combination with the previous α-ketoglutarate formation by oxidative deamination of glutamate (Glacken, 1988). Thereby pyruvate can either be converted to lactate or refueled into TCA cycle via acetyl-CoA. The metabolization of glutamine is defined as "glutaminolysis" (Glacken, 1988).

Cytosolic glucose is phosphorylated by hexokinase and resulting glucose-6-phosphate is either metabolized in Embden-Meyerhof-Parnas pathway of glycolysis or in pentose-phosphate pathway. In glycolysis (Fig. 2.3), glucose-6-phosphate is isomerized to fructose-6-phosphate (glucose-6-phosphate isomerase) which is subsequently phosphorylated (phosphofructokinase). Fructose-1,6-bisphosphate is then cleaved (aldolase) to produce the triose phosphate isomers glyceraldehyde-3-phosphate and dihydroxyacetone-phosphate which can be interconverted by triose phosphate isomerase.
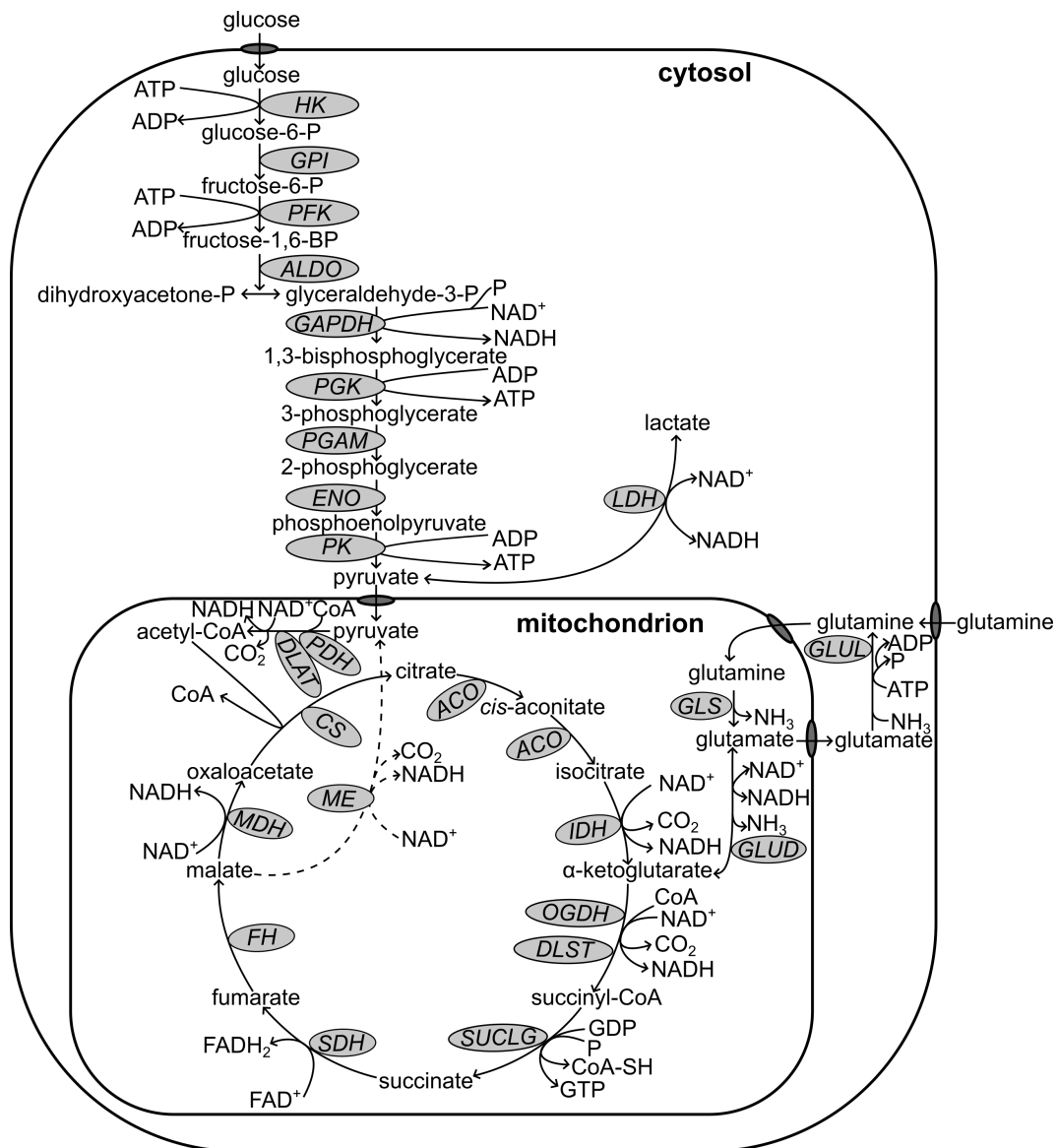
FIGURE 2.3: Central carbon metabolism of CHO cells. CHO cells grow on glucose and glutamine which are fueled into Emden-Meyerhof-Parnas pathway of glycolysis and tricarboxylic acid cycle (TCA), respectively. Exchange of metabolites between cytosol and mitochondrial matrix or cytosol and extracellular matrix requires specific transporters. Grey shaded ellipses symbolize the gene names of corresponding enzymes for each reaction. CoA = coenzyme A, P = (ortho)phosphate. *HK*: hexokinase, *GPI*: glucose-6-phosphate isomerase, *PFK*: phosphofructokinase, *ALDO*: aldolase, *GAPDH*: glyceraldehyde-3-phosphate dehydrogenase, *PGK*: phosphoglycerate kinase, *PGAM*: phospho-glycerate mutase, *ENO*: enolase, *PK*: pyruvate kinase, *LDH*: lactate dehydrogenase, *GLS*: glutaminase, *GLUL*: glutamate-ammonia ligase, *GLUD*: glutamate dehydrogenase, *PDH*: pyruvate dehydrogenase, *DLAT*: di-hydrolipoamide S-acetyltransferase, *CS*: citrate synthase, *ACO*: aconitase, *IDH*: isocitrate dehydrogenase, *OGDH*: α-ketoglutarate dehydrogenase, *DLST*: dihydrolipoamide S-succinyltransferase, *SUCLG*: succinate-CoA ligase, *SDH*: succinate dehydrogenase, *FH*: fumarate hydratase, *MDH*: malate dehydrogenase *ME*: malic enzyme. With modifications to Mulukutla et al. (2012) and KEGG pathway cge00010.

In the subsequent reactions of glycolysis, glyceraldehyde-3-phosphate is converted to pyruvate and two molecules of ATP are produced by substrate-level phosphorylation. Altogether the metabolization of one glucose molecule by glycolysis generates a net energy yield of two ATP molecules and leads to the reduction of one molecule of NAD^+ (oxidized nicotinamide adenine dinucleotide). (Berg et al., 2003; Klempnauer et al., 2011)

A substantial amount of produced pyruvate is not transported into mitochondrial matrix for further metabolization in TCA cycle but is instead converted to lactate, thereby regenerating NADH (reduced nicotinamide adenine dinucleotide) to NAD^+. This lactate formation is known as the "Warburg Effect" and is part of "aerobic glycolysis". Cell cultures were shown to metabolize the accumulated lactate after entering glucose and glutamine depletion. (Mulukutla et al., 2010; Seth et al., 2006; Vander Heiden et al., 2009)

Nevertheless, pyruvate is primarily metabolized in TCA cycle (Fig. 2.3) and therefore mitochondrial pyruvate uptake is mediated by a heterodimer of mitochondrial pyruvate carriers (MPC1/MPC2) (Bricker et al., 2012). Pyruvate dehydrogenase and dihydrolipoamide S-acetyltransferase mediate oxidative decarboxylation of pyruvate and thus acetyl-CoA formation. Thereafter citrate synthase uses the substrates oxaloacetate and acetyl-CoA for citrate formation. Aconitase isomerizes citrate via *cis*-aconitate to isocitrate. Two subsequent oxidative decarboxylation steps convert citrate to α-ketoglutarate (isocitrate dehydrogenase) and then to succinyl-CoA (α-ketoglutarate dehydrogenase, dihydrolipoamide S-succinyltransferase). α-ketoglutarate is the entry point for metabolization of glutamine by TCA cycle. Succinate-CoA ligase cleaves the energy-rich thioester bond of succinyl-CoA, thus phosphorylating guanine diphosphate (GDP) to form the energy-rich guanine triphosphate (GTP). Succinate is oxidized by succinate dehydrogenase to form fumarate which is subsequently hydrated by fumarate hydratase to form malate. Oxaloacetate is finally regenerated by oxidation of malate (malate dehydrogenase). (Berg et al., 2003; Klempnauer et al., 2011)

Altogether one round of TCA cycle generates one molecule of GTP, two molecules of carbon dioxide (CO_2) and reduces three molecules of NAD^+ to NADH during oxidation and oxidative decarboxylation steps. In addition, one molecule of FAD (oxidized flavin adenine dinucleotide) is

reduced ($FADH_2$) during oxidation of succinate to form fumarate. The acetyl-CoA formation by oxidative decarboxylation of pyruvate, upstream of TCA cycle, generates another NADH and CO_2 molecule. (Berg et al., 2003; Klempnauer et al., 2011)

Electron Transport Chain and Oxidative Phosphorylation

The regeneration of reducing equivalents NADH and $FADH_2$ to NAD^+ and FAD is a function of the electron-transport chain which is coupled to oxidative phosphorylation. The transfer of cytosolic NADH to mitochondrial matrix is mediated by the glycerol 3-phosphate shuttle and the malate-aspartate shuttle (Mulukutla et al., 2010; Passarella et al., 2003). The interaction of five complexes of the IMM (NADH dehydrogenase, succinate dehydrogenase, cytochrome bc1 complex, cytochrome c oxidase and ATP synthase) mediates regeneration of reducing equivalents, reduction of oxygen and ATP-synthesis (Fig. 2.4).

NADH binds to NADH dehydrogenase (complex I) and is regenerated to NAD^+, thereby transferring two electrons via the prosthetic groups flavin mononucleotide and iron-sulfur cluster to the hydrophobic molecule ubiquinone (UQ). Likewise complex II bound $FADH_2$ transfers two electrons via iron-sulfur complex to UQ, thus regenerating FAD. The reduced state of UQ takes up two protons (H^+) from the mitochondrial matrix to form ubiquinol (UQH_2). Due to its hydrophobic character UQH_2 diffuses within the IMM to cytochrome bc1 complex (complex III). UQH_2 binds to a distinct binding site of complex III and transfers one of its two electrons via iron-sulfur cluster and cytochrome c1 to oxidized cytochrome c. The other electron reduces a complex III bound UQ molecule to form a semi-ubiquinone anion ($UQ^{\cdot-}$). This electron transfer is mediated by cytochrome b. The resulting UQ is replaced by another UQH_2 molecule which again transfers one electron to cytochrome c and one electron to $UQ^{\cdot-}$ to form UQH_2 by uptake of two H^+ from the mitochondrial matrix. During the regeneration of NADH to NAD^+ and UQH_2 to UQ the released H^+ are pumped into the IMS by complex I and complex III, respectively. The electron transfer to UQ and via cytochrome c1 to cytochrome c in combination with the H^+ transport is defined as "Q cycle" (Brandt and Trumpower, 1994; Mitchell, 1975; Trumpower, 1990).
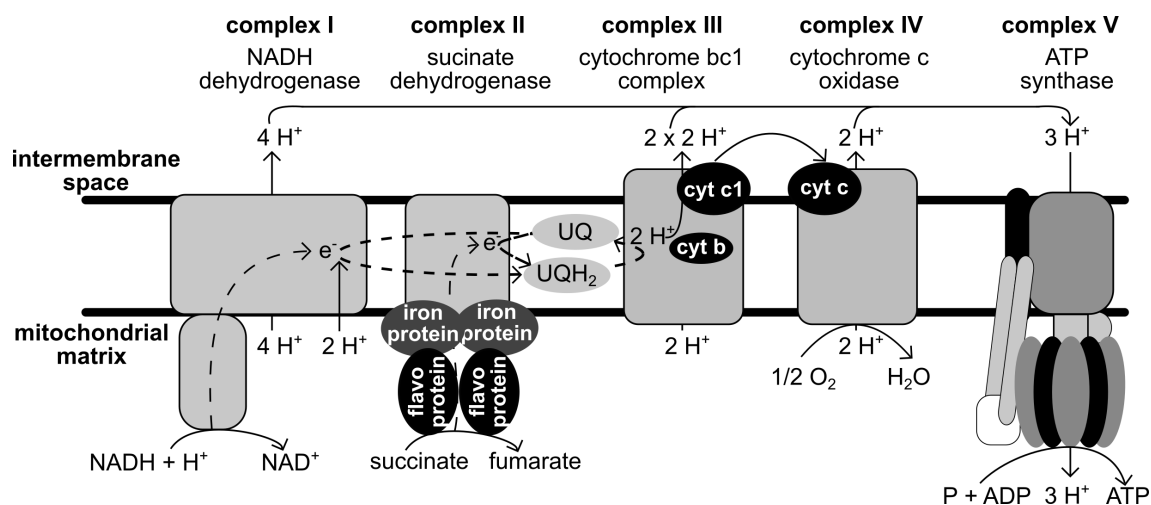
FIGURE 2.4: Electron-transport chain and oxidative phosphorylation. Complex I-IV build the electron transport chain which finally reduces oxygen (O_2) to water (H_2O). Electrons from NADH (complex I) and $FADH_2$ (complex II) are transferred to complex III via ubiquinone (UQ). Thus UQ is reduced to ubiquinol (UQH_2). UQH_2 transfers electrons to cytochrome b (cyt b) and through cytochrome c1 (cyt c1) to cytochrome c (cyt c). Cytochrome c oxidase oxidizes the reduced cyt c and reduces O_2 to H_2O. Electron transport leads to the transfer of protons (H^+) from mitochondrial matrix to IMS, thus forming a H^+-gradient across the IMM. The resulting proton motive force is utilized for oxidative phosphorylation by ATP synthase, thereby producing ATP. (Berg et al., 2003). With modifications to KEGG pathway cge00190.

Cytochrome c oxidase (complex IV) oxidizes cytochrome c molecules and transfers the released electrons via complex bound copper ions (Cu_A/Cu_A, Cu_B) and heme groups (heme a, heme a_3) to oxygen to form water. Thereby two H^+ per two oxidized cytochrome c molecules and one reduced oxygen atom, respectively, are transported from mitochondrial matrix to intermembrane space. (Berg et al., 2003)

The H^+-pumping function of complex I, III and IV was described to create a pH gradient and a mitochondrial membrane potential, thus generating a proton motive force. According to the "chemiosmotic theory" of Mitchell (1966), electron-transport chain and ATP synthesis are linked by this proton-motive force: oxidative phosphorylation. (Berg et al., 2003; Nath and Villadsen, 2015)

Mitochondrial ATP synthase (complex V) catalyzes the phosphorylation of ADP to form ATP and consists of the F0 domain (subunits: c-ring, a, b, d, f, A6L, F_6 and oligomycin sensitivity-conferring protein (OSCP)) which is located mainly in the inner mitochondrial membrane and the F1 domain

(subunits: α, β, γ, δ, ϵ) in the mitochondrial matrix. A hexameric ring of alternating α and β subunits in association with subunits a, b, d, F_6 and OSCP build the so called "stator" of ATP synthase, whereas the "rotor" is composed of c-ring, γ, δ and ϵ. H^+ flux through subunit a and c-ring into the mitochondrial matrix induces rotation of the γ subunit, thus changing the conformations of catalytic β sites of ATP synthesis. Rotation enables switching between ADP and orthophosphate binding, ATP synthesis and ATP release. (Berg et al., 2003; Jonckheere et al., 2012)

The coupling efficiency of electron-transport chain and oxidative phosphorylation is quantitatively described by the P/O ratio which defines the number of produced ATP molecules per reduced oxygen atom (Hinkle, 2005). The P/O ratio varies depending on the type of regenerated reducing equivalent. P/O ratios of 2.5 and 1.5 were mentioned in literature for NADH and $FADH_2$, respectively (Hinkle, 2005; Nath and Villadsen, 2015; Wahl et al., 2008).

Energy Yield

CHO cells catabolize glucose in part to lactate via "aerobic glycolysis" and in part to CO_2 via glycolysis and TCA cycle. The energy yield of glucose metabolization to lactate is 2 ATP molecules whereas a complete metabolization via TCA in combination with subsequent oxidative phosphorylation theoretically yields 36 ATP molecules (Berg et al., 2003; Klempnauer et al., 2011; Vander Heiden et al., 2009). Glacken (1988) and Altamirano et al. (2013) described a theoretical energy yield of 24 - 27 ATP molecules for complete oxidation of glutamine to carbon dioxide. This energy yield can be achieved via oxidative deamination of glutamate to α-ketoglutarate, conversion of α-ketoglutarate to malate in TCA, subsequent oxidative decarboxylation of malate to pyruvate and fueling of pyruvate into TCA cycle via conversion to acetyl-CoA (Glacken, 1988). In contrast an energy yield of 9 ATP was stated if pyruvate was catabolized to lactate or for the transaminase mediated metabolization of glutamine as this pathway requires further TCA intermediates, e. g. oxaloacetate (Altamirano et al., 2013; Glacken, 1988).

Biosynthesis of Purine Nucleotides

Nucleotides of the purine bases adenine (A) and guanine (G) are building blocks of DNA and RNA and therefore substantial amounts of purine nucleotides are required during DNA replication and transcription. Further, purine nucleoside triphosphates (ATP, GTP) are important cellular energy sources with ATP being the most abundant form, even in its own de novo biosynthesis pathway (Fig. 2.5). This elucidates the high energy requirement of the de novo purine nucleotide biosynthesis. Salvage pathways provide an opportunity to avoid de novo synthesis by recycling of purine bases (Berg et al., 2003). Adenine phosphoribosyltransferase and hypoxanthine-guanine phosphoribosyltransferase catalyze the formation of adenine monophosphate and guanine monophosphate, respectively. Enzymes catalyze the conversion of purine base and 5-phosphoribosyl-1-pyrophosphate to purine nucleoside monophosphate and pyrophosphate (Berg et al., 2003).
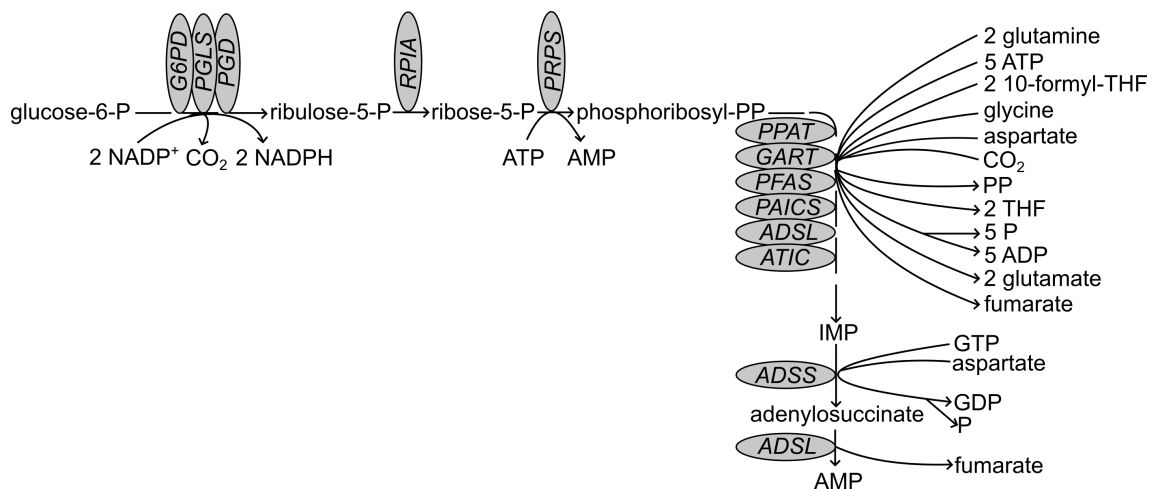
FIGURE 2.5: De novo biosynthesis of purine nucleotides. Grey shaded ellipses symbolize the gene names of corresponding enzymes for each reaction. P = (ortho)phosphate, PP = pyrophosphate, THF = tetrahydrofolate. *G6PD*: glucose-6-phosphate dehydrogenase, *PGLS*: 6-phosphogluconolactonase, *PGD*: phosphogluconate dehydrogenase, *RPIA*: ribose 5-phosphate isomerase A, *PRPS*: phosphoribosyl pyrophosphate synthetase, *PPAT*: phosphoribosyl pyrophosphate amidotransferase , *GART*: phosphoribosylglycinamide formyltransferase, *PFAS*: phosphoribosylformylglycinamidine synthase, *PAICS*: phosphoribosylaminoimidazole carboxylase, *ADSL*: adenylosuccinate lyase , *ATIC*: 5-aminoimidazole-4-carboxamide ribonucleotide formyltransferase, *ADSS*: adenylosuccinate synthase. With modifications to KEGG pathway cge00030 and cge00230.

De novo biosynthesis of purine nucleotides is located in the cytosol and includes the synthesis of ribose-5-phosphate, an important precursor of purine nucleotide synthesis, via pentose-phosphate pathway. Glucose-6-phosphate is converted to ribulose-5-phosphate by the enzymes glucose-6-phosphate dehydrogenase, 6-phosphogluconolactonase and phosphogluconate dehydrogenase. Ribulose-5-phosphate is isomerized to ribose-5-phosphate by ribose-5-phosphate isomerase and subsequently phosphorylated by phosphoribosyl pyrophosphate synthetase to form 5-phosphoribosyl-1-pyrophosphate (PRPP). PRPP is a central metabolite of purine nucleotide synthesis as the purine base ring structure is gradually constructed directly on PRPP. A variety of enzymes (Fig. 2.5) built up the base ring structure and thereby convert PRPP to inosine monophosphate (IMP). The required nitrogen atoms are provided by amino/amido groups of glutamine, glycine and aspartate while 10-formyl-tetrahydrofolate, glycine and CO_2 provide carbon groups. Synthesis of AMP is finally mediated by adenylosuccinate synthase and lyase and requires GTP and aspartate as substrates. In subsequent reactions adenylate kinases can transfer phosphate groups from ATP to AMP and ADP, respectively. Altogether the de novo synthesis of AMP from glucose requires 7 molecules of ATP, 1 molecule of GTP, 2 molecules of oxidized nicotinamide adenine dinucleotide phosphate ($NADP^+$) and a variety of nitrogen and carbon donors. (Berg et al., 2003; Lane and Fan, 2015)

Regulation of Metabolism by Adenine Nucleotides

Regulation at the level of enzymes is a common property of metabolic pathways. In this context, adenine nucleotides allosterically activate (AMP, ADP) or inhibit (ATP) a variety of enzymes of catabolic pathways. Further, metabolic enzymes are inactivated by kinase mediated phosphorylation. Therefore cellular ratios of adenine nucleotides, e. g. ADP/ATP ratio or energy charge, have an impact on the metabolization of the main cellular substrates glucose and glutamine (Fig. 2.3). The glycolytic enzymes phosphofructokinase (*PFK*) and pyruvate kinase (*PK*) are targets for allosteric inhibition by ATP (Berg et al., 2003; Brüser et al., 2012; Fenton and Hutchinson, 2009; Martínez-Costa et al., 2012). In addition, high ATP levels contribute inactivation of pyruvate kinase by phosphorylation (Berg et al.,

2003; Fenton and Hutchinson, 2009), whereas binding of AMP and ADP to allosteric sites stimulates phosphofructokinase. High energy charges, which correspond to high ATP levels, induce phosphorylation of pyruvate dehydrogenase (*PDH*) and α-ketoglutarate dehydrogenase (*OGDH*), thereby inactivating these enzymes of TCA cycle. The oxidative deamination of glutamate by glutamate dehydrogenase (*GLUD*) to form α-ketoglutarate is activated by high ADP levels and inactivated by high ATP levels (Fang et al., 2002).

In addition to the regulatory effect on the catabolic pathways glycolysis and TCA cycle, adenine nucleotide levels also influence their *de novo* biosynthesis pathway (Fig. 2.5). AMP, ADP and ATP are feedback inhibitors of PRPP amidotransferase (*PPAT*), where AMP also inhibits the enzymes PRPP synthetase (*PRPS*) and adenylosuccinate synthase (*ADSS*) (Lane and Fan, 2015; Van der Weyden and Kelly, 1974; Wyngaarden, 1976).

AMP/ATP ratio is a trigger of the AMP-activated protein kinase (AMPK) mediated regulation of catabolic and anabolic pathways (Carling, 2004; Corton et al., 1994; Mulukutla et al., 2010). AMPK, which is also defined as energy sensor, is activated by allosterical binding of AMP and a subsequent phosphorylation. High ATP levels hamper the binding of AMP to AMPK, thus inhibiting enzyme activity (Carling, 2004). In its active state, AMPK inactivates ATP-consuming anabolic pathways, stimulates ATP-producing catabolic pathways, e. g. by activation of glucose transporters, hexokinase and phosphofructokinase 2, and induces p53-mediated cell cycle arrest (2.2) (Barnes et al., 2002; Carling, 2004; Jones et al., 2005; Mulukutla et al., 2010). Stress conditions, e. g. heat shock, arsenite treatment or sorbitol induced hyperosmolality, were shown to activate the AMPK cascade independent from changes in AMP/ATP ratios (Carling, 2004; Corton et al., 1994; Fryer et al., 2002).

2.5 Industrial Relevance of CHO Cells

The approval of more than 100 biopharmaceuticals produced in CHO cells (Butler and Meneses-Acosta, 2012) illustrates the industrial relevance of these cells as mammalian host cell lines.

Several important cellular characteristics benefited this trend. CHO cells have the ability to grow in suspension in chemically defined culture medium without fetal calf serum reaching high cell densities in large scale bioreactors of up tp 20,000 L (Birch and Racher, 2006; Chu and Robinson, 2001; Jayapal et al., 2007; Kim et al., 2012; Li et al., 2010). In addition, suitable expression systems (2.5) are available for insertion of the gene of interest (GOI) into the host cell genome, for cell line selection and for amplification of the inserted genes (2.5) (Jayapal et al., 2007; Kim et al., 2012; Wurm, 2004).

Since the approval of the first biotherapeutic product in 1986, CHO cells have proven to be safe hosts showing high viral resistance and producing therapeutic proteins with low human immunogenicity (Butler and Meneses-Acosta, 2012; Jayapal et al., 2007; Kim et al., 2012). The immunogenicity is mediated by the post-translational modification (2.5) of a therapeutic protein. Therefore a low immunogenicity represents a high similarity of the human and CHO post-translational modification. This similarity is also responsible for the good bioactivity of CHO products for the treatment of human diseases.

The aforementioned characteristics contribute to the fact that CHO cells became the industry's "mammalian workhorse" (Jayapal et al., 2007; Kim et al., 2012).

Cell Line Development

The biotechnological production of therapeutic proteins requires cell lines which stably express a defined gene of interest (GOI) - the product. The development of such cell lines is a time consuming process which can take more than six months (Jayapal et al., 2007). The use of a host cell line which had been pre-adapted to the later cultivation conditions, e. g. growth in suspension, reduced this time span significantly (Birch and Racher, 2006). At first a CHO host cell line is transfected with an expression vector using electroporation, nucleofection or lipofection (Jayapal et al., 2007; Lattenmayer et al., 2007; Li et al., 2010).

Two common expression systems are described in CHO literature; the glutamine synthetase (GS) and the DHFR expression system where the DHFR system is the one which is most frequently used in CHO cell line development (Jayapal et al., 2007; Kim et al., 2012; Wurm, 2004).

The DHFR expression vector (Fig. 2.6) usually contains genetic information for the replication of the vector in bacteria (e. g. *E. coli*) and for the expression of the GOI in combination with *DHFR* as selection marker for gene amplification. The vector might as well contain a secondary antibiotic selection marker (e. g. aminoglycoside phosphotransferase gene, blasticidindeaminase, hydromycin phosphotransferase) in order to facilitate clone selection (Jayapal et al., 2007; Li et al., 2010). The gene of interest and the selection marker can be under the control of one promoter but usually their expression is controlled by individual promoters. While strong viral promoters (e. g. from human cytomegalovirus) are used to control the expression of the gene of interest, selection markers are commonly under the control of weak promoters (e. g. SV40) (Birch and Racher, 2006; Boshart et al., 1985).
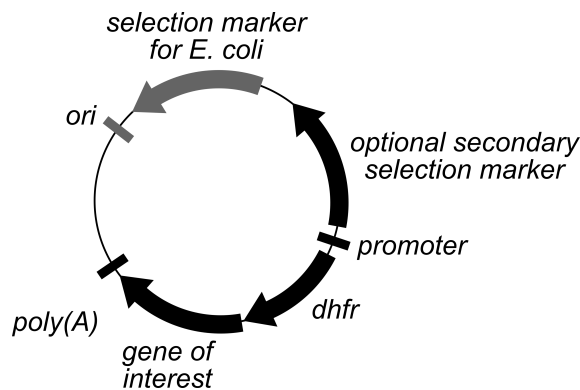
FIGURE 2.6: Vector design for DHFR (dihydrofolate reductase) expression system. ori = origin of replication for *E. coli*, selection markers represent genes mediating antibiotic resistance, poly(A) = 3' poly-adenine tail. With modifications to Jayapal et al. (2007)

The DHFR expression system is used in combination with DHFR deficient cell lines like CHO DXB11 and CHO DG44. Due to their deficiency of DHFR, the aforementioned cell lines are not able to synthesize glycine, hypoxanthine and thymidine (2.1). This auxotrophy is utilized in the cell selection process.

After transfection, the expression vector can enter the nucleus of the host cell line and random integration of the genetic information into the host cell genome might occur. In a subsequent

selection step transfected cells are grown in the presence of low concentrations of the folic acid analog methotrexate (MTX) which competitively inhibits DHFR (Jayapal et al., 2007). In addition the cultivation medium is free of glycine, hypoxanthine and thymidine thereby selecting for cells showing stable expression of DHFR due to vector integration. The surviving cells of the previous selection step are exposed to high concentrations of MTX and have to adapt to this intense selection pressure in order to survive. The cells most likely cope with this situation by amplifying the integration site of the DHFR gene or by genomic rearrangements. The gene of interest is supposed to be simultaneously amplified with the DHFR gene so that the amplification step results in cell clones often containing several hundreds of gene copies (Jayapal et al., 2007).

The resulting cell pool is screened for clones with high growth rate (μ), q_P and product quality. Pre-cultures of the resulting clones ($\sim$ 10 -30) are generated during several passages of cultivation and are finally used as inoculum for scale-down processes of the final industrial production process. The cell clone showing the best performance under this culture conditions is chosen for the generation of a cell bank of cryo cultures (Jayapal et al., 2007). The cell line development with the GS expression system proceeds in accordance to the previously described steps for the DHFR expression system. In contrast to the DHFR system, the GS expression vector contains DNA encoding for glutamine synthetase instead of *DHFR*. GS synthesizes glutamine from glutamate and ammonia and enables cell lines which are auxotrophic for glutamine to survive in glutamine-free medium. CHO cell lines commonly require a glutamine supplemented cultivation medium due to their low endogenous GS activity but GS-knockout CHO cell lines are utilized as well. Cells transfected with a GS expression vector can integrate the GS gene into their genome and may overcome this auxotrophy. Methionine sulphoximine (MSX), a competitive inhibitor of GS, can be applied to enforce the selection pressure. Selection and amplification step are therefore performed in glutamine-free cultivation medium supplemented with low or high concentrations of MSX.

Post-translational Modification

Several therapeutic proteins possess post-translational modifications (PTM, e. g. glycosylation) which are necessary for their bioactivity. A high similarity between the PTM pattern of biotechnologically produced therapeutics and the pattern of the organism undergoing medical treatment (e. g. humans) is important for a high bioactivity and a low immunogenicity. Therefore PTM is an important property of product quality.

The PTM of a therapeutic protein depends on the post-translational machinery of the host cell line. CHO cells have a highly similar post-translational machinery compared to humans and thus synthesize therapeutically applicable products (Butler and Meneses-Acosta, 2012; Walsh, 2010a,b). Butler and Meneses-Acosta (2012) mentioned that $\sim 99\%$ of the genes encoding glycosylating enzymes in the human genome had a CHO homolog. Böhm et al. (2015) analyzed the impact of the type of mammalian host cell line (BHK, CHO, HEK293) on q_P, c_P and the glycosylation pattern. In conclusion, CHO cells were shown to own the best properties in terms of formation, stability and bioactivity of the product.

The main types of PTMs associated with therapeutic proteins are amidation, sulfation, disulfide bond formation, γ-carboxylation, β-hydroxylation and glycosylation (Walsh, 2010b; Walsh and Jefferis, 2006). Disulfide bond formation affects the folding process and therefore the tertiary and quaternary structure of proteins. This folding process is located in the endoplasmic reticulum (ER) where covalent linkages between inter- or intramolecular cysteine residues of proteins are favored due to oxidizing conditions (Feige and Hendershot, 2011; Wittrup, 1995). This process is mediated by disulfide isomerases whereby a subsequent quality control mechanism in the ER ensures that only correctly folded proteins are passed on in the secretory pathway. Human IgG1 antibodies are examples for proteins requiring disulfide bond formation for a proper folding (Fig. 2.7).

Another important PTM of antibodies (Fig. 2.7) is glycosylation and in general it is the most complex and with $\sim 40\%$ of all approved biopharmaceutical products being glycosylated the most abundant type of PTM (Walsh, 2010a,b). Walsh (2010b) summarized cell- and protein-specific processes that were described to be affected by glycosylation. This involved serum half-life, folding,

targeting/trafficking and the stability and bioactivity of a protein. Two types of glycosylation are described in literature, O-linked and N-linked glycosylation. The O-linked glycosylation defines the attachment of a glycan structure to a protein's serine or threonine residue via the oxygen atom. This type of glycosylation occurs either in the ER or the Golgi and requires no consensus sequence. The more abundant N-linked glycosylation is located in the ER where an oligosaccharide is transferred from the donor molecule dolichol phosphate to an asparagine residue of a protein via the nitrogen atom (Fig. 2.8). The consensus sequence Asn-X-Ser/Thr, where X can be any amino acid but proline, determines the asparagine residues that can function as glycan recipients (Hossler et al., 2009; Walsh and Jefferis, 2006).
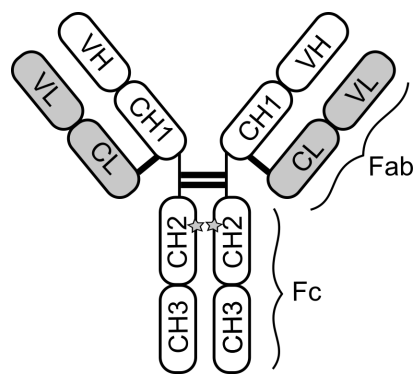
FIGURE 2.7: Structure of a human IgG1 antibody. White = domains of immunoglobulin heavy chain (H), grey = domains of immunoglobulin light chain (L), C = constant region, V = variable region, star = Fc-terminal glycosylation at asparagine residue 297 (Asn297). The antibody consists of two heavy and two light chains and is divided in two Fab and one Fc region. A flexible linker connects the Fc region with the two Fab regions (hinge). The heavy chains are covalently linked by disulfide bonds. The constant domains of a Fab region are also connected by a disulfide bond. The antigen binding site is formed by the Fab domains VH and VL. With Modifications to Natsume et al. (2009).

IgG antibodies are built up by two identical heavy and two identical light chains forming two antigen binding fragments (Fab) and a Fc moiety for the induction of effector mechanisms, e .g. antibody-dependent cellular cytotoxicity (ADCC), phagocytosis or complement-dependent cellular cytotoxicity (Fig. 2.7) (Walsh and Jefferis, 2006). The Fc region possesses conserved sites for N-linked glycosylation at asparagine residue 297 (Asn297) of each heavy chain (Fig. 2.7). Fab regions show as well N-linked

glycosylation but in a non-conserved manner and with a low frequency of $\sim$ 15 - 20% (Dwek et al., 1995; Mimura et al., 2007).
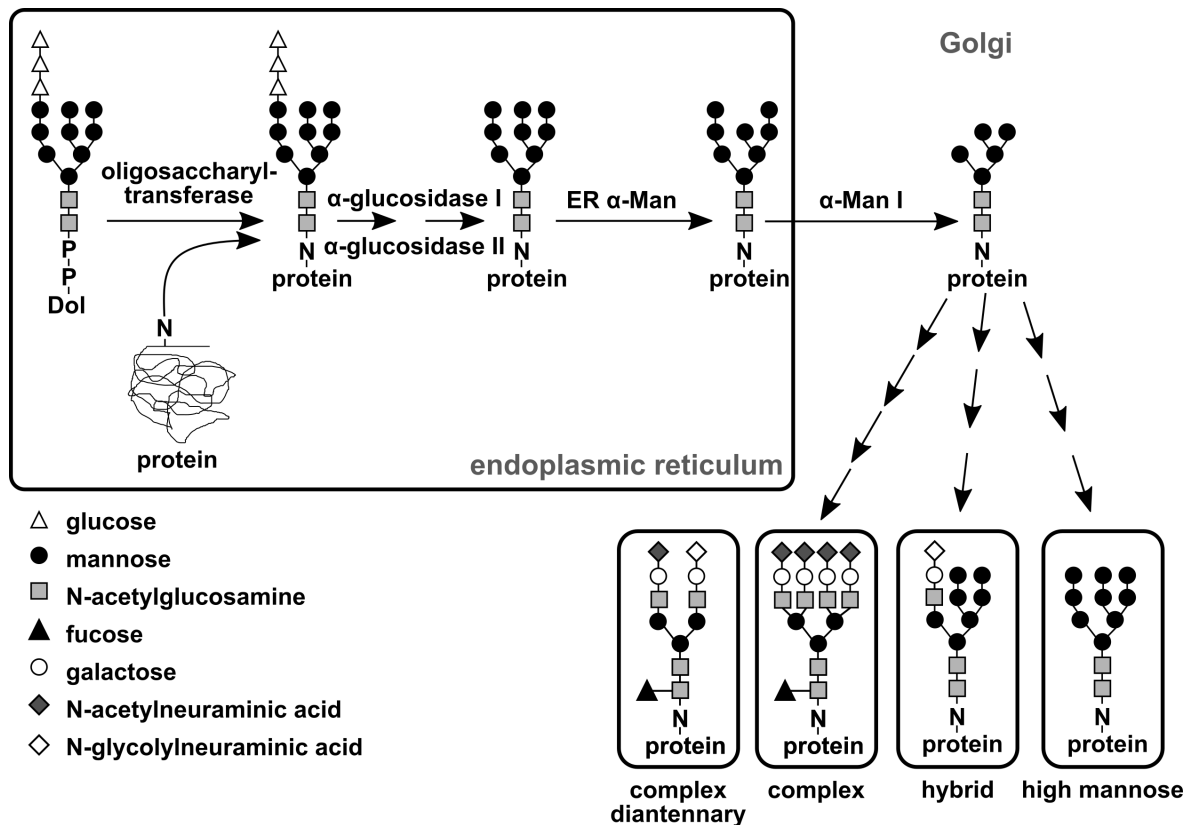
FIGURE 2.8: Glycosylation of proteins in the endoplasmic reticulum and the Golgi network. An Oligosaccharyltransferase transfers a glycan structure from the donor dolichol phosphate (Dol-P-P) to an asparagine residue of a protein via the nitrogen atom. Therefore this type of glycosylation is called N-linked glycosylation. Glucosidases and α-mannosidases (α-Man) trim the glycan structure in the ER thereby removing glucose and mannose molecules. The resulting glycoprotein (type mannose-5) is transported to the Golgi network where the glycan structure can be further modified by the enzymes galactosyl-, sialyl-, fucosyl- and mannosyl-glycoprotein N-acetylglucosaminyltransferase. Examples for the different types of N-linked glycan structures (complex, hybrid, high mannose) are shown. All glycan structures possess a pentasaccharide core structure (GlcNAc$_2$Man$_3$). With modifications to Hossler et al. (2009).

The N-linked glycosylation of proteins is located in the ER and is followed by the modification of the glycan structure by galactosyl-, sialyl-, fucosyl- and mannosyl-glycoprotein N-acetylglucosaminyltransferases in the Golgi network. The modification of glycan structures leads to the formation of

representative types of N-linked glycosylation - high mannose, hybrid and complex type (Hossler et al., 2009). A pentasaccharide core structure (GlcNAc$_2$Man$_3$) is specific for all types of N-linked glycosylation. The conserved N-linked glycan structures of IgG antibodies are assigned to the complex diantennary type (Fig. 2.7) (Dwek et al., 1995; Jefferis, 2009; Walsh and Jefferis, 2006). Culture conditions, e. g. temperature, dissolved oxygen (DO) level and/or composition of cultivation media, can cause alterations of the glycan structure (2.6). In the field of glycoengineering, targeted modifications of the glycan structure are utilized for the improvement of antibody properties, e. g. bioactivity or half-life (Ceaglio et al., 2008; Elliott et al., 2003).

Cell Culture Processes

The biotech industry utilizes recombinant cell lines as "cell factories" for the production of therapeutic proteins. The manufacturing process of these biotherapeutics is subdivided into the main sectors upstream processing and downstream processing. While the focus of downstream processing is placed on the isolation, purification and sometimes modification of the biotechnological product, upstream processing is more diversified (Butler and Meneses-Acosta, 2012; Walsh, 2010b). It includes the development of cell lines (2.5), media and process strategies, the realization of the final cultivation process and the separation of the cells from the cultivation medium. Therefore various possibilities for the improvement of specific product formation rates and product titers are available but likewise complicate an optimization in the sector of upstream processing.

Important issues of upstream processing are summarized in the following sections.

Cell Growth

All cell culture processes are based on a tremendous amount of viable cells. This biomass is generated from a cryo culture and scaled-up during a series of bioreactor processes defined as "seed train" and "inoculum train" (Li et al., 2010). The knowledge of the different phases of cell growth (Fig. 2.9) occurring during a bioprocess is essential for the production of large amounts of viable, metabolically active cells as inoculum for the production of therapeutic proteins.
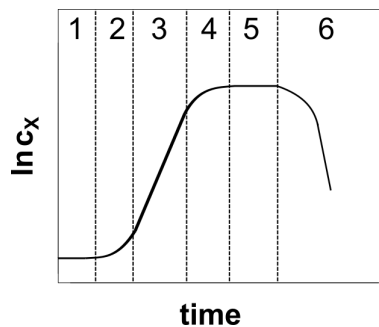
FIGURE 2.9: Phases of cell growth during a batch cultivation. 1: during "lag phase" cells show almost no growth as they adapt to new culture conditions after being inoculated into fresh medium, 2: in "acceleration phase" cells start growing with a steadily increasing growth rate, 3: a maximal and constant growth rate is characteristic for cells in the "exponential growth phase", 4: substrate limitation in "decelerating phase" causes a decline of cell growth, 5: no cell growth occurs in "stationary phase" due to complete substrate consumption, 6: in "declining phase" substrate deficiency hampers maintenance of important cellular functions and causes cell death. With modifications to Katoh et al. (2015)

Each bioprocess starts with the inoculation of cells into fresh cultivation medium. Commonly, cells require changes in gene/protein expression in order to adapt to the new culture conditions. Therefore they show almost no growth in this so called "lag phase" whose length depends for example on the type and number of the inoculated cells and the culture conditions. In the following "acceleration phase" cells start growing with a steadily increasing growth rate (μ) until they enter the "exponential growth phase" where cell growth is constant and maximal (μ_{max}). Cell growth subsequently declines ("deceleration phase") due to limitation of substrate (e. g. glucose (Glc), glutamine (Gln)) and stops when substrate is completely consumed in the "stationary phase". Finally, substrate deficiency hampers the maintenance of important cellular functions and causes cell death ("declining phase"). (Katoh et al., 2015)

Process Modes

Most mammalian production processes are either performed in fed batch or perfusion mode (Fig. 2.10). The simplest form of cultivation is a batch process where cells are inoculated into fresh medium and incubated without further manipulation (Fig. 2.10-A). Therefore batch cultures contain relatively high substrate concentrations (e. g. c_{Glc}, c_{Gln}) at the beginning of the cultivation ($c_{S,0}$), thereby

facilitating the production of by-products. Accumulation of the common by-products lactate (Lac) and ammonium (NH_4^+) was shown to be linked to inhibition of cell growth and impaired q_P and product quality (Lao and Toth, 1997; Yang and Butler, 2002). Despite the relatively high substrate level, high cell densities and product titers are hampered by substrate limitation occurring during the time of batch cultivation (Wlaschin and Hu, 2006). Lower $c_{S,0}$ in combination with the supply of substrates as required, limits the formation of by-products and prevents substrate limitations. This is realized in fed batch and perfusion mode thereby enabling high cell densities ($> 10^7$ cells mL^{-1}) and high product titers (Howaldt et al., 2011; Wlaschin and Hu, 2006). A fed batch process is based on a batch process with low $c_{S,0}$. Cells are grown without further manipulation until substrate concentrations approach limitation, thus the supply of concentrated substrate solutions (feeding) is started (Fig. 2.10-B) (Wlaschin and Hu, 2006).

In order to prevent by-product formation, the availability of the substrates glucose and glutamine is limited by controlled feeding strategies. The simple periodic feeding strategy is based on the addition of concentrated substrate solutions once or twice a day. The required volume for each interval can be calculated according to c_{Glc} and c_{Gln} in the bioreactor and the cell specific consumption of these metabolites. Although final substrate concentrations commonly show a wide range of variety, the simplicity of periodic feeding is still the reason for its application in large scale production (Li et al., 2010). A more precise adjustment of the availability of substrates can be realized by continuous feeding. Thereby feeding is executed as a function of an on-line measured process parameter (e. g. c_{Glc}, oxygen uptake rate) (Wlaschin and Hu, 2006).

The performance of a fed batch process relies not only on the feeding strategy but as well on the composition of the feed solution. A common approach for the preparation of feed solutions is to use a 10- to 15-fold concentrated version of the cultivation medium (Li et al., 2010; Wlaschin and Hu, 2006). As this most likely leads to a surplus (e. g. inorganic ions) or limitation (e. g. Mg^{2+} and vitamins) of certain nutrients, special feeding solutions are developed. Another important aspect of feed solution design is to reduce the feeding-mediated increase in culture osmolality as high osmotic conditions inhibit cell growth (> 350 mOsmol kg^{-1}) or even cause cell death (> 450 mOsmol kg^{-1}) (Han et al., 2010; Kim and Lee, 2002; Lee et al., 2003a; Ryu et al., 2000; Shen et al., 2010).
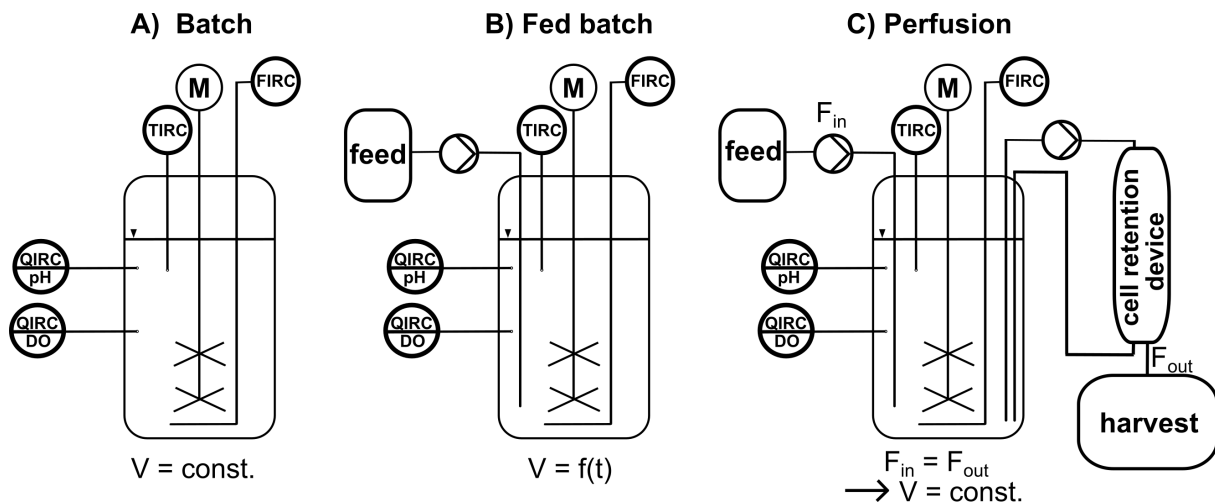
FIGURE 2.10: Bioreactor setups for batch (A), fed batch (B) and perfusion mode (C). Bioreactors are agitated (M), aerated (FIRC) and possess control modules for the adjustment of temperature (TIRC), pH and dissolved oxygen (DO). In batch mode (A), cells are inoculated into cultivation medium and incubated at defined growth conditions without further manipulations. A fed batch process (B) is an extension to the batch mode where concentrated nutrient solutions (feed) are added during the time of cultivation. Thus the accumulation of growth inhibiting amounts of by-products (e. g. ammonium, lactate) is limited. In perfusion mode (C) the system is supplied with concentrated nutrient solutions while an equal volume of cell suspension is withdrawn from the bioreactor (V = constant). Cells are subsequently separated from the cultivation broth (harvest) by an external cell retention device and are finally returned into the bioreactor. V = working volume of the bioreactor [L], F_{in} = influx [L h^{-1}], F_{out} = efflux [L h^{-1}], const. = constant. (Birch and Racher, 2006; Howaldt et al., 2011)

Continuous cultivations are characterized by withdrawal of the same amount of cell suspension as added by feeding. Thereby the equal influx and efflux lead to a constant working volume in the bioreactor. Perfusion mode (Fig. 2.10-C) is a special form of continuous cultivation where cells of the withdrawn cell suspension are aseptically separated from the culture broth and are returned into the bioreactor. Thus very high cell densities ($\geqslant 10^8$ cells mL^{-1}) can be achieved under defined and constant culture conditions. The steady replacement of cell suspension by fresh medium provides appropriate conditions for high µ , q$_P$ and product quality by preventing the accumulation of by-products.

A variety of cell retention systems, namely spin filters, centrifuges, alternating tangential filter systems (ATF), hydroclones and acoustic or gravity settlers, has been described in literature (Voisard et al., 2003; Warnock and Al-Rubeai, 2006). The retention of cells is either based on filtration, sedimentation or centrifugation and therefore cell size and density are important criteria for cell

separation. All of these systems, except spin filters, can only be used as external systems so that cells reside outside the bioreactor for a certain amount of time. Ideal cell retention devices show high perfusion rates (in L d^{-1}), high retention efficiencies, low residence times outside the bioreactor and a high robustness. In general, perfusion mode enables the cultivation of cells at defined and constant conditions for several months. Therefore the long-term stability of cell lines regarding μ and q_P is of utmost importance. Spin filters, centrifuges, gravity settlers and ATF are commonly applied for large scale biomanufacturing of mAbs, enzymes and blood factors (Ozturk, 2015).

In conclusion, fed batch mode is the most frequently used process strategy for industrial production as it yields high product titers, shows high robustness in large scale and as less time is required for process development and validation compared to perfusion mode (Howaldt et al., 2011). However, perfusion mode is utilized for the production of some biopharmaceuticals, e. g. for the rather instable blood coagulation factor VIII (Chu and Robinson, 2001; Howaldt et al., 2011).

Process Development

Process performance, in terms of cell growth, product formation and product quality, relies not only on the selected cell line but as well on culture conditions (Fig. 2.11). These depend on process mode, composition of media and on operating parameters (e. g. pH, agitation (N), temperature (T), dissolved oxygen (DO)). The synergy of this operational properties is investigated during process development in order to identify a process strategy that provides appropriate culture conditions for a selected cell line. Since 2009 the application of the quality by design (QbD) approach has been recommended for process development by the EMA and the FDA. The major purpose of this approach is the comprehensive understanding of biotechnological production processes and the identification of critical parameters and sources of variation in order to ensure that therapeutic products consistently meet predefined quality standards (EMA, Gronemeyer et al. (2014)). A multidimensional "design space" finally specifies the limits that a process must observe (Howaldt et al., 2011). The required experiments for process analysis are frequently planned on basis of the design of experiments (DOE)

approach (Castro et al., 1992; Fisher, 1935; Gronemeyer et al., 2014; Hammett et al., 2007; Horvath et al., 2010; Legmann et al., 2009; Li et al., 2010). Thus the number of experiments is reduced to an essential minimum and the financial burden and duration can be decreased as well. QbD is highly connected with Process Analytical Technology (PAT), an FDA initiative for the implementation of modern measurement devices with the objective of a better understanding of the influence of process parameters on product quality (Gnoth et al., 2007). PAT and QbD often apply multivariate data analysis (e. g. principle component analysis) for investigating the synergy of operational properties and the effect on product quality (Gnoth et al., 2007; Horvath et al., 2010; Schaub et al., 2012).
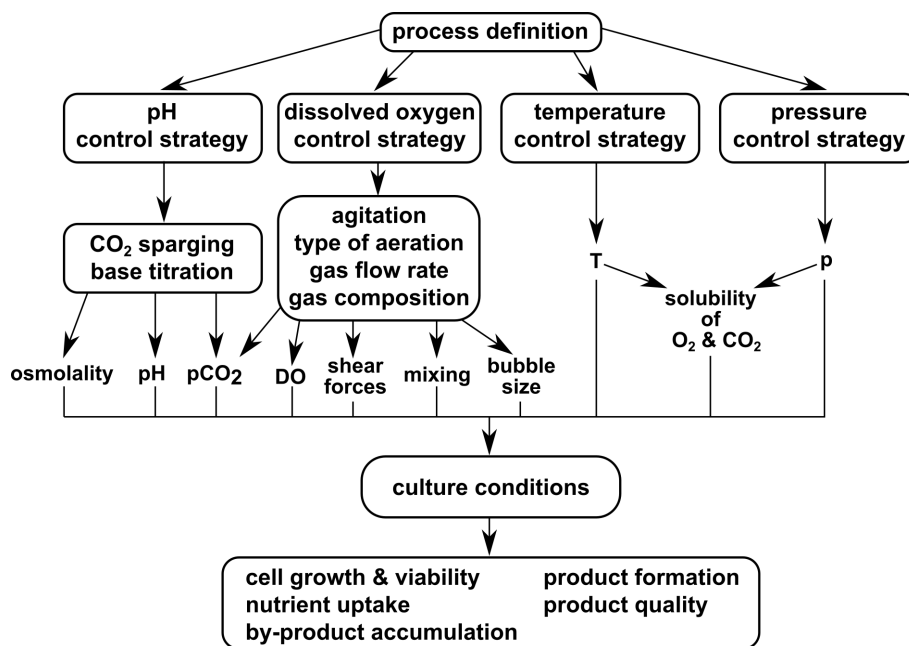
FIGURE 2.11: Correlation between operating parameters and process performance. DO = dissolved oxygen, pCO_2 = dissolved carbon dioxide level. With modifications to Li et al. (2010).

Stirred tank bioreactors (STRs) are most frequently applied during large scale biomanufacturing (1,000 - 20,000 L) and process development (Birch and Racher, 2006; Chu and Robinson, 2001; Li et al., 2010; Wurm, 2004). Usually STRs are equipped with sensors and devices that allow

measurement and adjustment of pH, T, N and DO. This enables a high grade of experimental reproducibility which is important during process optimization. Microscale (10 - 15 mL), benchtop scale (1 - 5 L) and pilot scale (80 - 100 L) STRs are standard cultivation vessels for industrial process development. Due to the low amount of required resources, microscale bioreactors are often utilized for screening experiments during development of cultivation media and parameter testing (Chen et al., 2009; Janakiraman et al., 2015; Legmann et al., 2009). Janakiraman et al. (2015) described a high consistency between the results of the microscale ambr15^{TM} system and benchtop scale STRs and even claimed that microscale STRs might replace benchtop scale STRs as traditional scale-down models. But at the moment the main experiments during process development are still performed in 1 - 2 L STRs (Li et al., 2010; Wurm, 2004). Pilot scale STRs are commonly applied at late stage in order to validate the developed process strategy at a larger scale and to provide higher quantities of cell suspension for the optimization of downstream processes.

Process development involves the optimization of operational properties that can in part be adjusted by specific control strategies during cultivation (Fig. 2.11). Common parameter set points for mammalian cell cultures are a culture osmolality of 270 - 330 mOsmol kg^{-1}, T = 37°C, 20 - 50% DO and pH 7.0. Most cell culture media are based on the bicarbonate buffering system and therefore pH can be reduced by carbon dioxide (CO_2) sparging while pH is increased by base titration. STRs are equipped with cooling devices which are utilized for temperature control. DO depends on agitation, the type of aeration, gas flow rate and the composition of gas. Usually the type of aeration and stirring device has been predetermined in accordance with the equipment of the manufacturing STRs and is therefore not changed during process development. Gas mixing modules enable the possibility to mix air, O_2, N_2 and CO_2 as required during a cultivation process. (Li et al., 2010)

Control strategies do not only regulate the targeted parameter but also influence other operational properties. Osmolality mainly depends on the osmolality of cultivation medium but it is usually increased by base titration and the addition of feed solutions in fed batch mode. A DO control strategy that involves changes in agitation speed will most likely influence the mixing of cell culture, bubble size and shear forces while changes in gas flow rate and composition affect the dissolved CO_2 level (p_{CO_2}). In addition, p_{CO_2} is influenced by pH control as CO_2 sparging and base titration influence the

balance between dissolved CO_2 and bicarbonate (HCO_3^-). The solubility of gasses, e. g. O_2, CO_2, is further increased by decreasing culture temperature and increasing pressure in the STR.

As process strategies are developed for large scale STRs, typical scale-up criteria have to be considered. Volume-independent operating parameters (e. g. DO, T, pH) can be maintained whereas volume-dependent parameters (e. g. agitation, aeration, feed volume) need to be scaled up (Li et al., 2010). Working volume and feed volume can proportionally be increased but due to differences in bioreactor setup (e. g. geometry, control capability, volume to surface ratio) this is not suitable for agitation and aeration. The intensity of shear forces and the accumulation of pCO_2 would significantly be increased by a linear scale-up of agitation speed and gas flow rate, thus causing cell disruption and inhibition of cell growth and product formation (DeZengotita et al., 2002; Kimura and Miller, 1996; Lara et al., 2006; Zhu et al., 2005). Commonly applied scale-up criteria for agitation and aeration are a sufficient oxygen supply, mixing of culture and stripping of CO_2. The resulting cell compatible volumetric power inputs are usually low and interfere with homogeneous mixing of the cell suspension. Local variations of process parameters, e. g. pH, osmolality, p_{CO_2} and T, are therefore common properties of large scale cell culture processes (Fig 3.1) and were described to influence the cellular performance (2.6).

2.6 Hyperosmolality

The separation of two solutions with different solute concentrations by a semipermeable membrane activates a process called osmosis. While solvent molecules are able to pass the semipermeable membrane, solute molecules are not. The differences in solute concentration cause a flow of solvent molecules across the semipermeable membrane. Although solvent molecules can pass the membrane in both directions, the flow rate from the less concentrated solution to the higher concentrated solution is significantly higher. This compensation process causes an increase in pressure on the side of the originally higher concentrated solution. A characteristic property in this context is the osmotic pressure which defines the pressure that would be required in order to stop the solvent flow across

the semipermeable membrane. (Florence and Attwood, 2016; Mortimer and Müller, 2003)

In 1887 Jacobus van't Hoff claimed that molecules of an ideal dilute solution behaved like the molecules of an ideal gas in a defined space (Mortimer and Müller, 2003). Therefore the van't Hoff equation for osmotic pressure of ideal dilute solutions equals the gas law,

$$\pi = c_{solute,i} \times R \times T \tag{2.1}$$

where π is the osmotic pressure, $c_{solute,i}$ represents the molal concentration of solute i, R is the ideal gas constant and T the absolute temperature (Florence and Attwood, 2016; Mortimer and Müller, 2003). Eq.2.1 was extended by factor ν and ω in order to consider the fact that solutions are commonly non ideal and may contain molecules that ionize when dissolved. In this context, ω represents the osmotic coefficient and ν the number of ions (e. g. ν = 2 for NaCl). (Florence and Attwood, 2016)

$$\pi = \omega_i \times \nu_i \times c_{solute,i} \times R \times T \tag{2.2}$$

The osmolality of a solution is defined as the mass of osmotically active particles in 1 kg of water and has the corresponding unit milliosmole per kg (mOsmol kg^{-1}) (Costanzo, 2014). Eq. 2.3 shows that osmolality equals the ratio of the osmotic pressure of a solution and the osmotic pressure of a 1 molal ideal unionized solution with $\nu_{ideal} = \omega_{ideal} = 1$ (Florence and Attwood, 2016).

$$\xi = \frac{\pi}{\pi_{ideal}} = \frac{\omega_i \times \nu_i \times c_{solute,i} \times R \times T}{\omega_{ideal} \times \nu_{ideal} \times c_{solute,ideal} \times R \times T} = \omega_i \times \nu_i \times c_{solute,i} \tag{2.3}$$

As cell membranes possess semipermeable properties, osmosis can occur between the cultivation medium and cytoplasm (Mortimer and Müller, 2003). An important aspect in this context is the difference in osmolality of cultivation medium and cytoplasm because this triggers osmosis. Cultivation media with similar osmolality (isotonic) as the cytoplasm ($\sim 290 \pm 20$ mOsmol kg^{-1}) prevent osmosis whereas cells exposed to cultivation media with significantly higher osmolality (hyperosmotic) have to cope with this phenomenon (Costanzo, 2014; Kiehl et al., 2011; Mortimer and Müller, 2003).

Cellular Response Upon Hyperosmotic Culture Conditions

In general, independent osmolality studies investigated the cellular response in a range of approximately 290 - 610 mOsmol kg^{-1}. Significant effects were commonly described above 350 mOsmol kg^{-1} which can be defined as the osmolality level where hyperosmotic stress begins. Characteristic phenomena of hyperosmotic conditions are a dose-dependent decrease in μ and the maximal viable cell density (DeZengotita et al., 2002; Han et al., 2010; Kiehl et al., 2011; Kim and Lee, 2002; Lee et al., 2003a; Ryu et al., 2000, 2001; Shen et al., 2010; Zhang et al., 2010; Zhu et al., 2005). This inhibition of cell growth was shown to be associated with DNA damage, thus inducing cell cycle arrest or even apoptosis (Cherlet and Marc, 1999; Han et al., 2010; Kim and Lee, 2002; Ryu et al., 2001). Specifically, p53-mediated arrest of CHO, murine hybridoma and renal inner medullary cells in G1-phase of cell cycle (Cherlet and Marc, 1999; Dmitrieva et al., 2001; Ryu et al., 2001) and arrest of murine hybridoma in S-phase (Sun et al., 2004) were described in literature. Hyperosmolality studies of Kim and Lee (2002) and Han et al. (2010) revealed that osmolalities $\sim$ 500 mOsmol kg^{-1} or higher activate caspase-3 and -7, thus mediating apoptosis (2.3) including fragmentation of chromosomal DNA via the caspase cascade.

Analysis of the cell metabolism of hyperosmotically stressed CHO cells highlighted an enhanced metabolic activity(Ryu et al., 2000; Shen et al., 2010; Zhu et al., 2005). In concurrence with increased consumption of metabolites and production of by-products, hyperosmotically stressed antibody producing CHO cells showed a dose-dependent increase in q_P (Kiehl et al., 2011; Kim and Lee, 2002; Lee et al., 2003a; Ryu et al., 2000, 2001; Shen et al., 2010). However, the combination of cell growth inhibition and increased q_P commonly hampered a significant enhancement of final c_P (Han et al., 2010; Kiehl et al., 2011; Kim and Lee, 2002; Lee et al., 2003a; Ryu et al., 2000; Shen et al., 2010). The influence of hyperosmotic culture conditions on product quality is another important aspect as variations in PTM may cause e. g. decrease of bioactivity or increase of immunogenicity (Hossler et al., 2009; Pacis et al., 2011; Walsh, 2010b). Pacis et al. (2011) revealed an increased number of antibodies with mannose-5 glycoform (2.8) at hyperosmotic culture conditions which is unusual for human IgGs. Therefore hyperosmolality may negatively affect the functional properties of the produced mAbs.

Cultivation of CHO cells in hyperosmotic cultivation medium exposes the cells to the process of osmosis. Kiehl et al. (2011) described a rapid and dose-dependent decrease in cell size of IgG producing CHO cells followed by an increase in cell size above the initial. This phenomenon had already been described and reviewed for other mammalian cells, thereby exhibiting that efflux of water resulted in a decrease in cell size within minutes whereas a long-term process called regulatory volume increase (RVI) caused the subsequent increase in cell size (Alfieri and Petronini, 2007; Burg et al., 2007; Kiehl et al., 2011; Lang et al., 1998). Ion transporters in the cytoplasmic membrane, e. g. sodium (Na^+)/hydrogen (H^+) exchanger, chloride (Cl^-)/hydrogen carbonate (HCO_3^-) exchanger and Na^+-potassium (K^+)-$2Cl^-$ co-transporter, enable an accumulation of Na^+, K^+ and Cl^- in the cytosol in combination with an influx of water, thus causing RVI. The resulting increased intracellular ionic strength is then compensated by an accumulation of organic osmolytes, e. g. glycine, sorbitol, *myo*-inositol, taurine and betaine. This synthesis or influx of osmolytes together with the increased synthesis of chaperones is an important adaptation process in order to prevent apoptosis as osmolytes and chaperones stabilize macromolecules. (Alfieri and Petronini, 2007; Lang et al., 1998)

The effect of hyperosmolality on the transcriptome will be described in section 2.7.

2.7 Transcriptomics

The genome of mammalian cells consists of protein encoding and non-coding sequences (Eddy, 2001). The expression patterns of both protein encoding (mRNA) and non-coding genomic sequences (e. g. miRNAs, transfer RNAs (tRNA) and ribosomal RNAs (rRNA)) are characteristic for a cell cultivated at defined conditions due to a process of adaptation. The research field of transcriptomics investigates changes in expression patterns, thereby focusing on changes in mRNA and miRNA expression in relation to product formation, cell growth, apoptosis and variations of process parameters,(Clarke et al., 2011, 2012; Doolan et al., 2013; Fischer et al., 2014; Gammell et al., 2007; Hammond et al., 2012; Harreither et al., 2015; Hernández Bort et al., 2012; Kelly et al., 2015b; Schaub et al., 2012, 2010; Shen et al., 2010; Vishwanathan et al., 2015; Wong et al., 2006; Yee et al., 2009). In terms of cell culture, re-

search results may contribute to an optimization of cell lines and production processes (Barron et al., 2011a; Datta et al., 2013; Fischer et al., 2014, 2015b,c; Fomina-Yadlin et al., 2015; Jadhav et al., 2014; Jamnikar et al., 2015; Kelly et al., 2015a; Lewis et al., 2016; Lin et al., 2011; Loh et al., 2014; Vishwanathan et al., 2014). Common methods in transcriptomics are 'quantitative real time polymerase chain reaction' (qRT-PCR), microarrays and RNA sequencing, where especially CHO studies were hampered by the lack of a publicly available CHO genome (Datta et al., 2013; Wuest et al., 2012). Before Xu et al. (2011) published the draft genomic sequence for CHO K1, cross species approaches applying genomic information from *Homo sapiens*, *Mus musculus* or *Rattus norvegicus* and custom-made CHO cDNA microarrays were commonly applied to investigate the CHO transcriptome. (Clarke et al., 2011, 2012; Doolan et al., 2013; Druz et al., 2011; Harreither et al., 2015; Hernández Bort et al., 2012; Lin et al., 2011; Melville et al., 2011; Nissom et al., 2006; Schaub et al., 2010; Yee et al., 2009).

The Link between miRNA and mRNA

Lee et al. (1993) discovered a genomic sequence which did not encode a protein but two transcripts of ∼ 22 and 61 nucleotides (nt). *LIN-4* was described as a negative regulator of *LIN-14* mRNA, thereby playing an important role in postembryonic development of the nematode *Caenorhabditis elegans* (*C. elegans*) . As *LIN-4* transcripts and the 3'untranslated region (UTR) of *LIN-14* mRNA revealed sequence complementarity, the negative regulation was suggested to be mediated by an interaction of the two RNAs. Wightman et al. (1993) confirmed this hypothesis, thereby revealing a functional conservation of seven elements in the *LIN-14* 3'UTR among *C. elegans* and *C. briggsae*. Seven years after the identification of *LIN-4*, Reinhart et al. (2000) described another short RNA (21 nt) which showed sequence complementarity to the 3'UTR of several mRNAs . This 21 nt RNA, named *LET-7*, was therefore hypothesized to control target mRNAs and to regulate the transition of *C. elegans* from the late-larval to the adult stage (Reinhart et al., 2000). An even more important discovery was made by Pasquinelli et al. (2000) who detected *LET-7* among a variety of different organisms including *Homo sapiens*, *Mus musculus* and *Drosophila melanogaster*, thereby revealing sequence conservation. More small RNAs with similarity to *LIN-4* and *LET-7* were identified and the group of these ∼ 22 nt short

RNAs was finally termed miRNAs (Lau et al., 2001; Lee and Ambros, 2001).

Sequence information for a variety of different miRNAs from 223 species, including vertebrates, viruses and plants, are currently deposited at the public miRNA database "miRBase" (http://www. mirbase.org) and may be used as reference sequences for the assignment of new miRNAs (Griffiths-Jones, 2004; Griffiths-Jones et al., 2006; Kozomara and Griffiths-Jones, 2011, 2014). Among these are 306 sequences from Chinese hamster which are based on an NGS study by Hackl et al. (2011). However, as mentioned in section 2.2 even more CHO-specific miRNAs have been described in literature (Diendorfer et al., 2015; Hackl et al., 2012, 2011; Johnson et al., 2011).

miRNA Processing Pathway

miRNA encoding genomic sequences are embedded in both non-coding and protein encoding transcripts, where both intronic and exonic localization of miRNA genes were described in literature (Barron et al., 2011b; Kim et al., 2009; Lagos-Quintana et al., 2001; Lau et al., 2001; Lee et al., 2002b). However, the majority of miRNAs is encoded in form of single miRNA genes or miRNA clusters in intronic regions of the genome (Barron et al., 2011b; Kim et al., 2009; Lee et al., 2002b). For most of the poly- and monocistronically encoded miRNAs a RNA polymerase II mediated transcription process was described in literature (Fig. 2.12) (Lee et al., 2004).

In this context the resulting primary miRNA transcripts (pri-miRNA) are characterized by a hairpin stem-loop structure with a cap motif at the 5' end and a polyadenylated tail at the 3' end (Lee et al., 2004). In addition to the RNA polymerase II mediated transcription, research studies revealed RNA polymerase III mediated transcription for a small group of human miRNAs which are associated to repetitive genomic elements (e. g. Alu) (Borchert et al., 2006).

The Microprocessor complex, including the RNase III enzyme Drosha and the double-stranded RNA binding protein DGCR8 (DiGeorge syndrome critical region 8), mediates cleavage nearby the stem structure of pri-miRNAs, thus forming $\sim$ 70 nt hairpin precursor miRNAs (pre-miRNAs) with a $\sim$ 22 nt stem and a two nucleotide overhang at the 3' end (Denli et al., 2004; Gregory et al., 2004; Lee et al., 2003b). While pri-miRNAs are located in the nucleus (Lee et al., 2002b), pre-miRNAs are

exported to the cytoplasm by the Ran-GTP-dependent importin-β-related transport receptor exportin-5 (Bartel, 2004; Kim, 2004; Lee et al., 2002b; Lund et al., 2004). In the cytoplasm, pre-miRNAs are recognized and further processed to $\sim$ 22 nt miRNA duplexes (miRNA:miRNA*) by another RNase III enzyme called Dicer (Barron et al., 2011b; Hutvágner et al., 2001; Kim et al., 2009).
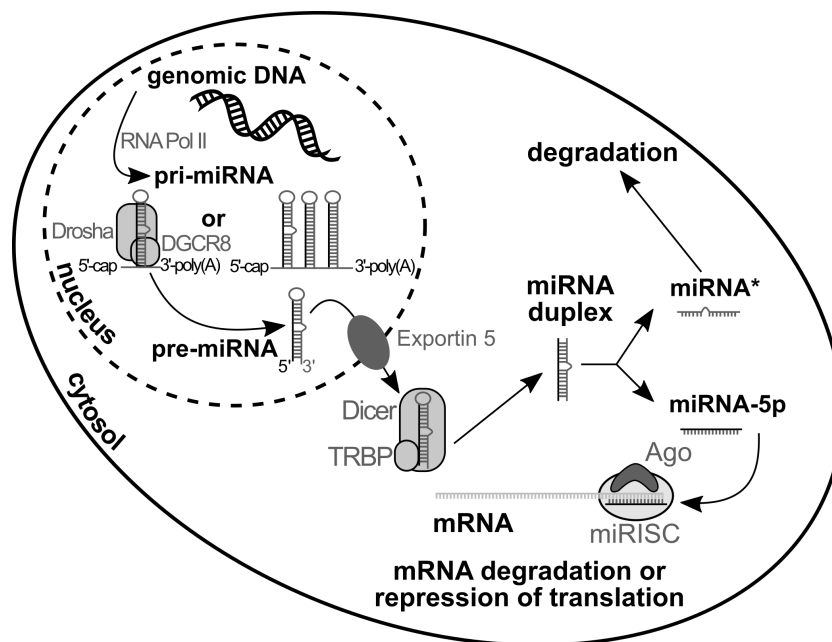
FIGURE 2.12: Biogenesis of miRNAs. miRNAs are encoded either mono- or polycistronically in the cellular genome. Commonly, miRNA genes are transcribed by RNA polymerase II (RNA PolII) so that the resulting hairpin stem-loop primary-miRNA transcripts (pri-miRNA) possess a 5'-cap and a polyadenylated 3' end. The Microprocessor complex which consists of the RNAse III Drosha and the double-stranded RNA binding protein DGCR8 (DiGeorge syndrome critical region 8) mediates the processing of pri-miRNA into a $\sim$ 70 nt precursor miRNA (pre-miRNA). Exportin-5 enables the transport of pre-miRNA into the cytoplasm where the RNAse III enzyme Dicer cleaves the terminal loop, thus forming a miRNA duplex. The assembly of the RNA-induced silencing complex (RISC), mediating mRNA degradation or repression of translation, is facilitated by Dicer, TRBP (TAR RNA-binding protein) and Ago (Argonaute). One of the strains of the miRNA duplex is loaded into RISC, thus being able to bind to complementary regions of target mRNAs. The other strain (miRNA*) is degraded. With modifications to Barron et al. (2011b); Jadhav et al. (2013); Kim et al. (2009); Sun et al. (2010).

In general, both strands of the miRNA duplex are capable of being assembled into the RNA-induced silencing complex (RISC) (Bartel, 2004; Khvorova et al., 2003; Kim et al., 2009; Schwarz et al., 2003). However, Schwarz et al. (2003) and Khvorova et al. (2003) revealed that the RNA strand with

thermodynamically less stable base pairing at the 5' end is commonly the miRNA that is part of RISC while the other RNA strand, designated as miRNA*, is degraded. The miRNA loading process is mediated by the miRNA loading complex consisting of an Argonaute protein (Ago) and transactivating response RNA-binding protein (TRBP) in association with Dicer (Chendrimada et al., 2005; Gregory et al., 2005; Maniataki and Mourelatos, 2005). Thereby TRBP recruits the endonuclease Ago to miRNA, thus forming the catalytic engine of RISC where the miRNA targets complementary mRNA regions and Ago is capable of cleaving the target mRNA in an ATP-independent manner(Chendrimada et al., 2005; Gregory et al., 2005; Maniataki and Mourelatos, 2005).

Recognition and Prediction of Target mRNAs

miRNAs regulate the expression of protein encoding genes at the posttranscriptional level. In this context, one miRNA was shown to possess multiple target sites, while an mRNA may contain several target sites for the same miRNA and different types of miRNAs, respectively (Brennecke et al., 2005; Doench and Sharp, 2004; Sun et al., 2010). Therefore, a cooperative effect of multiple miRNAs in mRNA repression was mentioned in literature (Sun et al., 2010).

The interaction between miRNA and mRNA commonly occurs at the 3'UTR of the mRNA where a completely complementary $\sim$ 7 nt miRNA segment (nucleotides 2 - 8), defined as seed-region, enables the formation of an RNA duplex which is however commonly not solely sufficient to initiate repression of mRNA (Lewis et al., 2003; Sun et al., 2010). In fact, miRNA-mRNA-interaction and consequently mRNA repression are promoted by additional features, e. g. accumulation of adenine-uracil-nucleotides close to the miRNA target site, pairing of miRNA nucleotides 13 - 16 with mRNA and proximity to other miRNA target sites (Grimson et al., 2007). In general, precise nucleotide pairing is required at the seed-region and at nucleotides 13 - 16, whereas wobbles, bulges or other nucleotide mismatches are tolerated at other segments of the miRNA-mRNA duplex (Brennecke et al., 2005; Grimson et al., 2007; Sun et al., 2010). This property of miRNA-mRNA interaction gives rise to the fact that target sites are suitable for multiple miRNAs (Oulas et al., 2012; Sun et al., 2010).

TABLE 2.1: Criteria of algorithms and tools for miRNA target prediction. * = sequence preference of target sites (TargetScan, DIANA-microT), combinatorial miRNA-mRNA interaction (PicTar), statistical significance of miRNA-mRNA interaction (RNAhybrid, mirWIP), target site accessibility (PITA, mirWIP), verified miRNA-mRNA interaction and trained model (TargetProfiler), machine learning framework with integrated features of miRNA-mRNA interaction (MirTarget2). With changes to Sun et al. (2010). (Hamzeiy et al., 2014; Oulas et al., 2012, 2015).

tool	seed match	sequence complementarity	binding energy of miRNA-mRNA duplex	others*
PicTar	x	x	x	x
TargetScan/TargetScanS	x	x	x	x
miRanda	x	x	x	
PITA	x	x	x	x
DIANA-microT	x	x	x	x
TargetProfiler	x	x	x	x
RNAhybrid		x	x	x
miRWIP	x	x	x	x
miRDB (MirTarget2)				x

The specific features of miRNA-mRNA interaction were utilized for the development of bioinformatic miRNA target prediction tools. Oulas et al. (2015), Hamzeiy et al. (2014) and Sun et al. (2010) reviewed common miRNA target prediction algorithms (Tab. 2.1) including PicTar, TargetScan/TargetScanS, miRanda, PITA, DIANA-microT, TargetProfiler, RNAhybrid, mirWIP, miRDB (MirTarget2). Most of these tools predict miRNA targets on basis of seed-region match, base complementarity of miRNA and mRNA as well as on the binding energy of miRNA-mRNA duplexes (Oulas et al., 2015; Sun et al., 2010). Although multiple miRNA target prediction tools are available, the low specificity in combination with a high sensitivity generates a high number of false positives (Sun et al., 2010). Therefore, it is desirable to compare the results of different target prediction tools in order to identify potential miRNA targets. In addition, experimental validation of predicted miRNA targets is required to confirm predicted miRNA targets. Reporter assays, e. g. luciferase reporter assay or green fluorescent protein reporter assay, may validate the direct interaction of miRNA and target mRNA, whereas qRT-PCR,

microarray and Northern blot are applied to investigate changes in mRNA and miRNA expression levels (Chou et al., 2015).

miRNA and mRNA Naming Conventions

In order to standardize the naming of conserved miRNAs from different organisms, the naming convention of Ambros et al. (2003) introduced the prefix "miR" in combination with a unique identifying number (e. g. miR-1). A similar naming convention is applied for miRNA encoding genes, where italics and the prefix in lower case are characteristic (e. g. *miR-1*) (Ambros et al., 2003). According to Ambros et al. (2003), miRNAs from different organisms but with identical or similar sequences are assigned the same number, whereas numeral/letter suffixes are added to identical and very similar miRNAs of an organism, respectively (e. g. *mir-1-1*, *mir-1-2* or *mir-10a*, *mir-10b*). Furthermore, an additional suffix (-3p/-5p) indicates whether the mature miRNA originated from the 3' or the 5' arm of the pre-miRNA (Griffiths-Jones et al., 2006). Commonly an additional species specific three- or four-letter prefix is added for clarification of the miRNA origin (Griffiths-Jones et al., 2006). In this context, *cgr* and *hsa* are examples for miRNAs from *Cricetulus griseus* (Chinese hamster) and *Homo sapiens*, respectively.

International nomenclature committees, e. g. HGNC (human), MGD (mouse), IUBMB (protein encoding genes) aim at standardizing the naming of genes and gene products across different species so that each gene/gene product has a single, unique and descriptive name and symbol (Povey et al., 1997). A gene name briefly describes the function or a specific property of the gene (e. g. lactate dehydrogenase - *LDH*) whereas the gene symbol is an abbreviation of the gene name (Shows et al., 1987). Gene symbols are characterized by a combination of Latin letters and Arabic numbers where numeral suffixes are used to indicate that different genes encode gene products of similar function (e. g. *HK1*, *HK2*). Historically, letter suffixes were used in this case so that this naming convention was maintained for the concerned gene symbols (e. g. *LDHA*, *LDHB*) (Shows et al., 1987). Genes which were annotated by database searching, thus lacking functional information, are designated with the suffix "L" (like) (Blake et al., 1997).

Transcriptomic Response of CHO Cells to Hyperosmotic Culture Conditions

Previous CHO specific transcriptome studies (mRNA and miRNA) focused on correlations between gene expression changes, μ and q_P as well as on time-dependent changes throughout the different phases of cell growth (Clarke et al., 2011; Hernández Bort et al., 2012; Schaub et al., 2010). Furthermore, research groups investigated the cellular response upon changing culture conditions (Baik et al., 2006; Barron et al., 2011b; Bedoya-López et al., 2016; Birzele et al., 2010; Druz et al., 2011; Gammell et al., 2007; Schaub et al., 2010; Yee et al., 2009). While several of the aforementioned studies investigated the effects of low culture temperature on mRNA and miRNA expression (Baik et al., 2006; Barron et al., 2011b; Bedoya-López et al., 2016; Gammell et al., 2007; Yee et al., 2009) only one research group has described the transcriptomic response of CHO cells upon hyperosmotic stimulus so far (Shen et al., 2010). In this context, mRNA expression analysis on basis of custom-made Affymetrix® CHO microarrays and qRT-PCR revealed differential expression (up- and downregulation) of genes encoding proteins involved in cell signaling, transport, transcriptional regulation and metabolism (Shen et al., 2010). Furthermore, the transcriptomic response upon changing culture conditions was hypothesized to be specific for a defined cell line and condition as minor similarities were observed in comparison to other stress responses (sodium butyrate treatment, low culture temperature) or mammalian cell lines (Shen et al., 2010).

2.8 Improving Cellular Performance of CHO Cells by Cell Line Engineering

Transcriptomic research studies reveal potential targets for the improvement of recombinant CHO cell lines by cell line engineering. The mutual aims of cell line engineering strategies are an enhancement of cell growth, productivity and yield as well as an improvement of cellular stress resistance (Fischer et al., 2015a). Modification of gene expression can be realized by transient or stable overexpression of target genes, by chromosomal deletion or by RNA interference (Barron et al., 2011b; Fischer et al., 2015a; Wuest et al., 2012). Furthermore, miRNA complementary oligonucleotides, called

antagomirs, are capable of inhibiting miRNA function by binding to their target miRNAs (Sun et al., 2010). Another technique utilizes synthetic RNAs (miRNA sponges) which competitively inhibit the binding of miRNAs to target sites, thus suppressing miRNA function (Sun et al., 2010).

Multiple research studies described enhancements in recombinant protein production by stable or transient overexpression of *cgr*-miR-17, *cgr*-miR-19b, *cgr*-miR-20a, *cgr*-miR-92a, *cgr*-miR-2861, *mmu*-miR-30 family members, *hsa*-miR-7, *hsa*-miR1287, *hsa*-miR-557 (Barron et al., 2011a; Fischer et al., 2014, 2015b,c; Jadhav et al., 2014; Loh et al., 2014; Strotbek et al., 2013) or inhibition of miR-23, miR-34 and *mmu*-466-5p (Druz et al., 2011, 2013; Kelly et al., 2015a,b) in CHO cells.

In comparison to the aforementioned miRNAs approximately 100 target genes for CHO cell engineering were summarized in a review by Fischer et al. (2015a). Related cell line engineering strategies for an improvement of cellular productivity focused on enhancement of apoptosis and stress resistance (Cost et al., 2010; Doolan et al., 2010; Fischer et al., 2015a; Kim and Lee, 2002; Lee et al., 2009; Sung et al., 2007; Tan et al., 2015), induction of cell cycle arrest (Bi et al., 2004; Fussenegger et al., 1998; Mazur et al., 1998) and reduced production of toxic by-products (Chong et al., 2010; Fogolin et al., 2004; Kim and Lee, 2007b; Lao and Toth, 1997; Tabuchi and Sugiyama, 2013; Tabuchi et al., 2010; Toussaint et al., 2016; Wlaschin and Hu, 2007a; Yang and Butler, 2002).

3 Motivation and Objectives

Chinese hamster ovary (CHO) cells are the "mammalian workhorses" of biopharmaceutical industry. Since the approval of the first CHO product in 1987 process development has contributed to a remarkable progress in cellular performance, e. g. cell growth and product formation. The switch from batch to fed batch mode and the improvement of cell lines, cultivation media and operating parameters resulted in $\sim$ 6-fold higher viable cell densities, 4- to 10-fold enhanced q_P and $\sim$ 100-fold higher c_P (Jayapal et al., 2007; Schaub et al., 2012; Seth et al., 2006; Tabuchi and Sugiyama, 2013; Wurm, 2004). Nevertheless, optimization strategies intensified culture conditions and therefore may cause stress conditions. While mixing of lab scale STRs (1 - 100 L) is usually efficient, inhomogeneous culture conditions are characteristic for large scale STRs ($\leqslant$ 20,000 L), thus facilitating the occurrence of stress conditions. In order to prevent cell disruption and inhibition of cell growth and product formation, volumetric power inputs usually have to be low in large scale STRs, thus contributing to inefficient mixing and inhomogeneous culture conditions (Gelves et al., 2014; Lara et al., 2006; Nienow, 2006). Fig. 3.1 exemplarily illustrates the formation of microenvironments in a 300 L STR with 180 L working volume on basis of a computational fluid dynamics (CFD) model.

Cells cultivated in large scale STRs are consequently exposed to gradients of different culture conditions (e. g. pH, T, DO, c_S, p_{CO_2}). Considering that mixing times are in the order of minutes, changing culture conditions might therefore induce a specific cellular response (Lara et al., 2006). As described in literature, conditions that differ from standard culture conditions, e. g. hypothermia (30 - 33°C), hyperosmolality ($\geqslant$ 350 mOsmol kg^{-1}), commonly inhibit cell growth or even induce apoptosis (Bollati-Fogolín et al., 2008; Fox et al., 2004; Han et al., 2010; Kaufmann et al., 1999; Lee et al., 2003a; Ryu et al., 2000, 2001; Shen et al., 2010; Trummer et al., 2006; Yoon et al., 2004, 2005).
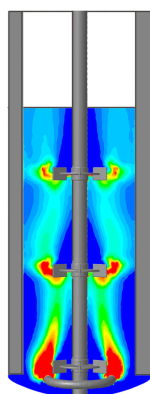
FIGURE 3.1: Calculated local k_La distribution for a STR with 180 L working volume. k_La distribution was calculated on basis of a computational fluid dynamics (CFD) model. The bioreactor had a defined working volume of 180 L and was equipped with a ring sparger and three Rushton turbines. Regions with high k_La values (0.54 h^{-1}) are colored in red, while green colored areas indicated mid-range k_La values of about 0.27 h^{-1}. Regions with extremely low k_La values ($\sim$ 0.0 h^{-1}) are illustrated in dark blue. With modifications to Gelves et al. (2014).

Surprisingly, stress conditions like for example hyperosmolality, which may occur in fed batch cultures, were shown to cause decrease in cell growth whereas q_P was enhanced (Fox et al., 2004; Furukawa and Ohsuye, 1998; Han et al., 2009; Kaufmann et al., 1999; Lee et al., 2003a; Ryu et al., 2000; Shen et al., 2010). However, this phenomenon has not been fully deciphered yet, although elucidating the connection between hyperosmolality and enhanced q_P may contribute to the identification of new strategies to further enhance the cellular performance.

Therefore this research project focuses on the effects of hyperosmotic culture conditions on antibody producing CHO cell lines in order to reveal toeholds for the improvement of therapeutic protein production.

High producing mammalian cell lines (q_P = 40 - 100 pg cell^{-1} d^{-1}) synthesize recombinant proteins in the order of $\sim$ 20% of the total cellular protein (Seth et al., 2006; Tabuchi and Sugiyama, 2013; Wurm, 2004). This substantial recombinant protein production is an energy consuming process. The formation of each peptide bond requires at least three ATP molecules which adds up to $\sim$ 4,000 ATP molecules per IgG1 antibody consisting of 12 domains with $\sim$ 110 amino acids each (Jefferis, 2009; Seth et al., 2006). Disregarding other energy dependent processes during antibody production (e. g. correct folding and disulfide bond formation in the ER) (Braakman et al., 1992; Mirazimi and Svensson, 2000), high producing cell lines utilize about 1.1 - 2.7 pmol$_{ATP}$ cell^{-1} d^{-1} for the

synthesis of recombinant antibodies. This daily cellular ATP consumption is an equivalent of $\sim 1 -$ 13.5% of the specific ATP formation rates (q_{ATP}, 20 - 108 $pmol_{ATP}$ $cell^{-1}$ d^{-1}) which have been described in literature for different mammalian cell lines (Lin et al., 1999; Miller et al., 1987; Mulukutla et al., 2010; Sidorenko et al., 2008; Wahl et al., 2008).

ATP formation is commonly based on substrate-level phosphorylation and on oxidative phosphorylation (2.4), the latter being located in mitochondria, the cellular "powerhouses" (2.3). A preliminary diploma thesis (Pfizenmaier, 2011) focused on the development of an antibody-mediated intracellular fluorescence labeling method for flow cytometric qualitative/quantitative analysis of mitochondrial number in CHO cells. The method was applied to investigate the effects of hyperosmotic culture conditions on the mitochondrial compartment of an anti-interleukin-8 (anti-IL-8) producing CHO DP-12 cell line (ATCC CRL-12445). Surprisingly research results revealed a decrease in mitochondrial fluorescence in response to a osmotic shift from ~ 290 to ~ 390 mOsmol kg^{-1} on day three of a batch cultivation, thus hypothesizing that the number of mitochondria might have decreased (Fig. 3.2). As a consequence the suggested hypothesis was the starting point of the present research project.
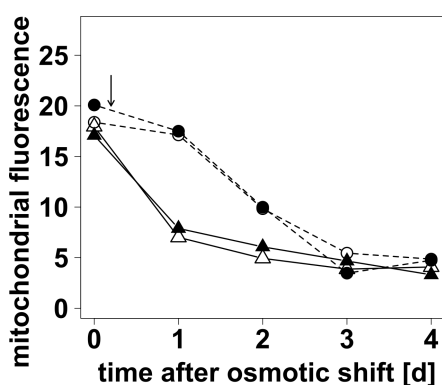
FIGURE 3.2: **Effect of hyperosmolality on mitochondrial fluorescence.** The cell line CHO DP-12 was cultivated in four bioreactors in batch mode. On day three of cultivation, osmolality was increased in two bioreactor from ~ 290 to ~ 390 mOsmol kg^{-1} ($\blacktriangle,\triangle$). The other two cultures served as references ($\bullet$, $\circ$). An antibody-based fluorescence labeling of intracellular mitochondria (4.2.5) was performed directly before as well as on the following four days after osmotic shift. The fluorescence intensities of isotype controls were used to correct the medians of mitochondrial fluorescence intensities (575 nm). With changes to Pfizenmaier (2011).

Effects of Hyperosmotic Culture Conditions on the Mitochondrial Compartment and the Phenotype of CHO DP-12 Cells

The mitochondrial compartment is a highly dynamic cellular component (2.3) whose morphology is shaped by fusion and fission of mitochondrial membranes as a function of the cellular state and requirements (Campello and Scorrano, 2010; Hock and Kralli, 2009; Pernas and Scorrano, 2016; Scheffler, 2001). A decrease in mitochondrial mass of hyperosmotically stressed CHO DP-12 cells was indicated by fluorescence labeling of the mitochondrial target protein TOM22 (translocase of the outer mitochondrial membrane) (Pfizenmaier, 2011). However, this result was based on two biological replicates (Pfizenmaier, 2011) and was contradictory to results of previous independent studies investigating the effects of hyperosmolality, oxidative stress and sodium butyrate treatment (Lee et al., 2002a, 2003a; Lin et al., 1999; McMurray-Beaulieu et al., 2009).

Therefore one of the main objectives of this thesis was to characterize the hyperosmotic phenotype of CHO DP-12 cells and to investigate whether mitochondrial fluorescence intensity truly correlated with mitochondrial mass. With mitochondria being the cellular "powerhouses" for ATP formation and recombinant protein production being an energy intensive process, analyses of intracellular adenine nucleotide pools and determination of q_{ATP} were major aspects while characterizing the phenotype of hyperosmotically stressed cells.

The Transcriptomic Response (mRNA/miRNA) of Antibody Producing CHO DP-12 Cells to Hyperosmotic Stimulus

In order to reveal the connection between hyperosmotic culture conditions and enhanced product formation, a complete picture of the cellular response is required. However, while hyperosmotic effects on cellular metabolism of CHO cells have extensively been investigated (Han et al., 2010; Lee et al., 2003a; Ryu et al., 2000, 2001; Shen et al., 2010), only Shen et al. (2010) have studied the CHO-specific hyperosmotic response at the level of mRNA expression so far. Therefore, a further objective

of the present research project was to characterize the transcriptomic response (mRNA/miRNA) to hyperosmotic culture conditions on basis of an NGS approach. In this context, NGS analyses were expected to identify superimposed transcriptional changes that induce characteristic phenotypes of hyperosmotically stressed cells. Furthermore, the combined analysis of mRNA and miRNA expression was supposed to reveal potential target mRNAs of significantly differentially expressed miRNAs.

Identification of Strategies for q_P Enhancing Cell Line Engineering Strategies

While the characterization of metabolic and transcriptomic response to hyperosmotic culture conditions most notably aimed at elucidating the reason for the q_P enhancing effect, the acquired knowledge served as well as a basis for the identification of potential strategies to improve cellular productivity even further. The leading objective was to identify energy providing cell line engineering strategies contributing to enhanced recombinant protein production.

4 Materials and Methods

4.1 Materials

4.1.1 Chemicals

TABLE 4.1: Chemicals

chemical	company
acetonitrile $\geqslant$ 99.9%	VWR, DE
cis-aconitate (*cis*-aco) $\geqslant$ 98%	Sigma-Aldrich, US
adenosine diphosphate disodium salt (ADP)	Gerbu, DE
adenosine monophosphate disodium salt (AMP)	Fluka, US
adenosine triphosphate disodium salt (ATP)	Gerbu, DE
algal lyophilized cells U-^{13}C > 99 atom% (lot no. 487945)	Sigma-Aldrich, US
amino acid standard (AAS18)	Sigma-Aldrich, US
ammonium cuvette test LCK303	Hach, DE
boric acid	Merck, DE
bovine serum albumin (BSA)	VWR, DE
calibration standard 300 mOsmol kg^{-1}	gonotec, DE
chloroform $\geqslant$ 98%	Sigma-Aldrich, US
digitonin 5%	Invitrogen, US
digitonin	Applichem, DE
dimethyl sulfoxide (DMSO)	Sigma-Aldrich, US
D-mannitol	Merck, DE
ethanol $\geqslant$ 96%	Carl Roth, DE
ethylenediaminetetraacetic acid (EDTA)	Carl Roth, DE
Flow-Check^{TM} fluorospheres	Beckman Coulter, US
Flow-Set^{TM} fluorospheres	Beckman Coulter, US
9-fluorenylmethyl chloroformate (FMOC)	Sigma-Aldrich, US
fructose-6-phosphate (F6P) $\geqslant$ 98%	Sigma-Aldrich, US
geneticin (G418)	Santa Cruz Biotechnology, US

TABLE 4.1: Chemicals (continued)

chemical	company
glucose-6-phosphate (G6P) $\geqslant$ 98%	Sigma-Aldrich, US
glucose/lactate standard	TRACEAnalytics, DE
hydrochloric acid 32%	Carl Roth, DE
hydrochloric acid 32%	Sigma-Aldrich, US
IsoFlow^{TM} sheath fluid	Beckman Coulter, US
L-asparagine (Asn) $\geqslant$ 99%	Sigma-Aldrich, US
L-glutamine (Gln) CELLPURE$^{®}$ $\geqslant$ 99%	Carl Roth, DE
L-norvaline $\geqslant$ 99%	Fluka, US
L-tryptophane $\geqslant$ 99%	Fluka, US
3-mercaptopropionic acid	Sigma-Aldrich, US
methanol $\geqslant$ 99.8%	VWR, DE
methotrexate (MTX)	Applichem, DE
methoxyamine hydrochloride $\geqslant$ 98%	Sigma-Aldrich, US
2-(N-morpholino)ethanesulfonic acid	Sigma-Aldrich, US
pH-buffer solution pH 7.00 $\pm$ 0.02	Carl Roth, DE
pH-buffer solution pH 4.00 $\pm$ 0.02	Carl Roth, DE
pH-buffer solution pH 9.00 $\pm$ 0.02	Carl Roth, DE
phosphoric acid 85%	Fluka, US
ortho-phthaldialdehyde (OPA)	Fluka, US
R-phycoerythrin	Santa Cruz Biotechnology, US
potassium hydroxide 45% (KOH)	Sigma-Aldrich, US
potassium phosphate dibasic (K_2HPO_4)	Sigma-Aldrich, US
potassium phosphate monobasic (KH_2PO_4)	Sigma-Aldrich, US
propidium iodide (PI)	Sigma-Aldrich, US
pyridine $\geqslant$ 99%	Sigma-Aldrich, US
pyruvate $\geqslant$ 99%	Sigma-Aldrich, US
^{13}C-pyruvate $\geqslant$ 99%	euriso-top, DE
RNaseA, Pure Link^{TM}	Invitrogen, US
RNAprotect cell reagent	Qiagen, DE
sample solution for LaboTRACE	TRACEAnalytics, DE
SeramunBlau$^{®}$	Seramun Diagnostica, DE
sodium azide	Sigma-Aldrich, US
sodium carbonate (Na_2CO_3)	Carl Roth, DE
sodium chloride CELLPURE$^{®}$ $\geqslant$ 99.8%	Carl Roth, DE
sodium hydrogen carbonate ($NaHCO_3$)	Carl Roth, DE
sodium hydroxide (NaOH)	Carl Roth, DE
sodium phosphate dibasic (Na_2HPO_4)	Carl Roth, DE

TABLE 4.1: Chemicals (continued)

chemical	company
sodium tetraborate decahydrate	Sigma-Aldrich, US
sulfuric acid $\geqslant$ 98%	Carl Roth, DE
TC-42-D medium	Xell, DE
N-tert-butyldimethylsilyl-N-methyltrifluoroacetamide (MTBSTFA)	Sigma-Aldrich, US
tetrabutylammonium bisulfate (TBAS)	Fluka, US
tris(hydroxymethyl)aminomethane (Tris) base	Carl Roth, DE
trypan blue solution 0.4%	Sigma-Aldrich, US
Tween 20	Fluka, US
water LC-MS grade	VWR, DE

4.1.2 Antibodies

TABLE 4.2: Antibodies

ELISA	
antibody	**company**
anti-human IgG F(c) goat antibody	biomol, DE
anti-human kappa chain goat antibody peroxidase conjugated	biomol, DE
intracellular staining of mitochondria	
antibody	**company**
anti-TOM22 mouse antibody	Abnova, Taiwan
mouse IgG2a isotype control	Sigma-Aldrich, US
anti-mouse-IgG2a goat antibody phycoerythrin conjugated	Santa Cruz Biotechnology, US

4.1.3 Buffers and Solutions

TABLE 4.3: Buffers and Solutions

buffer or solution			recipe
blocking buffer - ELISA	1	L	TBS
	10	g	BSA

TABLE 4.3: Buffers and Solutions (continued)

buffer or solution				recipe
coating buffer - ELISA		3.7	g	$NaHCO_3$
		0.64	g	Na_2CO_3
	ad	1.0	L	NANOpure water
cryo medium		10	%	DMSO (v/v)
		90	%	culture medium (v/v)
culture medium				TC-42-D medium
CHO DP-12		4	mM	Gln
		200	nM	MTX
culture medium				TC-42-D medium
BIBH1 preculture		4	mM	Gln
		200	nM	MTX
		200	$mg\,L^{-1}$	G418
culture medium				TC-42-D medium
BIBH1 bioreactor		6	mM	Gln
		200	nM	MTX
		200	$mg\,L^{-1}$	G418
dilution buffer - ELISA		1	L	TBS
		10	g	BSA
		5	mL	Tween 20 (10%)
filtration buffer		10	mM	KH_2PO_4
pH 7.1, 290 mOsmol kg^{-1}		10	mM	K_2HPO_4
		145	mM	NaCl
fixation buffer		70	%	ethanol
cell cycle analysis		30	%	PBS
FMOC reagent		2.5	mg	9-fluorenylmethyl chloroformate
amino acid analysis		1	mL	acetonitrile
HPLC elution buffer A		10	mM	Na_2HPO_4
amino acids, pH 8.2		10	mM	$Na_2B_4O_7$
		0.5	mM	NaN_3
HPLC elution buffer B		45	%	acetonitrile (v/v)
amino acids		45	%	methanol (v/v)
		10	%	water LC-MS grade (v/v)

TABLE 4.3: Buffers and Solutions (continued)

buffer or solution			recipe
HPLC elution buffer A	100	mM	KH_2PO_4
nucleotides, pH 6.0	100	mM	K_2HPO_4
	4	mM	TBAS
HPLC elution buffer B	70	%	elution buffer A, nucleotides (v/v)
nucleotides, pH 7.2	30	%	methanol (v/v)
LC-MS/MS elution buffer A	10	%	ammonium acetate buffer (10 mM) (v/v)
pH 9.2	90	%	acetonitrile (v/v)
LC-MS/MS elution buffer B	90	%	ammonium acetate buffer (10 mM) (v/v)
pH 9.2	10	%	acetonitrile (v/v)
lysis buffer	0.122	%	digitonin (m/v)
			in filtration buffer
MES-buffer	19.8	mM	2-(N-morpholino)ethanesulfonic acid
pH 7.4	250	mM	D-mannitol
OPA reagent	10	mg	*ortho*-phthaldialdialdehyde
amino acid analysis	1	mL	potassium borate buffer (0.4 M, pH 10.2)
	8.2	µL	3-mercaptopropionic acid
PBS (phosphate buffered saline)	1.0	mM	KH_2PO_4
pH 7.4	5.6	mM	Na_2HPO_4
	154.0	mM	NaCl
PEB-buffer	0.5	%	BSA (m/v)
	2	mM	EDTA
			in PBS pH 7.4
TBS (Tris buffered saline) - ELISA	6.06	g	Tris Base
pH 7.2 - 7.8	8.2	g	NaCl
	6.0	mL	HCl (6 M)
ad	1.0	L	NANOpure water
washing solution - ELISA	1	L	TBS
	5	mL	Tween 20 (10%)

4.1.4 Consumables

TABLE 4.4: Consumables

consumable	company
capillary column GC (26 m x 0.25 mm, 0.25 µm)	Phenomenex, US
Cedex smart slides	Roche, DE
cryo vials	Greiner, DE
glass fiber filter type A/D	Pall, US
measuring vessels for osmomat	gonotec, DE
metrigard™ filters	Pall, US
microtiter plates (ELISA MICROLON®200)	Greiner, DE
Microplate, 96 well, PS, F-bottom, µCLEAR®, black	Greiner, DE
Omnifix® luer lock connection (3 mL, 5 mL, 10 mL and 50 mL)	Braun Melsungen, DE
pipet tips (10µL, 200µL and 5000µL)	Sarstedt, DE
pipet tips (1000µL)	Greiner, DE
QIAshredder	Qiagen, DE
reaction tubes, safe-lock (1.5 mL)	Eppendorf, DE
reaction tubes black (1.5 mL)	Carl Roth, DE
reaction tubes flow cytometer (15 mL)	Beckman Coulter, US
reaction tubes (1.5 mL, 2 mL, 15 mL and 50 mL)	Sarstedt, DE
RNeasy Mini Kit	Qiagen, DE
SeQuant ZIC-pHILIC, 5 µm, PEEK 150 x 2.1 mm, metal-free	di2chrom, DE
serologic pipets (1 mL, 5 mL, 10 mL, 25 mL and 50 mL)	Carl Roth, DE and Sarstedt, DE
shake flasks (125 mL, 250 mL and 500 mL)	BD, US and Corning, US
sterilizing grade filter, PES, 0.22 µm	Carl Roth, DE
sterilizing grade filter, Sartolab-P20, 0.2 µm	Sartorius, DE
Supelcosil LC18, 3 µm, 15 cm x 4.6 mm	Sigma, US
ZelluTrans/Roth Mini Dialyzer MD 300 (5 mL)	Carl Roth, DE
Zorbax Eclipse Plus C18/250 x 4.6 mm	Agilent Technologies, US

4.1.5 Software

TABLE 4.5: Software

analytics	
ChemStation	Agilent Technologies, US
MassHunter B.04.00	Agilent Technologies, US
TurboMass 4.1	Perkin Elmer, US

_{TABLE} 4.5: **Software** (continued)

flow cytometry	
Cell Cycle Analysis of DNA histograms	Cylchred
CXP Analysis	Beckman Coulter, US

gene expression analysis	
DESeq2 1.8.1	Bioconductor
edgeR 3.10.2	Bioconductor (Robinson et al., 2010)
GOrilla	(Eden et al., 2009)
GOseq 1.20.0	Bioconductor (Young et al., 2010)
maSigPro 1.40.0	Bioconductor (Conesa et al., 2006; Nueda et al., 2014)
MGI Gene Ontology Term Finder	http://www.informatics.jax.org
VennDiagram 1.6.16	CRAN

general use	
DASGIP Control 4.0	DASGIP, DE
Excel 2010	Microsoft, US
Hmisc 3.17-0	CRAN
R 3.2.1	The R Foundation for Statistical Computing
RStudio 0.98.1103	RStudio

4.1.6 Equipment

_{TABLE} 4.6: **Equipment**

instrument	company
AutoSystem XL gas chromatograph	Perkin Elmer, US
bioblock	DASGIP, DE
bioreactor (DS1500ODSS)	DASGIP, DE
CEDEX cell counter	Roche, DE
centrifuge (Megafuge 1.0R)	Heraeus, DE
cryostat F3	Haake, DE
diode array detector (DAD)	Agilent Technologies, US
DR 2800 VIS spectrophotometer	Hach, DE
flow cytometer FC500	Beckman Coulter, US
fluorescence detector (FLD)	Agilent Technologies, US
gas mixing module (MX4/4)	DASGIP, DE

TABLE 4.6: **Equipment** (continued)

instrument	company
HPLC system (1200 series)	Agilent, Technologies, US
LaboTRACE	TRACEAnalytics, DE
membrane vacuum pump	Vaccubrand, DE
microcentrifuge 5417R, FA-45-30-11 rotor	Eppendorf, DE
Minitron shaker incubator	Infors, CH
module for pH/DO monitoring (PH4PO4)	DASGIP, DE
multi pump module (MP8)	DASGIP, DE
Nalgene® Cryo 1°C freezing container	Thermo Scientific, US
NanoDrop spectrophotometer	Thermo Scientific, US
NANOpure II	Barnstead, US
osmomat 030	Gonotec, DE
oxygen sensor	Mettler Toledo, US
pH probe	Mettler Toledo, US
Pipetboy acu	Integra Biosciences, CH
Research pipet 10, 20, 100, 200, 1000, 5000, 10000	Eppendorf, DE
rotary vacuum incubator (RVC 2-33)	Martin Christ, DE
Synergy^{TM} microplate reader	BioTek, US
temperature/agitation module TC4SC4	DASGIP, DE
thermomixer comfort	Eppendorf, DE
Triple Quad mass spectrometer 6410B with ESI ion source	Agilent Technologies, DE
TurboMass mass spectrometer	Perkin Elmer, US

4.2 Methods

Parts of this thesis have already been published. Some of the applied methods were described in these manuscripts which can be found in supporting information B. Where applicable, cross references are given.

4.2.1 Cell Lines and Adaptation

The anti-IL-8 producing cell line CHO DP-12 clone#1934 aIL8.92 NB 28605/14 (ATCC® CRL-12445[TM]) and the cell line BIBH1 producing a humanized IgG_1 antibody (kindly provided by Boehringer-Ingelheim Pharma GmbH & Co. KG, Germany) were adapted to grow in TC-42-D medium with designated supplementation of L-glutamine (Gln) and selective additives (methotrexate (MTX), G418) (Tab. 4.3). Cells were subcultured every two to three days in shake flasks with cell densities of 4×10^5 cells mL^{-1} upon inoculation. Cells were incubated at 37°C, 5% CO_2, with orbital shaking at 150 rpm and 50 mm displacement in a humidified shaker incubator (Infors, CH). After 34 (CHO DP-12) or 37 (BIBH1) passages, master cell banks with 1×10^7 cells mL^{-1} of cryo medium (Tab. 4.3) were generated. Cells were stored in liquid nitrogen and used to build up working cell banks.

4.2.2 Batch Cultivation with Osmotic Shift

Preparation of Inoculum

A cryo culture was thawed and washed once with appropriate culture medium for precultures (Tab. 4.3) ($300g$, 25°C, 5 min). The cells were seeded at a cell density of 4×10^5 cells mL^{-1} in 125 mL shake flasks. Shake flasks were incubated at 37°C, 5% CO_2, with orbital shaking at 150 rpm and 50 mm displacement in a humidified shaker incubator (Infors, CH) and cultures were scaled up every two to three days for four passages.

Batch Cultivation in Bioreactor

Exponentially growing cells were used to inoculate bioreactors (4×10^5 cells mL^{-1}) of a fourfold parallel DS15000ODSS bioreactor system (DASGIP, DE) equipped with two pitched-blade impellers (blade angle: 30°, $\phi_{impeller}$ = 50 mm), L-sparger, temperature sensor, dissolved oxygen (DO) sensor and pH probe (Mettler Toledo). Tab. 4.7 shows the set points of parameters for bioreactor cultivations. TC-42-D medium (Xell) supplemented with appropriate c_{Gln} and selective additives (MTX, G418) for CHO DP-12 or BIBH1 was used as culture medium (Tab. 4.3). The working volume (V_R) varied between 1.2 and 1.4 L. The percentage of DO at atmospheric pressure (Tab. 4.7) was controlled by MX4/4 gas mixing module (DASGIP). While the percentage of oxygen (x_{O_2}) in the inlet air was continuously increased, the aeration rate was controlled by a cascade (Fig. 4.1). pH was adjusted to pH 7.1 by sparging of CO_2 or titration with 1 M Na_2CO_3.

TABLE 4.7: Set points of parameters for bioreactor cultivations. N = agitation, DO = dissolved oxygen at atmospheric pressure, T = temperature.

parameter	CHO DP-12	BIBH1
N [rpm]	150	150
CO_2 overlay [%]	5	5
DO [%]	40	30
pH	7.1	7.1
T [°C]	37	37
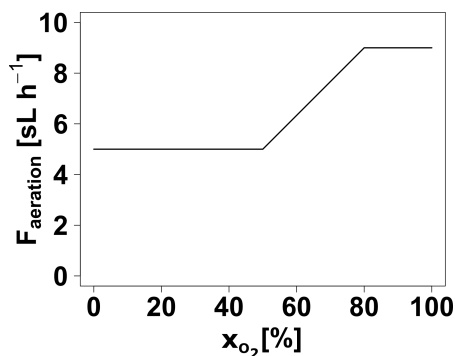
FIGURE 4.1: Cascade control for aeration rate during bioreactor cultivation. $F_{aeration}$ = aeration rate, x_{O_2} = percentage of oxygen in inlet air.

Osmotic Shift

Hyperosmotic conditions were induced by the addition of NaCl-enriched cultivation medium. The time point of osmotic shift during bioreactor cultivation as well as the intensity of the shift were dependent on the experiment (Tab. 4.8). In order to compensate dilution effects caused by osmotic shift, equal volumes of culture medium were added to the reference cultures.

TABLE 4.8: Time point and intensity of the osmotic shift during bioreactor cultivation. t = time between inoculation and osmotic shift.

parameter	reference	CHO DP-12 condition 1	condition 2	condition 3	BIBH1
Δt [h]	-	72	35	35	35
osmolality [mOsmol kg^{-1}]	280	380	380	430	445

4.2.3 Fast Filtration Approach

Fast filtration approaches (Matuszczyk et al., 2015; Pfizenmaier et al., 2015) were applied to prepare samples for quantification of intracellular and mitochondrial metabolic pool sizes. The fast filtration method enables a rapid separation of cells from cultivation medium and quenching of cell metabolism. Filtration parameters varied according to the type of sample and the number of cells (Tab. 4.9).

Cell suspension with a defined number of cells was applied on the moistened filter(s) of a filtration unit which was connected to a vacuum pump. A vacuum of 30 or 90 mbar (Tab. 4.9) was used to separate cells from medium. For mitochondrial samples, cells were permeabilized by the addition of lysis buffer (Tab. 4.3) in order to deplete cytosol during the final quenching and washing step with ice-cold filtration buffer (Tab. 4.9). Filters representing whole cell or mitochondrial samples were transferred to suitable containers for extraction (Carl Roth) and were frozen in liquid nitrogen. Samples were stored at -70°C.

The lysis buffer contained the detergent digitonin which was shown to permeabilize membranes by interacting with the cholesterol molecules inside the membrane (Kuznetsov et al., 2008). The molar ratio of cholesterol and phospholipids of the plasma membrane was stated to be 7 - 50-fold higher compared to the outer or inner mitochondrial membrane (Kuznetsov et al., 2008). Therefore the optimized fast filtration protocol by Matuszczyk et al. (2015) enabled depletion of cytosol while retaining the mitochondrial compartment. The efficiency of this approach was validated by quantification of cytosolic (glucose-6-phosphate (G6P), fructose-6-phosphate (F6P)) and mitochondrial (*cis*-aconitate (*cis*-aco)) marker metabolites in whole cell and mitochondrial samples.

TABLE 4.9: Parameters for fast filtration approaches. A/D = 47 mm borosilicate glass fiber filter type A/D with a pore size of 3 μm (Pall), M = 47 mm metrigard^{TM} filter with 0.5 μm pore size (Pall). Filtration buffer (Tab. 4.3) was used to moisten the filters. Lysis buffer (Tab. 4.3) contained 0.122% digitonin.

	whole cell sample		mitochondrial samples
parameter	10^7 cells	2×10^7 cells	2×10^7 cells
filter(s)	A/D	A/D	A/D + M
vacuum [mbar]	30	30	90
moistening of filter(s) [mL]	10	10	10
lysis buffer [mL]	-	-	12.5
filtration buffer [mL]	30	35	43.65

4.2.4 Extraction of Intracellular Metabolites

Metabolites of whole cell or mitochondrial samples which had been prepared by fast filtration were extracted by a combination of methanol (70%, -20°C, 90 min) and chloroform treatment. This method was described in Pfizenmaier et al. (2015) (manuscript 1, supporting information B.1). The extraction process included an evaporation step (Tab. 4.10) in order to concentrate the samples and to remove methanol. The protocol was optimized to keep the temperature of the samples ∼4°C (Illner, 2012).

TABLE 4.10: Evaporation protocol for cell extracts.

phase	pressure [mbar]	time [min]
1	20	1
2	20	9
3	15	1
4	15	4
5	10	1
6	10	9
7	8	1
8	8	4
9	6	1
10	6	4
11	4	1
12	4	74

4.2.5 Analytical Methods

The following paragraphs describe the analytical methods which were applied to characterize cell culture processes.

Viable Cell Density and Viability

The determination of viable cell density and viability was based on trypan blue staining and analysis with Cedex XS cell counter (Roche).

Osmolality

A freezing point osmometer (gonotec) was used to analyze osmolality of buffers, solutions and samples. The osmometer was calibrated with NANOpure water and a 300 mOsmol kg^{-1} standard solution (gonotec).

Glucose, Lactate and Ammonium

A biosensor with immobilized glucose and lactate oxidase was applied to determine glucose (Glc) and lactate (Lac) concentrations with the Glc/Lac-analyzer LaboTRACE (TRACEAnalytics). LCK303 cuvette test (Hach) was applied to analyze ammonium concentrations based on the indophenol blue method.

Amino Acids

Amino acid concentrations in supernatants of bioreactor cultivations were analyzed by reversed-phase high performance liquid chromatography (HPLC) with precolumn *ortho*-phthaldialdehyde/ 9-fluorenylmethyl chloroformate derivatization as described in detail by Henderson Jr and Brooks (2010). Analysis was performed with an Agilent 1200 series apparatus equipped with a fluorescence detector ($\lambda_{excitation}$ = 230 nm, $\lambda_{emission}$ = 450 nm), a Zorbax Eclipse Plus C_{18} guard column (Agilent, 12.5 x 4.6 mm, 5 µm) and a Zorbax Eclipse Plus C_{18} column (Agilent, 250 x 4.6 mm, 5 µm). Measurements were acquired at a column temperature of 40°C and a flow rate of 1.5 mL min^{-1} for the mobile phase. The percentage of elution buffer A (10 mM Na_2HPO_4, 10 mM $Na_2B_4O_7$, 0.5 mM NaN_3, pH 8.2) and elution buffer B (45% methanol, 45% acetonitrile, 10% water) in the mobile phase was changed according to a gradient (Henderson Jr and Brooks, 2010). The internal standard L-norvaline was added to the seven standard calibration levels (AAS18 (Sigma-Aldrich) + L-asparagine, L-glutamine and L-tryptophane) and diluted samples. Collected data were analyzed with ChemStation (Agilent).

Antibody

Enzyme linked immunosorbent assay (ELISA) was used to quantify antibody concentrations in the supernatants of bioreactor cultivations. ELISA MICROLON® 200 plates (Greiner) were coated with a 1:500 dilution of anti-human IgG F(c) goat antibody (biomol) in coating buffer (Tab. 4.3) for 1 h. Plates were washed three times with washing solution (Tab. 4.3) and non-specific binding sites were blocked with bovine serum albumin (BSA) containing blocking buffer for 30 min. Meanwhile the supernatants and the cell line specific standard were diluted (Tab. 4.3). After another three washing steps, the plates were incubated with diluted standards and samples for 1 h. The washing steps were followed by a 1 h

treatment with a diluted peroxidase conjugated anti-human kappa chain goat antibody (1:90 000, biomol). After five washing steps the substrate SeramunBlau® containing hydrogen peroxide and 3,3',5,5'-tetramethylbenzidine (TMB) was added to the plates. By catalyzing the decomposition of hydrogen peroxide, the antibody conjugated peroxidase withdraws electrons from TMB thereby forming dimerizing TMB radical cations (Gallati and Pracht, 1985). The enzymatic reaction was stopped after 30 min by the addition of 0.25 M sulfuric acid and dimerization of TMB was reversed. The absorbance of the resulting yellow TMB^{2+} cations was analyzed with a $Systec^{TM}$ microplate reader (BioTek) at 450 nm (reference 620 nm). The correlation between antibody concentration and absorbance was determined based on the results for different dilutions of the standard antibody solution. All steps were performed at room temperature.

TABLE 4.11: Elution buffer gradient during adenine nucleotide analysis by HPLC. Elution buffer A: 100 mM K_2HPO_4/ KH_2PO_4, 4 mM TBAS, pH 6.0. Elution buffer B: 70% elution buffer A, 30% methanol, pH 7.2.

time [min]	elution buffer A [%]	elution buffer B [%]
0	100	0
3.5	100	0
20	60	40
22	55	45
40	45	55
48	0	100
55	0	100
60	100	0
67	100	0

Adenine Nucleotides

Concentrations of adenine nucleotides in cell extracts were acquired by ion-pair reversed-phase HPLC with changes to a method described by Cserjan-Puschmann et al. (1999) (Pfizenmaier et al., 2015). Agilent 1200 Series apparatus was equipped with a diode array detector ($\lambda_{detection}$ = 260 nm) and a Supelcosil LC 18-T column (15 cm x 4.6 mm, 3 μm) protected by $Hypersil^{TM}$ BDS C18 guard-column. As

described in section 4.3, elution buffer A consisted of 100 mM K_2HPO_4/ KH_2PO_4 and 4 mM TBAS with a pH of 6.0. Elution buffer B (pH 7.2) was prepared of 70% elution buffer A and 30% methanol. A mixture of elution buffer A and B served as mobile phase for HPLC analysis (Tab. 4.11). The flow rate was 1 mL min^{-1} and the column was tempered at 30°C. The standard calibration levels (7-points) contained defined amounts of ATP, ADP and AMP. Selected samples were spiked with ATP, ADP and AMP in order to evaluate the influence of the sample matrix on the quantification of analytes. Collected data were analyzed with ChemStation (Agilent).

Glucose-6-Phosphate, Fructose-6-Phosphate and *cis*-Aconitate

The concentrations of G6P, F6P and *cis*-aco in extracts of whole cell and mitochondrial samples were determined based on hydrophilic interaction liquid chromatography-electrospray ionization-tandem mass spectrometry (HILIC-ESI-MS/MS) applying high selectivity in multiple reaction monitoring (MRM) mode as described by Teleki et al. (2015), Matuszczyk et al. (2015) and in manuscript 2 (supporting information B.2). Agilent 6410B Triple Quad mass spectrometer (Agilent Technologies, US) with ESI ion source was equipped with Sequant ZIC–pHILIC column (150 x 2.1 mm, 5 µm) protected by Sequant ZIC–pHILIC guard column (20 x 2.1 mm, 5 µm). Measurements were acquired in negative ionization mode with high selectivity.

The samples for HILIC-ESI-MS/MS analysis were prepared as described in Tab. 4.12.

TABLE 4.12: Composition of the samples for analysis by HILIC-ESI-MS/MS.

component	amount [%]
^{13}C-algal extract	10
cell extract/standard analytes	29
ammonium acetate (1 M, pH 9.2)	1
acetonitrile	60

Isotope dilution mass spectrometry (IDMS) method which had previously been described by Teleki et al. (2015) was used to analyze the data sets. The determination of metabolite concentrations with

this method is based on $^{12}C/^{13}C$-ratios. Therefore external calibration standards (8-point calibration) and samples had been supplemented with a defined amount of ^{13}C-labeled internal standard prior to LC-MS/MS measurement. Lyophilized U-^{13}C-labeled algal cells (> 99 atom% ^{13}C, Sigma-Aldrich) containing all analyzed metabolites served as substrate for the extraction of ^{13}C-labeled internal standard as described by Vielhauer et al. (2011). External calibration curves were prepared by linear regression thereby plotting $^{12}C/^{13}C$-ratios of analyte peak areas against the corresponding ^{12}C-concentration of the analyzed metabolite.

Pyruvate

Pyruvate concentrations in supernatants of bioreactor cultivations were analyzed by gas chromatography-mass spectrometry (GS-MS). An AutoSystem XL gas chromatograph (Perkin Elmer) with TurboMass mass spectrometer (Perkin Elmer) was equipped with a capillary column (26 m x 0.25 mm, 0.25 μm, Phenomenex). Helium was used as mobile phase with a flow rate of 1 mL min^{-1}. During the time of measurement the temperature of the column oven was controlled at 320°C.

The supernatants were thawed and diluted 1:50 with water (LC-MS grade). The internal standard (100 μM ^{13}C-pyruvate) was mixed 1:1 (V = 100 μL) with sample or ^{12}C-pyruvate standard calibration level and evaporated until complete dryness thereby keeping sample temperature below 10°C. Methoxamine hydrochlorid was dissolved in pyridine (20 mg mL^{-1}) and 60 μL each were used to dissolve the dried samples. The samples were incubated at 60°C and 12 000 rpm for 30 min (Thermomixer comfort, Eppendorf). Reaction tubes were centrifuged at 10 000g for 3 min and 30 μL of the received supernatant were transferred to GC-MS vials containing 60 μL N-tert-butyldimethyl-silyl-N-methyltrifluoroacetamide (MTBSTFA, Sigma-Aldrich). The vials were incubated at 60°C and 600 rpm for 60 min. A volume of 1 μL was injected for analysis by GC-MS.

The collected data were analyzed with TurboMass 4.1 (Perkin Elmer).

Antibody Dependent Fluorescence Labeling of Intracellular Mitochondria

Pfizenmaier (2011) developed a flow cytometric method for analyzation of changes of the mitochondrial compartment. Fluorescence labeling of mitochondria was based on the permeabilization of cells followed by antibody dependent fluorescence labeling of a mitochondrial target protein. Digitonin was used for the selective permeabilization of the plasma membrane. 1×10^7 cells were harvested (300g, 5 min, 4°C) and washed with 1 mL MES-buffer (Tab. 4.3). The cells were resuspended in 1 mL of MES-buffer containing 0.02% (v/v) digitonin and were incubated on ice for 10 min. The permeabilized cells were separated from the digitonin containing buffer by centrifugation (600g, 5 min, 4°C) and were resuspended in 1 mL PEB-buffer (Tab. 4.3). In order to block non-specific binding sites, the cells were incubated at 4°C for 15 min. Cells were pelleted (1 000g, 3 min, 4°C) and resuspended in 100 µL PBS (pH 7.4) containing 1 µg of IgG2a (mouse) antibody detecting translocase of the outer mitochondrial membrane 22 (TOM22, Abnova). The samples were incubated for 30 min at 4 °C followed by two washing steps with 1 mL of PEB-buffer. Thereafter, cells were incubated with an isotype specific anti-mouse-IgG2a (goat) phycoerythrin (PE) conjugated antibody (1 µg/10^7 cells, Santa Cruz Biotechnology) for 30 min at 4°C in the dark. The cells were washed three times with 1 mL PEB-buffer and were finally resuspended in 0.5 mL PEB-buffer. Isotype controls functioned as control for non-specific antibody binding. For this purpose, the primary antibody was replaced by a mouse IgG2a isotype control antibody (Sigma-Aldrich). Three technical replicates of the staining procedure were performed for each sample type and time point. Samples and isotype controls were analyzed by flow cytometry at low flow rate (FC500, Beckman Coulter).

Tab. 4.13 summarizes the flow cytometer settings which were used to detect 40 000 events for each analyzed sample. Fluorescence intensity of FlowSet calibration beads (Beckman Coulter) was determined with FC500 on each day of flow cytometric measurement in order to analyze variances of the flow cytometer. All fluorescence intensities were normalized on the fluorescence intensity of FlowSet beads.

TABLE 4.13: Flow cytometer settings for analyzing mitochondrial fluorescence intensity. $\lambda_{excitation}$ = 488 nm, FS = forward scatter, SS = sidewards scatter, FL2 = fluorescence channel 2 (575 nm), Lin = linear, Log = logarithmic

channel	voltage [V]	type of amplification	amplification factor
FS	750	Lin	2.0
SS	850	Lin	5.0
FL2	430	Log	1.0

Mitochondrial fluorescence intensity (Ψ_{mit}) was calculated according to Eq. 4.1

$$\Psi_{mit} = \frac{\overline{\Psi}_{sample_t} - \overline{\Psi}_{iso_t}}{\overline{\Psi}_{sample_t=0} - \overline{\Psi}_{iso_t=0}} \tag{4.1}$$

with $\overline{\Psi}_{sample}$ as the arithmetic mean (n = 3) of the normalized median fluorescence intensities of the sample and $\overline{\Psi}_{iso}$ as the arithmetic mean (n = 3) of the normalized median fluorescence intensities of the isotype control. The index t represents the time between osmotic shift and analysis.

Influence of Osmolality on the Fluorescence Intensity of Phycoerythrin

R-phycoerythrin (Santa Cruz Biotechnology) was dissolved in 500 µL of 10 mM potassium phosphate buffer (pH 7.1) with an osmolality of either 290 or 380 mOsmol kg^{-1} resulting in a final concentration of approximately 380 µg mL^{-1}. The suspensions were dialyzed (Mini Dialyzer MD300) against phosphate buffer with the corresponding osmolality for 8 h at 4°C in the dark, whereby buffers were replaced twice. Osmolalities of the phycoerythrin suspensions were subsequently confirmed with a freezing point osmometer (gonotec) followed by serial dilution of phycoerythrin suspensions in corresponding phosphate buffer on a 96 well microplate (Greiner). Fluorescence intensities were analyzed with Synergy^{TM} microplate reader (BioTek) with $\lambda_{excitation}$ = 485 nm and $\lambda_{emission}$ = 590 nm.

Apoptosis Assay

The Annexin V-FITC kit (Beckman Coulter) was used to perform testing for apoptosis according to the specifications of the manufacturer. In order to distinguish apoptotic or necrotic cells from viable cells, different kinds of controls were used to adjust flow cytometer settings. Apoptotic cells (positive control) were received by incubation of cells with 1 µM staurosporine for 6 h at 37°C, 5% CO_2 in a humidified shaker incubator (150 rpm, 50 mm displacement). Viable cells served as negative control. Control samples were either treated with both, Annexin V-FITC and propidium iodide or with just one of the components. Directly before (0 h) and 24 h after the induction of hyperosmotic conditions, 5×10^5 cells mL^{-1}) were incubated with Annexin V-FITC and propidium iodide for 15 min on ice followed by flow cytometric analysis of 50,000 events. A positive Annexin V-FITC signal indicates apoptosis and in combination with a positive propidium iodide signal necrosis.

TABLE 4.14: Flow cytometer settings for apoptosis assay. $\lambda_{excitation}$ = 488 nm, FS = forward scatter, SS = sidewards scatter, FL1 = fluorescence channel 2 (525 nm), FL3 = fluorescence channel 3 (620 nm) Lin = linear, Log = logarithmic

channel	voltage [V]	type of amplification	amplification factor
FS	690	Lin	2.0
SS	1000	Lin	5.0
FL1	370	Log	1.0
FL3	402	Log	1.0

Cell Cycle Analysis

Cells were harvested by centrifugation (300g, 5 min, 4°C) and were washed once with PBS. Fixation of cells was performed with -20°C-cold ethanol containing fixation buffer (Tab. 4.3) and cell samples (1×10^7 cells mL^{-1}) were stored at -20°C. Fixed cells were washed and resuspended with PBS, treated with RNase A and finally stained with propidium iodide (10 µg/10^7 cells). The stained cells were analyzed by flow cytometry detecting 35 000 events (Tab. 4.15).

Propidium iodide intercalates into the DNA and therefore the fluorescence intensity of a cell correlates with its DNA-content (Crissman and Steinkamp, 1973). Resulting histograms for fluorescence channel 3 (620 nm) were analyzed with the software Cylchred (4.5) in order to determine the percentage of cells in G1-, G2- and S-phase of cell cycle.

TABLE 4.15: Flow cytometer settings for cell cycle analysis. $\lambda_{excitation}$ = 488 nm, FS = forward scatter, SS = sidewards scatter, FL3 = fluorescence channel 3 (620 nm), Lin = linear, Log = logarithmic

channel	voltage [V]	type of amplification	amplification factor
FS	896	Lin	2.0
SS	1000	Lin	2.0
FL3	409	Log	1.0

4.2.6 Determination of Specific Metabolic Rates

Specific metabolic rates were determined for defined time intervals of bioreactor cultivations. Time variant process parameters, e. g. biomass, can be described by mass balances (Eq. 4.2)

$$\frac{m_X}{dt} = \frac{d(c_X \times V)}{dt} \tag{4.2}$$

with m_X as the amount of biomass (in g), t as the time of cultivation (in d), c_X as the concentration of biomass (in g L^{-1}) and V as the working volume of the bioreactor (in L).
Eq. 4.2 can be simplified by product rule and $\frac{dV}{dt} = 0$ which applies for batch cultivations. The resulting equation defines the specific growth rate (μ in d^{-1}) as follows

$$\mu = \frac{1}{c_X} \times \frac{dc_X}{dt} \tag{4.3}$$

μ was analyzed in the exponential growth phase where μ = constant applies. Therefore the integration of Eq. 4.3 leads to

$$\ln \frac{c_X}{c_{X_0}} = \mu \times t \tag{4.4}$$

For mammalian cell culture it was assumed that the number of cells (N_{cells}) approximates m_X. In accordance, the viable cell density (VCD in cells L^{-1}) approximates c_X.

Based on Eq. 4.4 plotting of $\ln \frac{VCD}{VCD_0}$ versus (vs.) t followed by linear regression reveals μ as the slope of the regression line.

The specific substrate formation rate (q_S in mol $cell^{-1}$ d^{-1}) is defined as follows:

$$q_S = \frac{1}{c_X} \times \frac{dc_S}{dt} \tag{4.5}$$

with c_S as the concentration of substrate (in mol L^{-1}).
The integration of Eq. 4.5 for a time interval i to i+1 leads to

$$q_S = \frac{1}{c_X(t)} \times \frac{c_{S,\,i+1} - c_{S,\,i}}{t_{i+1} - t_i} \tag{4.6}$$

q_S was determined by plotting c_S vs. the integral of viable cell density (IVCD) thereby analyzing q_S as the slope of the regression line.

In addition c_S was plotted vs. t and the resulting slope of the regression line was divided by the arithmetic mean of VCD in order to obtain q_S.

The specific product formation rate (q_P in mol $cell^{-1}$ d^{-1}) was determined in accordance to q_S.

4.2.7 Carbon/Oxygen Balancing and Calculation of ATP Formation Rates

Specific ATP formation rates (q_{ATP}) were estimated on basis of carbon and oxygen balancing. Therefore changes in the amount of substrates and by-products during time intervals of bioreactor cultivations were calculated in C-mol ($\Delta n_{metabolite(x),\ C-mol}$) as described by Eq. 4.7

$$\Delta n_{metabolite(x),\ C-mol} = N_{C,\ metabolite(x)} \times \left(c_{metabolite(x),\ t=i+1} \times V_{t=i+1} - c_{metabolite(x),\ t=i} \times V_{t=i} \right)$$

(4.7)

with $N_{C,\ metabolite(x)}$ as the number of carbon atoms of metabolite(x), $c_{metabolite(x),\ t=i}$ as concentration of metabolite(x) (in mol L^{-1}) at time point i and $V_{t=i}$ as the working volume in the bioreactor (in L) at time point i. Meinhold (2012) analyzed the molar composition of exponentially growing CHO DP-12 cells. Cells contained 1.51×10^{-11} mol carbon per cell. $\Delta n_{biomass,\ C-mol}$ was calculated on basis of Eq. 4.8 with $VCD_{t=i}$ as the viable cell density (in cells L^{-1}) at time point i of cultivation.

$$\Delta n_{biomass,\ C-mol} = 1.51 \times 10^{-11} \left[\frac{C-mol}{cell} \right] \times \left(VCD_{t=i+1} \times V_{t=i+1} - VCD_{t=i} \times V_{t=i} \right) \quad (4.8)$$

Changes in the amount of metabolite(x) in O-mol ($\Delta n_{metabolite(x)}$ in O-mol) were calculated as follows:

$$\Delta n_{metabolite(x),\ O-mol} = X_{O/C,\ metabolite(x)} \times \Delta n_{metabolite(x),\ C-mol} \quad (4.9)$$

$X_{O/C,\ metabolite(x)}$ represented the ratio of oxygen and carbon in metabolite(x), e. g. 1 for $C_6H_{12}O_6$ or 0.487 for biomass (Meinhold, 2012).

The sum of all negative $\Delta n_{metabolite(x),\,C-mol}$ or $\Delta n_{metabolite(x),\,O-mol}$ values formed the carbon or oxygen influx (Eq. 4.10) while carbon and oxygen efflux were represented by the sum of all positive values of $\Delta n_{metabolite(x),\,C-mol}$ or $\Delta n_{metabolite(x),\,O-mol}$ respectively (Eq. 4.11).

$$\text{carbon}_{influx} = \sum \Delta n_{metabolite(x),\,C-mol} \qquad \text{oxygen}_{influx} = \sum \Delta n_{metabolite(x),\,O-mol} \qquad (4.10)$$

$$\text{with } \Delta n_{metabolite(x),\,C-mol} < 0 \qquad\qquad \text{with } \Delta n_{metabolite(x),\,O-mol} < 0$$

$$\text{carbon}_{efflux} = \sum \Delta n_{metabolite(x),\,C-mol} \qquad \text{oxygen}_{efflux} = \sum \Delta n_{metabolite(x),\,O-mol} \qquad (4.11)$$

$$\text{with } \Delta n_{metabolite(x),\,C-mol} > 0 \qquad\qquad \text{with } \Delta n_{metabolite(x),\,O-mol} > 0$$

As the composition of the exhaust gas could not be analyzed for bioreactor cultivations it was assumed that the amount of produced CO_2 in a time interval (Δn_{CO_2} in C-mol) was represented by the difference between carbon_{influx} and carbon_{efflux} (Eq. 4.12). The same was assumed for Δn_{O_2} (4.13).

$$\Delta n_{CO_2} = (-1) \times \text{carbon}_{influx} - \text{carbon}_{efflux} \qquad (4.12)$$

$$\Delta n_{O_2} = (-1) \times \text{oxygen}_{influx} - \text{oxygen}_{efflux} \qquad (4.13)$$

Specific CO_2 and O_2 formation rates (q_{CO_2}, q_{O_2}) were calculated for different time intervals (Δt) according to Eq. 4.14 with $\overline{VCD}$ describing the geometric mean of viable cell density in the analyzed time interval.

$$q_{CO_2} = \frac{1}{\Delta t} \times \frac{\Delta n_{CO_2}}{\overline{VCD}} \qquad\qquad q_{O_2} = \frac{1}{\Delta t} \times \frac{\Delta n_{O_2}}{\overline{VCD}} \qquad (4.14)$$

q_{O_2} is connected to q_{ATP} as described by Eq. 4.15:

$$q_{ATP} = (-1) \times P/O \times q_{O_2} \tag{4.15}$$

where P/O represents the number of ATP molecules which is produced per reduced oxygen atom by the respiratory chain (Hinkle, 2005). Balcarcel and Clark (2003), Hinkle (2005) and Wahl et al. (2008) described a NADH-linked P/O-ratio of 2.5 and a $FADH_2$-linked P/O-ratio of 1.5. In general a P/O-ratio of 2.5 was considered in this study. Nevertheless P/O-ratios of 1.5 were also taken into consideration for a representative interpretation of data.

4.2.8 Calculation of Adenine Nucleotide Pool Sizes

Adenine nucleotide pools were determined for whole cell and mitochondrial samples which were acquired by fast filtration approaches and methanol/chloroform extraction (4.2.3, 4.2.4). The complete extraction process of intracellular metabolites was gravimetrically documented to determine the volume of extraction solute ($V_{extract.\ solute}$ in L) and the factor of concentration by evaporation ($C_{evap.}$). The intracellular amount of a metabolite ($n_{metabolite}$ in mol cell^{-1}), e. g. n_{ATP} or n_{G6P}, was calculated based on Eq. 4.16

$$n_{metabolite} = c_{metabolite} \times C_{evap.} \times V_{extract.\ solute} \times \frac{1}{N_{cells}} \tag{4.16}$$

with $c_{metabolite}$ (in mol L^{-1}) as the concentration of the metabolite in the cell extract which was analyzed by HPLC or LC-MS/MS (4.2.5) and N_{cells} as the number of cells which were used for the extraction of intracellular metabolites.

Mitochondrial ATP pools ($n_{ATP_{mit}}$ in mol cell^{-1}) were determined by Eq. 4.17 thereby considering the loss of mitochondrial compartment and the remaining cytosol on basis of specific marker metabolites. *cis*-aco was used as mitochondrial marker and G6P and F6P functioned as cytosolic marker metabolites. Index (C) defines whole cell samples and (M) mitochondrial samples. (M)/(C)-ratios represent the remaining fraction of mitochondrial or cytosolic marker metabolites in cytosol depleted/ mitochondrial samples.

$$n_{ATP_{mit}} = \frac{n_{cis-aco(C)}}{n_{cis-aco(M)}} \times n_{ATP\,(M)} \times \left(1 - 0.5 \times \frac{n_{G6P\,(M)}}{n_{G6P\,(C)}} - 0.5 \times \frac{n_{F6P\,(M)}}{n_{F6P\,(C)}} \right) \qquad (4.17)$$

Eq. 4.18 was used to calculate cytosolic ATP-contents ($n_{ATP_{cyt}}$ in mol cell^{-1}).

$$n_{ATP_{cyt}} = n_{ATP(C)} - n_{ATP_{mit}} \qquad (4.18)$$

Mitochondrial and cytosolic ADP ($n_{ADP_{mit}}$, $n_{ADP_{cyt}}$) and AMP ($n_{AMP_{mit}}$, $n_{AMP_{cyt}}$) contents were calculated in accordance to the equations used for ATP (Eq. 4.17 and 4.18). Intracellular adenine nucleotide concentrations were calculated on basis of intracellular adenine nucleotide contents and corresponding cell diameters (CEDEX), thereby assuming a spherical cellular morphology.

Adenylate energy charges for whole cell samples and the cytosolic and mitochondrial compartment were calculated according to Atkinson and Walton (1967), Eq. 4.19.

$$AEC = \frac{n_{ATP} + 0.5 \times n_{ADP}}{n_{ATP} + n_{ADP} + n_{AMP}} \qquad (4.19)$$

4.2.9 Calculation of Errors and Statistics

Analyzed metabolic parameters were based on three technical and at least three biological replicates if not stated otherwise.

As the calculation of the standard deviation for a metabolic parameter x (σ_x) was based on the assumption of normally distributed data, Shapiro-Wilk normality test was applied to validate normal distribution of data (P $\geqslant$ 0.05).

σ_x was calculated as follows:

$$\sigma_x = \sqrt{\frac{\sum_{i=1}^{n}(x_i - \bar{x})^2}{n-1}} \tag{4.20}$$

with x_i as an individual data point, $\bar{x}$ as the arithmetic mean of all data points and n as the number of data points.

The calculation of some metabolic quantities, e. g. $n_{ATP_{mit}}$ or AEC, (Eq. 4.21) was based on error-prone parameters like for example n_{G6P} or n_{ADP} . Standard deviations for aforementioned metabolic quantities ($\bar{\sigma}_f$) were calculated based on Gaussian error propagation as described in Eq. 4.22

$$f = f(\bar{x}, ..., \bar{n}) \tag{4.21}$$

$$\bar{\sigma}_f = \sqrt{\left(\frac{\partial f}{\partial \bar{x}} \times \sigma_x\right)^2 + ... + \left(\frac{\partial f}{\partial \bar{n}} \times \sigma_n\right)^2} \tag{4.22}$$

with x as error-prone metabolic parameter, $\frac{\delta f}{\delta \bar{x}}$ as partial derivative of f with respect to $\bar{x}$ and σ_x as standard deviation of $\bar{x}$.

A two-sided unequal variance t-test was applied to determine significant differences in metabolism of hyperosmotically treated cells compared to cells grown at reference conditions. According to the con-

vention described by Cumming et al. (2007), P-values (P) $\leqslant$ 0.05 indicated a statistically significant difference while P $\leqslant$ 0.01 represented a highly significant difference between the results for hyperosmotic and reference conditions.

4.2.10 miRNA and mRNA Expression Analysis

Next generation sequencing (NGS) was applied to investigate the effects of an osmotic upshift on mRNA and miRNA expression of CHO DP-12 cells.

Cells (2×10^6) were harvested by centrifugation (400g, 4°C, 5 min), resuspended in 300 µL RNAprotect Cell Reagent (Qiagen) and frozen in liquid nitrogen. Cell samples were stored at -70°C until isolation of RNA.

MFT-Services (http://www.mft-services.de) in Tübingen performed the steps from RNA-isolation to the lists of raw counts for miRNAs and mRNAs as described in manuscript 2, supporting information B.2.

Identification of Significantly Differentially Expressed miRNAs and mRNAs

miRNA and mRNA counts were further analyzed with edgeR (version 3.10.2) (Robinson et al., 2010) in RStudio (version 0.98.1103, R version 3.2.1). The detailed R scripts for miRNA and mRNA analysis can be found in supporting information A.2.2 and A.2.3.

In summary, 10 counts were added to each mRNA and miRNA raw count. Only those mRNAs which showed more than 10 counts in at least 12 of 25 samples were considered for further analysis. In accordance to the mRNA protocol, a minimal read count of 11 in each of the samples was the criterion to select a miRNA for further analysis.

In another step, only those genes and miRNAs which revealed at least one count per million (CPM) in 3 or more samples remained in the datasets for subsequent differential expression analyses. CPM were calculated as described in Eq. 4.23

$$\text{CPM} = \frac{\Gamma_i}{\sum_{i=1}^{n} \Gamma_i} \times 10^6 \tag{4.23}$$

with Γ_i as the number of counts for gene i and $\sum_{i=1}^{n} \Gamma_i$ as the sum of counts for gene i=1 to n. Differential expression analysis was performed with the negative binomial generalized linear model (GLM) method developed by McCarthy et al. (2012). Gene-specific variations were estimated with an empirical Bayes approach (McCarthy et al., 2012). Cox-Reid adjusted profile likelihood statistics, Pearson's chi-square test and Benjamini-Hochberg method (Benjamini and Hochberg, 1995) were used for identification of significantly differentially expressed genes (DEG). miRNAs and mRNAs showing log2-fold changes (log2(FC)) $\geqslant |1.0|$, P $\leqslant 0.02$ and false discovery rates (FDR) $\leqslant 0.02$ were defined as DEGs. Principal Component Analyses were performed for mRNA and miRNA datasets with DESeq2 (4.5).

Gene Expression Dynamics

The number of significantly up- and downregulated mRNAs at defined time points was visualized by VennDiagram (version 1.6.9). MaSigPro (version 1.40.0) with hierarchical clustering was applied to investigate expression dynamics of up- and downregulated mRNAs (Conesa et al., 2006; Nueda et al., 2014). Gene count datasets were filtered as described in the previous abstract and were CPM-normalized with edgeR before they were further analyzed with maSigPro. A detailed example of a maSigPro R script is shown in supporting information A.2.4. In 2014, Nueda et al. expanded the maSigPro supported models by GLMs thereby enabling the analysis of RNA count data sets. maSigPro analysis was based on a combination of two polynomial regression steps (Conesa et al., 2006; Nueda et al., 2014). In the first step a regression model was fit to each gene with least-square parameter esti-

mation and significant genes (P-value and FDR $\leqslant$ 0.02) were identified by F-statistic and Benjamini-Hochberg method (Nueda et al., 2014). The first step was followed by a stepwise regression in order to identify the best regression coefficients for each of the selected genes in step one. Genes were defined as statistically significant if the R-square value (R^2) for the regression model was greater than 0.7 and P-value and FDR were lower than 0.02. Finally genes were clustered with hierarchical clustering algorithm.

Gene Ontology Enrichment Analysis

Gene Ontology (GO) Enrichment Analysis was performed with GOseq (version 1.20.0, Young et al. (2010)), MGI Gene Ontology Term Finder (http://www.informatics.jax.org) and GOrilla (Eden et al., 2009). As *C. griseus* was not supported by the three tools, analyses were based on the GO data sets for *Homo sapiens*, *Mus musculus* and *Rattus norvegicus*.

miRNA Target Prediction

Validated mRNA targets of differentially expressed (DE) miRNAs were identified on basis of the miR-TarBase database (http://mirtarbase.mbc.nctu.edu.tw/, Chou et al. (2015)). mRNAs were assumed to be targets of a specific miRNA if their identification was based on luciferase or green fluorescent protein (GFP) reporter assay, Western blot and/or quantitative polymerase chain reaction (qPCR).
In addition, miRDB (http://mirdb.org/miRDB/, Wong and Wang (2015)), DIANA-microT web server version 5.0 (http://diana.imis.athena-innovation.gr/DianaTools/index.php?r=microT_CDS/index, Paraskevopoulou et al. (2013); Reczko et al. (2012)) and TargetScanHuman release 6.2 (http://www.targetscan.org/vert_61/) were applied to predict targets of DE miRNAs. Target prediction was performed for human or murine miRNA homologs.
MGI Gene Ontology Term Finder (http://www.informatics.jax.org), GOrilla (Eden et al., 2009) and AmiGO Term Enrichment Services (http://amigo.geneontology.org/rte) connected to **P**rotein **AN**alysis **TH**rough **E**volutionary **R**elationships (PANTHER) Classification System were applied for GO enrichment analysis of DE predicted targets.

5 Results

The production of heterologous proteins by mammalian host cell lines is an energy consuming process. The highest amount of cellular energy in form of ATP is produced by metabolic pathways (TCA cycle, electron transport chain, oxidative phosphorylation) located in the mitochondrial compartment: the cellular "powerhouse". Therefore, the key interest of a preliminary diploma thesis (Pfizenmaier, 2011) was the development of a flow cytometric method to investigate resizing of the mitochondrial compartment in relation to q_p enhancing hyperosmotic culture conditions. The translocase of the outer mitochondrial membrane 22 (TOM22) represented the target molecule for the developed antibody-based fluorescence labeling of intracellular mitochondria (4.2.5). This method was utilized by Pfizenmaier (2011) in order to investigate the mitochondrial response upon osmotic upshift from 290 to 390 mOsmol kg^{-1} during batch cultivation of an anti-IL-8-IgG1 producing CHO DP-12 cell line (4.2.2). Thus, a decline in mitochondrial fluorescence (Fig. 3.2) upon hyperosmotic stimulus was revealed and a reduced size of the mitochondrial compartment was assumed.

This hypothesis in relation to the q_P enhancing effect of hyperosmotic culture conditions represented the starting point to conduct further research concerning this complex of themes in the current study.

In the first part of this research study, experiments were performed to validate and to further characterize the phenotype of hyperosmotically stressed CHO DP-12 cells.

5.1 Phenotype of CHO DP-12 Cells Exposed to Hyperosmotic Stimulus (+ 100 mOsmol kg^{-1})

Results of this section have partially been published in Pfizenmaier et al. (2015) (manuscript 1 supporting information B.1).

5.1.1 G1-phase Arrest and Inhibition of Cell Growth due to Hyperosmolality

Bioreactor cultivations (4.2.2) were performed in batch mode to investigate the phenotype of hyperosmotically stressed CHO DP-12 cells. Hyperosmotic culture conditions (390 mOsmol kg^{-1}) were induced by adding NaCl-enriched cultivation medium to four of eight cell cultures (V_R = 1.2 L) 72 h after inoculation, thus resulting in a highly significant difference (P < 0.001) in osmolality of $\sim$ 100 mOsmol kg^{-1} compared to reference cultures (Fig. 5.1). Osmolality slightly increased with the time of cultivation whereby the $\sim$100 mOsmol kg^{-1} difference between reference and hyperosmotic batch cultures remained rather constant until the end of cultivation (Fig. 5.1).

Starting with approximately identical profiles of viable cell densities (VCD) in all batch cultures, hyperosmotic culture conditions lowered the VCD compared to reference cultures. However, post-shift profiles of VCD showed high inter-culture variances, thus alleviating the effect on VCD. While VCD reached a maximal level (VCD$_{max}$) of 9.0 $\pm$ 1.4 x 10^6 cells mL^{-1} on day 6 at reference conditions, hyperosmolality reduced VCD$_{max}$ to 6.4 $\pm$ 1.1 x 10^6 cells mL^{-1}. Analysis of cellular growth rates (μ) for the time interval day 4 to 6 revealed a significantly lower μ for hyperosmotically stressed cells compared to reference cells (μ =0.28 $\pm$ 0.04 d^{-1} vs. μ =0.48 $\pm$ 0.11 d^{-1}, P = 0.02, n = 4).

In contrast to VCD, the osmotic upshift from 290 to 390 mOsmol kg^{-1} did not affect the viability of CHO DP-12 cells. Viability of both, reference and hyperosmotically stressed CHO DP-12 cells, showed levels > 97% until culture day 6 where viability started to decline, consequently reaching levels below 90% on culture day 8 (Fig. 5.1).
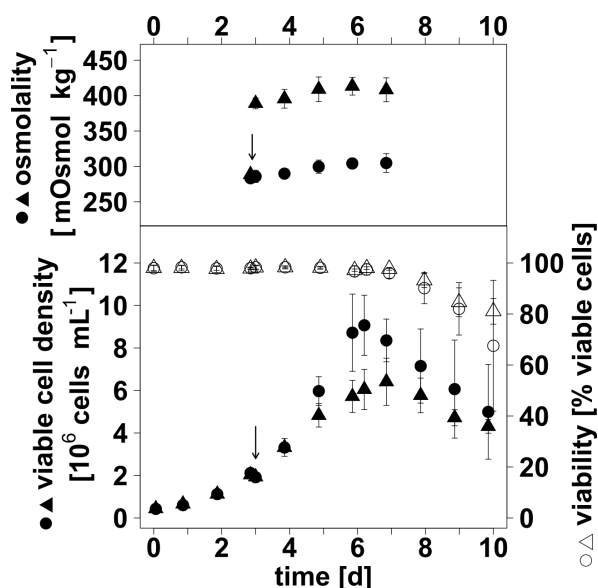
FIGURE 5.1: Profiles of osmolality, viable cell density and viability of CHO DP-12 cells cultivated in bioreactor. NaCl-enriched cultivation medium (Tab. 4.3) was added 72 h after inoculation (arrow) to defined cultures in order to induce hyperosmotic conditions (n = 4, ▲△). An equal volume of standard CHO DP-12 cultivation medium was added to reference cultures (n = 4, ● ○). Error bars represent standard deviations of four biological replicates thereby considering as well the technical error of measurement (n = 3). Highly significant difference in osmolality between day 3 and 7 (P < 0.001). With changes to Fig. 1AB of Pfizenmaier et al. (2015) (supporting information B.1).

A cell cycle arrest related inhibition of cell growth was described for CHO cells exposed to hyperosmotic culture conditions by Ryu et al. (2001). Therefore, the cell cycle distribution of reference and hyperosmotic cultures was analyzed in this study.

Directly before the osmotic stimulus, all CHO DP-12 batch cultures showed a similar population composition with respect to cell cycle distribution (Fig. 5.2). Thereafter, the percentage of hyperosmotically stressed cells in G1-phase increased from ∼ 40% on day 3 to 79% on day 7 (Fig. 5.2 A). In addition, the cell population in S-phase decreased significantly from 46% to 16% in the same time interval while a slight decrease from 14% to 5% was detected for G2-phase (Fig. 5.2 BC). An increase in the percentage of cells in G1-phase together with a decrease of cells in S- and G2-phase was also characteristic for reference cultures. However, a comparison of hyperosmotic and reference cultures

revealed significantly higher G1-phase populations and significantly lower S-phase populations (P < 0.005, n = 4) for hyperosmotically stressed cells on day 4 to 6 ((Fig. 5.2 AB). Consequently, the results suggest an induction of G1-phase arrest by osmotic upshift.
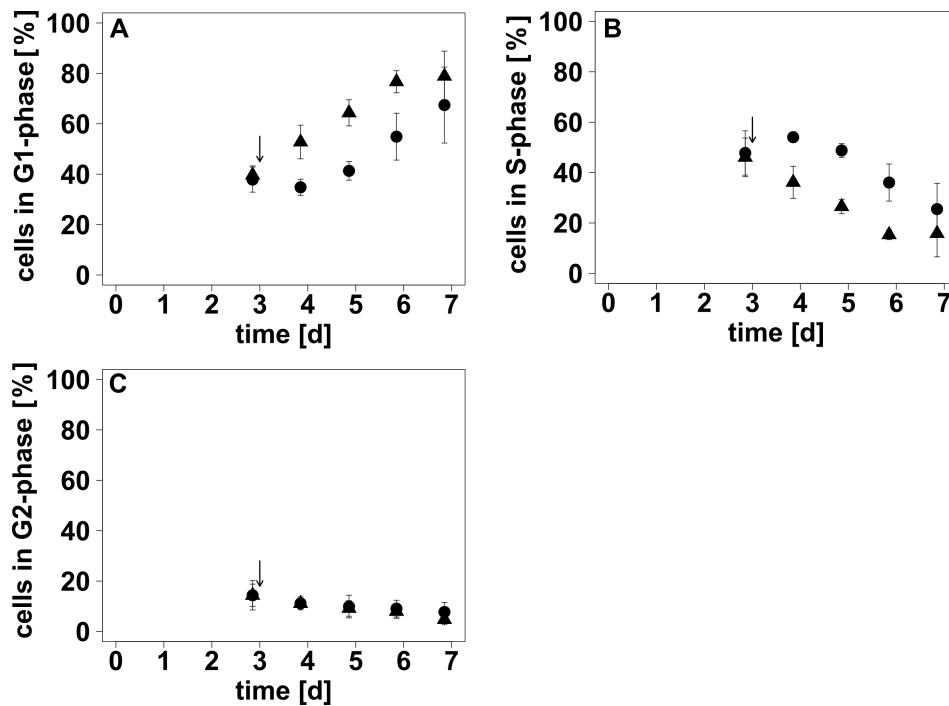
FIGURE 5.2: Effect of hyperosmolality (+ 100 mOsmol kg^{-1}) on the cell cycle distribution of CHO DP-12 cultures. NaCl-enriched cultivation medium (Tab. 4.3) was added 72 h after inoculation (arrow) resulting in an osmolality of $\sim$ 390 mOsmol kg^{-1} (▲) for hyperosmotic cultures. Osmolality of reference cultures was $\sim$ 290 mOsmol kg^{-1} (●). Determination of the distribution of cells in G1- (A), S- (B) and G2-phase (C) of cell cycle was based on propidium iodide staining and flow cytometric analysis (4.2.5). Error bars represent standard deviations of four biological replicates with three technical replicates each. Figure A is a modified version of Fig. 2 of Pfizenmaier et al. (2015) (supporting information B.1). Highly significant difference due to hyperosmolality for G1- and S-phase on days 4 to 6 (P < 0.005).

5.1.2 Metabolic Rates Increase Upon Osmotic Shift

To obtain a better idea of the metabolic activity and the productivity of hyperosmotically stressed CHO DP-12 cells (+ 100 mOsmol kg^{-1}), specific metabolic formation rates were determined for Glc, Lac and

the produced mAb (Tab. 5.1). Highly significantly reduced q_{Glc} and increased q_{Lac} were observed for cells exposed to hyperosmotic culture conditions in the post-shift period day 4 to 6. To be precise, q_{Glc} and q_{Lac} changed by 35 and 40%, respectively, thus maintaining the molar yield in Lac per consumed mol of Glc ($Y_{Lac/Glc}$, 1.10 ± 0.14 vs. 1.06 ± 0.25 mol_{Lac} mol_{Glc}^{-1} for reference cells). Limiting conditions with respect to the nutrient Glc (~ 5 mM, Ozturk and Hu (2005)) occurred on culture day 6 (supporting information Fig. A.1). Noteworthy, the concentration of the accumulated Lac in the culture broth started to decline at the same time point (supporting information Fig. A.1). In addition to the aforementioned changes, q_P improved from 3.69 to 5.55 pg_{mAb} $cell^{-1}$ d^{-1} in response to hyperosmotic stimulus resulting in a maximal c_P of ~ 90 mg L^{-1} compared to ~ 60 mg L^{-1} for reference cultures (supporting information Fig. A.2).

TABLE 5.1: Effect of hyperosmolality (390 mOsmol kg^{-1}) on q_{Glc}, q_{Lac} and q_P in the time interval day 4 - 6. Negative values indicate consumption whereas positive values stand for production. ** highly significant difference between reference and hyperosmotic conditions ($P \leqslant 0.002$, n = 4)

	q_{Glc} **	q_{Lac} **	q_P
	[pmol cell^{-1} d^{-1}]		[pg$_{mAb}$ cell^{-1} d^{-1}]
reference	- 1.55 $\pm$ 0.18	1.64 $\pm$ 0.19	3.69
hyperosmolal	- 2.09 $\pm$ 0.13	2.29 $\pm$ 0.12	5.55

5.1.3 Osmotic Upshift Reduces TOM22-Mediated Mitochondrial Fluorescence

Stress conditions affect the cellular response (2.6 and 2.7) and may therefore cause changes in energy demand and variations in the size of the mitochondrial compartment. An antibody-based technique for intracellular fluorescence labeling of mitochondria (4.2.5) was applied to investigate changes of the mitochondrial compartment as response to hyperosmotic stimulus. Directly before osmotic upshift, flow cytometric analyses revealed congruent histograms and equal median fluorescence intensities for cells of all batch cultures (Fig. 5.3 B, supporting information Fig. A.5). About 24 h after

hyperosmotic stimulus ($+100$ mOsmol kg^{-1}), osmotically stressed cells showed a more than 50% decrease in mitochondrial fluorescence intensity compared to reference cells which showed only slight changes (Fig. 5.3 B). More precisely, hyperosmotic culture conditions shifted the histogram to lower fluorescence intensities whereas similar histograms were observed for isotype controls of reference and hyperosmotic cultures (Fig. 5.3 A). Mitochondrial fluorescence intensities decreased with the time of cultivation, thereby showing significantly lower fluorescence levels for hyperosmotically stressed cells on day 4 and 5 ($P < 0.01$). In contrast, comparable values for both reference and hyperosmotically stressed cells were detected on day 6 and 7 (Fig. 5.3).

In summary, experiments validated the previously described decrease in mitochondrial fluorescence intensity at hyperosmotic culture conditions (Pfizenmaier, 2011).
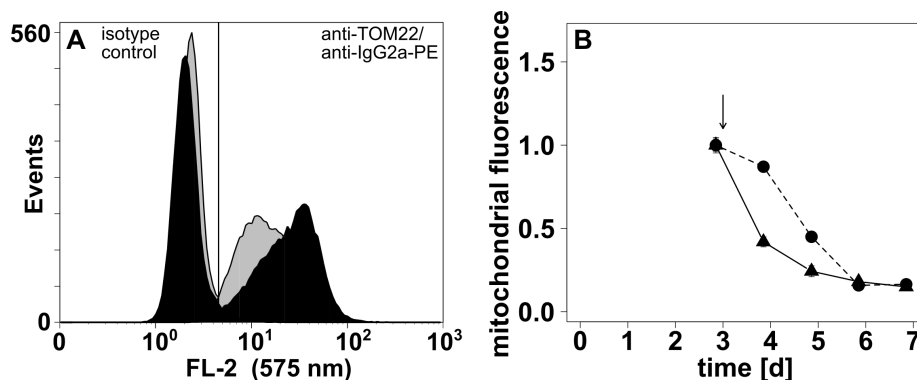
FIGURE 5.3: A: Histogram of flow cytomerically analyzed CHO DP-12 cells 24 h after osmotic shift. B: Time courses of mitochondrial fluorescence. Intracellular mitochondria were labeled by a combination of an anti-translocase of the outer mitochondrial membrane 22 (TOM22) and a phycoerythrin (PE)-conjugated isotype-specific anti-IgG2a antibody. The fluorescence intensity of the cells was analyzed by flow cytometry, thereby detecting 40,000 events (4.2.5). Mitochondria of CHO DP-12 cells were stained directly before osmotic shift (arrow) and on each of the following days of cultivation (4.2.2). Osmotic shift resulted in an osmolality of ~ 390 mOsmol kg^{-1} (grey, ▲, n=4) compared to ~ 290 mOsmol kg^{-1} for the reference cultures (black, ●, n = 4). Mitochondrial fluorescence (Fig. B) was normalized and corrected for non-specific binding as described in Eq. 4.1. Error bars were smaller than the symbols of the plotted data points. Highly significant difference in mitochondrial fluorescence on days 4 and 5 ($P < 0.01$).

5.1.4 Hyperosmotically Stressed Cells Show Enhanced Availability of ATP

Initial results for the hyperosmotic stimulus study revealed increased consumption of Glc and production of Lac in combination with a decrease in the mitochondrial fluorescence signal of osmotically stressed CHO DP-12 cells. As these results may indicate contradictory effects of hyperosmolality on the cellular energy level, cell specific O_2, CO_2 and ATP formation rates (q_{O_2}, q_{CO_2}, q_{ATP}) as well as intracellular adenine nucleotide pools were subsequently analyzed.

Carbon and oxygen balancing (4.2.7, supporting information Tab. A.2) were applied in order to calculate q_{O_2} and q_{CO_2} for both hyperosmotic and reference cultures. In the post-shift period day 3 to 4, q_{O_2} was approximately - 0.32 pmol cell^{-1} h^{-1} for reference and osmotically stressed cells whereas q_{CO_2} was as high as 0.25 pmol cell^{-1} h^{-1} (Fig. 5.4). Thereafter hyperosmolality resulted in even lower values for q_{O_2} and higher values for q_{CO_2}, thus depicting increased consumption of O_2 and production of CO_2, respectively (Fig. 5.4).
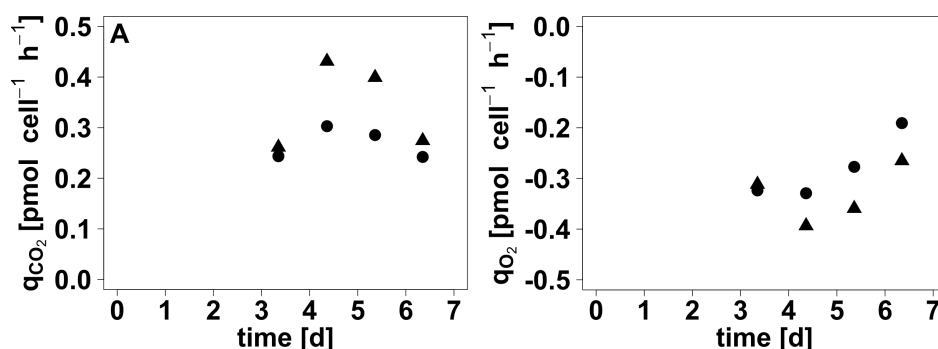
FIGURE 5.4: Effect of osmotic shift (+ 100 mOsmol kg^{-1}) on specific carbon dioxide (q_{CO_2}) and oxygen formation rates (q_{O_2}) of CHO DP-12 cells. Hyperosmotic conditions ($\sim$ 390 mOsmol kg^{-1}, ▲) were induced by the addition of NaCl-enriched cultivation medium (Tab. 4.3) 72 h after inoculation of bioreactors (4.2.2). Osmolality of reference cultures was $\sim$ 290 mOsmol kg^{-1}(●). The determination of q_{CO_2} and q_{O_2} was based on carbon and oxygen balancing (4.2.7) for defined time intervals. Data points are arithmetic means of two biological replicates.

To be precise, q_{O_2} reached -0.39 or -0.36 pmol cell^{-1} h^{-1} in the time interval day 4 to 5 and day 5 to 6 while values of 0.43 and 0.40 pmol cell^{-1} h^{-1} were calculated for q_{CO_2} (Fig. 5.4). In the same time

intervals, reference cells showed comparatively minor changes in q_{O_2} and q_{CO_2} (Fig. 5.4). Respiratory quotient (RQ $\approx$ 1) functioned as a quality standard for the calculated rates and therefore average RQs were analyzed for the time interval day 4 to 7. Noteworthy, the average RQ for reference cultures (1.07 $\pm$ 0.14) resembled the RQ at hyperosmotic conditions (1.08 $\pm$ 0.04).

To obtain q_{ATP} in relation to the determined q_{O_2} (Eq. 4.15, 4.2.7) a P/O-ratio of 2.5 was assumed on basis of values from literature (Balcarcel and Clark, 2003; Hinkle, 2005; Nath and Villadsen, 2015; Wahl et al., 2008). Starting from comparable q_{ATP} of approximately 19 pmol cell^{-1} d^{-1} in the post-shift interval day 3 to day 4, q_{ATP} of CHO DP-12 cells exposed to hyperosmolality increased by $\sim$ 20% whereas almost no change was observed for reference cells (Fig. 5.5). Although q_{ATP} declined from day 4 to 7, approximately 30 to 39% higher values were observed for hyperosmotically stressed cells.
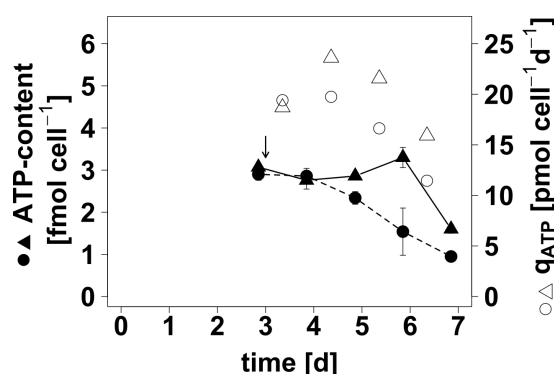
FIGURE 5.5: Influence of hyperosmolality ($+$100 mOsmol kg^{-1}) on intracellular ATP-content and specific ATP formation rate (q_{ATP}) of CHO DP-12. NaCl-enriched cultivation medium (Tab. 4.3) was added 72 h after inoculation (arrow) resulting in an osmolality of $\sim$ 390 mOsmol kg^{-1} ($\blacktriangle$ $\triangle$) for hyperosmotic cultures. Osmolality of reference cultures was $\sim$ 290 mOsmol kg^{-1}($\bullet$ $\circ$). Intracellular ATP-contents were determined by a combination of a fast filtration approach for 10^7 cells (4.2.3), methanol/chloroform extraction (4.2.4) and HPLC analysis (4.2.5). Two biological replicates with three technical replicates each were analyzed at all time points and were used to calculate the standard deviations represented by error bars. q_{ATP} was determined by carbon and oxygen balancing (4.2.7) and a P/O ratio of 2.5 (Balcarcel and Clark, 2003; Hinkle, 2005; Nath and Villadsen, 2015; Wahl et al., 2008). With changes to Fig. 3 of Pfizenmaier et al. (2015)(supporting information B.1.)

In concurrence with the enhanced q_{ATP}, CHO DP-12 cells exposed to hyperosmolality possessed higher intracellular ATP-contents (n_{ATP}) on day 5, 6 and 7 (Fig. 5.5). Precisely, all cell cultures showed similar n_{ATP} of ~ 3 fmol cell^{-1} directly before and 24 h after osmotic upshift. In the following time of cultivation, n_{ATP} of osmotically stressed cells increased up to 3.30 fmol cell^{-1} on day 6 and subsequently lowered to 1.60 fmol cell^{-1}. During the same time interval, n_{ATP} of reference cells decreased almost gradually from 2.86 to 0.95 fmol cell^{-1}, thus revealing a distinct enhancement of n_{ATP} at hyperosmotic culture conditions. In addition, analysis of intracellular adenine nucleotides revealed ADP-contents (n_{ADP}) between 0.15 and 0.29 fmol cell^{-1} whereby n_{ADP} tended to be higher for hyperosmotically stressed cells (supporting information Fig. A.4). Intracellular AMP levels were even lower than n_{ADP} and consequently the measured AMP values were below the reliable detection limit.

The adenylate energy charge (AEC) according to Atkinson and Walton (1967) is an important and highly stable metabolic control parameter that is defined as the sum of n_{ATP} and $1/2 \times n_{ADP}$ divided by the sum of n_{ATP}, n_{ADP} and n_{AMP} (Eq. 4.19 section 4.2.8). Therefore, AECs were determined directly before osmotic upshift (day 3) and in the post-shift period day 4 to 7, thereby disregarding AMP levels (Tab. 5.2). Reference and osmotically stressed CHO DP-12 cells showed equal and stable AECs of 0.97 ± 0.01 on day 3 to 5 (Tab. 5.2). Thereafter, AECs declined but still remained at levels above 0.90.

TABLE 5.2: Effect of osmotic upshift (+ 100 mOsmol kg^{-1}) on adenylate energy charges. Day 3 represents the time point directly before osmolality was increased from ~ 290 mOsmol kg^{-1} (reference) to ~ 390 mOsmol kg^{-1} (hyperosmolal) during batch cultivation of CHO DP-12.

	day 3	day 4	day 5	day 6	day 7
reference	0.97 ± 0.01	0.97 ± 0.01	0.97 ± 0.01	0.96 ± 0.01	0.93 ± 0.02
hyperosmolal	0.97 ± 0.01	0.97 ± 0.01	0.97 ± 0.01	0.92 ± 0.06	0.91 ± 0.02

According to independent studies (Alfieri and Petronini, 2007; Burg et al., 2007; Kiehl et al., 2011; Lang et al., 1998) hyperosmotic culture conditions can induce RVI (2.6), thus being able to affect intracellular metabolite concentrations and pool sizes, respectively. To review whether enhanced q_{ATP}

and n_{ATP} at hyperosmotic culture conditions were related to RVI, cell diameters and intracellular ATP-concentrations (c_{ATP}) were investigated (4.2.8). Reference and osmotically stressed cells showed comparable cell diameters of $\sim$ 11.6 µm in the pre-shift period and directly after osmotic upshift (Fig. 5.6 B). Subsequently, hyperosmolality induced a steady increase in cell diameter, reaching 13.5 µm on day 7. In contrast, cell diameters of reference cells remained rather constant until day 6, followed by a distinct increase to 12.9 µm on day 7. After culture day 7, cell diameters of both reference and osmotically stressed cells declined whereby cell diameters of cells exposed to hyperosmotic stimulus tended to be higher (Fig. 5.6 B).
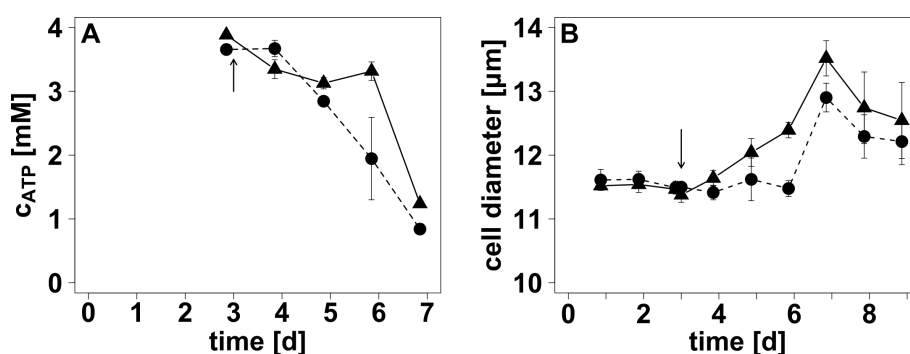
FIGURE 5.6: Changes in intracellular ATP-concentration (A) and cell diameter (B) of CHO DP-12 due to hyperosmolality (+100 mOsmol kg^{-1}). Osmolality was increased 72 h after inoculation by the addition of NaCl-enriched cultivation medium (arrow). This resulted in an osmolality of $\sim$ 390 mOsmol kg^{-1} (▲) compared to $\sim$ 290 mOsmol kg^{-1} for reference cultures (●). Cell diameters were determined by Cedex XS cell counter. Intracellular ATP-concentrations were analyzed by a combination of a fast filtration approach for 10^7 cells (4.2.3), methanol/chloroform extraction (4.2.4), HPLC analysis (4.2.5) and the assumption of spherical cells. Error bars of Fig. A represent standard deviations based on two biological replicates and three technical replicates each while error bars of Fig. B represent standard deviations of four biological replicates.

In accordance to the hyperosmotically induced 2-fold increase in n_{ATP} on culture day 6 (Fig. 5.5), osmotically stressed CHO DP-12 cells showed $\sim$ 1.7-fold elevated c_{ATP} at the same time point (Fig. 5.6 A). On day 5 and 7, however, the difference in c_{ATP} compared to reference cells was slightly less distinct as for n_{ATP} (Fig. 5.6 A). As the time course of cell diameters for osmotically stressed CHO DP-12 cells indicated RVI, the required q_{ATP} to compensate RVI ($q_{ATP,+}$) was estimated. Regarding the time in-

terval day 3 to 5, osmotically stressed cells showed a daily increase in cell volume of approximately 0.75 pL cell^{-1}. Considering the average c_{ATP} of 3.4 mM for this time interval, a $q_{ATP,+}$ of 0.26 fmol cell^{-1} d^{-1} would have been required to maintain c_{ATP}. Noteworthy, the enhancement of q_{ATP} was as high as 4910 fmol cell^{-1} d^{-1} for the time interval day 3 to 4, thus being several magnitudes higher than $q_{ATP,+}$.

Concluding, hyperosmotically stressed CHO DP-12 cells showed enhanced q_{ATP} in combination with increased n_{ATP} and c_{ATP}.

5.1.5 Reliability of the Mitochondrial Staining Procedure

The observed improved energetic capacity of hyperosmotically stressed CHO DP-12 cells was contrary to the hypothesized reduced size of the mitochondrial compartment as response to hyperosmotic culture conditions. In order to investigate whether the antibody-based mitochondrial staining procedure produced reliable results, additional flow cytometric parameters were analyzed and further control experiments were performed.

As part of the flow cytometric analysis of mitochondrial fluorescence intensities, signals of forward and sidewards scatter were investigated in order to reveal potential changes in cell size or cellular structure which may influence the binding of the anti-TOM22 antibody to its mitochondrial target. Both, reference and batch cultures undergoing hyperosmotic treatment, showed comparable histograms for forward and sidewards scatter prior to osmotic upshift on day 3 of cultivation (Fig. 5.7).

Broader but similar forward scatter histograms were received for reference and hyperosmotic cultures on day 7, thereby showing a tendency to elevated values for forward scatter which may correlate with enlarged cell size (Fig. 5.7). An increase in intra-culture variance was also observed for sidewards scatter from day 3 to 7. However, this effect was more pronounced at hyperosmotic culture conditions. Furthermore, the sidewards scatter histogram of osmotically stressed cells was shifted to higher values resulting in a distinct difference with respect to reference conditions (Fig. 5.7). Concluding, this difference in sidewards scatter which developed during the four day post-shift period may indicate

hyperosmotically induced changes in cellular structure.
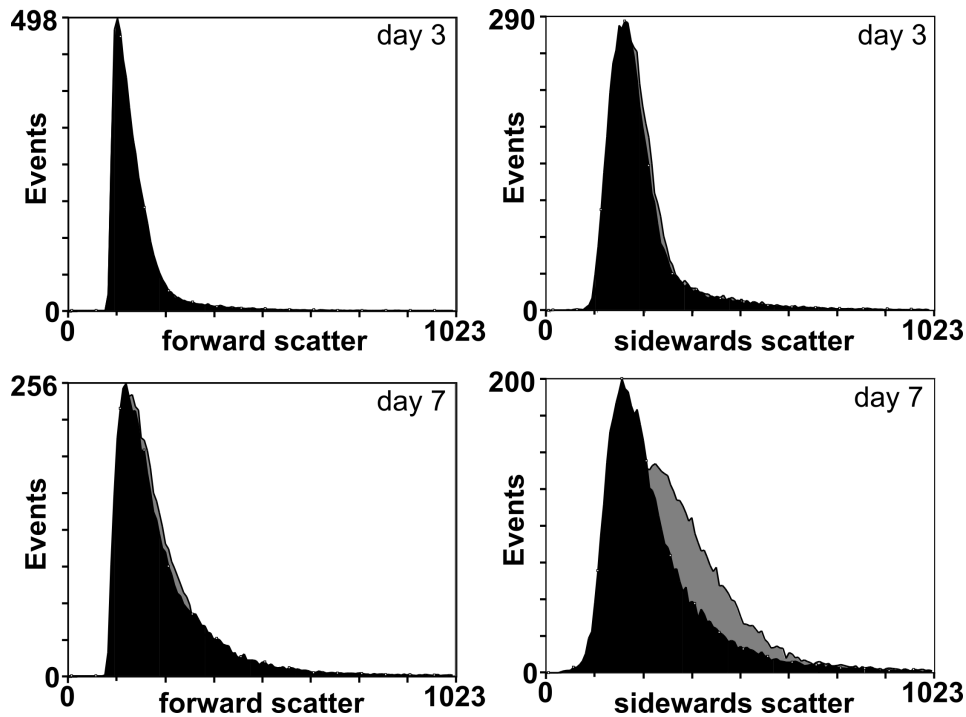
FIGURE 5.7: Effect of hyperosmotic stimulus on forward and sidewards scatter of CHO DP-12 cells. Information of forward and sidewards scatter was acquired as part of the flow cytometric analysis of mitochondrial fluorescence intensities (4.2.5). Measurements were performed directly before (day 3) as well as on the following four days after hyperosmotic stimulus (+100 mOsmol kg^{-1}). Addition of NaCl-enriched cultivation medium to four CHO DP-12 batch cultures resulted in an average culture osmolality of $\sim$ 390 mOsmol kg^{-1} (grey) compared to $\sim$ 290 mOsmol kg^{-1} for reference cultures (n = 4). Histograms for day 3 and 7 are based on at total of 40,000 events.

Additional experiments were performed in order to elucidate whether hyperosmotic culture conditions may affect the reliability of the staining procedure. Although all washing steps during the mitochondrial staining procedure should have resulted in comparable sample osmolalities, the influence of osmolality on the intensity of the fluorescent label phycoerythrin was investigated. The resulting data revealed that hyperosmolality had no effect on the fluorescence intensity of phycoerythrin (supporting information Fig. A.7). Furthermore, a potential interaction between the mitochondrial staining target TOM22 and the pro-apoptotic protein BAX (2.3) which might reduce

mitochondrial fluorescence, was rejected on basis of comparable amounts of apoptotic cells in both reference and hyperosmotic cultures (supporting information Fig. A.6).

Additional experiments eliminated a possible influence of sample osmolality or interaction of TOM22 and BAX on the antibody-mediated fluorescence staining of intracellular mitochondria. However, hyperosmolality caused changes in the flow cytometric sidewards scatter signal, thus indicating structural changes of CHO DP-12 cells which may in fact influence the binding of the anti-TOM22 antibody to its mitochondrial target.

5.2 Optimization of Experimental Setup for Further Analyses

This section describes how the experimental setup was adjusted in order to receive optimized conditions for further investigations of the effects of hyperosmolality on antibody producing CHO cells.

5.2.1 Determination of the Time Interval for Analyses

First experiments with hyperosmotic stimulus revealed a rather short post-shift time interval of $\sim$ 3 days before limiting c_{Glc} occurred. With respect to the detected differences in q_{ATP} and n_{ATP} in the time interval day 4 to 7 limiting c_{Glc} may influence the validity of these results. Therefore, the precise time interval of exponential growth was determined in order to identify an earlier time point for osmotic upshift. Likewise, the preparation of inoculum as well as the inoculation process itself were standardized to a greater extent to reduce inter-culture variance and to improve the comparability of results from different batch processes.
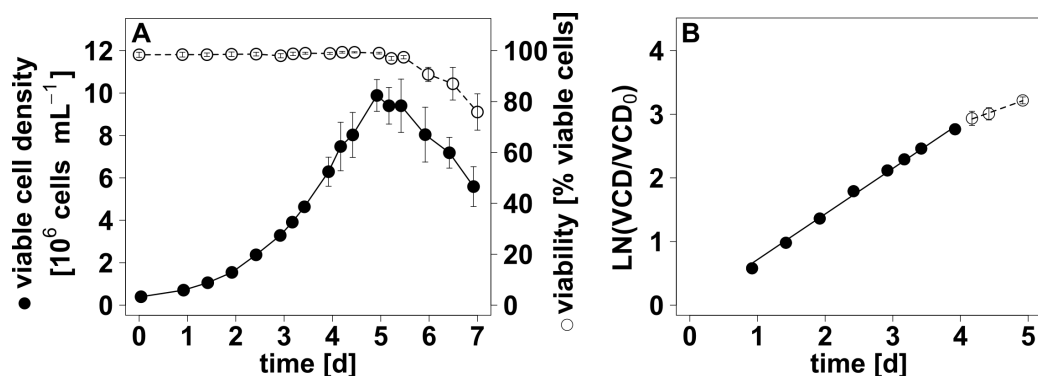
FIGURE 5.8: A: Time course of viable cell density and viability of a reference CHO DP-12 process. CHO DP-12 cells were cultivated in batch mode in bioreactors (4.2.2). Error bars represent standard deviations for three biological replicates considering as well the technical error of measurements. **B: Determination of "exponential growth phase" and specific growth rate (μ) by linear regression.** A μ of 0.72 d^{-1} was determined for "exponential growth phase" (●) and μ= 0.38 d^{-1} for "decelerating phase" (○). Regression lines showed R^2 > 0.99.

CHO DP-12 cells were inoculated in three STRs (V$_R$ = 1.2 L) and were cultivated in batch mode to monitor VCD and viability (4.2.2). Starting from a VCD of approximately 0.4 x 10^6 cells mL^{-1} upon inoculation, VCD reached a VCD$_{max}$ of $\sim$ 10 x 10^6 cells mL^{-1} during the first five days of cultivation (Fig. 5.8 A). This phase of cell growth was characterized by a constant and maximal μ of 0.72 d^{-1} for the time interval day 1 to 4, followed by a reduced μ of 0.38 d^{-1} between day 4 and 5 (Fig. 5.8 B). These two time intervals represent the "exponential growth phase" and the subsequent "decelerating phase" (Fig. 2.9). Instead of a significant "stationary phase" with rather constant VCD, decreasing VCD and viability indicated entry into "declining phase" nearly subsequent to "decelerating phase".

Concluding, induction of hyperosmotic stimulus during "exponential growth phase" could be realized as early as culture day 1 thereby extending the time for culture related analyses. However, the required amount of cells for intracellular metabolite analysis was with 1 - 2 x 10^7 cells per sample reasonably high (Tab. 4.9). Thus, low VCDs increase sample volumes and may prolong the filtration step which was utilized for a fast separation of cells and culture broth (4.2.3). In order to minimize this effect, VCD should at least reach 1 x 10^6 mL^{-1} before hyperosmotic culture conditions are induced. Consequently, the most adequate time for hyperosmotic stimulus according to experimental results

was stated to be 35 h after inoculation.

5.2.2 Preliminary Transcriptome Analysis

First research studies revealed a defined phenotype for CHO DP-12 cells exposed to hyperosmotic culture conditions (5.1). However, a holistic view seemed to be required to elucidate the reasons for enhanced energetic capacity and q_P of osmotically stressed cells. Therefore, a combined analysis of mRNA and miRNA expression of hyperosmotically stressed cultures was expected to contribute to a better understanding of superimposed transcriptional effects.

RNA-Content of CHO DP-12 Cells

An important aspect in this context was the determination of the RNA-content of CHO DP-12 cells during a batch process in order to provide sufficient amounts of RNA for NGS ($\sim 2\,\mu g$ RNA). Therefor, volumes corresponding to 1×10^6, 2×10^6 and 4×10^6 cells were centrifuged to receive cell pellets, which were subsequently resuspended in RNAprotect (Qiagen, US), frozen in liquid nitrogen and stored at -70°C. Isolation of RNA by a combination of QIAshredder and miRNeasy Mini Kit according to the instructions of the manufacturer (Qiagen, US) revealed RNA concentrations of approximately 230, 490 and 650 ng μL^{-1} in a total of 30 μL for the corresponding cell numbers 1×10^6, 2×10^6 and 4×10^6. In addition, RNA-contents remained rather constant from culture day 1 to 3. With respect to these results, even 1×10^6 cells provided a more than sufficient amount of RNA. However, considering the requirement for a rerun of sequencing or significantly reduced RNA-contents due to hyperosmotic culture conditions, a number of 2×10^6 cells per sample was selected for a preliminary transcriptome analysis.

Cell Growth and Metabolism

The preliminary transcriptome analysis was performed to validate sample preparation in terms of RNA-content and -quality as well as to determine the time interval and setup for the final NGS experiment. For this purpose, two batch processes ($V_R = 1.2$ L) with CHO DP-12 cells were performed in STR,

thereby increasing osmolality by $\sim$100 mOsmol kg^{-1} in one of the two batch cultures (Fig. 5.9). According to the results for the identification of an earlier time point for osmotic upshift (5.2.1), hyperosmotic culture conditions were induced 35 h after inoculation. The resulting osmolality of $\sim$380 mOsmol kg^{-1} increased over the time of cultivation, finally reaching $\sim$430 mOsmol kg^{-1} (Fig. 5.9). Likewise, osmolality of the reference culture changed from approximately 280 mOsmol kg^{-1} to $\sim$330 mOsmol kg^{-1} (Fig. 5.9).
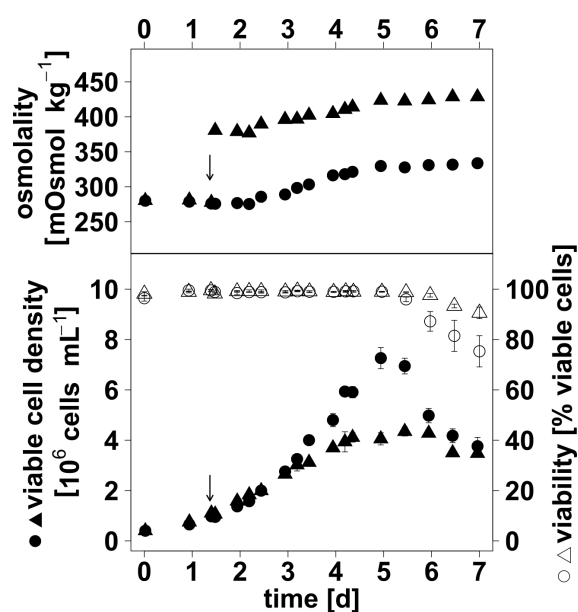
FIGURE 5.9: Time course of osmolality, viable cell density and viability during cultivation for preliminary transcriptome analysis. Two bioreactors were inoculated with the cell line CHO DP-12. 35 h thereafter, osmolality was increased in one bioreactor by the addition of NaCl-enriched medium (▲ △) (Tab. 4.3, 4.2.2). A comparable volume of standard cultivation medium was added to the reference bioreactor (● ○). Error bars represent the technical error of the measurement (n = 3).

In accordance with previous results (Fig. 5.1), hyperosmotic stimulus caused an inhibition of cell growth and consequently lowered VCD$_{max}$ from 7.3 $\pm$ 0.4 x 10^6 cells mL^{-1} to 4.3 $\pm$ 0.2 x 10^6 cells mL^{-1} (Fig. 5.9). First effects of this well-known phenomenon of hyperosmolality were observed on culture day 3.5 where VCD of reference culture tended to be higher compared to VCD of hyperosmotic culture. Noteworthy, two days lay between the hyperosmotic stimulus on day 1.5 and the occurrence of

reduced VCDs (Fig. 5.9). This was in accordance with the period of time observed for an osmotic shift on culture day 3 (Fig. 5.1). Viability of both reference and hyperosmotic culture remained at levels > 98% until day 5. Thereafter, reference cells showed a more distinct decline in viability than hyperosmotically stressed cells whose viability stayed above 90% (Fig. 5.9).

The decline in viability of reference culture was associated with significantly decreasing VCD, limiting c_{Glc} and slightly decreasing c_{Lac} (Fig. 5.10 A). Although the occurrence of Glc limitation seemed not to be influence by culture osmolality, VCD of hyperosmotically stressed cells decreased only slightly from day 6 to 7. Analysis of glutamine concentration (c_{Gln}) for reference and hyperosmotic culture revealed almost congruent time courses until day 3.5 of cultivation. Thereafter, c_{Gln} began to accumulate in hyperosmotic culture until day 5.5 (Fig. 5.10 B) whereas c_{Gln} of reference culture reached growth limiting levels (0.1 - 0.5 mM, Ozturk and Hu (2005)). This phenomenon was less characteristic for the previous experiment with osmotic upshift on day 3 of cultivation but seemed to be associated with growth inhibiting $c_{NH_4^+}$ of approximately 8 mM which were observed in both reference and hyperosmotic cultures on day 4 of cultivation (supporting information Fig. A.1 and A.3).
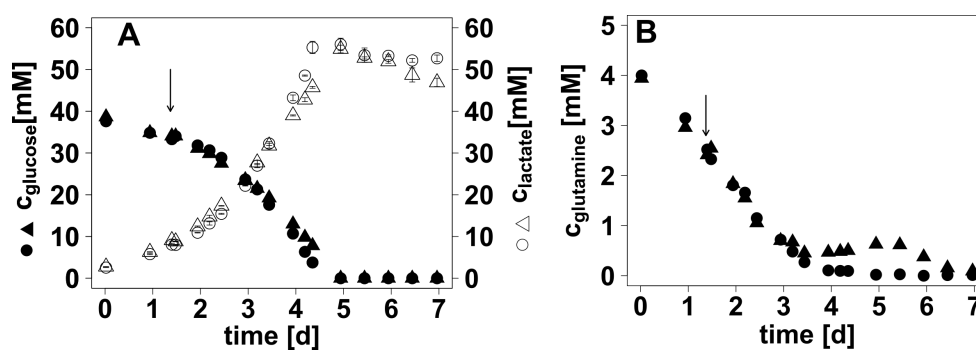
FIGURE 5.10: Effects of osmotic shift (+ 100 mOsmol kg^{-1}, 35 h) on the metabolites glucose, lactate (A) and glutamine. NaCl-enriched cultivation medium (Tab. 4.3) was added to the CHO DP-12 culture 35 h after inoculation (arrow). Osmolality was increased from $\sim$ 280 mOsmol kg^{-1} ($\bullet$ $\circ$) to $\sim$ 380 mOsmol kg^{-1} ($\blacktriangle$ $\triangle$). $c_{glucose}$ and $c_{lactate}$ were determined enzymatically with LaboTRACE. Error bars represent the technical error of the measurement (n = 3). $c_{glutamine}$ was analyzed by HPLC (4.2.5)

To examine whether the earlier osmotic upshift caused a similar increase in n_{ATP} and n_{ADP} as hyperosmotic stimulus on culture day 3, intracellular adenine nucleotide pools were analyzed directly

before and for the "exponential growth phase" after osmotic shift (Fig. 5.11). Similar n_{ATP} of ~ 3 fmol cell^{-1} were observed for both cultures prior to the induction of hyperosmolality. About 12 h after osmotic upshift, CHO DP-12 cells exposed to hyperosmotic conditions showed a slight decrease to 2.61 ± 0.04 fmol$_{ATP}$ cell^{-1} followed by a subsequent increase to 3.24 ± 0.15 fmol$_{ATP}$ cell^{-1} on culture day 4 (Fig. 5.11). Considering the technical error of analysis, n_{ATP} of reference cells remained relatively constant until day 3. Subsequently, a decline in n_{ATP} from 3.07 ± 0.09 fmol$_{ATP}$ cell^{-1} to 2.65 ± 0.06 fmol$_{ATP}$ cell^{-1} on day 4 was observed. Hyperosmotic stimulus resulted in 1.2-fold elevated n_{ATP} and 1.3-fold increased n_{ADP} on day 4 (Fig. 5.11).

In contrast to n_{ATP}, pre-shift intracellular ADP-pools differed between the two batch cultures showing $n_{ADP} = 0.27 \pm 0.03$ fmol cell^{-1} for the later reference culture and $n_{ADP} = 0.22 \pm 0.01$ fmol cell^{-1} for the culture undergoing osmotic upshift (Fig. 5.11). However, similar n_{ADP} were observed on day 2 and 3. While n_{ADP} of reference cells remained at ~ 0.20, n_{ADP} of hyperosmotically stressed cells increased from 0.22 ± 0.01 to 0.27 ± 0.02 fmol cell^{-1} on day 3 to 4 (Fig. 5.11).
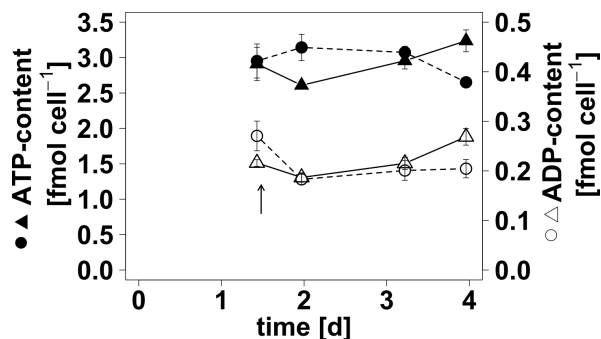
FIGURE 5.11: Influence of osmotic upshift (+ 100 mOsmol kg^{-1}, 35 h) on intracellular ATP- and ADP-contents of CHO DP-12 cells. Osmolality was increased from ~ 280 mOsmol kg^{-1} (●) to ~ 380 mOsmol kg^{-1} (▲) by addition of NaCl-enriched cultivation medium (Tab. 4.3) to CHO DP-12 batch culture 35 h after inoculation (arrow). Intracellular ATP- and ADP-contents were analyzed by a combination of a fast filtration approach for 10^7 cells (4.2.3), methanol/chloroform extraction (4.2.4) and HPLC (4.2.5). Error bars represent the technical error of the measurement (n = 3).

Quality of Isolated RNA and NGS Data

Analysis of mRNA and miRNA expression was performed directly before (day 1.4) as well as 12 and 42 h after osmotic upshift for reference and hyperosmotic culture. MFT-Services Tübingen was provided with cell samples (2×10^6 cells per sample) in order to perform NGS for mRNA and miRNA expression analysis.

In a first step, the quality of the isolate RNA was analyzed with Bioanalyzer 2100 (Agilent Technologies, US), revealing high values for the quality criterion RNA integrity number (RIN) and c_{RNA} levels between 441 and 799 ng µL^{-1} whereby three of six samples contained $\sim$ 530 ng$_{RNA}$ µL^{-1} (Tab. 5.3). With RINs $\geqslant$ 9.0 compared to an optimal RIN of 10.0 and c_{RNA} in the range of the preassigned level, the quality of samples was adequate for subsequent NGS. Furthermore, hyperosmotic culture condition did not tend to influence c_{RNA}.

TABLE 5.3: Quality of isolated RNA. Osmolality was increased 35 h (t = 0) after inoculation of CHO DP-12 cells. At given time points after the osmotic shift, RNA was isolated from 2×10^6 cells with miRNeasy kit. The quality of the isolated RNA was determined with Bioanalyzer 2100. c_{RNA} = RNA concentration, RIN = RNA integrity number.

osmolality [mOsmol kg^{-1}]	time [h]	c_{RNA} [ng µL^{-1}]	RIN
280	0	441	9.4
380	0	570	9.0
280	12	534	9.1
380	12	536	9.5
280	42	535	9.3
380	42	799	9.0

Isolated RNA was utilized for NGS, resulting in NGS data sizes of $\sim$ 10 million reads for mRNA samples and $\sim$ 1-2 million reads for miRNA samples, respectively. With FastQC quality scores $\geqslant$ 20 for each base and read, miRNA and mRNA NGS datasets revealed good sequencing qualities. Approximately 90% of mRNA reads were mapped to the CHO K1 reference genome whereby 60% of reads were mapped to annotated genes. In contrast, the percentage of mapped miRNA reads was signifi-

cantly lower (0.8 - 21%) and associated with the small number of total reads. Consequently, with less than 1% of reads mapped to miRNAs (e. g. *cgr*-miR-147, *cgr*-miR-184 and *cgr*-miR-1973), these datasets could not be utilized for reliable miRNA expression analyses. MFT-Services used the gained knowledge about NGS for miRNA expression analysis of CHO DP-12 cell samples to improve the sequencing protocol for future experiments. Comparison of NGS miRNA data for reference and hyperosmotic samples with respect to raw read counts of *cgr*-miR-147, *cgr*-miR-184 and *cgr*-miR-1973 revealed comparable read counts directly before hyperosmotic stimulus. In addition, miRNA read count levels of the aforementioned miRNAs increased over time in reference samples whereas reduced levels were detected in hyperosmotic samples. The most distinct differences were observed 42 h after osmotic upshift.

Processing and Analysis of NGS Data

In order to identify significantly differentially expressed genes (DEGs) with $\log_2(\text{FC}) \geqslant |1.0|$, $P \leqslant 0.02$ and FDR $\leqslant 0.02$, mRNA read count datasets were processed and analyzed with the Bioconductor package edgeR (4.2.10).

In a first step, low-abundance genes were removed from the dataset. More precisely, only those mRNAs with read counts greater than ten in more than three samples and mRNAs with more than 1 CPM in all samples were used for further analysis. The comparison of total read counts per sample (library size) before and after filtering revealed slightly lower values after filtering (Fig. 5.12 A).

However, the effect of filtering was less pronounced than the sample-specific differences in library size. Noteworthy, significantly reduced library sizes were observed for the sample which was drawn directly before osmotic upshift from reference culture and for the sample representing the hyperosmolal state 42 h after induction. TMM and CPM normalization were applied to compensate for sample-specific effects, e. g. differences in library size, sequencing depth or RNA-composition. Visualization of CPM normalized read counts for each sample in a boxplot revealed similar interquartile ranges for reference and hyperosmolal samples at different time points (Fig. 5.12 B). Thus, normalization effectively adjusted the aforementioned sample-specific differences.
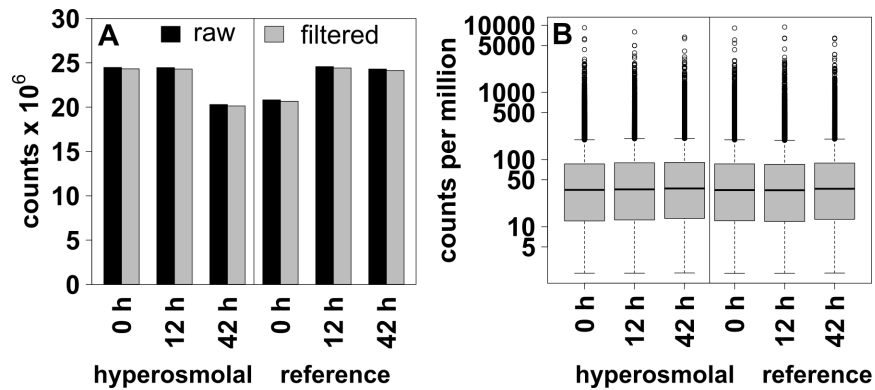
FIGURE 5.12: Processing of NGS data from preliminary experiments. A: Effect of filtering on number of counts. B: Boxplot for CPM normalized filtered data sets. Transcriptome analysis was performed during batch cultivation of CHO DP-12 cells directly before (0 h) as well as 12 and 42 h after osmotic upshift on day 1.45 (280 → 380 mOsmol kg^{-1}). The received NGS data were processed: mRNAs with read counts greater than 10 in more than three samples and mRNAs with more than 1 CPM in all samples were used for further analysis. Fig. A compares the total number of read counts for each sample before (raw) and after (filtered) the filtering step. Fig. B compares samples after counts per million mapped reads (CPM, Eq. 4.23 normalization, 4.2.10)
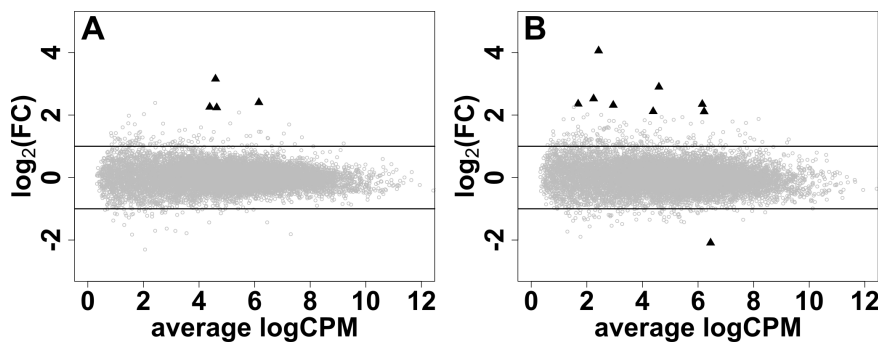
FIGURE 5.13: MA plot for gene expression changes 12 h (A) and 42 h (B) after hyperosmotic stimulus (+ 100 mOsmol kg^{-1}). Transcriptome analysis was performed during batch cultivation of CHO DP-12 cells directly before as well as 12 h (A) and 42 h (B) after osmotic upshift on day 1.45 (280 → 380 mOsmol kg^{-1}). EdgeR analysis of NGS data revealed changes in gene expression. Each symbol (○ ▲) stands for a gene with ▲ representing significantly differentially expressed genes (log$_2$(FC) ⩾ |1.0|, P ⩽ 0.02, FDR ⩽ 0.02).

Further steps of edgeR analysis considering a biological coefficient of variation (BCV) of 0.05 (4.2.10) served to identify DEGs due to hyperosmotic stimulus. Therefor, mRNA levels of hyperosmotically stressed cells were compared to those of reference cells at each time point of analysis (0 h, 12 h, 42 h). At the reference point directly before osmotic upshift, no DEGs were observed, thus

revealing comparable gene expression patterns for both reference and the subsequent hyperosmolal cell culture. Twelve hours after osmotic upshift, edgeR analysis identified 4 DEGs whereby all of these genes were upregulated (Fig. 5.13 A). An additional 30 h later, the number of DEGs increased to 9 with 8 genes being upregulated and 1 being downregulated (Fig. 5.13 B). Average logCPM values ranged between 1 and 12 for all genes which passed the previous data filtering step (Fig. 5.13). Genes defined as DEGs 12 h after osmotic upshift revealed average logCPM values of approximately 4 to 6. Similar average logCPM levels were observed for about half of the DEGs at time point 42 h past hyperosmotic stimulus whereas the other half of DEGs were less abundant in the RNA samples (Fig. 5.13).

TABLE 5.4: Preliminary experiment reveals significantly up-/ downregulated genes 12 and 42 h after osmotic upshift (+ 100 mOsmol kg^{-1}). Osmolality was increased 35 h after inoculation of CHO DP-12 from 280 to 380 mOsmol kg^{-1}. NGS and subsequent data analysis with edgeR revealed significantly upregulated genes compared to reference culture (280 mOsmol kg^{-1}). Data are based on single biological replicates whereby a biological coefficient of variation of 0.05 was assumed for data analysis. Values in bold met the significance criteria for differentially expressed genes (log2(FC) $\geqslant$ |1.0|, P $\leqslant$ 0.02 and FDR $\leqslant$ 0.02) whereas values in brackets did not.

gene	log2(FC) 12 h	42 h	gene	log2(FC) 12 h	42 h
CHN1	(1.7)	**2.4**	*IL1R2*	(2.4)	**4.1**
CITED1	(1.5)	**2.1**	*MATN4*	(-1.4)	**-2.1**
DDIT4	**2.4**	**2.4**	*OLFM1*	**2.2**	(1.6)
FIGF	(0.8)	**2.3**	*SEMA4D*	**3.2**	**2.9**
FMO4	**2.3**	**2.1**	*SUCNR1*	(1.1)	**2.5**

CHN1: chimerin 1, ***CITED1:*** CREB binding protein/p300-interacting transactivator, ***DDIT4:*** DNA damage inducible transcript 4, ***FIGF:*** c-fos induced growth factor, ***FMO4:*** flavin containing monooxygenase 4, ***IL1R2:*** interleukin 1 receptor type II, ***MATN4:*** matrilin 4, ***OLFM1:*** olfactomedin 1, ***RANBP3L:*** RAN binding protein 3-like, ***SEMA4D:*** semaphorin 4D, ***SUCNR1:*** succinate receptor 1

Three genes which were defined as DEG were significantly upregulated at both analyzed time points (Tab. 5.4): DNA damage inducible transcript 4 (*DDIT4*), flavin containing monooxygenase 4 (*FMO4*) and semaphorin 4D (*SEMA4D*) showed log$_2$(FC) between 2.1 and 3.2 due to osmotic upshift.

In general, $\log_2$(FC) of DEGs ranged between 2.1 and 4.1 for upregulated genes while a $\log_2$(FC) of -2.1 was observed for the only downregulated gene matrilin 4 (*MATN4*).

To identify a common biological function of significantly upregulated genes at hyperosmotic culture conditions, GO enrichment analysis was performed. Thus, 7 of 9 genes were assigned to "signal transduction" (GO:0007165), among these chimerin 1 (*CHN1*), CREB binding protein/p300-interacting transactivator (CITED1), c-fos inducing growth factor (*FIGF*),olfactomedin 1 (*OLFM1*) and succinate receptor 1 (*SUCNR1*) as well as *DDIT4* and *SEMA4D*.

5.2.3 Intensification of Hyperosmotic Stress

The earlier osmotic upshift did not benefit the elucidation of the reasons for enhanced energy supply and q_P of hyperosmotically stressed cells. More precisely, although increased n_{ATP} occurred at an earlier time point, proximity to Glc limitation could still not be neglected (Fig. 5.11, Fig. 5.10). Furthermore, results from the preliminary transcriptome analysis did not reveal an informative number of DEGs to describe the dynamic changes in gene expression due to hyperosmotic stimulus. Consequently, the decision to make was to intensify hyperosmotic stress in order to receive more significant results.

Therefore, osmolalities of CHO DP-12 batch cultures (V_R =1.2 L) were increased by 130 or 150 mOsmol kg^{-1} 35 h after inoculation in order to analyze the effect on cell growth, metabolism and cell cycle distribution.

Prior to osmotic upshift (day 1.4) the average osmolality of all three batch cultures was 278 $\pm$ 2 mOsmol kg^{-1} (Fig. 5.14). The subsequent hyperosmotic stimulus (day 1.45) resulted in culture osmolalities of 408 $\pm$ 3 mOsmol kg^{-1} or 425 $\pm$ 2 mOsmol kg^{-1} compared to an osmolality of 280 $\pm$ 2 mOsmol kg^{-1} for reference culture (Fig. 5.14). Osmolalities changed slightly with the time of cultivation reaching maximal values of approximately 290, 418 and 435 mOsmol kg^{-1}, respectively. Thus, reference and hyperosmotic cultures showed a comparable increase in osmolality of +10 mOsmol kg^{-1}.

The pre-shift period was characterized by similar VCDs and viabilities for all CHO DP-12 cell cultures, so that hyperosmotic stimulus occurred at an average VCD of 1.02 $\pm$ 0.05 x 10^6 cells mL^{-1} and at an average viability of 98.9 $\pm$ 0.6% (Fig. 5.14). Hyperosmotic stimulus reduced μ in both cultures from 0.81 d^{-1} (reference) to approximately 0.55 d^{-1} in the post-shift interval day 1.5 to 2.5 and from 0.83 d^{-1} (reference) to $\sim$ 0.40 d^{-1} in the time interval day 2.5 to 3.2. Thus, significantly lower VCD$_{max}$ were observed for cell cultures undergoing hyperosmotic stress. More precisely, the culture with the highest osmolality achieved the lowest VCD$_{max}$ while the highest VCD$_{max}$ was observed at reference conditions (3.2 x 10^6 cells mL^{-1} < 3.8 x 10^6 cells mL^{-1} < 14.0 x 10^6 cells mL^{-1}, Fig. 5.14). After reaching VCD$_{max}$ on culture day 5.5, reference culture showed a direct decline in VCD. In contrast, rather stationary VCDs were observed for hyperosmotic cultures in the same time interval (Fig. 5.14).
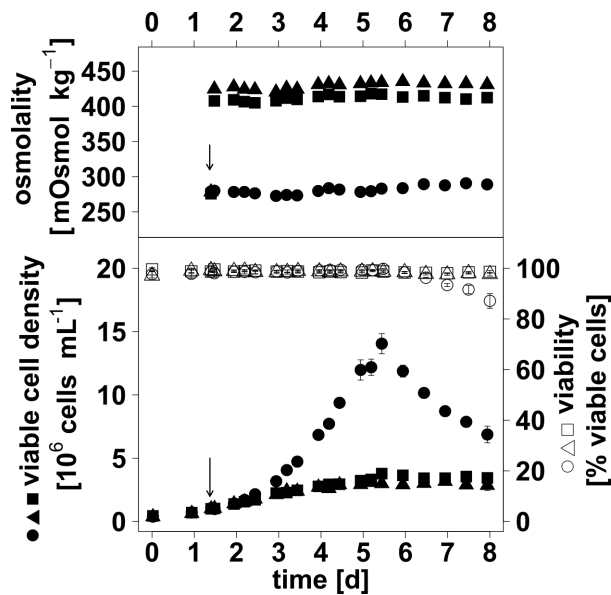
FIGURE 5.14: Increased hyperosmotic stress (+ 130/+ 150 mOsmol kg^{-1}) and its effect on viable cell density and viability of CHO DP-12. Osmolality was increased during bioreactor cultivations of CHO DP-12 (arrow) by the addition of NaCl-enriched TC-42-D cultivation medium 35 h after inoculation (Tab. 4.3). Compared to the reference culture ● ○) osmolality was increased by $\sim$ 130 mOsmol kg^{-1} (■ □) and $\sim$ 150 mOsmol kg^{-1} (▲ △), respectively. Data were determined as described in section 4.2.5. Error bars represent the technical error of the measurements (n = 3).

Viabilities $\geqslant$ 98% were observed for hyperosmotic cultures during the whole time of cultivation. The reference culture showed equally high viability until day 6 followed by a moderate decline which resulted in a viability below 90% on day 8 (Fig. 5.14).

Besides the effects of intensified hyperosmotic stress on cell growth and viability, the influence on n_{ATP} and c_{Glc} was investigated. Starting from an average pre-shift n_{ATP} of 2.51 $\pm$ 0.40 fmol cell^{-1} (day 1.4) intracellular ATP-content was not affected by hyperosmotic stimulus until culture day 4 where approximately 1.8-fold increased n_{ATP} were observed for hyperosmotically stressed cells independent of the exact osmolality (Fig. 5.15 A). CHO DP-12 cells exposed to osmotic upshift showed a further increase in n_{ATP} from day 4 to 5 while n_{ATP} of reference cells remained rather constant. Therefore the aforementioned 1.8-fold difference between n_{ATP} of reference and osmotically stressed cells raised to twofold (Fig. 5.15 A). Noteworthy, hyperosmotic stimulus of 130 or 150 mOsmol kg^{-1} enhanced n_{ATP} from approximately 2.4 to 4.5 fmol cell^{-1} on day 5 of cultivation. Thus, resulting n_{ATP}-levels were 23% higher on day 4 of cultivation compared to previously described levels for a batch culture with an osmolality of 380 mOsmol kg^{-1} (Fig. 5.11).
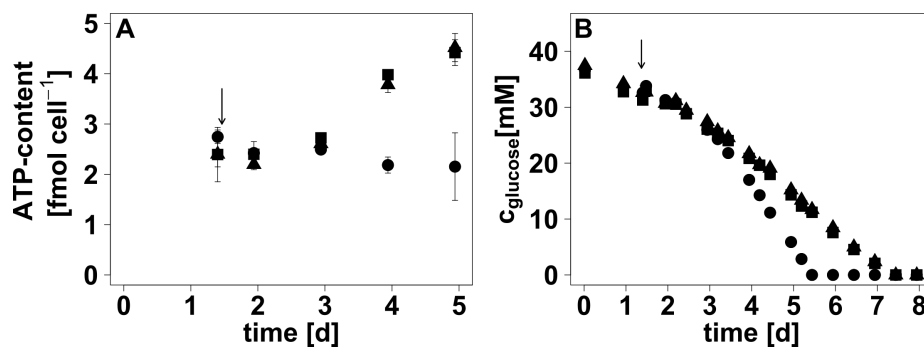
FIGURE 5.15: Influence of hyperosmolality (+ 130/+ 150 mOsmol kg^{-1}) on intracellular ATP-content (A) and glucose concentration (B). Osmolality was increased by the addition of NaCl-enriched cultivation medium 35 h after inoculation of bioreactors with the cell line CHO DP-12 (Tab. 4.3, 4.2.2). While the osmolality of the reference culture was $\sim$ 280 mOsmol kg^{-1} (●), hyperosmotic cultures showed values of $\sim$ 410 mOsmol kg^{-1} (■) or $\sim$ 430 mOsmol kg^{-1} (▲). Intracellular ATP-contents were determined by a combination of a fast filtration approach for 10^7 cells (4.2.3), methanol/chloroform extraction (4.2.4) and HPLC analysis (4.2.5). $c_{glucose}$ was measured enzymatically with LaboTRACE (TRACEAnalytics). Error bars represent the technical error of the measurements (n = 3).

Analysis of c_{Glc} revealed significantly different time courses for reference and hyperosmotic cultures. Starting with similar c_{Glc} profiles in the pre-shift and the 24 h post-shift period, faster decreasing c_{Glc} levels were observed for reference culture in the subsequent time interval. As a result a two days delayed time point for complete consumption of Glc was detected for hyperosmotic cultures which had not been demonstrated in the previous experiments (day 7.5 vs. day 5.5, Fig. 5.15 B). Limiting c_{Glc} occurred in reference culture after day 5 of cultivation with an associated decline in c_{Lac} from 39.1 mM on day 5.5 to 33.2 mM on day 8 (supporting information Fig. A.8). In contrast, hyperosmotic cultures showed lower levels of approximately 30 mM Lac on day 5.5 to 8.

With respect to these results, enhanced n_{ATP} of hyperosmotically stressed cells were observed prior to the Glc limitation of reference cells (Fig. 5.15).

To obtain an idea how osmolalities as high as 410 and 430 mOsmol kg^{-1}, respectively, affected the population composition with respect to cell cycle mapping, percentages of cells in G1-, G2- and S-phase were analyzed directly before and on the following four days of cultivation (Fig. 5.16, supporting information Fig. A.8 B).
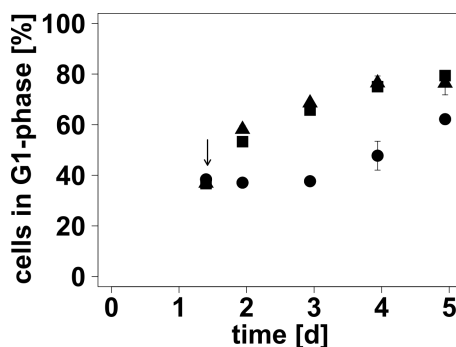
FIGURE 5.16: Effect of osmotic shift (+130/+150 mOsmol kg^{-1}) on the amount of CHO DP-12 cells in G1-phase of cell cycle. NaCl-enriched cultivation medium was added to batch cultures 35 h after inoculation (4.2.2). Osmolality was increased from $\sim$ 280 mOsmol kg^{-1} (reference condition, ●) to $\sim$ 410 (■) or 430 mOsmol kg^{-1} (▲). The determination of cell cycle distribution was based on propidium iodide staining and flow cytometric analysis of the cells (4.2.5). Error bars represent the technical error of the measurements (n = 3).

As previous experiments described an arrest of hyperosmotically stressed cells in G1-phase (5.1), cell cycle analysis focused on the influence of intensified hyperosmotic culture conditions on the percentage of cells in G1-phase. Directly before osmotic upshift in two of three CHO DP-12 batch cultures an average percentage of cells in G1-phase of $37 \pm 2\%$ was determined (Fig. 5.16). This percentage remained rather constant in reference culture until day 3 of cultivation, thus being in concurrence with the cell cycle analysis for the first hyperosmotic stress experiment of this thesis (Fig. 5.2 A). From culture day 3 to 5, cell cycle analysis revealed an increasing number of reference cells in G1-phase, finally reaching 62% (Fig. 5.16). In comparison, the percentages of cells in G1-phase increased approximately 1.5- to 1.6-fold within the first 12 h after osmotic upshift, thereby revealing a higher percentage for the 430 mOsmol kg^{-1} culture (Fig. 5.16). During the following two days of cultivation, a further accumulation of hyperosmotically stressed cells in G1-phase was observed. Thus, approximately 76 - 79% of cells were assigned to G1-phase on day 4 and 5. In contrast to the increasing percentage of cells in G1-phase, the number of cells in S-phase declined from ∼49% on day 1.4 to approximately 14% on day 5 while the percentage of cells in G2-phase decreased only slightly (supporting information Fig. A.8 B).

Concluding, intensified hyperosmotic culture conditions enhanced the previously described effects on cell growth and n_{ATP}. However, hyperosmotically stressed cultures still showed high viability and sufficient cell growth in order to provide enough cells for metabolic and transcriptome analyses. The selected 20 mOsmol kg^{-1} difference in osmotic upshift (+ 130/+ 150 mOsmol kg^{-1}) resulted in insignificant differences and therefore a hyperosmotic stimulus of + 150 mOsmol kg^{-1} was chosen for the subsequent main experiment (5.3). Another important aspect for this decision was that increased osmotic stress levels contributed to more significant results which had been the initial intention of this experiment.

5.3 Metabolic and Transcriptomic Response of CHO DP-12 upon Hyperosmotic Stimulus (+ 150 mOsmol kg^{-1}) 35 h After Inoculation

Results of this section have in parts been published in Pfizenmaier et al. (2016) (manuscript 2 supporting information B.2).

The pivotal results of this thesis were based on seven CHO DP-12 batch cultures (V_R =1.4 L) which were performed in STRs (4.2.2). In order to study the metabolic and transcriptomic response to hyperosmotic culture conditions, four of seven batch cultures were supplemented with NaCl-enriched cultivation medium to increase osmolality by approximately 150 mOsmol kg^{-1} 35 h after inoculation. The other three batch cultures were supplemented with an equal amount of standard cultivation medium and served as references.

5.3.1 Reduced Cell Growth Hampers an Increase in c_P by Enhanced q_P

Starting from an average osmolality of approximately 280 mOsmol kg^{-1} in all seven batch cultures, hyperosmotic stimulus resulted in a highly significantly elevated culture osmolality of $\sim$ 430 mOsmol kg^{-1} for batch cultures exposed to osmotic stress (P < 0.001, Fig. 5.17). The approximately 150 mOsmol kg^{-1} difference in osmolality of reference and hyperosmotic cultures enhanced over time as osmolality of hyperosmotic cultures increased by $\sim$ 10 mOsmol kg^{-1} whereas a slight decrease in osmolality was observed for reference cultures (Fig. 5.17). In response to hyperosmotic culture conditions, significantly reduced μ (Tab. 5.5) were revealed in the post-shift time intervals day 1.5 to 2.5 (0.60 $\pm$ 0.03 d^{-1} vs. 0.68 $\pm$ 0.03 d^{-1}, P < 0.05) and day 3 to 4 (0.26 $\pm$ 0.04 d^{-1} vs. 0.83 $\pm$ 0.08 d^{-1}, P < 0.01), thus resulting in highly significantly lower VCDs from day 2.5 to 8 (P < 0.001, Fig. 5.17). Based on an average VCD of 1.2 $\pm$ 0.1 x 10^6 mL^{-1}, the growth inhibiting effect of hyperosmotic culture conditions reduced VCD$_{max}$ by $\sim$ 67% from 12.0 x 10^6 cells mL^{-1} to 4.0 x 10^6 cells mL^{-1} (Fig. 5.17). After reaching a maximal level

on day 5, reference cultures showed a distinct decline in VCD on the subsequent days of cultivation whereas hyperosmotic cultures maintained VCDs similar to VCD_{max} (Fig. 5.17).
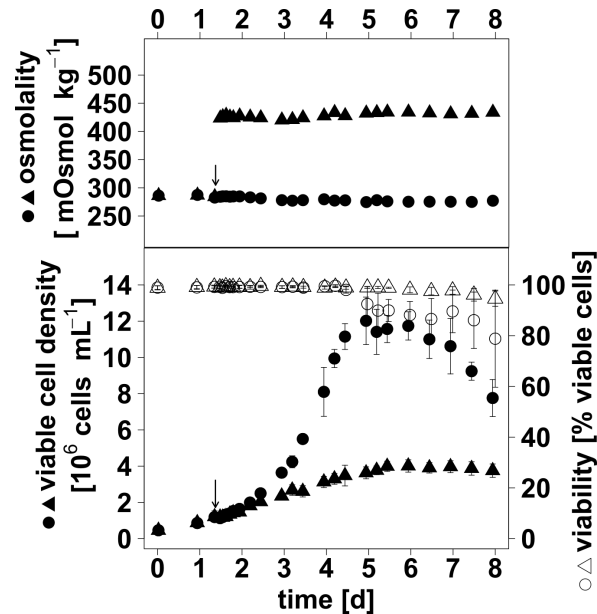
FIGURE 5.17: Profiles of osmolality, viable cell density and viability during batch cultivation of CHO DP-12 with osmotic shift (arrow, +150 mOsmol kg^{-1}). Cells were cultivated in STRs (4.2.2) and osmolality was increased 35 h after inoculation by the addition of NaCl-enriched cultivation medium (n = 4, ▲ △). An equal volume of cultivation medium (Tab. 4.3) was added to reference cultures (n = 3, ● ○). Error bars represent standard deviations for biological replicates considering as well the technical error of measurements (n = 3). Highly significant differences in osmolality (P<0.001, day 1.5 - 8), viable cell density (P<0.001, day 2.5 - 8) and viability (P < 0.001, day 5 - 6.5). With changes to Fig. 1 of manuscript 2 (supporting information B.2).

Analysis of the cellular viability revealed an average percentage of 99.3 ± 0.5% viable cells in batch cultures directly before osmotic upshift (Fig. 5.17). Thereafter similarly high levels (> 98%) were maintained in hyperosmotic cultures until day 6 of cultivation followed by a slight decline in viability to ∼ 95% on day 8. In contrast, an earlier onset (day 5) of decreasing viabilities was observed for reference cultures, thus being in concurrence with the aforementioned starting point for declining VCD (Fig. 5.17). Although the average percentage of viable cells tended to be lower in reference cultures, inter-culture variances hampered the validation of a significant difference compared to viabilities of hyperosmotic cultures (Fig. 5.17).

TABLE 5.5: Effect of hyperosmolality on specific product formation rate and growth rate of CHO DP-12 cells. ** = highly significant difference (P < 0.01), * = significant difference (P < 0.05).

		q_P [pg_{mAb} cell^{-1} d^{-1}]	μ [d^{-1}]
day 1.5 - 2.5 *	reference	13.77 ± 1.02	0.68 ± 0.03
	hyperosmolal	11.46 ± 0.76	0.60 ± 0.03
day 3.0 - 4.0 **	reference	8.05 ± 0.85	0.83 ± 0.08
	hyperosmolal	12.98 ± 0.18	0.26 ± 0.04
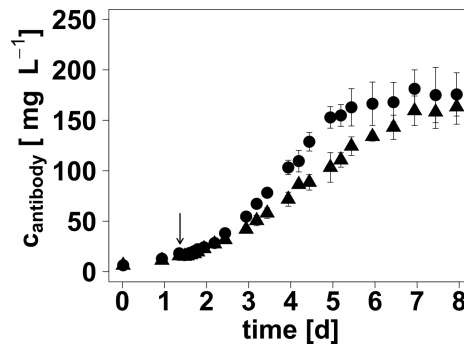
FIGURE 5.18: Time course of the antibody concentration during batch cultivation of CHO DP-12 with osmotic shift (+ 150 mOsmol kg^{-1}). Hyperosmotic culture conditions were induced 35 h after inoculation (arrow) by the addition of NaCl-enriched cultivation medium (Tab. 4.3, 4.2.2). Osmolality of hyperosmotic cultures was $\sim$ 430 mOsmol kg^{-1} (▲) compared to $\sim$ 280 mOsmol kg^{-1} for reference cultures (●). The concentration of the produced anti-IL-8-IgG1 antibody was determined by ELISA as described in 4.2.5. Error bars represent the standard deviation for four biological replicates thereby considering as well the technical error of measurements (n = 3). Highly significantly lower c_P were observed on day 3.5 to 5 (P $\leqslant$ 0.01)

As the cultivated CHO DP-12 cell line produced an anti-IL-8-IgG1 antibody, q_P was determined for the post-shift time intervals day 1.5 to 2.5 and day 3 to 4 (Tab. 5.5). While hyperosmotic stimulus induced significantly reduced q_P on day 1.5 to 2.5 (11.46 $\pm$ 0.76 pg_{mAb} cell^{-1} d^{-1} vs. 13.77 $\pm$ 1.02 pg_{mAb} cell^{-1} d^{-1}, P < 0.05), a highly significantly enhanced q_P was observed in the subsequent time interval (12.98 $\pm$ 0.18 pg_{mAb} cell^{-1} d^{-1} vs. 8.05 $\pm$ 0.85 pg_{mAb} cell^{-1} d^{-1}, P < 0.01). However, the combination of enhanced q_P and reduced μ did not improve c_P. Noteworthy, highly significantly reduced c_P were observed at hyperosmotic culture conditions in the post-shift period day 3.5 to 5.0 whereby this difference between reference and hyperosmotic cultures declined with the time of cultivation

(Tab. 5.18). Thus, final c_P did not significantly differ in hyperosmotic and reference cell cultures (163.3 ± 17.1 mg$_{mAb}$ L^{-1} vs. 175.7 ± 21.4 mg$_{mAb}$ L^{-1} on day 8).

5.3.2 Changes in Metabolic Rates

Concentrations of amino acids, Glc, Lac and NH$_4^+$ were analyzed throughout the time of cultivation, in order to identify characteristic changes in the occurrence of growth-inhibiting levels and in specific metabolite formation rates (q) of substrates (Glc, Gln, Asn) and by products (Lac, NH$_4^+$) due to hyperosmotic stimulus (Tab. 5.6, Fig. 5.19, Fig. 5.20). Furthermore, these analyses contributed to elucidating the relation between hyperosmotic stress and the previously identified enhanced energetic capacity of CHO DP-12 cells (5.1.4, 5.2.3) which as part of the pivotal experiments was studied in more detail (5.3.3).

Hyperosmotic stimulus did not affect metabolic rates in the post-shift time interval day 1.5 to 2.5 (Tab. 5.6). In contrast, significantly increased q_{Gln} (60%, P < 0.01) and $q_{NH_4^+}$ (240%, P < 0.001) were observed for CHO DP-12 cells exposed to hyperosmolality in the subsequent period day 3 to 4 whereas q_{Glc} was significantly reduced (56%, P = 0.05). Thus, hyperosmotic stimulus significantly increased the molar yield in NH$_4^+$ per consumed mol of Gln ($Y_{NH_4^+/Gln}$). Although CHO DP-12 cells metabolized Asn in a non-neglectable manner, Asn formation rates (q_{Asn}) were not affected by culture osmolality. Together with the increased consumption of Glc, hyperosmotically stressed cells showed an elevated q_{Lac} (139%, P = 0.07). With respect to the hyperosmotically induced changes in q_{Glc} and q_{Lac}, the decrease in $Y_{Lac/Glc}$ from one analyzed time interval to the other was less pronounced at hyperosmotic culture conditions. More precisely, $Y_{Lac/Glc}$ levels of approximately 1.32 mol$_{Lac}$ mol$_{Glc}^{-1}$ were revealed for both culture conditions in the post-shift period day 1.5 to 2.5 while $Y_{Lac/Glc}$ of reference and hyperosmotically stressed cells subsequently reduced to 0.73 ± 0.08 mol$_{Lac}$ mol$_{Glc}^{-1}$ and 1.11 ± 0.21 mol$_{Lac}$ mol$_{Glc}^{-1}$, respectively.

TABLE 5.6: Effect of a 150 mOsmol kg^{-1} hyperosmotic stimulus on metabolic rates of CHO DP-12. Hyperosmotic culture conditions were induced in 4 of 7 batch cultures 35 h after inoculation. Reference cultures showed an osmolality of $\sim$ 280 mOsmol kg^{-1} compared to $\sim$ 430 mOsmol kg^{-1} for hyperosmolal cultures. Metabolites were analyzed as described in section 4.2.5 and subsequently specific metabolite formation rates (q) were determined for define time intervals. Values in bold represent significant differences in response to hyperosmotic stimulus (P < 0.05).

	q [pmol cell^{-1} d^{-1}]										
	day 1.5 - 2.5						day 3.0 - 4.0				
metabolite	reference			hyperosmolal			reference			hyperosmolal		
glutamine	-0.96	±	0.08	-0.86	±	0.06	**-0.40**	**±**	**0.05**	**-0.16**	**±**	**0.03**
asparagine	-0.51	±	0.06	-0.46	±	0.03	-0.30	±	0.03	-0.35	±	0.04
glutamate	0.46	±	0.05	0.34	±	0.01	0.12	±	0.04	0.15	±	0.04
ammonium	0.86	±	0.08	0.91	±	0.07	**-0.10**	**±**	**0.02**	**0.14**	**±**	**0.02**
glucose	-3.01	±	0.19	-3.02	±	0.15	**-1.61**	**±**	**0.10**	**-2.52**	**±**	**0.35**
lactate	3.92	±	0.33	3.98	±	0.33	1.18	±	0.19	2.80	±	0.77

The aforementioned hyperosmotically induced differences in metabolic rates affected the profiles of metabolite concentrations. Despite significantly lower VCDs at hyperosmotic culture conditions (Fig. 5.17), elevated q_{Lac} resulted in similar c_{Lac} in hyperosmotic and reference cultures in the post-shift period day 1.5 to 5.5 (Fig. 5.19 A). Subsequently, a further increase in c_{Lac} was observed for hyperosmotic cell cultures, thus achieving a maximal c_{Lac} of 40.7 ± 5.0 mM compared to 34.5 ± 6.8 mM at reference conditions (Fig. 5.19 A). However, high inter-culture variances hampered the validation of significantly elevated c_{Lac} for the time interval day 6 to 8. Starting from rather congruent c_{Glc} profiles, significantly increased c_{Glc} were observed in hyperosmotic cultures in the time interval day 4.5 to 5.0 (P < 0.05). Consequently, hyperosmotic stimulus delayed the occurrence of limiting c_{Glc} by approximately 12 h (day 5.5 vs. day 5.0, Fig. 5.19 A).
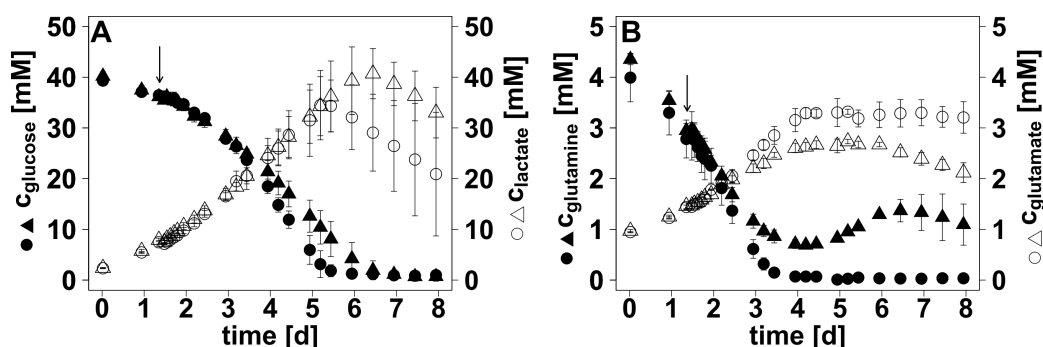
FIGURE 5.19: Profiles of metabolite concentrations during batch cultivation of CHO DP-12 with osmotic shift (arrow, + 150 mOsmol kg^{-1}). NaCl-enriched cultivation medium (Tab. 4.3) was used to increase osmolality 35 h after inoculation (4.2.2). This resulted in an osmolality of $\sim$ 430 mOsmol kg^{-1} for hyperosmotic cultures (n = 4, ▲ △) compared to $\sim$ 280 mOsmol kg^{-1} for reference cultures (n = 3, ● ○). $c_{glucose}$ and $c_{lactate}$ were analyzed enzymatically while $c_{glutamine}$ and $c_{glutamate}$ were determined by HPLC as described in 4.2.5. Error bars represent standard deviations for biological replicates considering as well the technical error of measurements (n = 3).

Starting from an average c_{Gln} of 2.9 $\pm$ 0.3 mM directly before osmotic upshift, reference cultures showed a more distinct decrease in c_{Gln} than hyperosmotic cultures, thus reaching limiting concentrations on culture day 3 (Fig. 5.19 B). Noteworthy, c_{Gln} of hyperosmotic cultures stopped to decline at approximately the same time point although c_{Gln} levels were in the range of $\sim$ 0.7 mM (Fig. 5.19 B). Consequently, no further accumulation of Glu was observed in reference and hyperosmotic cultures. In addition to the aforementioned phenomenon, hyperosmotic culture conditions induced a characteristic accumulation of Gln after reaching the minimal c_{Gln} of 0.7 mM (Fig. 5.19 B). Due to the link between metabolization of Gln and the formation of NH_4^+ which had been shown to be increased due to hyperosmolality in the time interval day 3 to 4, culture specific NH_4^+ levels were determined (Fig. 5.20).

Prior to osmotic upshift and in the post-shift period day 1.5 to 3.5, similar profiles for $c_{NH_4^+}$ were observed in all batch cultures whereby $c_{NH_4^+}$ tended to be slightly higher at hyperosmotic culture conditions (Fig. 5.20). On day 3.5, reference cultures showed a maximal $c_{NH_4^+}$ of 7.7 $\pm$ 0.3 mM compared to 8.3 $\pm$ 0.2 mM for hyperosmotic cultures. Thereafter, reference $c_{NH_4^+}$ declined to approximately 6 mM on day 5.5 whereas hyperosmotic $c_{NH_4^+}$ remained at levels of $\sim$ 8 mM. With respect to the c_{Gln} profile

for hyperosmotic culture conditions a timely concurrence with high $c_{NH_4^+}$ was observed (Fig. 5.19 B, Fig. 5.20).
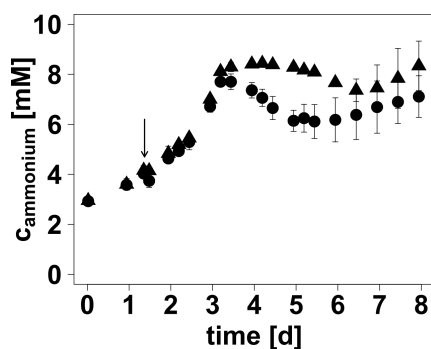
FIGURE 5.20: Effect of hyperosmolality on the accumulation of ammonium in CHO DP-12 culture. Osmolality was increased (arrow) by NaCl-enriched cultivation medium (Tab. 4.3) 35 h after the inoculation of bioreactors (4.2.2). Hyperosmotic cultures (n = 4) showed osmolalities of $\sim$ 430 mOsmol kg^{-1} (▲ △) compared to $\sim$ 280 mOsmol kg^{-1} for reference cultures (n = 3, ● ○). Ammonium concentrations were analyzed with LCK303 cuvette test (Hach) (4.2.5). Error bars represent standard deviations for biological replicates.

5.3.3 Enhanced q_{ATP} and Increased ATP-Pools Reveal a Surplus of Energy

Preliminary experiments indicated a relationship between hyperosmotic culture conditions and elevated intracellular adenine nucleotide pools as well as enhanced q_{ATP} (5.1.4, 5.2.3). Noteworthy, an increase in osmolality from $\sim$ 290 to $\sim$ 390 mOsmol kg^{-1} on day 3 of cultivation resulted in 20 to 39% enhanced q_{ATP} and 1.2- to 2.2-fold elevated n_{ATP} (5.1.4). Furthermore, 1.7- to 2.1-fold increased n_{ATP} were observed for a + 150 mOsmol kg^{-1} osmotic stimulus 35 h after inoculation (5.2.3). The phenomenon of enhanced energetic capacity in response to hyperosmotic culture conditions was examined in more detail on basis of three reference cultures and three cultures exposed to hyperosmotic stimulus (+ 150 mOsmol kg^{-1}) 35 h after inoculation. In this context, datasets were analyzed with respect to statistical significance.

Carbon and oxygen balancing (supporting information Tab. A.2) were applied to determine q_{CO_2} and q_{O_2}, thus revealing 1.4- to 3-fold increased q_{CO_2} at hyperosmotic culture conditions while q_{O_2} were

similarly reduced (supporting information Fig. A.9). Consequently, similar RQs close to the quality criterion RQ $\approx$ 1 (0.9 - 1.1) were determined for cells grown at reference or hyperosmotic culture conditions. q_{ATP} were subsequently calculated on basis of q_{O_2} and the assumption of a P/O ratio of 2.5 (Eq. 4.15, 4.2.7). Thereby, significantly enhanced q_{ATP} (+ 140 - 176%) were observed for hyperosmotically stressed cells in the post-shift time interval day 3 to 6 (Fig. 5.21). Noteworthy, q_{ATP} of osmotically stressed CHO DP-12 cells were in the range of approximately 32 to 44 pmol cell^{-1} d^{-1} compared to $\sim$ 12 to 25 pmol cell^{-1} d^{-1} for reference cells (Fig. 5.21). Considering the possibility of a reduced P/O ratio of 1.5 (2.4) for hyperosmotically stressed cells, q_{ATP} would nevertheless be significantly enhanced in the time intervals day 4 to 5 and day 5 to 6 (P < 0.03).

To obtain information on the subcellular distribution of adenine nucleotides, a compartment-specific fast filtration approach (4.2.3) was utilized to determine pool sizes for the two most important compartments in this context - cytosol and mitochondria. The mitochondrial marker *cis*-aco and the cytosolic markers G6P and F6P were utilized to evaluate the efficiency and quality of the cytosol depleted/mitochondrial samples. While intracellular amounts of G6P and F6P were depleted by approximately 75 - 87%, 81 - 96% of the whole cell *cis*-aco contents were retained in mitochondrial samples (supporting information Tab. A.3).

Starting from similar cytosolic ATP-contents ($n_{ATP_{cyt}}$) of approximately 2.7 fmol cell^{-1} on the pre-shift culture day 1.4, $n_{ATP_{cyt}}$ of hyperosmotically stressed cells steadily increased to 3.66 $\pm$ 0.24 fmol cell^{-1} on day 5 while reference cells showed a decline to 2.04 $\pm$ 0.28 fmol cell^{-1} (Fig. 5.21). Thus, hyperosmotic stimulus resulted in highly significantly elevated $n_{ATP_{cyt}}$ on day 4 and 5 (+1.6-/+1.8-fold, P < 0.01). In comparison, mitochondrial ATP-contents ($n_{ATP_{mit}}$) were $\sim$ 13.5-fold lower than $n_{ATP_{cyt}}$ on day 1.4 (Fig. 5.21, Tab. 5.7). This distinct difference increased even further in the subsequent post-shift period as $n_{ATP_{mit}}$ decreased in both reference and hyperosmotically stressed cells from day 1.4 to 3 followed by rather constant levels of approximately 0.12 $\pm$ 0.02 fmol cell^{-1} for reference cells and $\sim$ 0.19 $\pm$ 0.03 fmol cell^{-1} for hyperosmotically stressed cells (Fig. 5.21, Tab. 5.7). In concurrence with significantly elevated $n_{ATP_{cyt}}$, hyperosmotic stimulus resulted also in significantly increased $n_{ATP_{mit}}$ on day 4 and 5 of cultivation (+1.5-/+1.6-fold, P < 0.05).
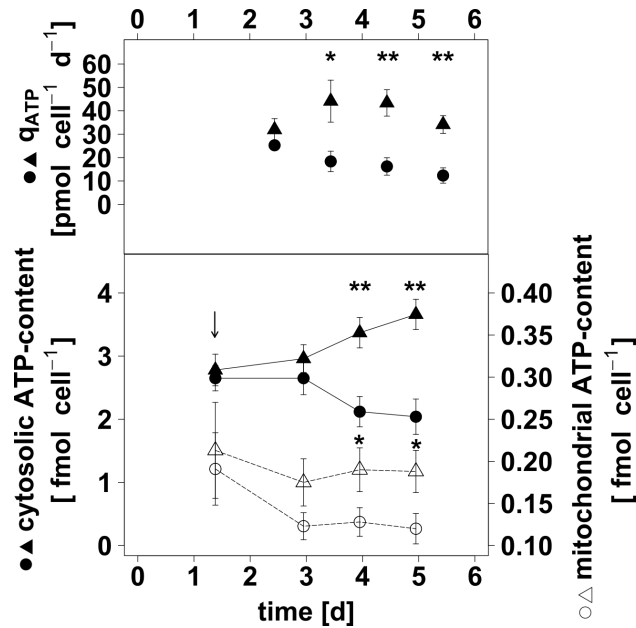
FIGURE 5.21: Changes in cytosolic and mitochondrial ATP-content and ATP formation rates (q$_{ATP}$) at hyperosmotic conditions. Directly before osmotic shift (arrow)and on each of the following days of cultivation a compartment-specific fast filtration approach for 2 x 10^7 cells (4.2.3) was applied to generate whole cell and mitochondrial samples of CHO DP-12. Extraction of metabolites was performed by methanol/chloroform treatment of cell samples (4.2.4) and ATP-concentrations of cell extracts were determined by HPLC (4.2.5). Cytosolic and mitochondrial ATP-contents were calculated according to Eq. 4.17 and Eq. 4.18 (4.2.8). Hyperosmotic cultures (▲ △) showed osmolalities ∼ 430 mOsmol kg^{-1} compared to reference cultures with ∼ 280 mOsmol kg^{-1} (● ○). Error bars represent standard deviations for biological replicates (n = 3). Determination of q$_{ATP}$ was based on C- and O-balancing (4.2.7) and the assumption of a P/O ratio of 2.5 (Balcarcel and Clark, 2003; Hinkle, 2005; Nath and Villadsen, 2015; Wahl et al., 2008). * statistically significant (P < 0.05), ** highly significant difference (P < 0.01) between hyperosmotic and reference conditions. With changes to Fig. 2 of manuscript 2 (supporting information B.2)

TABLE 5.7: Cellular distribution of ATP for reference and hyperosmotically stressed cells. n$_{ATP_{cyt}}$ = cytosolic ATP-content [fmol cell^{-1}], n$_{ATP_{mit}}$ = mitochondrial ATP-content [fmol cell^{-1}].

	n$_{ATP_{cyt}}$/n$_{ATP_{mit}}$	
t [d]	reference	hyperosmolal
1.4	13.9 ± 1.0	13.1 ± 1.2
3.0	21.6 ± 2.1	16.9 ± 1.3
4.0	16.6 ± 1.9	17.7 ± 1.3
5.0	17.0 ± 2.3	19.5 ± 1.3

Hyperosmotic culture conditions may induce changes in cell size, thus influencing intracellular metabolite pool sizes and concentrations. Hyperosmotically stressed CHO DP-12 cells revealed enlarged cell diameters in the post-shift time interval day 2.5 to 3.5. In the subsequent period (day 4) rather similar cell diameters were observed for reference and hyperosmotically stressed cells followed by significantly elevated cell diameters for reference cells from day 4.5 to 5.5 (supporting information Fig. A.10 B). In concurrence with these changes in cell size and previously identified elevated $n_{ATP_{cyt}}$ and $n_{ATP_{mit}}$, hyperosmotically stressed cells showed increased c_{ATP} on day 4 and 5 (day 4: 1.4-fold, P = 0.07, day 5: 2.3-fold, P = 0.001, supporting information Fig. A.10 A).

Regarding the effects of hyperosmotic stimulus on $n_{ATP_{cyt}}$ and $n_{ATP_{mit}}$, similar effects were observed for cytosolic and mitochondrial ADP-contents ($n_{ADP_{cyt}}$, $n_{ADP_{mit}}$, supporting information Fig. A.11), while AMP levels were commonly below the reliable detection limit of HPLC analysis. Noteworthy, with levels of 0.05 $\pm$ 0.01 $fmol_{ADP}$ $cell^{-1}$ and 0.06 $\pm$ 0.01 $fmol_{ADP}$ $cell^{-1}$, hyperosmotically stressed cells showed 1.8- and 2.0-fold higher $n_{ADP_{mit}}$ on culture day 4 and 5 (P < 0.05, Fig. A.11). $n_{ADP_{cyt}}$ were similarly elevated by osmotic upshift as $n_{ADP_{mit}}$ whereby a statistically significant difference could be validated for day 5 (0.31 $\pm$ 0.10 vs. 0.13 $\pm$ 0.02 $fmol_{ADP}$ $cell^{-1}$).
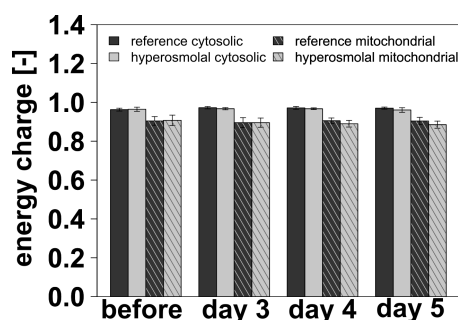
FIGURE 5.22: Cytosolic and mitochondrial adenylate energy charges of CHO DP-12 cells under isotonic and hyperosmotic conditions. Cytosolic and mitochondrial adenine nucleotide contents were analyzed (4.2.3, 4.2.4, 4.2.5, 4.2.8) directly before osmotic shift and on the following days of cultivation. Addition of NaCl-enriched medium 35 h after inoculation resulted in $\sim$ 430 mOsmol kg^{-1} compared to $\sim$ 280 mOsmol kg^{-1} for reference cultures. Energy charges were calculated according to Eq. 4.19 (Atkinson and Walton, 1967). Error bars represent standard deviations for biological replicates (n = 3). Statistically significant difference between mitochondrial and cytosolic energy charges (P < 0.05).

To obtain a better idea of the cellular state at hyperosmotic culture conditions, cytosolic and mitochondrial AEC (AEC_{cyt}, AEC_{mit}) were determined directly before (day 1.4) and in the post-shift period day 3 to 5 (Fig. 5.22). As reliable n_{AMP} were missing for multiple time points, the influence of n_{AMP} on AEC was analyzed on basis of available and reliable AMP data. Consideration of the rather low n_{AMP} levels reduced AEC by 0.01 - 0.02. Due to the minor differences in AECs calculated with or without consideration of n_{AMP}, the following AEC_{cyt} and AEC_{mit} were solely based on $n_{ATP_{cyt}}$ and $n_{ADP_{cyt}}$ or on $n_{ATP_{mit}}$ and $n_{ADP_{mit}}$ (Fig. 5.22).

CHO DP-12 cells of reference and hyperosmotic cultures showed similar physiological AEC_{cyt} and AEC_{mit} (≥ 0.9) directly before osmotic upshift and at all analyzed time points of the post-shift period (Fig. 5.22). More precisely, AEC_{cyt} of both reference and hyperosmotically stressed cells were in the range of 0.97 ± 0.01 compared to significantly lower AEC_{mit} of 0.90 ± 0.02 (P < 0.05, Fig. 5.22).
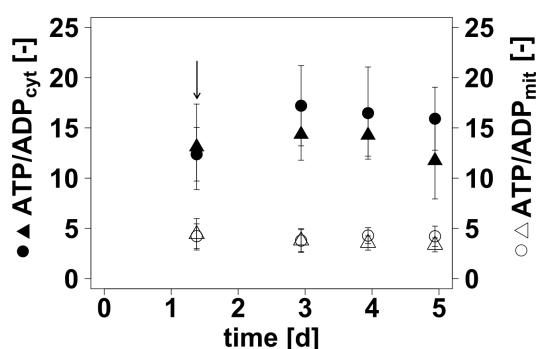
FIGURE 5.23: Cytosolic and mitochondrial ATP/ADP ratios of CHO DP-12. Results for hyperosmotic ($\sim$ 430 mOsmol kg^{-1}, ▲ △) and isotonic conditions ($\sim$ 280 mOsmol kg^{-1}, ● ○) were compared. NaCl-enriched cultivation medium (Tab. 4.3) was used to increase osmolality 35 h after inoculation (arrow) of batch cultures (4.2.2). Adenine nucleotide contents were determined by a combination of a compartment-specific fast filtration approach (4.2.3), methanol/chloroform extraction (4.2.4) as well as HPLC and LC-MS/MS analysis (4.2.5). Eq. 4.17 and Eq. 4.18 were applied to calculated cytosolic and mitochondrial adenine nucleotide pools. Error bars represent standard deviations for biological replicates (n = 3).

A similar result was obtained by comparison of cytosolic n_{ATP}/n_{ADP} ratios (ATP/ADP$_{cyt}$) of reference and hyperosmotically stressed cells as well as for the corresponding mitochondrial counterpart ATP/ADP$_{mit}$ (Fig. 5.23). Although ATP/ADP$_{cyt}$ of cells exposed to hyperosmotic culture conditions tended to be lower than for reference cells, no statistically significant difference was observed.

ATP/ADP$_{mit}$ were approximately 3- to 4.5-fold lower than ATP/ADP$_{cyt}$, whereby ATP/ADP$_{mit}$ of hyperosmotically stressed cell tended to be slightly reduced on day 4 and 5 compared to ATP/ADP$_{mit}$ of reference cells (day 4: 3.5 $\pm$ 0.7 vs. 4.3 $\pm$ 0.8, day 5: 3.4$\pm$ 0.8 vs. 4.2 $\pm$ 1.0).

5.3.4 Quality of RNA and NGS Raw Counts

Cell samples for transcriptome analysis were prepared directly before (0 h) as well as 2, 4, 6 and 8 h after osmotic upshift (+ 150 mOsmol kg^{-1}, 35 h) for three hyperosmotic and two reference batch cultures of antibody producing CHO DP-12 cells (4.2.10). The subsequent isolation, quantification and quality control of RNA by MFT-Services Tübingen revealed c_{RNA} levels between 286 and 1215 ng µL^{-1} with RINs of 9.8 - 10 (supporting information Tab. A.4). These results indicated a very good RNA quality in combination with sufficient amounts of RNA whereby no correlation between culture osmolality and c_{RNA} or RIN was observed (supporting information Tab. A.4).

While sequencing of mRNAs was performed at all aforementioned time points, sequencing of miRNAs was limited to the time point directly before osmotic upshift as well as to the time points 4 h and 8 h after hyperosmotic stimulus. This decision was a consequence of the relatively poor NGS quality for miRNAs in the preliminary transcriptome analysis in combination with a tendency to more distinct differences between reference and hyperosmotic cultures at the posterior of the two analyzed time points (5.2.2).

The quality scores across all bases of a read were in the range of 30 to 40 for all samples, thus showing very good base qualities. Despite the aforementioned problems during the preliminary transcriptome analysis, improvement in NGS for miRNA expression analysis resulted in library sizes of 6 - 13 million reads whereby $\sim$ 42% were mapped to annotated CHO miRNAs. In comparison, NGS for mRNA expression analysis produced libraries of 9 - 11 million reads with approximately 60% of reads being mapped to annotated CHO genes. The resulting mRNA and miRNA raw count datasets were processed according to defined protocols whereby especially low-abundance mRNAs and miRNAs were removed from datasets (supporting information A.2.2, A.2.3). In this context, only those mRNAs showing read counts greater than ten in more than 50% of samples and genes with more than

1 CPM in at least two samples were kept for subsequent analysis of DEGs. Similar filtering criteria were applied on miRNA raw count datasets (A.2.3).

Filtering of low-abundance mRNAs and miRNAs slightly reduced the total number of reads (supporting information Fig. A.15, Fig. A.17 A) However, this effect was less pronounced than the overall differences in library size. TMM and CPM normalization were applied to compensate for sample-specific effects like e. g. differences in library size. Visualization of CPM normalization of filtered mRNA datasets in a boxplot revealed rather similar medians for CPM of different samples (supporting information Fig. A.16, Fig. A.17 B). The same procedure was applied for filtered miRNA datasets, thus showing more distinct differences in median and interquartile regions compared to the results for mRNA. The final application of TMM normalization, negative binomial generalized linear model (GLM) method in combination with tagwise dispersion estimation resulted in a median tagwise BCV of 0.03 for mRNA (BCV_{min} = 0, BCV_{max} = 0.17) and median BCV = 0.11 for miRNA (BCV_{min} = 0.01, BCV_{max} = 0.46). In comparison, a BCV of 0.05 was applied for preliminary transcriptome analysis (5.2.2) due to the lack in biological replicates.

5.3.5 Principal Component and Differential Gene Expression Analysis

Prior to the detailed investigation of changes in mRNA (gene) expression, principal component analysis (PCA) of the rlog-transformed mRNA dataset enabled a more global view at the influence of hyperosmotic stimulus on gene expression of CHO DP-12 cells (Fig. 5.24). About 88% of data variability were preserved in the first and the second principal component (PC1, PC2) whereby projection of all samples onto these components revealed a distinct separation of samples. Noteworthy, all samples derived from batch cultures with osmolalities of approximately 280 mOsmol kg^{-1} clustered at a distinct position in the PC1-PC2-plot, thus indicating low variability in mRNA levels among these 13 samples. On the contrary, the significantly different projection of hyperosmotic and reference samples onto PC1 elucidated a high variability in gene expression due to hyperosmotic stimulus.

Furthermore, projection of samples onto PC2 illustrated a potential time-dependent variability in mRNA levels among hyperosmotic samples (Fig. 5.24).
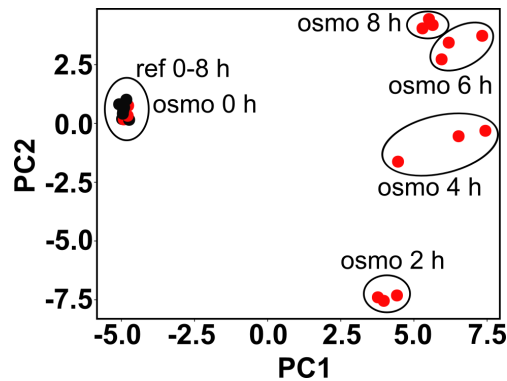
FIGURE 5.24: Principal component analysis for time series data of mRNA expression. The first principal component (PC1) contained 64% and PC2 24% of the variability in the dataset. mRNA expression data were analyzed directly before (0 h) as well as 2, 4, 6 and 8 h after osmotic upshift for reference (black symbols, ref, 280 mOsmol kg^{-1}) and hyperosmotic cultures (red symbols, osmo, 430 mOsmol kg^{-1}).

The subsequent detailed gene expression analysis confirmed the picture of the PCA. Reference cells showed no significant changes in gene expression from one analyzed time point to the other. Furthermore, similar gene expression patterns were observed for all cell cultures directly before osmotic upshift. Thereafter, hyperosmotic stimulus resulted in 4,200 to 4,900 DEGs (P $\leqslant$ 0.02 and FDR $\leqslant$ 0.02), whereby only 5 to 13% of DEGs showed a significant log2(FC) $\geqslant$ |1.0| (Tab. 5.8).

TABLE 5.8: Effect of hyperosmotic stimulus on the number of differentially expressed genes. DEG = differentially expressed gene with P $\leqslant$ 0.02 and FDR $\leqslant$ 0.02, UP = DEG with log2(FC) $\geqslant$ 1.0, DOWN = DEG with log2(FC) $\leqslant$ -1.0, NA = not applicable.

DEG 0 h		DEG 2 h		DEG 4 h		DEG 6 h		DEG 8 h	
0		4,228		4,256		4,876		4,606	
UP	DOWN	UP	DOWN	UP	DOWN	UP	DOWN	UP	DOWN
NA	NA	369	163	232	58	186	60	156	58

Two hours after induction of hyperosmotic culture conditions, 369 genes were significantly upregulated and 163 significantly downregulated with respect to mRNA levels of reference cells at the same time point. Thereafter the number of upregulated genes decreased during each 2 h interval (2 h: 369, 4 h: 232, 6 h: 186, 8 h: 156) whereas the number of downregulated genes decreased from 163 to 58 and remained rather constant afterwards (2 h: 163, 4 h: 58, 6 h: 60, 8 h: 58).

5.3.6 Gene Expression Dynamics and Relation to Biological Function

Hyperosmotic stimulus during batch cultivations of CHO DP-12 cells induced characteristic dynamic changes in gene expression which were illustrated by Venn diagrams (Fig. 5.25, supporting information A.2.7, A.2.8).
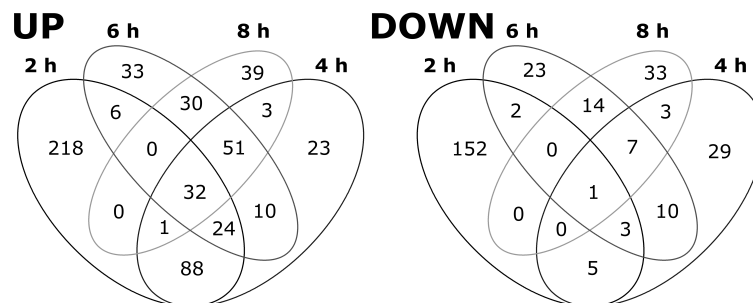
FIGURE 5.25: Venn diagrams for significantly up or downregulated mRNAs at hyperosmotic culture conditions. Osmolality was increased 35 h after inoculation of CHO DP-12 by the addition of NaCl-enriched cultivation medium (280 → 430 mOsmol kg^{-1}, Tab. 4.3, 4.2.2). Cell samples of reference and hyperosmotic cultures were prepared directly before and 2, 4, 6 and 8 h after osmotic shift. Gene expression analysis was based on NGS. Data were analyzed with edgeR and visualized with VennDiagram (4.2.10). mRNAs with log2(FC) $\geqslant$ |1.0|, P $\leqslant$ 0.02 and FDR $\leqslant$ 0.02 were defined as significantly differentially expressed (supporting information A.2.7, A.2.8). With changes to Fig. 3A of manuscript 2 (supporting information B.2)

While approximately 40% of upregulated (218 of 558) and $\sim$ 54% of downregulated genes (152 of 282) were exclusively significantly differentially expressed 2 h after hyperosmotic stimulus, the remaining genes showed different expression dynamics. In general, about 44% of upregulated genes showed significantly elevated mRNA levels at more than one of the four analyzed time points. In contrast, significantly reduced mRNA levels at more than a single time point were observed for only 16% of downregulated genes. In this context, *EGR1* (early growth response 1) was the only gene with significantly downregulated gene expression levels during the whole time of analysis compared to 32 genes (Tab. A.8) with significantly upregulated expression levels at all time points after osmotic upshift (Fig. 5.25).

To investigate dynamic changes in gene expression instead of the number of significantly up-/downregulated DEGs, maSigPro analysis with subsequent hierarchical clustering was applied on the 558 significantly upregulated and the 282 significantly downregulated genes (Fig. 5.26, supporting information Fig. A.18). Furthermore, Gene Ontology (GO) enrichment analyses (4.2.10) were performed for Venn diagram groups and maSigPro clusters in order to elucidate potential correlations between gene expression dynamics and biological functions (Tab. 5.9).

About 50% of the 558 upregulated genes were assigned to one of the nine clusters illustrating distinct gene expression dynamics at hyperosmotic culture conditions (Fig. 5.26, supporting information Fig. A.18). Accordingly, $\sim$ 40% of the 282 downregulated genes were part of one of the 6 clusters for downregulated genes (supporting information A.2.6). Noteworthy, maSigPro analysis revealed no significant time-dependent changes in gene expression for the majority of corresponding genes at reference conditions (Fig. 5.26, supporting information Fig. A.18). Only cluster 4 and 5 for downregulated genes showed a slight increase in the median gene expression from time point 6 h to 8 h.

Some gene groups of the Venn diagram for significantly downregulated genes were assigned to a distinct cluster, e. g. genes with significantly lowered expression levels at time points 6 h and 8 h were part of cluster 5. However, neither gene groups of the Venn diagram nor maSigPro clusters encompassed downregulated genes enriched in specific biological processes.
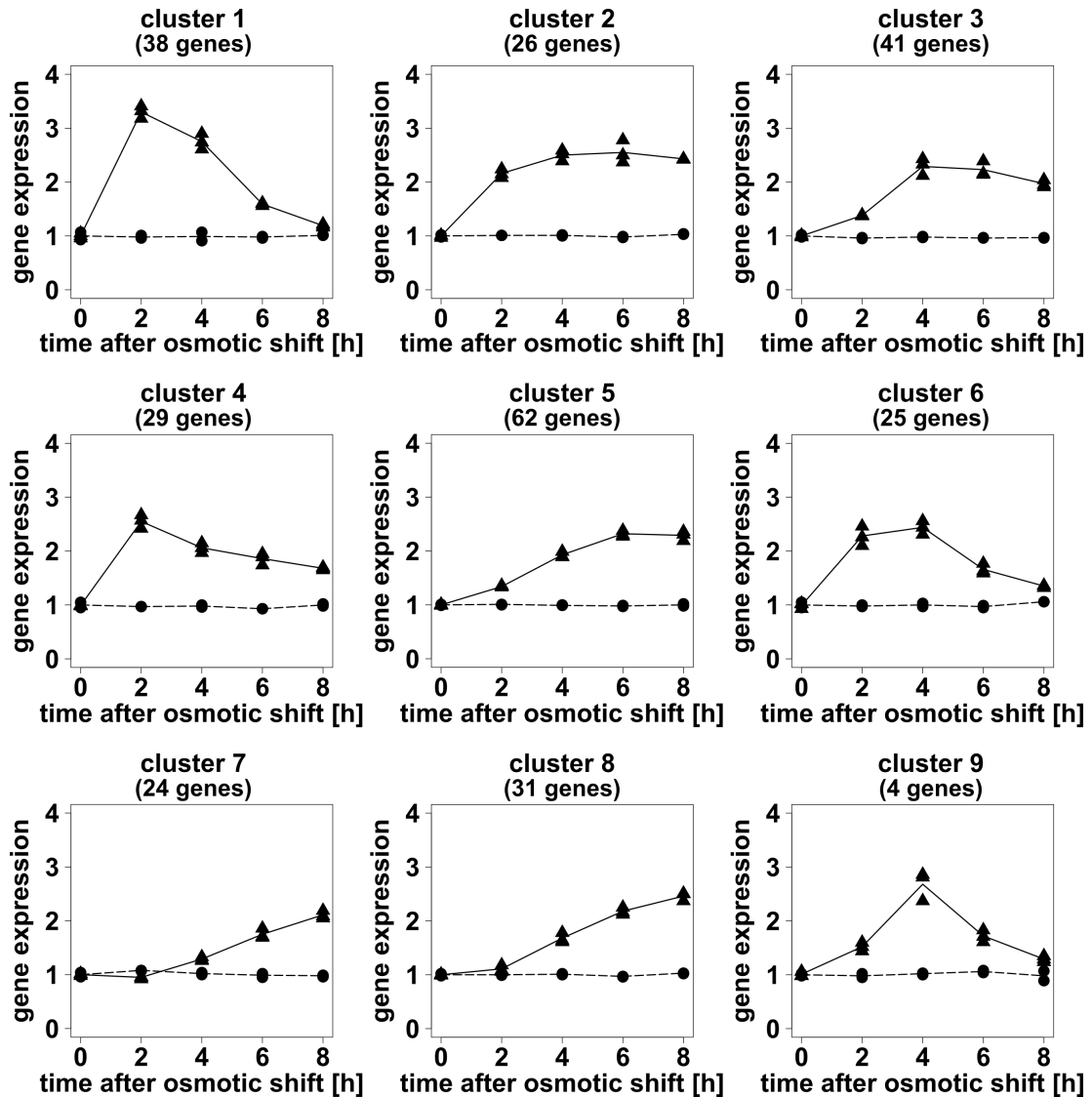
FIGURE 5.26: Clusters of gene expression dynamics of significantly upregulated mRNAs. Osmolality was increased during batch cultivation of CHO DP-12 by the addition of NaCl-enriched cultivation medium (Tab. 4.3, 4.2.2). This resulted in an osmolality of $\sim$ 430 mOsmol kg^{-1} for hyperosmotic cultures (n = 3, ▲) compared to $\sim$ 280 mOsmol kg^{-1} for reference cultures (n = 2, ●). Gene expression analysis was based on NGS and data were analyzed with edgeR and maSigPro (4.2.10). Diagrams show medians of the gene expression of clustered genes. With changes to Fig. 3B of manuscript 2 (supporting information B.2)

In general, results revealed little relation between gene expression dynamics and annotation of genes to defined biological processes. Only four groups of the Venn diagram for significantly upregulated genes as well as maSigPro cluster 3 revealed an enrichment of genes in specific GO-categories (Tab. 5.9).

Genes with significantly upregulated expression at all analyzed time points after hyperosmotic stimulus, were partially involved in "small anatomical structure development" and "negative regulation of cellular metabolic process". One of the genes of the latter GO-category was *CDK1A* which encodes the G1-phase arrest mediating cyclin dependent kinase inhibitor protein 1A (p21, Bedoya-López et al. (2016); Roobol et al. (2011)). Furthermore, *DDIT4* which had already been observed in the preliminary transcriptome analysis was annotated to both of the aforementioned GO-categories (Tab. 5.9). maSigPro analysis assigned 14 of the 32 genes to cluster 2, thus showing short time of response ($\leqslant 2$ h) in combination with rather constantly high gene expression levels (Fig. 5.26, supporting information Tab. A.8). The remaining 18 genes of this gene group were equally distributed among clusters 3, 4, 5 and 6. Significantly upregulated genes at the post-shift time points 4, 6 and 8 h after osmotic upshift were also members of cluster 3 and 5, whereby some of these genes were involved in "cell adhesion" (GO:0007155). A delayed and gradually enhancing gene expression response (cluster 5 or 8) was characteristic for genes encoding Na$^+$-transporting proteins (*ATP1B1*, *SLC28A1*, *SLC5A3* and *SLC6A13*) which were part of the GO-category "cation transport" (Fig. 5.26, Tab. 5.9). These genes were enriched in the Venn diagram group of genes with significantly elevated expression 6 and 8 h after hyperosmotic stimulus (Fig. 5.25). In contrast, genes involved in "cell surface receptor signaling" showed an immediate and short-term response ($\leqslant 2$ h) upon osmotic upshift (Tab. 5.9). The maSigPro cluster 3 was the only one which encompassed genes enriched in a specific biological process, namely "regulation of programmed cell death" (Fig. 5.26, Tab. 5.9).

Besides the aforementioned relations between gene expression dynamics and biological function, gene expression analysis revealed genes encoding proteins with strictly tissue related function. These genes, e. g. mucin 2 (*MUC2*), oviductal glycoprotein 1 (*OVGP1*), interleukin 15 (*IL15*), nebulin (*NEB*) and titin (*TTN*), showed a short time of response ($\leqslant 2$ h) in combination with significantly elevated mRNA levels for at least 6 h after hyperosmotic stimulus (supporting information Tab.A.8, Tab. A.10).

TABLE 5.9: GO enrichment analysis for upregulated genes at indicated time points or for gene cluster.

218 genes (2 h ↑) GO:0007166 cell surface receptor signaling	32 genes (2 h, 4 h, 6 h, 8 h ↑) GO:0048856 small anatomical structure development	GO:0031324 negative regulation of cellular metabolic process
ADORA2A	BCL6	BCL6
AMHR2	CRYAB	CDK1A
BAG3	DDIT4	CRYAB
BCL9L	DYRK3	DDIT4
CDK5R1	ETS2	DUSP1
CELSR3	HEXIM1	ETS2
CHRM4	HOXC6	GPD1L
CNTF	IL15	HEXIM1
DTX2	NEB	IER3
DUOX1	NUPR1	SMYD1
FGFR2	PHEX	SPOCD1
FZD9	SEMA6C	ZBTB38
GPR97	SMYD1	
GRIN2C	TTN	
HIC1		
HOXD3		
ID1	**30 genes (6 h, 8 h ↑) GO:0006812 cation transport**	**51 genes (4 h, 6 h, 8 h ↑) GO:0007155 cell adhesion**
IQUB		
ITGA10	AQP1	COL7A1
ITGAE	ATP1B1	CTGF
JMJD6	ITPR2	GPR98
KIF27	SERINC2	IL7R
KREMEN2	SLC28A1	KIFC3
L1CAM	SLC5A3	LMO7
MYO1G	SLC6A13	MERTK
RLTPR		SEMA4D
SPEN		
SPRY2	**cluster 3 GO:0043067 regulation of programmed cell death**	
TGIF1		
TGIF2		
TLE4		
TNFRSF4	AHI1	DUSP1
WNT5B	BTG2	MKL1
	CLN8	NUPR1
	CTGF	SERPINE1

5.3.7 Osmotic Upshift Induces Upregulation of Seven miRNAs

To obtain information on sample-specific differences in miRNA expression levels, a PCA in combination with subsequent projection of samples onto PC1 and PC2 was performed for the miRNA dataset. The resulting PC1-PC2-plot which preserved 71% of variability in these two PCs did not show distinct clustering of biological replicates, thus revealing considerable variability in miRNA expression levels of biological replicates (Fig. 5.27). The only exception in this context, were the 8 h hyperosmotic treatment samples which were located in close proximity to each other. However, the variability in PC1 seemed to be associated with culture osmolality due to a distinct separation of reference and hyperosmotic samples (Fig. 5.27).
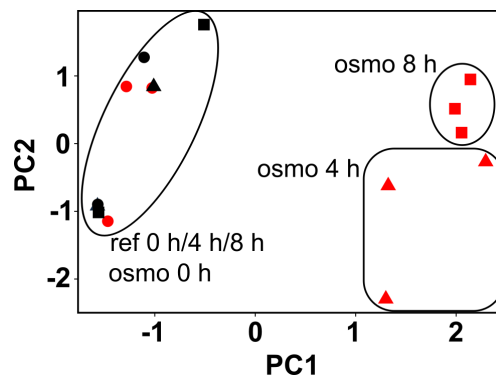
FIGURE 5.27: Principal component analysis for time series data of miRNA expression. The first principal component (PC1) contained 48% and PC2 23% of the variability in the dataset. miRNA expression data were analyzed directly before (0 h, ●, ●) as well as 4 h (▲, ▲) and 8 h (■, ■) after osmotic upshift for reference (ref, 280 mOsmol kg^{-1}, black symbols) and hyperosmotic cultures (osmo, 430 mOsmol kg^{-1}, red symbols).

Detailed analysis of miRNA expression of hyperosmotically stressed CHO DP-12 cells at time points 4 h and 8 h after osmotic upshift revealed seven miRNAs (miR-132-3p, miR-132-5p, miR-182, miR-183, miR-194, miR-215-3p, miR-215-5p) with significantly elevated expression levels (P $\leqslant$ 0.02, FDR $\leqslant$ 0.02, log2(FC) $\geqslant$ 1.0, Tab. 5.10). Noteworthy, hyperosmotic stimulus resulted in a 2.5- to 5.3-fold upregulation of the aforementioned seven miRNAs within the 4 h post-shift period (Tab.5.10). Another four hours later a decrease in differential expression levels was observed for miR-182 (-7%), miR-183 (-13%),

miR-215-5p (-13%), miR-194 (-19%) and miR-215-3p (-43%) whereas the differential expression level of miR-132-5p increased by 23%. In contrast, miR-132-3p showed a constant 4-fold upregulation at both analyzed time points after hyperosmotic stimulus (Tab. 5.10).

TABLE 5.10: Significantly differentially expressed miRNAs due to hyperosmotic shift. Osmolality was increased 35 h after inoculation of CHO DP-12 (280 → 430 mOsmol kg^{-1}). Next generation sequencing (4 and 8 h after osmotic shift) and subsequent data analysis with edgeR revealed significantly upregulated miRNAs in comparison to reference cultures (280 mOsmol kg^{-1}). miRNAs with log2(FC) $\geqslant$ 1.0, P $\leqslant$ 0.02 and FDR $\leqslant$ 0.02 were defined as significantly differentially expressed.

miRNA	log2(FC) 4 h	8 h
cgr-miR-132-3p	2.0	2.0
cgr-miR-132-5p	1.3	1.6
cgr-miR-182	2.4	2.3
cgr-miR-183	1.3	1.1
cgr-miR-194	2.3	2.0
cgr-miR-215-3p	2.3	1.5
cgr-miR-215-5p	2.5	2.3

5.3.8 Prediction of Potential miRNA Targets

miRNAs commonly repress translation of target mRNAs or induce mRNA degradation. To reveal correlations between the observed changes in mRNA and miRNA expression levels, target prediction tools were utilized to identify potential miRNA targets among the significantly up- or downregulated DEGs. Application of miRDB, TargetScan and DIANA-microT resulted in the prediction of 14 to 1609 miRNA targets for a single miRNA, whereby the highest numbers were commonly received from DIANA-microT (Tab. 5.11). However, the numbers of consistently predicted miRNA targets (core targets) on basis of the results of all three target prediction tools ranged between 0 (miR-132-5p, miR-215-3p) and 298. The subsequent comparison of core targets with the lists of significantly up- or downregulated mRNAs revealed a total of 26 potential miRNA targets (up: 17, down: 9). Concluding, miRNA target prediction revealed a total of 26 potential targets for miR-132-3p (5), miR-182 (13), miR-183 (6)

and miR-215-5p (2) whereas no miRNA targets were observed for miR-132-5p, miR-194 and miR-215-3p (Tab. 5.11).

TABLE 5.11: Summary of miRNA target prediction. The miRNA target prediction tools miRDB, TargetScan and DIANA-microT were applied to identify targets (mRNAs) for miRNAs showing significant upregulation in response to hyperosmotic stimulus (4.2.10). $N_{targets_{valid.}}$ = number of validated targets according to independent studies, N_{miRDB} = number of predicted miRNA targets by miRDB, $N_{TargetScan}$ = number of predicted miRNA targets by TargetScan, N_{microT} = number of predicted miRNA targets by DIANA-microT, $N_{core targets}$ = number of consistently predicted miRNA targets by all three tools, $N_{DE core targets}$ = number of consistently predicted miRNA targets and significantly up- or downregulated in the current study, $N_{DE targets_{valid.}}$ = number of targets which were differentially expressed in the current study and validated as miRNA targets in independent studies.

miRNA	$N_{targets_{valid.}}$	N_{miRDB}	$N_{targets_{predicted}}$ $N_{TargetScan}$	N_{microT}	$N_{core targets}$	$N_{DE core targets}$ up	down	$N_{DE targets_{valid.}}$
miR-132-3p	10	364	407	1108	114	3	2	0
miR-132-5p	0	40	407	57	0	NA	NA	NA
miR-182	22	634	1121	1609	298	8	5	2
miR-183	12	376	387	748	147	5	1	1
miR-194	18	291	14	810	9	0	0	0
miR-215-3p	0	212	110	545	0	NA	NA	NA
miR-215-5p	3	132	156	258	24	1	1	0

As all significantly differentially expressed miRNAs were upregulated in response to hyperosmotic culture conditions, gene expression data for predicted miRNA targets (mRNAs) were examined with respect to negative or declining log2(FC). As a result 17 of the 26 potential miRNA targets showed either significantly reduced gene expression levels or a time-dependent decline in differential gene expression (Fig. 5.28). A subsequent GO-enrichment analysis revealed that the majority of the predicted miRNA targets was involved in "regulation of cell proliferation and cell signaling". Altogether, potential miRNA targets were observed for four of the seven significantly upregulated miRNAs (miR-132-3p (3), miR-182 (9), miR-183 (3) and miR-215-5p (2)). Among these miRNA targets were the mRNAs of early growth response 1 (*EGR1*), snail family transcriptional repressor 2 (*SNAI2*) and metastasis suppressor 1 (*MTSS1*) which had been validated as targets of miR-183 or miR-182 in independent studies (Liu et al., 2012; Qu et al., 2013; Sarver et al., 2010; Wang et al., 2012).

		2 h	4 h	6 h	8 h	
cgr-miR-132-3p	FOXP2	-0.32	-1.63	-1.75	-1.35	
	SGK3	-0.17	-0.64	-1.13	-0.78	
	MTSS1*	-0.54	-1.25	-0.86	-0.79	
	ARRDC3	-1.22	-0.47	-0.24	-0.56	
cgr-miR-182	FGD4	-1.03	-0.98	-0.81	-0.55	regulation of cell proliferation and cell signaling
	L1CAM	1.3	0.82	0.31	0.12	
	SLC30A1	1.03	-0.02	-0.04	-0.01	
	SNAI2*	-1.33	-0.42	-0.02	-0.18	
	EGR1*	-2.19	-2.94	-3.25	-3.45	
cgr-miR-183	RHOBTB1	-0.8	-1.01	-0.59	-0.91	
	SPRY2	1.1	0.59	0.07	-0.3	
cgr-miR-215-5p	EREG	1.54	1.18	0.94	0.58	
cgr-miR-132-3p	SLC26A7	1.41	1.5	1.16	0.47	
	HOXA9	-1.23	-0.77	-0.46	-0.3	
cgr-miR-182	INO80D	0.48	0.85	1.04	0.79	miscellaneous
	PDZD2	0.93	1.1	-0.01	0.34	
cgr-miR-215-5p	FRMD4B	-1.05	-0.62	-0.5	-0.31	

FIGURE 5.28: Heatmap of predicted and differentially expressed miRNA targets. miRNA targets (mRNAs) were predicted for significantly upregulated miRNAs with miRDB, TargetScan and microT (4.2.10). The heatmap shows log2-fold-changes (log2(FC)) for consistently identified targets with downregulated or decreasing gene expression levels. All targets were significantly differentially expressed (log2(FC) $\geqslant |1.0|$, P $\leqslant$ 0.02 and FDR $\leqslant$ 0.02) at at least one point during the time of analysis. Functional clustering was based on GO-enrichment analysis (4.2.10). *FOXP2*: forkhead box protein 2, *SGK3*: serum/glucocorticoid regulated kinase 3, *MTSS1*: metastasis suppressor 1, *ARRDC3*: arrestin domain containing 3, *FGD4*: FYVE, RhoGEF and PH domain containing 4, *L1CAM*: L1 cell adhesion molecule, *SLC30A1*: solute carrier family 30 member 1, *SNAI2*: snail family transcriptional repressor 2, *EGR1*: early growth response 1, *RHOBTB1*: Rho related BTB domain containing 1, *SPRY2*: sprouty RTK signaling antagonist 2, *EREG*: epiregulin. $\ast$ = validated in independent studies.

5.4 Hyperosmotic Phenotype of a Cell Line with CHO DG44 Origin

Industrial CHO production cell lines originate from different parental backgrounds, e. g. CHO DG44 or CHO DXB11, and may therefore show differences in the response to changing culture conditions. As the CHO DP-12 cell line of the previous experiments originates from CHO DXB11 the following section investigates the phenotype of a CHO DG44 derived cell line named BIBH1 (kindly provided by Boehringer-Ingelheim Pharma GmbH & Co. KG) in response to hyperosmotic stimulus.

Suitable culture conditions for this purpose were determined in preliminary experiments as part of the bachelor thesis of Elena Bollgönn (Bollgönn, 2014).

5.4.1 Hyperosmolality Enhances Product Formation Rates at Reduced Cell Growth

Designated hyperosmotic culture conditions ($+155$ mOsmol kg^{-1}) were induced in four of eight BIBH1 batch cultures ($V_R = 1.3$ L) by the addition of NaCl-enriched cultivation medium 35 h after inoculation of bioreactors (4.2.2). Each of the other four reference cultures was supplemented with a comparable amount of standard cultivation medium (4.3) to compensate for diluting effects.

Directly before hyperosmotic stimulus (day 1.4) batch cultures showed an average culture osmolality of 283 ± 5 mOsmol kg^{-1} (Fig. 5.29).   Subsequently, addition of NaCl resulted in a significantly elevated culture osmolality of 435 ± 6 mOsmol kg^{-1} ($P \leqslant 0.02$, Fig. Fig.5.29) compared to 281 ± 3 mOsmol kg^{-1} for reference cultures. Osmolalities of both, reference and hyperosmotic cultures, increased by approximately 35 mOsmol kg^{-1} over the time of cultivation, still maintaining the approximately 155 mOsmol kg^{-1} difference between the two types of cultures (Fig. 5.29).

Starting with VCDs of approximately 0.4×10^6 cells mL^{-1} upon inoculation, an average VCD of $1.0 \pm 0.1 \times 10^6$ cells mL^{-1} was observed for batch cultures directly before osmotic upshift (Fig. 5.29). Significantly reduced μ ($P < 0.005$, n = 4, Tab. 5.12) were observed for the post-shift time intervals

day 1.5 to 2.5 (-36%) and day 3 to 4 (-47%), thus resulting in likewise lower VCD at hyperosmolal culture conditions subsequently to day 3 (day 3 - 5: P < 0.05, day 5 - 7: P < 0.01, n = 4). Consequently, an approximately 63% lower VCD_{max} was achieved in hyperosmolal BIBH1 cultures in comparison to reference cultures (3.1 ± 0.4 x 10^6 cells mL^{-1} vs. 8.5 ± 0.8 x 10^6 cells mL^{-1}). Rather similar viabilities ($\geqslant$ 95%) were determined until day 2 of cultivation followed by a tendency to reduced viabilities at hyperosmotic culture conditions whereby no statistically significant difference compared to reference conditions was observed (Fig. 5.29). Viabilities of both reference and hyperosmotic cultures started to decline on day 4.5 of cultivation. Thus, hyperosmotic cultures reached levels below 90% on day 5 and reference cultures on day 6 (Fig. 5.29).
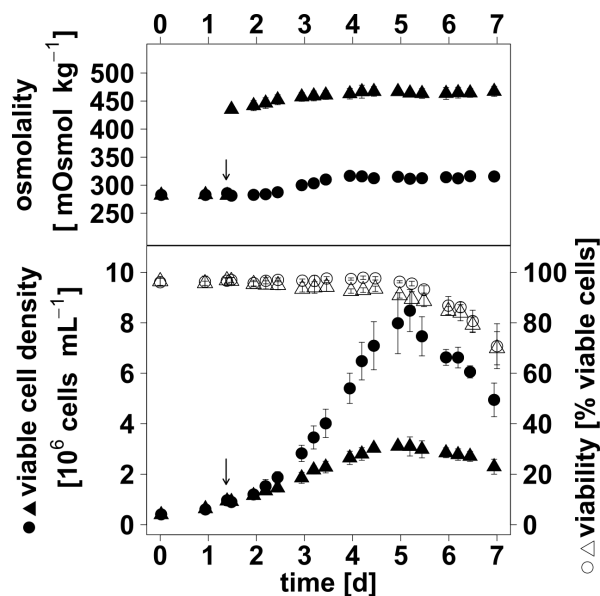
FIGURE 5.29: Influence of hyperosmolality on viable cell density and viability of BIBH1 cells. NaCl-enriched cultivation medium was used to induced hyperosmotic conditions (arrow, ▲ △) 35 h after inoculation of bioreactors (4.2.2). An equal volume of standard cultivation medium was added to reference cultures (● ○). Error bars represent standard deviations for biological replicates (n = 4) considering as well the technical error of measurements (n = 3). Highly significant difference in osmolality between reference and hyperosmotic cultures in the post-shift period (P ⩽ 0.02). Significant difference in viable cell density on day 3 - 5 (P < 0.05) and highly significant difference after day 5 (P < 0.01).

Together with the aforementioned inhibition of cell growth, hyperosmotic culture conditions in-duced a highly significant enhancement of q_P in the post-shift time intervals day 1.5 to 2.5 (+ 46%) and day 3 to 4 (+104%, Tab. 5.12). To be precise, q_P of BIBH1 cells exposed to $\sim$155 mOsmol kg^{-1} higher culture osmolality were as high as 34.55 ± 3.41 pg$_{mAb}$ cell^{-1} d^{-1} and 23.75 ± 3.30 pg$_{mAb}$ cell^{-1} d^{-1} in the aforementioned time intervals compared to 23.67 ± 1.15 pg$_{mAb}$ cell^{-1} d^{-1} and 11.67 ± 3.06 pg$_{mAb}$ cell^{-1} d^{-1} for reference BIBH1 cells (Tab. 5.12). However, enhanced q_P did not significantly improve the final c_P which reached a level of approximately 337 ± 25 mg L^{-1} compared to 320 ± 50 mg L^{-1} for reference culture (supporting information Fig. A.13).

TABLE 5.12: Effect of Hyperosmolality on specific product formation rate and growth rate of BIBH1 cells. Osmotic upshift resulted in an approximately 155 mOsmol kg$_{-1}$ difference in osmolality of reference (280 mOsmol kg^{-1}) and hyperosmolal cultures (435 mOsmol kg^{-1}). ** = highly significant difference (P < 0.005, n = 4), * = significant difference (P < 0.05)

		q_P ** [pg$_{mAb}$ cell^{-1} d^{-1}]			μ * [d^{-1}]		
day 1.5 - 2.5	reference	23.67	$\pm$	1.15	0.77	$\pm$	0.05
	hyperosmolal	34.55	$\pm$	3.41	0.49	$\pm$	0.03
day 3.0 - 4.0	reference	11.67	$\pm$	3.06	0.64	$\pm$	0.03
	hyperosmolal	23.75	$\pm$	3.30	0.34	$\pm$	0.03

5.4.2 Osmotic Upshift Increases the Number of BIBH1 Cells in G1-Phase

In order to analyze whether the DG44-derived BIBH1 cell line showed similar changes in population composition with respect to cell cycle mapping as the DXB11-derived CHO DP-12 cell line, the percent-ages of cells in G1-, S- and G2-phase were determined at the pre-shift time point day 1.4 and on the following days after osmotic upshift (Fig. 5.30).

Cell cycle analysis revealed similar population composition for all BIBH1 batch cultures for the pre-shift time point, with $40 \pm 6\%$ of cells in G1-phase, $43 \pm 6\%$ in S-phase and $17 \pm 2\%$ in G2-phase (Fig. 5.30). In the subsequent post-shift period, hyperosmotic culture conditions induced an accumu-

lation of BIBH1 cells in G1-phase. Noteworthy, on culture day 3.5 52 ± 4% of hyperosmotically stressed BIBH1 cells were assigned to G1-phase followed by a further increase to 71 ± 3% on day 4.5 (Fig. 5.30 A). Thus, the percentage of hyperosmotically stressed cells in G1-phase was significantly higher (P ≤ 0.01, n = 4) than those of reference cells (33 ± 5% and 57 ± 5%).

In conjunction with the accumulation of hyperosmotically stressed cells in G1-phase, the percentages of cells in S- and G2-phase declined from 43 ± 8% on day 1.4 to 22 ± 5% on day 4.5 and from 17 ± 2% to 7 ± 3%, respectively (Fig. 5.30 BC). Although hyperosmotic cultures tended to have lower percentages of cells in S- and G2-phase than reference cultures, elevated inter-culture variances hampered the identification of statistically significant differences (Fig. 5.30).
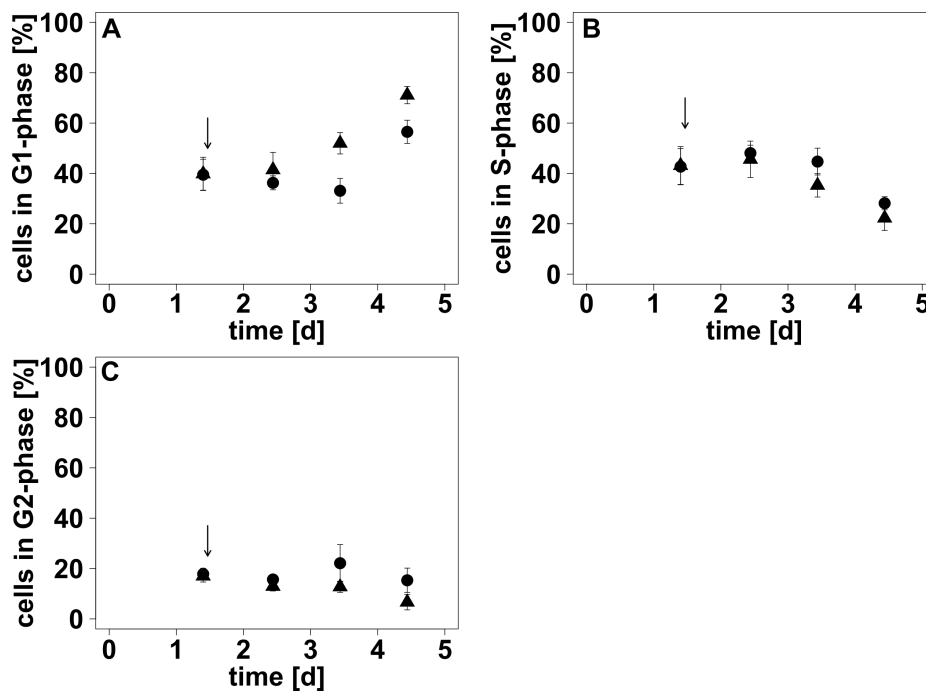
FIGURE 5.30: **Percentage of BIBH1 cells in G1- (A), S- (B) and G2-phase (C) of cell cycle.** Hyperosmotic culture conditions (∼ 435 mOsmol kg⁻¹, ▲) were induced 35 h after inoculation (arrow) by the addition of NaCl-enriched cultivation medium (Tab. 4.3, 4.2.2). Reference cultures showed osmolalities of ∼ 280 mOsmol kg⁻¹ (●). Cell cycle distribution was determined by propidium iodide staining and flow cytometric analysis of cells (4.2.5). Error bars represent standard deviations for biological replicates (n = 4) considering as well the technical error of measurements (n = 3). Highly significant difference in the amount of cells in G1-phase (A) on day 3.5 and 4.5 (P ≤ 0.01).

5.4.3 Hyperosmotically Stressed BIBH1 Cells Show Enhanced Metabolic Activity

Concentrations of the main metabolites Glc, Lac and Gln were analyzed throughout the time of cultivation (Fig. 5.31) and specific metabolite formation rates (q) were calculated for defined time intervals (Tab.5.13). Starting from c_{Glc} of approximately 36 mM in all batch cultures, hyperosmotic BIBH1 cultures showed a decelerated decrease in c_{Glc} and consequently an $\sim$ 12 h delayed entry into Glc limitation (day 4.5 vs. day 4, Fig. 5.31 A). In concurrence with the decelerated decrease in c_{Glc}, a delayed increase in c_{Lac} was observed at hyperosmotic culture conditions, finally reaching a maximal c_{Lac} of 47.1 $\pm$ 2.2 mM on day 5. In comparison, reference cultures revealed a maximal c_{Lac} of 52.1 $\pm$ 2.0 mM on day 4. After reaching maximal values, c_{Lac} declined to 33.3 $\pm$ 2.2 mM in reference cultures and to 38.7 $\pm$ 2.2 mM in hyperosmotic cultures until the end of cultivation (Fig. 5.31 A).

BIBH1 batch cultures showed congruent profiles for c_{Gln} in the pre-shift period day 0 to 1.4, followed by slightly faster decreasing c_{Gln} in hyperosmotic cultures from day 1.45 to 3 (Fig. 5.31 B). Subsequently, limiting c_{Gln} levels (c_{Gln} < 0.5 mM) were revealed for both reference and hyperosmotic cultures on day 3.5 (Fig. 5.31 B). While a further decrease in c_{Gln} was observed in reference cultures, hyperosmotic cultures showed a slight accumulation of Gln.
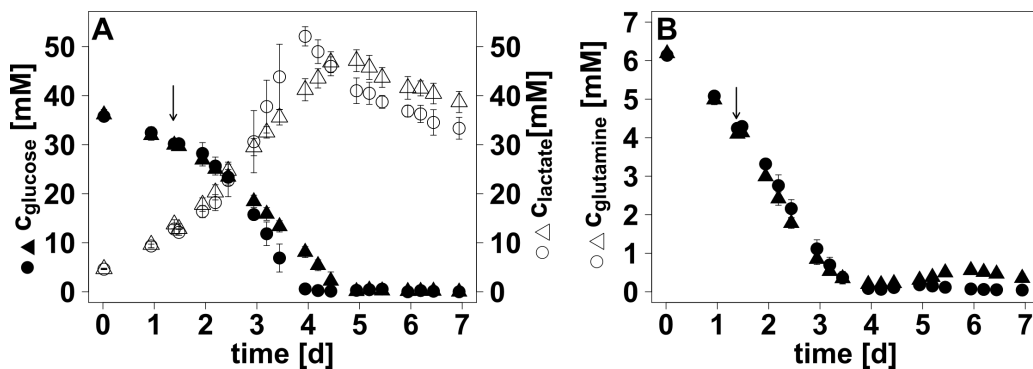
FIGURE 5.31: Concentrations of glucose, lactate (A) and glutamine (B) during batch cultivation of BIBH1 with osmotic shift. Osmolality was increased 35 h after inoculation of bioreactors (arrow, 4.2.2). Reference cultures showed osmolalities $\sim$ 280 mOsmol kg^{-1} ($\bullet$ $\circ$) compared to hyperosmotic cultures with $\sim$ 435 mOsmol kg^{-1} ($\blacktriangle$ $\triangle$). Metabolite concentrations were analyzed as described in 4.2.5. Error bars represent standard deviations for biological replicates (n = 4) considering as well the technical error of measurements (n = 3).

Although hyperosmotic culture conditions caused a decelerated decrease in c_{Glc}, hyperosmotically stressed cells showed significantly enhanced cell specific consumption of Glc in the time interval day 1.5 to 2.5 (q_{Glc} = -5.50 $\pm$ 0.20 vs. -4.40 $\pm$ 0.44 $pmol_{Glc}$ cell^{-1} d^{-1}, P < 0.05, n = 4) and on day 3 to 4 (q_{Glc} = -4.45 $\pm$ 0.10 vs. -3.23 $\pm$ 0.45 $pmol_{Glc}$ cell^{-1} d^{-1}, P < 0.05, n = 4). In concurrence to q_{Glc}, hyperosmotic stimulus resulted in a highly significantly reduced q_{Gln} in the post-shift period day 1.5 to 2.5 (-2.08 $\pm$ 0.01 $pmol_{Gln}$ cell^{-1} d^{-1} vs. -1.40 $\pm$ 0.05 $pmol_{Gln}$ cell^{-1} d^{-1}, P < 0.01, n = 4) and in a significantly lower q_{Gln} in the time interval day 3 to 4 (-0.48 $\pm$ 0.08 $pmol_{Gln}$ cell^{-1} d^{-1} vs. -0.20 $\pm$ 0.00 $pmol_{Gln}$ cell^{-1} d^{-1}, P < 0.05, n = 4). Furthermore, a highly significantly increased q_{Lac} was observed for hyperosmotically stressed cells (10.30 $\pm$ 1.04 $pmol_{Lac}$ cell^{-1} d^{-1} vs. 6.10 $\pm$ 0.89 $pmol_{Lac}$ cell^{-1} d^{-1}) in the post-shift period day 1.5 to 2.5 (Tab. 5.13).

The approximately 69% increase in q_{Lac} in the post-shift period day 1.5 to 2.5 together with the $\sim$ 25% enhanced consumption of Glc resulted in an $\sim$ 25% elevated $Y_{Lac/Glc}$ for hyperosmotically stressed BIBH1 cells (1.73 $\pm$ 0.15 mol_{Lac} mol_{Glc}^{-1} vs. 1.38 $\pm$ 0.07 $_{Lac}$ mol_{Glc}^{-1}, P < 0.05, n = 4). In the subsequent time interval day 3 to 4, $Y_{Lac/Glc}$ of osmotically stressed cells decreased to 1.12 $\pm$ 0.08 mol_{Lac} mol_{Glc}^{-1} while $Y_{Lac/Glc}$ of reference cells remained rather constant (1.33 $\pm$ 0.15 mol_{Lac} mol_{Glc}^{-1}). However, hyperosmotically induced significant differences in $Y_{Lac/Glc}$ could not be validated for the time interval day 3 to 4 (P = 0.12, n = 4).

TABLE 5.13: Effect of Hyperosmolality on metabolic rates of BIBH1 cells. Osmotic upshift resulted in an approximately 155 mOsmol kg^{-1} difference in osmolality of reference (280 mOsmol kg^{-1}) and hyperosmolal cultures (435 mOsmol kg^{-1}). Negative values represent consumption whereas positive values stand for formation. ** = highly significant difference (P < 0.01, n = 4), * = significant difference (P < 0.05, n = 4), ° = no significant difference

		q_{Glc}* [pmol cell^{-1} d^{-1}]			q_{Lac}**/° [pmol cell^{-1} d^{-1}]			q_{Gln}**/* [pmol cell^{-1} d^{-1}]		
day 1.5 - 2.5	reference	- 4.40	$\pm$	0.44	6.10	$\pm$	0.89	- 1.40	$\pm$	0.10
	hyperosmolal	- 5.50	$\pm$	0.20	10.30	$\pm$	1.04	- 2.08	$\pm$	0.05
day 3.0 - 4.0	reference	- 3.23	$\pm$	0.45	4.33	$\pm$	0.91	- 0.20	$\pm$	0.00
	hyperosmolal	- 4.45	$\pm$	0.10	4.98	$\pm$	0.24	- 0.48	$\pm$	0.08

5.4.4 Enhanced ATP Formation Rates Do Not Result in Elevated ATP-Contents

To identify whether BIBH1 would show a comparable enhancement in energetic capacity upon hyperosmotic stimulus as CHO DP-12 cells, q_{ATP}, n_{ATP} and c_{ATP} were determined.

While q_{ATP} of reference and hyperosmotically stressed BIBH1 cells did not differ in the post-shift interval day 2 to 3, significantly enhanced q_{ATP} (+114%/+157%) were determined for hyperosmotically stressed cells in the subsequent period day 3 to 4.5 (Fig. 5.32 A, P < 0.01, n = 4). Noteworthy, q_{ATP} increased from 27.8 ± 6.7 pmol cell^{-1} d^{-1} to 59.7 ± 7.0 pmol cell^{-1} d^{-1} and from 20.5 ± 1.9 pmol cell^{-1} d^{-1} to 52.7 ± 5.6 pmol cell^{-1} d^{-1}, respectively (Fig. 5.32 A).
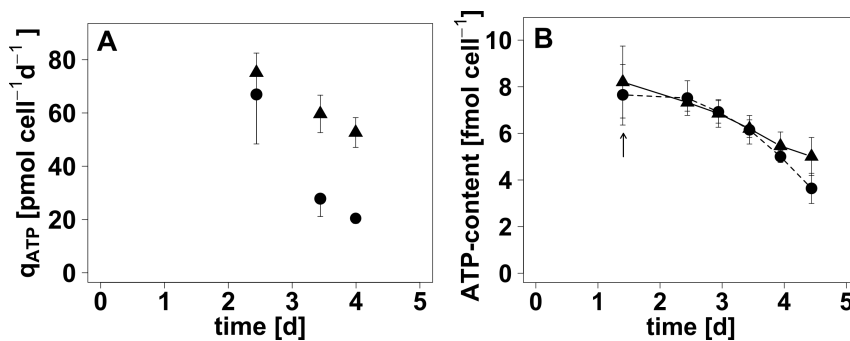
FIGURE 5.32: Effect of hyperosmolality on q_{ATP} (A) and n_{ATP} (B) of BIBH1 cells. Hyperosmotic culture conditions ($\sim$ 435 mOsmol kg^{-1}, ▲) were induced during batch cultivation by the addition of NaCl-enriched medium (arrow). Osmolality of reference cultures was $\sim$ 280 mOsmol kg^{-1} (●). **A**: Determination of q_{ATP} was based on C- and O-balancing (4.2.7) and the assumption of a P/O ratio of 2.5 (Balcarcel and Clark, 2003; Hinkle, 2005; Nath and Villadsen, 2015; Wahl et al., 2008). Error bars represent standard deviations based on four biological replicates each. q_{ATP} were highly significantly elevated in the post-shift time interval day 3 to 4.5 (P < 0.01). **B**: Intracellular ATP-content was determined by a combination of fast filtration approach for 10^7 cells (4.2.3), methanol/chloroform extraction (4.2.4) and HPLC analysis (4.2.5). Error bars represent standard deviations for biological replicates (n = 4) considering as well the technical error of measurements (n = 3).

However, this significant increase in q_{ATP} did not result in likewise elevated n_{ATP}. Starting from an average level of 7.97 ± 1.33 fmol cell^{-1} prior to osmotic upshift, n_{ATP} of reference and hyperosmotically stressed cells declined with the time of cultivation, thereby showing rather congruent profiles until culture day 4 (Fig. 5.32 B). An additional 12 h later, n_{ATP} of reference cells tended to be lower compared to n_{ATP} of cells exposed to hyperosmotic culture conditions (3.64 ± 0.65 fmol$_{ATP}$ cell^{-1} vs. $5.01 \pm$

0.82 fmol$_{ATP}$ cell^{-1}) but this effect was not statistically significant. Likewise, n$_{ADP}$ and n$_{AMP}$ of reference and hyperosmotically stressed BIBH1 cells did not differ significantly although values tended to be elevated at hyperosmotic culture conditions (supporting information Fig. A.14). Consequently, hyperosmotic stimulus did not affect AEC which showed values greater than 0.9 at all analyzed time points.

Analysis of cell diameters for the subsequent calculation of c$_{ATP}$ revealed similar cell sizes in the pre-shift period while significantly elevated cell diameters were determined for BIBH1 cells exposed to hyperosmotic culture conditions in the time interval day 2 to 3.5 (P < 0.05, n = 4, Fig. 5.33 B). In general, cell diameters of hyperosmotically stressed cells ($\sim$ 15 µm) tended to be larger than those of reference cells ($\sim$ 14.0 - 14.5 µm).
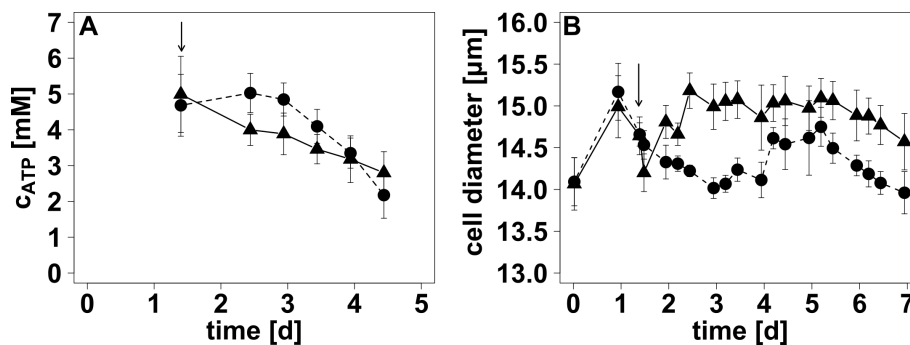
FIGURE 5.33: Time courses for intracellular ATP-concentration (A) and cell diameter (B) of hyperosmotically stressed BIBH1 cells. Osmolality was increased 35 h after inoculation by the addition of NaCl-enriched cultivation medium (arrow). This resulted in an osmolality of $\sim$ 435 mOsmol kg^{-1} (▲) compared to $\sim$ 280 mOsmol kg^{-1} for reference cultures (●). Intracellular ATP-concentrations were analyzed by a combination of a fast filtration approach for 10^7 cells (4.2.3), methanol/chloroform extraction (4.2.4), HPLC analysis (4.2.5) and the assumption of spherical cells. Error bars represent standard deviations for biological replicates (n = 4) considering as well the technical error of measurements (n = 3). Significant difference in cell diameters on day 2 and 2.5 (P < 0.05). Highly significant difference in cell diameters in the time interval day 3 to 3.5 (P $\leqslant$ 0.01).

The calculation of c$_{ATP}$ on basis of cell diameters and n$_{ATP}$ revealed a comparable c$_{ATP}$ level of approximately 4.8 mM for cultures undergoing hyperosmotic treatment and reference cultures on day 1.4 (Fig 5.33 A). Thereafter, hyperosmotically stressed cells showed a steady decline in c$_{ATP}$ finally reaching a value of 2.8 $\pm$ 0.6 mM on day 4.5. In contrast, c$_{ATP}$ of reference cells remained at high

levels of $\sim$ 4.9 mM until culture day 3 followed by a continuous decrease to 2.2 $\pm$ 0.6 mM on day 4.5 (Fig 5.33 A). However, differences in c_{ATP} were not regarded as statistically significant.

6 Discussion

Inhomogeneous mixing, base titration and feeding of concentrated substrate solutions may induce hyperosmotic culture conditions ($\geqslant 350$ mOsmol kg^{-1}) during large scale fed batch production processes of antibody producing CHO cells (Jayapal et al., 2007; Lara et al., 2006; Nienow, 2006; Wurm, 2004). Multiple independent hyperosmolality studies revealed an inhibition of cell growth in combination with a q_P enhancing effect (Han et al., 2010; Lee et al., 2003b; Ryu et al., 2000, 2001; Shen et al., 2010). However, the underlying reason for the enhancement of cellular productivity has not been elucidated so far.

Therefore this thesis characterized the hyperosmotic phenotype of an antibody-producing CHO DP-12 cell line. With respect to the energy consuming process of recombinant protein production, research focused on the analysis of hyperosmotic effects on mitochondrial compartment and cellular energetic capacity. Furthermore, this study combined mRNA and miRNA expression analysis in order to contribute to a better understanding of superimposed transcriptional changes regarding hyperosmotic stress response and to identify suitable targets for q_P enhancing cell line engineering strategies.

6.1 Hyperosmotic Phenotype of CHO DP-12 Cells

The characterization of the hyperosmotic phenotype of CHO DP-12 cells was based on different experimental setups regarding time point (35 h/72 h after inoculation) and intensity of hyperosmotic stimulus ($+100/+130/+150$ mOsmol kg^{-1}) during batch cultivations.

6.1.1 Cell Growth and Metabolism

Hyperosmotic stimulus reduced μ of CHO DP-12 cells in a dose-dependent manner whereby more characteristic differences were commonly observed after a 24 h latency. While a direct correlation between μ and VCD was observed for cell cultures exposed to an osmotic stimulus of +150 mOsmol kg^{-1} (5.3.1), high inter-culture variances hampered the validation of a comparable relation between μ and VCD for a 50 mOsmol kg^{-1} lower osmotic upshift, so that significantly reduced μ did not result in equally different VCD (5.1). In summary, the dose-dependent decrease in μ and VCD was in agreement with previous independent hyperosmolality studies which described decreasing μ and VCD with increasing culture osmolality (Lee et al., 2003a; Ryu et al., 2000, 2001; Shen et al., 2010).

Inhibition of cell growth by hyperosmolality was shown to be associated with DNA damage, thus inducing p53-mediated cell cycle arrest or even apoptosis at osmolalities of approximately 500 mOsmol kg^{-1} (Cherlet and Marc, 1999; Han et al., 2010; Kim and Lee, 2002; Ryu et al., 2001). In this context, first signs for a decline in viability were usually identified at culture osmolalities above 450 mOsmol kg^{-1} (Kim and Lee, 2002; Shen et al., 2010; Zhang et al., 2010). Hyperosmotic CHO DP-12 cultures which formed the basis for the majority of research studies of this thesis showed final culture osmolalities in the range of 380 to 430 mOsmol kg^{-1}, thus being below the critical limit of 450 mOsmol kg^{-1}. Consequently, the observation of similarly high viabilities for both, reference and hyperosmotic cultures (Fig. 5.1, Fig. 5.9, Fig. 5.14, Fig. 5.17), were in agreement with findings of previous independent studies (Kim and Lee, 2002; Shen et al., 2010; Zhang et al., 2010).

Furthermore, cell cycle analysis revealed a dose-dependent accumulation of hyperosmotically stressed CHO DP-12 cells in G1-phase (Fig. 5.2, Fig. 5.16) within the first 12 h after hyperosmotic stimulus followed by a further increase to approximately 75 - 80%. Thus, reduced μ and VCD of CHO DP-12 cells exposed to hyperosmotic culture conditions were shown to be a result of G1-arrest which had also been described by Ryu et al. (2001) for a hyperosmotically stressed antibody-producing CHO cell line.

Independent research studies linked deceleration of cell growth with enhanced cell specific consumption of the main metabolites Glc and Gln (q_{Glc}, q_{Gln} ↓) thereby anticipating a contribution to the

q_P enhancing effect of hyperosmotic culture conditions (Ozturk and Palsson, 1991; Ryu et al., 2000, 2001; Shen et al., 2010). Likewise, specific formation rates for the corresponding by-products Lac and NH_4^+ (q_{Lac}, $q_{NH_4^+}$) were shown to increase upon hyperosmotic stimulus. In this context, $Y_{Lac/Glc}$ and $Y_{NH_4^+/Gln}$ either remained at reference levels or showed significantly elevated values (Ozturk and Palsson, 1991; Shen et al., 2010). In accordance to the aforementioned findings of independent research studies for CHO and murine hybridoma cell lines, q_P of CHO DP-12 cells improved by 50% at 380 mOsmol kg^{-1} (+ 100 mOsmol kg^{-1},) and by 61% at 430 mOsmol kg^{-1} (+ 150 mOsmol kg^{-1}, Tab. 5.6). However, the reduced µ of osmotically stressed CHO DP-12 cells prevented likewise elevated c_P, thus being in agreement with unchanged or even decreased c_P which were described in literature (Kim and Lee, 2002; Lee et al., 2003a; Ozturk and Palsson, 1991; Ryu et al., 2000, 2001; Shen et al., 2010). The aforementioned enhancement in q_P for CHO DP-12 cells exposed to osmotic upshift of + 100 mOsmol kg^{-1} or + 150 mOsmol kg^{-1} (5.1.2, Tab. 5.6) was associated with significantly reduced q_{Glc} in combination with increased q_{Lac}. Furthermore, a hyperosmotic stimulus of 150 mOsmol kg^{-1} significantly elevated $q_{NH_4^+}$ (Tab. 5.6). While the effects of hyperosmolality on q_P, q_{Glc}, q_{Lac} and $q_{NH_4^+}$ of CHO DP-12 cells were in agreement with those described in literature (Ozturk and Palsson, 1991; Ryu et al., 2000, 2001; Shen et al., 2010), the contrary applied for q_{Gln}.

Hyperosmotically stressed CHO DP-12 cells (430 mOsmol kg^{-1}) consumed approximately 60% less Gln than reference cells, whereas Shen et al. (2010) described $\sim$ 40 to 46% enhanced q_{Gln} for a Fc-fusion protein producing CHO B0 cell line grown at comparable culture osmolalities of 410 and 450 mOsmol kg^{-1}, respectively. Strikingly, CHO DP-12 cells exposed to hyperosmotic stimulus 35 h after inoculation (380/430 mOsmol kg^{-1}) stopped metabolization of extracellular Gln on day 4 of cultivation and exported Gln instead, thus resulting in an accumulation in the culture broth (Fig. 5.10 B, Fig. 5.19 B). This phenomenon seemed to be related to high $c_{NH_4^+}$ levels ($\sim$ 8 mM) in combination with the availability of Asn as a second main amino acid substrate. Noteworthy, Asn is metabolized by deamidation in combination with a subsequent transamination of aspartate and α-ketoglutarate into Glu and oxaloacetate which is then fueled into TCA cycle (Zhang et al., 2016a). Consequently, the consumption of 1 mol Asn produces less NH_4^+ than the deamidation and oxidative deamination based metabolization of 1 mol Gln (1 mol instead of 2 mol NH_4^+, 2.4). Therefore, the relatively low

levels of Gln (~ 0.7 mM) compared to c_{Asn} of approximately 2 mM on day 4 in combination with high $c_{NH_4^+}$ (~ 8 mM) may have caused a switch from combined consumption of Asn and Gln towards an exclusive metabolization of Asn. As Glu is an intermediate of Asn metabolization, the observed increase in c_{Gln} may originate from the glutamate-ammonia ligase mediated synthesis of Gln from Glu and NH_4^+ (2.4). This assumption is in part confirmed by comparable but opposite changes in $c_{NH_4^+}$ (-0.7 mM) and c_{Gln} (+ 0.6 mM) in the post-shift period day 4 to 6 (Fig. 5.19 B, Fig. 5.20). In this context, metabolic flux analysis (MFA) would be a suitable tool to validate the aforementioned hypotheses.

Summarizing, except for q_{Gln} all other characteristic changes ($\mu \downarrow$, G1-arrest, $q_P \uparrow$, $q_{Glc} \downarrow$, $q_{Lac} \uparrow$, $q_{NH^+} \uparrow$) of hyperosmotically stressed anti-IL-8-IgG1 producing CHO DP-12 cells were in agreement with previous independent studies. In conclusion, the applied experimental setups provided appropriate conditions for the investigation of the cellular energetic capacity and the transcriptional response of hyperosmotically stressed CHO cells.

6.1.2 Mitochondrial Compartment and Cellular Energetic Capacity

Typical properties of hyperosmotically stressed mammalian cells, e. g. cell cycle arrest, increased cell size and decreased q_{Glc} and q_{Gln}, have been anticipated to contribute to the improvement of q_P (Han et al., 2009; Kiehl et al., 2011; Lee et al., 2003a; Ryu et al., 2000, 2001; Shen et al., 2010). Nevertheless, the extensive characterization of the hyperosmotic phenotype of CHO cells has not revealed the link between hyperosmolality and enhanced cell specific productivity so far. Despite the fact that recombinant protein production represents a metabolic burden for CHO production cell lines, the effect of hyperosmotic culture conditions on cellular energetic capacity has hardly ever been investigated.

The aforementioned circumstance was the motivation for a strong focus on hyperosmotically induced changes in q_{ATP} and intracellular adenine nucleotide pools as part of this research project. In this context, the results of a previous diploma thesis (Pfizenmaier, 2011) which investigated resizing of the mitochondrial compartment upon hyperosmotic stimulus represented the starting point for

further analysis. Strikingly, significantly reduced mitochondrial fluorescence intensities were revealed for CHO cells exposed to hyperosmotic stimulus ($+100$ mOsmol kg^{-1}, Fig. 3.2), thus assuming a reduced size of the mitochondrial compartment and consequently less mitochondrial activity.

These results were in contradiction to findings of previous research studies investigating the effects of hyperosmolality (Lee et al., 2003a; Lin et al.,1999), oxidative stress (Lee et al., 2002a), sodium butyrate treatment (McMurray-Beaulieu et al., 2009) and *CDK1A* overexpression (Bi et al., 2004). Proteome analysis of antibody producing CHO cells grown at a culture osmolality of 450 mOsmol kg^{-1} revealed increased expression levels for the glycolytic enzymes pyruvate kinase and glyceraldehyde-3-phosphate dehydrogenase, thus anticipating an increased production of ATP (Lee et al., 2003a). Lin et al. (1999) investigated energy metabolic fluxes from Glc and Gln in hyperosmotically stressed murine hybridoma cells, thereby assuming complete oxidation for the consumed Gln compared to only 5% complete oxidation for Glc. As a result, enhanced q_{ATP} were observed at hyperosmotic culture conditions and those were subsequently correlated with improved q_P (Lin et al., 1999). Furthermore, the q_P enhancing effect of sodium butyrate treatment was shown to be associated with increased cell specific consumption of O_2 as well as elevated n_{ATP} for recombinant CHO cells (McMurray-Beaulieu et al., 2009). An increase in mitochondrial mass was described for human lung fibroblasts exposed to oxidative stress on basis of mitochondrial fluorescence labeling with 10-n-nonyl-acridine orange and flow cytometric analysis (Lee et al., 2002a). Likewise, overexpression of *CDK1A* resulted in increased mitochondrial mass and mitochondrial dehydrogenase activity in relation to G1-arrest and enhanced q_P (Bi et al., 2004).

While 50% decreased mitochondrial fluorescence intensities were once more described for CHO DP-12 cells exposed to hyperosmotic stimulus ($290 \rightarrow 390$ mOsmol kg^{-1}, Fig. 5.3, $P < 0.01$, $n = 4$), the same experimental setup revealed 20 - 39% enhanced q_{O_2} and q_{ATP} as well as 1.2- to 2.1-fold increased n_{ATP} for hyperosmotically stressed cells (Fig. 5.5). Thus, the observed changes in q_{O_2}, q_{ATP} and n_{ATP} were in agreement with the aforementioned findings of independent hyperosmolality, oxidative stress, sodium butyrate treatment and *CDK1A* overexpression studies (Bi et al., 2004; Lee et al., 2002a, 2003a; Lin et al., 1999; McMurray-Beaulieu et al., 2009) whereas the decrease in mitochondrial fluorescence

intensity was not. Furthermore, the determined levels for q_{O_2}, q_{ATP} and n_{ATP} were in a similar range as values described in literature (Dietmair et al., 2010; Matuszczyk et al., 2015; Miller et al., 1987; Ozturk and Hu, 2005; Sidorenko et al., 2008; Volmer et al., 2011; Wahl et al., 2008). As a consequence, the reliability of the anti-TOM22 antibody-based mitochondrial staining procedure was questioned and additional analyses were performed (5.1.5).

However, control experiments solely revealed hyperosmotically induced changes in cellular structure (Fig. 5.7) which may hamper the binding of the anti-TOM22 antibody to its mitochondrial target. As the mitochondrial compartment was described as a highly dynamic system which changes its morphology by fusion and fission of mitochondrial membranes as a function of the cellular state and requirements, altered energy requirements at hyperosmotic culture conditions may have most likely affected mitochondrial morphology (Campello and Scorrano, 2010; Hock and Kralli, 2009; Pernas and Scorrano, 2016; Scheffler, 2001). Pernas and Scorrano (2016) linked enhanced energy production with proliferation of cristae, thus increasing the IMM area for oxidative phosphorylation. With respect to elevated q_{ATP} and decreased mitochondrial fluorescence one may anticipate that hyperosmotic culture conditions induced similar changes of the mitochondrial compartment, thus hampering the interaction of the anti-TOM22 antibody and OMM target TOM22. Furthermore, Mitra et al. (2009) described the mitochondrial morphology during cell cycle as a conversion from a giant, hyperfused network at G1-S transition to intermediate states of isolated/fragmented elements in S-, G2-, G2-M- and G1-phase. Regarding the arrest of hyperosmotically stressed CHO DP-12 cells in G1-phase of cell cycle, morphological changes of the mitochondrial compartment seemed to be obvious according to the description by Mitra et al. (2009). Nevertheless, declining mitochondrial fluorescence intensities did not directly correlate with changes in cell cycle distribution. Concluding, morphological changes rather than a reduced size of the mitochondrial compartment was anticipated to be the reason for the decrease in mitochondrial fluorescence intensity, thus revealing ineptness of the antibody-based staining procedure.

Enhanced q_{ATP} and n_{ATP} were also validated for an osmotic upshift of $+150$ mOsmol kg^{-1} 35 h after inoculation (Fig. 5.21). In accordance to sodium butyrate treated CHO cells (McMurray-Beaulieu et al.,

2009), osmotically stressed CHO DP-12 cells (390/430 mOsmol kg^{-1}), showed a general increase in intracellular adenine nucleotide pools (n_{ATP} ↑, n_{ADP} ↑), thus maintaining ATP/ADP ratios (e. g. AEC). This picture of increased n_{ATP}, n_{ADP} and unchanged AEC at hyperosmotic culture conditions was refined by analysis of mitochondrial and cytosolic adenine nucleotide pools (Fig. 5.21), thereby confirming that both cytosolic and mitochondrial pool sizes were significantly elevated upon hyperosmotic stimulus while ATP/ADP ratios (AEC, ATP/ADP) remained rather constant (Fig. 5.21, Fig. 5.22, Fig. 5.23). Consequently, research results emphasized the importance of conserved cellular distributions of adenine nucleotides. Strikingly, $n_{ATP_{mit}}$, AEC_{mit} and ATP/ADP$_{mit}$ of reference and hyperosmotically stressed CHO DP-12 cells were significantly lower than their cytosolic counterparts (Tab. 5.7). Nevertheless, these findings were in agreement with previous independent studies for CHO cells, heart myocytes and rat liver (Geisbuhler et al., 1984; Matuszczyk et al., 2015; Schwenke et al., 1981; Soboll et al., 1978) and probably mirrored the cellular strategy with mitochondria as the energy producing "powerhouses" which quickly provide cytosolic processes with the required amounts of ATP.

In accordance to independent research studies (Alfieri and Petronini, 2007; Burg et al., 2007; Kiehl et al., 2011; Lang et al., 1998), cell size of hyperosmotically stressed CHO DP-12 cells increased with the time of cultivation due to the induction of RVI (2.6, Fig. 5.6 B, supporting information Fig. A.10 B). However, changes in q_{ATP} upon hyperosmotic stimulus out-valued by far the required $q_{ATP, +}$ to maintain c_{ATP} with increasing cell size. Accordingly, elevated c_{ATP} were revealed for hyperosmotically stressed CHO DP-12 cells so that RVI was rejected as a reason for increased intracellular adenine nucleotide pools (2.6, Fig. 5.6 B, supporting information Fig. A.10 B).

Starting with the hypothesis of a reduced mitochondrial activity for hyperosmotically stressed CHO DP-12 cells (Pfizenmaier, 2011), further experiments revealed exactly the opposite: enhancement in q_{ATP}, n_{ATP} and c_{ATP} mirrored the improved energetic capacity of hyperosmotically stressed CHO DP-12 cells which may have benefited the increase in q_P as anticipated by independent research studies (Bi et al., 2004; Lee et al., 2003a; Lin et al., 1999; McMurray-Beaulieu et al., 2009). Furthermore, the combination of decelerated cell growth and elevated n_{ATP} revealed a surplus in energy supply which may be utilized to improve cellular productivity even further.

6.1.3 Cell Line Specificity

CHO production cell lines originate from different parental CHO cell lines with deviating genomic backgrounds. Thus, the cellular response upon changing culture conditions may differ from one CHO cell line to another. With respect to the CHO DXB11 origin of the previously discussed CHO DP-12 cell line, the hyperosmotic response of the CHO DG44 derived cell line BIBH1 (kindly provided by Boehringer-Ingelheim Pharma GmbH & Co. KG, Germany) was investigated.

In general, hyperosmotic culture conditions (435 mOsmol kg^{-1}) induced the same characteristic effects as described for CHO DP-12 (5.1, 5.3) and other CHO cell lines (Kim and Lee, 2002; Lee et al., 2003a; Ozturk and Palsson, 1991; Ryu et al., 2000, 2001; Shen et al., 2010). Noteworthy, BIBH1 cells exposed to hyperosmotic stimulus showed significantly increased q_{Lac}, q_P and percentages of cells in G1-phase of cell cycle while μ , q_{Glc} and q_{Gln} were decreased (Tab. 5.12, Tab. 5.13, Fig. 5.30). The latter was contrary to the effect observed for CHO DP-12 cells but was in agreement with findings by Shen et al. (2010). Despite the similarities in the hyperosmotic response of BIBH1 and CHO DP-12 cells the actual values for specific metabolite formation rates of BIBH1 cells were generally 1.4- to 3-fold higher (q_P, q_{Lac}) or lower (q_{Glc}) than those of CHO DP-12 cells, thus revealing an enhanced metabolic activity for BIBH1 cells. Accordingly, n_{ATP} of BIBH1 cells were significantly higher than those of CHO DP-12 cells (8 fmol$_{ATP}$ cell^{-1} vs. 3 fmol$_{ATP}$ cell^{-1}), while c_{ATP} tended to be higher as well (5 mM vs. 4 mM).

With respect to the effect of hyperosmolality on energetic capacity of BIBH1 cells, significantly enhanced q_{ATP} were observed in the post-shift period day 3 to 4.5 while n_{ATP} were not affected at all (Fig. 5.32). The reason for this difference in hyperosmotic response of CHO DP-12 and BIBH1 cells may be as simple as the circumstance that the cell line BIBH1 was developed on basis of Boehringer-Ingelheim's high expression (BI HEX^{TM}) platform, thus holding a potentially better cellular setup to overcome the metabolic burden of recombinant protein production than the low-producing CHO DP-12 cell line. As a consequence, BIBH1 cells are most likely capable of utilizing an existing surplus in energetic capacity directly - a property which seemed to be lacking in CHO DP-12 cells due to the intracellular accumulation of ATP at hyperosmotic culture conditions.

Several cell line engineering approaches focusing on improvement of CHO metabolism have al-

ready been described in literature (Chong et al., 2010; Fogolin et al., 2004; Jeong et al., 2001; Kim and Lee, 2007a,b; Park et al., 2000; Tabuchi and Sugiyama, 2013; Tabuchi et al., 2010; Wlaschin and Hu, 2007b; Zhou et al., 2011). Most of these approaches aimed at reducing the formation of the growth inhibiting by-products Lac and NH_4^+ by (over)expression of *MDH II,* pyruvate kinase, carbamoyl phosphate synthetase I and ornithine transcarbamoylase (Chong et al., 2010; Fogolin et al., 2004; Kim and Lee, 2007b; Park et al., 2000) or downregulation of *LDH* and pyruvate dehydrogenase kinase (Jeong et al., 2001; Kim and Lee, 2007a; Zhou et al., 2011). In comparison to q_{Lac} of optimized cell lines (4 - 5.6 pmol cell^{-1} d^{-1}), even lower values were determined for CHO DP-12 cells while BIBH1 cells showed a tendency to higher q_{Lac}. Nevertheless $Y_{Lac/Glc}$ of both cell lines were in accordance to those of optimized cell lines (Fogolin et al., 2004; Kim and Lee, 2007b), thus indicating that the cellular metabolism of CHO DP-12 and BIBH1 cells has already been optimized regarding in terms of Lac formation. Furthermore, Chong et al. (2010) linked overexpression of *MDH II* with 3.3-fold increased intracellular c_{ATP}. Concluding, even one single difference between two cell lines has the potential to cause significant differences in cellular energy metabolism and may therefore affect productivity.

In summary, the results of the BIBH1 study revealed a rather similar hyperosmotic stress response as observed for CHO DP-12 cells. Particularly, the confirmation of enhanced q_{ATP} upon hyperosmotic stimulus was of utmost importance as this result corroborated the hypothesized correlation between enhanced q_{ATP} and improved q_P.

6.2 Optimization of the Experimental Setup

6.2.1 Time of Analysis and Intensified Hyperosmotic Stress

Optimization of the experimental setup focused on extending the time between hyperosmotic stimulus and the occurrence of limiting c_{Glc} levels in order to diminish a potential influence on the results for cellular energetic capacity. In fact, a 37 h earlier time point for osmotic upshift of + 100 mOsmol kg^{-1} prolonged the time for analysis and revealed elevated n_{ATP} for hyperosmotically stressed CHO DP-12 cells before n_{ATP} of reference cells started to decline (Fig. 5.11). Thus, the differ-

ence in n_{ATP} was associated with hyperosmotic stimulus rather than with nutritional limitation of reference cells. Nevertheless, the differences between reference and hyperosmotic conditions were not as significant as expected at the first moment. Concluding, the time point of osmotic upshift did not significantly impact on the intensity of hyperosmotically induced changes of cell growth and metabolism. In addition, preliminary transcriptome analysis revealed a rather low number of DEGs upon hyperosmotic stimulus (Tab. 5.4). As a consequence, optimization of the experimental setup was applied to contribute to an enhancement of hyperosmotically induced effects. Intensification of hyperosmotic stress was chosen to achieve this aim and in fact hyperosmotic stimuli as high as + 130 or + 150 mOsmol kg^{-1} resulted in the desired significant difference between reference and hyperosmotically stressed CHO DP-12 cells (5.3). In conclusion, results were in agreement with independent hyperosmolality studies which described more significant effects with increasing culture osmolalities (Kim and Lee, 2002; Lee et al., 2003a; Ryu et al., 2000, 2001; Shen et al., 2010).

6.2.2 Transcriptome Analysis

Preliminary transcriptome analysis was performed in order to test sample preparation, sequencing quality, edgeR analysis and to receive a first idea of differential mRNA and miRNA expression upon hyperosmotic stimulus. Although quality and amount of isolated RNA were not affected by culture osmolality and were in an adequate range for subsequent sequencing, NGS for miRNA expression analysis resulted in poor data quality with pretty low numbers for total read counts. Thus, MFTServices Tübingen had to adjust the miRNA library preparation as well as the subsequent sequencing step. As a result, the quality of miRNA sequencing data was significantly improved and consequently provided suitable datasets for the analysis of differential miRNA expression upon hyperosmotic stimulus as part of the main experiment. However, sample-specific differences were still more significant than those of mRNA samples (Fig. 5.24, Fig. 5.27) and were not completely compensated by normalization (supporting information Fig. A.17). The miRNA-specific BCV varied between 0.01 and 0.46 and showed a median BCV of 0.11, thus revealing high sample-specific differences for part of the miRNAs. This may partially be associated to biological variations but may also be related to the fact

that miRNAs are even shorter than one read length ($\sim$ 22 nt vs. 61 nt). Therefore, the whole process of NGS for analysis of miRNA expression, including e. g. library preparation, sequencing, removal of adapter sequences, is far more critical than for mRNA samples and may most likely affect mapping efficiency and consequently sample-specific miRNA expression levels.

In contrast to miRNA datasets, NGS for mRNA expression analysis revealed similarly high total read counts and mapping efficiencies during the preliminary and the main experiment. Furthermore, the applied edgeR protocol efficiently normalized mRNA datasets with respect to differences in library size (supporting information Fig. A.16). Strikingly, preliminary transcriptome analysis revealed a low number of DEGs upon hyperosmotic stimulus, whereby 9 genes were significantly upregulated and one gene significantly downregulated. Unfortunately, the observed DEGs seemed not to contribute to the identification of reasonable transcriptional changes with respect to the hyperosmotic phenotype. These results were assumed to be related to the moderate osmotic upshift. As a consequence, a more intense hyperosmotic stimulus was chosen for the main experiment in order to observe more significant changes in mRNA and miRNA expression.

Regarding the high number of significantly differentially expressed mRNAs upon osmotic upshift in the main experiment, adjustment of hyperosmotic stress level and time of analysis revealed a more precise picture of hyperosmotically induced transcriptional response of CHO DP-12 cells, whereby 6 of the aforementioned 10 DEGs were again shown to be significantly upregulated (*CHN1*, *CITED1*, *DDIT4*, *FIGF*, *OLFM1*, *SEMA4D*). Thus, optimization of the experimental setup still maintained characteristic transcriptional changes of CHO DP-12 cells.

6.3 Transcriptional Response of CHO DP-12 Cells Upon Hyperosmotic Stimulus

NGS for mRNA and miRNA expression analysis revealed a total of 558 mRNAs (supporting information A.2.7) and 7 miRNAs (Tab. 5.10) with significantly upregulated expression levels during the 8 h time interval after osmotic upshift (280 $\rightarrow$ 430 mOsmol kg^{-1}). In contrast, 282 mRNAs were signifi-

cantly downregulated (supporting information A.2.8). However, while miRNAs were significantly upregulated at both of the analyzed time points after osmotic upshift (4 h, 8 h), a diversity of expression dynamics was revealed for differentially expressed mRNAs (Fig. 5.25, Fig. 5.26, supporting information Fig. A.18). Strikingly, genes with similar expression profiles were not necessarily assigned to specific biological processes.

6.3.1 Conserved Gene Expression Changes

Burg et al. (2007) reviewed the response of mammalian cells to hyperosmotic stresses and summarized characteristic changes in gene and protein expression. A comparison to the statistically significant gene expression changes of hyperosmotically stressed CHO DP-12 cells revealed similarly elevated mRNA levels for the eight genes ATPase Na^+/K^+ transporting beta 1 polypeptide (*ATP1B1*), aquaporin 1 (*AQP1*), solute carrier family 38 member 2 (*SLC38A2*), solute carrier family 6 member 6 (*SLC6A6* = *TAUT*), nuclear factor of activated T-cells 5 (*NFAT5*), crystallin alpha B (*CRYAB*), *HSP110* and *HSPA4L* encoding channel proteins, transporters, transcription factors and chaperones. According to independent studies (Alfieri and Petronini, 2007; Burg et al., 2007; Lang et al., 1998) the transporters ATP1B1, SLC38A2 and SLC6A6 were involved in osmoregulation and RVI (2.6), thus mediating replacement of intracellularly accumulated Na^+ with K^+ (ATP1B1) or influx of osmolytes, e. g. neutral amino acids (SLC38A2) or taurine (SLC6A6).

Furthermore, the differential expression of 57 genes (upregulated: 28, downregulated: 29) were in agreement with the microarray based transcriptional response of an osmotically stressed CHO B0 cell line producing Fc-fusion protein (Shen et al. (2010), Tab. A.2.9). Surprisingly, all genes which were assigned to cell metabolism (Tab. A.2.9), were downregulated although an increased metabolic activity was observed in the present and in several independent studies (Ryu et al., 2000; Shen et al., 2010; Zhu et al., 2005). However, none of these genes encoded a protein involved in central metabolism (2.4). In contrast, proteins related to cell death (*DDIT4*, *GLCCI1*) or cell proliferation (*PLK2*) were upregulated. Despite the similarity of gene expression changes for 57 genes, only 16 thereof were significantly differentially expressed regarding the applied threshold ($\log_2(\text{FC}) \geqslant |1.0|$, $P \leqslant 0.02$) and FDR $\leqslant 0.02$) and

were consequently defined as CHO specific expression markers for NaCl-induced hyperosmotic culture conditions (Tab. A.2.9). With respect to a total of 800 significantly up- or downregulated genes in the present study, the number of conserved gene expression changes was rather low. This might either be related to cell line specificity as anticipated by Shen et al. (2010) or to the limited number of genes that is commonly considered by microarray based transcriptome studies. Therefore, future NGS studies may reveal an additional number of CHO specific gene expression changes.

6.3.2 Gene Expression Dynamics and Relation to the Hyperosmotic Phenotype

Analysis of mRNA expression revealed a highly dynamic transcriptional response for CHO DP-12 cells exposed to hyperosmotic culture conditions (Fig. 5.24, Fig. 5.25, Fig. 5.26). Unfortunately, mRNAs with comparable expression patterns were not necessarily assigned to a specific biological process (Tab. 5.9). However, mRNA expression levels for genes encoding proteins involved in "negative regulation of cellular metabolic process" quickly responded upon osmotic upshift and were significantly upregulated at all analyzed post-shift time points. Among these was *CDK1A* which had been shown to induce G1-arrest and enhancement in q_P in CHO producer cell lines (Bi et al., 2004; Fussenegger et al., 1998). Likewise, independent research studies on q_P enhancing culture conditions revealed that cell cycle arrest upon temperature downshift (37°C $\rightarrow$ 30 - 33°C) or sodium butyrate treatment was associated with upregulation of genes encoding CDK inhibitors, e. g. *CDK1A, CDKN2C, CDKN2A* (Bedoya-López et al., 2016; Kaufmann et al., 1999; Klausing et al., 2011; Roobol et al., 2011; Trummer et al., 2006; Yee et al., 2008). Hence, targeted overexpression of *CDK1A* or upregulation of different CDK-inhibitors in response to cellular stress conditions were related to the same phenotypic effects which were induced by hyperosmolality. Furthermore, Bi et al. (2004) associated *CDK1A* overexpression with increased mitochondrial mass and mitochondrial dehydrogenase activity on basis of Mito Tracker Green FM or 3-(4, 5-dimethyliazol-2-yl)-2,5-diphenyl tetrazolium bromide (MTT) staining and subsequent flow cytometric analysis. Once more, these results were in agreement with the hyperosmotically induced enhancement of q_{O_2}, q_{ATP} and n_{ATP}. Thus, it is anticipated that upregulation of *CDK1A* expression upon hyperosmotic stimulus plays a central role in the hyperosmotic stress response and for the

development of the hyperosmotic phenotype of CHO DP-12 cells.

Regarding the regulatory network of mammalian cell cycle, mRNA expression levels of *CDK1A*'s transcriptional activator p53 (He et al., 2005; Poon, 2016) as well as expression of several genes encoding related protein kinases, e. g. ATM, CHK1/2, were not affected by hyperosmotic stimulus which might be due to a continuous basal expression to enable a quick activation by phosphorylation if required (Poon, 2016). In contrast, the components cyclin D and E of the CDK1A inhibited complexes cyclin D/CDK4 and cyclin E/CDK2 (He et al., 2005; Poon, 2016) showed significantly downregulated mRNA expression levels 4 h after osmotic upshift (*CCND1*, log2(FC): -0.6 (2 h), -1.2 (4 h), -1.0 (6 h), -1.1 (8 h)) or declining expression levels (*CCNE1*, log2(FC): -0.3 (2 h), -0.7 (4 h), -0.8 (6 h), -1.0 (8 h)).

In general, the group of genes with immediate and significant changes in gene expression levels upon hyperosmotic stimulus were expected to include sensors, inducers and regulators of major stress response pathways. In deed, the majority of DEGs with exclusively significantly elevated expression levels 2 h after hyperosmotic stimulus were assigned "cell surface receptor signaling" function. Strikingly, *SPRY2*, a predicted miR-183 target which had been described as negative regulator of *CDK1A* by Zhang et al. (2016b) was part of the aforementioned gene group, thus linking *SPRY2* gene expression dynamics to the occurrence of G1-arrest.

Steadily increasing mRNA expression levels were characteristic for genes involved in "cation transport" which finally reached significantly elevated log2(FC) ($\geqslant 1.0$) 6 h after osmotic upshift. According to independent research studies (Alfieri and Petronini, 2007; Kwon et al., 1992; Lang et al., 1998; Zhou et al., 2012), four of the seven genes of this group were involved in the process of RVI which was characteristic for CHO DP-12 cells undergoing hyperosmotic treatment. More precisely, the upregulated Na^+/*myo*-inositol transporter SLC5A3, Na^+/taurine transporter SLC6A13 and AQP1 were shown to mediate cellular influx of osmolytes and water while ATP1B1 enabled replacement of Na^+ with K^+, thus stabilizing cellular function (Alfieri and Petronini, 2007; Kwon et al., 1992; Lang et al., 1998; Zhou et al., 2012).

The only maSigPro cluster revealing enrichment of genes involved in a specific biological process was cluster 3 which encompassed several genes related to "regulation of programmed cell death". Among these was a gene encoding dual specificity phosphatase (*DUSP1*) which was shown to be in-

duced by p53 in response to cellular stress, e. g. oxidative or nutritional stress (Liu et al., 2008). DUSP1 itself inhibited mitogen-activated protein kinase (MAPK) by phosphorylation, thus hampering cell growth and proliferation (Liu et al., 2008) similar to the observed effects of hyperosmolality on CHO DP-12 cells. Likewise, p53-mediated induction was described for the BTG family member 2 (BTG2, Guardavaccaro et al. (2000)) which was significantly upregulated upon hyperosmotic stimulus in CHO DP-12 cells. Furthermore, expression of BTG2 in mouse embryo fibroblasts was shown to result in hypophosphorylated pRb protein, thus inducing G1-arrest accompanied with downregulation of CCND1 protein expression (Guardavaccaro et al., 2000). Therefore, hyperosmotically induced upregulation of BTG2 in combination with significantly downregulated *CCND1* expression and G1-arrest were in agreement with the aforementioned results of independent research studies.

Transcriptome analysis revealed no direct link between differential gene expression and elevated n_{ATP} and q_{ATP}. This may be due to the fact that the transcriptional response was analyzed about two days before significantly different n_{ATP} and q_{ATP} were detected for hyperosmotically stressed cells. Furthermore, metabolic pathways, e. g. glycolysis and TCA cycle, which contribute to the synthesis of ATP are highly regulated at the level of metabolic enzymes and metabolic flux. $n_{AMP/ATP}$ or $n_{ADP/ATP}$ influence the activity of metabolic enzymes as a measure of cellular energy demand (Berg et al., 2003; Brüser et al., 2012; Fenton and Hutchinson, 2009; Martínez-Costa et al., 2012). Thereby, AMP, ADP and ATP are common allosteric effector nucleotides of metabolic enzymes, thus enabling responses of cell metabolism at the second time scale (turnover rate of 1.5 mM s^{-1} for ATP) whereas the transcriptional response is several magnitudes slower (Oldiges et al., 2007; Wurm et al., 2010). Consequently, the identification of a direct link between gene expression and ATP synthesis is anticipated to be rather difficult.

In conclusion, gene groups with assigned biological functions contained genes which are anticipated to contribute to the observed hyperosmotic phenotype, e. g. G1-arrest, RVI, of CHO DP-12 cells with respect to research results of independent studies.

6.3.3 Correlations Between Differential miRNA Expression and the Hyperosmotic Phenotype of CHO DP-12 Cells

Hyperosmotic culture conditions induced inhibition of cell growth by G1-arrest while q_P was improved. During the last five years, miRNA-based cell line engineering approaches to enhance q_P of CHO cells applied transient or stable overexpression of a variety of different miRNAs, namely *cgr*-miR-17, *cgr*-miR-19b, *cgr*-miR-20a, *cgr*-miR-92a, *cgr*-miR-2861, *mmu*-miR-30 family members, *hsa*-miR-7, *hsa*-miR-1287 and *hsa*-miR-557 (Barron et al., 2011a; Fischer et al., 2015b,c; Jadhav et al., 2014; Loh et al., 2014; Meleady et al., 2012; Strotbek et al., 2013). Commonly, these approaches achieved 1.2 to 2.5-fold enhanced q_P together with improved or unchanged cell growth, thus resulting in significantly elevated c_P. In contrast, the cell growth inhibiting effect of miR-7 or miR-30 family members in combination with enhanced q_P hampered an improvement in final c_P (Barron et al., 2011a; Fischer et al., 2014, 2015b). Besides the enhancement of cellular productivity by overexpression of miRNAs, Kelly et al. (2015a) and Kelly et al. (2015b) were able to improve q_P by a miRNA sponge mediated functional inhibition of miR-23 and miR-34a, respectively. Another approach achieved increased VCD, prolonged viability and enhanced q_P by utilizing an antagomir to inhibit the pro-apoptotic function of *mmu*-miR-466-5p (Druz et al., 2011, 2013).

Despite the q_P enhancing effect of hyperosmotic culture conditions, none of the seven significantly differentially expressed miRNAs (Tab. 5.10) was among the finally applied cell line engineering targets of the aforementioned research studies. In addition, research studies on characteristic miRNA expression patterns in relation to µ, low cultivation temperature or histone deacetylase inhibition (Barron et al., 2011b; Clarke et al., 2012; Fischer et al., 2015c; Gammell et al., 2007) showed no similarities to the hyperosmotic stress response of CHO DP-12 cells. Nevertheless, Strotbek et al. (2013) transiently transfected an antibody producing CHO DG44 cell line with *hsa*-miR-183 during their miRNA screening studies, thus revealing significantly enhanced q_P in combination with decreased VCD. Strikingly, these effects of *hsa*-miR-183 were in accordance with the hyperosmotic phenotype of CHO DP-12 cells and therefore miR-183 was assumed to play an important role in cell cycle arrest and improvement of cellular productivity. The involvement in cell cycle arrest was corroborated by the fact that the three

predicted miR-183 targets were shown to be involved in cell proliferation. The most interesting one in this context was the transcription factor EGR1 which was validated as miR-183 target and was revealed to promote tumor migration (Sarver et al., 2010). Accordingly, Sells et al. (1995) described a EGR1-mediated delay of IL-1 induced G0/G1-arrest in human melanoma cells while Parpa et al. (2009) inhibited growth of human prostate carcinoma cell lines by downregulation of *EGR1*. Furthermore, hepatocytes of mice exposed to carbon tetrachloride required EGR1 for cell cycle entry from G0- to G1-phase and for G1-S transition (Pritchard et al., 2011). The aforementioned tumor growth enhancing function of EGR1 was confirmed by other research studies (Scharnhorst et al., 2000; Virolle et al., 2003).

Concluding, the hyperosmotically induced increase in *cgr*-miR-183 expression together with downregulation of *EGR1* and G1-arrest depicted exactly the same picture which had been described for multiple cancer cell lines (Parpa et al., 2009; Pritchard et al., 2011; Sarver et al., 2010; Sells et al., 1995). In contrast, some other research studies described EGR1 as positive regulator of *CDK1A* consequently inducing cell cycle arrest by inhibition of cyclin A/E/CDK2 and cyclin D/CDK4 (He et al., 2005; Poon, 2016; Ragione et al., 2003; Shin et al., 2010), thus being contrary to reduced expression levels for *EGR1* and upregulation of *CDK1A* which were observed in hyperosmotically stressed CHO DP-12 cells. However, a reverse correlation between the expression level of the miR-183 target sprouty RTK signaling antagonist 2 (*SPRY2*) and *CDK1A* expression was described for a colon cancer cell line by Zhang et al. (2016b). In general, further experiments, e. g. luciferase reporter assays, are required to validate the proposed interaction of *cgr*-miR-183 with *EGR1* and *SPRY2* mRNA, respectively. Furthermore, the anticipated correlations between *cgr*-miR-183 and the hyperosmotic phenotype may be confirmed by overexpression of miR-183 in CHO DP-12 cells and subsequent analysis of *CDK1A* expression levels, cell cycle distribution and q_P.

Besides miR-183, all other differentially expressed miRNAs were associated to p53-mediated tumor suppression or to cell proliferation (Braun et al., 2008; Georges et al., 2008; Jiang et al., 2015; Khella et al., 2013; Kong et al., 2012; Li et al., 2014; Park et al., 2011; Pichiorri et al., 2010; Wang et al., 2008, 2012, 2014a). However, depending on the type of cancer cell line miR-132 and miR-182 either induced suppression of proliferation or promoted tumor progression (Jiang et al., 2015; Kong et al.,

2012; Li et al., 2014; Park et al., 2011; Wang et al., 2012, 2014a). In contrast, miR-132 and the p53-inducible miRNAs miR-194 and miR-215 were shown to contribute to elevated gene expression levels of the G1-arrest inducing protein CDK1A (Braun et al., 2008; Georges et al., 2008; Jiang et al., 2015; Pichiorri et al., 2010) which was revealed to be significantly upregulated upon hyperosmotic stimulus in this research study. In return, miR-194 and miR-215 functioned as regulators of *TP53* expression (Braun et al., 2008; Pichiorri et al., 2010). According to independent studies, multiple of the predicted miRNA targets were either associated with tumor suppression, e. g. *ARRDC3, FOXP2, MTSS1, RHOBTB1* (Draheim et al., 2010; Gascoyne et al., 2015; Wang et al., 2012; Xu et al., 2012), or with cancer cell invasion, proliferation and cell cycle progression, e. g. SGK3, SNAI2 (Cheng et al., 2013; Wang et al., 2014b), thus illustrating the potential diversity of regulatory changes behind the inhibition of cell growth upon hyperosmotic stimulus.

6.3.4 Cell Line Engineering Strategies

With respect to the energy consuming process of recombinant protein production, cell line engineering strategies focus among others on approaches which improve the cellular energy supply in order to enhance q_P. In this context, previous independent studies applied genome reduction (Lieder et al., 2015; Mizoguchi et al., 2007; Sauer and Mattanovich, 2012), metabolic engineering of ATP consuming or producing pathways (Hara and Kondo, 2015; Seth et al., 2006) or methods to induce cell cycle arrest (Bi et al., 2004; Fussenegger et al., 1998; Kim et al., 2012; Seth et al., 2006) to optimize cellular productivity.

The surplus in energetic capacity of hyperosmotically stressed CHO DP-12 cells represents one starting point for cell line engineering as ATP may be utilized to improve cellular productivity. Nevertheless, further investigations, e. g. MFA, *in vivo* enzyme activity assays, metabolome and proteome analysis, are required to identify possibilities to fuel the surplus in ATP into product synthesis. Especially, allosteric regulation of enzyme activity by ATP should be considered in this context (2.4).

Enhanced availability of cellular energy seemed to be associated with G1-arrest as hyperosmotically stressed cells showed even higher q_{ATP} although the energetic demand in terms of reduced cell

proliferation declined. The revealed upregulation of *CDK1A* is anticipated to play a central role for the development of the hyperosmotic phenotype of CHO DP-12 cells as overexpression of *CDK1A* has already been described to induce G1-arrest and to improve q_P of CHO producer cell lines (Bi et al., 2004; Fussenegger et al., 1998). The finding of elevated q_{ATP} in combination with the aforementioned properties may elucidate the reason for CDK1A's q_P enhancing function and its suitability as cell line engineering target. However, the CDK1A-mediated inhibition of cell growth commonly hampers the improvement of c_P and therefore a suitable time point and strategy for the induction of *CDK1A* expression would be required to utilize the q_P enhancing effect for an improvement of c_P.

Besides *CDK1A*, the miRNAs *cgr*-miR-132, *cgr*-miR-194 and *cgr*-miR-215 may represent potential targets for cell line engineering as these miRNAs were significantly upregulated upon hyperosmotic stimulus and were shown to induce CDK1A-mediated G1-arrest in independent research studies (Braun et al., 2008; Georges et al., 2008; Jiang et al., 2015; Pichiorri et al., 2010). Consequently, overexpression of the aforementioned miRNAs in recombinant CHO cell lines is assumed to contribute to an enhancement in cellular productivity in regard of the q_P enhancing effect of *CDK1A*. Another promising miRNA for cell line engineering is expected to be miR-183 whose q_P enhancing effect has already been described for transient expression of *hsa*-miR-183 in an antibody producing CHO cell line, thus resulting in significantly enhanced q_P and reduced VCD (Strotbek et al., 2013). Furthermore, several independent research studies refined the involvement of miR-183 and its predicted miRNA targets EGR1 and SPRY2 in cell cycle arrest or progression.

In contrast to the aforementioned strategies, which focused on overexpression of genes or miRNAs, genome reduction may also be a suitable strategy to improve the cellular performance of CHO producer cell lines. Analysis of mRNA expression revealed increased expression levels for genes encoding proteins with dispensable function in suspension growing cells. Among these proteins were components for a protecting extracellular mucin layer (MUC2, OVGP1), members of the muscle sarcomere (NEB, TTN) as well as a protein which stimulates proliferation and differentiation of cells of the immune system (IL15). Regarding the dispensable function, the aforementioned proteins seemed to be potential candidates to enhance q_P by genome reduction. Especially the synthesis of the heavily O-glycosylated (>50%) proteins MUC2 and OVGP1 requires a great amount of energy (Hollingsworth

and Swanson, 2004; Lagow et al., 1999). For example, considering an energy demand of 3 molecules of ATP per peptide bond (Seth et al., 2006), the synthesis of 1 MUC2 molecule consisting of approximately 5100 amino acids (Lagow et al., 1999) would consume $\sim$ 15 300 mol_{ATP}. In contrast, only 3957 mol_{ATP} are required for 1 mol of IgG1 antibody ($\sim$1320 amino acids). Consequently, recombinant protein production might be hampered by the ATP intense production of proteins with dispensable function. Previous microbial genome reduction studies revealed an overall improvement of cellular performance including enhancement of recombinant protein production (Lieder et al., 2015; Mizoguchi et al., 2007; Sauer and Mattanovich, 2012). With respect to the mindset of microbial producers, deletion of *IL15, MUC2, NEB, OVGP1* and *TTN* may potentially contribute to an enhancement of the cellular performance of CHO DP-12 cells.

6.4 Conclusions and Future Perspectives

The aim of this thesis was to reveal the reason for the q_P enhancing effect of hyperosmotic culture conditions and to utilize the acquired knowledge to identify potential cell line engineering strategies for the improvement of the cellular performance of CHO producer cell lines. For this purpose an antibody producing CHO DP-12 cell line was cultivated in STRs in batch mode and hyperosmotic culture conditions were induced by the addition of NaCl-enriched cultivation medium. Strikingly, a decrease in anti-TOM22 mediated mitochondrial fluorescence intensity was observed whereas q_{ATP}, n_{ATP} and c_{ATP} increased upon hyperosmotic stimulus. With respect to findings of control experiments and independent research studies (Mitra et al., 2009; Pernas and Scorrano, 2016), the decrease in mitochondrial fluorescence is assumed to be attributed to sterically hampering structural changes rather than to a reduced size of the mitochondrial compartment. This may be validated by electron microscopic analysis or a combination of an alternative fluorescence staining procedure for mitochondria and confocal microscopy.

Comparison of the observed hyperosmotic phenotype of CHO DP-12 cells to findings of independent research studies indicated that the combination of G1-arrest and enhanced energetic capacity most likely plays the decisive role for the improvement of cell specific productivity in hyperosmoti-

cally stressed CHO DP-12 cells. Although arrested cells are expected to have an alleviated energy demand compared to exponentially growing cells, hyperosmotically stressed CHO DP-12 cells showed significantly increased q_{ATP} that exceeded by far the required ATP formation to compensate for the hyperosmotically induced RVI. Therefore, it is anticipated that hyperosmotically stressed CHO DP-12 cells partly utilize the observed surplus in ATP supply for recombinant protein production, thus improving q_P. This hypothesis is corroborated by the fact that stress related enhancement of q_P was frequently associated with cell cycle arrest

The hyperosmotically induced G1-arrest of CHO DP-12 cells is most likely mediated by the significant upregulation of *CDK1A*. In this context, *cgr*-miR-132, *cgr*-miR-194 and *cgr*-miR-215 may have superimposed regulatory function as these miRNAs were associated with enhanced *CDK1A* expression levels in independent research studies (Braun et al., 2008; Georges et al., 2008; Jiang et al., 2015; Pichiorri et al., 2010) which in turn was shown to improve q_P of CHO producer cell lines (Bi et al., 2004; Fussenegger et al., 1998). Furthermore, upregulation of *cgr*-miR-183 upon hyperosmotic stimulus may also be a reason for G1-arrest and the related enhancement in q_P as indicated by previous independent research results (Parpa et al., 2009; Pritchard et al., 2011; Sarver et al., 2010; Scharnhorst et al., 2000; Sells et al., 1995; Strotbek et al., 2013; Virolle et al., 2003; Zhang et al., 2016b).

Targeted overexpression of the aforementioned miRNAs and subsequent analysis of cell cycle distribution and *CDK1A* expression levels may confirm the proposed correlations between miRNAs, *CDK1A* and cell cycle arrest. In this context, validation of potential miRNA targets is anticipated to contribute to a more detailed picture of the regulatory processes behind the observed hyperosmotic phenotype. These studies will consequently reveal whether one of the miRNAs may be a suitable cell line engineering target to improve the cellular performance of CHO producer cell lines.

The immediate and long term upregulation of genes encoding proteins with dispensable function in suspension growing CHO cultures represents another starting point for cell line engineering. Thus, *MUC2*, *NEB*, *OVGP1* and *TTN* are expected to be ideal candidates for genome reduction in order to boost recombinant protein production likewise to approaches for microbial production hosts (Lieder et al., 2015; Mizoguchi et al., 2007; Sauer and Mattanovich, 2012). Future research studies have to show whether deletion of the aforementioned genes contributes to an improvement of cellular

productivity or availability of energy. Furthermore, analysis of mRNA expression upon hyperosmotic stimulus should be performed for multiple CHO producer cell lines in order to investigate if those exhibit conserved differential expression patterns for genes with strictly tissue related function.

Finally, further investigations like *in vivo* enzyme activity assays or metabolome and proteome analysis are required in order to reveal potential strategies to boost cellular productivity on basis of the hyperosmotically induced surplus in ATP supply.

7 Author Contribution

This chapter specifies my (Jennifer Pfizenmaier-Wu) contribution to manuscripts which have already been published in peer-reviewed international journals and in a book, respectively. Manuscript 1 and 2 are provided in appendix B.

Manuscript 1

Pfizenmaier, J., J.-C. Matuszczyk & R. Takors (2015). Changes in Intracellular ATP-Content of CHO Cells as Response to Hyperosmolality. Biotechnol. Prog., 31(5):1212-1216.

Jennifer Pfizenmaier-Wu (J. P.) designed and carried out all experiments described in this manuscript. In addition, J. P. analyzed and interpreted data and participated in the preparation of the manuscript.

Manuscript 2

Pfizenmaier, J., L. Junghans, A. Teleki & R. Takors (2016). Hyperosmotic Stimulus Study Discloses Benefits in ATP Supply and Reveals miRNA/mRNA Targets to Improve Recombinant Protein Production. Biotechnol. J., 11:1037-1047.

J. P. designed and carried out all experiments except for the (I) processing of cell samples for NGS, (II) sequencing of mRNAs and miRNAs and (III) preparation of mRNA and miRNA read count datasets. J. P. participated in data analysis, data interpretation and preparation of the manuscript.

Manuscript 3

Pfizenmaier, J. & Takors R. (2016). Host organisms: Mammalian Cells, In Industrial Biotechnology Microorganisms (volume 3, chapter 17), edited by C. Wittmann and J. C. Liao. Weinheim:Wiley-VCH.

J. P. wrote the sections "Basics of Cellular Structure and Metabolism", "The Genome of CHO cells" and "Molecular Biology Tools". Furthermore, J. P. prepared figure 4 as part of section "Intracellular Metabolome Analysis" and provided the paragraph about glycoengineering in section "Improving Cellular Performance by Genetic and Metabolic Engineering".

References

Acehan, D., X. Jiang, D. G. Morgan, J. E. Heuser, X. Wang, & C. W. Akey (2002). Three-Dimensional Structure of the Apoptosome: Implications for Assembly, Procaspase-9 Binding, and Activation. *Mol. Cell*, 9(2):423–432.

Aggarwal, R. S. (2014). What's fueling the biotech engine-2012 to 2013. *Nat. Biotechnol.*, 32(1):32–39.

Ahting, U., C. Thun, R. Hegerl, D. Typke, F. E. Nargang, W. Neupert, & S. Nussberger (1999). The TOM core complex: the general protein import pore of the outer membrane of mitochondria. *J. Cell Biol.*, 147(5):959–968.

Alexandrow, M. G. & J. L. Hamlin (2004). Cdc6 chromatin affinity is unaffected by serine-54 phosphorylation, S-phase progression, and overexpression of cyclin A. *Mol. Cell. Biol.*, 24(4):1614–1627.

Alfieri, R. R. & P. G. Petronini (2007). Hyperosmotic stress response: Comparison with other cellular stresses. *Pflugers Arch. Eur. J. Physiol.*, 454(2):173–185.

Altamirano, C., J. Berrios, M. Vergara, & S. Becerr (2013). Advances in improving mammalian cells metabolism for recombinant protein production. *Electron. J. Biotechnol.*, 16(3):1–14.

Ambros, V., B. Bartel, D. P. Bartel, C. B. Burge, J. C. Carrington, X. Chen, G. Dreyfuss, S. R. Eddy, S. Griffiths-Jones, M. Marshall, M. Matzke, G. Ruvkun, & T. Tuschl (2003). A uniform system for microRNA annotation. *RNA*, 9(3):277–279.

Atkinson, D. E. & G. M. Walton (1967). Adenosine triphosphate conservation in metabolic regulation. Rat liver citrate cleavage enzyme. *J Biol Chem*, 242(13):3239–3241.

Baik, J. Y., M. S. Lee, S. R. An, S. K. Yoon, E. J. Joo, Y. H. Kim, H. W. Park, & G. M. Lee (2006). Initial transcriptome and proteome analyses of low culture temperature-induced expression in CHO cells producing erythropoietin. *Biotechnol Bioeng*, 93(2):361–371.

Balcarcel, R. R. & L. M. Clark (2003). Metabolic screening of mammalian cell cultures using well-plates. *Biotechnol Prog*, 19(1):98–108.

Baldwin, S. A. (1993). Mammalian passive glucose transporters: members of an ubiquitous family of active and passive transport proteins. *Biochim. Biophys. Acta - Rev. Biomembr.*, 1154(1):17–49.

References

Barnes, K., J. C. Ingram, O. H. Porras, L. F. Barros, E. R. Hudson, L. G. D. Fryer, F. Foufelle, D. Carling, D. G. Hardie, & S. A. Baldwin (2002). Activation of GLUT1 by metabolic and osmotic stress: potential involvement of AMP-activated protein kinase (AMPK). *J. Cell Sci.,* 115(11):2433–2442.

Barron, N., N. Kumar, N. Sanchez, P. Doolan, C. Clarke, P. Meleady, F. O'Sullivan, & M. Clynes (2011a). Engineering CHO cell growth and recombinant protein productivity by overexpression of miR-7. *J Biotechnol,* 151(2):204–211.

Barron, N., N. Sanchez, P. Kelly, & M. Clynes (2011b). MicroRNAs: tiny targets for engineering CHO cell phenotypes? *Biotechnol Lett,* 33(1):11–21.

Bartel, D. P. (2004). MicroRNAs: genomics, biogenesis, mechanism, and function. *Cell,* 116(2):281–297.

Bauer, M. F., C. Sirrenberg, W. Neupert, & M. Brunner (1996). Role of Tim23 as Voltage Sensor and Presequence Receptor in Protein Import into Mitochondria. *Cell,* 87(1):33–41.

Bauer, N. C., P. W. Doetsch, & A. H. Corbett (2015). Mechanisms Regulating Protein Localization. *Traffic,* 16(10):1039–1061.

Becker, J., M. Hackl, O. Rupp, T. Jakobi, J. Schneider, R. Szczepanowski, T. Bekel, N. Borth, A. Goesmann, J. Grillari, C. Kaltschmidt, T. Noll, A. Puhler, A. Tauch, & K. Brinkrolf (2011). Unraveling the Chinese hamster ovary cell line transcriptome by next-generation sequencing. *J Biotechnol,* 156(3):227–235.

Bedoya-López, A., K. Estrada, A. Sanchez-Flores, O. T. Ramírez, C. Altamirano, L. Segovia, J. Miranda-Ríos, M. A. Trujillo-Roldán, & N. A. Valdez-Cruz (2016). Effect of Temperature Downshift on the Transcriptomic Responses of Chinese Hamster Ovary Cells Using Recombinant Human Tissue Plasminogen Activator Production Culture. *PLoS One,* 11(3):1–26.

Bellot, G., P.-F. Cartron, E. Er, L. Oliver, P. Juin, L. C. Armstrong, P. Bornstein, K. Mihara, S. Manon, & F. M. Vallette (2007). TOM22, a core component of the mitochondria outer membrane protein translocation pore, is a mitochondrial receptor for the proapoptotic protein Bax. *Cell Death Differ.,* 14(4):785–794.

Benjamini, Y. & Y. Hochberg (1995). Controlling the False Discovery Rate: A Practical and Powerful Approach to Multiple Testing. *J. R. Stat. Soc. Ser. B,* 57(1):289 − 300.

Berg, J., J. Tyomczko, & L. Stryer (2003). *Biochemie,* 5th edition. Spektrum Akademischer Verlag Heidelberg/Berlin.

Bertoli, C., J. M. Skotheim, & R. a. M. de Bruin (2013). Control of cell cycle transcription during G1 and S phases. *Nat. Rev. Mol. Cell Biol.,* 14(8):518–528.

Bhola, P. & A. Letai (2016). Mitochondria—Judges and Executioners of Cell Death Sentences. *Mol. Cell,* 61(5):695–704.

Bi, J.-X., J. Shuttleworth, & M. Al-Rubeai (2004). Uncoupling of cell growth and proliferation results in enhancement of productivity in p21CIP1-arrested CHO cells. *Biotechnol. Bioeng.,* 85(7):741–749.

Birch, J. R. & A. J. Racher (2006). Antibody production. *Adv Drug Deliv Rev,* 58(5-6):671–685.

Birzele, F., J. Schaub, W. Rust, C. Clemens, P. Baum, H. Kaufmann, A. Weith, T. W. Schulz, & T. Hildebrandt (2010). Into the unknown: expression profiling without genome sequence information in CHO by next generation sequencing. *Nucleic Acids Res,* 38(12):3999–4010.

Blake, J. A., M. T. Davisson, J. T. Eppig, L. J. Maltais, S. Povey, J. A. White, & J. E. Womack (1997). Report from the International Nomenclature Workshop. *Genomics,* 45(2):464–476.

Böhm, E., B. K. Seyfried, M. Dockal, M. Graninger, M. Hasslacher, M. Neurath, C. Konetschny, P. Matthiessen, A. Mitterer, & F. Scheiflinger (2015). Differences in N-glycosylation of recombinant human coagulation factor VII derived from BHK, CHO, and HEK293 cells. *BMC Biotechnol.,* 15(1):87.

Bollati-Fogolín, M., G. Forno, M. Nimtz, H. S. Conradt, M. Etcheverrigaray, & R. Kratje (2008). Temperature Reduction in Cultures of hGM-CSF-expressing CHO Cells: Effect on Productivity and Product Quality. *Biotechnol. Prog.,* 21(1):17–21.

Bollgönn, E. (2014). Effects of hyperosmolality on intracellular ATP content of antibody-producing CHO cells. *Bachelor Thesis, Insitute Biochem. Eng. Univ. Stuttgart.*

Borchert, G. M., W. Lanier, & B. L. Davidson (2006). RNA polymerase III transcribes human microRNAs. *Nat. Struct. Mol. Biol.,* 13(12):1097–1101.

Boshart, M., F. Weber, G. Jahn, K. Dorsch-Häsler, B. Fleckenstein, & W. Schaffner (1985). A very strong enhancer is located upstream of an immediate early gene of human cytomegalovirus. *Cell,* 41(2):521–530.

Braakman, I., J. Helenius, & A. Helenius (1992). Role of ATP and disulphide bonds during protein folding in the endoplasmic reticulum. *Nature,* 356(6366):260–262.

Brandt, U. & B. Trumpower (1994). The protonmotive Q cycle in mitochondria and bacteria. *Crit. Rev. Biochem. Mol. Biol.,* 29(3):165–197.

Braun, C. J., X. Zhang, I. Savelyeva, S. Wolff, U. M. Moll, T. Schepeler, T. F. Orntoft, C. L. Andersen, & M. Dobbelstein (2008). p53-Responsive micrornas 192 and 215 are capable of inducing cell cycle arrest. *Cancer Res.,* 68(24):10094–104.

Brennecke, J., A. Stark, R. B. Russell, & S. M. Cohen (2005). Principles of MicroRNA–Target Recognition. *PLoS Biol.*, 3(3):e85.

Bricker, D. K., E. B. Taylor, J. C. Schell, T. Orsak, A. Boutron, Y.-C. Chen, J. E. Cox, C. M. Cardon, J. G. Van Vranken, N. Dephoure, C. Redin, S. Boudina, S. P. Gygi, M. Brivet, C. S. Thummel, & J. Rutter (2012). A mitochondrial pyruvate carrier required for pyruvate uptake in yeast, Drosophila, and humans. *Science*, 337(6090):96–100.

Brüser, A., J. Kirchberger, M. Kloos, N. Sträter, & T. Schöneberg (2012). Functional linkage of adenine nucleotide binding sites in mammalian muscle 6-phosphofructokinase. *J. Biol. Chem.*, 287(21):17546–17553.

Burg, M. B., J. D. Ferraris, & N. I. Dmitrieva (2007). Cellular response to hyperosmotic stresses. *Physiol. Rev.*, 87(4):1441–1474.

Butler, M. & A. Meneses-Acosta (2012). Recent advances in technology supporting biopharmaceutical production from mammalian cells. *Appl Microbiol Biotechnol*, 96(4):885–894.

Campello, S. & L. Scorrano (2010). Mitochondrial shape changes: orchestrating cell pathophysiology. *EMBO Rep.*, 11(9):678–684.

Candé, C., N. Vahsen, I. Kouranti, E. Schmitt, E. Daugas, C. Spahr, J. Luban, R. T. Kroemer, F. Giordanetto, C. Garrido, J. M. Penninger, & G. Kroemer (2004). AIF and cyclophilin A cooperate in apoptosis-associated chromatinolysis. *Oncogene*, 23(8):1514–1521.

Cao, Y., S. Kimura, T. Itoi, K. Honda, H. Ohtake, & T. Omasa (2012). Construction of BAC-based physical map and analysis of chromosome rearrangement in Chinese hamster ovary cell lines. *Biotechnol. Bioeng.*, 109(6):1357–1367.

Carling, D. (2004). The AMP-activated protein kinase cascade–a unifying system for energy control. *Trends Biochem. Sci.*, 29(1):18–24.

Castro, P., P. Hayter, A. Ison, & A. Bull (1992). Application of a statistical design to the optimization of culture medium for recombinant interferon-gamma production by Chinese hamster ovary cells. *Appl. Microbiol. Biotechnol.*, 38(1):88–90.

Ceaglio, N., M. Etcheverrigaray, R. Kratje, & M. Oggero (2008). Novel long-lasting interferon alpha derivatives designed by glycoengineering. *Biochimie*, 90(3):437–449.

Chen, A., R. Chitta, D. Chang, & A. Amanullah (2009). Twenty-four well plate miniature bioreactor system as a scale-down model for cell culture process development. *Biotechnol. Bioeng.*, 102(1):148–160.

Chendrimada, T. P., R. I. Gregory, E. Kumaraswamy, J. Norman, N. Cooch, K. Nishikura, & R. Shiekhattar (2005). TRBP recruits the Dicer complex to Ago2 for microRNA processing and gene silencing. *Nature*, 436(7051):740–744.

Cheng, J.-C., H.-M. Chang, & P. C. K. Leung (2013). Egr-1 mediates epidermal growth factor-induced downregulation of E-cadherin expression via Slug in human ovarian cancer cells. *Oncogene*, 32(8):1041–1049.

Cherlet, M. & A. Marc (1999). Hybridoma cell behaviour in continuous culture under hyperosmotic stress. *Cytotechnology*, 29(1):71–84.

Chong, W. P. K., S. G. Reddy, F. N. K. Yusufi, D.-Y. Lee, N. S. C. Wong, C. K. Heng, M. G. S. Yap, & Y. S. Ho (2010). Metabolomics-driven approach for the improvement of Chinese hamster ovary cell growth: overexpression of malate dehydrogenase II. *J. Biotechnol.*, 147(2):116–121.

Chou, C.-H., N.-W. Chang, S. Shrestha, S.-D. Hsu, Y.-L. Lin, W.-H. Lee, C.-D. Yang, H.-C. Hong, T.-Y. Wei, S.-J. Tu, T.-R. Tsai, S.-Y. Ho, T.-Y. Jian, H.-Y. Wu, P.-R. Chen, N.-C. Lin, H.-T. Huang, T.-L. Yang, C.-Y. Pai, C.-S. Tai, W.-L. Chen, C.-Y. Huang, C.-C. Liu, S.-L. Weng, K.-W. Liao, W.-L. Hsu, & H.-D. Huang (2015). miRTarBase 2016: updates to the experimentally validated miRNA-target interactions database. *Nucleic Acids Res.*, 44(D4):D239–247.

Chu, L. & D. K. Robinson (2001). Industrial choices for protein production by large-scale cell culture. *Curr. Opin. Biotechnol.*, 12(2):180–187.

Clarke, C., P. Doolan, N. Barron, P. Meleady, F. O'Sullivan, P. Gammell, M. Melville, M. Leonard, & M. Clynes (2011). Large scale microarray profiling and coexpression network analysis of CHO cells identifies transcriptional modules associated with growth and productivity. *J Biotechnol*, 155(3):350–359.

Clarke, C., M. Henry, P. Doolan, S. Kelly, S. Aherne, N. Sanchez, P. Kelly, P. Kinsella, L. Breen, S. F. Madden, L. Zhang, M. Leonard, M. Clynes, P. Meleady, & N. Barron (2012). Integrated miRNA, mRNA and protein expression analysis reveals the role of post-transcriptional regulation in controlling CHO cell growth rate. *BMC Genomics*, 13(656):1–14.

Cogliati, S., C. Frezza, M. E. Soriano, T. Varanita, R. Quintana-Cabrera, M. Corrado, S. Cipolat, V. Costa, A. Casarin, L. C. Gomes, E. Perales-Clemente, L. Salviati, P. Fernandez-Silva, J. A. Enriquez, & L. Scorrano (2013). Mitochondrial cristae shape determines respiratory chain supercomplexes assembly and respiratory efficiency. *Cell*, 155(1):160–171.

Conesa, A., M. J. Nueda, A. Ferrer, & M. Talón (2006). maSigPro: A method to identify significantly differential expression profiles in time-course microarray experiments. *Bioinformatics*, 22(9):1096–1102.

Corton, J. M., J. G. Gillespie, & D. Hardie (1994). Role of the AMP-activated protein kinase in the cellular stress response. *Curr. Biol.*, 4(4):315–324.

Cost, G. J., Y. Freyvert, A. Vafiadis, Y. Santiago, J. C. Miller, E. Rebar, T. N. Collingwood, A. Snowden, & P. D. Gregory (2010). BAK and BAX Deletion Using Zinc-Finger Nucleases Yields Apoptosis-Resistant CHO Cells. *Biotechnol Bioeng*, 105(2):330–340.

Costanzo, L. S. (2014). Cellular Physiology. In *Physiology*, chapter 1, Pp. 12–14. Philadelphia: Saunders.

Crissman, H. A. & J. A. Steinkamp (1973). Rapid, simultaneous measurement of DNA, protein, and cell volume in single cells from large mammalian cell populations. *J. Cell Biol.*, 59(3):766–771.

Cserjan-Puschmann, M., W. Kramer, E. Duerrschmid, G. Striedner, & K. Bayer (1999). Metabolic approaches for the optimisation of recombinant fermentation processes. *Appl Microbiol Biotechnol*, 53(1):43–50.

Cumming, G., F. Fidler, & D. L. Vaux (2007). Error bars in experimental biology. *J Cell Biol*, 177(1):7–11.

Datta, P., R. J. Linhardt, & S. T. Sharfstein (2013). An 'omics approach towards CHO cell engineering. *Biotechnol Bioeng*, 110(5):1255–1271.

Denli, A. M., B. B. J. Tops, R. H. A. Plasterk, R. F. Ketting, & G. J. Hannon (2004). Processing of primary microR-NAs by the Microprocessor complex. *Nature*, 432(7014):231–235.

Derouazi, M., D. Martinet, N. Besuchet Schmutz, R. Flaction, M. Wicht, M. Bertschinger, D. L. Hacker, J. S. Beckmann, & F. M. Wurm (2006). Genetic characterization of CHO production host DG44 and derivative recombinant cell lines. *Biochem. Biophys. Res. Commun.*, 340(4):1069–1077.

Dewey, W. C. & M. A. Fuhr (1976). Quantification of Mitochondria During the Cell Cycle of Chinese Hamster Cells. *Exp. Cell Res.*, 99:23 – 30.

DeZengotita, V. M., A. E. Schmelzer, & W. M. Miller (2002). Characterization of hybridoma cell responses to elevated pCO(2) and osmolality: intracellular pH, cell size, apoptosis, and metabolism. *Biotechnol Bioeng*, 77(4):369–380.

Diendorfer, A. B., M. Hackl, G. Klanert, V. Jadhav, M. Reithofer, F. Stiefel, F. Hesse, J. Grillari, & N. Borth (2015). Annotation of additional evolutionary conserved microRNAs in CHO cells from updated genomic data. *Biotechnol. Bioeng.*, 112(7):1488–1493.

Dietmair, S., N. E. Timmins, P. P. Gray, L. K. Nielsen, & J. O. Kromer (2010). Towards quantitative metabolomics of mammalian cells: development of a metabolite extraction protocol. *Anal Biochem*, 404(2):155–164.

Dimitrova, D. S., I. T. Todorov, T. Melendy, & D. M. Gilbert (1999). Mcm2, but not RPA, is a component of the mammalian early G1-phase prereplication complex. *J. Cell Biol.*, 146(4):709–722.

Dmitrieva, N., L. Michea, & M. Burg (2001). p53 Protects renal inner medullary cells from hypertonic stress by restricting DNA replication. *Am. J. Physiol. Renal Physiol.*, 281(3):F522–F530.

Doench, J. G. & P. A. Sharp (2004). Specificity of microRNA target selection in translational repression. *Genes Dev.*, 18(5):504–511.

Doolan, P., C. Clarke, P. Kinsella, L. Breen, P. Meleady, M. Leonard, L. Zhang, M. Clynes, S. T. Aherne, & N. Barron (2013). Transcriptomic analysis of clonal growth rate variation during CHO cell line development. *J Biotechnol*, 166(3):105–113.

Doolan, P., P. Meleady, N. Barron, M. Henry, R. Gallagher, P. Gammell, M. Melville, M. Sinacore, K. McCarthy, M. Leonard, T. Charlebois, & M. Clynes (2010). Microarray and proteomics expression profiling identifies several candidates, including the valosin-containing protein (VCP), involved in regulating high cellular growth rate in production CHO cell lines. *Biotechnol. Bioeng.*, 106(1):42–56.

Draheim, K. M., H.-B. Chen, Q. Tao, N. Moore, M. Roche, & S. Lyle (2010). ARRDC3 suppresses breast cancer progression by negatively regulating integrin beta4. *Oncogene*, 29(36):5032–5047.

Druz, A., C. Chu, B. Majors, R. Santuary, M. Betenbaugh, & J. Shiloach (2011). A novel microRNA mmu-miR-466h affects apoptosis regulation in mammalian cells. *Biotechnol. Bioeng.*, 108(7):1651–1661.

Druz, A., Y. J. Son, M. Betenbaugh, & J. Shiloach (2013). Stable inhibition of mmu-miR-466h-5p improves apoptosis resistance and protein production in CHO cells. *Metab Eng*, 16:87–94.

Du, C., M. Fang, Y. Li, L. Li, & X. Wang (2000). Smac, a Mitochondrial Protein that Promotes Cytochrome c–Dependent Caspase Activation by Eliminating IAP Inhibition. *Cell*, 102(1):33–42.

Dwek, R. A., A. C. Lellouch, & M. R. Wormald (1995). Glycobiology: 'the function of sugar in the IgG molecule'. *J. Anat.*, 187:279–292.

Eddy, S. R. (2001). Non–coding RNA genes and the modern RNA world. *Nat. Rev. Genet.*, 2(12):919–929.

Eden, E., R. Navon, I. Steinfeld, D. Lipson, & Z. Yakhini (2009). GOrilla: a tool for discovery and visualization of enriched GO terms in ranked gene lists. *BMC Bioinformatics*, 10(48):1–6.

Elliott, S., T. Lorenzini, S. Asher, K. Aoki, D. Brankow, L. Buck, L. Busse, D. Chang, J. Fuller, J. Grant, N. Hernday, M. Hokum, S. Hu, A. Knudten, N. Levin, R. Komorowski, F. Martin, R. Navarro, T. Osslund, G. Rogers, N. Rogers, G. Trail, & J. Egrie (2003). Enhancement of therapeutic protein in vivo activities through glyco-engineering. *Nat Biotechnol*, 21(4):414–421.

Endo, T. & D. Kohda (2002). Functions of outer membrane receptors in mitochondrial protein import. *Biochim. Biophys. Acta - Mol. Cell Res.*, 1592(1):3–14.

Fang, J., B. Y. L. Hsu, C. M. MacMullen, M. Poncz, T. J. Smith, & C. A. Stanley (2002). Expression, purification and characterization of human glutamate dehydrogenase (GDH) allosteric regulatory mutations. *Biochem. J.*, 363(1):81–87.

Feige, M. J. & L. M. Hendershot (2011). Disulfide bonds in ER protein folding and homeostasis. *Curr. Opin. Cell Biol.*, 23(2):167–175.

Fenton, A. W. & M. Hutchinson (2009). The pH dependence of the allosteric response of human liver pyruvate kinase to fructose-1,6-bisphosphate, ATP, and alanine. *Arch. Biochem. Biophys.*, 484(1):16–23.

Fischer, S., T. Buck, A. Wagner, C. Ehrhart, J. Giancaterino, S. Mang, M. Schad, S. Mathias, A. Aschrafi, R. Handrick, & K. Otte (2014). A functional high-content miRNA screen identifies miR-30 family to boost recombinant protein production in CHO cells. *Biotechnol. J.*, 9(10):1279–1292.

Fischer, S., R. Handrick, & K. Otte (2015a). The art of CHO cell engineering: A comprehensive retrospect and future perspectives. *Biotechnol. Adv.*, 33(8):1878–1896.

Fischer, S., S. Mathias, S. Schaz, V. V. Emmerling, T. Buck, M. Kleemann, M. Hackl, J. Grillari, A. Aschrafi, R. Handrick, & K. Otte (2015b). Enhanced protein production by microRNA-30 family in CHO cells is mediated by the modulation of the ubiquitin pathway. *J. Biotechnol.*, 212:32–43.

Fischer, S., A. J. Paul, A. Wagner, S. Mathias, M. Geiss, F. Schandock, M. Domnowski, J. Zimmermann, R. Handrick, F. Hesse, & K. Otte (2015c). miR-2861 as novel HDAC5 inhibitor in CHO cells enhances productivity while maintaining product quality. *Biotechnol. Bioeng.*, 112(10):2142–2153.

Fisher, R. A. (1935). *The Design of Experiments*, 1st edition. Edinburgh: Oliver and Boyd Ltd.

Florence, A. T. & D. Attwood (2016). *Physicochemical principles of pharmacy*, 6th edition. London: Pharmaceutical Press.

Fogolin, M. B., R. Wagner, M. Etcheverrigaray, & R. Kratje (2004). Impact of temperature reduction and expression of yeast pyruvate carboxylase on hGM-CSF-producing CHO cells. *J. Biotechnol.*, 109(1-2):179–191.

Fomina-Yadlin, D., M. Mujacic, K. Maggiora, G. Quesnell, R. Saleem, & J. T. McGrew (2015). Transcriptome analysis of a CHO cell line expressing a recombinant therapeutic protein treated with inducers of protein expression. *J. Biotechnol.*, 212:106–115.

Fox, S. R., U. A. Patel, M. G. Yap, & D. I. Wang (2004). Maximizing interferon-gamma production by Chinese hamster ovary cells through temperature shift optimization: experimental and modeling. *Biotechnol Bioeng*, 85(2):177–184.

Friedman, J. R. & J. Nunnari (2014). Mitochondrial form and function. *Nature*, 505(7483):335–343.

Fryer, L. G. D., A. Parbu-Patel, & D. Carling (2002). The Anti-diabetic drugs rosiglitazone and metformin stimulate AMP-activated protein kinase through distinct signaling pathways. *J. Biol. Chem.*, 277(28):25226–25232.

Fulda, S. & K.-M. Debatin (2006). Extrinsic versus intrinsic apoptosis pathways in anticancer chemotherapy. *Oncogene*, 25:4798–4811.

Furukawa, K. & K. Ohsuye (1998). Effect of culture temperature on a recombinant CHO cell line producing a C-terminal alpha-amidating enzyme. *Cytotechnology*, 26(2):153–164.

Fussenegger, M., S. Schlatter, D. Dätwyler, X. Mazur, & J. E. Bailey (1998). Controlled proliferation by multigene metabolic engineering enhances the productivity of Chinese hamster ovary cells. *Nat. Biotechnol.*, 16(5):468–472.

Gallati, H. & I. Pracht (1985). [Horseradish peroxidase: kinetic studies and optimization of peroxidase activity determination using the substrates H2O2 and 3,3',5,5'-tetramethylbenzidine]. *J. Clin. Chem. Clin. Biochem.*, 23(8):453–460.

Gammell, P., N. Barron, N. Kumar, & M. Clynes (2007). Initial identification of low temperature and culture stage induction of miRNA expression in suspension CHO-K1 cells. *J Biotechnol*, 130(3):213–218.

Gascoyne, D. M., H. Spearman, L. Lyne, R. Puliyadi, M. Perez-Alcantara, L. Coulton, S. E. Fisher, P. I. Croucher, & A. H. Banham (2015). The Forkhead Transcription Factor FOXP2 Is Required for Regulation of p21WAF1/CIP1 in 143B Osteosarcoma Cell Growth Arrest. *PLoS One*, 10(6):e0128513.

Geisbuhler, T., R. A. Altschuld, R. W. Trewyn, A. Z. Ansel, K. Lamka, & G. P. Brierley (1984). Adenine nucleotide metabolism and compartmentalization in isolated adult rat heart cells. *Circ. Res.*, 54(5):536–546.

Gelves, R., A. Dietrich, & R. Takors (2014). Modeling of gas-liquid mass transfer in a stirred tank bioreactor agitated by a Rushton turbine or a new pitched blade impeller. *Bioprocess Biosyst. Eng.*, 37(3):365–375.

Georges, S. A., M. C. Biery, S.-Y. Kim, J. M. Schelter, J. Guo, A. N. Chang, A. L. Jackson, M. O. Carleton, P. S. Linsley, M. A. Cleary, & B. N. Chau (2008). Coordinated regulation of cell cycle transcripts by p53-Inducible microRNAs, miR-192 and miR-215. *Cancer Res.*, 68(24):10105–10112.

Glacken, M. W. (1988). Catabolic Control of Mammalian-Cell Culture. *Bio-Technology*, 6(9):1041–1050.

Gnoth, S., M. Jenzsch, R. Simutis, & A. Lübbert (2007). Process Analytical Technology (PAT): batch-to-batch reproducibility of fermentation processes by robust process operational design and control. *J. Biotechnol.*, 132(2):180–186.

Gregory, R. I., T. P. Chendrimada, N. Cooch, & R. Shiekhattar (2005). Human RISC Couples MicroRNA Biogenesis and Posttranscriptional Gene Silencing. *Cell*, 123(4):631–640.

Gregory, R. I., K.-p. Yan, G. Amuthan, T. Chendrimada, B. Doratotaj, N. Cooch, & R. Shiekhattar (2004). The Microprocessor complex mediates the genesis of microRNAs. *Nature*, 432(7014):235–240.

Griffiths-Jones, S. (2004). The microRNA Registry. *Nucleic Acids Res.*, 32:D109–D111.

Griffiths-Jones, S., R. J. Grocock, S. van Dongen, A. Bateman, & A. J. Enright (2006). miRBase: microRNA sequences, targets and gene nomenclature. *Nucleic Acids Res.*, 34:D140–D144.

Grimson, A., K. K.-H. Farh, W. K. Johnston, P. Garrett-Engele, L. P. Lim, & D. P. Bartel (2007). MicroRNA Targeting Specificity in Mammals: Determinants beyond Seed Pairing. *Mol. Cell*, 27(1):91–105.

Gronemeyer, P., R. Ditz, & J. Strube (2014). Trends in Upstream and Downstream Process Development for Antibody Manufacturing. *Bioengineering*, 1(4):188–212.

Gross, A., J. M. McDonnell, & S. J. Korsmeyer (1999). BCL-2 family members and the mitochondria in apoptosis. *Genes Dev.*, 13:1899–1911.

Guardavaccaro, D., G. Corrente, F. Covone, L. Micheli, I. D'Agnano, G. Starace, M. Caruso, & F. Tirone (2000). Arrest of G1-S progression by the p53-inducible gene PC3 is Rb dependent and relies on the inhibition of cyclin D1 transcription. *Mol. Cell. Biol.*, 20(5):1797–1815.

Hackl, M., V. Jadhav, T. Jakobi, O. Rupp, K. Brinkrolf, A. Goesmann, A. Puhler, T. Noll, N. Borth, & J. Grillari (2012). Computational identification of microRNA gene loci and precursor microRNA sequences in CHO cell lines. *J Biotechnol*, 158(3):151–155.

Hackl, M., T. Jakobi, J. Blom, D. Doppmeier, K. Brinkrolf, R. Szczepanowski, S. H. Bernhart, C. Honer Zu Siederdissen, J. A. Bort, M. Wieser, R. Kunert, S. Jeffs, I. L. Hofacker, A. Goesmann, A. Puhler, N. Borth, & J. Grillari (2011). Next-generation sequencing of the Chinese hamster ovary microRNA transcriptome: Identification, annotation and profiling of microRNAs as targets for cellular engineering. *J Biotechnol*, 153(1-2):62–75.

Hamlin, J. L. & C. Ma (1990). The mammalian dihydrofolate reductase locus. *Biochim Biophys Acta*, 1087(2):107–125.

Hammett, K., J. Kuchibhatla, C. Hunt, S. Holdread, & J. Brooks (2007). Developing Chemically Defined Media Through DOE: Complete Optimization with Increased Protein Production in Less than 8 Months. In *Cell Technol. Cell Prod.*, R. Smith, ed., chapter 6, Pp. 683–691. Dordrecht: Springer Netherlands.

Hammond, S., J. C. Swanberg, M. Kaplarevic, & K. H. Lee (2011). Genomic sequencing and analysis of a Chinese hamster ovary cell line using Illumina sequencing technology. *BMC Genomics*, 12(67):1–8.

Hammond, S., J. C. Swanberg, S. W. Polson, & K. H. Lee (2012). Profiling conserved microRNA expression in recombinant CHO cell lines using Illumina sequencing. *Biotechnol Bioeng*, 109(6):1371–1375.

Hamzeiy, H., J. Allmer, & M. Yousef (2014). Computational Methods for MicroRNA Target Prediction. *Methods Mol Biol.*, 1107:207–221.

Han, Y. K., Y. G. Kim, J. Y. Kim, & G. M. Lee (2010). Hyperosmotic stress induces autophagy and apoptosis in recombinant Chinese hamster ovary cell culture. *Biotechnol Bioeng*, 105(6):1187–1192.

Han, Y. K., T. Y. Koo, & G. M. Lee (2009). Enhanced Interferon-beta Production by CHO Cells Through Elevated Osmolality and Reduced Culture Temperature. *Biotechnol. Prog.*, 25(5):1440–1447.

Hara, K. Y. & A. Kondo (2015). ATP regulation in bioproduction. *Microb. Cell Fact.*, 14(198):1–9.

Harreither, E., M. Hackl, J. Pichler, S. Shridhar, N. Auer, P. P. Łabaj, M. Scheideler, M. Karbiener, J. Grillari, D. P. Kreil, & N. Borth (2015). Microarray profiling of preselected CHO host cell subclones identifies gene expression patterns associated with increased production capacity. *Biotechnol. J.*, 10(10):1625–1638.

Hartl, F.-U., N. Pfanner, D. W. Nicholson, & W. Neupert (1989). Mitochondrial protein import. *Biochim. Biophys. Acta - Rev. Biomembr.*, 988(1):1–45.

He, G., Z. H. Siddik, Z. Huang, R. Wang, J. Koomen, R. Kobayashi, A. R. Khokhar, & J. Kuang (2005). Induction of p21 by p53 following DNA damage inhibits both Cdk4 and Cdk2 activities. *Oncogene*, 24(18):2929–2943.

Henderson Jr, J. W. & A. Brooks (2010). Improved Amino Acid Methods using Agilent ZORBAX Eclipse Plus C18 Columns for a Variety of Agilent LC Instrumentation and Separation Goals. *Agil. Technol. Wilmington, DE, USA.*

Hernández Bort, J. A., M. Hackl, H. Höflmayer, V. Jadhav, E. Harreither, N. Kumar, W. Ernst, J. Grillari, & N. Borth (2012). Dynamic mRNA and miRNA profiling of CHO-K1 suspension cell cultures. *Biotechnol. J.*, 7(4):500–515.

Hinkle, P. C. (2005). P/O ratios of mitochondrial oxidative phosphorylation. *Biochim Biophys Acta*, 1706(1-2):1–11.

Hock, M. B. & A. Kralli (2009). Transcriptional control of mitochondrial biogenesis and function. *Annu. Rev. Physiol.*, 71:177–203.

Hoitzing, H., I. G. Johnston, & N. S. Jones (2015). What is the function of mitochondrial networks? A theoretical assessment of hypotheses and proposal for future research. *Bioessays,* 37(6):687–700.

Hollingsworth, M. A. & B. J. Swanson (2004). Mucins in cancer: protection and control of the cell surface. *Nat. Rev. Cancer,* 4(1):45–60.

Horvath, B., M. Mun, & M. W. Laird (2010). Characterization of a monoclonal antibody cell culture production process using a quality by design approach. *Mol. Biotechnol.,* 45(3):203–206.

Hossler, P., S. F. Khattak, & Z. J. Li (2009). Optimal and consistent protein glycosylation in mammalian cell culture. *Glycobiology,* 19(9):936–949.

Howaldt, M., F. Walz, & R. Kempken (2011). Kultivierung von Säugetierzellen. In *Bioprozesstechnik,* H. Chmiel, ed., chapter 11, Pp. 373–425. Heidelberg: Spektrum Akademischer Verlag.

Hutvágner, G., J. McLachlan, A. E. Pasquinelli, E. Bálint, T. Tuschl, & P. D. Zamore (2001). A cellular function for the RNA-interference enzyme Dicer in the maturation of the let-7 small temporal RNA. *Science,* 293(5531):834–838.

Illner, M. (2012). Design and optimization of a method for metabolite extraction from CHO cells. *Diploma Thesis, Inst. Biochem. Eng. Univ. Stuttgart.*

Jadhav, V., M. Hackl, A. Druz, S. Shridhar, C. Y. Chung, K. M. Heffner, D. P. Kreil, M. Betenbaugh, J. Shiloach, N. Barron, J. Grillari, & N. Borth (2013). CHO microRNA engineering is growing up: Recent successes and future challenges. *Biotechnol Adv,* 31(8):1501–1513.

Jadhav, V., M. Hackl, G. Klanert, J. A. Hernandez Bort, R. Kunert, J. Grillari, & N. Borth (2014). Stable overexpression of miR-17 enhances recombinant protein production of CHO cells. *J. Biotechnol.,* 175:38–44.

Jamnikar, U., P. Nikolic, A. Belic, M. Blas, D. Gaser, A. Francky, H. Laux, A. Blejec, S. Baebler, & K. Gruden (2015). Transcriptome study and identification of potential marker genes related to the stable expression of recombinant proteins in CHO clones. *BMC Biotechnol.,* 15(98):1–10.

Janakiraman, V., C. Kwiatkowski, R. Kshirsagar, T. Ryll, & Y.-M. Huang (2015). Application of high-throughput mini-bioreactor system for systematic scale-down modeling, process characterization, and control strategy development. *Biotechnol. Prog.,* 31(6):1623–1632.

Jayapal, K. R., K. F. Wlaschin, W. S. Hu, & M. G. S. Yap (2007). Recombinant protein therapeutics from CHO cells - 20 years and counting. *Chem. Eng. Prog.,* 103(10):40–47.

Jefferis, R. (2009). Glycosylation as a strategy to improve antibody-based therapeutics. *Nat. Rev. Drug Discov.,* 8(3):226–234.

Jeong, D.-w., T. S. Kim, J. W. Lee, K. T. Kim, H. J. Kim, I.-H. Kim, & I. Y. Kim (2001). Blocking of Acidosis-Mediated Apoptosis by a Reduction of Lactate Dehydrogenase Activity through Antisense mRNA Expression. *Biochem. Biophys. Res. Commun.*, 289(5):1141–1149.

Jiang, X., X. Chen, L. Chen, Y. Ma, L. Zhou, Q. Qi, Y. Liu, S. Zhang, J. Luo, & X. Zhou (2015). Upregulation of the miR-212/132 cluster suppresses proliferation of human lung cancer cells. *Oncol. Rep.*, 33(2):705–712.

Johnson, K. C., N. M. Jacob, P. M. Nissom, M. Hackl, L. H. Lee, M. Yap, & W. S. Hu (2011). Conserved microRNAs in Chinese hamster ovary cell lines. *Biotechnol Bioeng*, 108(2):475–480.

Jonckheere, A. I., J. A. M. Smeitink, & R. J. T. Rodenburg (2012). Mitochondrial ATP synthase: architecture, function and pathology. *J. Inherit. Metab. Dis.*, 35(2):211–225.

Jones, R. G., D. R. Plas, S. Kubek, M. Buzzai, J. Mu, Y. Xu, M. J. Birnbaum, & C. B. Thompson (2005). AMP-activated protein kinase induces a p53-dependent metabolic checkpoint. *Mol. Cell*, 18(3):283–293.

Kantardjieff, A., P. M. Nissom, S. H. Chuah, F. Yusufi, N. M. Jacob, B. C. Mulukutla, M. Yap, & W.-S. Hu (2009). Developing genomic platforms for Chinese hamster ovary cells. *Biotechnol. Adv.*, 27(6):1028–1035.

Katoh, S., J.-i. Horiuchi, & F. Yoshida (2015). *Biochemical Engineering*, 2nd edition. Weinheim: Wiley-VCH.

Kaufmann, H., X. Mazur, M. Fussenegger, & J. E. Bailey (1999). Influence of low temperature on productivity, proteome and protein phosphorylation of CHO cells. *Biotechnol Bioeng*, 63(5):573–582.

Kelly, P. S., L. Breen, C. Gallagher, S. Kelly, M. Henry, N. T. Lao, P. Meleady, D. O'Gorman, M. Clynes, & N. Barron (2015a). Re-programming CHO cell metabolism using miR-23 tips the balance towards a highly productive phenotype. *Biotechnol. J.*, 10(7):1029–1040.

Kelly, P. S., C. Gallagher, M. Clynes, & N. Barron (2015b). Conserved microRNA function as a basis for Chinese hamster ovary cell engineering. *Biotechnol. Lett.*, 37(4):787–798.

Khella, H. W. Z., M. Bakhet, G. Allo, M. A. S. Jewett, A. H. Girgis, A. Latif, H. Girgis, I. Von Both, G. A. Bjarnason, & G. M. Yousef (2013). miR-192, miR-194 and miR-215: a convergent microRNA network suppressing tumor progression in renal cell carcinoma. *Carcinogenesis*, 34(10):2231–2239.

Khvorova, A., A. Reynolds, & S. D. Jayasena (2003). Functional siRNAs and miRNAs Exhibit Strand Bias. *Cell*, 115(2):209–216.

Kiehl, T. R., D. Shen, S. F. Khattak, Z. Jian Li, & S. T. Sharfstein (2011). Observations of cell size dynamics under osmotic stress. *Cytom. A*, 79(7):560–569.

Kim, J. Y., Y. G. Kim, & G. M. Lee (2012). CHO cells in biotechnology for production of recombinant proteins: current state and further potential. *Appl Microbiol Biotechnol*, 93(3):917–930.

Kim, N. S. & G. M. Lee (2002). Response of recombinant Chinese hamster ovary cells to hyperosmotic pressure: effect of Bcl-2 overexpression. *J Biotechnol*, 95(3):237–248.

Kim, S. H. & G. M. Lee (2007a). Down-regulation of lactate dehydrogenase-A by siRNAs for reduced lactic acid formation of Chinese hamster ovary cells producing thrombopoietin. *Appl. Microbiol. Biotechnol.*, 74(1):152–159.

Kim, S. H. & G. M. Lee (2007b). Functional expression of human pyruvate carboxylase for reduced lactic acid formation of Chinese hamster ovary cells (DG44). *Appl Microbiol Biotechnol*, 76(3):659–665.

Kim, V. N. (2004). MicroRNA precursors in motion: exportin-5 mediates their nuclear export. *Trends Cell Biol.*, 14(4):156–159.

Kim, V. N., J. Han, & M. C. Siomi (2009). Biogenesis of small RNAs in animals. *Nat. Rev. Mol. Cell Biol.*, 10(2):126–139.

Kimura, R. & W. M. Miller (1996). Effects of elevated pCO(2) and/or osmolality on the growth and recombinant tPA production of CHO cells. *Biotechnol. Bioeng.*, 52(1):152–160.

Klausing, S., O. Krämer, & T. Noll (2011). Bioreactor cultivation of CHO DP-12 cells under sodium butyrate treatment – comparative transcriptome analysis with CHO cDNA microarrays. *BMC Proc.*, 5(Suppl 8):P98.

Klempnauer, K.-H., L. Fischer, & M. K. Otto (2011). Einführung in die Biochemie. In *Bioprozesstechnik*, H. Chmiel, ed., chapter 2, Pp. 23–65. Heidelberg: Spektrum Akademischer Verlag.

Klingenberg, M. & H. Rottenberg (1977). Relation between the Gradient of the ATP/ADP Ratio and the Membrane Potential across the Mitochondrial Membrane. *Eur. J. Biochem.*, 73(1):125–130.

Kong, W.-Q., R. Bai, T. Liu, C.-L. Cai, M. Liu, X. Li, & H. Tang (2012). MicroRNA-182 targets cAMP-responsive element-binding protein 1 and suppresses cell growth in human gastric adenocarcinoma. *FEBS J.*, 279(7):1252–60.

Kozomara, A. & S. Griffiths-Jones (2011). miRBase: integrating microRNA annotation and deep-sequencing data. *Nucleic Acids Res*, 39:D152–D157.

Kozomara, A. & S. Griffiths-Jones (2014). miRBase: annotating high confidence microRNAs using deep sequencing data. *Nucleic Acids Res.*, 42:D68–D73.

Kuwana, T., M. R. Mackey, G. Perkins, M. H. Ellisman, M. Latterich, R. Schneiter, D. R. Green, & D. D. Newmeyer (2002). Bid, Bax, and Lipids Cooperate to Form Supramolecular Openings in the Outer Mitochondrial Membrane. *Cell*, 111(3):331–342.

Kuznetsov, A. V., V. Veksler, F. N. Gellerich, V. Saks, R. Margreiter, & W. S. Kunz (2008). Analysis of mitochondrial function in situ in permeabilized muscle fibers, tissues and cells. *Nat. Protoc.*, 3(6):965–976.

Kwon, H. M., A. Yamauchi, S. Uchida, A. S. Preston, A. Garcia-Perez, M. B. Burg, & J. S. Handler (1992). Cloning of the cDNa for a Na+/myo-inositol cotransporter, a hypertonicity stress protein. *J. Biol. Chem.*, 267(9):6297–6301.

Lagos-Quintana, M., R. Rauhut, W. Lendeckel, & T. Tuschl (2001). Identification of novel genes coding for small expressed RNAs. *Science*, 294(5543):853–858.

Lagow, E., M. M. DeSouza, & D. D. Carson (1999). Mammalian reproductive tract mucins. *Hum. Reprod. Update*, 5(4):280–292.

Lane, A. N. & T. W.-M. Fan (2015). Regulation of mammalian nucleotide metabolism and biosynthesis. *Nucleic Acids Res.*, 43(4):2466–2485.

Lang, F., G. L. Busch, M. Ritter, H. Volkl, S. Waldegger, E. Gulbins, & D. Haussinger (1998). Functional significance of cell volume regulatory mechanisms. *Physiol Rev*, 78(1):247–306.

LaNoue, K. F. & A. C. Schoolwerth (1979). Metabolite Transport in Mitochondria. *Annu. Rev. Biochem.*, 48:871–922.

Lao, M. S. & D. Toth (1997). Effects of ammonium and lactate on growth and metabolism of a recombinant Chinese hamster ovary cell culture. *Biotechnol Prog*, 13(5):688–691.

Lara, A. R., E. Galindo, O. T. Ramírez, & L. A. Palomares (2006). Living with heterogeneities in bioreactors: understanding the effects of environmental gradients on cells. *Mol. Biotechnol.*, 34(3):355–381.

Lattenmayer, C., M. Loeschel, K. Schriebl, W. Steinfellner, T. Sterovsky, E. Trummer, K. Vorauer-Uhl, D. Muller, H. Katinger, & R. Kunert (2007). Protein-free transfection of CHO host cells with an IgG-fusion protein: selection and characterization of stable high producers and comparison to conventionally transfected clones. *Biotechnol Bioeng*, 96(6):1118–1126.

Lau, N. C., L. P. Lim, E. G. Weinstein, & D. P. Bartel (2001). An abundant class of tiny RNAs with probable regulatory roles in Caenorhabditis elegans. *Science*, 294(5543):858–862.

Lavrik, I., A. Golks, & P. H. Krammer (2005). Death receptor signaling. *J. Cell Sci.*, 118(2):265–267.

Le, H., C. Chen, & C. T. Goudar (2015). An evaluation of public genomic references for mapping RNA-Seq data from Chinese hamster ovary cells. *Biotechnol. Bioeng.*, 112(11):2412–2416.

Lee, H.-C., P.-H. Yin, C.-W. Chi, & Y.-H. Wei (2002a). Increase in mitochondrial mass in human fibroblasts under oxidative stress and during replicative cell senescence. *J. Biomed. Sci.*, 9(6):517–526.

Lee, M. S., K. W. Kim, Y. H. Kim, & G. M. Lee (2003a). Proteome analysis of antibody-expressing CHO cells in response to hyperosmotic pressure. *Biotechnol Prog*, 19(6):1734–1741.

Lee, R. C. & V. Ambros (2001). An extensive class of small RNAs in Caenorhabditis elegans. *Science*, 294(5543):862–864.

Lee, R. C., R. L. Feinbaum, & V. Ambros (1993). The C. elegans heterochronic gene lin-4 encodes small RNAs with antisense complementarity to lin-14. *Cell*, 75(5):843–854.

Lee, S., S. Kim, X. Sun, J. H. Lee, & H. Cho (2007). Cell cycle-dependent mitochondrial biogenesis and dynamics in mammalian cells. *Biochem. Biophys. Res. Commun.*, 357(1):111–117.

Lee, Y., C. Ahn, J. Han, H. Choi, J. Kim, J. Yim, J. Lee, P. Provost, O. Radmark, S. Kim, & V. N. Kim (2003b). The nuclear RNase III Drosha initiates microRNA processing. *Nature*, 425(6956):415–419.

Lee, Y., K. Jeon, J.-T. Lee, S. Kim, & V. N. Kim (2002b). MicroRNA maturation: stepwise processing and subcellular localization. *EMBO J.*, 21(17):4663–4670.

Lee, Y., M. Kim, J. Han, K.-H. Yeom, S. Lee, S. H. Baek, & V. N. Kim (2004). MicroRNA genes are transcribed by RNA polymerase II. *EMBO J.*, 23(20):4051–4060.

Lee, Y. Y., K. T. K. Wong, J. Tan, P. C. Toh, Y. Mao, V. Brusic, & M. G. S. Yap (2009). Overexpression of heat shock proteins (HSPs) in CHO cells for extended culture viability and improved recombinant protein production. *J. Biotechnol.*, 143(1):34–43.

Legmann, R., H. B. Schreyer, R. G. Combs, E. L. McCormick, A. P. Russo, & S. T. Rodgers (2009). A predictive high-throughput scale-down model of monoclonal antibody production in CHO cells. *Biotechnol. Bioeng.*, 104(6):1107–1120.

Leung, A. K. & P. A. Sharp (2010). MicroRNA functions in stress responses. *Mol Cell*, 40(2):205–215.

Lewis, A. M., N. R. Abu-Absi, M. C. Borys, & Z. J. Li (2016). The use of 'Omics technology to rationally improve industrial mammalian cell line performance. *Biotechnol. Bioeng.*, 113(1):26–38.

Lewis, B. P., I.-h. Shih, M. W. Jones-Rhoades, D. P. Bartel, & C. B. Burge (2003). Prediction of Mammalian MicroRNA Targets. *Cell*, 115(7):787–798.

Lewis, N. E., X. Liu, Y. Li, H. Nagarajan, G. Yerganian, E. O'Brien, A. Bordbar, A. M. Roth, J. Rosenbloom, C. Bian, M. Xie, W. Chen, N. Li, D. Baycin-Hizal, H. Latif, J. Forster, M. J. Betenbaugh, I. Famili, X. Xu, J. Wang, & B. O. Palsson (2013). Genomic landscapes of Chinese hamster ovary cell lines as revealed by the Cricetulus griseus draft genome. *Nat. Biotechnol.*, 31(8):759–765.

Li, F., N. Vijayasankaran, A. Y. Shen, R. Kiss, & A. Amanullah (2010). Cell culture processes for monoclonal antibody production. *MAbs*, 2(5):466–479.

Li, P., C. Sheng, L. Huang, H. Zhang, L. Huang, Z. Cheng, & Q. Zhu (2014). MiR-183/-96/-182 cluster is up-regulated in most breast cancers and increases cell proliferation and migration. *Breast cancer Res.*, 16(473):1–17.

Lieder, S., P. I. Nikel, V. de Lorenzo, & R. Takors (2015). Genome reduction boosts heterologous gene expression in Pseudomonas putida. *Microb. Cell Fact.*, 14(23):1–14.

Lin, J., M. Takagi, Y. Qu, P. Gao, & T. Yoshida (1999). Metabolic flux change in hybridoma cells under high osmotic pressure. *J Biosci Bioeng*, 87(2):255–257.

Lin, N., A. Davis, S. Bahr, T. Borgschulte, K. Achtien, & K. Kayser (2011). Profiling highly conserved microrna expression in recombinant IgG-producing and parental Chinese hamster ovary cells. *Biotechnol Prog*, 27(4):1163–1171.

Liu, Y.-X., J. Wang, J. Guo, J. Wu, H. B. Lieberman, & Y. Yin (2008). DUSP1 Is Controlled by p53 during the Cellular Response to Oxidative Stress. *Mol. Cancer Res.*, 6(4):624–633.

Liu, Z., J. Liu, M. F. Segura, C. Shao, P. Lee, Y. Gong, E. Hernando, & J.-J. Wei (2012). MiR-182 overexpression in tumourigenesis of high-grade serous ovarian carcinoma. *J. Pathol.*, 228(2):204–215.

Loh, W. P., B. Loo, L. Zhou, P. Zhang, D.-Y. Lee, Y. Yang, & K. P. Lam (2014). Overexpression of microRNAs enhances recombinant protein production in Chinese hamster ovary cells. *Biotechnol. J.*, 9(9):1140–1151.

Lund, E., S. Güttinger, A. Calado, J. E. Dahlberg, & U. Kutay (2004). Nuclear export of microRNA precursors. *Science*, 303(5654):95–98.

Ma, H. T. & R. Y. C. Poon (2011). How protein kinases co-ordinate mitosis in animal cells. *Biochem. J.*, 435(1):17–31.

Malumbres, M. & M. Barbacid (2005). Mammalian cyclin-dependent kinases. *Trends Biochem Sci*, 30(11):630–641.

Maniataki, E. & Z. Mourelatos (2005). A human, ATP-independent, RISC assembly machine fueled by pre-miRNA. *Genes Dev.*, 19(24):2979–2990.

Mannella, C. A. (1992). The 'ins' and 'outs' of mitochondrial membrane channels. *Trends Biochem Sci*, 17(8):315–320.

Martínez-Costa, O. H., V. Sánchez, A. Lázaro, E. D. Hernández, K. Tornheim, & J. J. Aragón (2012). Distinct functional roles of the two terminal halves of eukaryotic phosphofructokinase. *Biochem. J.*, 445(2):213–218.

Masai, H., S. Matsumoto, Z. You, N. Yoshizawa-Sugata, & M. Oda (2010). Eukaryotic chromosome DNA replication: where, when, and how? *Annu. Rev. Biochem.*, 79:89–130.

Matuszczyk, J.-C., A. Teleki, J. Pfizenmaier, & R. Takors (2015). Compartment-specific metabolomics for CHO reveals that ATP pools in mitochondria are much lower than in cytosol. *Biotechnol. J.*, 10(10):1639–1650.

Mazur, X., M. Fussenegger, W. A. Renner, & J. E. Bailey (1998). Higher productivity of growth-arrested Chinese hamster ovary cells expressing the cyclin-dependent kinase inhibitor p27. *Biotechnol. Prog.*, 14(5):705–713.

McCarthy, D. J., Y. Chen, & G. K. Smyth (2012). Differential expression analysis of multifactor RNA-Seq experiments with respect to biological variation. *Nucleic Acids Res.*, 40(10):4288–4297.

McClatchey, P. M., A. C. Keller, R. Bouchard, L. A. Knaub, & J. E. B. Reusch (2015). Fully automated software for quantitative measurements of mitochondrial morphology. *Mitochondrion*, 26:58–71.

McMurray-Beaulieu, V., S. Hisiger, C. Durand, M. Perrier, & M. Jolicoeur (2009). Na-butyrate sustains energetic states of metabolism and t-PA productivity of CHO cells. *J Biosci Bioeng*, 108(2):160–167.

Meinhold, H. (2012). Metabolic flux analysis in mammalian cells: Impact of compartments on intracellular flux patterns in CHO DP12 cells. *Master Thesis, Inst. Biochem. Eng. Univ. Stuttgart*.

Meleady, P., M. Gallagher, C. Clarke, M. Henry, N. Sanchez, N. Barron, & M. Clynes (2012). Impact of miR-7 over-expression on the proteome of Chinese hamster ovary cells. *J. Biotechnol.*, 160(3-4):251–262.

Melville, M., P. Doolan, W. Mounts, N. Barron, L. Hann, M. Leonard, M. Clynes, & T. Charlebois (2011). Development and characterization of a Chinese hamster ovary cell-specific oligonucleotide microarray. *Biotechnol. Lett.*, 33(9):1773–1779.

Miller, W. M., C. R. Wilke, & H. W. Blanch (1987). Effects of dissolved oxygen concentration on hybridoma growth and metabolism in continuous culture. *J Cell Physiol*, 132(3):524–530.

Mimura, Y., P. R. Ashton, N. Takahashi, D. J. Harvey, & R. Jefferis (2007). Contrasting glycosylation profiles between Fab and Fc of a human IgG protein studied by electrospray ionization mass spectrometry. *J. Immunol. Methods*, 326(1-2):116–126.

Mirazimi, A. & L. Svensson (2000). ATP is required for correct folding and disulfide bond formation of rotavirus VP7. *J. Virol.*, 74(17):8048–8052.

Mitchell, P. (1966). Chemiosmotic coupling in oxidative and photosynthetic phosphorylation. *Biol. Rev.*, 41(3):445–501.

Mitchell, P. (1975). The protonmotive Q cycle: a general formulation. *FEBS Lett.*, 59(2):137–139.

Mitra, K., C. Wunder, B. Roysam, G. Lin, & J. Lippincott-Schwartz (2009). A hyperfused mitochondrial state achieved at G1-S regulates cyclin E buildup and entry into S phase. *Proc. Natl. Acad. Sci.*, 106(29):11960–11965.

Mizoguchi, H., H. Mori, & T. Fujio (2007). Escherichia coli minimum genome factory. *Biotechnol. Appl. Biochem.*, 46(Pt 3):157–167.

Moro, F., C. Sirrenberg, H. Schneider, W. Neupert, & M. Brunner (1999). The TIM17-23 preprotein translocase of mitochondria: composition and function in protein transport into the matrix. *EMBO J.*, 18(13):3667–3675.

Mortimer, C. E. & U. Müller (2003). Osmose. In *Chemie Das Basiswissen der Chemie*, chapter 13.9, Pp. 215–216. Stuttgart: Georg Thieme Verlag.

Mulukutla, B. C., M. Gramer, & W. S. Hu (2012). On metabolic shift to lactate consumption in fed-batch culture of mammalian cells. *Metab Eng*, 14(2):138–149.

Mulukutla, B. C., S. Khan, A. Lange, & W. S. Hu (2010). Glucose metabolism in mammalian cell culture: new insights for tweaking vintage pathways. *Trends Biotechnol*, 28(9):476–484.

Nass, M. M. & S. Nass (1963). Intramitochondrial fibers with DNA characteristics. I. fixation and electron staining reactions. *J. Cell Biol.*, 19:593–611.

Nath, S. & J. Villadsen (2015). Oxidative phosphorylation revisited. *Biotechnol. Bioeng.*, 112(3):429–437.

Natsume, A., R. Niwa, & M. Satoh (2009). Improving effector functions of antibodies for cancer treatment: Enhancing ADCC and CDC. *Drug Des Devel Ther*, 3:7–16.

Neupert, W. & J. M. Herrmann (2007). Translocation of proteins into mitochondria. *Annu. Rev. Biochem.*, 76:723–749.

Nielsen, J. & M. C. Jewett (2008). Impact of systems biology on metabolic engineering of Saccharomyces cerevisiae. *FEMS Yeast Res*, 8(1):122–131.

Nienow, A. W. (2006). Reactor engineering in large scale animal cell culture. *Cytotechnology*, 50(1-3):9–33.

Nigg, E. A. (2001). Mitotic kinases as regulators of cell division and its checkpoints. *Nat. Rev. Mol. Cell Biol.*, 2(1):21–32.

Nissom, P. M., A. Sanny, Y. J. Kok, Y. T. Hiang, S. H. Chuah, T. K. Shing, Y. Y. Lee, K. T. Wong, W. S. Hu, M. Y. Sim, & R. Philp (2006). Transcriptome and proteome profiling to understanding the biology of high productivity CHO cells. *Mol Biotechnol*, 34(2):125–140.

Nueda, M. J., S. Tarazona, & A. Conesa (2014). Next maSigPro: updating maSigPro bioconductor package for RNA-seq time series. *Bioinformatics*, 30(18):2598–2602.

Oldiges, M., S. Lütz, S. Pflug, K. Schroer, N. Stein, & C. Wiendahl (2007). Metabolomics: current state and evolving methodologies and tools. *Appl. Microbiol. Biotechnol.*, 76(3):495–511.

Oulas, A., N. Karathanasis, A. Louloupi, I. Iliopoulos, K. Kalantidis, & P. Poirazi (2012). A new microRNA target prediction tool identifies a novel interaction of a putative miRNA with CCND2. *RNA Biol.*, 9(9):1196–1207.

Oulas, A., N. Karathanasis, A. Louloupi, G. A. Pavlopoulos, P. Poirazi, K. Kalantidis, & I. Iliopoulos (2015). Prediction of miRNA targets. *Methods Mol. Biol.*, 1269:207–229.

Ozturk, S. S. (2015). Oportunities and Challenges for the Implementation of Continuous Processing in Biomanufacturing. In *Contin. Process. Pharm. Manuf.*, G. Subramanian, ed., Pp. 457–476. Weinheim: Wiley-VCH.

Ozturk, S. S. & W.-S. Hu, eds. (2005). *Cell culture technology for pharmaceutical and cell-based therapies*, 1st edition. Boca Raton: CRC Press.

Ozturk, S. S. & B. O. Palsson (1991). Effect of medium osmolarity on hybridoma growth, metabolism, and antibody production. *Biotechnol Bioeng*, 37(10):989–993.

Pacis, E., M. Yu, J. Autsen, R. Bayer, & F. Li (2011). Effects of cell culture conditions on antibody N-linked glycosylation-what affects high mannose 5 glycoform. *Biotechnol. Bioeng.*, 108(10):2348–2358.

Paraskevopoulou, M. D., G. Georgakilas, N. Kostoulas, I. S. Vlachos, T. Vergoulis, M. Reczko, C. Filippidis, T. Dalamagas, & a. G. Hatzigeorgiou (2013). DIANA-microT web server v5.0: service integration into miRNA functional analysis workflows. *Nucleic Acids Res.*, 41:169–173.

Park, H.-S., I.-H. Kim, I.-Y. Kim, K.-H. Kim, & H.-J. Kim (2000). Expression of carbamoyl phosphate synthetase I and ornithine transcarbamoylase genes in Chinese hamster ovary dhfr-cells decreases accumulation of ammonium ion in culture media. *J. Biotechnol.*, 81(2):129–140.

Park, J.-K., J. C. Henry, J. Jiang, C. Esau, Y. Gusev, M. R. Lerner, R. G. Postier, D. J. Brackett, & T. D. Schmittgen (2011). miR-132 and miR-212 are increased in pancreatic cancer and target the retinoblastoma tumor suppressor. *Biochem. Biophys. Res. Commun.*, 406(4):518–523.

Parpa, E., A. Ortega, & L. Saenz (2009). Down-regulation of Egr-1 by siRNA inhibits growth of human prostate carcinoma cell line PC-3. *Oncol. Rep.*, 22(6):1513–1518.

Partridge, M. A., M. M. Davidson, & T. K. Hei (2007). The complete nucleotide sequence of Chinese hamster (Cricetulus griseus) mitochondrial DNA. *DNA Seq*, 18(5):341–346.

Pasquinelli, A. E., B. J. Reinhart, F. Slack, M. Q. Martindale, M. I. Kuroda, B. Maller, D. C. Hayward, E. E. Ball, B. Degnan, P. Muller, J. Spring, A. Srinivasan, M. Fishman, J. Finnerty, J. Corbo, M. Levine, P. Leahy, E. Davidson, & G. Ruvkun (2000). Conservation of the sequence and temporal expression of let-7 heterochronic regulatory RNA. *Nature*, 408(6808):86–89.

Passarella, S., A. Atlante, D. Valenti, & L. de Bari (2003). The role of mitochondrial transport in energy metabolism. *Mitochondrion*, 2(5):319–343.

Pernas, L. & L. Scorrano (2016). Mito-Morphosis: Mitochondrial Fusion, Fission, and Cristae Remodeling as Key Mediators of Cellular Function. *Annu. Rev. Physiol.*, 78:505–531.

Pfanner, N., K. Hill, K. Model, M. T. Ryan, K. Dietmeier, F. Martin, & R. Wagner (1998). Tom40 forms the hydrophilic channel of the mitochondrial import pore for preproteins. *Nature*, 395(6701):516–521.

Pfizenmaier, J. (2011). Tool development for flow cytometric qualitative/quantitative analysis of mitochondrial number in CHO cells. *Diploma Thesis, Inst. Biochem. Eng. Univ. Stuttgart*.

Pfizenmaier, J., L. Junghans, A. Teleki, & R. Takors (2016). Hyperosmotic Stimulus Study Discloses Benefits in ATP Supply and Reveals miRNA/mRNA Targets to Improve Recombinant Protein Production of CHO Cells. *Biotechnol. J.*, 11:1037–1047.

Pfizenmaier, J., J.-C. Matuszczyk, & R. Takors (2015). Changes in Intracellular ATP-Content of CHO Cells as Response to Hyperosmolality. *Biotechnol. Prog.*, 31(5):1212–1216.

Pfizenmaier, J. & R. Takors (2016). Host organisms: Mammalian Cells. In *Ind. Biotechnol. Microorg. Adv. Biotechnol. (Volume 3)*, J. Liao and C. Wittmann, eds., chapter 17. Weinheim: Wiley-VCH.

Pichiorri, F., S.-S. Suh, A. Rocci, L. De Luca, C. Taccioli, R. Santhanam, W. Zhou, D. M. Benson, C. Hofmainster, H. Alder, M. Garofalo, G. Di Leva, S. Volinia, H.-J. Lin, D. Perrotti, M. Kuehl, R. I. Aqeilan, A. Palumbo, & C. M. Croce (2010). Downregulation of p53-inducible microRNAs 192, 194, and 215 Impairs the p53-MDM2 Autoregulatory Loop in Multiple Myeloma Development. *Cancer Cell*, 18(4):367–381.

Poon, R. Y. C. (2016). Cell Cycle Control: A System of Interlinking Oscillators. *Methods Mol. Biol.*, 1342:3–19.

Povey, S., J. White, J. Nahmias, & H. Wain (1997). Problems of nomenclature. *Nature*, 390(6658):329.

Pritchard, M. T., R. N. Malinak, & L. E. Nagy (2011). Early growth response (EGR)-1 is required for timely cell-cycle entry and progression in hepatocytes after acute carbon tetrachloride exposure in mice. *Am. J. Physiol. Gastrointest. Liver Physiol.*, 300(6):1124–1131.

Puck, T. T., S. J. Cieciura, & A. Robinson (1958). Genetics of somatic mammalian cells. III. Long-term cultivation of euploid cells from human and animal subjects. *J Exp Med*, 108(6):945–956.

Qu, Y., W.-C. Li, M. R. Hellem, K. Rostad, M. Popa, E. McCormack, A. M. Oyan, K.-H. Kalland, & X.-S. Ke (2013). MiR-182 and miR-203 induce mesenchymal to epithelial transition and self-sufficiency of growth signals via repressing SNAI2 in prostate cells. *Int. J. Cancer*, 133(3):544–555.

Ragione, F. D., V. Cucciolla, V. Criniti, S. Indaco, A. Borriello, & V. Zappia (2003). p21Cip1 gene expression is modulated by Egr1: a novel regulatory mechanism involved in the resveratrol antiproliferative effect. *J. Biol. Chem.*, 278(26):23360–23368.

Reczko, M., M. Maragkakis, P. Alexiou, I. Grosse, & A. G. Hatzigeorgiou (2012). Functional microRNA targets in protein coding sequences. *Bioinformatics*, 28(6):771–776.

Reinhart, B. J., F. J. Slack, M. Basson, A. E. Pasquinelli, J. C. Bettinger, A. E. Rougvie, H. R. Horvitz, & G. Ruvkun (2000). The 21-nucleotide let-7 RNA regulates developmental timing in Caenorhabditis elegans. *Nature*, 403(6772):901–906.

Renault, T. T., X. Grandier-Vazeille, H. Arokium, G. Velours, N. Camougrand, M. Priault, O. Teijido, L. M. Dejean, & S. Manon (2012). The cytosolic domain of human Tom22 modulates human Bax mitochondrial translocation and conformation in yeast. *FEBS Lett.*, 586(2):116–121.

Robinson, M. D., D. J. McCarthy, & G. K. Smyth (2010). edgeR: a Bioconductor package for differential expression analysis of digital gene expression data. *Bioinformatics*, 26(1):139–140.

Roobol, A., J. Roobol, M. J. Carden, A. Bastide, A. E. Willis, W. B. Dunn, R. Goodacre, & C. M. Smales (2011). ATR (ataxia telangiectasia mutated-and Rad3-related kinase) is activated by mild hypothermia in mammalian cells and subsequently activates p53. *Biochem. J*, 435:499–508.

Ross, D. W. & H. C. Mel (1972). Growth dynamics of mitochondria in synchronized Chinese hamster cells. *Biophys. J.*, 12(11):1562–1572.

Rupp, O., J. Becker, K. Brinkrolf, C. Timmermann, N. Borth, A. Pühler, T. Noll, & A. Goesmann (2014). Construction of a public CHO cell line transcript database using versatile bioinformatics analysis pipelines. *PLoS One*, 9(1):e85568.

Ryu, J. S., T. K. Kim, J. Y. Chung, & G. M. Lee (2000). Osmoprotective effect of glycine betaine on foreign protein production in hyperosmotic recombinant chinese hamster ovary cell cultures differs among cell lines. *Biotechnol Bioeng*, 70(2):167–175.

Ryu, J. S., M. S. Lee, & G. M. Lee (2001). Effects of cloned gene dosage on the response of recombinant CHO cells to hyperosmotic pressure in regard to cell growth and antibody production. *Biotechnol Prog*, 17(6):993–999.

Saelens, X., N. Festjens, L. V. Walle, M. van Gurp, G. van Loo, & P. Vandenabeele (2004). Toxic proteins released from mitochondria in cell death. *Oncogene*, 23(16):2861–2874.

Santel, A. & M. T. Fuller (2001). Control of mitochondrial morphology by a human mitofusin. *J. Cell Sci.*, 114(5):867–874.

Sarver, A. L., H. Li, & S. Subramanian (2010). MicroRNA miR-183 functions as an oncogene by targeting the transcription factor EGR1 and promoting tumor cell migration. *Cancer Res.*, 70(23):9570–9580.

Sauer, M. & D. Mattanovich (2012). Construction of microbial cell factories for industrial bioprocesses. *J. Chem. Technol. Biotechnol.*, 87(4):445–450.

Scharnhorst, V., A. L. Menke, J. Attema, J. K. Haneveld, N. Riteco, G. J. van Steenbrugge, A. J. van der Eb, & A. G. Jochemsen (2000). EGR-1 enhances tumor growth and modulates the effect of the Wilms' tumor 1 gene products on tumorigenicity. *Oncogene*, 19(6):791–800.

Schaub, J., C. Clemens, H. Kaufmann, & T. W. Schulz (2012). Advancing biopharmaceutical process development by system-level data analysis and integration of omics data. *Adv Biochem Eng Biotechnol*, 127:133–163.

Schaub, J., C. Clemens, P. Schorn, T. Hildebrandt, W. Rust, D. Mennerich, H. Kaufmann, & T. W. Schulz (2010). CHO gene expression profiling in biopharmaceutical process analysis and design. *Biotechnol Bioeng*, 105(2):431–438.

Scheffler, I. E. (2001). A century of mitochondrial research: achievements and perspectives. *Mitochondrion*, 1(1):3–31.

Schmitt, S., U. Ahting, L. Eichacker, B. Granvogl, N. E. Go, F. E. Nargang, W. Neupert, & S. Nussberger (2005). Role of Tom5 in Maintaining the Structural Stability of the TOM Complex of Mitochondria. *J. Biol. Chem.*, 280(15):14499–14506.

Schwarz, D. S., G. Hutvágner, T. Du, Z. Xu, N. Aronin, & P. D. Zamore (2003). Asymmetry in the Assembly of the RNAi Enzyme Complex. *Cell*, 115(2):199–208.

Schwenke, W. D., S. Soboll, H. J. Seitz, & H. Sies (1981). Mitochondrial and cytosolic ATP/ADP ratios in rat liver in vivo. *Biochem. J.*, 200(2):405–408.

Sells, S. F., S. Muthukumar, V. P. Sukhatme, S. A. Crist, & V. M. Rangnekar (1995). The zinc finger transcription factor EGR-1 impedes interleukin-1-inducible tumor growth arrest. *Mol. Cell. Biol.*, 15(2):682–692.

Seth, G., P. Hossler, J. C. Yee, & W. S. Hu (2006). Engineering cells for cell culture bioprocessing–physiological fundamentals. *Adv Biochem Eng Biotechnol*, 101:119–164.

Shen, D., T. R. Kiehl, S. F. Khattak, Z. J. Li, A. He, P. S. Kayne, V. Patel, I. M. Neuhaus, & S. T. Sharfstein (2010). Transcriptomic responses to sodium chloride-induced osmotic stress: a study of industrial fed-batch CHO cell cultures. *Biotechnol Prog*, 26(4):1104–1115.

Shi, Y. (2001). A structural view of mitochondria-mediated apoptosis. *Nat Struct Biol*, 8(5):394–401.

Shin, S. Y., C. G. Kim, S. H. Kim, Y. S. Kim, Y. Lim, & Y. H. Lee (2010). Chlorpromazine activates p21 (Waf1/Cip1) gene transcription via early growth response-1 (Egr-1) in C6 glioma cells. *Exp. Mol. Med.*, 42(5):395–405.

Shotwell, M. A., D. W. Jayme, M. S. Kilberg, & D. L. Oxender (1981). Neutral amino acid transport systems in Chinese hamster ovary cells. *J. Biol. Chem.*, 256(11):5422–5427.

Shows, T. B., P. J. McAlpine, C. Boucheix, F. S. Collins, P. M. Conneally, J. Frézal, H. Gershowitz, P. N. Goodfellow, J. G. Hall, P. Issitt, C. A. Jones, B. B. Knowles, M. Lewis, V. A. McKusick, M. Meisler, N. E. Morton, P. Rubenstein, M. S. Schanfield, R. D. Schmickel, M. H. Skolnick, M. A. Spence, G. R. Sutherland, M. Traver, N. Van Cong, & H. F. Willard (1987). Guidelines for human gene nomenclature. An international system for human gene nomenclature (ISGN, 1987). *Cytogenet. Cell Genet.*, 46(1-4):11–28.

Sidorenko, Y., A. Wahl, M. Dauner, Y. Genzel, & U. Reichl (2008). Comparison of metabolic flux distributions for MDCK cell growth in glutamine- and pyruvate-containing media. *Biotechnol Prog*, 24(2):311–320.

Sieck, J. B., T. Cordes, W. E. Budach, M. H. Rhiel, Z. Suemeghy, C. Leist, T. K. Villiger, M. Morbidelli, & M. Soos (2013). Development of a Scale-Down Model of hydrodynamic stress to study the performance of an industrial CHO cell line under simulated production scale bioreactor conditions. *J. Biotechnol.*, 164(1):41–9.

Sirrenberg, C., M. F. Bauer, B. Guiard, W. Neupert, & M. Brunner (1996). Import of carrier proteins into the mitochondrial inner membrane mediated by Tim22. *Nature*, 384(6609):582–585.

Soboll, S., R. Scholz, & H. W. Heldt (1978). Subcellular metabolite concentrations. Dependence of mitochondrial and cytosolic ATP systems on the metabolic state of perfused rat liver. *Eur. J. Biochem.*, 87(2):377–390.

Srinivasula, S. M., M. Ahmad, T. Fernandes-Alnemri, & E. S. Alnemri (1998). Autoactivation of Procaspase-9 by Apaf-1-Mediated Oligomerization. *Mol. Cell*, 1(7):949–957.

Stark, G. R. & W. R. Taylor (2006). Control of the G2/M transition. *Mol. Biotechnol.*, 32(3):227–248.

Strotbek, M., L. Florin, J. Koenitzer, A. Tolstrup, H. Kaufmann, A. Hausser, & M. A. Olayioye (2013). Stable microRNA expression enhances therapeutic antibody productivity of Chinese hamster ovary cells. *Metab Eng*, 20:157–166.

Sun, W., Y.-S. Julie Li, H.-D. Huang, J. Y.-J. Shyy, & S. Chien (2010). microRNA: a master regulator of cellular processes for bioengineering systems. *Annu. Rev. Biomed. Eng.*, 12:1–27.

Sun, Z., R. Zhou, S. Liang, K. M. McNeeley, & S. T. Sharfstein (2004). Hyperosmotic stress in murine hybridoma cells: effects on antibody transcription, translation, posttranslational processing, and the cell cycle. *Biotechnol Prog*, 20(2):576–589.

Sung, Y. H., H. J. Kim, & H. W. Lee (2007). Identification of a novel Rb-regulated gene associated with the cell cycle. *Mol Cells*, 24(3):409–415.

Tabuchi, H. & T. Sugiyama (2013). Cooverexpression of alanine aminotransferase 1 in Chinese hamster ovary cells overexpressing taurine transporter further stimulates metabolism and enhances product yield. *Biotechnol Bioeng*, 110(8):2208–2215.

Tabuchi, H., T. Sugiyama, S. Tanaka, & S. Tainaka (2010). Overexpression of taurine transporter in Chinese hamster ovary cells can enhance cell viability and product yield, while promoting glutamine consumption. *Biotechnol. Bioeng.*, 107(6):998–1003.

Tan, J. G., Y. Y. Lee, T. Wang, M. G. S. Yap, T. W. Tan, & S. K. Ng (2015). Heat shock protein 27 overexpression in CHO cells modulates apoptosis pathways and delays activation of caspases to improve recombinant monoclonal antibody titre in fed-batch bioreactors. *Biotechnol. J.*, 10(5):790–800.

Teleki, A., A. Sánchez-Kopper, & R. Takors (2015). Alkaline conditions in hydrophilic interaction liquid chromatography for intracellular metabolite quantification using tandem mass spectrometry. *Anal. Biochem.*, 475:4–13.

Toussaint, C., O. Henry, & Y. Durocher (2016). Metabolic engineering of CHO cells to alter lactate metabolism during fed-batch cultures. *J. Biotechnol.*, 217:122–131.

Trummer, E., K. Fauland, S. Seidinger, K. Schriebl, C. Lattenmayer, R. Kunert, K. Vorauer-Uhl, R. Weik, N. Borth, H. Katinger, & D. Müller (2006). Process parameter shifting: Part I. Effect of DOT, pH, and temperature on the performance of Epo-Fc expressing CHO cells cultivated in controlled batch bioreactors. *Biotechnol. Bioeng.*, 94(6):1033–1044.

Trumpower, B. L. (1990). The protonmotive Q cycle. Energy transduction by coupling of proton translocation to electron transfer by the cytochrome bc1 complex. *J. Biol. Chem.*, 265(20):11409–11412.

Urlaub, G. & L. a. Chasin (1980). Isolation of Chinese hamster cell mutants deficient in dihydrofolate reductase activity. *Proc. Natl. Acad. Sci. U. S. A.*, 77(7):4216–4220.

Urlaub, G., E. Käs, a. M. Carothers, & L. a. Chasin (1983). Deletion of the diploid dihydrofolate reductase locus from cultured mammalian cells. *Cell*, 33(2):405–412.

Urlaub, G., P. J. Mitchell, E. Kas, L. a. Chasin, V. L. Funanage, T. T. Myoda, & J. Hamlin (1986). Effect of gamma rays at the dihydrofolate reductase locus: deletions and inversions. *Somat. Cell Mol. Genet.*, 12(6):555–566.

Van der Weyden, M. B. & W. N. Kelly (1974). Human adenylosuccinate synthetase. Partial purification, kinetic and regulatory properties of the enzyme from placenta. *J. Biol. Chem.*, 249(22):7282–7289.

Vander Heiden, M. G., L. C. Cantley, & C. B. Thompson (2009). Understanding the Warburg effect: the metabolic requirements of cell proliferation. *Science*, 324(5930):1029–1033.

Vielhauer, O., M. Zakhartsev, T. Horn, R. Takors, & M. Reuss (2011). Simplified absolute metabolite quantification by gas chromatography-isotope dilution mass spectrometry on the basis of commercially available source material. *J. Chromatogr. B Anal. Technol. Biomed. Life Sci.*, 879(32):3859–3870.

Virolle, T., A. Krones-Herzig, V. Baron, G. De Gregorio, E. D. Adamson, & D. Mercola (2003). Egr1 promotes growth and survival of prostate cancer cells. Identification of novel Egr1 target genes. *J. Biol. Chem.*, 278(14):11802–11810.

Vishwanathan, N., H. Le, T. Le, & W. S. Hu (2014). Advancing biopharmaceutical process science through transcriptome analysis. *Curr. Opin. Biotechnol.*, 30:113–119.

Vishwanathan, N., A. Yongky, K. C. Johnson, H.-Y. Fu, N. M. Jacob, H. Le, F. N. K. Yusufi, D. Y. Lee, & W.-S. Hu (2015). Global insights into the Chinese hamster and CHO cell transcriptomes. *Biotechnol. Bioeng.*, 112(5):965–976.

Voisard, D., F. Meuwly, P.-A. Ruffieux, G. Baer, & A. Kadouri (2003). Potential of cell retention techniques for large-scale high-density perfusion culture of suspended mammalian cells. *Biotechnol. Bioeng.*, 82(7):751–765.

Volmer, M., S. Northoff, S. Scholz, T. Thute, H. Buntemeyer, & T. Noll (2011). Fast filtration for metabolome sampling of suspended animal cells. *Biotechnol Lett*, 33(3):495–502.

Wahl, A., Y. Sidorenko, M. Dauner, Y. Genzel, & U. Reichl (2008). Metabolic flux model for an anchorage-dependent MDCK cell line: characteristic growth phases and minimum substrate consumption flux distribution. *Biotechnol Bioeng*, 101(1):135–152.

Walsh, G. (2010a). Biopharmaceutical benchmarks 2010. *Nat Biotechnol*, 28(9):917–924.

Walsh, G. (2010b). Post-translational modifications of protein biopharmaceuticals. *Drug Discov. Today*, 15(17-18):773–780.

Walsh, G. (2014). Biopharmaceutical benchmarks 2014. *Nat. Biotechnol.*, 32(10):992–1000.

Walsh, G. & R. Jefferis (2006). Post-translational modifications in the context of therapeutic proteins. *Nat. Biotechnol.*, 24(10):1241–1252.

Wang, G., W. Mao, & S. Zheng (2008). MicroRNA-183 regulates Ezrin expression in lung cancer cells. *FEBS Lett.*, 582(25-26):3663–3668.

Wang, J., J. Li, J. Shen, C. Wang, L. Yang, & X. Zhang (2012). MicroRNA-182 downregulates metastasis suppressor 1 and contributes to metastasis of hepatocellular carcinoma. *BMC Cancer*, 12:227.

Wang, J., G. Xu, F. Shen, & Y. Kang (2014a). miR-132 targeting cyclin E1 suppresses cell proliferation in osteosarcoma cells. *Tumour Biol.*, 35(5):4859–4865.

Wang, Y., D. Zhou, & S. Chen (2014b). SGK3 is an androgen-inducible kinase promoting prostate cancer cell proliferation through activation of p70 S6 kinase and up-regulation of cyclin D1. *Mol. Endocrinol.*, 28(6):935–948.

Warnock, J. N. & M. Al-Rubeai (2006). Bioreactor systems for the production of biopharmaceuticals from animal cells. *Biotechnol. Appl. Biochem.*, 45:1–12.

Wenz, L.-S., L. Opaliński, N. Wiedemann, & T. Becker (2015). Cooperation of protein machineries in mitochondrial protein sorting. *Biochim. Biophys. Acta - Mol. Cell Res.*, 1853(5):1119–1129.

Wiedemann, N., V. Kozjak, A. Chacinska, B. Schönfisch, S. Rospert, M. T. Ryan, N. Pfanner, & C. Meisinger (2003). Machinery for protein sorting and assembly in the mitochondrial outer membrane. *Nature*, 424(6948):565–571.

Wightman, B., I. Ha, & G. Ruvkun (1993). Posttranscriptional regulation of the heterochronic gene lin-14 by lin-4 mediates temporal pattern formation in C. elegans. *Cell*, 75(5):855–862.

Wittrup, K. D. (1995). Disulfide bond formation and eukaryotic secretory productivity. *Curr. Opin. Biotechnol.*, 6(2):203–208.

Wlaschin, K. F. & W.-S. Hu (2006). Fedbatch culture and dynamic nutrient feeding. *Adv. Biochem. Eng. Biotechnol.*, 101:43–74.

Wlaschin, K. F. & W. S. Hu (2007a). A scaffold for the Chinese hamster genome. *Biotechnol Bioeng*, 98(2):429–439.

Wlaschin, K. F. & W.-S. Hu (2007b). Engineering cell metabolism for high-density cell culture via manipulation of sugar transport. *J. Biotechnol.*, 131(2):168–176.

Wlaschin, K. F., P. M. Nissom, L. Gatti Mde, P. F. Ong, S. Arleen, K. S. Tan, A. Rink, B. Cham, K. Wong, M. Yap, & W. S. Hu (2005). EST sequencing for gene discovery in Chinese hamster ovary cells. *Biotechnol Bioeng*, 91(5):592–606.

Wolter, K. G., Y. T. Hsu, C. L. Smith, A. Nechushtan, X. G. Xi, & R. J. Youle (1997). Movement of Bax from the cytosol to mitochondria during apoptosis. *J. Cell Biol.*, 139(5):1281–1292.

Wong, D. C., K. T. Wong, Y. Y. Lee, P. N. Morin, C. K. Heng, & M. G. Yap (2006). Transcriptional profiling of apoptotic pathways in batch and fed-batch CHO cell cultures. *Biotechnol Bioeng*, 94(2):373–382.

Wong, N. & X. Wang (2015). miRDB: an online resource for microRNA target prediction and functional annotations. *Nucleic Acids Res.*, 43:D146–152.

Worton, R. G., C. C. Ho, & C. Duff (1977). Chromosome stability in CHO cells. *Somatic Cell Genet.*, 3(1):27–45.

Wuest, D. M., S. W. Harcum, & K. H. Lee (2012). Genomics in mammalian cell culture bioprocessing. *Biotechnol. Adv.*, 30(3):629–638.

Wurm, F. M. (2004). Production of recombinant protein therapeutics in cultivated mammalian cells. *Nat Biotechnol*, 22(11):1393–1398.

Wurm, F. M. & D. Hacker (2011). First CHO genome. *Nat. Biotechnol.*, 29(8):718–720.

Wurm, M., B. Schöpke, D. Lutz, J. Müller, & A.-P. Zeng (2010). Microtechnology meets systems biology: the small molecules of metabolome as next big targets. *J. Biotechnol.*, 149(1-2):33–51.

Wyngaarden, J. B. (1976). Regulation of purine biosynthesis and turnover. *Adv. Enzyme Regul.*, 14:25–42.

Xu, R.-S., X.-D. Wu, S.-Q. Zhang, C.-F. Li, L. Yang, D.-D. Li, B.-G. Zhang, Y. Zhang, J.-P. Jin, & B. Zhang (2012). The tumor suppressor gene RhoBTB1 is a novel target of miR-31 in human colon cancer. *Int. J. Oncol.*, 42(2):676–682.

Xu, X., H. Nagarajan, N. E. Lewis, S. Pan, Z. Cai, X. Liu, W. Chen, M. Xie, W. Wang, S. Hammond, M. R. Andersen, N. Neff, B. Passarelli, W. Koh, H. C. Fan, J. Wang, Y. Gui, K. H. Lee, M. J. Betenbaugh, S. R. Quake, I. Famili, & B. O. Palsson (2011). The genomic sequence of the Chinese hamster ovary (CHO)-K1 cell line. *Nat Biotechnol*, 29(8):735–741.

Yang, M. & M. Butler (2002). Effects of ammonia and glucosamine on the heterogeneity of erythropoietin glycoforms. *Biotechnol. Prog.*, 18(1):129–138.

Yano, M., N. Hoogenraad, K. Terada, & M. Mori (2000). Identification and functional analysis of human Tom22 for protein import into mitochondria. *Mol. Cell. Biol.*, 20(19):7205–7213.

Yee, J. C., M. de Leon Gatti, R. J. Philp, M. Yap, & W. S. Hu (2008). Genomic and proteomic exploration of CHO and hybridoma cells under sodium butyrate treatment. *Biotechnol Bioeng*, 99(5):1186–1204.

Yee, J. C., Z. P. Gerdtzen, & W. S. Hu (2009). Comparative transcriptome analysis to unveil genes affecting recombinant protein productivity in mammalian cells. *Biotechnol Bioeng*, 102(1):246–263.

Yoon, S., S. Hwang, & G. Lee (2004). Enhancing Effect of Low Culture Temperature on Specific Antibody Productivity of Recombinant Chinese Hamster Ovary Cells: Clonal Variation. *Biotechnol. Prog.*, 20(6):1683–1688.

Yoon, S. K., S. L. Choi, J. Y. Song, & G. M. Lee (2005). Effect of culture pH on erythropoietin production by Chinese hamster ovary cells grown in suspension at 32.5 and 37.0°C. *Biotechnol. Bioeng.*, 89(3):345–356.

Young, M. D., M. J. Wakefield, G. K. Smyth, & A. Oshlack (2010). Gene ontology analysis for RNA-seq: accounting for selection bias. *Genome Biol.*, 11(R14):1–16.

Zander, C., Z. Zhang, T. Albers, & C. Grewer (2015). Amino acid transporters and glutamine. In *Glutamine Clin. Nutr.*, R. Rajendram, V. R. Preedy, and V. B. Patel, eds., chapter 2, Pp. 21–36. New York: Springer Science+Business Media.

Zetterberg, A., O. Larsson, & K. G. Wiman (1995). What is the restriction point? *Curr. Opin. Cell Biol.*, 7(6):835–842.

Zhang, L.-X., W.-Y. Zhang, C. Wang, J.-T. Liu, X.-C. Deng, X.-P. Liu, L. Fan, & W.-S. Tan (2016a). Responses of CHO-DHFR cells to ratio of asparagine to glutamine in feed media: cell growth, antibody production, metabolic waste, glutamate, and energy metabolism. *Bioresour. Bioprocess.*, 3(1):5.

Zhang, Q., K. Shim, K. Wright, A. Jurkevich, & S. Khare (2016b). Atypical role of sprouty in p21 dependent inhibition of cell proliferation in colorectal cancer. *Mol. Carcinog.*, 55(9):1355–1368.

Zhang, X., I. F. Garcia, L. Baldi, D. L. Hacker, & F. M. Wurm (2010). Hyperosmolarity enhances transient recombinant protein yield in Chinese hamster ovary cells. *Biotechnol. Lett.*, 32(11):1587–1592.

Zhou, M., Y. Crawford, D. Ng, J. Tung, A. F. Pynn, A. Meier, I. H. Yuk, N. Vijayasankaran, K. Leach, J. Joly, B. Snedecor, & A. Shen (2011). Decreasing lactate level and increasing antibody production in Chinese Hamster Ovary cells (CHO) by reducing the expression of lactate dehydrogenase and pyruvate dehydrogenase kinases. *J Biotechnol*, 153(1-2):27–34.

Zhou, Y., S. Holmseth, C. Guo, B. Hassel, G. Höfner, H. S. Huitfeldt, K. T. Wanner, & N. C. Danbolt (2012). Deletion of the gamma-aminobutyric acid transporter 2 (GAT2 and SLC6A13) gene in mice leads to changes in liver and brain taurine contents. *J. Biol. Chem.*, 287(42):35733–35746.

Zhu, M. M., A. Goyal, D. L. Rank, S. K. Gupta, T. Vanden Boom, & S. S. Lee (2005). Effects of elevated pCO2 and osmolality on growth of CHO cells and production of antibody-fusion protein B1: A case study. *Biotechnol. Prog.*, 21(1):70–77.

Zou, H., Y. Li, X. Liu, & X. Wang (1999). An APAF-1 Cytochrome c Multimeric Complex Is a Functional Apoptosome That Activates Procaspase-9. *J. Biol. Chem.*, 274(17):11549–11556.

A Supporting Information

A.1 Figures and Data of Cultivations
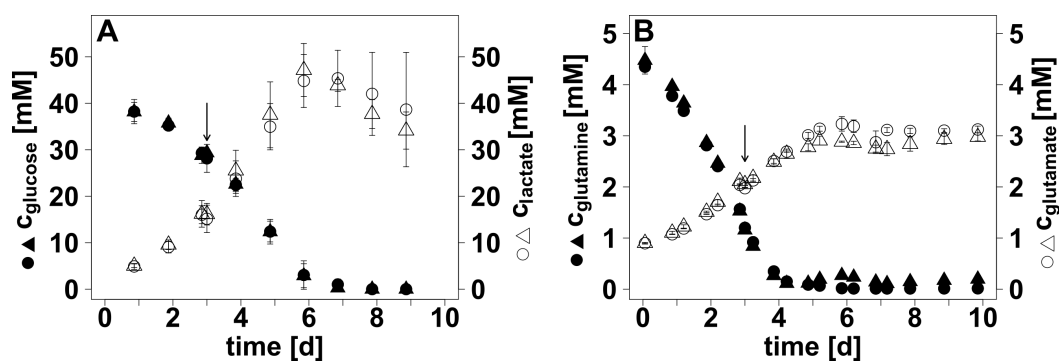
FIGURE A.1: Profiles of metabolite concentrations during batch cultivation of CHO DP-12 with osmotic shift (+ 100 mOsmol kg^{-1}). NaCl-enriched cultivation medium (Tab. 4.3) was added 72 h (arrow) after inoculation in order to induce hyperosmotic conditions ($\sim$ 390 mOsmol kg^{-1}, ▲ △). Osmolality of reference cultures was $\sim$ 290 mOsmol kg^{-1} (● ○). $c_{glucose}$ and $c_{lactate}$ were determined enzymatically by LaboTRACE (TRACEAnalytics) while $c_{glutamine}$ and $c_{glutamate}$ were analyzed by HPLC (4.2.5). Error bars of Fig. A represent standard deviations for four biological replicates thereby considering as well the technical error of measurements (n = 3). Error bars of Fig. B represent the standard deviation based on two biological replicates and three technical replicates each.
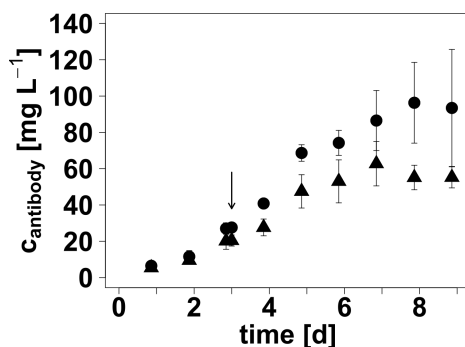
FIGURE A.2: Time course of c_P for CHO DP-12 cells exposed to hyperosmolality (390 mOsmol kg^{-1}). Hyperosmotic culture conditions were induced 72 h after inoculation (arrow) by the addition of NaCl-enriched cultivation medium (Tab. 4.3, 4.2.2). Osmolality of hyperosmotic cultures was $\sim$ 390 mOsmol kg^{-1} ($\blacktriangle$) compared to $\sim$ 290 mOsmol kg^{-1} for reference cultures ($\bullet$). The concentration of the produced anti-IL-8-IgG1 antibody was determined by ELISA as described in 4.2.5. Error bars combine biological (n = 2) and technical error (n = 3).
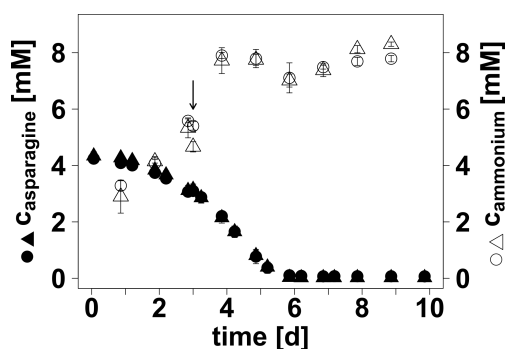
FIGURE A.3: Profiles for the metabolites asparagine and ammonium during batch cultivation of CHO DP-12 with osmotic shift (+ 100 mOsmol kg^{-1}). Hyperosmotic culture conditions ($\sim$ 390 mOsmol kg^{-1}, $\blacktriangle$ $\triangle$) were induced by the addition of NaCl-enriched medium (Tab. 4.3) 72 h after inoculation of bioreactors (arrow). An equal volume of standard cultivation medium was added to reference cultures ($\sim$ 290 mOsmol kg^{-1}, $\bullet$ $\circ$). $c_{asparagine}$ was analyzed by HPLC while LCK303 cuvette test (Hach) was applied for the determination of $c_{ammonium}$. Error bars combine biological (n = 2) and technical error (n = 3).

TABLE A.1: Data of carbon (A) and oxygen (B) balance for hyperosmotically stressed CHO DP-12 cells (390 mOsmol kg^{-1}). Values were calculated as described in section 4.2.7. Negative values represent carbon/oxygen influx while positive values represent carbon/oxygen efflux.

A

metabolite	$\Delta n_{metabolite}$ [C-mol] - hyperosmolal				$\Delta n_{metabolite}$ [C-mol] - reference			
	day 3 - day 4	day 4 - day 5	day 5 - day 6	day 6 - day 7	day 3 - day 4	day 4 - day 5	day 5 - day 6	day 6 - day 7
alanine	5.73E-04	3.65E-04	3.74E-04	-1.76E-03	9.00E-04	5.53E-04	-7.52E-04	-1.15E-03
arginine	-1.95E-03	-3.84E-03	-2.40E-03	-1.55E-03	-1.38E-03	-3.36E-03	-2.63E-03	-2.79E-03
asparagine	-5.00E-03	-6.57E-03	-3.44E-03	-4.23E-05	-4.45E-03	-7.01E-03	-2.96E-03	-1.68E-04
aspartate	1.49E-05	-1.31E-03	-1.99E-03	-2.41E-03	2.93E-04	-8.13E-04	-1.73E-03	-2.14E-03
glutamate	2.36E-03	6.66E-04	-2.50E-04	-1.44E-03	2.94E-03	1.84E-03	2.01E-04	-2.63E-03
glutamine	-5.37E-03	-9.24E-04	7.55E-04	-7.05E-04	-5.16E-03	-1.57E-03	-3.91E-04	-3.60E-05
glycine	-6.43E-04	-7.51E-04	-3.04E-04	4.40E-04	-5.34E-04	-7.09E-04	-3.05E-04	6.88E-04
histidine	-7.36E-04	-1.11E-03	-8.17E-04	-4.31E-04	-5.79E-04	-9.80E-04	-9.43E-04	-6.25E-04
isoleucine	-1.62E-03	-3.02E-03	-2.51E-03	-1.33E-03	-1.27E-03	-2.67E-03	-2.52E-03	-1.52E-03
leucine	-2.46E-03	-4.30E-03	-3.71E-03	-2.05E-03	-2.02E-03	-3.91E-03	-3.83E-03	-1.79E-03
phenylalanine	-1.31E-03	-2.10E-03	-1.69E-03	-7.20E-04	-1.02E-03	-1.87E-03	-1.76E-03	-7.77E-04
proline	-5.86E-04	-1.69E-03	-8.09E-04	-6.85E-05	-4.65E-04	-1.14E-03	-5.39E-04	-9.20E-04
serine	-1.66E-03	-2.88E-03	-2.61E-03	-2.10E-03	-9.45E-04	-2.33E-03	-2.57E-03	-2.64E-03
threonin	-9.87E-04	-2.03E-03	-1.32E-03	-4.85E-04	-7.50E-04	-1.45E-03	-1.24E-03	-6.77E-04
tryptophan	-5.23E-04	-7.76E-04	-6.36E-04	-3.05E-04	-3.56E-04	-7.10E-04	-8.09E-04	-3.28E-04
tyrosine	-1.19E-03	-2.02E-03	-1.53E-03	-7.67E-04	-8.85E-04	-1.78E-03	-1.67E-03	-9.84E-04
valine	-1.54E-03	-2.54E-03	-2.03E-03	-1.10E-03	-1.04E-03	-2.23E-03	-2.09E-03	-1.10E-03
glucose	-6.01E-02	-8.18E-02	-6.43E-02	-4.97E-02	-5.52E-02	-7.17E-02	-6.03E-02	-2.45E-02
lactate	3.78E-02	4.12E-02	2.07E-02	-3.26E-02	3.14E-02	3.01E-02	2.13E-02	2.30E-03
pyruvate	-7.16E-04	-5.49E-04	-1.32E-03	-1.49E-03	-1.27E-03	-8.94E-04	-1.99E-03	-6.94E-05
biomass	2.74E-02	2.22E-02	1.13E-02	1.01E-02	2.61E-02	3.49E-02	1.99E-02	-1.31E-03
antibody	6.46E-04	1.26E-03	-5.84E-06	3.41E-04	3.43E-04	9.00E-04	6.14E-06	-1.72E-04
carbon$_{influx}$	-8.64E-02	-1.18E-01	-9.17E-02	-5.78E-02	-7.73E-02	-1.05E-01	-8.91E-02	-4.63E-02
carbon$_{efflux}$	6.88E-02	6.57E-02	3.31E-02	1.09E-02	6.20E-02	6.83E-02	4.14E-02	2.96E-03
n_{CO2}	1.76E-02	5.25E-02	5.85E-02	4.69E-02	1.53E-02	3.68E-02	4.77E-02	4.33E-02

B

metabolite	$\Delta n_{metabolite}$ [O-mol] - hyperosmolal				$\Delta n_{metabolite}$ [O-mol] - reference			
	day 3 - day 4	day 4 - day 5	day 5 - day 6	day 6 - day 7	day 3 - day 4	day 4 - day 5	day 5 - day 6	day 6 - day 7
alanine	-6.01E-02	-8.18E-02	-6.43E-02	-4.97E-03	-5.52E-02	-6.26E-02	-6.03E-02	-2.45E-02
arginine	3.78E-02	4.12E-02	2.07E-02	-3.26E-02	3.14E-02	2.40E-02	2.13E-02	2.30E-03
asparagine	1.34E-02	1.08E-02	5.53E-03	4.94E-03	1.27E-02	1.23E-02	9.68E-03	-6.37E-04
aspartate	-7.16E-04	-5.49E-04	-1.32E-03	-1.49E-03	-1.27E-03	-1.55E-03	-1.99E-03	-6.94E-05
glutamate	-3.22E-03	-5.54E-04	4.53E-04	-4.23E-04	-3.09E-03	-6.51E-04	-2.35E-04	-2.16E-05
glutamine	1.89E-03	5.33E-04	-2.00E-04	-1.15E-03	2.35E-03	6.41E-04	1.61E-04	-2.10E-03
glycine	1.49E-05	-1.31E-03	-1.99E-03	-2.41E-03	2.93E-04	-1.32E-03	-1.73E-03	-2.14E-03
histidine	-3.75E-03	-4.93E-03	-2.58E-03	-3.18E-05	-3.34E-03	-3.26E-03	-2.22E-03	-1.26E-04
isoleucine	-1.66E-03	-2.88E-03	-2.61E-03	-2.10E-03	-9.45E-04	-2.50E-03	-2.57E-03	-2.64E-03
leucine	-2.45E-04	-3.70E-04	-2.72E-04	-1.44E-04	-1.93E-04	-2.99E-04	-3.14E-04	-2.08E-04
phenylalanine	-6.43E-04	-7.51E-04	-3.04E-04	4.40E-04	-5.34E-04	-4.09E-04	-3.05E-04	6.88E-04
proline	-7.40E-04	-1.52E-03	-9.91E-04	-3.64E-04	-5.63E-04	-9.60E-04	-9.30E-04	-5.08E-04
serine	-6.52E-04	-1.28E-03	-8.01E-04	-5.17E-04	-4.61E-04	-9.40E-04	-8.75E-04	-9.29E-04
threonin	-3.95E-04	-6.72E-04	-5.09E-04	-2.56E-04	-2.95E-04	-5.45E-04	-5.57E-04	-3.28E-04
tryptophan	-6.17E-04	-1.02E-03	-8.12E-04	-4.42E-04	-4.17E-04	-8.35E-04	-8.34E-04	-4.40E-04
tyrosine	-9.51E-05	-1.41E-04	-1.16E-04	-5.55E-05	-6.47E-05	-1.30E-04	-1.47E-04	-5.96E-05
valine	-2.91E-04	-4.67E-04	-3.76E-04	-1.60E-04	-2.26E-04	-3.80E-04	-3.91E-04	-1.73E-04
glucose	-5.40E-04	-1.01E-03	-8.37E-04	-4.43E-04	-4.23E-04	-8.30E-04	-8.41E-04	-5.08E-04
lactate	-8.22E-04	-1.43E-03	-1.24E-03	-6.83E-04	-6.73E-04	-1.25E-03	-1.28E-03	-5.97E-04
pyruvate	-2.34E-04	-6.74E-04	-3.23E-04	-2.74E-05	-1.86E-04	-3.91E-04	-2.16E-04	-3.68E-04
biomass	3.82E-04	2.43E-04	2.49E-04	-1.17E-03	6.00E-04	-2.36E-04	-5.01E-04	-7.68E-04
antibody	3.29E-04	6.40E-04	-2.97E-06	1.74E-04	1.74E-04	2.59E-04	3.12E-06	-8.76E-05
oxygen$_{influx}$	-7.47E-02	-1.01E-01	-7.96E-02	-4.94E-02	-6.79E-02	-7.91E-02	-7.63E-02	-3.72E-02
oxygen$_{efflux}$	5.38E-02	5.35E-02	2.69E-02	5.52E-03	4.76E-02	3.72E-02	3.11E-02	2.97E-03
n_{O2}	2.09E-02	4.79E-02	5.27E-02	4.39E-02	2.03E-02	4.19E-02	4.52E-02	3.42E-02
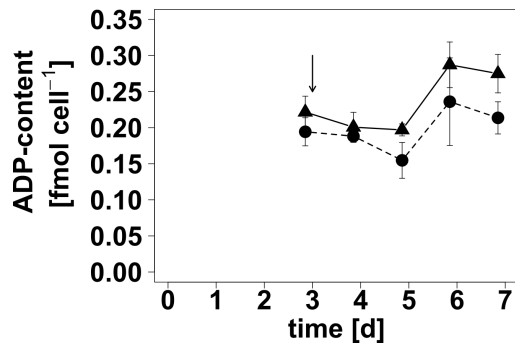
FIGURE A.4: Effect of hyperosmotic culture conditions on intracellular ADP-content of CHO DP-12 cells. NaCl-enriched cultivation medium (Tab. 4.3) was added 72 h after inoculation (arrow) resulting in an osmolality of $\sim$ 390 mOsmol kg^{-1} ($\blacktriangle$ $\triangle$) for hyperosmotic cultures. The osmolality of reference cultures was $\sim$ 290 mOsmol kg^{-1}($\bullet$ $\circ$). Intracellular ADP-contents were determined by a combination of a fast filtration approach for 10^7 cells (4.2.3), methanol/chloroform extraction (4.2.4) and HPLC analysis (4.2.5). Two biological replicates with three technical replicates each were analyzed at all time points and were used to calculated standard deviations represented by error bars.
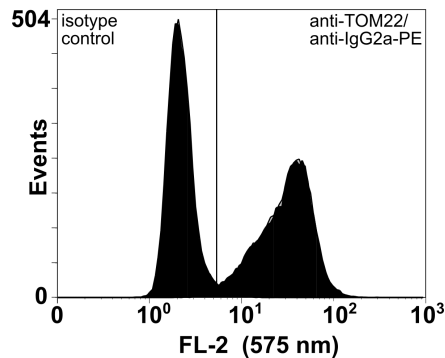
FIGURE A.5: Reference measurement of mitochondrial fluorescence directly before osmotic shift (+ 100 mOsmol kg^{-1}). Intracellular mitochondria of CHO DP-12 cells were labeled by a combination of an anti-translocase of the outer mitochondrial membrane 22 (TOM22) and a phycoerythrin (PE)-conjugated isotype-specific anti-IgG2a antibody. The fluorescence intensity of the cells was analyzed by flow cytometry (4.2.5). The received histograms (fluorescence channel 2 (FL-2), 575 nm) of samples and isotype control were overlaid. Black histograms correspond to reference cultures while grey histograms represent the results for hyperosmotic cultures.
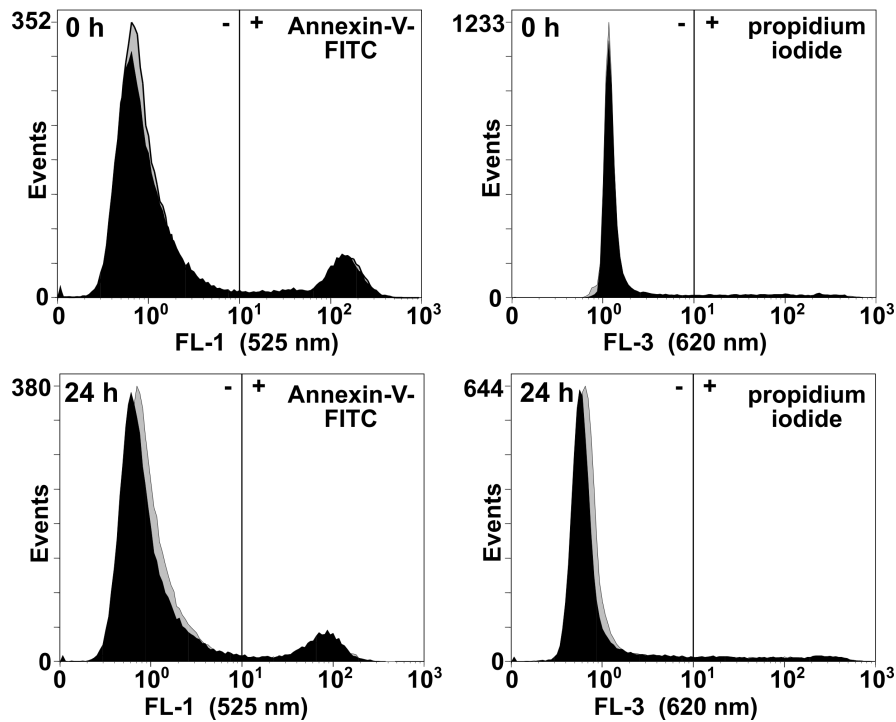
FIGURE A.6: Effect of osmotic shift (+100 mOsmol kg^{-1}) on the amount of apoptotic cells. The Annexin V-FITC kit (Beckman Coulter) was used to perform testing for apoptosis according to the specifications of the manufacturer. In order to distinguish apoptotic or necrotic cells from viable cells, different kinds of controls were used to adjust flow cytometer settings. Apoptotic cells (positive control) were received by incubation of cells with 1 μM staurosporine for 6 h at 37°C, 5% CO_2 in a humidified shaker incubator (150 rpm, 50 mm displacement). Viable cells served as negative control. Control samples were either treated with both, Annexin V-FITC and propidium iodide (PI) or with just one of the components. Directly before (0 h) and 24 h after the induction of hyperosmotic conditions, cells (5 x 10^5 mL^{-1}) were incubated with Annexin V-FITC and PI for 15 min on ice followed by flow cytometric analysis. A positive Annexin V-FITC signal indicates apoptosis and in combination with a positive PI-signal necrosis. black = reference, grey = hyperosmotic
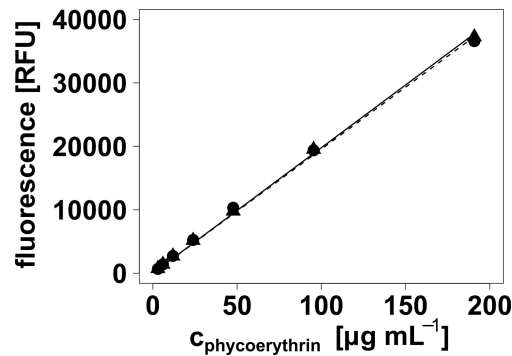
FIGURE A.7: Influence of osmolality on the fluorescence intensity of phycoerythrin. The fluorophore phycoerythrin was diluted in 0.01 M potassium phosphate buffer (pH 7.1) with an osmolality of 294 mOsmol kg^{-1} (●) or 381 mOsmol kg^{-1} (▲). Fluorescence intensity was determined with a Synergy^{TM} microplate reader (BioTek). $\lambda_{excitation} = 485/20$, $\lambda_{emission} = 590/35$, RFU = relative fluorescence units.
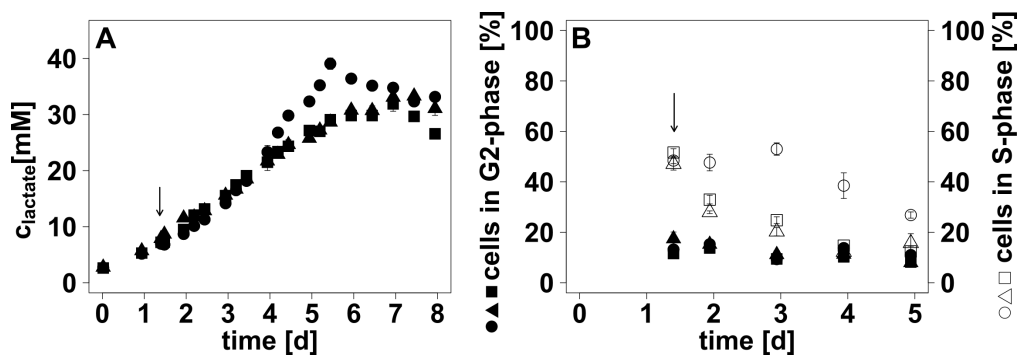
FIGURE A.8: Time courses of the lactate concentration (A) and the percentage of CHO DP-12 cells in S- and G2-phase (B) for cultivations with osmotic shift (+120/140 mOsmol kg^{-1}). Hyperosmotic conditions were induced 35 h after inoculation (arrow) by the addition of NaCl-enriched cultivation medium (Tab. 4.3, 4.2.2). Diagrams show data for reference conditions (∼290 mOsmol kg^{-1}, ● ○), and two different hyperosmotic conditions (∼410 mOsmol kg^{-1}, ■ □, ∼430 mOsmol kg^{-1}, ▲ △). $c_{lactate}$ was analyzed enzymatically by Labo-TRACE (TRACEAnalytics) while cell cycle distribution was determined by propidium iodide staining and flow cytometric analysis (4.2.5).

TABLE A.2: Data of carbon (A) and oxygen (B) balance for hyperosmotically stressed CHO DP-12 cells (430 mOsmol kg^{-1}). Values were calculated as described in section 4.2.7. Negative values represent carbon/oxygen influx while positive values represent carbon/oxygen efflux.

A

metabolite	$\Delta n_{metabolite}$ [C-mol] - reference				$\Delta n_{metabolite}$ [C-mol] - hyperosmolal			
	day 2 - day 3	day 3 - day 4	day 4 - day 5	day 5 - day 6	day 2 - day 3	day 3 - day 4	day 4 - day 5	day 5 - day 6
alanine	7.00E-04	5.23E-04	-9.34E-04	-1.24E-03	7.63E-04	5.86E-04	4.93E-04	7.08E-04
arginine	-3.03E-03	-3.39E-03	-3.83E-03	-1.84E-03	-1.41E-03	-2.62E-03	-3.27E-03	-1.55E-03
asparagine	-5.80E-03	-8.46E-03	-4.79E-03	-2.14E-04	-4.04E-03	-5.34E-03	-5.18E-03	-3.02E-03
aspartate	-2.66E-04	-1.09E-03	-2.85E-03	-2.25E-03	8.37E-05	-1.09E-03	-1.95E-03	-1.85E-03
glutamate	3.63E-03	2.39E-03	-5.91E-04	-1.62E-03	2.71E-03	9.58E-04	-8.89E-04	-9.75E-04
glutamine	-9.68E-03	-3.14E-03	-3.16E-04	9.91E-05	-6.95E-03	-2.93E-03	2.57E-04	1.70E-03
glycine	-8.14E-04	-9.13E-04	-3.45E-04	8.30E-04	-5.71E-04	-4.82E-04	-3.04E-04	-1.20E-04
histidine	-9.91E-04	-1.09E-03	-1.05E-03	-3.06E-04	-6.15E-04	-7.50E-04	-7.38E-04	-3.31E-04
isoleucine	-2.33E-03	-3.11E-03	-3.61E-03	-1.47E-03	-1.30E-03	-2.18E-03	-2.41E-03	-1.34E-03
leucine	-3.55E-03	-4.76E-03	-5.44E-03	-1.92E-03	-2.00E-03	-3.12E-03	-3.27E-03	-1.87E-03
phenylalanine	-1.70E-03	-2.21E-03	-2.21E-03	-6.69E-04	-9.79E-04	-1.42E-03	-1.48E-03	-8.61E-04
proline	-4.35E-04	-1.98E-03	-1.33E-03	3.61E-05	-2.06E-04	-1.65E-03	-1.11E-03	-1.29E-03
serine	-1.64E-03	-2.42E-03	-3.82E-03	-2.91E-03	-1.16E-03	-2.11E-03	-2.36E-03	-1.39E-03
threonine	-1.30E-03	-1.68E-03	-1.65E-03	-6.24E-04	-7.81E-04	-1.21E-03	-1.26E-03	-6.99E-04
tryptophan	-6.73E-04	-9.54E-04	-8.76E-04	-3.05E-04	-4.40E-04	-5.82E-04	-5.51E-04	-3.60E-04
tyrosin	-1.69E-03	-2.13E-03	-2.32E-03	-8.56E-04	-9.41E-04	-1.49E-03	-1.65E-03	-9.12E-04
valine	-2.01E-03	-2.63E-03	-3.01E-03	-1.14E-03	-1.10E-03	-1.79E-03	-1.99E-03	-1.12E-03
glucose	-5.23E-02	-7.53E-02	-8.15E-02	-2.75E-02	-4.57E-02	-6.11E-02	-6.08E-02	-5.02E-02
lactate	2.24E-02	1.87E-02	1.55E-02	-6.52E-03	2.04E-02	1.89E-02	1.58E-02	1.07E-02
biomass	3.37E-02	6.42E-02	4.64E-02	-1.91E-02	1.43E-02	8.60E-03	3.28E-03	5.64E-04
antibody	1.54E-03	2.04E-03	1.76E-03	-6.44E-05	9.66E-04	1.20E-03	1.09E-03	8.22E-04
carbon$_{influx}$	-8.82E-02	-1.15E-01	-1.20E-01	-7.06E-02	-6.82E-02	-8.99E-02	-8.92E-02	-6.79E-02
carbon$_{efflux}$	6.19E-02	8.79E-02	6.37E-02	9.65E-04	3.93E-02	3.03E-02	2.09E-02	1.45E-02
n$_{CO2}$	2.63E-02	2.73E-02	5.67E-02	6.96E-02	2.89E-02	5.96E-02	6.83E-02	5.34E-02

B

metabolite	$\Delta n_{metabolite}$ [O-mol] - reference				$\Delta n_{metabolite}$ [O-mol] - hyperosmolal			
	day 2 - day 3	day 3 - day 4	day 4 - day 5	day 5 - day 6	day 2 - day 3	day 3 - day 4	day 4 - day 5	day 5 - day 6
alanine	4.66E-04	3.49E-04	-6.23E-04	-8.26E-04	5.08E-04	3.91E-04	3.29E-04	4.72E-04
arginine	-1.01E-03	-1.13E-03	-1.28E-03	-6.12E-04	-4.72E-04	-8.73E-04	-1.09E-03	-5.16E-04
asparagine	-4.35E-03	-6.34E-03	-3.59E-03	-1.61E-04	-3.03E-03	-4.01E-03	-3.89E-03	-2.26E-03
aspartate	-2.66E-04	-1.09E-03	-2.85E-03	-2.25E-03	8.37E-05	-1.09E-03	-1.95E-03	-1.85E-03
glutamate	2.91E-03	1.91E-03	-4.73E-04	-1.30E-03	2.17E-03	7.66E-04	-7.11E-04	-7.80E-04
glutamine	-5.81E-03	-1.88E-03	-1.90E-04	5.95E-05	-4.17E-03	-1.76E-03	1.54E-04	1.02E-03
glycine	-8.14E-04	-9.13E-04	-3.45E-04	8.30E-04	-5.71E-04	-4.82E-04	-3.04E-04	-1.20E-04
histidine	-3.30E-04	-3.62E-04	-3.49E-04	-1.02E-04	-2.05E-04	-2.50E-04	-2.46E-04	-1.10E-04
isoleucine	-7.77E-04	-1.04E-03	-1.20E-03	-4.88E-04	-4.34E-04	-7.28E-04	-8.05E-04	-4.47E-04
leucine	-1.18E-03	-1.59E-03	-1.81E-03	-6.41E-04	-6.65E-04	-1.04E-03	-1.09E-03	-6.23E-04
phenylalanine	-3.77E-04	-4.90E-04	-4.91E-04	-1.49E-04	-2.18E-04	-3.16E-04	-3.30E-04	-1.91E-04
proline	-1.74E-04	-7.92E-04	-5.33E-04	1.44E-05	-8.23E-05	-6.59E-04	-4.43E-04	-5.14E-04
serine	-1.64E-03	-2.42E-03	-3.82E-03	-2.91E-03	-1.16E-03	-2.11E-03	-2.36E-03	-1.39E-03
threonine	-9.76E-04	-1.26E-03	-1.24E-03	-4.68E-04	-5.86E-04	-9.05E-04	-9.44E-04	-5.25E-04
tryptophan	-1.22E-04	-1.74E-04	-1.59E-04	-5.55E-05	-8.00E-05	-1.06E-04	-1.00E-04	-6.55E-05
tyrosin	-5.65E-04	-7.10E-04	-7.73E-04	-2.85E-04	-3.14E-04	-4.98E-04	-5.49E-04	-3.04E-04
valine	-8.05E-04	-1.05E-03	-1.20E-03	-4.56E-04	-4.38E-04	-7.16E-04	-7.94E-04	-4.48E-04
glucose	-5.23E-02	-7.53E-02	-8.15E-02	-2.75E-02	-4.57E-02	-6.11E-02	-6.08E-02	-5.02E-02
lactate	2.24E-02	1.87E-02	1.55E-02	-6.52E-03	2.04E-02	1.89E-02	1.58E-02	1.07E-02
biomass	1.64E-02	3.13E-02	2.26E-02	-9.31E-03	6.99E-03	4.19E-03	1.60E-03	2.75E-04
antibody	7.84E-04	1.04E-03	8.96E-04	-3.28E-05	4.92E-04	6.11E-04	5.56E-04	4.19E-04
oxygen$_{influx}$	-7.15E-02	-9.65E-02	-1.02E-01	-5.41E-02	-5.82E-02	-7.67E-02	-7.64E-02	-6.04E-02
oxygen$_{efflux}$	4.29E-02	5.33E-02	3.91E-02	9.04E-04	3.07E-02	2.49E-02	1.84E-02	1.29E-02
n$_{O2}$	2.86E-02	4.32E-02	6.34E-02	5.32E-02	2.75E-02	1.91E-03	5.80E-02	4.75E-02
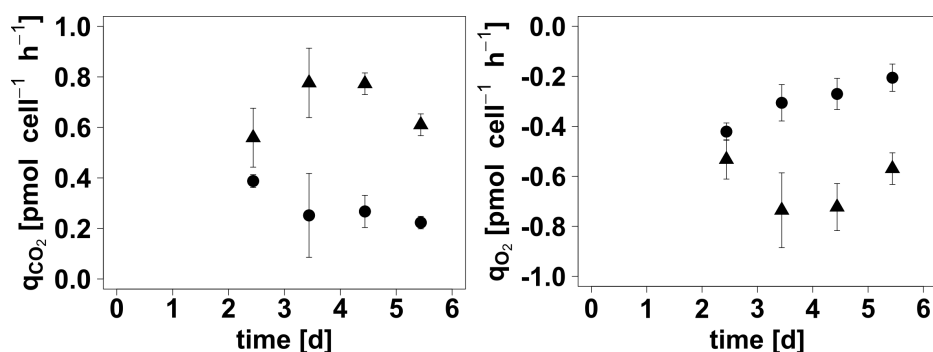
FIGURE A.9: Influence of hyperosmotic culture conditions (+ 150 mOsmol kg^{-1}) on specific carbon dioxide formation (q$_{CO_2}$) and oxygen uptake rate (q$_{O_2}$). NaCl-enriched cultivation medium (Tab. 4.3) was added to batch cultures of CHO DP-12 in order to induce hyperosmotic conditions 35 h after inoculation (4.2.2). Osmolality of reference cultures was $\sim$ 280 mOsmol kg^{-1} (n = 3, ●) compared to $\sim$ 430 mOsmol kg^{-1} for hyperosmotic cultures (n = 4, ▲). The determination of q$_{CO_2}$ and q$_{O_2}$ was based on carbon and oxygen balancing as described in 4.2.7. Errors represent standard deviations for biological replicates.
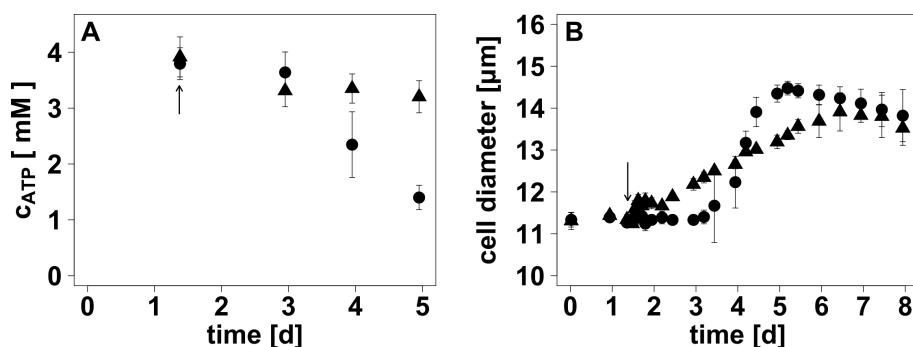
FIGURE A.10: Effect of hyperosmolality (+ 150 mOsmol kg^{-1}) on intracellular ATP-concentration and cell diameter of CHO DP-12. Osmolality was increased 35 h after inoculation by the addition of NaCl-enriched cultivation medium (arrow). This resulted in an osmolality of $\sim$ 430 mOsmol kg^{-1} (▲) compared to $\sim$ 280 mOsmol kg^{-1} for reference cultures (●). Cell diameters were determined by Cedex XS cell counter (Roche). Intracellular ATP-concentrations were analyzed by a combination of a fast filtration approach for 10^7 cells (4.2.3), methanol/chloroform extraction (4.2.4), HPLC analysis (4.2.5) and the assumption of spherical cells. Error bars represent standard deviations for four biological replicates thereby considering as well the technical error of measurements (n = 3). Hyperosmotic culture conditions resulted in highly significantly elevated c$_{ATP}$ on day 5 (P = 0.001).

TABLE A.3: Efficiency of cytosol depletion and retention of mitochondria for compartment-specific fast filtration approach. X_Y = ratio of the amount of metabolite Y in cytosol-depleted and whole cell sample, *cis*-aco = *cis*-aconitate, G6P = glucose-6-phosphate, F6P = fructose-6-phosphate.

	$X_{cis\text{-}aco}$		X_{G6P}		X_{F6P}	
t [d]	reference	hyperosmolal	reference	hyperosmolal	reference	hyperosmolal
1.4	0.81	0.81	0.16	0.16	0.23	0.22
3.0	0.83	0.85	0.16	0.17	0.25	0.16
4.0	0.87	0.81	0.16	0.18	0.24	0.14
5.0	0.96	0.82	0.21	0.19	0.13	0.15
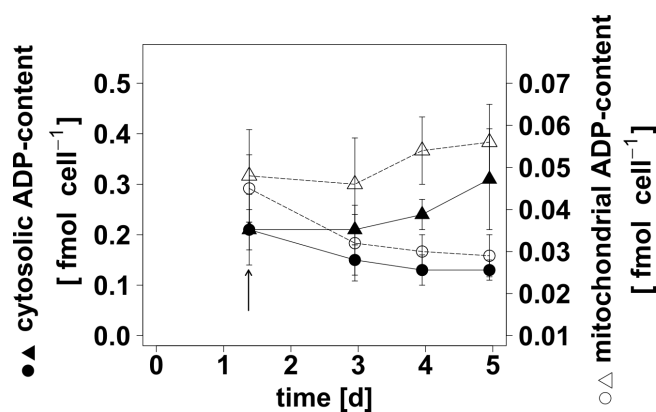
FIGURE A.11: Effect of hyperosmolality on cytosolic and mitochondrial ADP-content. Directly before osmotic shift (arrow)and on each of the following days of cultivation a compartment-specific fast filtration approach for 2×10^7 cells (4.2.3) was applied to generate whole cell and mitochondrial samples of CHO DP-12. Extraction of metabolites was performed by methanol/chloroform treatment of cell samples (4.2.4) and ADP-concentrations of cell extracts were determined by HPLC (4.2.5). Cytosolic and mitochondrial ADP-contents (ADP$_{cyt}$, ADP$_{mit}$) were calculated in accordance with Eq. 4.17 and Eq. 4.18 (4.2.8). Hyperosmotic cultures (▲ △) showed osmolalities $\sim$ 430 mOsmol kg^{-1} compared to reference cultures with $\sim$ 280 mOsmol kg^{-1} (● ○).Error bars represent standard deviations for biological replicates (n = 3). Statistically significant difference between hyperosmotic and reference conditions (P < 0.05) for ADP$_{cyt}$ on day four and for ADP$_{mit}$ on days four and five.
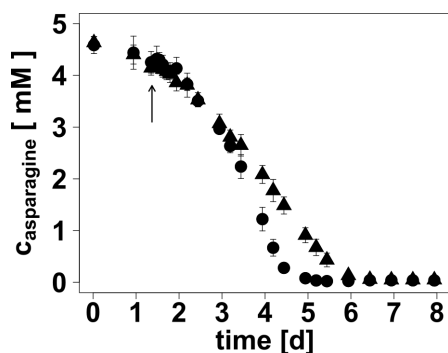
FIGURE A.12: Time course of extracellular asparagine concentration during batch cultivation of CHO DP-12 with osmotic shift (+150 mOsmol kg⁻¹). Hyperosmotic culture conditions ($\sim$ 430 mOsmol kg^{-1}, ▲ △) were induced by the addition of NaCl-enriched medium (Tab. 4.3) 35 h after inoculation of bioreactors (arrow). An equal volume of standard cultivation medium was added to reference cultures ($\sim$ 280 mOsmol kg^{-1}, ● ○). $c_{asparagine}$ was analyzed by HPLC. Error bars represent standard deviations based on three biological replicates for reference conditions and four biological replicates for hyperosmotic conditions .
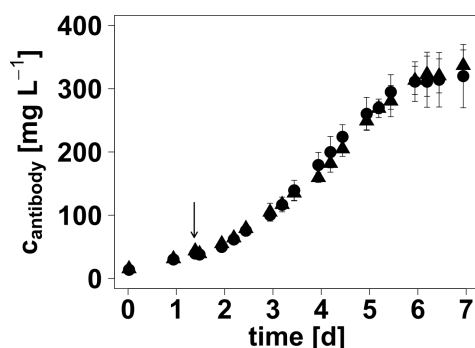
FIGURE A.13: Profile of antibody concentration during cultivation of BIBH1 with osmotic shift (+ 155 mOsmol kg⁻¹). NaCl-enriched cultivation medium (Tab. 4.3) was added 35 h after inoculation (arrow) resulting in an osmolality of $\sim$ 435 mOsmol kg^{-1} (▲ △) for hyperosmotic cultures. The osmolality of reference cultures was $\sim$ 280 mOsmol kg^{-1}(● ○). The concentration of the produced IgG1 antibody was determined by ELISA as described in 4.2.5. Error bars represent the standard deviation for four biological replicates thereby considering as well the technical error of measurements (n = 3).
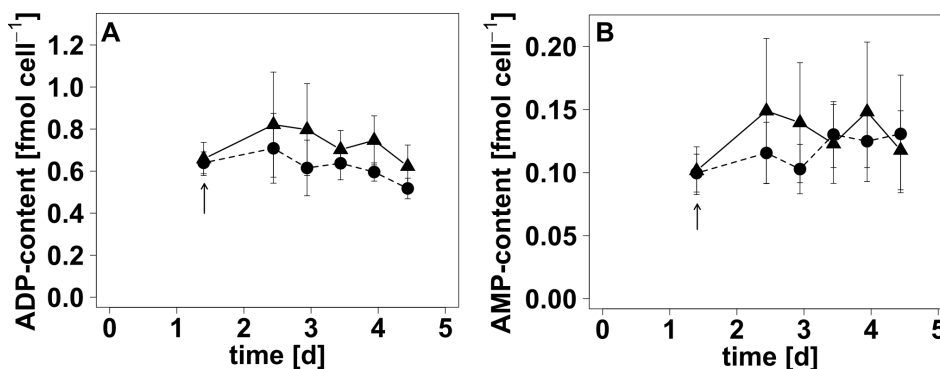
FIGURE A.14: Effect of hyperosmolality on intracellular ADP- and AMP-content of BIBH1. NaCl-enriched cultivation medium (Tab. 4.3) was added 35 h after inoculation (arrow) resulting in an osmolality of $\sim$ 435 mOsmol kg^{-1} ($\blacktriangle$ $\triangle$) for hyperosmotic cultures. The osmolality of reference cultures was $\sim$ 280 mOsmol kg^{-1}($\bullet$ $\circ$). Intracellular ADP- and AMP-contents were determined by a combination of a fast filtration approach for 10^7 cells (4.2.3), methanol/chloroform extraction (4.2.4) and HPLC analysis (4.2.5). Error bars represent standard deviations for four biological replicates thereby considering as well the technical error of measurements (n = 3).

A.2 Transcriptomic Analysis

A.2.1 Quality Information for Next Generation Sequencing

TABLE A.4: Quality of isolated RNA. Osmolality was increased 35 h (t = 0) after inoculation of CHO DP-12 cells. At given time points after the osmotic shift, RNA was isolated from 2×10^6 cells with miRNeasy kit (Qiagen). The quality of the isolated RNA was determined with Bioanalyzer 2100 (Agilent). c_{RNA} = RNA concentration, RIN = RNA integrity number.

sample	osmolality [mOsmol kg^{-1}]	time [h]	c_{RNA} [ng µL^{-1}]	RIN
E14R027a01	290	0	328	9.8
E14R027b01	290	0	716	10
E14R027c01	290	0	939	10
E14R027a02	430	2	291	9.9
E14R027b02	430	2	345	9.9
E14R027c02	430	2	380	9.8
E14R027a03	430	4	626	9.9
E14R027b03	430	4	717	10
E14R027c03	430	4	336	9.9
E14R027a04	430	6	580	9.9
E14R027b04	430	6	286	9.9
E14R027c04	430	6	971	10
E14R027a05	430	8	599	10
E14R027b05	430	8	813	10
E14R027c05	430	8	1215	10
E14R027d01	290	0	986	10
E14R027e01	290	0	270	9.9
E14R027d02	290	2	961	9.9
E14R027e02	290	2	365	9.8
E14R027d03	290	4	313	9.9
E14R027e03	290	4	491	9.7
E14R027d04	290	6	362	9.9
E14R027e04	290	6	309	9.9
E14R027d05	290	8	1067	10
E14R027e05	290	8	455	10
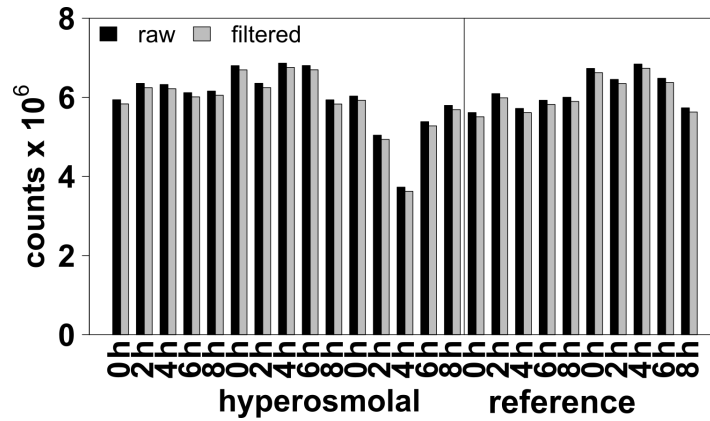
FIGURE A.15: Effect of data filtering on the number of counts for mRNA data sets from main experiments
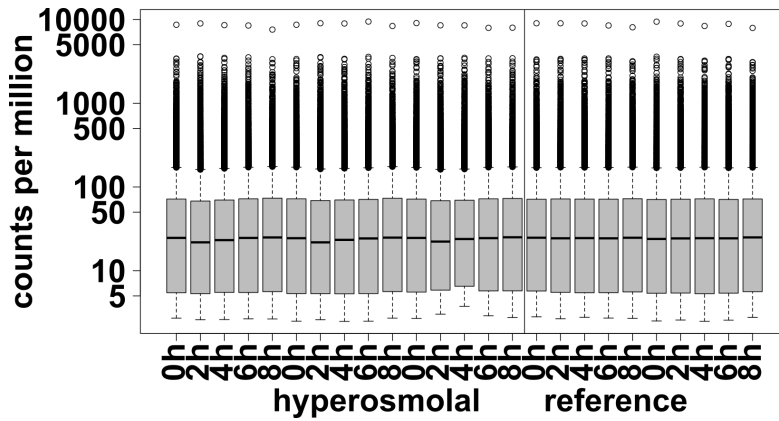
FIGURE A.16: Comparison of counts per million (mRNA) at different time points and conditions during main experiments.
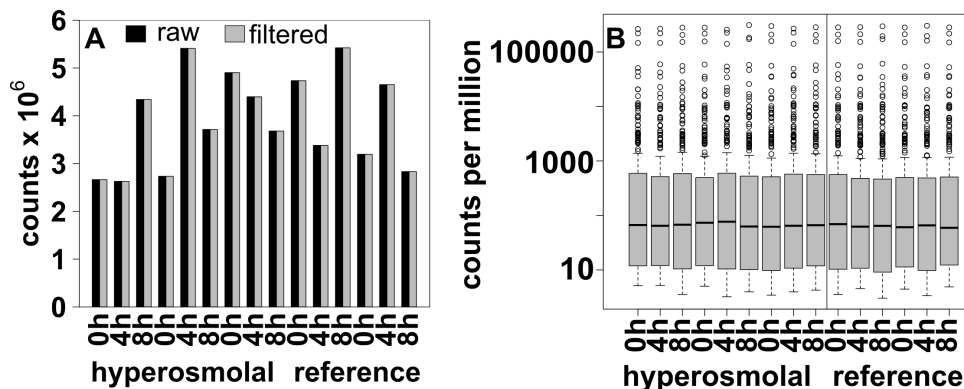
FIGURE A.17: Processing of miRNA data for main experiments. A: Effect of filtering on the number of counts. B: Comparison of counts per million at different time points and conditions

A.2.2 R Script for mRNA Expression Analysis

```
> library(edgeR)
> targets = read.table("E14R027_targets.txt", header = T, sep = "\t")
> RawCounts = read.table("E14R027_RawCounts_mRNA.txt", sep = "\t", col.names = ,1)
> rownames(RawCounts) = RawCounts$Identifier
> RawCounts = RawCounts[,c(-1)]
> all(targets$sampleID == colnames(RawCounts))
> keep = rowSums(RawCounts>10) >= 12
> filtCounts1 = RawCounts[keep,]
> filtCounts = cpm(filtCounts1)
> cpm = cpm(filtCounts1)
> keep = rowSums(cpm>1) >= 2
> filtCounts = filtCounts1[keep,]
> dim(filtCounts);dim(filtCounts1)
> group = as.factor(targets$group)
> DGE = DGEList(counts = filtCounts, group = group, genes = rownames(filtCounts))
> dim(DGE)
> DGE = calcNormFactors(DGE)
> design = model.matrix( ~ 0+group)
> rownames(design) = rownames(DGE$samples)
> colnames(design) = levels(group)
>    contrasts    =    makeContrasts("hyper_0h-iso_0h", "hyper_2h-iso_2h", "hyper_4h-iso_4h","hyper_
    6h-iso_6h", "hyper_8h-iso_8h", "hyper_2h-hyper_0h","hyper_4h-hyper_2h", "hyper_6h-hyper_4h",
    "hyper_8h-hyper_6h", "iso_2h-iso_0h", "iso_4h-iso_2h", "iso_6h-iso_4h", "iso_8h-iso_6h", levels         =
     design)
> DGE = estimateGLMCommonDisp(DGE, design)
> DGE = estimateGLMTrendedDisp(DGE, design)
> DGE = estimateGLMTagwiseDisp(DGE, design)
> print(DGE$common.dispersion)
> print(summary(DGE$tagwise.dispersion))
> fit = glmFit(DGE, design, dispersion = DGE$tagwise.dispersion)
> print(fit)
> lrt = glmLRT(fit, contrast = as.vector(contrasts[,n]))
> tt = topTags(lrt, n = dim(DGE)[1])
> print(head(tt$table))
> tt = tt$table
> print(head(tt$table))
> tt=tt$table
> DEG = subset(tt, PValue < 0.02&FDR < 0.02)
> DEGUp = subset(DEG, logFC >= log2(2))
```

> DEGDown = subset(DEG,logFC <= -log2(2))

A.2.3 R Script for miRNA Expression Analysis

```
> library(edgeR)
> targets = read.table("E14R027_targets_modified.txt", header = T, sep = "\t")
> RawCounts = read.table("E14R027_RawCounts_miRNA.txt", sep = "\t", col.names = ,1)
> rownames(RawCounts) = RawCounts$Gene
> RawCounts = RawCounts[,c(-1)]
> all(targets$sampleID == colnames(RawCounts))
> keep = rowSums(RawCounts > 10) >= 15
> filtCounts1 = RawCounts[keep,]
> cpm = cpm(filtCounts1)
> keep = rowSums(cpm > 1) >= 2
> filtCounts = filtCounts1[keep,]
> dim(filtCounts);dim(filtCounts1)
> cpmfiltCounts = cpm(filtCounts)
> group = as.factor(targets$group1)
> DGE = DGEList(counts = filtCounts, group = group, genes = rownames(filtCounts))
> dim(DGE)
> DGE = calcNormFactors(DGE)
> design = model.matrix( ~ 0+group)
> rownames(design) = rownames(DGE$samples)
> colnames(design) = levels(group)
>    contrasts    =    makeContrasts("hyper_0h-iso_0h", "hyper_4h-iso_4h","hyper_8h-iso_8h", "hyper_4h-
    hyper_0h","hyper_8h-hyper_4h","iso_4h-iso_0h","iso_8h-iso_4h", levels = design)
> DGE = estimateGLMCommonDisp(DGE, design)
> DGE = estimateGLMTrendedDisp(DGE, design)
> DGE = estimateGLMTagwiseDisp(DGE, design)
> print(DGE$common.dispersion)
> print(summary(DGE$tagwise.dispersion))
> fit = glmFit(DGE, design, dispersion=DGE$tagwise.dispersion)
> lrt = glmLRT(fit, contrast = as.vector(contrasts[,n]))
> tt = topTags(lrt, n = dim(DGE)[1])
> tt = tt$table
> DEG = subset(tt, PValue < 0.02 & FDR < 0.02)
> DEGUp = subset(DEG, logFC >= log2(2))
```

A.2.4 R Script for maSigPro Analysis

```
> library(maSigPro)
> design = read.table("edesign.txt", header = T, sep = "\t")
> head(design)
> rownames(design) = design$X
> head(design)
> edesign = design[,c(-1)]
> head(edesign)
> data = read.table("maSigPro_data.txt", header = T, sep = "\t")
> head(data)
> rownames(data) = data$X
> head(data)
> data = data[,c(-1)]
> head(data)
> design = make.design.matrix(edesign)
> design$groups.vector
> fit = p.vector(data, design, Q = 0.02, MT.adjust = "BH", counts = TRUE)
> fit$i
> tstep <- T.fit(fit, step.method = "backward", alfa = 0.02)
> sigs = get.siggenes(tstep, vars = "all")
> names(sigs$sig.genes)
> cluster = see.genes(sigs$sig.genes, k = 9)
> genes.cluster = cluster$cut
> head(genes.cluster)
```

A.2.5 maSigPro Clusters for Significantly Upregulated Genes

TABLE A.5: maSigPro gene clusters for significantly upregulated genes in response to hyperosmotic stimulus.

cluster 1 (38 genes)	cluster 2 (26 genes)	cluster 3 (41 genes)	cluster 4 (29 genes)	cluster 5 (62 genes)	cluster 6 (25 genes)	cluster 7 (24 genes)	cluster 8 (31 genes)	cluster 9 (4 genes)
ACSBG1	BCL6	AHI1	APC2	AKR1B1	ANXA9	ABCG1	ATP1B1	LOC100758641
ADAMTS3	BOD1	ARL4A	ATP2A1	AQP1	ARMCX4	ARHGEF37	CHN1	MYO3B
ALDH8A1	CDK1A	ASAP3	DTX2	AXIN2	CHRNB2	CALCOCO1	CITED1	NXPE4
ALPK3	CRYAB	BTG2	EDRF1	BCL2L11	DUOX2	DCN	COL4A2	PLCXD3
AMZ1	DDIT4	CABLES2	EREG	BMF	FOXP4	DDX59	FAM188B	
ANKRD61	DYRK3	CACNB3	ETS2	BPGM	HSPA4L	FYCO1	FOSL2	
ASL	FAT4	CCDC101	FAM132A	C3AR1	KIAA1522	HEATR7B2	GALM	
BAIAP3	GFOD1	CCDC69	HEXIM1	CCPG1	LOC100751769	HEXIM2	ITPR2	
CCDC164	GNL1	CCNG2	HOXC6	CDC42EP2	LOC100767001	HR	KIAA0513	
CEL	HSP110	CLN8	IRF2BPL	CDHR4	LOC100768165	LOC100752032	LOC100769997	
COL20A1	IER3	CREBRF	ITGA7	COL7A1	LOC100768757	LOC100754646	LOC100772072	
DUOXA2	IL15	CTGF	LOC100771158	CORNIFIN-A	LOC100771708	LOC100757262	MAOA	
FAM46C	LOC100755533	DUSP1	LOC100773107	CREM	LOC100772170	METTL20	MOXD1	
HEATR7B1	LOC100770289	DZANK1	MEPCE	CXCL3	LOC100772394	NOTUM	NADK2	
HHIPL2	LOC100771908	FAM117A	MYO1G	DAG1	MEX3B	NUDT6	NDRG2	
ID1	MBNL2	FGD3	NCKAP5L	DTX3	MKKS	NXPE3	NEURL1B	
ISLR2	PHEX	GFOD2	NFKBIZ	DYRK1B	NEB	PLA2G4F	NQO1	
ITGAX	RFX3	KCTD14	PAPD7	FAM131A	NFAT5	RAB7L1	PCX	
LMAN1L	SEMA6C	KLHL24	PER1	FIGF	PLCH2	RBM44	PDGFRA	
LOC100757105	SLC6A6	LOC100760433	PHF6	FMO4	SLC26A7	RGL1	PDK2	
LOC100762996	SMYD1	LOC100763833	PIF6	FOXN3	SPTBN5	SEPT4	PGM2L1	
LOC100764872	SRCAP	LOC100764334	SCAF4	GGCX	TEK	STXBP4	PTGES	
LOC100765388	WASF1	LPAR1	SETD1A	GPD1L	TMEM232	SUCNR1	RANBP3L	
LOC100769359	ZBTB38	MERTK	SLC38A2	GPR98	USP53	TLR3	RBM14	
LOC100773054	ZBTB43	MKL1	SPOCD1	GPRASP1			RHOB	
MMRN2	ZFP710	MYLIP	SPRED2	IFI204			RRAS2	
MUC2		NDST2	TMEM51	IL7R			SERINC2	
MXRA8		NUPR1	TOB1	JADE2			SLC6A13	
NXF3		RFX1	ZNF608	KIFC3			SRPX2	
PTHLH		RGMA		LAYN			SYNM	
RNF182		RGS16		LMO7			TNRC6B	
SCN4A		RNF24		LOC100760218				
TOR1AIP2		SEC14L1		LOC100761102				
TRIM72		SERPINE1		LOC100767397				
VMN2R1		SLC40A1		LOC100769915				
VWA3A		SLC6A9		LOC100772405				
WFIKKN2		SSH1		LYSMD3				
WNT2B		TRIB3		MAOB				
		TTBK2		MTUS1				
		TTN		NRP2				
		UVRAG		NXPE2				
				OASL				
				OLFM1				
				PCNXL4				
				PKD2				
				PRDM10				
				PRMT2				
				RPGRIP1				
				SEMA4D				
				SLC25A45				
				SLC28A1				
				SLC39A2				
				SLC5A3				
				SNX33				
				SQRDL				
				SRD5A1				
				TCP11L2				
				TJP3				
				TOM1				
				UAP1				
				WDFY2				
				WDR59				

A.2.6 maSigPro Clusters for Significantly Downregulated Genes
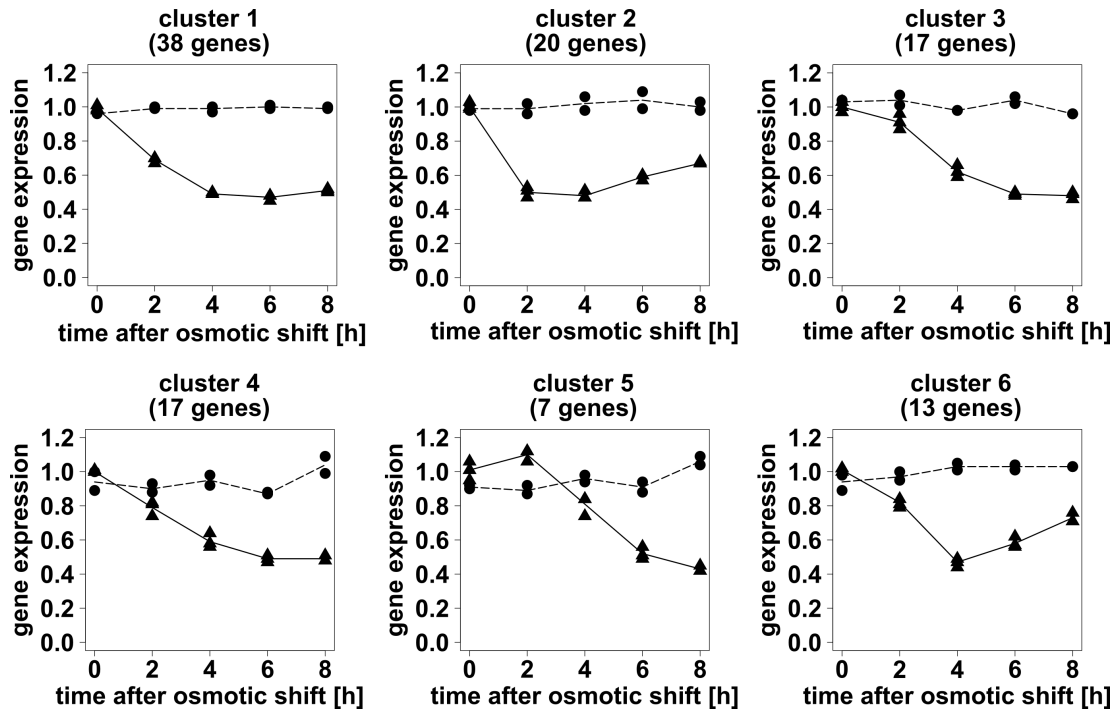
FIGURE A.18: Clusters of gene expression dynamics of significantly downregulated mRNAs. Osmolality was increased during batch cultivation of CHO DP-12 by the addition of NaCl-enriched cultivation medium (Tab. 4.3, 4.2.2). This resulted in an osmolality of $\sim$ 425 mOsmol kg^{-1} for hyperosmotic cultures (n = 3, ▲) compared to $\sim$ 285 mOsmol kg^{-1} for reference cultures (n = 2, ●). Gene expression analysis was based on next generation sequencing and data were analyzed with edgeR and maSigPro (4.2.10). Diagrams show medians of the gene expression of clustered genes.

TABLE A.6: maSigPro gene clusters for significantly downregulated genes upon to hyperosmotic stimulus.

cluster 1 (38 genes)	cluster 2 (20 genes)	cluster 3 (17 genes)	cluster 4 (17 genes)	cluster 5 (7 genes)	cluster 6 (13 genes)
ARVCF	ALS2CL	DPH6	ADAM19	ANKMY1	ARHGEF28
BZRAP1	ANGEL1	FOXP2	DCLK1	CDK14	ESR1
CASP1	B3GALNT1	HEATR4	DFNA5	ENOX1	ETL4
CAV2	DSEL	HELLS	F3	FUBP1	GULP1
CCND1	FAM161A	HNRNPA1	GLI1	KCNQ5	KDM8
CDH7	FGD4	IGDCC4	HIVEP3	TNFRSF12A	KIF13A
CIRBP	IKBKG	JADE3	LOC100756141	ZNF469	LOC100752991
DPH1	IL6	LOC100756717	LOC100768211		PEX14
DUSP5	LGALSL	LOC100771660	LOC100771726		PLEKHA6
EGR1	LOC100751006	MATN4	LOC100772063		PTER
EGR3	MKS1	OSCP1	LRRK1		SCAPER
ENDOD1	MURC	PION	NAV2		SRBD1
EPS8	NAV3	SLC29A1	SCNN1A		SYNE1
FAM114A1	NFKBIE	STXBP6	SLC12A5		
FAM198B	PLEKHN1	TMEM44	TNFRSF25		
FHL3	RAB7B	TTC39A	TTC28		
GLMN	RBM43	ZHX1	ZCCHC3		
HMGCS1	RHOBTB1				
LOC100758301	TAF1B				
LOC100761052	THBS1				
LOC100768278					
LYPLAL1					
MIDN					
MTSS1					
NAB2					
NAIP1					
PKDCC					
PMP22					
PTX3					
RELB					
SEC16B					
SGK3					
SLC16A6					
SLC25A43					
ST3GAL3					
TPBG					
TRP63					
ZDHHC15					

A.2.7 Significantly Upregulated Genes

TABLE A.7: Results of gene expression analysis for 51 significantly upregulated genes 4, 6 and 8 h after osmotic shift. log2(FC) $\geqslant$ 1, P and FDR $\leqslant$ 0.02, C = cluster (maSigPro)

	C	2 h log2(FC)	P-value	FDR	4 h log2(FC)	P-value	FDR	6 h log2(FC)	P-value	FDR	8 h log2(FC)	P-value	FDR
Ahi1	3	0.54	4.6E-08	6.4E-07	1.02	4.1E-26	6.1E-24	1.13	2.1E-31	3.4E-29	1.15	2.9E-31	4.7E-29
Akr1b1	5	0.82	9.2E-25	7.9E-23	1.26	3.2E-55	1.5E-52	1.57	1.8E-82	1.6E-79	1.80	1.3E-105	1.7E-102
Arl4a	3	0.47	5.1E-03	2.1E-02	1.27	2.9E-16	1.6E-14	1.01	1.7E-11	3.8E-10	1.02	8.1E-11	1.8E-09
Asap3	3	0.69	2.7E-05	2.1E-04	1.71	7.1E-30	1.3E-27	1.54	2.0E-23	1.7E-21	1.15	2.4E-14	8.9E-13
Bmf	5	0.07	8.2E-01	9.3E-01	1.27	2.1E-06	2.3E-05	1.79	1.4E-12	3.6E-11	1.59	1.6E-09	2.8E-08
Bod1	2	0.93	2.6E-40	5.5E-38	1.05	7.4E-51	3.0E-48	1.31	3.5E-80	3.0E-77	1.36	9.8E-84	1.0E-80
Cables2	3	0.93	1.6E-27	1.7E-25	1.30	4.1E-57	2.2E-54	1.32	2.9E-60	1.5E-57	1.11	1.9E-42	5.2E-40
Cacnb3	3	0.82	9.9E-09	1.5E-07	1.26	3.7E-24	4.6E-22	1.62	1.5E-37	3.1E-35	1.25	2.5E-24	2.5E-22
Cdhr4	5	0.41	2.6E-01	4.7E-01	1.41	4.3E-06	4.3E-05	1.91	1.5E-12	4.0E-11	1.68	3.8E-09	6.4E-08
Chn1	8	0.87	1.1E-03	5.7E-03	1.23	2.8E-08	4.3E-07	1.62	4.3E-14	1.4E-12	1.82	3.1E-18	1.7E-16
Cited1	8	0.33	4.9E-03	2.0E-02	1.16	2.7E-23	3.0E-21	1.75	1.3E-50	4.4E-48	2.04	1.7E-67	1.1E-64
Col7a1	5	0.62	7.6E-04	4.0E-03	1.13	5.8E-11	1.5E-09	1.36	5.4E-16	2.2E-14	1.24	1.8E-14	6.7E-13
Crebrf	3	0.42	1.6E-02	5.4E-02	1.58	5.7E-27	8.8E-25	1.28	1.9E-18	1.0E-16	1.15	1.2E-12	3.5E-11
Ctgf	3	0.09	8.2E-01	9.2E-01	1.91	1.8E-10	4.3E-09	1.97	1.7E-11	3.9E-10	1.55	6.6E-07	7.1E-06
Cxcl3	5	0.16	1.8E-01	3.7E-01	1.66	3.1E-52	1.3E-49	1.66	2.9E-61	1.5E-58	1.61	7.8E-56	3.3E-53
Dyrk1b	5	0.57	4.4E-04	2.5E-03	1.30	6.1E-18	4.2E-16	1.44	6.2E-22	4.8E-20	1.18	4.1E-16	1.8E-14
Fam117a	3	0.67	2.0E-06	2.0E-05	1.29	3.7E-22	3.8E-20	1.27	1.4E-21	1.0E-19	1.13	1.2E-15	5.3E-14
Fgd3	3	0.33	3.5E-03	1.5E-02	1.06	1.9E-22	2.0E-20	1.26	8.6E-32	1.5E-29	1.17	2.2E-27	2.7E-25
Gpr98	5	0.09	7.9E-01	9.1E-01	1.41	9.7E-07	1.1E-05	1.68	5.0E-09	7.7E-08	1.73	2.2E-09	3.8E-08
Il7r	5	0.07	7.2E-01	8.7E-01	1.18	3.4E-11	9.0E-10	1.56	2.6E-21	1.9E-19	1.90	1.3E-25	1.4E-23
Kiaa0513	8	0.07	6.1E-01	8.1E-01	1.13	1.0E-18	7.4E-17	1.37	5.6E-28	6.7E-26	1.52	2.6E-35	5.8E-33
Kifc3	5	0.56	3.7E-05	2.8E-04	1.34	2.3E-26	3.4E-24	2.21	5.2E-68	3.3E-65	1.92	2.1E-55	8.7E-53
Klhl24	3	0.53	2.1E-03	9.8E-03	1.18	9.2E-15	4.0E-13	1.33	2.5E-17	1.2E-15	1.30	3.1E-16	1.4E-14
Layn	5	0.60	3.9E-15	1.4E-13	1.37	9.7E-73	1.0E-69	1.71	5.1E-113	8.2E-110	1.80	1.1E-122	1.8E-119
Lmo7	5	0.74	6.9E-17	3.0E-15	1.22	4.2E-45	1.5E-42	1.41	1.3E-63	7.0E-61	1.57	2.2E-78	2.0E-75
LOC100754646	7	0.24	5.0E-01	7.2E-01	1.03	1.3E-03	6.3E-03	1.36	1.4E-06	1.3E-05	1.38	1.9E-06	1.9E-05
LOC100769915	5	0.26	4.1E-01	6.4E-01	1.13	2.2E-05	1.8E-04	1.01	1.2E-04	6.9E-04	1.03	5.2E-05	3.5E-04
LOC100772072	8	0.13	1.8E-01	3.7E-01	1.10	4.4E-33	9.5E-31	1.60	1.2E-69	8.4E-67	1.74	8.7E-81	8.4E-78
LOC100772405	5	0.40	1.9E-03	9.0E-03	1.02	2.9E-16	1.6E-14	1.05	2.8E-19	1.6E-17	1.23	2.9E-23	2.6E-21
Lpar1	3	0.65	1.4E-08	2.1E-07	1.30	1.0E-30	1.9E-28	1.52	2.2E-40	4.8E-38	1.30	1.3E-30	2.0E-28
Maoa	8	0.63	3.8E-03	1.6E-02	1.07	5.5E-08	7.9E-07	1.39	2.3E-14	7.9E-13	1.77	2.6E-23	2.3E-21
Mertk	3	0.86	2.7E-09	4.5E-08	1.65	2.5E-36	6.5E-34	1.65	8.0E-38	1.7E-35	1.47	1.7E-30	2.6E-28
Mkl1	3	0.52	1.1E-04	7.7E-04	1.35	1.4E-25	1.9E-23	1.15	7.1E-19	3.9E-17	1.26	7.0E-22	5.5E-20
Moxd1	8	0.51	1.6E-01	3.4E-01	1.34	1.6E-05	1.8E-04	2.15	3.0E-14	1.0E-12	2.36	4.4E-18	2.4E-16
Ndrg2	8	0.81	2.1E-02	6.7E-02	1.43	4.1E-06	4.1E-05	2.37	1.2E-19	7.4E-18	2.48	3.4E-23	3.0E-21
Nrp2	5	0.69	4.0E-14	1.3E-12	1.14	4.7E-40	1.4E-37	1.50	1.1E-68	7.5E-66	1.51	4.4E-71	3.0E-68
Nxpe2	5	0.72	4.0E-02	1.2E-01	1.38	1.1E-05	9.5E-05	1.98	3.1E-12	7.8E-11	1.83	6.0E-10	1.2E-08
Oasl	5	0.61	1.1E-03	5.7E-03	1.13	9.8E-13	3.3E-11	1.79	1.4E-30	2.1E-28	1.68	1.1E-26	1.4E-24
Olfm1	5	0.83	1.4E-08	2.1E-07	2.23	1.7E-66	1.3E-63	2.77	2.6E-109	3.8E-106	2.88	2.3E-115	3.4E-112
Pgm2l1	8	0.03	8.6E-01	9.4E-01	1.07	1.2E-10	2.8E-09	1.66	1.8E-24	1.7E-22	1.78	3.5E-32	6.3E-30
Ranbp3l	8	0.18	5.9E-01	7.9E-01	2.29	1.1E-18	8.1E-17	3.16	9.5E-49	2.9E-46	3.80	3.8E-78	3.2E-75
Rnf24	3	0.80	2.1E-07	2.5E-06	1.39	5.8E-21	5.0E-19	1.24	8.9E-18	4.4E-16	1.30	1.8E-17	8.9E-16
Rpgrip1	5	0.45	1.5E-01	3.2E-01	1.27	9.3E-06	8.5E-05	1.04	9.2E-05	5.4E-04	1.37	3.0E-06	2.8E-05
Sec14l1	3	0.87	3.3E-12	8.5E-11	1.36	1.1E-28	1.8E-26	1.44	3.7E-33	6.7E-31	1.26	4.2E-26	4.8E-24
Sema4d	5	0.95	2.0E-10	4.1E-09	2.67	1.5E-87	2.0E-84	3.36	2.7E-150	5.7E-147	3.10	9.7E-146	2.0E-142
Serpine1	3	0.34	1.9E-02	6.2E-02	1.19	1.6E-20	1.3E-18	1.56	1.0E-33	1.9E-31	1.51	9.8E-30	1.4E-27
Slc6a9	3	0.87	3.9E-13	1.1E-11	1.43	1.0E-34	2.3E-32	1.75	2.3E-49	7.3E-47	1.42	1.9E-33	3.8E-31
Srcap	2	0.92	9.9E-22	6.8E-20	1.08	3.7E-29	6.3E-27	1.18	2.4E-34	4.6E-32	1.07	1.1E-28	1.5E-26
Tcp11l2	5	0.48	7.2E-02	1.8E-01	1.14	6.6E-07	7.7E-06	1.11	1.3E-07	1.5E-06	1.54	5.9E-12	1.6E-10
Tjp3	5	0.43	1.2E-01	2.8E-01	1.08	8.3E-06	7.7E-05	1.45	3.9E-10	7.1E-09	1.02	8.9E-06	7.3E-05
Uvrag	3	0.93	1.2E-35	2.1E-33	1.41	8.8E-83	1.1E-79	1.11	1.6E-53	6.7E-51	1.18	5.1E-58	2.3E-55

TABLE A.8: Results of gene expression analysis for 32 significantly upregulated genes 2, 4, 6 and 8 h after osmotic shift. log2(FC) $\geqslant$ 1, P and FDR $\leqslant$ 0.02, C = cluster (maSigPro)

	C	2 h log2(FC)	P-value	FDR	4 h log2(FC)	P-value	FDR	6 h log2(FC)	P-value	FDR	8 h log2(FC)	P-value	FDR
Aldh8a1	1	2.94	1.2E-41	2.7E-39	2.40	1.2E-23	1.5E-21	1.27	7.7E-06	6.0E-05	1.15	1.0E-04	6.2E-04
Bcl6	2	1.73	6.5E-74	5.6E-71	1.65	3.6E-66	2.6E-63	1.85	3.9E-87	4.4E-84	1.59	2.1E-59	9.7E-57
Cdk1a	2	1.82	1.1E-51	3.6E-49	2.02	2.8E-62	1.7E-59	1.88	2.8E-57	1.4E-54	1.73	5.2E-45	1.5E-42
Cryab	2	1.31	2.3E-08	3.3E-07	1.20	2.1E-07	2.8E-06	1.48	1.6E-10	3.0E-09	1.16	2.3E-07	2.7E-06
Ddit4	2	3.57	6.9E-298	5.1E-294	3.84	0.0E+00	0.0E+00	3.99	0.0E+00	0.0E+00	3.34	1.0E-279	1.5E-275
Dusp1	3	1.37	2.0E-38	3.8E-36	2.16	2.7E-101	4.3E-98	2.13	2.8E-96	3.4E-93	1.86	4.9E-74	3.8E-71
Dyrk3	2	1.22	2.6E-18	1.3E-16	1.20	9.2E-20	7.2E-18	1.35	5.3E-25	5.2E-23	1.38	1.1E-21	8.9E-20
Ets2	4	2.12	2.2E-86	3.0E-83	1.79	1.3E-62	8.9E-60	1.74	7.6E-56	3.6E-53	1.27	1.3E-29	1.9E-27
Fmo4	5	1.93	2.6E-63	1.3E-60	2.53	1.2E-137	3.5E-134	2.62	7.6E-165	1.8E-161	2.77	9.2E-177	2.7E-173
Gfod1	2	2.16	3.5E-34	5.8E-32	2.84	1.5E-58	8.7E-56	2.64	2.9E-53	1.1E-50	2.08	7.2E-33	1.4E-30
Gnl1	2	1.25	1.7E-48	5.0E-46	1.42	2.7E-64	1.9E-61	1.64	1.9E-84	1.8E-81	1.40	1.6E-62	8.3E-60
Gpd1l	5	1.32	2.3E-37	4.4E-35	1.97	3.8E-109	6.9E-106	2.46	5.5E-192	2.0E-188	2.42	4.5E-189	1.6E-185
Hexim1	4	1.48	1.5E-94	2.7E-91	1.11	1.2E-54	5.6E-52	1.28	1.6E-70	1.2E-67	1.10	6.1E-53	2.2E-50
Hoxc6	4	1.89	5.3E-34	8.6E-32	1.53	2.1E-21	1.9E-19	1.80	5.8E-28	6.8E-26	1.32	3.0E-16	1.4E-14
Ier3	2	3.68	2.84E-313	0.0E+00	4.08	0.0E+00	0.0E+00	3.99	0.0E+00	0.0E+00	3.23	2.4E-250	1.7E-246
Il15	2	2.00	6.6E-29	8.1E-27	2.40	6.1E-36	1.5E-33	2.76	4.9E-52	1.8E-49	2.16	4.4E-30	6.6E-28
LOC100767397	5	1.87	1.2E-09	2.2E-08	1.89	5.7E-11	1.4E-09	2.48	2.0E-20	1.4E-18	2.42	4.6E-20	3.0E-18
LOC100772394	6	3.21	9.7E-49	2.9E-46	3.80	4.2E-70	3.8E-67	2.71	6.6E-26	7.0E-24	1.55	5.0E-08	6.6E-07
Mbnl2	2	1.25	2.6E-60	1.1E-57	1.31	9.7E-67	8.3E-64	1.10	1.7E-46	4.8E-44	1.17	1.1E-50	3.7E-48
Neb	6	3.78	3.4E-81	3.5E-78	4.15	9.7E-111	2.0E-107	2.24	2.3E-20	1.5E-18	1.31	2.1E-06	2.0E-05
Nupr1	3	1.61	1.1E-65	5.9E-63	2.53	8.0E-169	2.9E-165	2.58	2.3E-185	6.7E-182	2.58	2.2E-165	5.3E-162
Phex	2	1.05	9.4E-04	4.9E-03	1.38	2.7E-05	2.2E-04	1.11	5.9E-04	2.8E-03	1.74	2.1E-08	3.0E-07
Rgs16	3	1.97	7.8E-33	1.2E-30	2.33	1.1E-51	4.6E-49	2.37	1.5E-56	7.3E-54	2.17	2.5E-41	6.8E-39
Sema6c	2	1.13	9.6E-23	7.1E-21	1.41	9.3E-38	2.5E-35	1.57	4.0E-45	1.1E-42	1.19	2.9E-28	3.8E-26
Slc38a2	4	2.84	6.5E-224	3.2E-220	1.97	1.2E-116	3.0E-113	1.78	1.4E-96	1.9E-93	1.57	1.7E-76	1.3E-73
Slc39a2	5	1.13	1.8E-04	1.2E-03	2.80	1.1E-29	2.0E-27	3.32	1.4E-50	4.6E-48	3.08	1.4E-40	3.6E-38
Slc6a6	2	1.28	4.8E-32	6.8E-30	1.50	7.3E-44	2.4E-41	1.60	2.6E-48	7.8E-46	1.30	1.0E-33	2.1E-31
Smyd1	2	1.76	3.3E-14	1.1E-12	1.93	4.2E-17	2.6E-15	1.86	8.0E-16	3.3E-14	1.26	8.3E-08	1.1E-06
Spocd1	4	1.69	1.3E-08	2.0E-07	1.63	1.2E-07	1.7E-06	1.09	9.5E-04	4.3E-03	1.08	6.4E-04	3.2E-03
Tmem232	6	1.64	2.0E-10	4.0E-09	2.36	2.2E-20	1.8E-18	1.71	1.1E-09	1.9E-08	1.36	4.0E-06	3.6E-05
Ttn	3	2.09	1.1E-11	2.7E-10	3.95	1.2E-56	6.4E-54	3.68	1.1E-45	3.1E-43	3.16	1.5E-29	2.1E-27
Zbtb38	2	1.85	8.0E-82	9.0E-79	1.81	6.0E-80	6.7E-77	2.16	1.9E-117	3.5E-114	1.91	6.1E-90	7.4E-87

TABLE A.9: Results of gene expression analysis for 1 significantly upregulated gene 2, 4 and 8 h after osmotic shift. log2(FC) $\geqslant$ 1, P and FDR $\leqslant$ 0.02, C = cluster (maSigPro)

	C	2 h log2(FC)	P-value	FDR	4 h log2(FC)	P-value	FDR	6 h log2(FC)	P-value	FDR	8 h log2(FC)	P-value	FDR
Kansl1l		1.85	1.8E-65	9.2E-63	1.30	1.9E-29	3.4E-27	0.83	5.9E-13	1.6E-11	1.09	1.4E-20	9.8E-19

TABLE A.10: Results of gene expression analysis for 24 significantly upregulated genes 2, 4 and 6 h after osmotic shift. log2(FC) $\geqslant$ 1, P and FDR $\leqslant$ 0.02, C = cluster (maSigPro)

	C	2 h log2(FC)	P-value	FDR	4 h log2(FC)	P-value	FDR	6 h log2(FC)	P-value	FDR	8 h log2(FC)	P-value	FDR
Adamts3	1	2.53	1.5E-25	1.4E-23	2.18	1.2E-19	9.1E-18	1.11	2.4E-04	1.3E-03	0.48	1.4E-01	2.9E-01
Alpk3	1	2.56	1.9E-24	1.6E-22	1.93	1.8E-11	5.0E-10	1.12	9.1E-04	4.1E-03	0.38	3.1E-01	5.3E-01
Baiap3	1	2.11	2.6E-19	1.5E-17	1.81	1.6E-13	6.1E-12	1.05	7.2E-05	4.4E-04	0.74	8.9E-03	3.1E-02
Cspg5		2.95	4.3E-35	7.3E-33	1.51	1.7E-07	2.3E-06	1.19	2.5E-04	1.3E-03	0.32	3.6E-01	5.8E-01
Fam132a	4	1.61	1.8E-10	3.7E-09	1.44	8.1E-09	1.4E-07	1.26	3.2E-06	2.7E-05	0.94	3.9E-04	2.1E-03
Hspa4l	6	1.16	1.4E-08	2.1E-07	1.40	2.0E-11	5.5E-10	1.16	2.3E-08	3.1E-07	0.44	4.5E-02	1.2E-01
Itga7	4	1.28	4.6E-19	2.5E-17	1.08	1.0E-12	3.4E-11	1.12	3.7E-12	9.0E-11	0.91	3.4E-09	5.8E-08
LOC100762996		2.36	6.9E-17	3.0E-15	2.27	9.8E-16	5.1E-14	1.03	2.9E-03	1.1E-02	0.17	6.2E-01	8.2E-01
LOC100767001	6	1.19	9.8E-07	1.1E-05	1.53	4.0E-10	9.0E-09	1.67	3.9E-10	7.2E-09	0.83	7.2E-03	2.6E-02
LOC100768165	6	1.49	2.1E-06	2.1E-05	1.51	3.2E-07	3.9E-06	1.01	2.1E-03	8.5E-03	0.21	5.1E-01	7.4E-01
LOC100771158	4	1.61	2.1E-23	1.7E-21	1.39	1.8E-16	1.1E-14	1.32	3.1E-14	1.0E-12	0.93	1.6E-07	1.9E-06
LOC100771908	2	1.22	4.9E-11	1.1E-09	1.22	2.0E-12	6.6E-11	1.26	3.9E-13	1.1E-11	0.83	8.3E-07	8.8E-06
Mmrn2	1	1.54	2.4E-08	3.5E-07	1.33	1.2E-05	1.0E-04	1.07	9.9E-04	4.4E-03	0.02	9.6E-01	9.9E-01
Muc2	1	3.52	3.7E-52	1.3E-49	3.52	2.1E-54	9.6E-52	1.69	6.3E-08	7.7E-07	0.84	2.0E-02	6.0E-02
Nckap5l	4	1.68	2.3E-55	8.5E-53	1.12	8.8E-26	1.3E-23	1.02	6.1E-21	4.3E-19	0.91	7.6E-17	3.7E-15
Ovgp1		3.21	6.6E-58	2.8E-55	1.65	3.3E-10	7.5E-09	1.21	4.7E-05	3.0E-04	0.63	6.5E-02	1.6E-01
Plcxd3	9	1.23	2.2E-04	1.4E-03	1.50	1.3E-07	1.8E-06	1.10	3.1E-04	1.6E-03	0.68	4.5E-02	1.2E-01
Pygm		3.24	3.2E-71	2.4E-68	2.13	1.2E-24	1.6E-22	1.06	3.2E-05	2.1E-04	0.38	1.3E-01	2.7E-01
Rbm15	4	1.60	2.0E-34	3.3E-32	1.21	1.2E-20	1.0E-18	1.26	5.7E-22	4.4E-20	0.88	1.6E-11	3.9E-10
Slc26a7	6	1.41	3.3E-06	3.2E-05	1.50	2.4E-07	3.1E-06	1.16	6.6E-04	3.1E-03	0.47	1.8E-01	3.6E-01
Sptbn5	6	2.06	3.5E-32	5.0E-30	2.63	2.8E-50	1.1E-47	1.37	5.8E-13	1.6E-11	0.32	1.7E-01	3.4E-01
Tek	6	1.57	6.8E-09	1.1E-07	1.87	1.8E-11	5.0E-10	1.16	8.6E-05	5.1E-04	0.38	2.5E-01	4.6E-01
Tmem51	4	1.73	2.3E-57	9.1E-55	1.43	2.7E-38	7.7E-36	1.11	6.3E-24	5.6E-22	0.88	1.9E-15	7.8E-14
Tor1aip2	1	2.30	2.4E-75	2.3E-72	1.84	4.7E-49	1.7E-46	1.03	1.8E-14	6.2E-13	0.33	2.2E-02	6.6E-02

TABLE A.11: Results of gene expression analysis for 88 significantly upregulated genes 2 and 4 h after osmotic shift. log2(FC) $\geqslant$ 1, P and FDR $\leqslant$ 0.02, C = cluster (maSigPro)

	C	2 h log2(FC)	P-value	FDR	4 h log2(FC)	P-value	FDR	6 h log2(FC)	P-value	FDR	8 h log2(FC)	P-value	FDR
Aifm3		1.20	4E-07	5E-06	1.25	1.7E-05	1.4E-04	1.25	1.7E-05	1.4E-04	0.21	5.2E-01	7.4E-01
Ampd1		2.39	2E-17	1E-15	1.10	1.4E-03	6.9E-03	0.36	3.5E-01	5.7E-01	0.15	7.1E-01	8.8E-01
Amz1	1	1.37	1E-05	1E-04	1.12	7.9E-04	4.2E-03	0.77	3.4E-02	9.0E-02	0.27	4.7E-01	7.0E-01
Ankrd61	1	1.22	2E-10	4E-09	1.05	2.1E-07	2.8E-06	0.04	8.5E-01	9.5E-01	-0.21	3.8E-01	6.1E-01
Apc2	4	1.36	1E-11	3E-10	1.11	1.9E-07	2.5E-06	0.94	5.6E-05	3.5E-04	0.56	1.9E-02	5.9E-02
Armcx4	6	1.05	3E-03	1E-02	1.12	7.9E-04	4.2E-03	0.29	4.4E-01	6.6E-01	0.19	6.3E-01	8.3E-01
Asl	1	1.83	2E-20	1E-18	1.27	8.6E-09	1.5E-07	0.43	7.8E-02	1.8E-01	0.43	1.1E-01	2.3E-01
Bsn	6	1.73	4E-09	7E-08	1.49	5.5E-08	8.0E-07	0.00	1.0E+00	1.0E+00	0.35	3.2E-01	5.4E-01
Ccdc164	1	1.86	1E-10	2E-09	1.36	4.7E-06	4.6E-05	0.43	2.4E-01	4.3E-01	0.14	7.0E-01	8.7E-01
Cd101		2.60	1E-25	1E-23	1.37	2.0E-05	1.7E-04	0.46	2.2E-01	4.1E-01	0.01	9.8E-01	9.9E-01
Cd46		1.97	2E-15	7E-14	1.33	8.4E-07	9.6E-06	0.65	2.6E-02	7.3E-02	0.19	4.8E-01	7.1E-01
Cel	1	1.98	6E-12	2E-10	1.15	3.3E-04	1.9E-03	0.33	3.7E-01	5.9E-01	0.01	9.8E-01	9.9E-01
Chadl		2.18	7E-25	6E-23	1.04	2.9E-04	1.7E-03	-0.17	5.8E-01	7.8E-01	-0.32	3.0E-01	5.1E-01
Chrnb2	6	1.13	4E-04	2E-03	1.17	6.0E-04	3.3E-03	0.51	1.4E-01	2.8E-01	0.21	5.8E-01	8.0E-01
Cmya5		1.75	2E-08	4E-07	1.10	1.4E-03	6.9E-03	0.22	5.7E-01	7.8E-01	0.11	7.8E-01	9.2E-01
Col20a1	1	1.77	4E-09	6E-08	1.64	8.5E-08	1.2E-06	0.78	1.7E-02	5.0E-02	0.60	9.9E-02	2.2E-01
Cpm		1.47	3E-06	3E-05	1.04	1.8E-03	8.4E-03	0.36	3.3E-01	5.5E-01	0.11	7.8E-01	9.2E-01
Crocc		1.49	9E-18	4E-16	1.40	2.2E-15	1.1E-13	0.59	2.7E-03	1.1E-02	-0.13	4.7E-01	7.0E-01
Dnah12		2.30	2E-36	4E-34	1.67	2.0E-13	7.4E-12	0.07	8.1E-01	9.3E-01	0.16	5.7E-01	7.9E-01
Dnahc17		2.41	2E-25	1E-23	1.54	1.1E-08	1.8E-07	0.50	1.2E-01	2.5E-01	0.41	2.3E-01	4.2E-01
Duox2	6	1.55	1E-10	2E-09	1.76	1.0E-12	3.4E-11	0.64	1.9E-02	5.5E-02	0.18	5.1E-01	7.4E-01
Dysf		1.62	2E-07	3E-06	1.14	8.0E-04	4.2E-03	0.46	2.1E-01	3.9E-01	0.58	1.2E-01	2.6E-01
Edrf1	4	1.18	3E-69	2E-66	1.08	4.3E-54	1.9E-51	0.85	5.0E-35	9.9E-33	0.86	6.6E-34	1.3E-31
Emilin2		1.30	2E-07	3E-06	1.08	6.8E-05	4.9E-04	0.26	3.7E-01	5.9E-01	0.01	9.9E-01	9.9E-01
Epha2		1.58	5E-30	7E-28	1.19	3.1E-14	1.3E-12	0.79	2.7E-06	2.3E-05	0.45	6.8E-03	2.5E-02
Ereg	4	1.54	1E-66	8E-64	1.18	1.4E-39	4.2E-37	0.94	6.7E-26	7.2E-24	0.58	1.0E-10	2.2E-09
Evpl		2.73	3E-66	2E-63	1.42	4.5E-11	1.2E-09	0.01	9.5E-01	9.8E-01	-0.33	1.8E-01	3.5E-01
Fam179a		3.76	1E-70	1E-67	1.71	2.0E-08	3.1E-07	0.64	7.3E-02	1.7E-01	0.20	5.6E-01	7.8E-01
Fam46c	1	2.06	1E-12	4E-11	1.37	2.0E-05	1.7E-04	0.94	5.5E-03	1.9E-02	0.48	2.0E-01	3.9E-01
Farp2		2.31	2E-72	2E-69	1.43	3.7E-21	3.3E-19	0.50	3.3E-03	1.3E-02	0.23	1.8E-01	3.6E-01
Fer1l4		2.01	4E-15	1E-13	1.07	5.5E-04	3.1E-03	0.29	3.8E-01	6.0E-01	0.18	5.9E-01	8.0E-01
Gareml		2.34	1E-20	6E-19	1.07	2.2E-04	1.4E-03	0.45	1.6E-01	3.1E-01	0.25	4.1E-01	6.4E-01
Heatr7b1	1	2.59	7E-27	8E-25	2.42	9.4E-21	8.0E-19	0.85	9.5E-03	3.1E-02	0.01	9.9E-01	9.9E-01
Hhipl2	1	1.46	2E-14	6E-13	1.61	1.1E-16	6.8E-15	0.47	5.0E-02	1.2E-01	-0.48	5.8E-02	1.4E-01
Hkdc1		2.73	5E-25	5E-23	1.39	4.2E-05	3.2E-04	0.46	2.3E-01	4.2E-01	0.27	4.8E-01	7.1E-01
Il12rb2		2.48	2E-22	2E-20	1.11	4.3E-04	2.4E-03	0.46	1.9E-01	3.7E-01	0.35	3.6E-01	5.9E-01
Impg2		2.06	1E-14	4E-13	1.09	7.7E-04	4.0E-03	0.31	3.7E-01	5.9E-01	0.16	6.5E-01	8.4E-01
Islr2	1	2.11	8E-14	3E-12	1.42	5.7E-06	5.5E-05	0.89	1.1E-02	3.5E-02	0.01	9.9E-01	9.9E-01
Itgam		2.72	4E-24	3E-22	1.83	5.7E-09	1.0E-07	0.55	1.3E-01	2.7E-01	0.31	4.3E-01	6.7E-01
Itgax	1	1.54	1E-06	1E-05	1.30	1.3E-04	8.7E-04	0.66	7.7E-02	1.8E-01	0.10	7.9E-01	9.3E-01
Kiaa0319		2.55	2E-23	2E-21	1.28	1.8E-04	1.1E-03	0.53	1.6E-01	3.2E-01	0.09	8.1E-01	9.3E-01
Lman1l	1	1.39	8E-06	7E-05	1.23	2.4E-04	1.5E-03	0.39	2.9E-01	5.0E-01	0.24	5.4E-01	7.6E-01
LOC100751769	6	1.15	4E-04	2E-03	1.61	3.2E-07	4.0E-06	0.63	7.1E-02	1.7E-01	0.41	2.6E-01	4.7E-01
LOC100752478		1.17	7E-04	4E-03	1.04	1.8E-03	8.4E-03	0.10	8.0E-01	9.2E-01	0.31	4.3E-01	6.6E-01
LOC100757105		2.61	7E-22	5E-20	2.06	6.0E-12	1.8E-10	0.73	4.1E-02	1.1E-01	0.12	7.6E-01	9.1E-01
LOC100763491		3.06	5E-34	9E-32	1.98	2.5E-11	7.0E-10	0.80	2.7E-02	7.6E-02	0.58	1.2E-01	2.6E-01
LOC100764872	1	1.30	9E-05	6E-04	1.30	1.3E-04	8.7E-04	0.39	3.0E-01	5.1E-01	0.27	4.7E-01	7.0E-01
LOC100765388	1	1.67	6E-15	2E-13	1.71	1.3E-12	4.4E-11	0.35	2.1E-01	3.9E-01	0.38	2.4E-01	4.4E-01
LOC100769359	1	1.15	5E-04	3E-03	1.21	3.3E-04	2.0E-03	0.36	3.0E-01	5.2E-01	0.03	9.4E-01	9.8E-01
LOC100771708		1.08	1E-03	6E-03	1.17	6.0E-04	3.3E-03	0.49	1.9E-01	3.7E-01	0.27	4.7E-01	7.0E-01
LOC100773054	1	1.32	2E-08	3E-07	1.20	2.2E-06	2.3E-05	0.48	8.3E-02	1.9E-01	0.22	4.6E-01	6.9E-01
LOC100773845		1.89	2E-13	5E-12	1.04	2.9E-04	1.7E-03	0.08	7.9E-01	9.2E-01	-0.06	8.5E-01	9.5E-01
Map3k15		2.32	1E-21	8E-20	1.71	4.2E-09	7.5E-08	0.55	8.9E-02	2.0E-01	0.21	5.4E-01	7.6E-01
Mcf2		1.22	4E-04	2E-03	1.12	1.1E-03	5.4E-03	0.16	6.7E-01	8.6E-01	0.05	8.9E-01	9.6E-01
Mex3b	6	1.24	6E-08	8E-07	1.06	1.2E-07	1.7E-06	0.73	3.9E-04	2.0E-03	0.54	1.3E-02	4.2E-02
Mkks	6	1.12	2E-14	5E-13	1.38	1.5E-21	1.4E-19	0.84	2.6E-08	3.4E-07	0.69	2.8E-05	2.0E-04
Mxra8	1	1.33	4E-07	5E-06	1.26	6.9E-06	6.5E-05	0.73	3.2E-02	8.7E-02	0.12	7.3E-01	8.9E-01
Myo1a		1.47	4E-09	7E-08	1.02	5.0E-04	2.8E-03	0.06	8.3E-01	9.4E-01	-0.10	7.0E-01	8.8E-01
Myrfl		1.65	1E-07	2E-06	1.07	2.6E-03	1.1E-02	0.43	2.6E-01	4.6E-01	0.01	9.8E-01	9.9E-01
N4bp2l1		2.05	6E-18	3E-16	1.30	9.0E-06	8.2E-05	0.63	3.1E-02	8.4E-02	0.23	4.8E-01	7.1E-01
Nek10		2.10	4E-13	1E-11	1.19	6.0E-04	3.3E-03	0.35	3.7E-01	5.9E-01	-0.12	7.6E-01	9.1E-01
Nup210l		3.65	3E-92	4E-89	1.55	1.3E-09	2.6E-08	0.62	2.9E-02	8.0E-02	0.25	4.6E-01	6.9E-01
Pik3cd		1.78	3E-09	4E-08	1.09	1.9E-03	9.0E-03	0.46	2.3E-01	4.2E-01	0.04	9.3E-01	9.8E-01
Pkhd1l1		2.37	2E-18	1E-16	1.29	7.5E-05	5.4E-04	0.73	4.1E-02	1.1E-01	0.03	9.4E-01	9.8E-01
Plch2	6	1.56	1.4E-13	4.3E-12	1.86	2.0E-23	2.4E-21	0.87	1.7E-04	9.4E-04	0.19	4.0E-01	6.3E-01
Ppfia4		2.06	2.5E-21	1.7E-19	1.42	3.5E-09	6.5E-08	0.63	3.2E-02	8.6E-02	0.09	7.8E-01	9.2E-01
Ptprh		2.43	1.4E-19	8.1E-18	1.68	4.1E-08	6.2E-07	0.77	3.4E-02	9.0E-02	0.45	2.3E-01	4.3E-01
Qrich2		1.65	5.8E-12	1.4E-10	1.41	1.8E-06	1.9E-05	0.37	2.7E-01	4.7E-01	0.78	1.6E-02	5.2E-02
Rap1gap		2.39	2.3E-17	1.1E-15	1.23	1.3E-04	8.9E-04	0.78	2.7E-02	7.5E-02	0.12	7.6E-01	9.1E-01
Rnf182	1	1.86	5.3E-28	5.8E-26	1.92	6.3E-27	9.7E-25	0.98	1.1E-06	1.1E-05	0.12	6.0E-01	8.1E-01
Scn4a	1	3.39	9.0E-49	2.7E-46	2.50	4.0E-20	3.2E-18	0.73	4.1E-02	1.1E-01	0.58	1.2E-01	2.6E-01
Sema4g		2.46	1.4E-19	8.1E-18	1.21	4.5E-04	2.5E-03	0.19	6.1E-01	8.1E-01	0.10	7.9E-01	9.3E-01
Serpinc1		1.85	2.6E-11	5.9E-10	1.15	4.4E-04	2.5E-03	0.51	1.4E-01	2.8E-01	0.18	6.3E-01	8.3E-01
Setd1a	4	1.36	4.2E-52	1.4E-49	1.22	1.8E-42	5.7E-40	0.98	5.5E-28	6.6E-26	0.52	5.8E-09	9.4E-08
Slc3a1		1.92	1.7E-11	4.0E-10	1.07	5.5E-04	3.1E-03	0.29	3.8E-01	6.0E-01	0.23	5.2E-01	7.4E-01
Spatc1l		2.27	6.2E-24	5.0E-22	1.15	3.3E-04	1.9E-03	0.50	1.2E-01	2.5E-01	0.45	1.4E-01	3.0E-01
Sptbn2		1.46	3.4E-09	5.6E-08	1.07	3.6E-05	2.8E-04	0.04	8.9E-01	9.6E-01	-0.31	3.1E-01	5.3E-01
Tdrd5		2.05	1.9E-15	7.0E-14	1.37	3.4E-06	3.4E-05	-0.19	5.9E-01	7.9E-01	-0.15	6.7E-01	8.5E-01
Tgm3		1.33	3.7E-05	2.8E-04	1.17	6.0E-04	3.3E-03	0.39	3.2E-01	5.3E-01	0.31	4.2E-01	6.5E-01
Tlr7		1.80	9.5E-09	1.5E-07	1.19	2.6E-04	1.6E-03	0.85	1.1E-02	3.6E-02	0.25	5.0E-01	7.3E-01

TABLE A.11 (continued)

	C	2 h log2(FC)	P-value	FDR	4 h log2(FC)	P-value	FDR	6 h log2(FC)	P-value	FDR	8 h log2(FC)	P-value	FDR
Tnfsf9		1.08	1.7E-39	3.4E-37	1.06	2.3E-39	6.5E-37	1.00	2.4E-34	4.6E-32	0.81	1.5E-22	1.2E-20
Tob1	4	1.37	9.0E-32	1.3E-29	1.16	1.6E-21	1.5E-19	0.71	7.4E-09	1.1E-07	0.57	6.1E-06	5.2E-05
Trim72		2.34	6.2E-18	3.0E-16	1.60	2.2E-08	3.4E-07	0.99	2.7E-03	1.1E-02	0.19	6.0E-01	8.1E-01
Vwa3a	1	2.50	2.0E-34	3.3E-32	1.54	1.3E-13	4.9E-12	0.97	1.3E-04	7.2E-04	0.40	1.6E-01	3.3E-01
Wdr66		2.04	3.0E-17	1.4E-15	1.60	2.2E-08	3.4E-07	0.26	4.6E-01	6.8E-01	0.05	8.9E-01	9.6E-01
Wfikkn2	1	2.02	1.8E-11	4.2E-10	1.76	2.2E-08	3.4E-07	0.94	6.9E-03	2.4E-02	0.48	2.0E-01	3.9E-01
Wnt2b	1	1.29	6.9E-05	4.9E-04	1.21	1.4E-04	9.0E-04	0.33	3.7E-01	5.9E-01	0.38	3.2E-01	5.5E-01
Zbtb2		1.98	4.2E-94	6.8E-91	1.19	1.1E-29	2.1E-27	0.65	2.7E-08	3.6E-07	0.37	2.2E-03	9.5E-03

TABLE A.12: Results of gene expression analysis for 30 significantly upregulated genes 6 and 8 h after osmotic shift. log2(FC) $\geqslant$ 1, P and FDR $\leqslant$ 0.02, C = cluster (maSigPro)

	C	log2(FC)	P-value	FDR	log2(FC)	P-value	FDR	log2(FC)	P-value	FDR	log2(FC)	P-value	FDR
Abcg1	7	0.12	7.0E-01	8.6E-01	0.57	4.6E+00	3.2E-02	2.12	5.1E-20	3.2E-18	2.14	1.2E-24	1.3E-22
Aqp1	5	0.38	2.5E-01	4.6E-01	0.73	2.1E-02	6.6E-02	1.50	2.1E-07	2.3E-06	1.47	2.0E-06	1.9E-05
Atp1b1	8	0.51	1.4E-01	3.1E-01	0.59	6.6E-02	1.7E-01	1.14	1.1E-04	6.5E-04	1.25	5.2E-06	4.5E-05
Axin2	5	0.86	3.1E-04	1.9E-03	0.76	1.0E-03	5.3E-03	1.36	1.8E-09	3.0E-08	1.20	1.2E-07	1.5E-06
Bpgm	5	0.25	7.1E-03	2.8E-02	0.82	5.3E-21	4.6E-19	1.16	4.0E-44	1.0E-41	1.35	1.4E-55	5.7E-53
C3ar1	5	0.03	9.3E-01	9.7E-01	0.87	5.3E-03	2.1E-02	1.34	3.0E-06	2.5E-05	1.15	2.3E-04	1.3E-03
Dag1		0.52	1.4E-13	4.2E-12	0.89	6.4E-36	1.6E-33	1.08	1.7E-51	6.0E-49	1.11	1.8E-54	6.7E-52
Fam131a	5	0.52	2.0E-02	6.5E-02	0.68	3.9E-04	2.3E-03	1.18	6.5E-10	1.2E-08	1.10	2.9E-09	5.0E-08
Figf	5	0.71	1.5E-04	9.7E-04	0.91	1.6E-06	1.8E-05	1.60	6.7E-18	3.3E-16	1.61	7.4E-20	4.7E-18
Galm	8	0.10	2.9E-01	5.2E-01	0.57	3.2E-10	7.2E-09	1.24	1.6E-45	4.4E-43	1.44	6.0E-63	3.2E-60
Il1rl1		0.04	7.4E-01	8.8E-01	0.93	2.8E-15	1.3E-13	1.25	3.5E-28	4.3E-26	1.54	9.4E-40	2.3E-37
Itpr2	8	0.39	3.1E-06	3.0E-05	0.81	8.0E-23	8.7E-21	1.14	1.0E-43	2.6E-41	1.15	2.9E-47	9.2E-45
Neurl1b	8	-0.14	5.4E-01	7.5E-01	0.92	6.7E-06	6.3E-05	1.20	1.4E-10	2.7E-09	1.22	8.2E-12	2.1E-10
Notum	7	0.04	9.1E-01	9.6E-01	0.65	2.8E-02	8.4E-02	1.16	4.3E-05	2.8E-04	1.13	3.0E-05	2.2E-04
Nqo1	8	-0.06	3.4E-01	5.7E-01	0.56	1.9E-21	1.8E-19	1.01	9.2E-71	7.5E-68	1.48	3.5E-144	6.4E-141
Pcx	8	0.19	3.1E-02	9.3E-02	0.71	1.4E-15	6.8E-14	1.01	5.6E-30	7.6E-28	1.01	3.9E-30	5.9E-28
Pdk2	8	0.06	7.2E-01	8.7E-01	0.56	2.0E-04	1.3E-03	1.11	6.9E-14	2.2E-12	1.04	5.5E-13	1.7E-11
Pla2g4f	7	-0.24	4.0E-01	6.3E-01	0.48	1.1E-01	2.5E-01	1.18	1.7E-05	1.2E-04	1.07	5.5E-05	3.7E-04
Ptges	8	0.06	8.7E-01	9.5E-01	0.77	1.9E-02	6.1E-02	1.16	8.6E-05	5.1E-04	1.21	3.5E-05	2.5E-04
Rbm44	7	0.51	1.5E-01	3.3E-01	0.95	7.3E-03	2.8E-02	1.63	6.7E-08	8.1E-07	1.36	4.0E-06	3.6E-05
Serinc2	8	0.51	1.2E-06	1.3E-05	0.88	4.1E-19	3.1E-17	1.57	2.3E-55	1.0E-52	1.61	5.4E-61	2.6E-58
Slc28a1	5	0.31	4.1E-01	6.4E-01	0.97	5.6E-03	2.2E-02	1.10	1.5E-03	6.3E-03	1.07	1.5E-03	6.7E-03
Slc5a3	5	-0.07	7.9E-01	9.1E-01	0.93	2.7E-05	2.1E-04	1.24	2.6E-10	4.9E-09	1.06	2.0E-07	2.4E-06
Slc6a13	8	0.06	6.4E-01	8.3E-01	0.50	5.8E-05	4.3E-04	1.10	7.1E-20	4.4E-18	1.21	8.6E-25	9.2E-23
Sqrdl	5	0.14	4.1E-02	1.2E-01	0.70	1.2E-24	1.5E-22	1.05	5.9E-54	2.5E-51	1.20	2.9E-69	1.9E-66
Synm		-0.53	3.0E-03	1.4E-02	0.90	7.4E-09	1.3E-07	1.69	1.1E-27	1.3E-25	1.48	8.0E-23	6.7E-21
Tom1	5	0.52	3.7E-05	2.8E-04	0.75	6.6E-10	1.4E-08	1.13	2.4E-20	1.6E-18	1.10	1.7E-20	1.2E-18
Uap1	5	0.60	4.4E-21	2.8E-19	0.78	2.5E-35	5.8E-33	1.07	5.4E-67	3.1E-64	1.26	9.5E-87	1.1E-83
Wdfy2	5	0.37	7.2E-04	3.9E-03	0.84	1.7E-18	1.2E-16	1.45	2.7E-52	1.0E-49	1.37	2.2E-47	7.0E-45
Wdr59	5	0.37	5.7E-04	3.1E-03	0.74	2.5E-12	7.9E-11	1.02	3.5E-24	3.2E-22	1.05	4.1E-25	4.6E-23

TABLE A.13: Results of gene expression analysis for 3 significantly upregulated genes 4 and 8 h after osmotic shift. log2(FC) $\geqslant$ 1, P and FDR $\leqslant$ 0.02, C = cluster (maSigPro)

	C	2 h log2(FC)	P-value	FDR	4 h log2(FC)	P-value	FDR	6 h log2(FC)	P-value	FDR	8 h log2(FC)	P-value	FDR
Col4a2	8	0.17	6.4E-01	8.3E-01	1.02	3.3E-03	1.4E-02	0.89	5.6E-03	2.0E-02	1.86	5.1E-11	1.2E-09
Nuak1		0.62	1.0E-03	5.4E-03	1.11	1.4E-07	1.9E-06	0.91	1.8E-06	1.6E-05	1.06	6.0E-08	7.9E-07
Tp53inp1		-0.27	4.6E-01	6.9E-01	1.31	3.9E-05	3.0E-04	0.91	2.3E-03	9.2E-03	1.02	1.1E-03	5.1E-03

TABLE A.14: Results of gene expression analysis for 10 significantly upregulated genes 4 and 6 h after osmotic shift. log2(FC) $\geqslant$ 1, P and FDR $\leqslant$ 0.02, C = cluster (maSigPro)

	C	2 h log2(FC)	P-value	FDR	4 h log2(FC)	P-value	FDR	6 h log2(FC)	P-value	FDR	8 h log2(FC)	P-value	FDR
Cornifin-A	5	0.18	6.5E-01	8.3E-01	1.09	1.9E-03	9.0E-03	1.16	5.3E-04	2.6E-03	0.79	1.6E-02	5.2E-02
LOC100752904		-0.50	1.2E-02	4.3E-02	1.40	1.7E-19	1.3E-17	1.59	1.3E-22	1.0E-20	0.95	2.4E-09	4.3E-08
LOC100763833	3	0.05	5.4E-01	7.6E-01	1.26	5.0E-45	1.8E-42	1.25	2.2E-44	5.6E-42	0.91	2.9E-24	2.9E-22
LOC100770289	2	0.95	3.2E-12	8.1E-11	1.03	1.2E-15	6.1E-14	1.17	6.8E-18	3.4E-16	0.75	5.5E-08	7.3E-07
Mylip	3	0.75	2.2E-03	1.0E-02	1.63	3.1E-15	1.4E-13	1.50	2.1E-12	5.6E-11	0.96	8.1E-06	6.7E-05
Ndst2		0.54	4.0E-11	9.0E-10	1.15	8.7E-51	3.4E-48	1.13	6.3E-48	1.8E-45	0.71	2.0E-20	1.4E-18
Rgma	3	0.53	7.4E-06	6.6E-05	1.13	8.6E-25	1.1E-22	1.09	1.0E-21	7.7E-20	0.63	2.6E-08	3.6E-07
Snx33	5	0.26	2.3E-02	7.2E-02	1.03	8.6E-22	8.3E-20	1.15	2.5E-28	3.1E-26	0.86	2.5E-16	1.2E-14
Trib3	3	0.62	4.0E-11	9.0E-10	1.10	7.5E-32	1.5E-29	1.05	1.0E-28	1.3E-26	0.85	1.2E-18	6.9E-17
Ttbk2	3	0.67	1.7E-04	1.1E-03	1.36	1.3E-15	6.4E-14	1.11	6.3E-11	1.3E-09	0.91	1.0E-07	1.3E-06

TABLE A.15: Results of gene expression analysis for 6 significantly upregulated genes 2 and 6 h after osmotic shift. log2(FC) $\geqslant$ 1, P and FDR $\leqslant$ 0.02, C = cluster (maSigPro)

	C	2 h log2(FC)	P-value	FDR	4 h log2(FC)	P-value	FDR	6 h log2(FC)	P-value	FDR	8 h log2(FC)	P-value	FDR
Fat4		1.04	1.0E-04	6.9E-04	0.98	1.3E-04	8.4E-04	1.20	6.3E-06	5.0E-05	0.88	2.9E-04	1.6E-03
Irf2bpl	4	1.47	8.2E-33	1.2E-30	0.83	5.9E-12	1.8E-10	1.08	1.0E-18	5.6E-17	0.61	3.7E-07	4.2E-06
LOC100773107	4	1.37	5.8E-13	1.6E-11	1.00	1.4E-06	1.5E-05	1.13	1.9E-07	2.1E-06	0.94	3.0E-05	2.2E-04
Nfkbiz	4	1.38	3.8E-19	2.1E-17	0.96	1.3E-10	3.2E-09	1.17	6.5E-14	2.1E-12	0.98	2.3E-09	4.1E-08
Nlgn3		1.09	6.0E-05	4.3E-04	0.76	6.6E-03	2.6E-02	1.04	8.2E-04	3.7E-03	-0.26	4.2E-01	6.5E-01
Znf608	4	1.77	3.9E-32	5.6E-30	0.96	1.5E-09	3.1E-08	1.21	1.4E-13	4.3E-12	0.86	2.7E-07	3.2E-06

TABLE A.16: Results of gene expression analysis for 39 significantly upregulated genes 8 h after osmotic shift. log2(FC) $\geqslant$ 1, P and FDR $\leqslant$ 0.02, C = cluster (maSigPro)

	C	2 h log2(FC)	P-value	FDR	4 h log2(FC)	P-value	FDR	6 h log2(FC)	P-value	FDR	8 h log2(FC)	P-value	FDR
Arhgef37	7	0.09	7.8E-01	9.0E-01	0.30	2.7E-01	4.8E-01	0.82	1.5E-03	6.2E-03	1.28	4.1E-07	4.6E-06
Arsk		-0.29	2.5E-01	4.6E-01	0.35	1.2E-01	2.7E-01	0.50	2.9E-02	7.9E-02	1.13	2.1E-06	2.0E-05
Calcoco1	7	0.05	7.6E-01	9.0E-01	0.35	2.4E-02	7.3E-02	0.92	3.6E-09	5.8E-08	1.05	8.8E-13	2.6E-11
Ccpg1	5	0.34	4.1E-03	1.8E-02	0.74	1.0E-10	2.5E-09	0.92	2.4E-17	1.2E-15	1.03	1.0E-20	7.2E-19
Cdc42ep2	5	0.46	2.5E-02	7.9E-02	0.65	1.1E-03	5.7E-03	0.99	1.1E-07	1.3E-06	1.10	1.7E-07	2.0E-06
Crem	5	0.37	6.3E-03	2.5E-02	0.79	3.8E-09	6.9E-08	0.90	8.0E-13	2.2E-11	1.05	3.8E-16	1.7E-14
Dcn	7	0.26	2.3E-01	4.3E-01	0.11	6.1E-01	7.9E-01	0.90	7.6E-06	5.9E-05	1.09	4.1E-08	5.6E-07
Ddx59	7	-0.28	2.6E-02	8.0E-02	0.19	1.2E-01	2.7E-01	0.81	1.5E-12	4.0E-11	1.15	4.6E-23	4.0E-21
Fam188b	8	-0.18	2.0E-01	4.0E-01	0.76	7.1E-09	1.2E-07	0.95	7.5E-18	3.7E-16	1.16	9.8E-24	9.4E-22
Fyco1	7	-0.34	7.2E-06	6.4E-05	0.16	2.6E-02	8.1E-02	0.90	5.8E-38	1.3E-35	1.04	1.7E-50	5.9E-48
Ggcx	5	0.23	1.2E-02	4.4E-02	0.62	6.5E-11	1.6E-09	0.83	1.3E-19	7.6E-18	1.15	1.2E-35	2.8E-33
Gprasp1	5	0.68	1.2E-12	3.3E-11	0.78	1.4E-17	9.2E-16	0.98	2.1E-30	3.0E-28	1.21	2.5E-40	6.2E-38
Heatr7b2	7	0.04	9.2E-01	9.7E-01	0.71	2.6E-02	7.9E-02	0.87	5.6E-03	2.0E-02	1.41	6.6E-06	5.6E-05
Hexim2	7	-0.90	1.1E-05	9.4E-05	0.29	9.5E-02	2.2E-01	0.71	2.4E-05	1.6E-04	1.17	5.9E-13	1.8E-11
Hr	7	-0.07	7.9E-01	9.1E-01	0.42	1.2E-01	2.7E-01	0.67	3.0E-03	1.1E-02	1.31	8.7E-09	1.4E-07
Ifi204	5	0.19	5.5E-01	7.6E-01	0.59	4.0E-02	1.1E-01	0.69	8.6E-03	2.9E-02	1.04	2.1E-04	1.2E-03
LOC100752032	7	-0.73	4.9E-03	2.0E-02	-0.31	2.4E-01	4.4E-01	0.56	9.0E-03	3.0E-02	1.17	5.1E-08	6.7E-07
LOC100756955		-0.67	1.7E-03	8.1E-03	0.58	7.4E-04	3.9E-03	0.84	6.3E-07	6.3E-06	1.19	1.0E-10	2.3E-09
LOC100757262		0.05	7.9E-01	9.1E-01	0.28	1.5E-01	3.2E-01	0.60	7.2E-04	3.4E-03	1.07	3.2E-08	4.4E-07
LOC100760218	5	0.67	6.2E-02	1.6E-01	0.78	3.2E-02	9.5E-02	0.95	2.2E-03	9.0E-03	1.08	7.8E-04	3.8E-03
LOC100761102	5	0.17	2.3E-01	4.3E-01	0.34	1.6E-02	5.5E-02	0.58	3.6E-05	2.4E-04	1.06	5.5E-13	1.7E-11
LOC100769997	8	0.38	6.5E-06	5.9E-05	0.63	5.2E-15	2.3E-13	0.92	2.0E-32	3.5E-30	1.31	6.6E-62	3.3E-59
Lysmd3	5	0.14	3.1E-01	5.3E-01	0.89	1.9E-10	4.5E-09	0.95	6.9E-12	1.6E-10	1.16	8.3E-16	3.7E-14
Mettl20	7	-0.38	1.4E-01	3.1E-01	0.22	3.8E-01	6.0E-01	0.75	4.3E-04	2.1E-03	1.19	1.2E-08	1.9E-07
Nadk2	8	0.22	1.3E-01	2.9E-01	0.59	1.4E-05	1.2E-04	0.99	4.3E-14	1.4E-12	1.20	2.9E-20	2.0E-18
Nudt6	7	-0.34	1.2E-01	2.7E-01	0.32	1.2E-01	2.7E-01	0.51	1.2E-02	3.7E-02	1.07	3.6E-07	4.1E-06
Nxpe3	7	-0.17	4.5E-01	6.9E-01	0.09	6.5E-01	8.2E-01	0.86	4.6E-06	3.8E-05	1.39	2.4E-12	6.9E-11
Pdgfra	8	-0.21	5.9E-02	1.6E-01	0.73	5.1E-12	1.6E-10	0.95	1.6E-19	9.3E-18	1.02	5.4E-22	4.3E-20
Prmt2	5	0.23	8.8E-02	2.1E-01	0.65	2.5E-07	3.1E-06	0.95	6.0E-15	2.2E-13	1.04	7.4E-17	3.6E-15
Rab7l1	7	-0.20	2.9E-01	5.2E-01	0.12	4.8E-01	6.9E-01	0.73	7.3E-06	5.7E-05	1.08	1.1E-11	2.7E-10
Rfx3	2	0.63	9.3E-03	3.5E-02	0.70	6.5E-03	2.6E-02	0.64	8.7E-03	2.9E-02	1.17	2.0E-06	2.0E-05
Rgl1	7	-0.43	8.0E-04	4.2E-03	0.02	8.8E-01	9.4E-01	0.86	1.4E-15	5.4E-14	1.04	1.7E-21	1.3E-19
Sept4	7	-0.35	5.2E-02	1.4E-01	0.16	3.4E-01	5.6E-01	0.56	1.1E-03	4.7E-03	1.03	3.2E-10	6.4E-09
Srd5a1	5	0.24	2.4E-01	4.5E-01	0.65	6.9E-04	3.7E-03	0.90	1.6E-06	1.4E-05	1.08	2.1E-08	3.0E-07
Srpx2	8	0.16	1.3E-01	2.9E-01	0.46	7.4E-06	6.9E-05	0.99	6.1E-23	5.1E-21	1.18	2.1E-31	3.6E-29
Stxbp4	7	-0.08	7.0E-01	8.6E-01	0.38	4.7E-02	1.3E-01	0.71	6.0E-05	3.7E-04	1.18	6.5E-11	1.5E-09
Sucnr1	7	-0.45	1.3E-01	2.8E-01	0.24	3.5E-01	5.7E-01	0.86	6.2E-04	2.9E-03	1.02	3.5E-05	2.5E-04
Tlr3	7	0.03	8.5E-01	9.4E-01	0.57	1.6E-03	7.7E-03	0.58	5.7E-04	2.7E-03	1.04	8.6E-10	1.6E-08
Zcwpw2		-0.39	1.9E-01	3.8E-01	0.55	5.0E-02	1.4E-01	0.46	8.0E-02	1.8E-01	1.11	7.2E-05	4.7E-04

TABLE A.17: Results of gene expression analysis for 23 significantly upregulated genes 4 h after osmotic shift. log2(FC) ⩾ 1, P and FDR ⩽ 0.02, C = cluster (maSigPro)

	C	2 h			4 h			6 h			8 h		
		log2(FC)	P-value	FDR	log2(FC)	P-value	FDR	log2(FC)	P-value	FDR	log2(FC)	P-value	FDR
Akap17a		0.11	6.7E-01	8.5E-01	1.08	1.1E-05	1.0E-04	0.79	9.1E-04	4.1E-03	0.65	6.3E-03	2.3E-02
Btg2	3	0.10	7.0E-01	8.6E-01	1.07	1.1E-05	9.8E-05	0.87	1.7E-04	9.3E-04	0.73	4.8E-03	1.8E-02
Ccdc69	3	0.23	4.9E-01	7.2E-01	1.11	5.8E-04	3.2E-03	0.86	4.5E-03	1.6E-02	0.66	4.3E-02	1.1E-01
Ccng2	3	-0.07	6.5E-01	8.4E-01	1.09	5.0E-16	2.7E-14	0.87	1.9E-11	4.2E-10	0.98	5.5E-12	1.5E-10
Cln8	3	0.36	6.7E-02	1.7E-01	1.01	2.1E-08	3.4E-07	0.88	3.7E-07	3.9E-06	0.67	2.7E-04	1.5E-03
Dzank1	3	0.84	6.6E-04	3.6E-03	1.03	5.3E-06	5.1E-05	0.94	8.6E-05	5.1E-04	0.68	3.7E-03	1.5E-02
Hsp110	2	0.92	7.0E-75	6.3E-72	1.03	1.6E-93	2.4E-90	0.98	2.6E-86	2.7E-83	0.90	1.2E-71	8.7E-69
Kiaa1522	6	0.91	9.2E-20	5.6E-18	1.04	1.7E-25	2.3E-23	0.66	4.2E-11	8.8E-10	0.40	6.3E-05	4.2E-04
LOC100754104		0.44	1.8E-01	3.7E-01	1.10	1.1E-03	5.3E-03	0.40	2.5E-01	4.5E-01	0.38	2.4E-01	4.4E-01
LOC100758641	9	0.40	1.3E-02	4.5E-02	1.19	3.2E-17	2.0E-15	0.67	4.6E-06	3.8E-05	0.12	4.6E-01	6.9E-01
LOC100760433	3	0.39	2.6E-02	8.0E-02	1.12	8.0E-13	2.7E-11	0.92	6.8E-09	1.0E-07	0.62	7.5E-05	4.8E-04
LOC100762312		0.05	8.1E-01	9.2E-01	1.10	1.8E-10	4.3E-09	0.59	8.7E-05	5.2E-04	0.68	4.9E-05	3.3E-04
LOC100764334	3	0.62	6.1E-06	5.6E-05	1.00	6.1E-15	2.7E-13	0.98	1.0E-14	3.6E-13	0.94	5.4E-13	1.7E-11
LOC100772170	6	0.60	2.2E-02	7.1E-02	1.23	3.9E-06	3.9E-05	0.95	9.3E-04	4.2E-03	0.19	4.8E-01	7.1E-01
Muc5b		0.84	1.3E-03	6.3E-03	1.27	1.2E-07	1.6E-06	0.80	1.1E-02	3.5E-02	0.40	1.4E-01	2.8E-01
Myo3b	9	0.51	1.8E-01	3.6E-01	1.21	3.3E-04	2.0E-03	0.56	1.4E-01	2.8E-01	0.34	3.8E-01	6.0E-01
Nfat5	6	1.00	1.1E-09	1.9E-08	1.06	8.9E-11	2.2E-09	0.88	6.6E-08	8.0E-07	0.74	4.6E-06	4.1E-05
Nxpe4	9	0.33	4.9E-02	1.3E-01	1.53	1.5E-23	1.7E-21	0.81	6.5E-07	6.5E-06	0.46	1.8E-02	5.5E-02
Pdzd2		0.93	1.4E-03	6.8E-03	1.10	3.1E-04	1.9E-03	-0.01	9.7E-01	9.9E-01	0.34	2.6E-01	4.6E-01
Pkd2	5	0.65	1.9E-03	8.8E-03	1.08	9.9E-08	1.4E-06	0.97	4.7E-07	4.8E-06	0.77	9.2E-05	5.8E-04
Slc40a1	3	-0.07	5.4E-01	7.5E-01	1.08	2.7E-22	2.8E-20	0.85	6.2E-15	2.3E-13	0.89	1.2E-15	5.2E-14
Usp53	6	0.64	3.6E-04	2.1E-03	1.06	6.8E-09	1.2E-07	0.75	3.0E-05	2.0E-04	0.36	6.3E-02	1.5E-01
Zscan2		0.13	6.5E-01	8.4E-01	1.02	4.3E-05	3.3E-04	0.80	1.8E-03	7.3E-03	0.76	4.9E-03	1.9E-02

TABLE A.18: Results of gene expression analysis for 33 significantly significantly upregulated genes 6 h after osmotic shift. log2(FC) ⩾ 1, P and FDR ⩽ 0.02, C = cluster (maSigPro)

	C	2 h			4 h			6 h			8 h		
		log2(FC)	P-value	FDR	log2(FC)	P-value	FDR	log2(FC)	P-value	FDR	log2(FC)	P-value	FDR
Adat3		0.10	5.7E-01	7.8E-01	0.80	7.1E-07	8.3E-06	1.31	5.5E-15	2.1E-13	0.55	6.9E-04	3.4E-03
Bcl2l11	5	0.53	6.0E-02	1.6E-01	0.86	8.4E-04	4.4E-03	1.13	1.9E-05	1.4E-04	0.83	1.2E-03	5.6E-03
Ccdc101	3	0.18	2.1E-01	4.0E-01	0.61	5.4E-06	5.2E-05	1.06	2.0E-16	8.8E-15	0.55	6.4E-05	4.2E-04
Dlgap1		0.57	8.3E-02	2.0E-01	0.63	3.6E-02	1.0E-01	1.06	6.9E-05	4.2E-04	0.61	3.1E-02	8.8E-02
Dock6		-0.33	2.6E-01	4.8E-01	0.04	8.6E-01	9.3E-01	1.06	1.9E-05	1.3E-04	0.96	1.4E-04	8.3E-04
Dtx3	5	0.48	1.5E-04	1.0E-03	0.99	9.6E-16	5.0E-14	1.31	1.8E-26	2.0E-24	0.95	1.2E-15	5.3E-14
Elf3		0.05	8.7E-01	9.5E-01	0.54	8.8E-02	2.1E-01	1.28	3.1E-05	2.0E-04	0.49	1.1E-01	2.4E-01
Flg2		-0.76	8.6E-03	3.2E-02	0.92	1.7E-04	1.1E-03	1.17	1.0E-05	7.8E-05	0.91	7.5E-04	3.7E-03
Fosl2		-0.33	5.4E-02	1.5E-01	0.79	6.9E-07	8.0E-06	1.08	4.9E-12	1.2E-10	0.90	3.7E-09	6.3E-08
Foxn3	5	0.08	5.3E-01	7.5E-01	0.37	1.8E-03	8.4E-03	1.07	4.2E-19	2.4E-17	0.56	6.9E-07	7.4E-06
Gfod2	3	0.28	3.3E-02	9.7E-02	0.76	4.4E-09	7.8E-08	1.24	3.7E-19	2.1E-17	0.84	3.5E-10	7.1E-09
Ino80d		0.48	3.3E-02	9.8E-02	0.85	1.6E-04	1.0E-03	1.04	5.3E-06	4.3E-05	0.79	3.7E-04	2.0E-03
Jade2	5	0.50	1.8E-04	1.1E-03	0.87	2.7E-11	7.4E-10	1.32	1.6E-24	1.5E-22	0.82	4.8E-11	1.1E-09
Kctd14	3	0.34	3.5E-02	1.0E-01	0.96	1.1E-12	3.6E-11	1.00	1.9E-13	5.8E-12	0.98	1.2E-11	3.1E-10
LOC100750374		-0.17	5.2E-01	7.4E-01	0.62	2.1E-02	6.7E-02	1.06	5.6E-05	3.5E-04	0.65	6.3E-03	2.3E-02
LOC100755533	2	0.70	2.1E-07	2.5E-06	0.92	3.0E-12	9.5E-11	1.01	5.0E-15	1.9E-13	0.88	5.7E-11	1.3E-09
LOC100756910		-0.01	9.7E-01	9.9E-01	0.40	2.1E-01	4.0E-01	1.05	1.3E-03	5.5E-03	0.58	4.5E-02	1.2E-01
LOC100769566		0.38	2.5E-01	4.6E-01	0.79	2.9E-03	1.3E-02	1.24	5.6E-06	4.4E-05	0.80	2.7E-03	1.1E-02
Maob	5	0.21	3.4E-01	5.8E-01	0.48	2.4E-02	7.5E-02	1.04	4.1E-07	4.3E-06	0.93	6.7E-06	5.7E-05
Mtus1	5	-0.19	4.8E-01	7.1E-01	0.66	7.5E-03	2.9E-02	1.02	1.7E-05	1.2E-04	0.83	4.6E-04	2.4E-03
Pcnxl4	5	-0.13	3.8E-01	6.2E-01	0.52	2.0E-04	1.3E-03	1.02	1.8E-14	6.3E-13	0.77	9.1E-09	1.4E-07
Pgap1		-0.12	5.5E-01	7.6E-01	0.63	3.0E-04	1.8E-03	1.13	8.2E-10	1.4E-08	0.86	3.7E-06	3.3E-05
Prdm10	5	0.58	2.8E-05	2.2E-04	0.91	4.5E-12	1.4E-10	1.27	3.0E-22	2.4E-20	0.88	5.0E-12	1.4E-10
Rbm14	8	-0.19	2.0E-02	6.5E-02	0.63	1.5E-16	8.8E-15	1.18	6.6E-55	2.8E-52	0.92	9.8E-35	2.1E-32
Rfx1	3	0.38	1.9E-04	1.2E-03	0.92	4.4E-21	3.8E-19	1.18	4.9E-33	8.7E-31	0.83	7.1E-18	3.8E-16
Rhob	8	-0.29	1.2E-01	2.7E-01	0.52	2.6E-03	1.1E-02	1.13	7.9E-12	1.8E-10	0.79	9.9E-07	1.0E-05
Rras2	8	-0.16	3.8E-02	1.1E-01	0.57	1.6E-15	8.1E-14	1.08	1.5E-55	6.6E-53	0.99	5.6E-47	1.7E-44
Slc25a45	5	-0.01	9.7E-01	9.9E-01	0.44	4.9E-02	1.3E-01	1.07	1.1E-06	1.0E-05	0.96	1.1E-05	8.7E-05
Ssh1	3	0.11	3.6E-01	5.9E-01	0.81	3.4E-13	1.3E-11	1.08	1.9E-23	1.6E-21	0.60	2.2E-08	3.2E-07
Tmem104		-0.59	2.2E-04	1.4E-03	0.83	7.7E-09	1.3E-07	1.23	2.5E-17	1.2E-15	0.74	7.9E-08	1.0E-06
Tnrc6b	8	0.14	1.4E-01	3.0E-01	0.65	2.3E-12	7.5E-11	1.14	7.3E-35	1.4E-32	0.99	1.3E-27	1.7E-25
Zbtb5		-0.30	2.0E-01	3.9E-01	0.37	7.1E-02	1.8E-01	1.10	2.7E-07	2.9E-06	0.52	1.7E-02	5.3E-02
Zfp710	2	0.65	5.4E-06	5.0E-05	0.66	2.8E-06	2.9E-05	1.04	8.3E-14	2.6E-12	0.77	1.6E-08	2.4E-07

TABLE A.19: Results of gene expression analysis for 218 significantly upregulated genes 2 h after osmotic shift. log2(FC) ⩾ 1, P and FDR ⩽ 0.02, C = cluster (maSigPro)

	C	2 h log2(FC)	P-value	FDR	4 h log2(FC)	P-value	FDR	6 h log2(FC)	P-value	FDR	8 h log2(FC)	P-value	FDR
Acsbg1	1	1.03	2.9E-03	1.3E-02	0.93	9.9E-03	3.6E-02	0.39	3.0E-01	5.1E-01	-0.09	8.1E-01	9.3E-01
Acta1		1.84	2.2E-15	8.0E-14	0.94	1.4E-04	9.1E-04	0.68	1.4E-02	4.2E-02	0.06	8.4E-01	9.5E-01
Adora2a		1.30	5.6E-06	5.1E-05	0.53	1.2E-01	2.6E-01	-0.27	4.5E-01	6.7E-01	0.03	9.4E-01	9.8E-01
Ahdc1		2.12	1.2E-70	8.3E-68	0.26	3.8E-02	1.1E-01	-0.02	9.0E-01	9.7E-01	0.13	3.0E-01	5.2E-01
Amhr2		1.15	3.9E-06	3.7E-05	0.89	1.1E-03	5.4E-03	0.17	5.6E-01	7.7E-01	0.03	9.3E-01	9.8E-01
Ankrd13d		1.61	4.2E-12	1.1E-10	-0.20	4.5E-01	6.7E-01	-0.81	1.0E-02	3.3E-02	-0.36	2.4E-01	4.4E-01
Ano7		1.91	1.6E-10	3.3E-09	0.84	1.4E-02	4.8E-02	0.36	3.5E-01	5.7E-01	0.12	7.6E-01	9.1E-01
Anxa9	6	1.13	4.1E-04	2.4E-03	0.83	8.9E-03	3.3E-02	0.65	5.7E-02	1.4E-01	0.18	6.0E-01	8.1E-01
Aoc2		1.23	2.5E-09	4.2E-08	0.26	3.1E-01	5.3E-01	0.03	9.3E-01	9.7E-01	-0.31	2.5E-01	4.6E-01
Arhgap4		1.36	3.5E-05	2.7E-04	0.83	1.3E-02	4.6E-02	0.15	6.9E-01	8.6E-01	-0.21	5.7E-01	7.9E-01
Asah2		1.86	1.8E-09	3.1E-08	0.97	5.6E-03	2.2E-02	0.84	1.7E-02	5.2E-02	0.26	4.8E-01	7.1E-01
Aspn		1.01	2.8E-03	1.3E-02	0.56	1.2E-01	2.7E-01	0.06	8.8E-01	9.6E-01	0.18	6.3E-01	8.3E-01
Atp2a1	4	1.15	1.4E-08	2.1E-07	0.73	8.0E-04	4.2E-03	0.78	3.7E-04	1.9E-03	0.15	5.2E-01	7.5E-01
Atp6v0a4		1.10	9.6E-04	5.0E-03	0.67	5.1E-02	1.4E-01	0.22	5.7E-01	7.8E-01	0.31	4.3E-01	6.6E-01
Avil		1.23	1.3E-04	8.6E-04	0.39	3.0E-01	5.1E-01	-0.20	6.1E-01	8.1E-01	0.17	6.5E-01	8.4E-01
B3gnt2		1.33	1.7E-71	1.3E-68	0.55	1.5E-12	4.9E-11	0.44	1.9E-08	2.7E-07	0.16	3.7E-02	1.0E-01
Baat		1.18	3.9E-08	5.5E-07	0.94	3.9E-05	3.0E-04	0.56	2.3E-02	6.6E-02	0.15	5.5E-01	7.7E-01
Bag3		1.14	5.9E-29	7.3E-27	0.34	8.0E-04	4.2E-03	0.42	3.7E-05	2.4E-04	0.35	5.5E-04	2.8E-03
Bcl9l		1.27	6.7E-33	1.0E-30	0.43	3.3E-05	2.6E-04	0.57	4.6E-08	5.9E-07	0.38	2.0E-04	1.2E-03
Cacna1b		1.37	2.0E-05	1.6E-04	0.52	1.7E-01	3.5E-01	-0.05	9.0E-01	9.6E-01	-0.01	9.8E-01	9.9E-01
Casc1		1.19	8.8E-17	3.7E-15	0.29	6.5E-02	1.7E-01	-0.01	9.6E-01	9.9E-01	0.08	6.2E-01	8.3E-01
Ccdc11		1.01	2.8E-03	1.3E-02	0.25	4.9E-01	7.1E-01	-0.17	6.6E-01	8.4E-01	-0.12	7.6E-01	9.1E-01
Ccdc120		1.04	2.8E-09	4.7E-08	0.58	7.5E-04	4.0E-03	0.53	2.8E-03	1.1E-02	0.27	1.2E-01	2.7E-01
Ccdc141		1.52	3.4E-06	3.3E-05	0.97	5.6E-03	2.2E-02	0.27	4.9E-01	7.1E-01	0.23	5.6E-01	7.8E-01
Ccdc154		1.56	1.2E-09	2.2E-08	0.29	3.6E-01	5.8E-01	-0.30	3.7E-01	5.9E-01	-0.40	2.6E-01	4.7E-01
Ccdc27		1.19	5.3E-04	3.0E-03	0.62	9.6E-02	2.3E-01	0.28	4.6E-01	6.9E-01	0.06	8.8E-01	9.6E-01
Ccdc28b		1.94	2.6E-18	1.3E-16	0.63	9.1E-03	3.4E-02	-0.11	6.9E-01	8.7E-01	-0.09	7.3E-01	8.9E-01
Ccdc62		1.01	3.8E-03	1.6E-02	0.28	4.6E-01	6.8E-01	-0.09	8.1E-01	9.3E-01	-0.05	8.9E-01	9.6E-01
Cdk5r1		1.05	5.4E-04	3.0E-03	-0.14	6.6E-01	8.2E-01	0.05	8.9E-01	9.6E-01	0.09	8.0E-01	9.3E-01
Celsr3		1.60	5.9E-12	1.5E-10	0.73	7.3E-03	2.8E-02	0.17	5.8E-01	7.9E-01	0.26	4.1E-01	6.4E-01
Cemip		1.13	7.2E-04	3.9E-03	0.41	2.7E-01	4.8E-01	0.19	6.3E-01	8.2E-01	-0.12	7.6E-01	9.1E-01
Chrm4		1.59	2.7E-07	3.2E-06	0.65	7.8E-02	1.9E-01	0.36	3.3E-01	5.5E-01	-0.29	4.2E-01	6.5E-01
Cntf		1.14	2.0E-05	1.6E-04	0.36	2.4E-01	4.4E-01	0.17	5.8E-01	7.9E-01	-0.11	7.5E-01	9.0E-01
Col6a2		1.59	8.5E-07	9.3E-06	0.91	1.3E-02	4.5E-02	0.08	8.4E-01	9.5E-01	-0.07	8.5E-01	9.5E-01
Col9a3		1.03	1.2E-03	6.1E-03	0.73	3.3E-02	9.8E-02	0.33	3.7E-01	5.9E-01	0.06	8.7E-01	9.6E-01
Colec11		1.15	7.2E-04	3.9E-03	0.55	1.5E-01	3.2E-01	0.18	6.4E-01	8.3E-01	-0.01	9.8E-01	9.9E-01
Crtam		1.79	4.6E-09	7.4E-08	0.84	2.0E-02	6.5E-02	0.15	7.1E-01	8.8E-01	0.10	7.9E-01	9.3E-01
Ctsk		1.39	8.0E-23	5.9E-21	0.88	4.5E-08	6.6E-07	0.71	5.7E-05	3.6E-04	0.66	1.7E-04	9.9E-04
Cul9		1.27	1.0E-05	8.8E-05	0.68	5.9E-02	1.5E-01	0.03	9.3E-01	9.7E-01	-0.47	1.9E-01	3.7E-01
Ddx3x		1.01	2.8E-56	1.1E-53	0.59	2.0E-20	1.6E-18	0.14	2.4E-02	6.9E-02	0.15	1.5E-02	4.8E-02
Dido1		1.03	3.2E-58	1.4E-55	0.15	2.5E-02	7.7E-02	0.05	4.9E-01	7.1E-01	0.09	1.6E-01	3.2E-01
Dmkn		1.06	2.2E-03	1.0E-02	0.44	2.5E-01	4.5E-01	-0.09	8.1E-01	9.3E-01	0.10	7.9E-01	9.3E-01
Dnah7		1.89	8.5E-10	1.5E-08	0.84	2.0E-02	6.5E-02	0.35	3.7E-01	5.9E-01	0.05	8.9E-01	9.6E-01
Dnai2		1.11	5.5E-04	3.0E-03	0.37	3.0E-01	5.1E-01	-0.04	9.1E-01	9.7E-01	0.17	6.2E-01	8.2E-01
Dok3		1.38	6.7E-10	1.2E-08	0.40	1.8E-01	3.6E-01	-0.30	3.4E-01	5.5E-01	-0.21	5.0E-01	7.3E-01
Drp2		1.42	7.6E-06	6.8E-05	0.45	2.3E-01	4.3E-01	0.25	5.0E-01	7.2E-01	-0.03	9.4E-01	9.8E-01
Dtx2	4	1.18	5.7E-20	3.5E-18	0.88	2.1E-11	5.7E-10	0.78	1.5E-08	2.1E-07	0.48	4.6E-04	2.4E-03
Duox1		1.72	1.1E-08	1.7E-07	0.73	3.5E-02	1.0E-01	0.59	1.1E-01	2.3E-01	0.15	7.1E-01	8.8E-01
Duoxa2	1	1.10	9.6E-04	5.0E-03	0.95	7.3E-03	2.8E-02	0.59	1.1E-01	2.3E-01	-0.03	9.4E-01	9.8E-01
Dusp16		1.10	6.4E-37	1.2E-34	0.33	1.8E-04	1.2E-03	-0.03	7.4E-01	8.9E-01	0.21	2.2E-02	6.5E-02
Dusp8		1.00	2.2E-04	1.4E-03	0.91	4.5E-03	1.9E-02	0.23	4.5E-01	6.7E-01	0.67	3.5E-02	9.8E-02
Ecm1		1.37	5.3E-18	2.6E-16	0.39	2.7E-02	8.3E-02	-0.01	9.8E-01	9.9E-01	-0.25	1.7E-01	3.3E-01
Ecm2		1.14	1.2E-05	9.9E-05	0.50	1.0E-01	2.4E-01	0.19	5.5E-01	7.7E-01	0.24	5.0E-01	7.2E-01
Elf1		1.41	5.8E-49	1.8E-46	0.46	8.6E-06	7.9E-05	0.45	9.9E-06	7.4E-05	0.36	5.5E-04	2.8E-03
Esrp2		1.00	2.1E-03	9.8E-03	0.56	1.1E-01	2.4E-01	0.23	5.4E-01	7.6E-01	0.24	5.2E-01	7.4E-01
Fam184b		1.52	3.4E-06	3.3E-05	0.85	2.1E-02	6.7E-02	0.19	6.1E-01	8.1E-01	0.23	5.6E-01	7.8E-01
Fgfr2		1.28	1.9E-06	2.0E-05	0.52	9.1E-02	2.2E-01	0.68	2.2E-02	6.4E-02	0.42	1.5E-01	3.0E-01
Fndc7		1.23	8.2E-06	7.2E-05	0.41	1.8E-01	3.6E-01	0.29	3.3E-01	5.5E-01	0.06	8.6E-01	9.5E-01
Foxp4	6	1.06	3.9E-19	2.1E-17	0.88	5.3E-14	2.1E-12	0.69	8.2E-09	1.2E-07	0.29	1.4E-02	4.7E-02
Foxred2		1.22	7.5E-05	5.3E-04	0.49	1.9E-01	3.8E-01	0.06	8.8E-01	9.6E-01	0.13	7.3E-01	8.9E-01
Ftcd		1.15	9.5E-04	4.9E-03	0.79	3.4E-02	1.0E-01	0.23	5.6E-01	7.7E-01	0.06	8.8E-01	9.6E-01
Fzd9		1.06	2.2E-03	1.0E-02	0.62	9.6E-02	2.3E-01	0.23	5.6E-01	7.7E-01	-0.12	7.6E-01	9.1E-01
Gdpd1		1.02	3.9E-04	2.3E-03	0.36	3.2E-01	5.4E-01	-0.33	3.7E-01	5.9E-01	-0.03	9.3E-01	9.8E-01
Gem		1.36	2.5E-13	7.3E-12	0.73	1.7E-04	1.1E-03	0.89	2.9E-06	2.5E-05	0.90	1.3E-05	1.0E-04
Gnat2		1.57	2.2E-08	3.2E-07	0.30	3.7E-01	5.9E-01	-0.34	3.5E-01	5.7E-01	-0.19	5.9E-01	8.1E-01
Gnrh1		1.01	1.6E-03	7.7E-03	0.40	2.9E-01	5.1E-01	0.09	8.1E-01	9.3E-01	0.24	5.4E-01	7.6E-01
Gpr97		1.30	9.0E-05	6.2E-04	0.55	1.4E-01	3.0E-01	0.04	9.3E-01	9.7E-01	-0.12	7.6E-01	9.1E-01
Grin2c		1.29	7.5E-06	6.7E-05	0.42	1.9E-01	3.8E-01	0.34	3.4E-01	5.5E-01	-0.03	9.3E-01	9.8E-01
Hal		1.72	2.8E-08	4.1E-07	0.52	1.7E-01	3.5E-01	0.08	8.4E-01	9.4E-01	0.06	8.8E-01	9.6E-01
Hic1		1.06	1.2E-11	3.0E-10	0.06	6.8E-01	8.4E-01	0.72	2.7E-06	2.4E-05	0.33	2.7E-02	7.8E-02
Hic2		1.02	1.4E-14	4.8E-13	0.12	3.7E-01	5.9E-01	0.49	3.3E-04	1.7E-03	0.17	2.2E-01	4.2E-01
Hk3		1.14	1.4E-04	9.0E-04	0.42	1.8E-01	3.6E-01	0.23	5.1E-01	7.3E-01	0.13	7.0E-01	8.8E-01
Hnf1a		1.05	5.4E-04	3.0E-03	0.45	1.5E-01	3.2E-01	-0.12	7.0E-01	8.7E-01	0.02	9.4E-01	9.8E-01
Hoxd3		1.07	1.3E-04	8.9E-04	-0.09	7.9E-01	9.0E-01	-0.35	2.9E-01	5.0E-01	-0.27	4.3E-01	6.6E-01
Icam2		1.29	6.9E-05	4.9E-04	0.82	2.7E-02	8.2E-02	-0.05	9.0E-01	9.6E-01	-0.09	8.1E-01	9.3E-01
Id1	1	1.20	5.4E-12	1.3E-10	0.85	3.4E-06	3.4E-05	0.53	5.4E-03	1.9E-02	0.01	9.7E-01	9.9E-01
Iqub		1.06	1.7E-03	8.0E-03	0.51	1.9E-01	3.7E-01	0.16	6.7E-01	8.6E-01	0.10	7.9E-01	9.3E-01
Itga10		1.33	2.2E-08	3.2E-07	0.30	2.7E-01	4.8E-01	0.10	7.6E-01	9.0E-01	-0.47	1.1E-01	2.4E-01
Itgae		1.05	5.4E-04	3.0E-03	0.52	1.5E-01	3.1E-01	0.43	2.1E-01	3.9E-01	0.30	3.5E-01	5.7E-01
Itgb1bp2		1.02	9.1E-04	4.7E-03	0.40	2.5E-01	4.6E-01	0.11	7.4E-01	8.9E-01	-0.15	6.9E-01	8.7E-01
Itih4		1.59	2.7E-07	3.2E-06	0.38	3.2E-01	5.4E-01	-0.03	9.4E-01	9.8E-01	0.19	6.3E-01	8.3E-01
Jmjd6		1.15	1.3E-26	1.4E-24	0.41	1.2E-04	8.4E-04	-0.13	2.8E-01	4.8E-01	-0.30	1.0E-02	3.4E-02
Kcnk5		1.43	1.8E-60	8.4E-58	0.52	8.9E-08	1.2E-06	0.69	3.1E-12	7.6E-11	0.40	8.6E-05	5.5E-04
Kif27		1.02	5.6E-05	4.0E-04	0.74	5.2E-03	2.1E-02	-0.14	6.3E-01	8.3E-01	-0.31	3.1E-01	5.2E-01

228

TABLE A.19 (continued)

	C	2 h log2(FC)	P-value	FDR	4 h log2(FC)	P-value	FDR	6 h log2(FC)	P-value	FDR	8 h log2(FC)	P-value	FDR
Kmt2d		1.13	1.4E-21	9.4E-20	0.85	5.7E-13	2.0E-11	0.80	9.8E-12	2.2E-10	0.53	5.1E-06	4.4E-05
Kremen2		1.13	6.0E-05	4.3E-04	0.03	9.3E-01	9.7E-01	-0.02	9.5E-01	9.9E-01	-0.73	2.8E-02	8.2E-02
L1cam		1.30	9.0E-05	6.2E-04	0.82	2.7E-02	8.2E-02	0.31	4.2E-01	6.5E-01	0.12	7.6E-01	9.1E-01
L3mbtl1		1.85	6.1E-18	3.0E-16	0.86	1.7E-03	8.1E-03	0.59	8.0E-02	1.8E-01	-0.25	4.3E-01	6.6E-01
Lct		1.39	3.4E-05	2.6E-04	0.30	4.3E-01	6.5E-01	-0.07	8.5E-01	9.5E-01	0.10	7.9E-01	9.3E-01
Lmod2		1.19	3.1E-04	1.8E-03	0.91	6.4E-03	2.5E-02	0.39	2.8E-01	4.8E-01	0.10	7.9E-01	9.3E-01
LOC100751390		2.20	1.1E-39	2.2E-37	0.64	7.3E-04	3.9E-03	0.48	4.0E-02	1.0E-01	-0.22	3.4E-01	5.6E-01
LOC100751452		1.19	3.1E-04	1.8E-03	0.78	3.2E-02	9.5E-02	0.49	1.8E-01	3.5E-01	-0.20	6.1E-01	8.1E-01
LOC100752122		1.19	2.3E-04	1.4E-03	0.39	3.0E-01	5.1E-01	-0.26	4.7E-01	7.0E-01	-0.05	8.9E-01	9.6E-01
LOC100756748		1.19	4.0E-04	2.3E-03	0.89	8.6E-03	3.2E-02	0.33	3.5E-01	5.7E-01	0.14	7.0E-01	8.7E-01
LOC100756763		1.01	8.0E-06	7.1E-05	0.31	2.2E-01	4.1E-01	0.33	2.2E-01	4.1E-01	-0.42	1.1E-01	2.4E-01
LOC100757378		1.21	4.9E-22	3.4E-20	0.68	4.0E-07	4.9E-06	0.95	5.3E-13	1.5E-11	0.68	1.4E-07	1.7E-06
LOC100760294		1.24	4.7E-06	4.4E-05	0.28	3.9E-01	6.1E-01	-0.24	4.6E-01	6.9E-01	-0.37	2.7E-01	4.8E-01
LOC100761806		1.07	7.2E-04	3.8E-03	0.49	1.6E-01	3.4E-01	0.25	5.0E-01	7.2E-01	-0.09	8.1E-01	9.3E-01
LOC100762686		1.50	2.0E-07	2.5E-06	0.46	1.5E-01	3.1E-01	0.32	3.4E-01	5.5E-01	0.04	9.1E-01	9.7E-01
LOC100762980		1.04	1.0E-04	6.9E-04	0.73	1.1E-02	3.9E-02	0.86	4.5E-03	1.6E-02	0.69	1.6E-02	5.0E-02
LOC100763618		1.15	2.4E-04	1.5E-03	0.18	6.3E-01	8.0E-01	0.29	4.4E-01	6.6E-01	-0.01	9.7E-01	9.9E-01
LOC100764246		1.16	2.3E-08	3.4E-07	-0.27	3.5E-01	5.7E-01	-0.51	8.8E-02	2.0E-01	-0.42	1.8E-01	3.5E-01
LOC100765133		1.20	4.5E-36	8.1E-34	0.27	6.0E-03	2.4E-02	0.31	2.0E-03	8.0E-03	-0.02	8.2E-01	9.4E-01
LOC100766009		1.19	1.8E-04	1.1E-03	0.51	1.3E-01	2.9E-01	0.10	7.8E-01	9.1E-01	0.11	7.6E-01	9.1E-01
LOC100768297		1.54	1.3E-06	1.4E-05	0.38	3.2E-01	5.4E-01	0.10	8.0E-01	9.2E-01	-0.35	3.7E-01	6.0E-01
LOC100768757	6	1.04	4.0E-04	2.3E-03	0.99	8.7E-04	4.5E-03	0.88	4.5E-03	1.6E-02	0.55	6.5E-02	1.6E-01
LOC100769139		1.12	1.3E-03	6.3E-03	0.59	1.2E-01	2.6E-01	0.23	5.6E-01	7.7E-01	0.15	7.1E-01	8.8E-01
LOC100769633		1.42	7.6E-06	6.8E-05	0.76	2.8E-02	8.6E-02	0.05	8.9E-01	9.6E-01	0.31	4.3E-01	6.6E-01
LOC100770786		1.30	1.2E-04	7.9E-04	0.45	2.3E-01	4.3E-01	0.20	5.8E-01	7.9E-01	0.08	8.4E-01	9.5E-01
LOC100770921		1.28	5.3E-05	3.9E-04	0.41	2.7E-01	4.8E-01	-0.14	7.3E-01	8.8E-01	0.04	9.3E-01	9.8E-01
LOC100771947		1.01	5.1E-04	2.9E-03	0.50	8.8E-02	2.1E-01	-0.02	9.4E-01	9.8E-01	0.45	1.5E-01	3.1E-01
LOC100771996		1.08	1.3E-03	6.3E-03	0.62	1.0E-01	2.4E-01	0.23	5.6E-01	7.7E-01	0.22	5.6E-01	7.8E-01
LOC100772948		1.06	3.9E-06	3.7E-05	0.49	3.3E-02	9.6E-02	-0.03	9.1E-01	9.7E-01	0.31	2.6E-01	4.6E-01
LOC100774252		1.48	9.0E-07	9.8E-06	0.97	2.1E-03	9.7E-03	0.85	8.8E-03	2.9E-02	0.34	2.7E-01	4.7E-01
LOC100774601		1.16	4.5E-05	3.4E-04	0.74	2.2E-02	7.0E-02	-0.30	4.1E-01	6.3E-01	-0.17	6.5E-01	8.4E-01
Lrig3		1.19	2.7E-63	1.3E-60	0.40	6.7E-08	9.6E-07	0.34	9.2E-06	7.0E-05	0.06	4.1E-01	6.5E-01
Lrrc43		1.11	7.2E-04	3.9E-03	0.61	6.2E-02	1.6E-01	0.36	3.3E-01	5.5E-01	-0.07	8.5E-01	9.5E-01
Lrriq4		1.82	3.4E-10	6.7E-09	0.69	3.6E-02	1.0E-01	0.16	6.5E-01	8.4E-01	-0.14	7.0E-01	8.7E-01
Masp2		1.44	5.5E-06	5.1E-05	0.62	9.6E-02	2.3E-01	0.12	7.5E-01	9.0E-01	0.13	7.3E-01	8.9E-01
Mast1		1.45	6.7E-10	1.2E-08	0.65	8.6E-03	3.2E-02	0.48	7.7E-02	1.8E-01	0.32	1.9E-01	3.6E-01
Matn2		1.34	7.4E-07	8.2E-06	0.99	1.6E-03	7.8E-03	0.40	2.4E-01	4.4E-01	0.15	6.6E-01	8.5E-01
Matn3		1.03	2.9E-03	1.3E-02	0.72	5.0E-02	1.4E-01	0.42	2.7E-01	4.7E-01	0.11	7.8E-01	9.2E-01
Mepce	4	1.43	6.8E-83	8.2E-80	0.96	3.9E-36	9.8E-34	0.86	2.7E-28	3.3E-26	0.67	5.2E-17	2.5E-15
Mfi2		1.79	6.5E-11	1.4E-09	0.77	2.0E-02	6.5E-02	0.65	4.4E-02	1.1E-01	0.51	1.2E-01	2.6E-01
Msantd1		1.26	7.1E-05	5.0E-04	0.74	3.8E-02	1.1E-01	0.07	8.5E-01	9.5E-01	0.01	9.8E-01	9.9E-01
Muc13		2.36	8.3E-17	3.5E-15	0.66	8.4E-02	2.0E-01	0.56	1.4E-01	2.8E-01	0.04	9.3E-01	9.8E-01
Mxd1		1.08	3.4E-05	2.6E-04	0.72	6.0E-03	2.4E-02	0.60	3.5E-02	9.2E-02	0.33	2.5E-01	4.5E-01
Mybpc3		1.65	1.5E-08	2.3E-07	0.76	2.7E-02	8.1E-02	0.36	3.3E-01	5.5E-01	-0.09	8.1E-01	9.3E-01
Myh15		1.06	2.2E-03	1.0E-02	0.75	4.3E-02	1.2E-01	0.19	6.3E-01	8.2E-01	0.08	8.4E-01	9.5E-01
Myo1g	4	1.14	2.6E-05	2.1E-04	0.80	6.7E-03	2.6E-02	0.85	2.9E-03	1.1E-02	0.52	9.7E-02	2.2E-01
Myo7a		1.62	1.3E-07	1.7E-06	0.99	2.2E-01	1.0E-02	0.03	9.3E-01	9.7E-01	0.13	7.3E-01	8.9E-01
Naaa		1.10	5.1E-06	4.8E-05	-0.03	9.2E-01	9.6E-01	-0.23	4.3E-01	6.5E-01	-0.82	4.8E-03	1.8E-02
Nek5		1.02	9.1E-04	4.7E-03	0.74	2.2E-02	7.0E-02	0.22	5.3E-01	7.5E-01	-0.07	8.5E-01	9.5E-01
Nfil3		1.07	8.3E-48	2.4E-45	0.51	2.1E-11	5.8E-10	0.50	4.4E-11	9.2E-10	0.28	2.4E-04	1.4E-03
Nhedc2		1.19	4.4E-05	3.3E-04	0.91	1.2E-03	5.8E-03	0.14	6.8E-01	8.6E-01	-0.16	6.3E-01	8.3E-01
Nkrf		1.13	1.5E-24	1.3E-22	0.70	2.6E-09	5.0E-08	0.71	5.1E-10	9.3E-09	0.40	6.5E-04	3.3E-03
Npm2		1.32	6.0E-07	6.7E-06	0.67	4.5E-02	1.2E-01	-0.25	4.7E-01	6.9E-01	-0.22	5.3E-01	7.5E-01
Nt5e		1.13	7.2E-04	3.9E-03	0.30	4.3E-01	6.5E-01	0.08	8.4E-01	9.5E-01	0.38	3.2E-01	5.5E-01
Ntn3		1.00	2.1E-03	9.8E-03	0.76	2.8E-02	8.6E-02	0.07	8.5E-01	9.5E-01	0.25	5.0E-01	7.2E-01
Nxf3	1	1.28	1.6E-04	1.0E-03	0.96	5.4E-03	2.2E-02	0.30	4.2E-01	6.4E-01	0.20	6.1E-01	8.1E-01
Olfm2		1.00	3.8E-04	2.2E-03	0.70	1.2E-02	4.2E-02	0.37	2.0E-01	3.8E-01	0.40	1.9E-01	3.6E-01
Oser1		1.02	7.4E-28	8.2E-26	0.52	6.4E-08	9.2E-07	0.38	9.6E-05	5.7E-04	0.42	2.2E-05	1.6E-04
Pabpc1l		1.76	2.2E-09	3.7E-08	0.93	5.0E-03	2.0E-02	0.55	1.3E-01	2.6E-01	0.41	2.8E-01	4.9E-01
Papd7		1.09	1.4E-19	8.1E-18	0.73	1.4E-09	2.8E-08	0.63	1.5E-07	1.7E-06	0.37	2.1E-03	8.9E-03
Pde8a		1.13	4.1E-04	2.4E-03	0.42	2.2E-01	4.1E-01	0.01	9.7E-01	9.9E-01	0.07	8.3E-01	9.5E-01
Per1	4	1.12	6.1E-19	3.3E-17	0.63	3.4E-07	4.2E-06	0.96	2.0E-14	7.1E-13	0.48	1.0E-04	6.4E-04
Phf1		1.23	6.4E-19	3.4E-17	0.78	5.1E-07	6.1E-06	0.81	3.6E-07	3.8E-06	0.65	2.0E-05	1.5E-04
Phf13		1.28	4.4E-29	5.5E-27	0.51	1.0E-04	7.1E-04	0.31	1.7E-02	5.1E-02	0.11	4.0E-01	6.3E-01
Phf6	4	1.13	1.6E-45	4.5E-43	0.84	2.8E-23	3.2E-21	0.70	1.8E-16	7.8E-15	0.97	1.6E-30	2.6E-28
Pi16		1.19	4.0E-04	2.3E-03	0.75	4.3E-02	1.2E-01	0.59	1.1E-01	2.4E-01	0.31	4.2E-01	6.5E-01
Pigz		1.07	1.8E-04	1.1E-03	0.48	1.6E-01	3.3E-01	0.63	7.1E-02	1.7E-01	0.12	7.0E-01	8.8E-01
Pla2g4c		1.36	7.1E-07	7.8E-06	0.91	1.3E-02	4.5E-02	-0.15	6.7E-01	8.6E-01	-0.05	8.9E-01	9.6E-01
Plcd4		1.58	1.5E-08	2.3E-07	0.56	6.9E-02	1.7E-01	-0.13	7.2E-01	8.8E-01	-0.32	3.6E-01	5.8E-01
Plekhd1		1.21	2.3E-04	1.4E-03	0.53	1.4E-01	3.0E-01	0.28	4.6E-01	6.9E-01	-0.01	9.8E-01	9.9E-01
Ppef2		1.82	2.2E-09	3.7E-08	0.91	1.3E-02	4.5E-02	0.01	9.7E-01	9.9E-01	-0.03	9.4E-01	9.8E-01
Ppm1d		1.25	3.0E-32	4.4E-30	0.67	4.8E-09	8.5E-08	0.38	6.4E-04	3.0E-03	0.24	3.7E-02	1.0E-01
Pthlh	1	1.17	2.7E-42	6.6E-40	0.85	3.9E-22	3.9E-20	0.49	1.0E-07	1.2E-06	0.18	5.5E-02	1.4E-01
Rapsn		1.96	1.3E-10	2.6E-09	0.72	5.0E-02	1.4E-01	0.16	6.7E-01	8.6E-01	0.20	6.1E-01	8.1E-01
Rbbp6		1.45	1.1E-120	2.2E-117	0.49	4.2E-15	1.9E-13	-0.33	6.1E-07	6.1E-06	-0.44	1.0E-11	2.7E-10
Rfx4		1.22	9.8E-05	6.8E-04	0.55	1.5E-01	3.2E-01	0.12	7.5E-01	9.0E-01	-0.05	8.9E-01	9.6E-01
Rfx7		1.42	1.2E-42	2.9E-40	0.98	3.2E-21	2.8E-19	0.15	1.4E-01	2.9E-01	-0.10	3.2E-01	5.4E-01
Rltpr		1.04	1.6E-06	1.7E-05	0.42	8.2E-02	2.0E-01	0.43	1.1E-01	2.3E-01	-0.17	5.3E-01	7.5E-01
Rxfp4		1.43	2.0E-08	3.0E-07	0.79	6.0E-03	2.4E-02	-0.15	6.3E-01	8.2E-01	-0.57	8.0E-02	1.9E-01
Samd14		1.22	4.0E-04	2.3E-03	0.80	2.4E-02	7.4E-02	0.32	3.9E-01	6.1E-01	0.16	6.8E-01	8.6E-01
Satb2		1.16	7.1E-17	3.1E-15	0.04	7.6E-01	8.8E-01	-0.07	6.4E-01	8.3E-01	-0.29	2.5E-01	4.5E-01
Scaf4	4	1.27	6.7E-42	1.5E-39	0.95	2.1E-24	2.7E-22	0.64	9.6E-12	2.2E-10	0.27	4.2E-03	1.6E-02
Scube2		1.06	2.2E-03	1.0E-02	0.55	1.4E-01	3.0E-01	0.15	7.1E-01	8.8E-01	0.15	7.1E-01	8.8E-01
Sdcbp2		1.93	2.2E-16	9.0E-15	0.59	2.5E-02	7.7E-02	0.46	9.6E-02	2.1E-01	0.54	6.2E-02	1.5E-01

TABLE A.19 (continued)

	C	2 h log2(FC)	P-value	FDR	4 h log2(FC)	P-value	FDR	6 h log2(FC)	P-value	FDR	8 h log2(FC)	P-value	FDR
Sds		1.22	1.6E-06	1.7E-05	0.30	3.1E-01	5.3E-01	0.00	1.0E+00	1.0E+00	-0.23	4.8E-01	7.1E-01
Selplg		1.24	2.9E-04	1.8E-03	0.81	2.5E-02	7.8E-02	0.35	3.7E-01	5.9E-01	0.15	7.1E-01	8.8E-01
Septin-12		1.74	3.6E-11	8.2E-10	0.99	8.7E-04	4.5E-03	0.77	2.1E-02	6.1E-02	-0.12	7.1E-01	8.8E-01
Sgk2		1.07	9.5E-04	4.9E-03	0.49	1.9E-01	3.8E-01	0.08	8.4E-01	9.4E-01	0.05	8.9E-01	9.6E-01
Sh2d3a		1.13	9.6E-04	5.0E-03	0.52	1.7E-01	3.5E-01	0.23	5.6E-01	7.7E-01	0.04	9.3E-01	9.8E-01
Sh3d21		1.54	2.0E-11	4.6E-10	0.21	4.7E-01	6.8E-01	-0.70	1.2E-02	3.8E-02	-0.32	2.9E-01	5.1E-01
Sh3gl2		1.06	2.2E-03	1.0E-02	0.65	7.2E-02	1.8E-01	0.14	7.2E-01	8.8E-01	-0.09	8.1E-01	9.3E-01
Shisa4		1.30	6.2E-07	7.0E-06	-0.21	4.3E-01	6.5E-01	-0.03	9.2E-01	9.7E-01	0.40	1.5E-01	3.1E-01
Slc30a1		1.03	1.8E-17	8.5E-16	-0.02	8.7E-01	9.4E-01	-0.04	7.9E-01	9.2E-01	-0.01	9.5E-01	9.8E-01
Slc4a11		1.84	9.4E-11	2.0E-09	0.84	9.4E-03	3.5E-02	0.27	4.1E-01	6.4E-01	-0.21	5.4E-01	7.6E-01
Slc5a5		2.36	6.4E-61	3.0E-58	1.00	1.1E-08	1.9E-07	0.07	7.2E-01	8.8E-01	-0.63	1.8E-03	7.7E-03
Slc6a5		1.39	3.4E-05	2.6E-04	0.75	4.3E-02	1.2E-01	0.15	7.1E-01	8.8E-01	0.06	8.8E-01	9.6E-01
Spdef		1.46	9.1E-06	8.0E-05	0.32	3.7E-01	5.9E-01	-0.26	4.7E-01	7.0E-01	-0.07	8.5E-01	9.5E-01
Spen		1.12	1.8E-27	1.9E-25	0.54	9.6E-08	1.3E-06	0.27	8.0E-03	2.7E-02	0.08	4.1E-01	6.4E-01
Spi1		1.08	2.2E-03	1.0E-02	0.11	7.7E-01	8.9E-01	0.15	7.1E-01	8.8E-01	0.06	8.8E-01	9.6E-01
Spred2	4	1.05	1.3E-29	1.7E-27	0.74	2.6E-16	1.5E-14	0.86	6.5E-21	4.6E-19	0.32	3.5E-04	1.9E-03
Spry2		1.10	5.1E-12	1.3E-10	0.59	3.4E-04	2.0E-03	0.07	6.9E-01	8.7E-01	-0.30	7.5E-02	1.8E-01
Susd1		1.20	1.3E-04	8.7E-04	0.77	3.0E-02	9.0E-02	0.23	5.2E-01	7.4E-01	0.16	6.5E-01	8.4E-01
Susd2		1.06	2.2E-03	1.0E-02	0.59	1.3E-01	2.8E-01	0.04	9.3E-01	9.7E-01	0.02	9.7E-01	9.9E-01
Sytl1		1.17	3.1E-04	1.9E-03	0.62	8.3E-02	2.0E-01	0.35	3.7E-01	5.9E-01	-0.07	8.5E-01	9.5E-01
Tas1r2		1.35	6.3E-05	4.5E-04	0.82	2.7E-02	8.2E-02	0.27	4.9E-01	7.1E-01	-0.07	8.5E-01	9.5E-01
Tbkbp1		2.00	3.9E-11	8.8E-10	0.69	6.7E-02	1.7E-01	0.31	4.2E-01	6.5E-01	0.02	9.7E-01	9.9E-01
Tbx19		1.10	1.7E-03	8.1E-03	0.62	1.0E-01	2.4E-01	0.46	2.3E-01	4.2E-01	0.16	6.8E-01	8.6E-01
Tecta		1.57	6.8E-07	7.5E-06	0.59	1.1E-01	2.5E-01	0.24	5.3E-01	7.5E-01	0.08	8.4E-01	9.5E-01
Tfcp2l1		1.39	1.9E-05	1.5E-04	0.85	2.1E-02	6.7E-02	0.19	6.3E-01	8.2E-01	0.19	6.3E-01	8.3E-01
Tgif1		1.10	1.7E-43	4.4E-41	0.51	7.5E-10	1.6E-08	0.43	3.1E-07	3.3E-06	0.09	3.0E-01	5.2E-01
Tgif2		1.11	1.8E-19	1.0E-17	-0.11	3.8E-01	6.0E-01	-0.17	1.8E-01	3.5E-01	-0.49	1.4E-04	8.4E-04
Tle4		1.23	1.2E-30	1.7E-28	0.39	9.3E-04	4.8E-03	0.20	9.3E-02	2.1E-01	0.32	6.3E-03	2.3E-02
Tmed6		1.57	2.1E-07	2.6E-06	0.11	7.4E-01	8.7E-01	0.32	4.0E-01	6.3E-01	-0.17	6.5E-01	8.4E-01
Tmem191c		1.03	9.2E-04	4.8E-03	-0.12	7.2E-01	8.6E-01	-0.08	8.3E-01	9.4E-01	-0.11	7.4E-01	9.0E-01
Tnfrsf18		1.95	2.1E-12	5.6E-11	0.25	4.9E-01	7.0E-01	0.01	9.7E-01	9.9E-01	0.19	6.3E-01	8.3E-01
Tnfrsf4		2.06	1.3E-15	4.9E-14	0.66	4.1E-02	1.2E-01	0.06	8.6E-01	9.5E-01	-0.01	9.7E-01	9.9E-01
Tob2		2.12	9.2E-43	2.4E-40	0.81	9.5E-07	1.1E-05	0.85	2.5E-07	2.7E-06	0.30	6.8E-02	1.6E-01
Tph2		1.30	1.2E-04	7.9E-04	0.33	4.0E-01	6.2E-01	0.27	4.9E-01	7.1E-01	0.10	7.9E-01	9.3E-01
Trim10		1.06	2.2E-03	1.0E-02	0.55	1.4E-01	3.0E-01	0.06	8.8E-01	9.6E-01	0.06	8.8E-01	9.6E-01
Ttc36		1.02	1.4E-05	1.2E-04	0.16	5.5E-01	7.5E-01	0.32	2.8E-01	4.9E-01	-0.45	1.0E-01	2.3E-01
Unc13d		1.11	1.8E-04	1.2E-03	-0.02	9.6E-01	9.8E-01	-0.32	3.5E-01	5.7E-01	-0.22	5.3E-01	7.5E-01
Usp50		1.15	9.5E-04	4.9E-03	0.18	6.4E-01	8.1E-01	0.39	3.0E-01	5.1E-01	-0.03	9.4E-01	9.8E-01
Vmn2r1	1	1.24	2.9E-04	1.8E-03	0.91	1.3E-02	4.5E-02	0.32	4.0E-01	6.3E-01	-0.05	8.9E-01	9.6E-01
Vwce		1.25	1.3E-04	8.4E-04	0.40	3.2E-01	5.4E-01	0.36	3.5E-01	5.7E-01	-0.03	9.4E-01	9.8E-01
Wasf1	2	1.11	9.7E-14	3.0E-12	0.86	4.2E-09	7.6E-08	0.72	5.0E-07	5.1E-06	0.86	1.0E-09	2.0E-08
Wfikkn1		1.86	3.2E-40	6.5E-38	0.90	2.1E-09	4.1E-08	0.36	4.1E-02	1.1E-01	0.22	2.1E-01	4.0E-01
Wnt5b		1.03	5.2E-04	2.9E-03	0.40	1.9E-01	3.8E-01	0.16	6.5E-01	8.4E-01	-0.29	4.2E-01	6.5E-01
Zbtb43	2	1.05	4.3E-35	7.3E-33	0.95	2.5E-29	4.4E-27	0.99	2.9E-33	5.4E-31	0.87	8.8E-24	8.5E-22
Zbtb7a		1.22	4.2E-21	2.8E-19	0.23	7.6E-02	1.9E-01	0.36	7.1E-03	2.4E-02	0.11	4.1E-01	6.4E-01
Zmynd10		1.55	1.7E-09	3.0E-08	0.99	2.4E-04	1.5E-03	0.72	1.5E-02	4.6E-02	0.42	1.4E-01	2.9E-01
Znf185		1.13	4.1E-04	2.4E-03	0.56	1.1E-01	2.6E-01	0.03	9.3E-01	9.7E-01	-0.05	8.9E-01	9.6E-01
Zswim6		1.05	2.3E-22	1.7E-20	0.24	4.9E-02	1.3E-01	0.32	8.9E-03	2.9E-02	0.02	8.7E-01	9.6E-01

A.2.8 Significantly Downregulated Genes

TABLE A.20: Results of gene expression analysis for 1 significantly downregulated gene 2, 4, 6 and 8 h after osmotic shift. log2(FC) $\leqslant$ -1, P and FDR $\leqslant$ 0.02, C = cluster (maSigPro)

	C	2 h log2(FC)	P-value	FDR	4 h log2(FC)	P-value	FDR	6 h log2(FC)	P-value	FDR	8 h log2(FC)	P-value	FDR
Egr1	1	-2.19	1.0E-121	2.5E-118	-2.94	2.3E-173	1.1E-169	-3.25	9.0E-199	4.4E-195	-3.45	2.7E-235	1.3E-231

TABLE A.21: Results of gene expression analysis for 3 significantly downregulated gene 2, 4 and 6 h after osmotic shift. log2(FC) $\leqslant$ -1, P and FDR $\leqslant$ 0.02, C = cluster (maSigPro)

	C	2 h log2(FC)	P-value	FDR	4 h log2(FC)	P-value	FDR	6 h log2(FC)	P-value	FDR	8 h log2(FC)	P-value	FDR
Cdh7	1	-1.04	2.4E-09	4.1E-08	-1.09	1.8E-09	3.6E-08	-1.24	2.2E-12	5.6E-11	-1.00	1.2E-08	1.8E-07
Murc	2	-1.34	2.2E-19	1.3E-17	-1.18	9.9E-16	5.1E-14	-1.13	6.7E-16	2.8E-14	-0.97	1.5E-11	3.8E-10
Nav3	2	-1.05	3.0E-40	6.2E-38	-1.44	5.5E-71	5.4E-68	-1.07	8.4E-43	2.0E-40	-0.77	1.6E-23	1.4E-21

TABLE A.22: Results of gene expression analysis for 7 significantly downregulated gene 4, 6 and 8 h after osmotic shift. log2(FC) $\leqslant$ -1, P and FDR $\leqslant$ 0.02, C = cluster (maSigPro)

		2 h			4 h			6 h			8 h		
	C	log2(FC)	P-value	FDR	log2(FC)	P-value	FDR	log2(FC)	P-value	FDR	log2(FC)	P-value	FDR
Bzrap1	1	-0.70	4.1E-10	7.9E-09	-1.45	2.6E-35	5.9E-33	-1.18	1.4E-24	1.4E-22	-1.32	2.9E-32	5.3E-30
Egr3	1	-0.59	9.0E-03	3.4E-02	-1.28	6.1E-09	1.1E-07	-1.48	2.5E-10	4.7E-09	-1.57	5.7E-12	1.5E-10
Foxp2	3	-0.32	6.0E-03	2.4E-02	-1.63	7.1E-26	1.0E-23	-1.75	3.3E-30	4.7E-28	-1.35	2.8E-20	1.9E-18
Midn	1	-0.68	1.1E-15	4.4E-14	-1.07	1.9E-36	4.8E-34	-1.07	3.8E-35	7.5E-33	-1.14	7.4E-43	2.1E-40
Nav2	4	0.11	3.9E-01	6.3E-01	-1.32	6.1E-22	6.0E-20	-1.02	3.0E-14	1.0E-12	-1.27	3.0E-22	2.4E-20
Ptx3	1	-0.47	7.2E-03	2.8E-02	-1.02	7.9E-08	1.1E-06	-1.15	4.8E-10	8.8E-09	-1.11	1.0E-08	1.5E-07
Relb	1	-0.19	1.6E-01	3.4E-01	-1.10	8.2E-14	3.2E-12	-1.34	6.5E-19	3.6E-17	-1.41	4.5E-20	2.9E-18

TABLE A.23: Results of gene expression analysis for 14 significantly downregulated gene 6 and 8 h after osmotic shift. log2(FC) $\leqslant$ -1, P and FDR $\leqslant$ 0.02, C = cluster (maSigPro)

		2 h			4 h			6 h			8 h		
	C	log2(FC)	P-value	FDR	log2(FC)	P-value	FDR	log2(FC)	P-value	FDR	log2(FC)	P-value	FDR
Cdk14	5	0.48	7.6E-07	8.3E-06	-0.29	3.4E-03	1.5E-02	-1.39	2.3E-36	4.6E-34	-1.44	1.8E-36	4.0E-34
Cpt1c		0.80	6.9E-13	1.9E-11	-0.70	5.0E-08	7.4E-07	-1.10	2.5E-14	8.4E-13	-1.68	1.4E-34	2.9E-32
F3	4	-0.05	6.7E-01	8.5E-01	-0.49	1.6E-05	1.3E-04	-1.01	5.3E-17	2.5E-15	-1.03	4.6E-18	2.5E-16
Heatr4	3	-0.09	6.7E-01	8.5E-01	-0.42	5.5E-02	1.5E-01	-1.04	7.9E-06	6.1E-05	-1.00	5.8E-05	3.9E-04
LOC100756717	3	-0.33	1.0E-06	1.1E-05	-0.77	7.7E-24	9.5E-22	-1.17	2.2E-53	8.6E-51	-1.01	1.1E-39	2.7E-37
Matn4	3	-0.09	3.8E-01	6.2E-01	-0.62	1.1E-08	1.8E-07	-1.02	2.5E-20	1.6E-18	-1.30	4.8E-30	7.2E-28
Prdm16		0.73	1.0E-05	8.8E-05	0.22	2.1E-01	4.1E-01	-1.07	7.5E-07	7.3E-06	-1.23	4.1E-09	6.9E-08
Sec16b	1	-0.47	5.6E-02	1.5E-01	-0.86	8.6E-04	4.5E-03	-1.32	7.3E-07	7.1E-06	-1.07	3.4E-05	2.5E-04
Slc16a6	1	-0.48	7.3E-04	3.9E-03	-0.91	2.8E-08	4.3E-07	-1.23	3.1E-16	1.3E-14	-1.16	1.3E-13	4.4E-12
Tmem44	3	-0.33	7.6E-02	1.9E-01	-0.88	4.9E-05	3.6E-04	-1.43	1.1E-11	2.5E-10	-1.20	1.7E-07	2.0E-06
Ttc39a	3	-0.06	6.5E-01	8.3E-01	-0.40	9.4E-03	3.5E-02	-1.01	1.7E-10	3.4E-09	-1.04	3.9E-10	7.7E-09
Zdhhc15	1	-0.55	5.8E-05	4.2E-04	-0.92	2.1E-09	4.1E-08	-1.60	4.9E-25	4.9E-23	-1.01	9.4E-12	2.4E-10
Zhx1	3	-0.27	7.5E-04	4.0E-03	-0.65	4.2E-15	1.9E-13	-1.16	1.5E-42	3.5E-40	-1.12	1.8E-38	4.2E-36
Znf469	5	0.23	6.5E-03	2.6E-02	-0.21	1.6E-02	5.4E-02	-1.14	1.0E-29	1.3E-27	-1.68	3.1E-64	1.7E-61

TABLE A.24: Results of gene expression analysis for 3 significantly downregulated gene 4 and 8 h after osmotic shift. log2(FC) $\leqslant$ -1, P and FDR $\leqslant$ 0.02, C = cluster (maSigPro)

		2 h			4 h			6 h			8 h		
	C	log2(FC)	P-value	FDR	log2(FC)	P-value	FDR	log2(FC)	P-value	FDR	log2(FC)	P-value	FDR
Ccnd1	1	-0.62	5.7E-13	1.6E-11	-1.24	1.5E-43	4.8E-41	-0.98	6.5E-28	7.6E-26	-1.06	5.1E-33	9.9E-31
LOC100771726	4	-0.56	1.7E-04	1.1E-03	-1.06	2.5E-10	5.8E-09	-0.92	5.2E-07	5.3E-06	-1.15	2.4E-11	5.8E-10
Ttc28	4	-0.20	2.8E-02	8.5E-02	-1.09	2.3E-28	3.8E-26	-0.94	2.8E-20	1.8E-18	-1.02	1.7E-28	2.2E-26

TABLE A.25: Results of gene expression analysis for 10 significantly downregulated gene 4 and 6 h after osmotic shift. log2(FC) $\leqslant$ -1, P and FDR $\leqslant$ 0.02, C = cluster (maSigPro)

		2 h			4 h			6 h			8 h		
	C	log2(FC)	P-value	FDR	log2(FC)	P-value	FDR	log2(FC)	P-value	FDR	log2(FC)	P-value	FDR
Fam198b	1	-0.68	8.9E-10	1.6E-08	-1.07	4.4E-19	3.2E-17	-1.32	1.3E-29	1.7E-27	-0.92	3.4E-14	1.2E-12
Glmn	1	-0.60	7.7E-08	1.0E-06	-1.08	5.2E-19	3.8E-17	-1.10	4.6E-22	3.6E-20	-0.53	3.6E-06	3.3E-05
Hmgcs1	1	-0.49	5.9E-12	1.5E-10	-1.20	1.2E-61	7.3E-59	-1.09	9.5E-52	3.4E-49	-0.86	5.7E-33	1.1E-30
Kif13a	6	-0.09	3.1E-01	5.4E-01	-1.45	4.2E-42	1.3E-39	-1.01	1.4E-23	1.3E-21	-0.65	3.4E-12	9.5E-11
Lgalsl		-0.90	6.7E-20	4.1E-18	-1.19	5.9E-32	1.2E-29	-1.08	1.9E-31	3.1E-29	-0.77	2.4E-16	1.1E-14
LOC100768278	1	-0.45	7.1E-05	5.0E-04	-1.07	2.3E-17	1.5E-15	-1.12	1.6E-20	1.1E-18	-0.83	1.1E-11	2.8E-10
Lyplal1	1	-0.43	5.6E-04	3.1E-03	-1.08	2.4E-14	9.8E-13	-1.47	2.7E-25	2.7E-23	-0.96	3.9E-11	9.1E-10
Slc25a43	1	-0.52	4.5E-03	1.9E-02	-1.43	4.3E-13	1.5E-11	-1.52	7.2E-15	2.7E-13	-0.87	8.9E-06	7.3E-05
St3gal3	1	-0.32	3.5E-03	1.5E-02	-1.10	1.6E-20	1.3E-18	-1.08	1.3E-19	7.8E-18	-0.90	6.7E-15	2.6E-13
Tpbg	1	-0.67	3.1E-16	1.3E-14	-1.27	2.8E-44	9.6E-42	-1.12	8.0E-37	1.7E-34	-0.91	4.5E-26	5.1E-24

TABLE A.26: Results of gene expression analysis for 2 significantly downregulated gene 2 and 6 h after osmotic shift. log2(FC) ⩽ -1, P and FDR ⩽ 0.02, C = cluster (maSigPro)

	C	2 h log2(FC)	P-value	FDR	4 h log2(FC)	P-value	FDR	6 h log2(FC)	P-value	FDR	8 h log2(FC)	P-value	FDR
Il6	2	-1.21	6.0E-11	1.3E-09	-0.78	5.5E-06	5.3E-05	-1.04	6.3E-09	9.5E-08	-0.79	1.0E-05	8.1E-05
LOC100758352		-1.95	4.5E-52	1.5E-49	-0.49	1.6E-05	1.4E-04	-1.11	9.5E-22	7.2E-20	-0.95	4.4E-17	2.2E-15

TABLE A.27: Results of gene expression analysis for 5 significantly downregulated gene 2 and 4 h after osmotic shift. log2(FC) ⩽ -1, P and FDR ⩽ 0.02, C = cluster (maSigPro)

	C	2 h log2(FC)	P-value	FDR	4 h log2(FC)	P-value	FDR	6 h log2(FC)	P-value	FDR	8 h log2(FC)	P-value	FDR
Dsel	2	-1.26	9.1E-25	7.8E-23	-1.30	1.7E-25	2.3E-23	-0.95	1.7E-16	7.5E-15	-0.36	1.4E-03	6.2E-03
LOC100751006	2	-1.91	2.2E-44	5.9E-42	-1.08	1.1E-16	6.5E-15	-0.87	3.0E-12	7.5E-11	-0.57	5.0E-06	4.3E-05
LOC100775101		-1.39	5.3E-09	8.5E-08	-1.02	4.2E-06	4.1E-05	-0.77	8.4E-04	3.8E-03	-0.64	2.2E-03	9.3E-03
Mks1	2	-1.28	1.2E-09	2.2E-08	-1.11	3.2E-07	3.9E-06	-0.54	6.6E-03	2.3E-02	-0.64	1.5E-03	6.9E-03
Plekhn1	2	-1.28	5.4E-10	1.0E-08	-1.27	1.1E-10	2.7E-09	-0.66	7.8E-04	3.6E-03	-0.91	2.3E-07	2.7E-06

TABLE A.28: Results of gene expression analysis for 33 significantly downregulated gene 8 h after osmotic shift. log2(FC) ⩽ -1, P-value and FDR ⩽ 0.02, C = cluster (maSigPro)

	C	2 h log2(FC)	P-value	FDR	4 h log2(FC)	P-value	FDR	6 h log2(FC)	P-value	FDR	8 h log2(FC)	P-value	FDR
Acsl6		-0.08	7.2E-01	8.7E-01	-0.31	2.0E-01	4.0E-01	-0.90	3.6E-04	1.8E-03	-1.22	1.6E-06	1.5E-05
Adam19	4	-0.11	4.7E-01	7.0E-01	-0.56	4.5E-04	2.6E-03	-0.54	2.0E-03	8.0E-03	-1.24	5.7E-14	2.0E-12
Ankmy1	5	0.24	3.0E-01	5.3E-01	-0.19	4.3E-01	6.5E-01	-0.38	1.4E-01	2.9E-01	-1.05	4.4E-05	3.1E-04
Arhgap25		0.18	4.4E-01	6.7E-01	0.14	5.5E-01	7.5E-01	-0.05	8.2E-01	9.4E-01	-1.10	4.7E-06	4.1E-05
Cacna1i		0.98	1.4E-10	2.8E-09	0.26	1.2E-01	2.6E-01	-0.68	1.5E-03	6.4E-03	-1.35	7.1E-12	1.9E-10
Ccdc24		-0.13	6.0E-01	8.1E-01	-0.99	1.3E-04	8.9E-04	-0.54	4.5E-02	1.2E-01	-1.07	7.4E-05	4.8E-04
Cirbp	1	-0.44	3.2E-09	5.4E-08	-0.89	2.2E-28	3.7E-26	-0.84	5.9E-26	6.3E-24	-1.09	5.8E-40	1.4E-37
Dclk1	4	0.01	9.4E-01	9.8E-01	-0.59	4.7E-06	4.6E-05	-0.80	4.5E-08	5.7E-07	-1.05	4.6E-15	1.9E-13
Dfna5	4	-0.71	1.2E-04	8.1E-04	-0.79	2.1E-05	1.8E-04	-0.70	1.9E-04	1.0E-03	-1.07	1.1E-08	1.7E-07
Dusp5	1	-0.90	4.1E-06	3.9E-05	-0.67	5.7E-04	3.1E-03	-0.97	7.7E-07	7.5E-06	-1.21	2.3E-10	4.8E-09
Enox1	5	0.33	4.3E-03	1.8E-02	-0.07	5.6E-01	7.5E-01	-0.62	4.7E-07	4.9E-06	-1.12	4.6E-17	2.2E-15
Fubp1	5	0.11	2.1E-01	4.1E-01	-0.33	1.0E-04	7.0E-04	-0.86	1.8E-22	1.5E-20	-1.01	1.4E-30	2.3E-28
Gli1	4	0.06	5.6E-01	7.7E-01	-0.49	2.2E-05	1.8E-04	-0.79	1.8E-11	4.0E-10	-1.01	9.9E-19	5.7E-17
Hivep3		-0.02	8.8E-01	9.5E-01	-0.61	1.3E-06	1.4E-05	-0.99	5.8E-14	1.9E-12	-1.16	2.1E-18	1.2E-16
Hnrnpa1	3	-0.15	2.6E-02	8.1E-02	-0.49	5.4E-13	1.9E-11	-0.91	1.8E-41	4.2E-39	-1.16	1.8E-64	1.1E-61
LOC100756141	4	-0.13	3.2E-01	5.5E-01	-0.61	7.1E-06	6.7E-05	-0.63	4.8E-06	3.9E-05	-1.03	2.1E-14	7.7E-13
LOC100758779		-0.98	1.1E-06	1.2E-05	-0.48	1.0E-02	3.8E-02	-0.69	5.4E-04	2.6E-03	-1.02	1.1E-07	1.3E-06
LOC100768211	4	-0.52	8.2E-05	5.7E-04	-0.29	2.9E-02	8.6E-02	-0.76	7.8E-08	9.3E-07	-1.07	6.6E-14	2.3E-12
LOC100769865		-0.39	1.5E-01	3.3E-01	-0.41	1.0E-01	2.4E-01	-0.09	7.2E-01	8.8E-01	-1.25	3.8E-06	3.4E-05
LOC100772063	4	-0.10	1.5E-01	1.4E-01	-0.41	8.5E-09	1.4E-07	-0.69	1.0E-21	7.7E-20	-1.05	4.1E-48	1.4E-45
Mlph		0.71	5.0E-05	3.7E-04	0.29	1.3E-01	2.8E-01	-0.70	7.1E-04	3.3E-03	-1.24	7.4E-09	1.2E-07
Nab2	1	-0.51	1.6E-07	2.0E-06	-0.81	1.7E-16	1.0E-14	-0.93	2.4E-20	1.6E-18	-1.03	5.4E-24	5.3E-22
Nabp1		-0.42	3.2E-02	9.6E-02	-0.70	1.0E-04	8.1E-04	-0.54	4.3E-03	1.6E-02	-1.04	4.4E-08	5.9E-07
Oscp1	3	-0.22	8.4E-02	2.1E-01	-0.50	5.1E-04	2.9E-03	-0.64	3.4E-06	2.9E-05	-1.06	1.5E-11	3.7E-10
Pion	3	-0.25	2.2E-01	4.2E-01	-0.79	3.1E-04	1.8E-03	-1.00	5.8E-07	5.8E-06	-1.16	1.6E-07	2.0E-06
Scnn1a	4	-0.37	1.1E-01	2.6E-01	-0.62	1.2E-02	4.3E-02	-0.89	3.4E-04	1.7E-03	-1.22	1.0E-06	1.0E-05
Slc12a5	4	-0.25	2.5E-01	3.7E-01	-0.24	2.5E-01	4.5E-01	-0.58	5.4E-03	1.9E-02	-1.16	7.4E-09	1.2E-07
Slc29a1	3	-0.07	3.0E-01	5.2E-01	-0.50	6.5E-14	2.6E-12	-0.91	7.9E-42	1.9E-39	-1.05	3.8E-52	1.3E-49
Slc7a5		0.10	1.2E-01	2.7E-01	-0.37	1.5E-08	2.5E-07	-0.72	2.6E-28	3.3E-26	-1.02	1.4E-53	5.2E-51
Tmc8		-0.46	1.9E-03	9.0E-03	-0.38	5.2E-03	2.1E-02	-0.40	9.5E-03	3.1E-02	-1.09	5.5E-14	1.9E-12
Tnfrsf12a	5	0.27	1.7E-04	1.1E-03	-0.33	4.1E-06	4.1E-05	-0.80	6.6E-29	8.5E-27	-1.14	2.6E-55	1.0E-52
Tnfrsf25	4	0.01	9.6E-01	9.8E-01	-0.85	1.0E-03	5.3E-03	-0.72	7.3E-03	2.5E-02	-1.21	9.3E-06	7.6E-05
Zcchc3	4	-0.09	6.7E-01	8.5E-01	-0.62	3.1E-03	1.3E-02	-0.71	1.5E-03	6.4E-03	-1.07	4.6E-06	4.1E-05

TABLE A.29: Results of gene expression analysis for 23 significantly downregulated gene 6 h after osmotic shift. log2(FC) ⩽ -1, P and FDR ⩽ 0.02, C = cluster (maSigPro)

	C	2 h			4 h			6 h			8 h		
		log2(FC)	P-value	FDR	log2(FC)	P-value	FDR	log2(FC)	P-value	FDR	log2(FC)	P-value	FDR
Casp1	1	-0.34	6.4E-04	3.5E-03	-0.94	2.4E-18	1.7E-16	-1.17	1.7E-28	2.2E-26	-0.75	1.6E-12	4.7E-11
Cav2	1	-0.41	7.9E-04	4.2E-03	-0.83	2.8E-10	6.4E-09	-1.05	3.6E-16	1.5E-14	-0.71	3.1E-08	4.3E-07
Ccdc122		-0.10	5.4E-01	7.6E-01	-0.82	3.9E-05	3.0E-04	-1.11	2.8E-08	3.7E-07	-0.96	6.5E-06	5.5E-05
Dph6	3	-0.10	4.6E-01	6.9E-01	-0.40	8.6E-03	3.2E-02	-1.12	3.6E-13	1.0E-11	-0.81	2.0E-07	2.3E-06
Endod1	1	-0.45	2.0E-05	1.6E-04	-0.73	2.0E-11	5.7E-10	-1.02	3.2E-20	2.1E-18	-0.80	3.3E-13	1.1E-11
Eps8	1	-0.49	1.6E-16	6.6E-15	-0.99	3.6E-58	2.0E-55	-1.08	3.4E-69	2.4E-66	-0.98	1.5E-57	6.4E-55
Fam114a1	1	-0.26	2.8E-02	8.5E-02	-0.72	1.6E-08	2.6E-07	-1.00	2.6E-15	1.0E-13	-0.74	2.9E-09	5.1E-08
Fhl3	1	-0.45	5.3E-08	7.2E-07	-0.69	1.2E-15	5.9E-14	-1.03	2.0E-30	3.0E-28	-0.91	7.4E-27	9.1E-25
Gulp1	6	-0.18	1.4E-01	3.0E-01	-0.93	2.0E-12	6.5E-11	-1.10	1.1E-17	5.4E-16	-0.54	1.4E-05	1.1E-04
Hells	3	0.01	9.4E-01	9.8E-01	-0.79	9.1E-22	8.7E-20	-1.23	2.7E-49	8.5E-47	-0.92	1.3E-28	1.8E-26
Igdcc4	3	-0.11	6.0E-01	8.0E-01	-0.74	7.3E-04	3.9E-03	-1.22	3.9E-08	5.0E-07	-0.73	1.9E-03	8.1E-03
Jade3	3	0.00	9.9E-01	1.0E+00	-0.47	8.5E-03	3.2E-02	-1.14	1.9E-11	4.2E-10	-0.72	3.8E-05	2.7E-04
Kcnq5	5	0.49	4.9E-05	3.6E-04	-0.26	5.3E-02	1.4E-01	-1.14	1.4E-12	3.7E-11	-0.99	1.2E-10	2.5E-09
LOC100753714		0.22	3.5E-01	5.8E-01	-0.08	7.0E-01	8.5E-01	-1.17	7.3E-07	7.1E-06	-0.91	3.9E-04	2.1E-03
LOC100758301	1	-0.75	3.5E-08	4.9E-07	-0.98	3.5E-13	1.3E-11	-1.39	6.0E-19	3.3E-17	-1.00	7.5E-12	2.0E-10
LOC100761052	1	-0.21	1.6E-02	5.4E-02	-0.80	8.5E-19	6.1E-17	-1.04	1.7E-30	2.5E-28	-0.85	2.4E-20	1.6E-18
LOC100771660	3	-0.21	9.6E-03	3.6E-02	-0.73	2.4E-18	1.7E-16	-1.10	1.5E-37	3.1E-35	-0.97	1.5E-29	2.2E-27
Lrrk1	4	-0.16	1.4E-01	3.0E-01	-0.98	6.1E-17	3.7E-15	-1.08	4.5E-18	2.3E-16	-0.88	7.4E-15	2.9E-13
Naip1	1	-0.68	1.9E-06	2.0E-05	-0.57	3.3E-04	2.0E-03	-1.05	2.4E-12	6.2E-11	-0.77	1.5E-07	1.8E-06
Pmp22	1	-0.37	2.1E-02	6.8E-02	-0.82	3.3E-06	3.4E-05	-1.04	7.2E-10	1.3E-08	-0.80	3.6E-06	3.3E-05
Sgk3	1	-0.17	2.5E-01	4.7E-01	-0.64	2.9E-05	2.3E-04	-1.13	2.2E-14	7.5E-13	-0.78	6.2E-07	6.6E-06
Slc2a13		-0.23	2.4E-01	4.5E-01	-0.66	2.8E-03	1.2E-02	-1.12	1.7E-06	1.5E-05	-0.44	5.5E-02	1.4E-01
Stxbp6	3	-0.18	2.7E-01	4.9E-01	-0.85	3.2E-06	3.3E-05	-1.08	3.7E-09	5.9E-08	-0.91	7.4E-07	7.9E-06

TABLE A.30: Results of gene expression analysis for 29 significantly downregulated gene 4 h after osmotic shift. log2(FC) ⩽ -1, P and FDR ⩽ 0.02, C = cluster (maSigPro)

	C	2 h			4 h			6 h			8 h		
		log2(FC)	P-value	FDR	log2(FC)	P-value	FDR	log2(FC)	P-value	FDR	log2(FC)	P-value	FDR
Angel1	2	-0.70	1.1E-11	2.7E-10	-1.06	1.4E-23	1.6E-21	-0.49	3.2E-07	3.4E-06	-0.38	4.3E-05	3.0E-04
Arhgap24		0.25	8.2E-02	2.0E-01	-1.04	4.5E-11	1.2E-09	-0.16	3.1E-01	5.2E-01	-0.39	8.7E-03	3.0E-02
Arhgef28	6	-0.06	6.2E-01	8.1E-01	-1.08	3.0E-15	1.4E-13	-0.57	3.7E-06	3.1E-05	-0.38	2.2E-03	9.4E-03
Arvcf	1	-0.76	1.2E-05	1.0E-04	-1.03	4.6E-08	6.7E-07	-0.82	1.8E-05	1.3E-04	-0.74	3.8E-05	2.7E-04
B3galnt1	2	-0.82	1.0E-05	8.7E-05	-1.11	2.2E-09	4.2E-08	-0.94	1.7E-09	2.8E-08	-0.26	1.1E-01	2.5E-01
Dph1	1	-0.72	1.3E-28	1.6E-26	-1.18	1.1E-66	8.6E-64	-0.94	4.2E-45	1.1E-42	-0.93	2.5E-44	7.1E-42
Elp4		-0.19	8.6E-02	2.1E-01	-1.03	6.8E-16	3.6E-14	-0.77	1.3E-10	2.5E-09	-0.22	6.0E-02	1.5E-01
Esr1	6	-0.39	1.9E-02	6.3E-02	-1.21	3.4E-12	1.1E-10	-0.75	1.3E-05	9.5E-05	-0.62	1.0E-04	6.3E-04
Etl4	6	-0.36	3.1E-02	9.2E-02	-1.02	1.8E-08	2.8E-07	-0.87	4.0E-07	4.2E-06	-0.35	3.3E-02	9.2E-02
Fry		0.05	7.3E-01	8.8E-01	-1.21	1.6E-11	4.6E-10	-0.70	9.4E-05	5.6E-04	-0.73	2.9E-05	2.1E-04
Ikbkg	2	-0.87	2.7E-11	6.2E-10	-1.02	9.9E-15	4.3E-13	-0.75	3.6E-09	5.7E-08	-0.55	9.2E-06	7.5E-05
Kdm8	6	-0.59	2.0E-07	2.5E-06	-1.13	6.5E-20	5.2E-18	-0.61	1.5E-07	1.7E-06	-0.29	1.1E-02	3.6E-02
LOC100752991	6	-0.30	1.3E-01	2.9E-01	-1.24	3.0E-08	4.6E-07	-0.87	4.9E-05	3.1E-04	-0.57	8.3E-03	2.9E-02
Mtss1	1	-0.54	8.5E-06	7.5E-05	-1.25	5.2E-19	3.8E-17	-0.86	8.7E-12	2.0E-10	-0.79	1.0E-10	2.2E-09
Nfkbie	2	-0.71	1.3E-06	1.4E-05	-1.06	4.5E-13	1.1E-11	-0.65	3.3E-06	2.8E-05	-0.51	1.8E-04	1.0E-03
Pex14	6	-0.26	1.5E-02	5.3E-02	-1.01	5.6E-18	3.9E-16	-0.40	3.0E-04	1.5E-03	-0.31	3.7E-03	1.5E-02
Pkdcc	1	-0.80	4.2E-07	4.9E-06	-1.41	2.0E-17	1.3E-15	-0.76	1.6E-06	1.5E-05	-0.99	5.7E-11	1.3E-09
Plekha6	6	-0.21	1.9E-01	3.8E-01	-1.30	7.1E-13	2.5E-11	-0.91	2.5E-07	2.8E-06	-0.67	4.6E-05	3.2E-04
Pter	6	-0.50	3.9E-06	3.7E-05	-1.20	7.5E-22	7.3E-20	-0.85	8.3E-15	3.1E-13	-0.71	7.6E-10	1.5E-08
Rab7b	2	-0.43	3.4E-02	9.9E-02	-1.61	1.0E-14	4.4E-13	-0.93	2.1E-06	1.9E-05	-0.54	1.2E-02	3.9E-02
Rbm43	2	-0.73	1.5E-07	1.9E-06	-1.13	3.0E-13	1.1E-11	-0.70	6.7E-07	6.6E-06	-0.36	6.0E-03	2.2E-02
Rhobtb1	2	-0.80	6.6E-07	7.4E-06	-1.01	1.2E-09	2.4E-08	-0.59	1.2E-04	6.9E-04	-0.91	1.6E-10	3.3E-09
Scaper	6	-0.19	1.9E-02	6.3E-02	-1.16	1.6E-35	3.9E-33	-0.93	8.9E-28	1.0E-25	-0.25	3.1E-03	1.3E-02
Srbd1	6	-0.42	6.3E-06	5.8E-05	-1.16	2.7E-28	4.2E-26	-0.78	2.6E-16	1.1E-14	-0.38	4.6E-05	3.2E-04
Syne1	6	-0.16	6.8E-02	1.8E-01	-1.07	4.1E-29	6.9E-27	-0.86	4.1E-21	2.9E-19	-0.69	1.1E-14	4.4E-13
Taf1b	2	-0.98	2.3E-13	6.7E-12	-1.03	5.7E-14	2.3E-12	-0.56	1.4E-05	1.0E-04	-0.29	2.2E-02	6.7E-02
Taf9b		-0.21	3.5E-01	5.8E-01	-1.10	3.0E-06	3.1E-05	-0.90	1.4E-04	8.0E-04	-0.49	4.2E-02	1.1E-01
Thbs1	2	-0.77	2.7E-06	2.7E-05	-1.03	4.9E-10	1.1E-08	-0.68	8.7E-06	6.6E-05	-0.67	2.4E-05	1.8E-04
Trp63	1	-0.18	2.5E-01	4.7E-01	-1.32	5.5E-13	1.9E-11	-0.89	2.5E-07	2.7E-06	-0.77	4.7E-06	4.2E-05

TABLE A.31: Results of gene expression analysis for 152 significantly downregulated gene 2 h after osmotic shift. log2(FC) ⩽ -1, P and FDR ⩽ 0.02, C = cluster (maSigPro)

	C	2 h log2(FC)	P-value	FDR	4 h log2(FC)	P-value	FDR	6 h log2(FC)	P-value	FDR	8 h log2(FC)	P-value	FDR
Acsm3		-1.15	1.8E-05	1.5E-04	-0.35	1.4E-01	3.0E-01	0.08	7.3E-01	8.8E-01	0.12	6.2E-01	8.2E-01
Afap1l2		-1.05	4.7E-23	3.5E-21	-0.51	5.8E-07	6.8E-06	-0.24	1.3E-02	4.1E-02	-0.14	1.5E-01	3.1E-01
Als2cl	2	-1.32	1.4E-22	1.0E-20	-0.82	2.0E-10	4.6E-09	-0.61	2.0E-06	1.8E-05	-0.38	2.0E-03	8.5E-03
Amotl2		-2.84	6.0E-160	2.2E-156	-0.96	1.1E-32	2.3E-30	-0.45	1.7E-08	2.3E-07	-0.27	2.4E-04	1.4E-03
Ankrd28		-1.09	3.3E-26	3.2E-24	-0.46	2.8E-06	2.9E-05	-0.17	7.4E-02	1.7E-01	-0.18	5.0E-02	1.3E-01
Ankrd49		-1.23	5.8E-25	5.2E-23	-0.52	9.7E-07	1.1E-05	-0.27	5.9E-03	2.1E-02	-0.41	9.7E-05	6.1E-04
Arrdc3		-1.22	1.5E-08	2.2E-07	-0.47	1.4E-02	4.8E-02	-0.24	1.9E-01	3.6E-01	-0.56	5.3E-03	2.0E-02
Aste1		-1.08	2.9E-10	5.7E-09	-0.35	2.0E-02	6.5E-02	0.19	1.6E-01	3.2E-01	0.33	2.6E-02	7.5E-02
Atp9b		-1.09	1.1E-15	4.2E-14	-0.39	2.9E-03	1.3E-02	0.16	1.9E-01	3.7E-01	-0.04	7.3E-01	8.9E-01
Bbs10		-1.54	1.3E-22	9.5E-21	-0.89	1.2E-10	2.8E-09	-0.71	3.3E-08	4.3E-07	-0.29	3.1E-02	8.8E-02
Bbs12		-1.13	1.1E-13	3.3E-12	0.04	7.7E-01	8.8E-01	0.32	6.5E-03	2.2E-02	0.20	1.1E-01	2.5E-01
Birc2		-1.52	2.3E-30	3.1E-28	-0.09	4.1E-01	6.3E-01	0.21	3.7E-02	9.8E-02	0.41	1.3E-04	8.0E-04
Brca2		-1.05	1.3E-21	9.0E-20	-0.74	1.2E-11	3.6E-10	-0.25	1.9E-02	5.7E-02	-0.26	1.4E-02	4.4E-02
Card6		-1.20	9.7E-07	1.1E-05	-0.06	7.8E-01	8.9E-01	0.27	2.1E-01	4.0E-01	0.03	8.9E-01	9.6E-01
Ccdc14		-1.34	1.2E-20	7.3E-19	-0.27	3.6E-02	1.0E-01	-0.23	4.2E-02	1.1E-01	0.00	9.9E-01	1.0E+00
Ccdc15		-1.12	5.8E-07	6.5E-06	0.42	1.6E-02	5.4E-02	0.72	1.8E-05	1.2E-04	0.25	1.2E-01	2.6E-01
Ccdc71		-1.13	3.3E-16	1.3E-14	-0.47	1.7E-04	1.1E-03	-0.07	5.7E-01	7.8E-01	-0.26	3.6E-02	9.8E-02
Cgn		-1.09	2.1E-06	2.1E-05	-0.15	4.6E-01	6.6E-01	0.21	2.6E-01	4.6E-01	0.41	2.1E-02	6.4E-02
Ckap2l		-1.42	4.6E-37	8.5E-35	-0.61	1.4E-08	2.2E-07	-0.18	8.3E-02	1.9E-01	-0.23	2.2E-02	6.6E-02
Clk2		-1.04	3.1E-26	3.0E-24	-0.09	2.6E-01	4.7E-01	0.04	6.7E-01	8.5E-01	-0.51	2.2E-10	4.4E-09
Cluap1		-1.11	1.9E-24	1.6E-22	-0.35	4.3E-04	2.5E-03	0.13	1.4E-01	2.8E-01	0.43	2.7E-06	2.5E-05
Csf1		-1.03	9.7E-26	9.3E-24	-0.57	1.7E-10	3.9E-09	-0.41	2.0E-06	1.8E-05	-0.36	3.5E-05	2.5E-04
Cstf2t		-1.20	1.6E-56	6.2E-54	-0.43	1.6E-10	3.7E-09	-0.17	9.4E-03	3.1E-02	-0.05	4.4E-01	6.7E-01
Cxcr7		-1.17	8.5E-14	2.7E-12	-0.82	1.1E-07	1.5E-06	-0.41	6.8E-03	2.3E-02	-0.31	3.8E-02	1.0E-01
Cyr61		-1.59	1.1E-18	5.8E-17	-0.54	1.9E-04	1.2E-03	-0.34	1.3E-02	3.9E-02	-0.40	3.7E-03	1.5E-02
Dennd6b		-1.37	4.1E-20	2.6E-18	-0.64	3.1E-06	3.2E-05	-0.25	5.6E-02	1.4E-01	-0.45	3.4E-04	1.8E-03
Dus4l		-1.96	7.2E-66	4.1E-63	-0.81	4.2E-16	2.3E-14	-0.37	7.2E-05	4.4E-04	-0.50	1.1E-07	1.4E-06
Enc1		-1.08	1.5E-12	4.0E-11	-0.39	3.9E-03	1.6E-02	-0.51	3.8E-04	1.9E-03	-0.78	7.8E-08	9.9E-07
Eri2		-1.58	7.7E-34	1.2E-31	-0.35	2.1E-03	9.6E-03	-0.03	8.1E-01	9.3E-01	0.10	3.4E-01	5.7E-01
Fam161a	2	-1.07	3.6E-24	2.9E-22	-0.94	4.8E-17	3.0E-15	-0.63	6.8E-11	1.4E-09	-0.24	1.5E-02	4.8E-02
Fam186a		-1.15	2.2E-07	2.7E-06	-0.82	7.0E-05	5.1E-04	-0.39	5.8E-02	1.4E-01	-0.42	2.5E-02	7.4E-02
Fgd4	2	-1.03	7.9E-08	1.0E-06	-0.98	5.2E-08	7.6E-07	-0.81	3.0E-06	2.5E-05	-0.55	2.0E-03	8.4E-03
Fignl1		-1.12	9.9E-13	2.7E-11	0.16	2.4E-01	4.4E-01	0.18	1.7E-01	3.3E-01	0.06	6.8E-01	8.6E-01
Foxr2		-1.08	1.6E-05	1.3E-04	-0.74	1.8E-03	8.6E-03	-0.59	1.2E-02	3.7E-02	-0.14	5.2E-01	7.5E-01
Foxs1		-1.18	5.8E-17	2.5E-15	-0.23	5.8E-02	1.5E-01	-0.15	2.2E-01	4.1E-01	-0.31	9.6E-03	3.3E-02
Fpgt		-1.08	2.9E-08	4.2E-07	-0.23	1.9E-01	3.7E-01	-0.21	1.8E-01	3.4E-01	0.36	3.1E-02	8.9E-02
Frmd4b		-1.05	3.5E-28	3.9E-26	-0.62	1.1E-11	3.3E-10	-0.50	9.9E-09	1.4E-07	-0.31	3.9E-04	2.1E-03
Gen1		-1.01	5.4E-24	4.3E-22	-0.30	1.9E-03	8.9E-03	0.02	8.0E-01	9.2E-01	-0.01	8.9E-01	9.6E-01
Gtf2e1		-1.24	4.6E-36	8.3E-34	-0.51	3.4E-08	5.1E-07	-0.05	5.5E-01	7.7E-01	-0.11	2.2E-01	4.1E-01
Helb		-1.00	1.7E-17	7.8E-16	-0.40	2.8E-04	1.7E-03	-0.16	1.4E-01	2.9E-01	-0.31	4.6E-03	1.8E-02
Hmgxb4		-1.33	7.8E-44	2.1E-41	-0.57	1.9E-10	4.5E-09	-0.29	6.0E-04	2.8E-03	-0.06	4.8E-01	7.1E-01
Hoxa9		-1.23	7.8E-11	1.7E-09	-0.77	2.8E-05	2.2E-04	-0.46	5.2E-03	1.9E-02	-0.30	5.4E-02	1.4E-01
Hus1		-1.03	4.4E-24	3.6E-22	-0.36	2.5E-04	1.5E-03	-0.14	1.5E-01	3.0E-01	-0.37	1.2E-04	7.3E-04
Inip		-1.16	2.3E-28	2.6E-26	-0.38	1.3E-04	8.6E-04	-0.47	2.5E-06	2.2E-05	-0.37	2.7E-04	1.5E-03
Itpripl2		-1.10	1.3E-10	2.7E-09	-0.51	5.0E-04	2.8E-03	-0.26	6.3E-02	1.5E-01	-0.42	1.9E-03	8.2E-03
Jrk		-1.14	4.2E-08	5.9E-07	0.00	1.0E+00	1.0E+00	0.22	2.3E-01	4.1E-01	-0.07	6.9E-01	8.7E-01
Jrkl		-1.04	1.7E-16	7.1E-15	0.20	9.2E-02	2.2E-01	0.27	1.7E-02	5.0E-02	0.32	6.7E-03	2.4E-02
Kbtbd3		-1.38	3.5E-12	9.0E-11	0.06	7.4E-01	8.7E-01	-0.17	3.2E-01	5.4E-01	0.24	1.8E-01	3.5E-01
Kctd12		-1.17	2.9E-20	1.8E-18	-0.05	6.5E-01	8.2E-01	0.20	5.2E-02	1.3E-01	0.68	2.9E-11	7.0E-10
Khnyn		-1.13	9.3E-09	1.4E-07	-0.18	3.1E-01	5.3E-01	0.11	5.4E-01	7.6E-01	0.01	9.7E-01	9.9E-01
Kiaa1430		-1.32	9.1E-16	3.6E-14	-0.30	4.6E-02	1.3E-01	0.18	2.1E-01	3.9E-01	-0.05	7.2E-01	8.9E-01
Klf6		-1.14	1.7E-14	5.7E-13	-0.50	3.5E-04	2.1E-03	-0.42	2.5E-03	1.0E-02	-0.57	3.7E-05	2.6E-04
Klhl17		-1.39	2.3E-13	6.6E-12	-0.27	1.1E-01	2.6E-01	0.41	1.5E-02	4.7E-02	-0.29	5.6E-02	1.4E-01
Lca5		-1.17	2.4E-05	1.9E-04	0.11	6.7E-01	8.3E-01	0.39	8.5E-02	1.9E-01	0.51	3.6E-02	9.8E-02
Lfng		-1.24	2.9E-10	5.7E-09	0.11	4.9E-01	7.1E-01	0.11	5.1E-01	7.3E-01	-0.26	1.2E-01	2.5E-01
LOC100750581		-1.57	3.8E-33	5.8E-31	-0.66	1.0E-08	1.7E-07	-0.42	7.2E-05	4.4E-04	-0.24	3.9E-02	1.1E-01
LOC100750925		-1.27	3.2E-21	2.1E-19	-0.34	1.6E-03	7.6E-03	-0.72	1.1E-09	1.9E-08	-0.91	1.6E-13	5.3E-12
LOC100751788		-1.46	5.4E-10	1.0E-08	-0.29	1.4E-01	3.0E-01	-0.19	3.0E-01	5.2E-01	-0.60	1.4E-03	6.4E-03
LOC100752154		-1.04	4.4E-07	5.1E-06	0.03	8.6E-01	9.3E-01	-0.19	3.1E-01	5.3E-01	-0.28	1.6E-01	3.2E-01
LOC100752763		-1.14	1.8E-06	1.8E-05	0.23	2.5E-01	4.5E-01	-0.05	8.0E-01	9.2E-01	0.20	3.4E-01	5.6E-01
LOC100752852		-1.08	7.5E-14	2.3E-12	-0.47	8.3E-04	4.4E-03	-0.50	1.7E-04	9.1E-04	-0.38	7.1E-03	2.6E-02
LOC100752942		-1.05	4.6E-06	4.3E-05	-0.64	3.4E-03	1.5E-02	-0.51	9.9E-03	3.2E-02	0.22	2.6E-01	4.7E-01
LOC100752946		-1.09	1.2E-10	2.6E-09	0.19	1.7E-01	3.5E-01	0.15	2.5E-01	4.5E-01	0.47	8.8E-04	4.3E-03
LOC100753112		-1.19	1.1E-13	3.3E-12	-0.19	2.0E-01	3.9E-01	-0.08	5.5E-01	7.7E-01	-0.10	4.6E-01	6.9E-01
LOC100755006		-1.65	2.9E-10	5.7E-09	-0.03	8.9E-01	9.5E-01	-0.08	7.0E-01	8.7E-01	-0.28	1.8E-01	3.5E-01
LOC100755415		-1.04	1.7E-21	1.1E-19	-0.61	1.4E-08	2.3E-07	-0.15	1.4E-01	2.9E-01	-0.13	2.1E-01	4.0E-01
LOC100756316		-1.17	3.9E-20	2.4E-18	-0.44	1.2E-04	7.9E-04	-0.54	4.8E-06	3.9E-05	-0.55	2.0E-06	1.9E-05
LOC100756518		-1.39	5.0E-33	7.7E-31	-0.37	2.0E-04	1.3E-03	-0.15	1.1E-01	2.4E-01	-0.24	1.7E-02	5.4E-02
LOC100756571		-1.06	1.9E-10	3.9E-09	-0.02	8.9E-01	9.5E-01	-0.14	3.6E-01	5.8E-01	-0.03	8.4E-01	9.5E-01
LOC100756838		-1.08	3.0E-06	2.9E-05	-0.04	8.5E-01	9.3E-01	-0.14	4.7E-01	7.0E-01	-0.21	2.8E-01	4.9E-01
LOC100757376		-1.40	1.4E-06	1.5E-05	-0.57	3.3E-02	9.7E-02	0.37	1.8E-01	3.4E-01	0.16	5.4E-01	7.6E-01
LOC100757435		-1.05	1.8E-11	4.2E-10	-0.46	1.5E-03	7.2E-03	-0.07	6.0E-01	8.1E-01	0.00	9.8E-01	9.9E-01
LOC100757661		-1.10	7.7E-08	1.0E-06	-0.70	4.1E-04	2.3E-03	-0.30	1.2E-01	2.5E-01	0.05	8.1E-01	9.3E-01
LOC100758375		-1.11	4.1E-07	4.8E-06	0.07	7.0E-01	8.5E-01	-0.05	8.0E-01	9.3E-01	0.00	9.9E-01	1.0E+00
LOC100759388		-1.22	2.7E-10	5.4E-09	-0.41	2.1E-02	6.8E-02	-0.23	1.8E-01	3.4E-01	-0.09	6.2E-01	8.2E-01
LOC100759790		-1.95	3.2E-15	1.2E-13	-0.36	7.0E-02	1.8E-01	-0.40	7.5E-02	1.7E-01	-0.74	2.1E-04	1.2E-03
LOC100760958		-1.43	3.7E-42	8.9E-40	-0.37	7.7E-05	5.5E-04	-0.14	1.2E-01	2.5E-01	-0.15	1.1E-01	2.3E-01
LOC100761022		-1.45	4.8E-16	1.9E-14	-0.38	9.6E-03	3.5E-02	0.29	4.1E-02	1.1E-01	0.12	3.8E-01	6.1E-01
LOC100761451		-1.38	8.3E-11	1.8E-09	-0.25	1.8E-01	3.7E-01	-0.59	1.4E-03	6.0E-03	-0.48	1.2E-02	3.9E-02

TABLE A.31 (continued)

	2 h			4 h			6 h			8 h		
	C log2(FC)	P-value	FDR	log2(FC)	P-value	FDR	log2(FC)	P-value	FDR	log2(FC)	P-value	FDR
LOC100761566	-1.06	5.4E-10	1.0E-08	0.28	6.3E-02	1.6E-01	0.65	3.7E-06	3.1E-05	0.54	1.1E-04	6.6E-04
LOC100762097	-1.23	2.1E-07	2.6E-06	-0.05	8.1E-01	9.1E-01	0.59	2.3E-03	9.3E-03	0.40	3.0E-02	8.5E-02
LOC100762680	-1.55	4.9E-31	6.8E-29	-0.64	8.4E-08	1.2E-06	0.09	4.1E-01	6.3E-01	0.20	6.9E-02	1.7E-01
LOC100762940	-1.40	2.1E-52	7.3E-50	-0.73	2.9E-17	1.9E-15	-0.67	1.7E-15	6.6E-14	-0.79	4.0E-20	2.7E-18
LOC100762957	-1.46	7.8E-11	1.7E-09	-0.30	1.4E-01	3.0E-01	0.33	1.0E-01	2.2E-01	0.28	1.6E-01	3.2E-01
LOC100763247	-1.50	5.0E-11	1.1E-09	-0.83	2.6E-04	1.6E-03	-0.60	7.8E-03	2.6E-02	-0.75	8.8E-04	4.2E-03
LOC100764000	-1.30	1.2E-10	2.6E-09	-0.62	2.0E-03	9.4E-03	-0.13	5.1E-01	7.3E-01	-0.20	3.3E-01	5.5E-01
LOC100764206	-1.23	9.8E-20	5.9E-18	-0.13	3.0E-01	5.2E-01	-0.16	1.6E-01	3.1E-01	0.07	5.6E-01	7.8E-01
LOC100765641	-1.72	3.8E-42	9.0E-40	-0.19	5.5E-02	1.5E-01	0.07	4.5E-01	6.7E-01	0.23	2.0E-02	6.2E-02
LOC100765869	-1.09	6.3E-07	7.1E-06	0.19	3.6E-01	5.6E-01	0.38	7.1E-02	1.7E-01	0.41	5.5E-02	1.4E-01
LOC100767679	-1.74	1.8E-23	1.4E-21	0.12	3.8E-01	5.9E-01	-0.06	6.3E-01	8.2E-01	0.10	4.2E-01	6.5E-01
LOC100767757	-1.37	1.6E-15	6.1E-14	-0.44	3.5E-03	1.5E-02	0.08	5.5E-01	7.7E-01	0.17	2.2E-01	4.2E-01
LOC100767949	-1.42	2.3E-10	4.6E-09	-0.14	4.2E-01	6.4E-01	0.44	1.1E-02	3.4E-02	0.03	8.5E-01	9.5E-01
LOC100768488	-1.11	4.6E-18	2.3E-16	-0.85	1.1E-11	3.3E-10	-0.40	1.1E-03	4.7E-03	-0.45	1.9E-04	1.1E-03
LOC100768835	-1.06	5.6E-19	3.0E-17	-0.38	4.7E-04	2.6E-03	0.11	2.5E-01	4.5E-01	0.41	2.3E-05	1.7E-04
LOC100769329	-1.01	2.6E-05	2.1E-04	-0.54	2.3E-02	7.1E-02	-0.08	7.3E-01	8.9E-01	-0.12	6.2E-01	8.2E-01
LOC100769471	-1.00	3.1E-49	9.9E-47	-0.03	6.6E-01	8.3E-01	-0.12	6.6E-02	1.6E-01	-0.03	6.0E-01	8.1E-01
LOC100769782	-1.20	2.0E-07	2.4E-06	0.13	5.4E-01	7.4E-01	0.35	8.1E-02	1.9E-01	0.58	4.5E-03	1.7E-02
LOC100770072	-1.14	2.2E-13	6.4E-12	-0.62	2.6E-05	2.1E-04	-0.71	5.0E-07	5.1E-06	-0.60	3.4E-05	2.4E-04
LOC100770926	-1.22	5.8E-10	1.1E-08	0.19	2.2E-01	4.2E-01	0.13	3.7E-01	5.9E-01	0.22	1.5E-01	3.1E-01
LOC100771790	-1.38	1.3E-09	2.3E-08	-0.72	8.8E-04	4.6E-03	-0.69	1.9E-03	7.7E-03	-0.54	1.1E-02	3.7E-02
LOC100772116	-1.37	1.7E-16	7.1E-15	-0.56	4.2E-04	2.4E-03	-0.03	8.7E-01	9.6E-01	0.24	1.0E-01	2.3E-01
LOC100773301	-1.57	1.6E-27	1.7E-25	-0.70	1.7E-08	2.8E-07	-0.81	8.1E-10	1.4E-08	-0.92	1.3E-13	4.3E-12
LOC100773418	-1.09	1.1E-05	9.4E-05	0.27	2.0E-01	3.9E-01	0.59	2.3E-03	9.3E-03	0.34	1.2E-01	2.5E-01
LOC100773542	-1.46	1.2E-10	2.5E-09	-0.58	9.5E-03	3.5E-02	-0.60	3.1E-03	1.2E-02	-0.39	7.1E-02	1.7E-01
LOC100774429	-1.07	1.4E-06	1.4E-05	-0.14	4.3E-01	6.4E-01	-0.36	4.5E-02	1.1E-01	-0.40	2.1E-02	6.3E-02
LOC100774589	-1.06	7.2E-08	9.6E-07	-0.47	1.8E-02	5.4E-02	-0.62	1.6E-03	6.9E-03	-0.60	2.0E-03	8.6E-03
Lysmd4	-1.20	1.0E-09	1.8E-08	-0.10	5.5E-01	7.5E-01	0.09	5.2E-01	7.4E-01	0.05	7.1E-01	8.8E-01
Map10	-1.22	5.7E-08	7.7E-07	0.43	2.1E-02	6.8E-02	0.54	3.4E-03	1.3E-02	0.71	2.5E-04	1.4E-03
Mcf2l	-1.07	2.1E-08	3.1E-07	0.00	9.9E-01	9.9E-01	0.09	5.7E-01	7.8E-01	0.36	2.2E-02	6.6E-02
Med7	-1.17	1.2E-12	3.3E-11	-0.16	2.7E-01	4.8E-01	-0.34	1.7E-02	5.2E-02	-0.14	3.5E-01	5.8E-01
Mettl21a	-1.60	2.2E-29	2.8E-27	-0.39	1.5E-03	7.1E-03	-0.35	2.9E-03	1.1E-02	-0.25	3.9E-02	1.1E-01
Mkrn3	-1.72	1.5E-14	5.0E-13	-0.14	4.0E-01	6.2E-01	0.35	3.4E-02	9.2E-02	0.24	1.5E-01	3.0E-01
Mlh3	-1.24	1.2E-10	2.5E-09	-0.68	2.6E-04	1.6E-03	-0.72	3.5E-05	2.3E-04	-0.38	3.1E-02	8.7E-02
Mus81	-1.10	3.8E-07	4.5E-06	0.00	9.9E-01	9.9E-01	0.23	2.1E-01	3.9E-01	0.09	6.2E-01	8.2E-01
Nanp	-1.34	1.5E-18	7.7E-17	-0.28	4.3E-02	1.2E-01	-0.14	2.9E-01	5.0E-01	-0.09	4.9E-01	7.2E-01
Papolg	-1.02	1.0E-15	3.9E-14	-0.30	1.3E-02	4.6E-02	-0.12	2.7E-01	4.7E-01	0.03	8.1E-01	9.3E-01
Pars2	-1.44	2.3E-28	2.6E-26	-0.01	9.4E-01	9.7E-01	0.06	5.8E-01	7.8E-01	-0.15	2.1E-01	3.8E-01
Pde4b	-1.28	4.9E-07	5.6E-06	-0.45	3.5E-02	1.0E-01	-0.20	3.6E-01	5.8E-01	-0.40	7.5E-02	1.8E-01
Pex12	-1.02	1.8E-08	2.7E-07	-0.10	5.1E-01	7.2E-01	0.11	4.6E-01	6.8E-01	0.36	9.4E-03	3.2E-02
Pex13	-1.50	1.1E-28	1.3E-26	-0.51	1.4E-01	1.2E-04	0.02	8.7E-01	9.6E-01	0.21	4.8E-02	1.2E-01
Pim1	-1.04	4.2E-14	1.4E-12	-0.18	1.3E-01	2.8E-01	-0.12	3.4E-01	5.5E-01	-0.46	1.5E-04	9.0E-04
Ranbp6	-1.17	3.6E-30	4.8E-28	-0.29	2.7E-03	1.2E-02	-0.10	2.6E-01	4.6E-01	-0.10	2.8E-01	5.0E-01
Rg9mtd1	-1.11	9.4E-41	2.0E-38	-0.36	3.5E-06	3.6E-05	-0.18	1.8E-02	5.3E-02	-0.23	2.9E-03	1.2E-02
Rnasel	-1.04	6.2E-15	2.2E-13	-0.20	1.0E-01	2.4E-01	0.02	8.6E-01	9.5E-01	0.23	5.4E-02	1.4E-01
Rpp38	-1.21	1.4E-16	5.8E-15	-0.47	3.9E-04	2.3E-03	-0.17	1.8E-01	3.5E-01	-0.23	7.8E-02	1.8E-01
Senp8	-1.26	1.3E-07	1.7E-06	-0.83	4.2E-04	2.4E-03	-0.73	3.8E-04	1.9E-03	-0.48	2.9E-02	8.4E-02
Sgol1	-1.44	1.7E-41	3.8E-39	-0.25	5.2E-03	2.1E-02	-0.03	6.8E-01	8.6E-01	-0.30	7.4E-04	3.6E-03
Sh3rf2	-1.10	4.6E-09	7.4E-08	-0.83	7.7E-07	8.9E-06	-0.45	9.3E-03	3.1E-02	-0.81	2.3E-06	2.2E-05
Slc16a4	-1.01	3.6E-05	2.8E-04	-0.35	1.5E-01	3.1E-01	-0.04	8.8E-01	9.6E-01	-0.04	8.4E-01	9.5E-01
Slc9a5	-1.14	2.2E-18	1.1E-16	-0.17	1.5E-01	3.2E-01	0.19	1.1E-01	2.3E-01	-0.04	7.2E-01	8.9E-01
Snai2	-1.33	3.7E-18	1.8E-16	-0.42	1.5E-03	7.2E-03	-0.02	8.6E-01	9.5E-01	-0.18	1.6E-01	3.3E-01
Spice1	-1.28	2.0E-11	4.6E-10	-0.45	1.2E-02	4.2E-02	-0.20	2.3E-01	4.2E-01	-0.37	4.1E-02	1.1E-01
Taf1c	-1.06	8.9E-10	1.6E-08	0.21	1.3E-01	2.9E-01	0.04	7.8E-01	9.2E-01	-0.33	2.1E-02	6.4E-02
Tfcp2	-1.05	4.1E-10	7.8E-09	-0.23	1.3E-01	2.8E-01	-0.12	3.7E-01	5.9E-01	-0.06	6.8E-01	8.6E-01
Thap3	-1.35	5.9E-39	1.2E-36	-0.73	2.8E-13	1.0E-11	-0.11	2.5E-01	4.5E-01	-0.13	1.6E-01	3.3E-01
Tnip2	-1.02	8.0E-10	1.5E-08	-0.11	5.0E-01	7.1E-01	-0.23	1.3E-01	2.7E-01	0.12	4.2E-01	6.5E-01
Trib1	-1.75	4.7E-46	1.3E-43	-0.26	1.0E-02	3.7E-02	-0.47	3.1E-06	2.6E-05	-0.56	3.0E-08	4.2E-07
Trim21	-1.25	2.7E-10	5.3E-09	-0.44	1.1E-02	3.9E-02	-0.06	7.1E-01	8.8E-01	0.26	1.1E-01	2.4E-01
Txnip	-1.71	9.2E-153	2.7E-149	-0.62	6.1E-24	7.5E-22	-0.56	1.1E-19	6.9E-18	-0.59	1.4E-21	1.1E-19
Vcl	-1.08	6.0E-25	5.4E-23	-0.51	2.8E-07	3.5E-06	-0.22	2.0E-02	5.8E-02	-0.08	3.8E-01	6.0E-01
Wdr89	-1.58	1.3E-16	5.5E-15	-0.36	2.9E-02	8.7E-02	-0.23	1.4E-01	2.8E-01	0.13	4.4E-01	6.8E-01
Zbtb24	-1.49	1.6E-14	5.5E-13	0.02	9.0E-01	9.5E-01	0.17	2.5E-01	4.5E-01	0.07	6.5E-01	8.4E-01
Zbtb26	-1.22	7.6E-13	2.1E-11	0.28	5.0E-02	1.4E-01	0.27	5.1E-02	1.3E-01	0.27	4.8E-02	1.2E-01
Zcchc7	-1.24	1.5E-07	1.9E-06	-0.68	1.6E-03	7.6E-03	0.17	3.7E-01	5.9E-01	0.26	1.7E-01	3.4E-01
Zfp62	-1.34	2.3E-25	2.1E-23	-0.24	2.2E-02	6.9E-02	-0.21	3.9E-02	1.0E-01	0.16	1.2E-01	2.5E-01
Zkscan7	-1.41	6.5E-09	1.0E-07	-0.54	2.3E-02	7.1E-02	-0.11	5.9E-01	7.9E-01	0.02	9.4E-01	9.8E-01
Znf26	-1.11	7.3E-05	5.2E-04	-0.23	3.5E-01	5.7E-01	-0.07	8.0E-01	9.2E-01	-0.13	6.2E-01	8.2E-01
Znf317	-1.02	1.9E-19	1.1E-17	-0.56	4.1E-07	4.9E-06	-0.27	9.3E-03	3.0E-02	-0.11	2.9E-01	5.1E-01
Znf449	-1.34	2.1E-20	1.3E-18	0.12	2.8E-01	4.9E-01	0.51	9.5E-07	9.1E-06	0.88	2.1E-15	8.8E-14
Znf483	-2.34	5.8E-56	2.2E-53	0.21	9.7E-02	2.3E-01	0.33	8.1E-03	2.7E-02	0.46	2.6E-04	1.5E-03
Znf672	-1.04	3.3E-08	4.7E-07	-0.10	5.4E-01	7.4E-01	-0.03	8.6E-01	9.5E-01	-0.16	3.3E-01	5.5E-01
Znf746	-1.06	1.2E-15	4.5E-14	-0.22	6.5E-02	1.7E-01	-0.12	2.9E-01	5.0E-01	0.05	6.4E-01	8.4E-01

A.2.9 CHO specific Gene Expression Changes Upon Hyperosmotic Stimulus

TABLE A.32: Genes with similar changes in differential expression upon hyperosmotic stimulus as described by Shen et al. (2010). Underlined genes were defined as significantly differentially expressed (log2(FC) $\geq$ 1.0, P and FDR $\leq$ 0.02) in the current study. Blue = downregulated, red = upregulated.

cell proliferation/ cell death	cellular response	transporters/ signaling pathway	gene expression regulation	metabolism	miscellaneous
DDIT4	_CIRBP_	ATP1B3	_ANKRD49_	AMDHD2	ACYP
GLCCI1	HERPUD1	_ARL4C_	ARID4B	AZIN1	_AMOTL2_
PLK2	NFIB	_DUSP1_	ARID5B	GTPBP3	CKMT1
	NQO1	_GLMN_	_BCL6_	POLA2	CPEB4
	NSMCE1	_GPRASP1_	CREBBP	SYNCRIP	EFHD2
		RALGDS	EIF2C2	TK1	FBXW2
		SLC1A5	_ELF1_	UMPS	GLIPR2
		SLC38A2	HBS1L		KLC1
		TCIRG1	HES1		KLC2
		WSB1	HIPK2		KLC4
			MED8		LUC7L
			MXD4		_MBNL2_
			SUB1		PAPD4
			ZKSCAN1		_RBBP6_
					RG9MTD1
					RNF138
					RSBN1
					TMEM51

ACYP: acylphosphatase, **AMDHD2:** amidohydrolase domain containing 2, **AMOTL2:** angiomotin like 2, **ANKRD49:** ankyrin repeat domain 49, **ARID4B:** AT-rich interaction domain 4B, **ARID5B:** AT-rich interaction domain 5B, **ARL4C:** ADP ribosylation factor like GTPase 4C, **ATP1B3:** ATPase Na$^+$/K$^+$ transporting beta 3 polypeptide, **AZIN1:** antizyme inhibitor 1, **BCL6:** B cell leukemia/lymphoma 6, CIRBP: cold inducible RNA binding protein, **CKMT1:** creatine kinase, mitochondrial 1, **CPEB4:** cytoplasmic polyadenylation element binding protein 4, **CREBBP:** CREB (cAMP-response element binding protein) binding protein, **DDIT4:** DNA damage inducible transcript 4, **DUSP1:** dual specificity phosphatase 1, **EFHD2:** EF-hand domain family member D2, **EIF2C2:** eukaryotic translation initiation factor 2C 2, **ELF1:** E74-like factor 1, **FBXW2:** F-box and WD repeat domain containing 2, **GLCCI1:** glucocorticoid induced 1, **GLIPR2:** GLI pathogenesis-related 2, **GLMN:** glomulin, FKBP associated protein, **GPRASP1:** G protein-coupled receptor associated sorting protein 1, **GTPBP3:** GTP binding protein 3, **HBS1L:** HBS1 like translational GTPase, **HERPUD1:** homocysteine-inducible endoplasmic reticulum stress-inducible ubiquitin-like domain member 1, **HES1:** hes family bHLH transcription factor 1, **HIPK2:** homeodomain interacting protein kinase 2, **KLC1/2/4:** kinesin light chain 1/2/4, **LUC7L:** LUC7-like, **MBNL2:** muscleblind-like splicing regulator 2, **MED8:** mediator complex subunit 8, **MXD4:** Max dimerization protein 4, **NFIB:** nuclear factor I/B, **NQO1:** NAD(P)H dehydrogenase, quinone 1, **NSMCE1:** non-SMC element 1 homolog, **PAPD4:** PAP associated domain containing 4, **PLK2:** polo-like kinase 2, **POLA2:** polymerase (DNA directed) alpha 2 accessory subunit, **RALGDS:** ral guanine nucleotide dissociation stimulator, **RBBP6:** retinoblastoma binding protein 6, **RG9MTD1:** tRNA methyltransferase 10 homolog C, **RNF138:** ring finger protein 138 E3 ubiquitin protein ligase, **RSBN1:** round spermatid basic protein 1, **SLC1A5:** solute carrier family 1 (neutral amino acid transporter) member 5, **SLC38A2:** solute carrier family 38 member 2, **SUB1:** SUB1 homolog transcriptional regulator, **SYNCRIP:** synaptotagmin binding cytoplasmic RNA interacting protein, **TCIRG1:** T-cell immune regulator 1 ATPase H$^+$ transporting lysosomal V0 subunit A3, **TK1:** soluble thymidine kinase 1, **TMEM51:** transmembrane protein 51, **UMPS:** uridine monophosphate synthetase, **WSB1:** WD repeat and SOCS box containing 1, **ZKSCAN1:** zinc finger with KRAB and SCAN domains 1.

B Publications

B.1 Manuscript 1

Changes in Intracellular ATP-Content of CHO Cells as Response to Hyperosmolality

Jennifer Pfizenmaier, Jens-Christoph Matuszczyk and Ralf Takors*

Institute of Biochemical Engineering, University of Stuttgart, 70569 Stuttgart, Germany

*Corresponding author;   takors@ibvt.uni-stuttgart.de

A variety of approaches has been published to enhance specific productivity (q_p) of recombinant Chinese hamster ovary (CHO) cells. Changes in culture conditions, e. g. temperature shifts, sodium butyrate treatment and hyperosmolality, were shown to improve q_p. In order to contribute to a better understanding of the correlation between hyperosmolality and enhanced q_p, we analyzed cellular kinetics and intracellular adenine nucleotide pools during osmotic shift periods. Known phenotypes like increased formation rates for lactate and product (anti-IL-8 antibody; $q_{lactate}$, q_p) as well as increased cell specific uptake rate for glucose ($q_{glucose}$) were found - besides inhibition of cell growth and G1 arrest occurred during batch cultivations with osmotic shift. The analysis of intracellular AXP pools revealed enlarged ATP amounts for cells as response to hyperosmolality while energy charges remained unchanged. Enhanced ATP-pools coincided with severely increased ATP formation rates (q_{ATP}) which outweighed by far the putative requirements attributed to regulatory volume increase. Therefore elevated q_{ATP} mirrored an increased cellular demand for energy while experiencing hyperosmotic shift.

Introduction

The production of biopharmaceuticals is strongly based on mammalian cells, such as Chinese

hamster ovary (CHO), human embryonic kidney (HEK), baby hamster kidney (BHK) or mouse myeloma (NS0) cells[1,2]. Despite the variety of different cell lines, recombinant therapeutic proteins are predominantly produced in CHO[3]. While in 1986 maximum product titers did not exceed $\sim$ 0.05 g L[1], improvements in host cell engineering, cultivation media and process engineering resulted in a twenty- to hundredfold increase in product titer as well as in enhanced specific productivities (q_p)[3]. Several approaches showed that changes in culture conditions increased q_p of recombinant CHO cells. Reducing the cultivation temperature from 37°C to $\sim$ 30°C significantly improved q_p of different proteins[4-7]. This coincided with a reduction of cell growth and prolonged cultivation periods finally yielding increased product titers[6]. Comparable effects were achieved by the addition of sodium butyrate[8] as well as in combination with temperature shift[9]. By analogy, the addition of cheap salts like NaCl, resulting in improved q_p, is commonly applied as well[10-12]. However, hyperosmolality was shown to induce inhibition of cell growth, increase in fraction of cells in S-phase, cell cycle arrest in G1-phase or even cell death in a dose-dependent manner, the latter obviously hampering improvement of total product yield[10,13-16]. While osmolality of cell culture medium typically shows $\sim$ 290 mOsmol kg^{-1}, hyperosmotic studies encompassed elevated levels of about 350 – 450 mOsmol kg^{-1} without severe impacts on cell viability. On the other hand intense stress was found for osmolalities $\geqslant$ 500 mOsmol kg^{-1} even inducing cell death. To prevent negative consequences of intense osmotic stress, osmoprotective substances like glycine betaine were added[13] or apoptosis inhibiting genes like bcl-2 were overexpressed[17]. Hyperosmotic effects like G1-phase arrest[15], enhanced glucose and glutamine consumption rates[12,15,18] and increased cell size[19] were suspected to improve q_p[20]. Lee at al. anticipated alleviated energy (ATP) availability by observation of increased expression levels of glycolytic enzymes such as glyceraldehyde-3-phosphate dehydrogenase (GAPDH) and pyruvate kinase[11]. Likewise, Lin et al. found increased ATP production rates (q_{ATP}) for osmotically stressed cells applying metabolic flux analysis (MFA) for hybridoma cells[18]. Motivated by this findings our studies focused on the effect of hyperosmotic conditions on intracellular AMP, ADP and ATP-contents in antibody producing CHO cells. To be precise, studies challenged the hypothesis whether hyperosmotic conditions may be mirrored by increasing AXP pools in conjunction with likewise increased ATP formation rates as an indicator of energetic capacity changes.

Materials and Methods

Cell Line, Medium and Cultivation with Shift in Osmolality

An anti-IL-8-producing CHO DP-12 cell line (ATCC® CRL 12445[TM]) adapted to grow in suspension was cultivated in TC-42-D medium (Xell, Germany) supplemented with 4 mM L-glutamine and 200 nM

methotrexate. Cells were thawed and cultivated in shake flasks (Corning Incorporated, USA) for 3 passages in a humidified Minitron incubator shaker (Infors HT, Germany) at 37°C, 5% CO_2 and 150 rpm as inoculum for bioreactor cultivations. Batch cultivations with induction of hyperosmolal conditions were performed in a fourfold parallel bioreactor system (DS1500ODSS, DASGIP, Germany) with working volumes of 0.7 or 1.2 L and viable cell densities of 0.4 x 10^6 cells mL^{-1} upon inoculation. Cultivation parameters were controlled at 150 rpm agitation speed, 40% dissolved oxygen (at environmental pressure), 37°C and pH 7.1. Two quadruplicate experiments (2 x 4) with same inoculum were carried out and osmolality was increased by the addition of NaCl-enriched in two bioreactors 3 days after inoculation. The resulting difference in volume between bioreactors with or without shift in osmolality was compensated by adding an equal volume of TC-42-D medium to each control bioreactor. Osmolality was $\sim$ 290 mOsmol kg^{-1} in control reactors and was increased by 100 mOsmol kg^{-1} in bioreactors with osmotic shift.

Sampling

Cell suspension was withdrawn from bioreactor once or twice a day as well as shortly after the rise in osmolality. A small aliquot was used to analyze viable cell density and the rest was centrifuged at 800g, 4°C for 5 min (Heraeus Megafuge 1.0R). While osmolality was analyzed immediately, the rest of supernatant was stored at $-$70°C in aliquots. Immediately before and on each of the following 4 days, cell samples for determination of cell cycle distribution and intracellular nucleotide pools were generated. With modifications of a previously published approach[21], 10^7 cells were separated from cultivation medium by fast filtration using 47 mm borosilicate glass fiber filters type A/D with a pore size of 3 μm (Pall, Germany) and a vacuum of 30 mbar. Afterwards cells were quenched using 30 mL of ice-cold washing buffer (10 mM K_2HPO_4/KH_2PO_4, 290 mOsmol kg^{-1}, pH 7.1), filters with cells were immediately transferred to 120 mL screw cap containers (Carl Roth, Germany), frozen in liquid nitrogen and stored at $-$70°C. Ten million cells were separated from cultivation medium by centrifugation (300g, 4°C, 5 min), washed with 1 x phosphate buffered saline pH 7.4 (PBS), fixed with $-$20 °C cold 70% ethanol in PBS and stored at $-$20°C until further preparation for cell cycle analysis.

Extraction of intracellular metabolites

For extraction of intracellular nucleotides, 5 mL ice-cold 70% methanol were added to screw cap containers with filters followed by a 90-minute incubation at $-$20°C in a cryostat (Haake F3 Fisons, Germany). Cell extract was separated from filter using a vacuum pump. Screw cap container and filter were rinsed with 2 mL 50% methanol and 0.5 mL chloroform were added to the permeate. After 20 sec of mixing, the methanol-chloroform mixture was centrifuged at 3200g, 0°C for 10 min

(Heraeus Megafuge 1.0R) and 1 mL aliquots of the aqueous phase were transferred to 1.5 mL reaction tubes (Eppendorf, Germany) followed by evaporation (RVC 2-33 IR, Martin Christ GmbH, Germany). Cell extracts were stored at $-70°C$

Analytical Methods

Viable cell density and viability were analyzed by Cedex XS cell analyzer (Roche, Germany). Determination of glucose and lactate concentrations was performed using a LaboTRACE (TRACE Analytics, Germany). An Osmomat 030 (Gonotec, Germany) was used to analyze osmolality. Antibody concentrations were determined by enzyme-linked immunosorbent assay (ELISA) using goat anti-human IgG F(c) as well as goat anti-human kappa chain peroxidase conjugated antibody (Rockland, USA) and SeramunBlau® (Seramun, Germany) as substrate. Absorption at 450 nm was measured by Infinite® 200 PRO series microplate reader (Tecan, Switzerland). Ion-pair reversed-phase HPLC (RP-HPLC) based on a modified protocol of a formerly published method[22] was used to quantify AMP, ADP and ATP concentrations of cell extracts. Analyses were carried out with an Agilent 1200 series apparatus equipped with Supelcosil LC 18-T column (15 cm x 4.6 mm, 3 μm) protected by Hypersil™ BDS C18 guard-column. HPLC was performed at 30°C and a flow rate of 1 mL min^{-1} using two eluents as mobile phase. Buffer A (pH 6) contained 100 mM K_2HPO_4/KH_2PO_4 and 4 mM tetrabutylammonium bisulfate while buffer B (pH 7.2) consisted of 70% buffer A and 30% methanol. A diode array detector (DAD) was used for detection of nucleotides at 260 nm. Energy charges were calculated according to Atkinson et al.[23]. For determination of cell cycle distribution, ethanol fixed cells were washed and finally resuspended in PBS. Cells were incubated with RNAse A and propidium iodide followed by flow cytometric analysis of $10,000-20,000$ events at low flow rate (FC 500, Beckman Coulter). Histograms of FL-3 (620 nm) were analyzed by Cylchred software (Cardiff) to determine the percentage of cells in G1-, S-, and G2-phase of cell cycle.

**Calculation of Specific Rates and Statistics**

Specific rates were calculated for the most sensitive time interval day 4 to day 6. More data points were available for the second run of cultivations than for the first one as sampling frequency was increased from once to twice a day (six compared to three). Nevertheless calculation methods resulted in similar results. Logarithm of viable cell density was plotted versus cultivation time in order to determine specific growth rate (μ). Changes in glucose, lactate and antibody concentration over time were determined by linear regression ($R^2 > 0.98$) and were divided by arithmetic mean of viable cell density in order to calculate specific glucose consumption ($q_{glucose}$), lactate production ($q_{lactate}$) and antibody production rate (q_P). Standard deviations were calculated based on four biolog-

ical replicates. Unpaired student's t test was used to investigate data for statistical significance. The calculation of oxygen uptake (q_{O_2}), carbon dioxide formation (q_{CO_2}) and ATP formation rates (q_{ATP}) is summarized in the supplemental file. A P/O ratio of 2.5 was used for calculating q_{ATP} according to literature[24,25].

Results and Discussion

Hyperosmolality, especially the lower, non-lethal range (350 − 450 mOsmol kg^{-1}) is an extensively studied research field in cell culture. Nevertheless it is not yet completely understood how hyperosmotic conditions stimulate increase in q_p. Based on MFA with antibody producing hybridoma cells Lin et al. linked increased osmolality with enhanced q_{ATP} even anticipating co-stimulation of q_p[18]. Starting from ~ 290 mOsmol kg^{-1} (reference condition), osmolality was increased by adding NaCl enriched medium to four of eight batch cultures three days after inoculation (Figure 1A). Consequently, related osmolality levels increased to ~ 390 mOsmol kg^{-1} maintaining the constant difference of ~ 100 mOsmol kg^{-1} until the end of the experiment (Figure 1A). Noteworthy, tendencies of osmolality profiles were fairly similar in the hyperosmotic and the reference batches. Only slight osmolality increases were observed reflecting the impact of 1 M Na_2CO_3 titration (Figure 1A). Therefore a statistically sound difference (P < 0.001) in osmolality was given across the whole time of process.
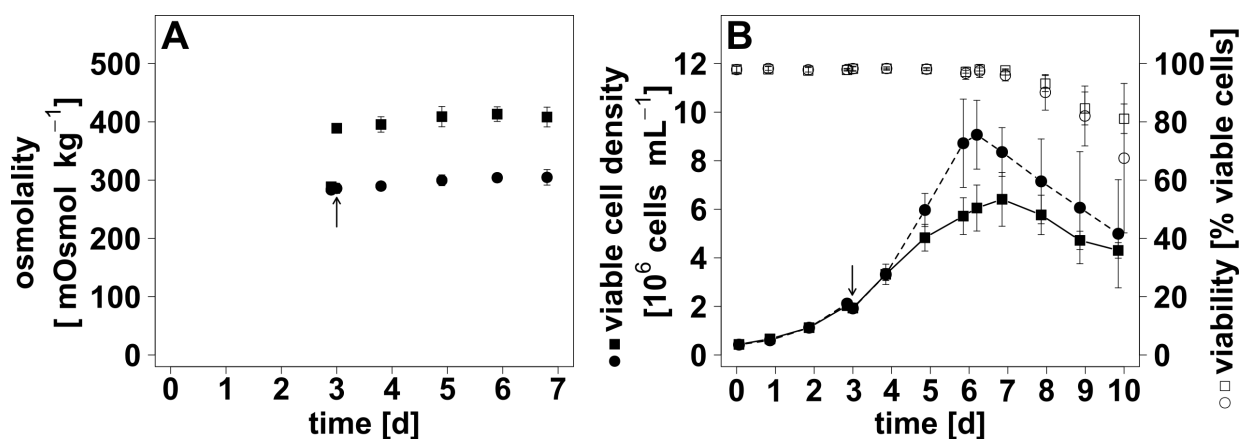
Figure 1. Profile of osmolality (A), viable cell density and viability (B). During batch cultivations of CHO DP-12 sodium chloride was added (arrow) to increase osmolality by ~ 100 mOsmol kg^{-1} (■, □) compared to reference (●, ○). A: Measurement of osmolality was based on cryoscopy using Osmomat 030 (Gonotec). Error bars represent standard deviations based on four biological replicates. B: Viable cell density (●, ■) and viability (○, □) of cultures were determined by trypan blue staining and Cedex XS (Roche). Error bars represent standard deviations based on four biological replicates.

Profiles of viable cell densities were similar in all cultures until the osmotic shift was performed

on day 3 (Figure 1B). Thereafter cells exposed to hyperosmolality showed lower viable cell densities compared to isotonic (reference) batch cultures (Figure 1B). However, discrepancies of viable cell densities did not result in likewise different cell viabilities. Instead, viability was not influenced by osmotic shift at all and stayed above 90% until day 8 (Figure 1B). In the post-shift interval day 4 to day 6, cells exposed to osmotic shift showed a growth rate of $\mu = 0.28 \pm 0.04\,d^{-1}$ while $\mu = 0.48 \pm 0.11\,d^{-1}$ was determined for reference cells. Considering these significant growth differences, equally different viable cell densities might have been expected. However, direct correlation between growth rate and viable cell density is not fully enabled because of superimposing high inter-culture variances. Nevertheless, imposing hyperosmolality apparently hampered cell growth (P = 0.02, n = 4). This finding is in agreement with independent studies[11-13,15] although the effect is less pronounced which is presumably due to inter-culture variance and the moderate stress imposed in our experiments. On the other hand, previously published effects of hyperosmolality on $q_{glucose}$ and $q_{lactate}$ could be verified[12,13,15]. Cells grown under hyperosmotic conditions showed increased $q_{glucose}$ (2.09 $\pm$ 0.13 vs. 1.55 $\pm$ 0.18 pmol cell^{-1} d^{-1}, P = 0.002, n = 4) and $q_{lactate}$ (2.29 $\pm$ 0.12 vs. 1.64 $\pm$ 0.19 pmol cell^{-1} d^{-1}, P = 0.001, n = 4) for the time interval day 4 to day 6. Hyperosmotic culture conditions enhanced q_P from 3.69 pg mAB cell^{-1} d^{-1} under isotonic conditions to 5.55 pg mAB cell^{-1} d^{-1} (n = 2) again confirming findings of independent studies[11-13,15,17,20].
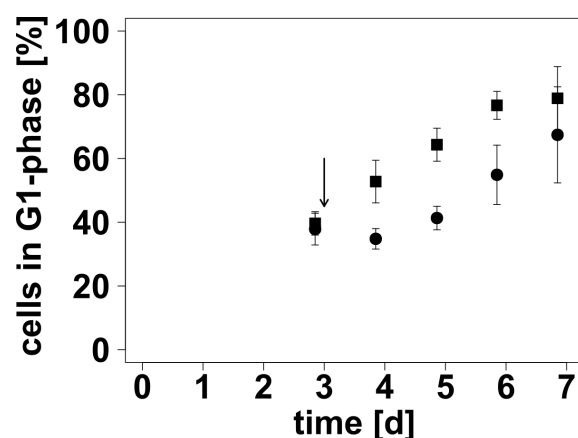

Figure 2. Time evolution of cells in G1-phase during batch cultivations of CHO DP-12 with osmotic shift. Addition of sodium chloride resulted in an osmolality of $\sim$ 390 mOsmol kg^{-1} (■) compared to $\sim$ 290 mOsmol kg^{-1} in control bioreactors (●). Ethanol fixed cells were stained with propidium iodide and analyzed by flow cytometry (FC500, Beckman Coulter). Error bars represent standard deviations based on four biological replicates.

The analysis of population composition with respect to cell cycle mapping revealed significant differences between hyperosmotic and reference cultures. Directly before the osmotic shift similar

cell fractions ($\sim$ 40%) were assigned to G1-phase. The post-pulse period revealed the opposite: a significantly higher fraction of hyperosmotically stimulated cells was observed to be in G1-phase (P < 0.005, n = 4, Figure 2). This observation was found to be in accordance with previous independent studies[15]. In addition, intracellular AXP pools and energy charges were monitored analyzing two biological replicates of each condition. The pre-shift period, represented by sample analysis on the third day of cultivation, disclosed ATP-contents of $\sim$ 3 fmol ATP cell^{-1} (Figure 3). Noteworthy, this amount was almost identical in all cultures. Reference cells unraveled continuous decline of ATP cell^{-1} values reaching about 1/3 of their original level on day 7 (Figure 3). Interestingly, hyperosmotically stimulated cells showed no decrease but rather an increase in intracellular ATP-contents until day 6 (Figure 3). Thereafter intracellular ATP-contents dropped to $\sim$ 1.6 fmol cell^{-1} (Figure 3). Intracellular ATP-concentrations, taking real cell volumes into account, showed similar profiles (supplemental Figure 4).

The amount of AMP in analyzed samples was below detection limit. Calculation of energy charges, disregarding AMP, resulted in no significant difference between hyperosmotic and reference conditions as intracellular ADP-contents tended to be higher for cells undergoing osmotic shift than for reference cells (Figure 3). Altogether, energy charges were at high level (> 0.9) during the whole period of analysis and declined only slightly on day 6 and 7 (Figure 3). This correlates as well with the previously described high cell viability (> 90%) for reference cells and cells exposed to hyperosmolality in the same time interval (Figure 1). In order to determine q_{ATP} on a daily basis (day 3 to day 7), specific carbon dioxide production (q_{CO_2}) and oxygen consumption (q_{O_2}) rates were calculated based on carbon and oxygen balancing (supplemental material). Respiratory quotient (RQ $\approx$ 1) as well as literature values were used as quality standards for the determined rates. For the time interval day 4 to day 7 RQs were close to 1 with an average RQ of 1.08 $\pm$ 0.04 for hyperosmolal conditions and 1.07 $\pm$ 0.14 for reference state. q_{O_2} and q_{CO_2} ranged from $0.2 - 0.4$ pmol cell^{-1} h^{-1} which was in concurrence with values from literature (0.2 - 0.8 pmol cell^{-1} h^{-1})[26]. A P/O ratio of 2.5[24,25] was assumed for the calculation of q_{ATP}. Comparable values of $\sim$ 19 pmol ATP cell^{-1} d^{-1} were determined for the time interval day 3 to day 4 (Figure 3) and lay in a comparable range of values published in literature[27-29]. Thereafter osmotically stimulated cells showed an increase in q_{ATP} of $\sim$ 21% while q_{ATP} of reference cells remained almost constant (Figure 3). On average, hyperosmotic shift lead to 30% higher q_{ATP} from day 4 to day 7. In this interval, cell volumes increased as well due to regulatory volume increase (RVI) under hyperosmotic culture conditions (supplemental Figure 3)[19,30]. Nevertheless, the calculation of the required amount of ATP to compensate RVI ($q_{ATP,+}$) (supplemental) showed that the increase in q_{ATP} was orders of magnitude higher than $q_{ATP,+}$ (4910 fmol cell^{-1} d^{-1} vs. 0.26 fmol cell^{-1} d^{-1}).
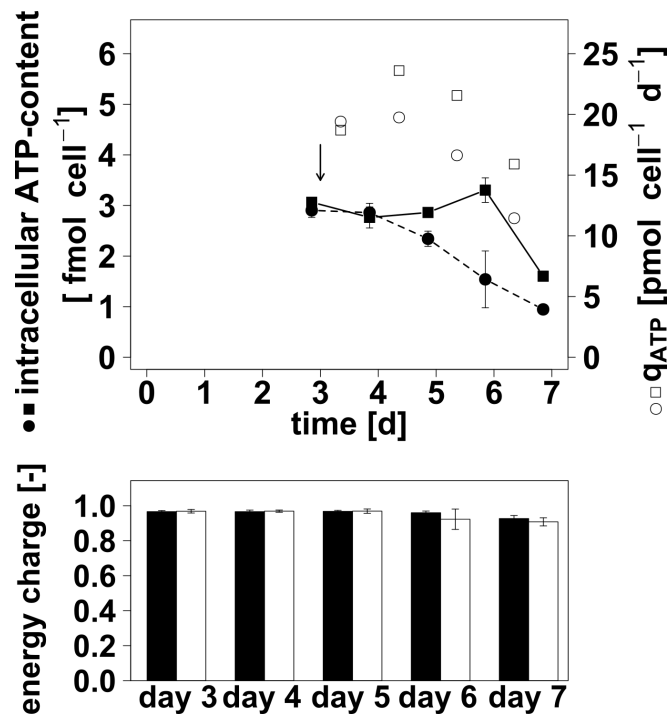
Figure 3. Effect of osmotic shift on intracellular ATP-content and energy charge during batch cultivation of CHO DP-12. Addition of sodium chloride (arrow) resulted in an osmolality of $\sim$ 390 mOsmol kg^{-1} ($\blacksquare$, $\square$, black) compared to $\sim$ 290 mOsmol kg^{-1} in control bioreactors ($\bullet$, $\bigcirc$, white). Fast filtration was used for cell sampling followed by methanol/chloroform extraction and RP-HPLC-quantification. Energy charges were calculated according to Atkinson et al.[23]. Error bars represent standard deviations based on two biological replicates as well as three technical replicates each. q_{ATP} was calculated as stated in supplemental. A P/O ratio of 2.5 was assumed[24,25].

In conclusion, our studies are in agreement with well-known effects of hyperosmolality, such as inhibition of cell growth, increased q_p and G1-arrest[11-13,15,17,20]. Besides, increased ATP levels and ATP formation rates (q_{ATP}) which had been determined during the post-shift period confirmed the hypothesis of Lin et al.[18] and Lee et al.[11]. Based on MFA and gene expression measurements, increased q_{ATP} were anticipated in antibody producing hybridoma and CHO, respectively[11,18]. Increased intracellular ATP-contents have been described before relating to high passage cultivation[31], addition of sodium butyrate[32] and changes in media composition[33]. These facts in combination with our results of an increased intracellular ATP-content together with elevated q_{ATP} reveal the connection between changing culture conditions and the cells' energetic capacity. On the one hand this could be interpreted as an effect of an increased demand for energy and on the other hand higher intracellular ATP-contents might mirror the cells' adaptation to changing culture conditions. Further studies are required to clarify whether the enhancement of ATP formation could be exploited to boost

antibody formation even further.

Literature Cited

1. Wurm FM. Production of recombinant protein therapeutics in cultivated mammalian cells. Nature biotechnology. 2004;22(11):1393-1398.

2. Kim JY, Kim YG, Lee GM. CHO cells in biotechnology for production of recombinant proteins: current state and further potential. Applied microbiology and biotechnology. 2012;93(3):917-930.

3. Jayapal KR, Wlaschin KF, Hu WS, Yap MGS. Recombinant protein therapeutics from CHO cells - 20 years and counting. Chem Eng Prog. 2007;103(10):40-47.

4. Furukawa K, Ohsuye K. Effect of culture temperature on a recombinant CHO cell line producing a C-terminal alpha-amidating enzyme. Cytotechnology. 1998;26(2):153-164.

5. Furukawa K, Ohsuye K. Enhancement of productivity of recombinant alpha-amidating enzyme by low temperature culture. Cytotechnology. 1999;31(1-2):85-94.

6. Kaufmann H, Mazur X, Fussenegger M, Bailey JE. Influence of low temperature on productivity, proteome and protein phosphorylation of CHO cells. Biotechnology and bioengineering. 5 1999;63(5):573-582.

7. Fox SR, Patel UA, Yap MG, Wang DI. Maximizing interferon-gamma production by Chinese hamster ovary cells through temperature shift optimization: experimental and modeling. Biotechnology and bioengineering. 20 2004;85(2):177-184.

8. Sung YH, Song YJ, Lim SW, Chung JY, Lee GM. Effect of sodium butyrate on the production, heterogeneity and biological activity of human thrombopoietin by recombinant Chinese hamster ovary cells. J Biotechnol. 9 2004;112(3):323-335.

9. Hendrick V, Winnepenninckx P, Abdelkafi C, et al. Increased productivity of recombinant tissular plasminogen activator (t-PA) by butyrate and shift of temperature: a cell cycle phases analysis. Cytotechnology. 2001;36(1-3):71-83.

10. Ozturk SS, Palsson BO. Effect of medium osmolarity on hybridoma growth, metabolism, and antibody production. Biotechnology and bioengineering. 25 1991;37(10):989-993.

11. Lee MS, Kim KW, Kim YH, Lee GM. Proteome analysis of antibody-expressing CHO cells in response to hyperosmotic pressure. Biotechnol Prog. 2003;19(6):1734-1741.

12. Shen D, Kiehl TR, Khattak SF, et al. Transcriptomic responses to sodium chloride-induced osmotic stress: a study of industrial fed-batch CHO cell cultures. Biotechnol Prog. 2010;26(4):1104-1115.

13. Ryu JS, Kim TK, Chung JY, Lee GM. Osmoprotective effect of glycine betaine on foreign protein production in hyperosmotic recombinant Chinese hamster ovary cell cultures differs among cell lines. Biotechnology and bioengineering. 20 2000;70(2):167-175.

14. Han YK, Kim YG, Kim JY, Lee GM. Hyperosmotic stress induces autophagy and apoptosis in recombinant Chinese hamster ovary cell culture. Biotechnology and bioengineering. 15 2010;105(6):1187-1192.

15. Ryu JS, Lee MS, Lee GM. Effects of cloned gene dosage on the response of recombinant CHO cells to hyperosmotic pressure in regard to cell growth and antibody production. Biotechnol Prog. 2001;17(6): 993-999.

16. Kim NS, Lee GM. Response of recombinant Chinese hamster ovary cells to hyperosmotic pressure: effect of Bcl-2 overexpression. Journal of biotechnology. 23 2002;95(3):237-248.

17. Lin J, Takagi M, Qu Y, Gao P, Yoshida T. Metabolic flux change in hybridoma cells under high osmotic pressure. Journal of bioscience and bioengineering. 1999;87(2):255-257.

18. Kiehl TR, Shen D, Khattak SF, Jian Li Z, Sharfstein ST. Observations of cell size dynamics under osmotic stress. Cytometry. Part A : the journal of the International Society for Analytical Cytology. 2011;79(7):560-569.

19. Han YK, Koo TY, Lee GM. Enhanced interferon-beta production by CHO cells through elevated osmolality and reduced culture temperature. Biotechnol Prog. 2009;25(5):1440-1447.

20. Volmer M, Northoff S, Scholz S, Thute T, Buntemeyer H, Noll T. Fast filtration for metabolome sampling of suspended animal cells. Biotechnology letters. 2011;33(3):495-502.

21. Cserjan-Puschmann M, Kramer W, Duerrschmid E, Striedner G, Bayer K. Metabolic approaches for the optimisation of recombinant fermentation processes. Applied microbiology and biotechnology. 1999;53(1):43-50.

B.2 Manuscript 2

The following manuscript was published in Biotechnology Journal 11:1037-1047 in 2016.

Hyperosmotic Stimulus Study Discloses Benefits in ATP Supply and Reveals miRNA/mRNA Targets to Improve Recombinant Protein Production of CHO Cells

Jennifer Pfizenmaier[1], Lisa Junghans[1], Attila Teleki[1] and Ralf Takors[1]

[1] University of Stuttgart, Institute of Biochemical Engineering, Stuttgart, Germany

Correspondence: Prof. Dr.-Ing. Ralf Takors, University of Stuttgart, Institute of Biochemical Engineering, Allmandring 31, 70569 Stuttgart, Germany.
E-Mail: takors@ibvt.uni-stuttgart.de

Abbreviations: AEC, adenylate energy charge; **ATP_{cyt}**, cytosolic ATP-content; **ATP_{mit}**, mitochondrial ATP-content; **CHO**, Chinese hamster ovary; **DEG**, differentially expressed gene; **FDR**, false discovery rate; **GO**, gene ontology; **mAB**, monoclonal antibody; **NGS**, next generation sequencing; **q_p**, specific product formation rate; **q_{ATP}**, specific ATP formation rate; **RVI**, regulatory volume increase; **VCD**, viable cell density

Abstract

Biopharmaceuticals are predominantly produced by Chinese hamster ovary (CHO) cells cultivated in fed-batch mode. Hyperosmotic culture conditions ($\geqslant$ 350 mOsmol kg^{-1}) resulting from feeding of nutrients may enhance specific product formation rates (q_p). As an improved ATP supply was anticipated to enhance q_p this study focused on the identification of suitable miRNA/mRNA targets to increase ATP levels. Therefor next generation sequencing and a compartment specific metabolomics approach were applied to analyze the response of an antibody (mAB) producing CHO cell line upon osmotic shift (280 $\rightarrow$ 430 mOsmol kg^{-1}). Hyperosmotic culture conditions caused a $\sim$ 2.6-fold increase of specific ATP formation rates together with a $\sim$ 1.7-fold rise in cytosolic and mitochondrial ATP-pools, thus showing increased ATP supply. mRNA expression analysis identified several genes encoding glycosylated proteins with strictly tissue related function. In addition, hyperosmotic culture conditions induced an upregulation of miR-132-3p, miR-132-5p, miR-182, miR-183, miR-194, miR-215-3p, miR-215-5p which have all been related to cell cycle arrest/proliferation in cancer studies. In relation to a previous independent CHO study miR-183 may be the most promising target to enhance q_p by stable overexpression. Furthermore, deletion of genes with presumably dispensable function in suspension growing CHO cells may enhance mAB formation by increased ATP levels.

1 Introduction

The annual global biopharmaceuticals market increased from \$94 billion in 2007 (1) to \$140 billion in 2013 (2). With Chinese hamster ovary (CHO) cells being the predominant mammalian expression platform for biopharmaceuticals (2) the importance of a permanent improvement in performance gets obvious. Thanks to intensive cell and process engineering, productivity of CHO based monoclonal antibody (mAB) production has increased about 100-fold during the last two decades reaching more than 5 g L^{-1} today (3,4). Such improvements of process performance coincide with more and more challenging cultivation conditions like hyperosmolality ($\geqslant$ 350 mOsmol kg^{-1}) as one of several putative stress factors.

The impact of hyperosmolality on cellular performance is a matter of steady interest often focusing on metabolic phenotypes. According to different studies, osmolalities ranging from 350$-$450 mOsmol kg^{-1}

did not severely affect viability of CHO cells. However, further increase in osmolality induced severe stress conditions finally causing cell death (5–8). The link between hyperosmolality and improved product formation rate (q_p) has not been fully deciphered so far. Increased glucose and glutamine consumption rates ($q_{glucose}$, $q_{glutamine}$) as well as cell cycle arrest and increase in cell size have been anticipated to contribute to an enhanced q_p (6–9). Recently Pfizenmaier et al. (2015) refined this picture by outlining that hyperosmolality coincides with the increased availability of energy (ATP) which is supposed to play a crucial role for the improved cellular performance .

Hence metabolic studies have already created a valuable basis to understand the complex interplay of regulatory schemes occurring in CHO under osmotic stress. However, the picture necessarily remains incomplete as long as the link to superimposed transcriptional control is missing. Related studies are comparatively rare which is certainly caused by the ‚late' publication of the CHO K1 genome sequence (10) which opened the door for today's next generation sequencing (NGS) studies. Prior to that, microarrays from related species like mouse or rat (11–13) were used and custom-made CHO cDNA microarrays were constructed (14–17). Transcriptomic studies were applied to investigate apoptotic pathways, variations of growth rate and productivity and to analyze the effects of process variations, e. g. low cultivation temperature, hyperosmolality and sodium butyrate treatment (3,8,18–26). Thus correlations between gene expression changes and enhanced productivity were elucidated and potential targets for cell line engineering were identified. One aim of cell line engineering is to provide additional energy for the synthesis of recombinant proteins in order to enhance cellular productivity. This can be realized e. g. by metabolic engineering of ATP generating or consuming pathways (27,28), genome reduction (29–31) or induction of a state of cellular senescence (28,32). To identify suitable target genes for these strategies, this study combines analysis of mRNA and miRNA expression of hyperosmotically stressed cell cultures. We suppose that understanding the transcriptional dynamics and mechanisms behind the characteristic hyperosmotic phenotype (enhanced q_p, cell cycle arrest and increased ATP formation rates) would provide a high capability for the identification of suitable targets to improve the energetic capacity of recombinant CHO cells. In order to get a more precise idea of the hyperosmotic effect on adenine nucleotide levels as a measure of energetic capacity, this study further applies a novel compartment

specific approach (33) to distinguish between cytosolic and mitochondrial adenine nucleotide pool sizes.

2 Materials and methods

2.1 Cell line, medium, and bioreactor cultivation with osmotic shift

A CHO DP-12 cell line (ATCC®CRL-12445[TM]) producing anti-IL-8 IgG1 antibody was cultivated in suspension in TC-42-D medium (Xell, Bielefeld, Germany) supplemented with 4 mM glutamine (Carl Roth, Karlsruhe, Germany) and 200 nM methotrexate (Applichem, Darmstadt, Germany). Cryo culture was thawed, scaled up in shake flasks (Corning, NY, USA) and used as inoculum for batch cultivations. Shake flasks were incubated at 37°C, 150 rpm and 5% CO_2 in a humidified Minitron incubator shaker (Infors HAT, Einsbach, Germany). Two series of batch cultivations were performed in a fourfold parallel DS1500ODSS bioreactor system (DASGIP, Jülich, Germany). Each series included one or two reference cultivations ($\sim$ 280 mOsmol kg^{-1}1) as well as two cultivations with osmotic shift ($\sim$ 430 mOsmol kg^{-1}). The seeding density was 0.4 x 10^6 cells mL^{-1} (V_0 = 1.4 L). Osmolality was increased by adding NaCl-enriched TC 42 D medium 35 h past inoculation. The set point for temperature was 37°C and dissolved oxygen was controlled at 40% (environmental pressure) using a DASGIP®MX4/4 module. pH was controlled at pH 7.1 by addition of 1 M Na_2CO_3 or sparging of CO_2 while the set point for agitation speed was 150 rpm.

2.2 Sampling

Over the whole time of cultivation, samples were withdrawn from the bioreactor twice or three times a day to analyze viable cell density, osmolality and concentrations of substrates and products. Directly before (0) as well as 2, 4, 6 and 8 h after osmotic shift 2 x 10^6 cells were pelleted by centrifugation, resuspended in RNAprotect (Qiagen, Hilden, Germany), frozen in liquid nitrogen and stored at 70°C until isolation of RNA. Whole cell and subcellular cell samples (2 x 10^7 cells/sample) for quantification of intracellular metabolite pools were generated by previously described fast filtration methods (33,34) directly before and 1.5, 2.5 and 3.5 days after osmotic shift. A 47 mm borosilicate glass fiber filter type A/D with a pore size of 3 μm (Pall, Dreieich, Germany) was used for whole cell

samples applying a vacuum of 30 mbar and 35 mL of ice-cold washing buffer (10 mM K_2HPO_4/KH_2PO_4, 290 mOsmol kg^{-1}, pH 7.1). A combination of the aforementioned A/D type filter and a Metrigard^{TM} glass fiber filter (Pall, Dreieich, Germany) with a pore size of 0.5 μm was applied for subcellular samples. Vacuum was increased to 90 mbar and digitonin containing washing-buffer (0.122% (m/v)) was added followed by regular washing buffer. Filters with cells were frozen in liquid nitrogen and stored at 70°C.

2.3 Extraction of intracellular cell metabolites

Intracellular metabolites were extracted from cells by a combination of incubation of filters with methanol at 20°C and treatment of the extract with chloroform as described before (34).

2.4 Analytics

Viable cell density and viability (Cedex XS, Roche innovatis, Bielefeld, Germany), glucose and lactate (LaboTRACE, TRACEAnalytics, Braunschweig, Germany), osmolality (Osmomat 030, Gonotec, Berlin, Germany) and antibody concentrations as well as intracellular adenine nucleotide pools were determined as described previously (34). Concentration of ammonium was measured with LCK303 cuvette test (Hach, Düsseldorf, Germany). Reversed-phase HPLC with an automated pre-column ortho-phthalaldehyde/9 fluorenylmethyl chloroformate derivatization was used for determination of amino acid concentrations with an Agilent 1200 series apparatus as described before [35]. L-norvaline (Sigma-Aldrich, Taufkirchen, Germany) functioned as internal standard. Hydrophilic interaction liquid chromatography-electrospray ionization-tandem mass spectrometry (HILIC-ESI-MS/MS) was performed with high selectivity in multiple reaction monitoring (MRM) mode to quantify intracellular and subcellular pool sizes of *cis*-aconitate (*cis*-Aco), glucose-6-phosphate (G6P) and fructose-6-phosphate (F6P) (33,36). Measurements were acquired with an Agilent 6410B Triple Quad mass spectrometer (Agilent, Waldbronn, Germany) with ESI ion source in negative ionization mode with high selectivity based on pre-optimized MRM transitions (36). The Instrument was equipped with a Sequant ZIC–pHILIC column (150 x 2.1 mm, 5 μm) protected by Sequant ZIC–pHILIC guard column (20 x 2.1 mm, 5 μm). Elution buffer A consisted of 10% (v/v) aqueous buffer solution

(10 mM ammonium acetate) and 90% (v/v) acetonitrile while eluent B contained 90% (v/v) aqueous buffer solution and 10% (v/v) acetonitrile. The pH of both eluents was adjusted to pH 9.2 (with 25% (v/v) ammonium hydroxide). The resulting data sets were analyzed with MassHunter B.04.00 software. Analysis was based on a previously described isotope dilution mass spectrometry (IDMS) method [36] using 13C-labeled internal standard which was extracted from U-13C labeled algal cells (> 99 atom% ^{13}C, lot no. 487945, Sigma-Aldrich, Taufkirchen, Germany) (37). Internal standard was added to external calibration levels as well as to cell extract samples during preparation for LC-MS analysis. Analyte peak areas (^{12}C/^{13}C-ratios) were plotted against ^{12}C concentration levels of the corresponding analyte and linear regression was used to prepare external calibration curves (36).

2.5 Calculation of specific rates, adenine nucleotide content, energy charge and statistics

Specific rates were analyzed for two different time intervals (day 1.5 − 2.5, day 3.0 − 4.0) following hyperosmotic shifts. Specific growth rate (μ) was determined by plotting the logarithm of viable cell density vs. time of cultivation. Metabolite concentrations were plotted vs. integrated viable cell density in order to analyze specific metabolite formation rates (q). Mitochondrial and cytosolic ATP content were calculated according to equations 1a and 1b (Supporting Information). Amounts of *cis*-Aco, G6P and F6P were used to correct measured adenine nucleotide contents for loss of mitochondrial compartment or remaining cytosol. Adenylate energy charge (AEC) was calculated according to Atkinson and Walton (38). Specific ATP formation rate (q_{ATP}) was determined according to equation 2 (Supporting Information) assuming a P/O ratio of 2.5 (39,40). Standard deviations were calculated based on three (reference) or four (hyperosmolal) biological replicates. Gaussian error propagation was applied in order to determine errors of calculated data. Unpaired student's t-test was applied to determine statistical significance.

2.6 RNA samples and sequencing

The cell samples of three biological replicates of cultivations with osmotic shift and two biological replicates of reference cultivations were chosen for gene expression analysis by NGS. miRNeasy kit

(Qiagen, Hilden, Germany) was used to isolate RNA. The quality of isolated RNA was determined with Bioanalyzer 2100 (Agilent, Taufkirchen, Germany). Preparation of samples for sequencing was performed with TruSeq®RNA Sample Pre Kit v2 (mRNA) and TruSeq® Small RNA Sample Prep Kit (miRNA) (Illumina, USA). Samples were sequenced on Illumina HiSeq2500 platform using Rapid Run Mode (62 cycles/library) resulting in 7 – 10 million reads per sample. The software FastQC served as quality control for sequencing (www.bioinformatics.babraham.ac.uk/projects). Cutadapt (41), spliced transcripts alignment to a reference (STAR) (42) and HTSeq-count (43) were used to prepare the received NGS data for differential gene expression analysis. CHO K1 genome and miRNA data for *Cricetulus griseus* (www.chogenome.org, miRBase (release 21)) functioned as references for STAR.

2.7 Software and Tools

RStudio (version 0.98.1103, R version 3.2.1) was used predominantly for data analysis and visualization. Differential gene expression analysis was performed with the package edgeR (version 3.10.2) (44). Negative binomial generalized linear model (GLM) method in combination with tagwise dispersion estimation was applied for differential expression analysis. Genes were defined as significantly up- or downregulated if they showed a log2-fold change $\geqslant |1|$ and passed the GLM likelihood ratio test with a P value $\leqslant 0.02$ and a false discovery rate (FDR) $\leqslant 0.02$. VennDiagram (version 1.6.9) was used for visualization. Gene expression dynamics were analyzed with maSigPro (version 1.40.0) (45,46). GO-enrichment analyses were performed with GOrilla (47) and MGI Gene Ontology Term Finder (www.informatics.jax.org).

3 Results

3.1 Changes in cell growth, metabolism and product formation

Hyperosmotic culture conditions ($\geqslant 350$ mOsmol kg^{-1}) can easily be induced by the addition of common salts like NaCl. Consequently this trigger is typically applied in related studies.

Accordingly, NaCl was as well used to increase osmolality during batch cultivations of an antibody producing CHO DP-12 cell line in this study. NaCl enriched medium was added to four of seven cultures 35 h after inoculation (Figure 1).
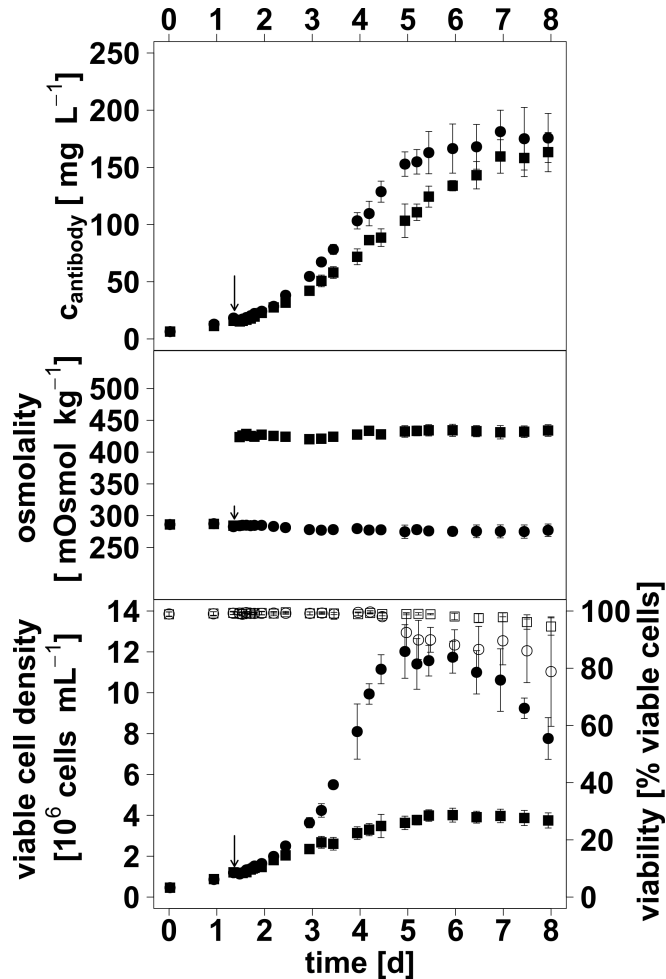
Figure 1. Time courses for antibody titer, osmolality, viable cell density and viability. Osmolality was increased by the addition of NaCl during batch cultivations of CHO DP-12 (arrow). Viable cell density (■ ●) and viability (○ □) were analyzed by Cedex XS, osmolality was determined with Osmomat 030 antibody titers were analyzed by ELISA. Error bars represent standard deviations for four (hyperosmolal, ■ □) or three biological replicates (reference, ● ○) also considering the technical error of measurements (n=3). Osmotic shift induced significantly higher osmolalities on day 1.5 − 8 (student's t-test, P-value < 0.001), a significantly lower viable cell density on day 2.5 - 8 (student's t-test, P value < 0.001) and a significantly higher viability on day 5 − 6.5 (student's t-test, P-value < 0.001).

Osmolality was increased from ∼ 280 mOsmol kg^{-1} (reference condition) to ∼ 430 mOsmol kg^{-1} resulting in a significant difference (P < 0.001) of ∼ 150 mOsmol kg^{-1} (Figure 1). During the first time

interval (day 1.5 to 2.5), specific growth rate (μ) was slightly lowered (0.60 $\pm$ 0.03 vs. 0.68 $\pm$ 0.03 d^{-1}) and lead to a significant difference in viable cell density (VCD) on day 2.5 (P < 0.001) (Figure 1).

From day 3 to 4 μ decreased even further to 0.26 $\pm$ 0.04 d^{-1} compared to 0.83 $\pm$ 0.08 d^{-1} for reference cultures. Starting on day 2.5, hyperosmotic cultures showed significantly lower VCD (P < 0.001) reaching a maximal VCD of 4.01 $\pm$ 0.34 x 10^6 cells mL^{-1} compared to 12.02 $\pm$ 1.31 x 10^6 cells mL^{-1} (Figure 1). As glucose concentrations reached limiting levels on day 5, reference cultures entered a phase of declining viability and VCD whereas the viability of hyperosmotically stressed cells was not affected at all (Figure 1).

Analysis of product formation rate (q_p) revealed no significant difference during the first 24 h after osmotic shift. Thereafter hyperosmolality resulted in a $\sim$1.6-fold higher q_p (12.98 $\pm$ 0.18 vs. 8.05 $\pm$ 0.85 pg cell^{-1} d^{-1}) and a comparable final antibody titer of 163 $\pm$ 17 mg L^{-1} compared to 176 $\pm$ 21 mg L^{-1} for reference cultures (Figure 1). Specific metabolite formation rates (q) did not significantly differ during time interval day 1.5 − 2.5 (Supporting Information Table I). From day 3 to 4, hyperosmotically stressed cells showed increased consumption of glucose (2.52 $\pm$ 0.35 vs. 1.61 $\pm$ 0.10 pmol cell^{-1} d^{-1}, P-value < 0.05) and production of lactate (2.80 $\pm$ 0.77 vs 1.18 $\pm$ 0.19 pmol cell^{-1} d^{-1}, P-value < 0.07). In the same interval, $q_{asparagine}$ and $q_{glutamate}$ were not affected by culture conditions whereas hyperosmotically stressed cells consumed less glutamine than reference cells (Supporting Information Table I).

3.2 Hyperosmotic stress causes an increase in mitochondrial and cytosolic adenine nucleotide pools

In previous studies, intracellular ATP-contents and q_{ATP} of CHO DP-12 cells increased after an osmotic shift from $\sim$290 to $\sim$390 mOsmol kg^{-1} on day 3 of cultivation (34). This study focused on the effects of an 1.5 d earlier and higher increase in osmolality ($\sim$280 to 430 mOsmol kg^{-1}) applying a compartment-specific approach to analyze the distribution of adenine nucleotide pools in the cell.

Starting from comparable cytosolic (2.7 fmol cell^{-1}) or mitochondrial (0.20 fmol cell^{-1}) pool sizes, cytosolic ATP-content (ATP$_{cyt}$) of hyperosmotic cultures increased (3.7 fmol cell^{-1}) while mitochondrial ATP-content (ATP$_{mit}$) did not change significantly (Figure 2).
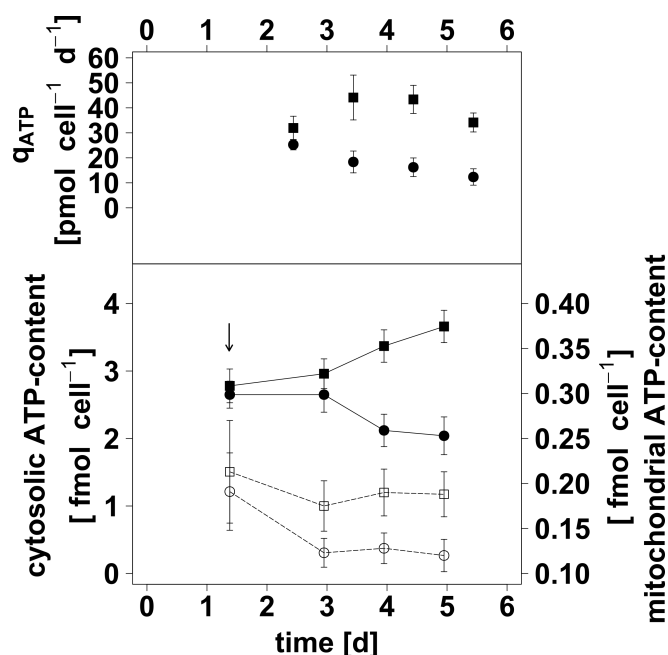
Figure 2. Effect of hyperosmolality on cytosolic (■ ●) and mitochondrial (○ □) ATP-content and q_{ATP}. Osmolality was increased by addition of NaCl (arrow) resulting in an osmolality of ~430 mOsmol kg^{-1} (■, □) compared to ~280 mOsmol kg^{-1} (●, ○) for reference cultivations. Cell sampling was performed by a compartment-specific fast filtration approach and intra- and subcellular metabolites were extracted by methanol/chloroform treatment. ATP was quantified by RP-HPLC. ATP data were corrected for sampling efficiency based on measurement of *cis*-aconitate (mitochondrial marker metabolite), glucose-6-phosphate and fructose-6-phosphate (cytosolic marker metabolite) using LC-IDMS method. q_{ATP} was calculated according to equation 8 (Supporting Information) with an assumed P/O ratio of 2.5 (42,43). Error bars represent standard deviations for three biological replicates considering the technical errors (n=3) by Gaussian error propagation. Student's t-test revealed significantly higher ATP$_{mit}$ (P-Value < 0.05) and ATP$_{cyt}$ (P-Value < 0.001) on days 4 and 5 for hyperosmotically stressed cells.

Due to decreasing ATP$_{cyt}$ and ATP$_{mit}$ of cells grown under reference conditions, hyperosmolality resulted in significantly higher ATP$_{cyt}$ (P < 0.001) and ATP$_{mit}$ (P < 0.05) on day 4 and 5 of cultivation. Comparable results were received for ADP (Supporting Information Figure 1) while AMP levels were frequently below the reliable detection limit. Noteworthy, the determined intracellular ATP-concentrations of hyperosmotically stressed cells were also increased compared to reference cells (Supporting Information Figure 2).

Analysis of subcellular distribution of adenine nucleotides revealed $13-20$-fold lower values for ATP_{mit} than for ATP_{cyt} (Table 1). In addition, ATP_{mit}/ADP_{mit}-ratios were $3-5$-fold smaller than cytosolic ratios (Table 1). Subcellular distributions of adenine nucleotides of hyperosmotically stressed cells did not significantly differ from reference cells. Before and after osmotic shift, physiological adenylate energy charges (AEC) were calculated for both conditions (AEC $\pm$ 0.9). AEC was not affected by osmotic shift and remained at levels of 0.97 $\pm$ 0.01 for cytosol or 0.90 $\pm$ 0.02 for mitochondrial compartment (Supporting Information Figure 3). AEC_{mit} were significantly lower than AEC_{cyt} (P-value < 0.05).

Table 1. Cytosolic and mitochondrial ratios for adenine nucleotides.

t [d]	reference	hyperosmolal	reference		hyperosmolal	
	ATP_{cyt}/ATP_{mit}		ATP/ADP_{mit}	ATP/ADP_{cyt}	ATP/ADP_{mit}	ATP/ADP_{cyt}
1.5	13.9 $\pm$ 1.0	13.1 $\pm$ 1.2	4.2 $\pm$ 1.2	12.4 $\pm$ 2.7	4.4 $\pm$ 1.6	13.1 $\pm$ 4.3
3.0	21.6 $\pm$ 2.1	16.9 $\pm$ 1.3	3.8 $\pm$ 1.2	17.2 $\pm$ 4.0	3.8 $\pm$ 1.1	14.4 $\pm$ 2.6
4.0	16.6 $\pm$ 1.9	17.7 $\pm$ 1.3	4.3 $\pm$ 0.8	16.5 $\pm$ 4.6	3.5 $\pm$ 0.7	14.3 $\pm$ 2.1
5.0	17.0 $\pm$ 2.3	19.5 $\pm$ 1.3	4.2 $\pm$ 1.0	15.9 $\pm$ 3.1	3.4 $\pm$ 0.7	11.7 $\pm$ 3.8

3.3 Correlations between gene expression dynamics and functional annotation of DEGs

Changes in mRNA expression were investigated directly before (0) and 2, 4, 6 and 8 h after osmotic shift from $\sim$ 280 to $\sim$ 430mOsmol kg^{-1}. In addition, miRNA expression was analyzed directly before (0) and at time points 4 and 8 h after increase in osmolality. While no differentially expressed genes (DEG, P-value $\leqslant$ 0.02, FDR $\leqslant$ 0.02) were identified directly before osmotic shift, hyperosmotic conditions induced dynamic changes in gene expression which were illustrated by Venn diagrams and maSigPro clusters (Figure 3AB, Supporting Information Table II).
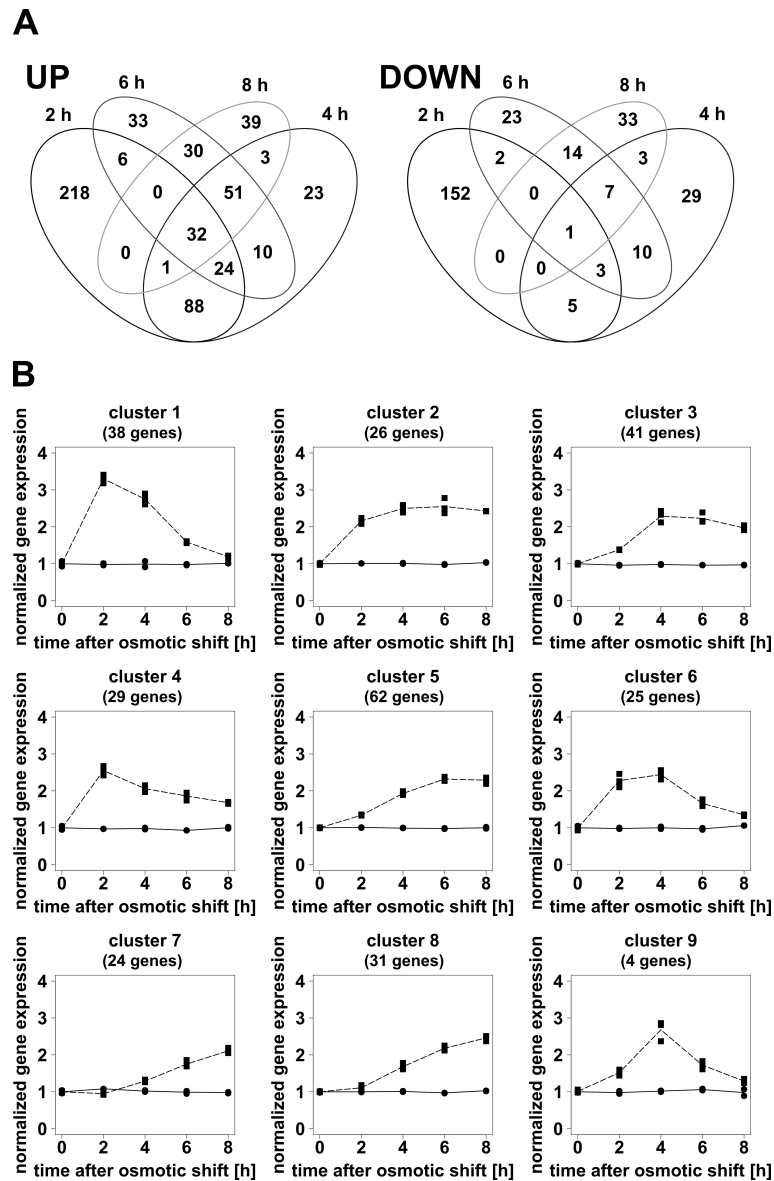
Figure 3. A: Venn diagrams for up- and downregulated genes with respect to the exposure period after hyperosmotic shift. Osmotic shift was performed by addition of NaCl ~35 h after inoculation of CHO DP-12 batch cultures. Gene expression analysis based on next generation sequencing (NGS) data was performed directly before, as well as 2, 4, 6 and 8 h after osmotic shift. NGS data were analyzed with edgeR package in order to identify significantly differentially expressed genes (P-value and FDR $\leqslant$ 0.02, log2(fold-change) $\geqslant |1|$). **B:** Clusters of gene expression dynamics of upregulated genes. Genes which were upregulated at some time point after increase in osmolality from ~280 to ~430 mOsmol kg^{-1} were analyzed with R package maSigPro and hierarchically clustered (n = 9).

About 40% of upregulated and 54% of downregulated genes were exclusively significantly differentially expressed 2 h after osmotic shift (Figure 3A). The remaining genes showed different expression dynamics with 32 genes being significantly upregulated and only one gene (*EGR1*) being significantly downregulated over the whole time of analysis. Gene ontology (GO) enrichment analysis for identified groups and clusters showed little relation between gene expression dynamics and annotation of genes to a specific biological process. Only four groups of the Venn diagram for upregulated genes as well as cluster 3 of maSigPro analysis encompassed genes enriched in specific biological processes (Supporting Information Table III). These biological processes were "cell surface receptor signaling", "negative regulation of cellular metabolic process", "cell adhesion", "cation transport" and "regulation of programmed cell death" (Supporting Information Table III). Several genes encoding Na^+-transporting proteins (*ATP1B1*, *SLC28A1*, *SLC5A3* and *SLC6A13*) were part of the GO-category "cation transport" and belonged to cluster 5 or 8. This response to elevated Na^+-concentrations due to osmotic shift was a delayed one which enhanced gradually (Supporting Information Table III, Figure 3B). "Negative regulation of cellular metabolic process" was an immediate and long term effect of hyperosmolality with almost half of the genes showing dynamics of cluster 2 and the rest of genes being distributed on clusters 3, 4 and 5 (Supporting Information Table III, Figure 3B). One of the genes of this GO-category was CDK1A which encodes the G1-phase arrest mediating cyclin dependent kinase inhibitor protein 1A (p21) (48,49). Genes of cell surface receptor signaling were characterized by an immediate upregulation ($\leqslant$ 2 h) and a following decline in expression level (Supporting Information Table IV).

In addition to the upregulated genes of the aforementioned biological processes, hyperosmolality induced as well upregulation of genes encoding proteins with tissue related function *IL15*, *MUC2*, *NEB*, *OVGP1* and *TTN* are exemplary genes with a short time of response and significantly upregulated expression levels over a time of at least 6 h.

3.4 Hyperosmotic stimulus induces upregulation of 7 miRNAs

The analysis of miRNA expression revealed 7 miRNAs (miR-132-3p, miR-132-5p, miR-182, miR-183, miR-194, miR-215-3p, miR-215-5p) that were significantly upregulated in hyperosmotically stressed cells

(Table 2). Four hours after osmotic shift, miRNA expression levels were more than 2.5-fold higher compared to reference cells. After another four hour time interval, a decrease in differential expression of miR-182 (-7%), miR-183 (-13%), miR-215-5p (-13%), miR194 (-19%) and miR-215-3p (-43%) was determined. In contrast, the differential expression of miR-132-3p stayed constant, while the osmotically induced upregulation of miR-132-5p increased by 23% (Table 2).

Table 2. Significantly upregulated miRNAs (P-value $\leqslant$ 0.02, FDR $\leqslant$ 0.02).

miRNA	fold change	
	4 h	8 h
cgr-miR-132-3p	4.0	4.0
cgr-miR-132-5p	2.5	3.0
cgr-miR-182	5.3	4.9
cgr-miR-183	2.5	2.1
cgr-miR-194	4.9	4.0
cgr-miR-215-3p	4.9	2.8
cgr-miR-215-5p	5.7	4.9

4 Discussion

4.1 CHO DP-12 cells show well-known hyperosmotic effects regarding cell growth and metabolism

Hyperosmotically stressed cells showed mainly the same characteristics as described in previous independent studies (6–8,34,9). Cell growth was most likely influenced by arrest of CHO DP-12 cells in G1-phase of cell cycle which had been detected in preliminary experiments (data not shown) as well as for a different experimental setup (34) or cell line (7). Although Shen et al. described an increased $q_{glutamine}$ for hyperosmotically stressed cells, CHO DP-12 showed a contrary effect. This might be due to the fact that CHO DP-12 cells consume asparagine as well in a non-neglectable manner.

Summarizing, the experimental setup provided appropriate conditions for further investigations concerning adenine nucleotide pools and gene expression dynamics.

4.2 Hyperosmotic stress provides a surplus in ATP supply

Previous independent studies (50,51) described acute cell shrinkage upon hyperosmotic shift followed by an increase in cell volume which commonly exceeded the pre-shift state. This cellular process of regulatory volume increase (RVI) was shown to be induce by activation of e. g. Na^+/K^+-ATPase, Na^+/H^+ exchange or the uptake of other electrolytes (50). RVI as a putative reason for increased ATP-content was rejected as hyperosmotically stressed cells showed as well increased c_{ATP} (Supporting Information Figure 2) and $36-41\%$ higher q_{ATP} (Figure 2) which outweighed by far the required amount of ATP to compensate RVI. In general values for intracellular ATP-contents were in agreement with previous findings (33,34,52,53). Noteworthy the possibility to distinguish between mitochondrial and cytosolic pools significantly refines our understanding of cellular energy management. In accordance with previous independent studies for rat liver or heart myocytes ATP_{mit} and ATP_{mit}/ADP_{mit}-ratios were lower than in cytosol highlighting the conservation and importance of the cellular distribution of adenine nucleotides (33,54–56). In addition, significantly lower AEC_{mit} than AEC_{cyt} were in agreement with independent measurements for CHO batch cultures without hyperosmotic stress (33).

While hyperosmotic culture conditions increased subcellular ATP and ADP pool sizes the subcellular distribution of ATP and ADP (ATP_{cyt}/ATP_{mit}, ATP/ADP, AEC) was not affected. This finding may reflect the cellular strategy with mitochondria serving as ATP provider quickly secreting ATP to the spots of consumption which are inside the cytosol. Consequently, it seems likely that ATP sensors which are incorporated in cellular regulation are located in the cytosol and not in mitochondria.

4.3 Conserved gene expression changes among mammalian and CHO cells

In comparison to a summarized list of genes and proteins associated with the response of mammalian cells to hyperosmolality (57) CHO DP-12 cells showed equal expression patterns for eight genes: *AQP1, SLC38A2, SLC6A6, ATP1B1, NFAT5, CRYAB, HSP110* and *HSPA4L*, comprising the categories channels, transporters, transcription factors and chaperones, were upregulated due to hyperosmolality (57). Further, differential changes in the expression of 57 genes (Supporting Information Table V) were in agreement with the microarray based transcriptomic studies of Shen et al., thus revealing CHO specific changes upon hyperosmotic treatment (8). Nevertheless only 16 of the aforementioned 57 genes

passed the threshold for DEGs and may therefore serve as CHO specific expression markers for NaCl-induced hyperosmolality. As microarray based expression studies consider a limited number of genes, future NGS studies may reveal higher numbers of conserved gene expression changes for hyperosmotically stressed CHO cells.

4.4 Identification of suitable mRNA targets to enhance q_p

EdgeR and maSigPro analysis revealed that even common changes in culture conditions like hyperosmolality resulted in a diversity of gene expression dynamics (Figure 3) not necessarily confirming the gene affiliation to a specific biological process (Supporting Information Table III). Genes showing immediate gene expression response might be more relevant for cell line engineering as these genes are most likely members of the early stress response and may as well be sensors, regulators or inducers of subsequent stress response pathways. In fact the majority of DEGs at time point 2 h after osmotic shift were related to cell surface receptor signaling. To the group of genes showing early and long term response ($\geqslant 6$ h) belonged several genes encoding proteins which seemed to have a dispensable function in suspension growing cells. *MUC2* and *OVGP1* encode heavily O-glycosylated ($> 50\%$) secretory proteins which form epithelial mucin layers to protect cells e. g. from microbial attack (58,59). The cultivation of CHO cells in suspension in stirred tank bioreactors most likely prevents the formation of this protecting mucin layer but nevertheless cells seem to spend a great amount of energy to synthesize large glycoproteins like *MUC2* (~ 5100 amino acids) (58). As the formation of one peptide bond was declared to require at least 3 molecules of ATP (28), about 15,300 mol ATP are consumed for the synthesis of 1 mol of MUC2 compared to 3,957 mol ATP for 1 mol of IgG1 antibody (~ 1320 amino acids). Hence the performance of industrial mAB producing cell lines, which is supposed to be much more ATP challenging than the one of the DP-12 cells of our study, might be hampered by this ATP consuming but dispensable expression of genes/proteins. Following the mindset and findings for microbial producers, genome reduction may enable an overall improvement in performance (29–31). Therefore the deletion of *MUC2* and *OVGP1* may potentially enhance the productivity of recombinant CHO cells. In addition, interleukin 15 which stimulates proliferation and differentiation of cells of the immune system and components of the

muscle sarcomere (*NEB*, *TTN*), may also be potential targets for genome reduction (60–62). Another gene of early and long term response was *CDK1A*. In previous independent studies hyperosmolality was shown to activate p53, the transcriptional activator of *CDK1A* encoding a protein that inhibits cyclin dependent kinase 2 and 4 (CDK4) thus inducing G1-phase arrest (48,49). Nevertheless, the expression of p53 and several related protein kinases, e. g. ATM, CHK1/2, did not change significantly in this study which might be due to a steady expression to realize a quick activation by phosphorylation if required (49). In contrast the gene encoding cyclin D1 (*CCND1*) which commonly binds and activates CDK4 was significantly downregulated 4 h after osmotic shift. Overexpression of *CDK1A* has already been applied as cell cycle engineering target to enhance q_p of recombinant CHO cells (63,64).

4.5 Linkage between upregulated miRNAs, cell cycle arrest and increase in q_p

Recent miRNA studies commonly enhanced q_p of recombinant CHO cells by stable overexpression of miRNAs (cgr-miR-17, cgr-miR-19b, cgr-miR-20a, cgr-miR-92a, cgr-miR-2861, mmu-miR-30 family members, hsa-miR-7, hsa-miR1287, hsa-miR-557) (65–70). In this context miR-7 and miR-30 had a negative impact on cell growth (66,69). Kelly et al. (2015) depleted miR-23 in recombinant CHO cells, thus increasing mitochondrial activity and q_p (71). Druz et al. (2013) improved apoptosis resistance and productivity of CHO cells by stable inhibition of mmu-miR-466-5p (72).

None of the seven significantly upregulated miRNAs (Table 2) was among the previously mentioned q_p enhancing miRNA targets of independent studies. Furthermore none of the significantly differently expressed miRNAs of this study was among the miRNAs related to low cultivation temperature, cell growth rate, histone deacetylase inhibition, or osmoregulation of mouse collecting duct epithelial cells (25,26,68,73,74). Surprisingly, all seven differentially expressed miRNAs were frequently shown to be involved in cell proliferation and p53 mediated tumor suppression in cancer cells (75–85). p53 was described to induce the expression of miR-194 and miR-215, which in turn were reported to be positive regulators of p53 (77–80). An either oncogenic or tumor suppressive role in cancer cells was reported for miR-132, miR-183 and miR-182 (75,76,81–85). Overexpression of miR-132, miR-194 and miR-215 resulted in a p53/CDK1A mediated cell cycle arrest in G1-phase (75,77,78,81). Increased product titers and enhanced q_p in combination with a decrease in cell growth was reported

for recombinant CHO cell lines which had transiently been transfected with human miR-183 (70). *EGR1* encoding the early growth response protein 1 was significantly downregulated at all analyzed time points after osmotic shift and was described to be involved in G1/S transition of cell cycle (86–89). Sarver et al. (2010) validated EGR1 as a target of miR-183 by luciferase reporter assay in different tumor cell lines (76). On basis of the research of Sarver et al. (2010) and Strotbek et al. (2013), one could wonder whether EGR1 may potentially be a target of miR-183 in CHO DP-12 as well and whether they might be involved in regulation or induction of G1-phase arrest, thus resulting in enhanced q_p (70,76). Nevertheless further experiments, e. g. luciferase reporter assay, have to validate these hypotheses.

4.6 Concluding remarks

In conclusion, we were able to show that hyperosmolality elevated qATP, thus resulting in increased cytosolic and mitochondrial adenine nucleotide pools while ATP/ADP-ratios remained constant. Our findings support the hypothesis that increased ATP-content together with deceleration of cell growth provides a surplus in ATP supply which may be used to boost productivity.

The immediate and long term upregulation of *MUC2*, *OVGP1*, *TTN* and *NEB* seemed to be a dispensable but energy consuming stress response for suspension growing cells. Therefore these genes might be ideal candidates for genomic deletion thus reducing the CHO genome in order to enhance productivity as it has already been shown for microorganisms (29–31). Further the significant upregulation of *CDK1A* in osmotically stressed CHO cells together with G1-phase arrest, increased q_{ATP} and enhanced q_p may elucidate *CDK1A*'s q_p enhancing role that had been described in previous cell cycle engineering studies (63,64). Overexpression of miR-132, miR-194 and miR-215 may potentially enhance as this was shown to induce p53/CDK1A(p21) mediated cell cycle arrest in G1-phase (75,77,78,81), these miRNAs may potentially be targets to enhance q_p by cell cycle engineering. The hypothesized regulatory connection between miR-183, EGR1 and cell cycle arrest together with the q_p enhancing effect described by Strotbek et al. (2013) give point to miR-183 as the most promising candidate for subsequent cell line engineering studies.

5 References

(1) Walsh, G., Biopharmaceutical benchmarks 2010. Nat. Biotechnol. 2010, 28, 917–924.

(2) Walsh, G., Biopharmaceutical benchmarks 2014. Nat. Biotechnol. 2014, 32, 992–1000.

(3) Schaub, J., Clemens, C., Kaufmann, H., Schulz, T.W., Advancing biopharmaceutical process development by system-level data analysis and integration of omics data. Adv. Biochem. Eng. Biotechnol. 2012, 127, 133–163.

(4) Wurm, F.M., Production of recombinant protein therapeutics in cultivated mammalian cells. Nat. Biotechnol. 2004, 22, 1393–1398.

(5) Han, Y.K., Kim, Y.G., Kim, J.Y., Lee, G.M., Hyperosmotic stress induces autophagy and apoptosis in recombinant Chinese hamster ovary cell culture. Biotechnol. Bioeng. 2010, 105, 1187–1192.

(6) Ryu, J.S., Kim, T.K., Chung, J.Y., Lee, G.M., Osmoprotective effect of glycine betaine on foreign protein production in hyperosmotic recombinant Chinese hamster ovary cell cultures differs among cell lines. Biotechnol. Bioeng. 2000, 70, 167–175.

(7) Ryu, J.S., Lee, M.S., Lee, G.M., Effects of cloned gene dosage on the response of recombinant CHO cells to hyperosmotic pressure in regard to cell growth and antibody production. Biotechnol. Prog. 2001, 17, 993–999.

(8) Shen, D., Kiehl, T.R., Khattak, S.F., Li, Z.J., et al., Transcriptomic responses to sodium chloride-induced osmotic stress: a study of industrial fed-batch CHO cell cultures. Biotechnol. Prog. 2010, 26, 1104–1115.

(9) Lee, M.S., Kim, K.W., Kim, Y.H., Lee, G.M., Proteome analysis of antibody-expressing CHO cells in response to hyperosmotic pressure. Biotechnol. Prog. 2003, 19, 1734–1741.

(10) Xu, X., Nagarajan, H., Lewis, N.E., Pan, S., et al., The genomic sequence of the Chinese hamster ovary (CHO)-K1 cell line. Nat. Biotechnol. 2011, 29, 735–741.

(11) Baik, J.Y., Lee, M.S., An, S.R., Yoon, S.K., et al., Initial transcriptome and proteome analyses of low culture temperature-induced expression in CHO cells producing erythropoietin. Biotechnol. Bioeng. 2006, 93, 361–371.

(12) Ernst, W., Trummer, E., Mead, J., Bessant, C., et al., Evaluation of a genomics platform for cross-species transcriptome analysis of recombinant CHO cells. Biotechnol. J. 2006, 1, 639–650.

(13) Yee, J.C., Wlaschin, K.F., Chuah, S.H., Nissom, P.M., Hu, W.S., Quality assessment of cross-species hybridization of CHO transcriptome on a mouse DNA oligo microarray. Biotechnol. Bioeng. 2008, 101, 1359–1365.

(14) Wlaschin, K.F., Nissom, P.M., Gatti Mde, L., Ong, P.F., et al., EST sequencing for gene discovery in Chinese hamster ovary cells. Biotechnol. Bioeng. 2005, 91, 592–606.

(15) Bahr, S.M., Borgschulte, T., Kayser, K.J., Lin, N., Using microarray technology to select housekeeping genes in Chinese hamster ovary cells. Biotechnol. Bioeng. 2009, 104, 1041–1046.

(16) Melville, M., Doolan, P., Mounts, W., Barron, N., et al., Development and characterization of a Chinese hamster ovary cell-specific oligonucleotide microarray. Biotechnol. Lett. 2011, 33, 1773–1779.

(17) Kantardjieff, A., Nissom, P.M., Chuah, S.H., Yusufi, F., et al., Developing genomic platforms for Chinese hamster ovary cells. Biotechnol. Adv. 2009, 27, 1028–1035.

(18) Schaub, J., Clemens, C., Schorn, P., Hildebrandt, T., et al., CHO gene expression profiling in biopharmaceutical process analysis and design. Biotechnol. Bioeng. 2010, 105, 431–438.

(19) Yee, J.C., Gerdtzen, Z.P., Hu, W.S., Comparative transcriptome analysis to unveil genes affecting recombinant protein productivity in mammalian cells. Biotechnol. Bioeng. 2009, 102, 246–263.

(20) Yee, J.C., de Leon Gatti, M., Philp, R.J., Yap, M., Hu, W.S., Genomic and proteomic exploration of CHO and hybridoma cells under sodium butyrate treatment. Biotechnol. Bioeng. 2008, 99, 1186–1204.

(21) Clarke, C., Doolan, P., Barron, N., Meleady, P., et al., Large scale microarray profiling and coexpression network analysis of CHO cells identifies transcriptional modules associated with growth and productivity. J. Biotechnol. 2011, 155, 350–359.

(22) Doolan, P., Clarke, C., Kinsella, P., Breen, L., et al., Transcriptomic analysis of clonal growth rate variation during CHO cell line development. J. Biotechnol. 2013, 166, 105–113.

(23) Wong, D.C., Wong, K.T., Lee, Y.Y., Morin, P.N., et al., Transcriptional profiling of apoptotic pathways in batch and fed-batch CHO cell cultures. Biotechnol. Bioeng. 2006, 94, 373–382.

(24) Druz, A., Chu, C., Majors, B., Santuary, R., et al., A novel microRNA mmu-miR-466h affects apoptosis regulation in mammalian cells. Biotechnol. Bioeng. 2011, 108, 1651–1661.

(25) Gammell, P., Barron, N., Kumar, N., Clynes, M., Initial identification of low temperature and culture stage induction of miRNA expression in suspension CHO-K1 cells. J. Biotechnol. 2007, 130, 213–218.

(26) Clarke, C., Henry, M., Doolan, P., Kelly, S., et al., Integrated miRNA, mRNA and protein expression analysis reveals the role of post-transcriptional regulation in controlling CHO cell growth rate. BMC Genomics 2012, 13, 1–14.

(27) Hara, K.Y., Kondo, A., ATP regulation in bioproduction. Microb. Cell Fact. 2015, 14, 198.

(28) Seth, G., Hossler, P., Yee, J.C., Hu, W.S., Engineering cells for cell culture bioprocessing–physiological fundamentals. Adv. Biochem. Eng. Biotechnol. 2006, 101, 119–164.

(29) Lieder, S., Nikel, P.I., de Lorenzo, V., Takors, R., Genome reduction boosts heterologous gene expression in Pseudomonas putida. Microb. Cell Fact. 2015, 14, 1–14.

(30) Mizoguchi, H., Mori, H., Fujio, T., Escherichia coli minimum genome factory. Biotechnol. Appl. Biochem. 2007, 46, 157–167.

(31) Sauer, M., Mattanovich, D., Construction of microbial cell factories for industrial bioprocesses. J. Chem. Technol. Biotechnol. 2012, 87, 445–450.

(32) Kim, J.Y., Kim, Y.G., Lee, G.M., CHO cells in biotechnology for production of recombinant proteins: current state and further potential. Appl. Microbiol. Biotechnol. 2012, 93, 917–930.

(33) Matuszczyk, J.-C., Teleki, A., Pfizenmaier, J., Takors, R., Compartment-specific metabolomics for CHO reveals that ATP pools in mitochondria are much lower than in cytosol. Biotechnol. J. 2015, 10, 1639–1650.

(34) Pfizenmaier, J., Matuszczyk, J.-C., Takors, R., Changes in Intracellular ATP-Content of CHO Cells as Response

to Hyperosmolality. Biotechnol. Prog. 2015, 31, 1212–1216.

(35) Buchholz, J., Schwentner, A., Brunnenkan, B., Gabris, C., et al., Platform engineering of Corynebacterium glutamicum with reduced pyruvate dehydrogenase complex activity for improved production of L-lysine, L-valine, and 2-ketoisovalerate. Appl. Env. Microbiol. 2013, 79, 5566–5575.

(36) Teleki, A., Sanchez-Kopper, A., Takors, R., Alkaline conditions in hydrophilic interaction liquid chromatography for intracellular metabolite quantification using tandem mass spectrometry. Anal Biochem 2015, 475, 4–13.

(37) Vielhauer, O., Zakhartsev, M., Horn, T., Takors, R., Reuss, M., Simplified absolute metabolite quantification by gas chromatography-isotope dilution mass spectrometry on the basis of commercially available source material. J. Chromatogr. B Anal. Technol. Biomed. Life Sci. 2011, 879, 3859–3870.

(38) Atkinson, D.E., Walton, G.M., Adenosine triphosphate conservation in metabolic regulation. Rat liver citrate cleavage enzyme. J. Biol. Chem. 1967, 242, 3239–3241.

(39) Balcarcel, R.R., Clark, L.M., Metabolic screening of mammalian cell cultures using well-plates. Biotechnol. Prog. 2003, 19, 98–108.

(40) Hinkle, P.C., P/O ratios of mitochondrial oxidative phosphorylation. Biochim. Biophys. Acta 2005, 1706, 1–11.

(41) Martin, M., Cutadapt removes adapter sequences from high-throughput sequencing reads. EMBnet.journal 2011, 17, 10–12.

(42) Dobin, A., Davis, C.A., Schlesinger, F., Drenkow, J., et al., STAR: Ultrafast universal RNA-seq aligner. Bioinformatics 2013, 29, 15–21.

(43) Anders, S., Pyl, P.T., Huber, W., HTSeq - A Python framework to work with high-throughput sequencing data. Bioinformatics 2014, 31, 166–169.

(44) Robinson, M.D., McCarthy, D.J., Smyth, G.K., edgeR: a Bioconductor package for differential expression analysis of digital gene expression data. Bioinformatics 2010, 26, 139–140.

(45) Nueda, M.J., Tarazona, S., Conesa, A., Next maSigPro: updating maSigPro bioconductor package for RNA-seq time series. Bioinformatics 2014, 30, 2598–2602.

(46) Conesa, A., Nueda, M.J., Ferrer, A., Talón, M., maSigPro: A method to identify significantly differential expression profiles in time-course microarray experiments. Bioinformatics 2006, 22, 1096–1102.

(47) Eden, E., Navon, R., Steinfeld, I., Lipson, D., Yakhini, Z., GOrilla: a tool for discovery and visualization of enriched GO terms in ranked gene lists. BMC Bioinformatics 2009, 10, 48.

(48) He, G., Siddik, Z.H., Huang, Z., Wang, R., et al., Induction of p21 by p53 following DNA damage inhibits both Cdk4 and Cdk2 activities. Oncogene 2005, 24, 2929–2943.

(49) Poon, R.Y.C., Cell Cycle Control: A System of Interlinking Oscillators. Methods Mol. Biol. 2016, 1342, 3–19.

(50) Schliess, F., Reinehr, R., Häussinger, D., Osmosensing and signaling in the regulation of mammalian cell

function. FEBS J. 2007, 274, 5799–803.

(51) Kiehl, T.R., Shen, D., Khattak, S.F., Jian Li, Z., Sharfstein, S.T., Observations of cell size dynamics under osmotic stress. Cytom. A 2011, 79, 560–569.

(52) Volmer, M., Northoff, S., Scholz, S., Thute, T., et al., Fast filtration for metabolome sampling of suspended animal cells. Biotechnol. Lett. 2011, 33, 495–502.

(53) Dietmair, S., Timmins, N.E., Gray, P.P., Nielsen, L.K., Kromer, J.O., Towards quantitative metabolomics of mammalian cells: development of a metabolite extraction protocol. Anal. Biochem. 2010, 404, 155–164.

(54) Schwenke, W.D., Soboll, S., Seitz, H.J., Sies, H., Mitochondrial and cytosolic ATP/ADP ratios in rat liver in vivo. Biochem. J. 1981, 200, 405–408.

(55) Soboll, S., Scholz, R., Heldt, H.W., Subcellular metabolite concentrations. Dependence of mitochondrial and cytosolic ATP systems on the metabolic state of perfused rat liver. Eur. J. Biochem. 1978, 87, 377–390.

(56) Geisbuhler, T., Altschuld, R.A., Trewyn, R.W., Ansel, A.Z., et al., Adenine nucleotide metabolism and compartmentalization in isolated adult rat heart cells. Circ. Res. 1984, 54, 536–546.

(57) Burg, M.B., Ferraris, J.D., Dmitrieva, N.I., Cellular response to hyperosmotic stresses. Physiol. Rev. 2007, 87, 1441–1474.

(58) Lagow, E., DeSouza, M.M., Carson, D.D., Mammalian reproductive tract mucins. Hum. Reprod. Update 1999, 5, 280–292.

(59) Hollingsworth, M.A., Swanson, B.J., Mucins in cancer: protection and control of the cell surface. Nat. Rev. Cancer 2004, 4, 45–60.

(60) Trinick, J., Titin and nebulin: Protein rulers in muscle? Trends Biochem. Sci. 1994, 19, 405–409.

(61) Pappas, C.T., Bliss, K.T., Zieseniss, A., Gregorio, C.C., The Nebulin family: An actin support group. Trends Cell Biol. 2011, 21, 29–37.

(62) Waldmann, T.A., The biology of interleukin-2 and interleukin-15: implications for cancer therapy and vaccine design. Nat. Rev. Immunol. 2006, 6, 595–601.

(63) Fussenegger, M., Schlatter, S., Dätwyler, D., Mazur, X., Bailey, J.E., Controlled proliferation by multigene metabolic engineering enhances the productivity of Chinese hamster ovary cells. Nat. Biotechnol. 1998, 16, 468–472.

(64) Bi, J.-X., Shuttleworth, J., Al-Rubeai, M., Uncoupling of cell growth and proliferation results in enhancement of productivity in p21CIP1-arrested CHO cells. Biotechnol. Bioeng. 2004, 85, 741–749.

(65) Loh, W.P., Loo, B., Zhou, L., Zhang, P., et al., Overexpression of microRNAs enhances recombinant protein production in Chinese hamster ovary cells. Biotechnol. J. 2014, 9, 1140–1151.

(66) Fischer, S., Mathias, S., Schaz, S., Emmerling, V.V., et al., Enhanced protein production by microRNA-30 family in CHO cells is mediated by the modulation of the ubiquitin pathway. J. Biotechnol. 2015, 212, 32–43.

(67) Jadhav, V., Hackl, M., Klanert, G., Hernandez Bort, J.A., et al., Stable overexpression of miR-17 enhances

recombinant protein production of CHO cells. J. Biotechnol. 2014, 175, 38–44.

(68) Fischer, S., Paul, A.J., Wagner, A., Mathias, S., et al., miR-2861 as novel HDAC5 inhibitor in CHO cells enhances productivity while maintaining product quality. Biotechnol. Bioeng. 2015, 112, 2142–2153.

(69) Meleady, P., Gallagher, M., Clarke, C., Henry, M., et al., Impact of miR-7 over-expression on the proteome of Chinese hamster ovary cells. J. Biotechnol. 2012, 160, 251–262.

(70) Strotbek, M., Florin, L., Koenitzer, J., Tolstrup, A., et al., Stable microRNA expression enhances therapeutic antibody productivity of Chinese hamster ovary cells. Metab. Eng. 2013, 20, 157–166.

(71) Kelly, P.S., Breen, L., Gallagher, C., Kelly, S., et al., Re-programming CHO cell metabolism using miR-23 tips the balance towards a highly productive phenotype. Biotechnol. J. 2015, 10, 1029–1040.

(72) Druz, A., Son, Y.J., Betenbaugh, M., Shiloach, J., Stable inhibition of mmu-miR-466h-5p improves apoptosis resistance and protein production in CHO cells. Metab. Eng. 2013, 16, 87–94.

(73) Barron, N., Kumar, N., Sanchez, N., Doolan, P., et al., Engineering CHO cell growth and recombinant protein productivity by overexpression of miR-7. J. Biotechnol. 2011, 151, 204–211.

(74) Huang, W., Liu, H., Wang, T., Zhang, T., et al., Tonicity-responsive microRNAs contribute to the maximal induction of osmoregulatory transcription factor OREBP in response to high-NaCl hypertonicity. Nucleic Acids Res. 2011, 39, 475–485.

(75) Jiang, X., Chen, X., Chen, L., Ma, Y., et al., Upregulation of the miR-212/132 cluster suppresses proliferation of human lung cancer cells. Oncol. Rep. 2015, 33, 705–712.

(76) Sarver, A.L., Li, H., Subramanian, S., MicroRNA miR-183 functions as an oncogene by targeting the transcription factor EGR1 and promoting tumor cell migration. Cancer Res. 2010, 70, 9570–9580.

(77) Braun, C.J., Zhang, X., Savelyeva, I., Wolff, S., et al., p53-Responsive micrornas 192 and 215 are capable of inducing cell cycle arrest. Cancer Res. 2008, 68, 10094–104.

(78) Georges, S.A., Biery, M.C., Kim, S.-Y., Schelter, J.M., et al., Coordinated regulation of cell cycle transcripts by p53-Inducible microRNAs, miR-192 and miR-215. Cancer Res. 2008, 68, 10105–10112.

(79) Khella, H.W.Z., Bakhet, M., Allo, G., Jewett, M.A.S., et al., miR-192, miR-194 and miR-215: a convergent microRNA network suppressing tumor progression in renal cell carcinoma. Carcinogenesis 2013, 34, 2231–2239.

(80) Pichiorri, F., Suh, S.-S., Rocci, A., De Luca, L., et al., Downregulation of p53-inducible microRNAs 192, 194, and 215 Impairs the p53/MDM2 Autoregulatory Loop in Multiple Myeloma Development. Cancer Cell 2010, 18, 367–381.

(81) Wang, J., Xu, G., Shen, F., Kang, Y., miR-132 targeting cyclin E1 suppresses cell proliferation in osteosarcoma cells. Tumour Biol. 2014, 35, 4859–4865.

(82) Kong, W.-Q., Bai, R., Liu, T., Cai, C.-L., et al., MicroRNA-182 targets cAMP-responsive element-binding protein 1 and suppresses cell growth in human gastric adenocarcinoma. FEBS J. 2012, 279, 1252–60.

(83) Wang, G., Mao, W., Zheng, S., MicroRNA-183 regulates Ezrin expression in lung cancer cells. FEBS Lett. 2008,

582, 3663–3668.

(84) Li, P., Sheng, C., Huang, L., Zhang, H., et al., MiR-183/-96/-182 cluster is up-regulated in most breast cancers and increases cell proliferation and migration. Breast cancer Res. 2014, 16, 473.

(85) Park, J.-K., Henry, J.C., Jiang, J., Esau, C., et al., miR-132 and miR-212 are increased in pancreatic cancer and target the retinoblastoma tumor suppressor. Biochem. Biophys. Res. Commun. 2011, 406, 518–523.

(86) Gashler, A.L., Swaminathan, S., Sukhatme, V.P., A novel repression module, an extensive activation domain, and a bipartite nuclear localization signal defined in the immediate-early transcription factor Egr-1. Mol. Cell. Biol. 1993, 13, 4556–4571.

(87) Parpa, E., Ortega, A., Saenz, L., Down-regulation of Egr-1 by siRNA inhibits growth of human prostate carcinoma cell line PC-3. Oncol. Rep. 2009, 22, 1513–1518.

(88) Pritchard, M.T., Malinak, R.N., Nagy, L.E., Early growth response (EGR)-1 is required for timely cell-cycle entry and progression in hepatocytes after acute carbon tetrachloride exposure in mice. Am. J. Physiol. Gastrointest. Liver Physiol. 2011, 300, 1124–1131.

(89) Sells, S.F., Muthukumar, S., Sukhatme, V.P., Crist, S.A., Rangnekar, V.M., The zinc finger transcription factor EGR-1 impedes interleukin-1-inducible tumor growth arrest. Mol. Cell. Biol. 1995, 15, 682–692.

C Complete List of Publications

Pfizenmaier, J. & Takors R. (2016). Host organisms: Mammalian Cells, In Industrial Biotechnology Microorganisms (volume 3, chapter 17), edited by C. Wittmann and J. C. Liao. Weinheim:Wiley-VCH.

Sanchez-Kopper A., M. Becker, **Pfizenmaier, J.**, C. Kessler, A. Karau & R. Takors (2016). Tracking dipeptides at work-uptake and intracellular fate in CHO culture. AMB Express, 6(1):48.

Pfizenmaier, J., L. Junghans, A. Teleki & R. Takors (2016). Hyperosmotic Stimulus Study Discloses Benefits in ATP Supply and Reveals miRNA/mRNA Targets to Improve Recombinant Protein Production. Biotechnol. J., 11:1037-1047

Pfizenmaier, J., J.-C. Matuszczyk & R. Takors (2015). Changes in Intracellular ATP-Content of CHO Cells as Response to Hyperosmolality. Biotechnol. Prog., 31(5):1212-1216

Matuszczyk, J.-C., A. Teleki, **J. Pfizenmaier** & R. Takors (2015). Compartment-specific metabolomics for CHO reveals that ATP pools in mitochondria are much lower than in cytosol. Biotechnol. J., 10(10): 1639 - 1650

Quan, S., P. Koldewey, T. Tapley, N. Kirsch, K.M. Ruane, **J. Pfizenmaier**, R. Shi, S. Hofmann, L. Foit, G. Ren, U. Jakob, Z. Xu, M. Cygler & J.C.A. Bardwell (2011). Genetic selection designed to stabilize proteins uncovers a chaperone called Spy. Nat. Struct. Mol. Biol., 18:262 - 269